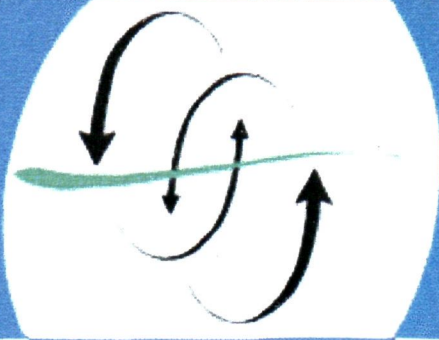




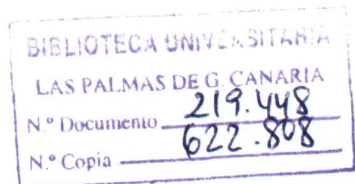
Universidad de Las Palmas de Gran Canaria



Año 1998



Coleccion de Separatas



**Facultad de Ciencias del Mar
Biblioteca de Ciencias Básicas**

Depósito Legal: G.C. 905-1999

ISBN 84-699-0790-5

Imprime: Servicio de Reprografía de la U.L.P.G.C.

<http://www.cbb.ulpgc.es/ccmar>

ÍNDICE

X Barton, E.D.; Arístegui, J.; Tett, P.; Cantón, M.; García Braun, J.; Hernández León, S.; Nykjaer, L.; Almeida, C.; Almunia, J.; Ballesteros, S.; Basterretxea, G. Escánez, J.; García Weill, L.; Hernandez Guerra, A.; López Laatzen, F.; Molina, R.; Montero, M.F.; Navarro Pérez, E.; Rodríguez, J.M.; Van Lenning, K.; Vélez, H. and Wild, K. The transition zone of the Canary Current upwelling region. **Progress in Oceanography**, 1998, vol. 41, p. 455-504

X Campo, Elena del; García Reina, Guillermo; Correa, Juan. Degradative disease in *Ulva Rigida* (Chlorophyceae) associated with *Agrochaete Genuculata* (Chlorophyceae). **Journal of Phycology**, 1998, vol. 34, p. 160-166

✓ Carbonell, E.; Castro, J.J. and Massuti, E. *Floriceps saccatus* plerocerci (Trypanorhyncha, Lacistorhynchidae) as parasites of dolphin fish (*Coryphaena hippurus* L.) and ponpano dolphin (*Coryphaena equiselis* L.) in Western Mediterranean and Eastern Atlantic waters. Ecological and Biological Aspects. **Journal of Parasitology**, 1998, vol. 84, nº 5, p. 1035-1039

X Carracedo, J.C.; Day, S.; Guillou, H.; Rodríguez Badiolas, E.; Canas, J.A. and Pérez Torrado, J. Hotspot volcanism close to a passive continental margin: the Canary Islands. **Geological Magazine**, 1998, vol. 5, p. 591-604

X Castro, José J. ; Caballero, Catalina. Dominance structure in small groups of juvenile white-seabream (*Diplodus sargus cadenati* de la Paz, Bauchot and Daget 1974). **Aggressive Behavior**, 1998, vol. 24, p. 197-204

X Castro, José J. ; Santiago José A. The influence of food distribution on the aggressive behaviour of juvenile white-seabream (*Diplodus sargus cadenati* de la Paz, Bauchot and Daget, 1974). **Aggressive Behaviour**, 1998, vol. 24, p. 379-384 189248

X Eiguren Fernández, A.; Sosa Ferrera, Z. y Santana Rodríguez, J.J. Determination of polychlorinated biphenyls by liquid chromatography following cloud-point extraction. **Analytica Chimica Acta**, 1998, vol. 358, p. 145-155 189249

X García Jiménez, Pilar; Rodrigo, Marta; Robaina, Rafael. Influence of plant growth regulators, polyamines and glycerol interaction on growth and morphogenesis of carposporelings of *Grateloupia* cultured in vitro. **Journal of Applied Phycology**, 1998, vol. 10, p. 95-100 189250

X García, J.L.; Fernández, I. y Pacheco, J.M. Análisis gráfico del comportamiento dinámico de pautas espaciales en sistemas de reacción-difusión. **Información tecnológica**, 1998, vol. 9, nº 6, p. 337-342 190785

X Gómez Pinchetti, Juan Luis; Del Campo Fernández, Elena; Moreno Díez Paula; García Reina, Guillermo. Nitrogen availability influences the biochemical composition and photosynthesis of tank-cultivated *Ulva rigida* (Chlorophyta). **Journal of Applied Phycology**, 1998, vol. 10, p. 383-389 190786

X Gómez, May y Hernández León, Santiago. Estudio de la comunidad mesozooplanctónica en relación a un efecto de isla en aguas de Gran Canaria. **Vieraea**, mayo 1998, vol. 26, p. 11-21 190787

X Hernández García V.; Hernández López, J.L.; Castro, J.J. The octopus (*Octopus vulgaris*) in the small-scale trap fishery off the Canary Islands (Central-East Atlantic). **Fisheries Research**, 1998, vol. 35, p. 183-189 190788

X Hernández García, V.; Castro, J.J. Morphological variability in *Illex coindetii* (Cephalopoda: Ommastrephidae) along the North-West coast of Africa. **Journal of Marine Biology Association U.K.**, 1998, vol. 78, p. 1259-1268

X Hernández-León, Santiago. Annual cycle of epiplanktonic copepods in Canary Island waters. **Fisheries Oceanography**, 1998, vol. 7, n° 3/4, p. 252-257

X Kaye, A. (UK); Stepto, R.F.T. (UK); Work, W.J. (USA); Alemán, J.V. (Spain); Malkin, A. Ya. (Russia). Definition of terms relating to the non-ultimate mechanical properties of polymers. **Pure and Applied Chemistry**, 1998, vol. 70, n° 3, p. 701-754. 190460

X Lindgren, A. ; Bouza, N.; Aberg, P. y Sosa, P. Spatial and temporal variation in distribution of *Gelidium canariensis* (Rhodophyta) from natural population of the Canary Islands. **Journal of Applied Phycology**, 1998, vol. 10, p. 273-278 190470

⊗ Montero, D.; Tort, L.; Izquierdo, M.S.; Robaina, L. and Vergara, J.M. Depletion of serum alternative complement pathway activity in gilthead seabream caused by a-tocopherol and n-3 HUFA dietary deficiencies. **Fish Physiology and Biochemistry**, 1998, vol. 18, p. 399-407 190470

⊗ Moreno, P.; Petkov, G.; Ramazanov, Z.; García, G. Lipids, fatty acids and sterols of *Cystoseira abies-marina*. **Botanica Marina**, 1998, vol. 41, p. 375-378 190427

X Pacheco Castelao, José M. El trabajo de los días. **Epsilon**, 1998, n°41, p. 321-329 190077

X Pacheco Castelao, José M. Matemáticas y biología. **Epsilon**, 1998, n° 40, p. 101-118 JJJ 190077

X Pajuelo, J.G. and Lorenzo, J.M. Population biology of the common pandora *Pagellus erythrinus* (Pisces: Sparidae) off the Canary Islands. **Fisheries Research**, 1998, vol. 36, p. 75-86 190078

✓ Pelegrí, J.L. y Sangrá, P. A mechanism for layer formation in stratified geophysical flows. **Journal of Geophysical Research**, 1998, vol. 103, nº C13, p.30.679-30. 693 19024

✓ Pelegrí, J.L.; Rodríguez Santana, A.; Sangrá, P. y Marrero-Díaz, A. Modeling of shear-induced diapycnal mixing in frontal systems. **Applied Scientific Research**, 1998, vol. 59, p. 159-175 19067

✓ Robaina, L.; Izquierdo, M.S.; Moyano, F.J.; Socorro, J.; Vergara, J.M.; Montero, D. Increase of the dietary n – 3/n – 6 fatty acid ratio and addition of phosphorus improves liver histological alterations induced by feeding diets containing soybean meal to gilthead seabream, *Sparus aurata*. **Aquaculture**, 1998, vol. 161, p. 281-293 19038

✗ Sosa, P. A.; Valero, M. Batista, F. Y González-Pérez, M.A. Genetic structure of natural populations of *Gelidium* species: a re-evaluation of results. **Journal of Applied Phycology**, 1998, vol. 10, 279-284 19045

✗ Uiblein, Franz; Bordes, Fernando; Castillo, Ricardo and G. Ramos, Antonio. Spatial distribution of shelf-and slope-dwelling fishes collected by bottom longline off Lanzarote and Fuerteventura, Canary Islands. **Marine Ecology**, 1998, vol. 19, nº 1, p. 53-66 19075



The transition zone of the Canary Current upwelling region

E.D. Barton^{a,*}, J. Arístegui^b, P. Tett^c, M. Cantón^d,
J. García-Braun^c, S. Hernández-León^b, L. Nykjaer^f,
C. Almeida^b, J. Almunia^b, S. Ballesteros^b, G. Basterretxea^b,
J. Escáñez^g, L. García-Weill^b, A. Hernández-Guerra^b,
F. López-Laatzén^g, R. Molina^g, M.F. Montero^b,
E. Navarro-Pérez^a, J.M. Rodríguez^g, K. van Lenning^b,
H. Vélez^a, K. Wild^a

^a*School of Ocean Sciences, University of Wales, Bangor, Wales, UK*

^b*Facultad de Ciencias del Mar, Universidad de Las Palmas de Gran Canaria, Spain*

^c*Department of Biological Sciences, Napier University, Edinburgh, Scotland, UK*

^d*Universidad de Almería, Spain*

^e*Universidad de La Laguna, Tenerife, Spain*

^f*Joint Research Centre, Ispra, Italy*

^g*Centro Oceanográfico de Canarias, Instituto Español de Oceanografía, Tenerife, Spain*

Abstract

Like all the major upwelling regions, the Canary Current is characterised by intense meso-scale structure in the transition zone between the cool, nutrient-rich waters of the coastal upwelling regime and the warmer, oligotrophic waters of the open ocean. The Canary Island archipelago, which straddles the transition, introduces a second source of variability by perturbing the general southwestward flow of both ocean currents and Trade winds. The combined effects of the flow disturbance and the eddying and meandering of the boundary between upwelled and oceanic waters produce a complex pattern of regional variability. On the basis of historical data and a series of interdisciplinary field studies, the principal features of the region are described. These include a prominent upwelling filament originating near 28°N off the African coast, cyclonic and anti-cyclonic eddies downstream of the archipelago, and warm wake regions protected from the Trade winds by the high volcanic peaks of the islands. The filament is shown to be a recurrent feature, apparently arising from the interaction of a topographically trapped cyclonic eddy with the outer edge of the coastal upwelling zone. Its role

* Corresponding author.

in the transport and exchange of biogenic material, including fish larvae, is considered. Strong cyclonic eddies, observed throughout the year, drift slowly southwestward from Gran Canaria. One sampled in late summer was characterised by large vertical isopycnal displacements, apparent surface divergence and strong upwelling, producing a fourfold increase in chlorophyll concentrations over background values. Such intense eddies can be responsible for a major contribution to the vertical flux of nitrogen. The lee region of Gran Canaria is shown to be a location of strong pycnocline deformation resulting from Ekman pumping on the wind shear boundaries, which may contribute to the eddy formation process. © 1998 Elsevier Science Ltd. All rights reserved.

Contents

1. Introduction	456
2. Data	458
3. Large scale context	460
3.1. Seasonal variation	460
3.2. Regional variation	466
4. Mesoscale variability	468
4.1. Upwelling filaments	469
4.2. Island eddies	482
4.3. Island lee	490
5. Discussion	492
6. Acknowledgements	501
7. References	501

1. Introduction

In recent years the richness of mesoscale structure associated with upwelling areas has been revealed by the use of satellite observations of sea surface temperature patterns and ocean colour (Traganza, Nestor, & McDonald, 1980). The interaction between the coastal upwelling regime over the continental shelf and the offshore oceanic regime has been shown to be highly variable and to take place in a zone several hundred kilometres wide. The boundary between the cool, nutrient-rich upwelled waters and the warmer, nutrient-poor offshore waters is irregular and often contorted to form long, narrow, offshore-flowing streamers or filaments of upwelled water which may reach far offshore. Much effort has been expended on examining these features typical of the 'Coastal Transition Zones' in terms of their in situ characteristics and role in shelf–ocean exchange of biota and nutrients (Brink, & Cowles, 1991). Filaments appear to arise from more than one cause, however, and may differ between sites and regions (Strub, Kosro, & Huyer, 1991).

The northwest African upwelling region is typical in terms of the obvious presence of filaments (Van Camp, Nykjaer, Mittelstaedt, & Schlittenhardt, 1991), though so far they have been little studied there. It differs from other upwelling zones because

of the presence of the Canary Islands, which provide another major source of meso-scale activity (Aristegui, Sangrá, Hernández-León, Cantón, Hernández-Guerra, & Kerling, 1994; Aristegui, Tett, Hernández-Guerra, Basterretxea, Montero, Wild, Sangrá, Hernández-León, Cantón, García Braun, Pacheco, & Barton, 1997). The archipelago consists of seven main islands distributed zonally across the eastern limb of the subtropical gyre of the North Atlantic at a latitude near 28°N (Fig. 1). The volcanic islands rise steeply from sea floor depths in excess of 2000 m with deep

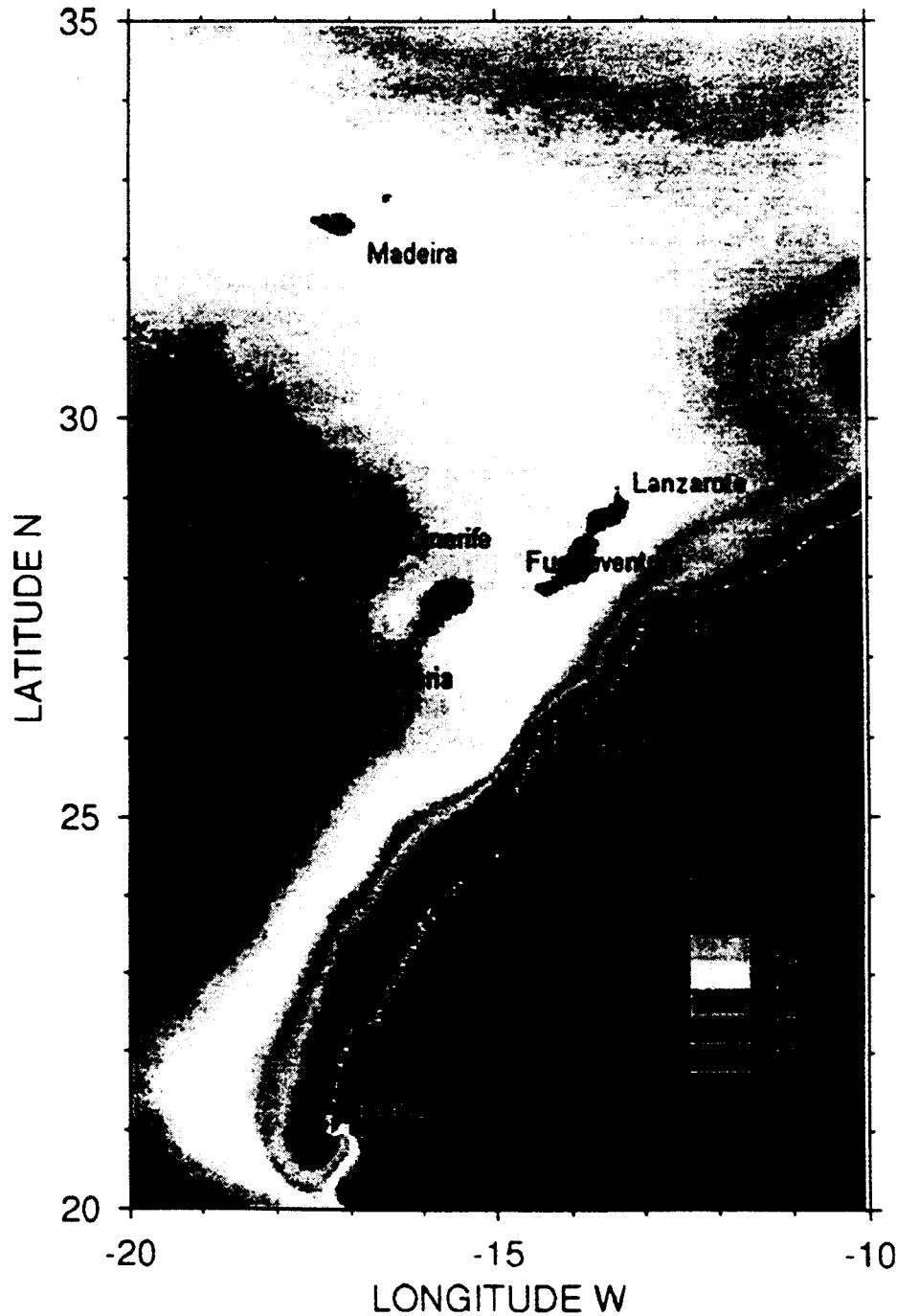


Fig. 1. Long term (1981–1991) mean sea surface temperature derived from Global Area Coverage AVHRR data.

channels separating them. Their summits reach a maximum height of 3718 m on Tenerife, where Teide is the highest mountain in all Spain. Fuerteventura is separated by a distance of some 90 km from the African mainland coast, and the archipelago extends some 400 km further west. The islands thus span the transitional zone linking the continental shelf upwelling region of northwest Africa to the open ocean waters of the subtropical gyre. They present a barrier to both the weak equatorward flow of the Canary Current and to the flow generated by the Trade winds, thus giving rise to a variety of mesoscale phenomena.

Early studies described the Canary region as 'oligotrophic', comparable to the open ocean subtropical gyres (De León, & Braun, 1973; Braun, 1980). However, this general view has changed during recent years, following the analyses of sea-surface temperature and chlorophyll derived from satellite images, and the study of physical and biological data gathered during shipboard sampling of the mesoscale variability of the region.

In this paper we discuss the results of a recent inter-disciplinary European project to study the Canary Island region in terms of its annual cycle and the various sources of mesoscale variability. The work is based on data collected during a series of three cruises carried out in different seasons, and supplemented by archived data from a variety of sources. The cruises had different individual emphases but all three sampled a dense grid south of Gran Canaria to study island wakes and eddies, two measured conditions along transects across the entire archipelago, and one made intensive measurements between the islands and the African coast to sample an upwelling filament (Fig. 2). Notionally the area can be divided into four sub-regions, waters north of the archipelago, affected (1) and unaffected (2) by the NW African coastal upwelling system; and southern waters, perturbed after flowing through the islands chain, affected (3) and unaffected (4) by the African upwelling. As will become apparent, the upwelling-open ocean boundary is contorted and subject to significant variability. This region affected by the boundary, constitutes the transition zone.

We provide an up-to-date overview of the area as a basis for more specialised reports and process studies in preparation, to document in some detail the major processes influencing mesoscale activity and to evaluate the importance of those processes. This zone of transition between coastal upwelling and open ocean conditions is important not only for its regional significance (for example in supporting a fishery through enhanced primary production), but also because it provides a convenient site for the study of two globally important processes. These are: (1) shelf-ocean exchange associated with eastern boundary upwelling; and (2) the disproportionate contribution of continental margin and island stirring to horizontal and upper-ocean vertical mixing in the subtropical ocean gyres. 'Mesoscale activity' is another way of labelling this stirring and its immediate consequences.

2. Data

Field data were obtained during three cruises on board R.V. *García del Cid*, 9–17 March 1991, on R.V. *Ignat Pavlyuchenkov*, 25 October–25 November 1991 and

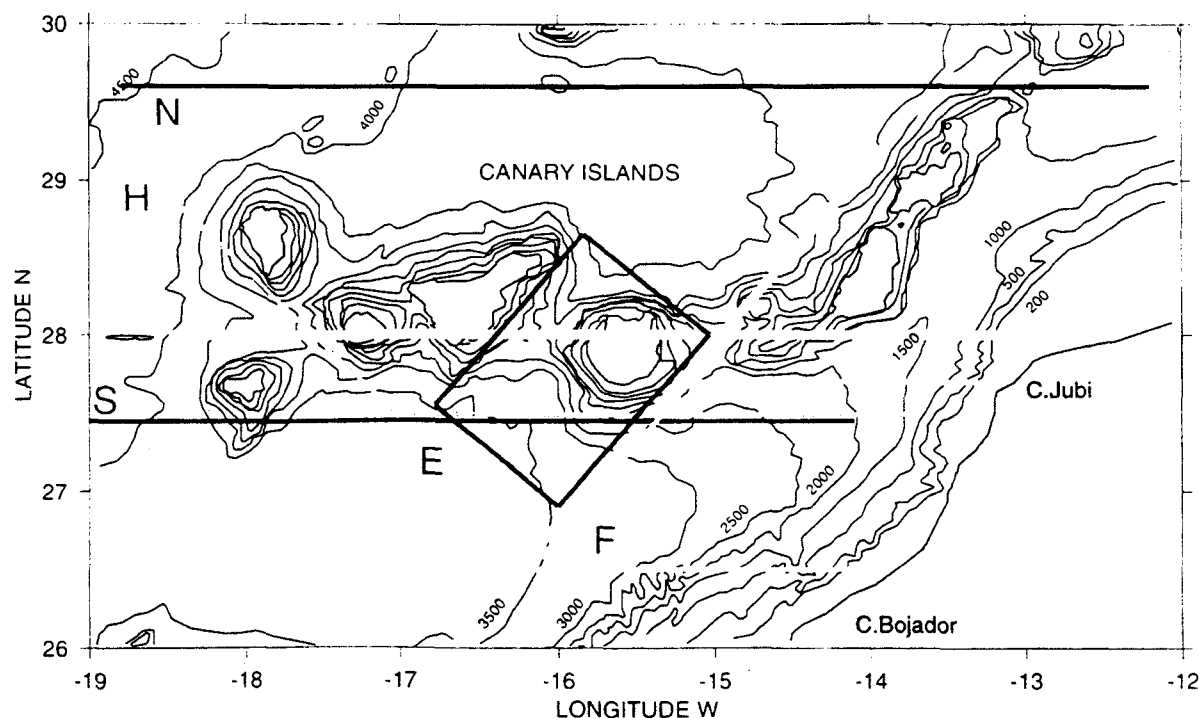


Fig. 2. Canary Islands region showing study areas for eddy surveys (E), filament survey (F) and long sections (N and S in October 1991 and H in August 1993). The region can conceptually be divided into four zones of influence: (1) dominated by coastal upwelling, (2) undisturbed oceanic, (3) upwelling and island influenced and (4) oceanic island influenced. Depth contours are marked in metres.

on R.V. *Hespérides*, 5–26 August 1993. The cruises took place during the three representative phases of the seasonal development of production in the Canaries region. These are: (1) the end of the winter period, when a bloom takes place; (2) the strongest Trade wind period, when coastal upwelling is most developed; and (3) early autumn, when winds are weakest and stratification is strongest. Wind data were obtained from the airport on the exposed east coast of Gran Canaria supplied by the Spanish Instituto Nacional de Meteorología.

Cruise observations consisted of interdisciplinary surveys as represented in Fig. 2. Each cruise included a grid of about 50 Conductivity-Temperature-Depth (CTD) stations at roughly 20 km spacing around Gran Canaria to observe island-induced eddies and other downstream effects (Box E). The October–November cruise included the two zonal transects (N and S) of stations at 20 km intervals to compare conditions upstream and downstream of the archipelago. The August cruise re-sampled most of transect S and a line extending northwest between the outer islands (Line H). Additionally this cruise made a survey of the northwest African coastal upwelling between Cabo Jubi, Cabo Bojador and 200 km offshore. Data were gathered with a SeaBird SB-19 CTD probe in the first cruise (Arístegui, Tett, Hernández-Guerra, Basterretxea, Montero, Wild, Sangrá, Hernández-León, Cantón, García Braun, Pacheco, & Barton, 1997), with a Niel Brown Mk III in the second cruise (Vélez-Muñoz, 1992) and with a SeaBird SB9-11 + probe in the August 1993 cruise (Navarro-Pérez, Vélez-Muñoz, & Wild, 1994). Casts were made generally to 600 m

or the sea bed, where shallower, though some were made to 1000 m. Ship board ADCP (Acoustic Doppler Current Profiler) observations made from the R.V. *Hespérides* in August 1993 are reported by Navarro-Pérez, & Barton (1995).

At many stations other variables were sampled with additional sensors and Niskin bottles on the CTD rosette, with separate bottle casts and with assorted net hauls. Properties determined included chlorophyll-*a* (Wild, 1992; Navarro-Pérez, Vélez-Muñoz, & Wild, 1994), oxygen and nutrients (Braun, & Escánez, 1996), primary production (Basterretxea, 1994), Electron Transport System activity in microplankton (Montero, 1992), phytoplankton and bacteria (Wild, 1995; Ballesteros, 1992; Kennaway, & Tett, 1994), zooplankton biomass (Hernández-León, 1988) and fish larvae (Rodríguez, 1996).

Sea Surface Temperature (SST) images were obtained from High Resolution Picture Transmission (HRPT) data from the Advanced Very High Resolution Radiometer (AVHRR) sensors onboard the National Oceanic and Atmospheric Administration (NOAA) satellites. A split window algorithm designed by Castagné, Le Borgne, Le Vouch, & Olry (1986) was used to correct for atmospheric water vapour. SST is calculated with an accuracy of about 0.5°C by this algorithm (Le Borgne, Le Vouch, & Marsouin, 1988). The images were plotted on a Mercator Projection with a 1 km pixel resolution.

3. Large scale context

3.1. Seasonal variation

In the North Atlantic throughout most of their meridional extent the Trade winds have a strong alongshore component which drives upwelling at the eastern boundary. The large scale upwelling is seen in mean sea surface temperature fields for the years 1981–1991 derived from AVHRR Global Area Coverage data (4 km resolution) from the NOAA satellites (Fig. 1). The overall isotherm pattern reflects the form of the eastern limb of the subtropical gyre. Lower mean temperatures occur in a coastal boundary zone that includes at least the inner Canary Islands. The southern limit of the year round upwelling is seen at Cabo Blanco. A disturbance effect by the islands is evident even in this long term mean picture, in which regions of higher temperature form wake-like patterns southwest of the five outer islands and to a lesser extent the inner two.

Wooster, Bakun, & McLain (1976); Speth, Detlefsen, & Sierts (1978); Nykjaer, & Van Camp (1994) have shown that during the months of June to September the Trade wind band affects the African coast between about 35°N and 20°N and have demonstrated the strong relation between the coastal temperature anomaly with respect to mid-ocean and the Ekman transport normal to the coast. In November to April the Trades, located further south in response to the southward shift and strengthening of the Azores High–Saharan Low system, affect the coast between about 30°N and 12°N. This annual cycle is manifest in the locality of the Canaries as a variation in strength and orientation of the Trade winds, leading to a strong

annual rhythm in wind forcing. In contrast to temperate latitudes, however, the strongest wind forcing is in the boreal summer, at about the same time as the strongest heating.

The annual march of sea surface temperature, wind vectors and estimated Ekman transport for latitude 29°N from the African coast to west of the Canaries is shown in Fig. 3. Monthly means of all available data from COADS, the Comprehensive Ocean-Atmosphere Data Set (Roy, & Mendelssohn, 1995), are shown for one degree squares. Ekman transport is calculated from the monthly mean wind stresses. The intensification of winds is evident between June and September as their direction changes from northeasterly to northerly. At these latitudes the monthly mean winds blow with an equatorward component along the African coast year round with the peak intensity occurring in July–August. The accompanying strengthening of the zonal temperature gradient is also clear. Maximum temperature contrast between coast and 20°W is seen in August–September. The latter is largely a result of the strengthening of the increased upwelling during summer at the African coast, though surface temperatures increase generally because of summertime insolation and heat gain by the ocean. Conditions are upwelling favourable throughout the year therefore, though less so in the winter months when the winds are weakest and most variable in direction. The strongest nearshore cooling is not revealed by the 1 degree grid resolution of this data set.

Realisations of the mean fields of sea surface wind, Ekman transport and temperature for the seasons corresponding to the project cruises show the major geographic and annual variation (Fig. 4). The intensity of the monthly mean winds increases significantly during the summer (August) throughout the area, although they remain conducive to upwelling in all months. The winds are weakest in November but are almost as weak in March. The general form of the temperature field shows that the typical cooler region of upwelling near the African coast persists year round. The southern limit of the upwelling in summer is clearly seen at Cabo Blanco (20° 50' N). A striking difference between the summer and other periods is that the isotherms show a weaker meridional temperature gradient across and north of the Canaries in August. During the other seasons they lie almost zonally, but in summer they trend northwest to southeast. This change represents the large scale seasonal alteration of the shape and location of the eastern limb of the subtropical gyre reported by Stramma, & Siedler (1988).

The mean Ekman transport (Fig. 4) shows significant zonal and meridional gradients, which decrease generally from the coast towards open ocean and from south to north. The wind stress curl and hence the vertical velocity at the base of the Ekman layer were calculated at 1° intervals by a centred difference scheme from the COADS pseudo-stress data. Sources of error in such calculations are discussed by Bakun, & Nelson (1991). The upwelling velocity, shown as contours overlaid on the wind stress maps in Fig. 4, shows the Ekman layer is divergent within 100–150 km of the African coast. This indicates an upward velocity and implies upwelling occurs year round as suggested by the temperature distributions. The temperature contours tend to parallel the coast within the region of divergence. Maximum values of estimated monthly mean upwelling velocity were around 0.4 m d⁻¹, but the diver-

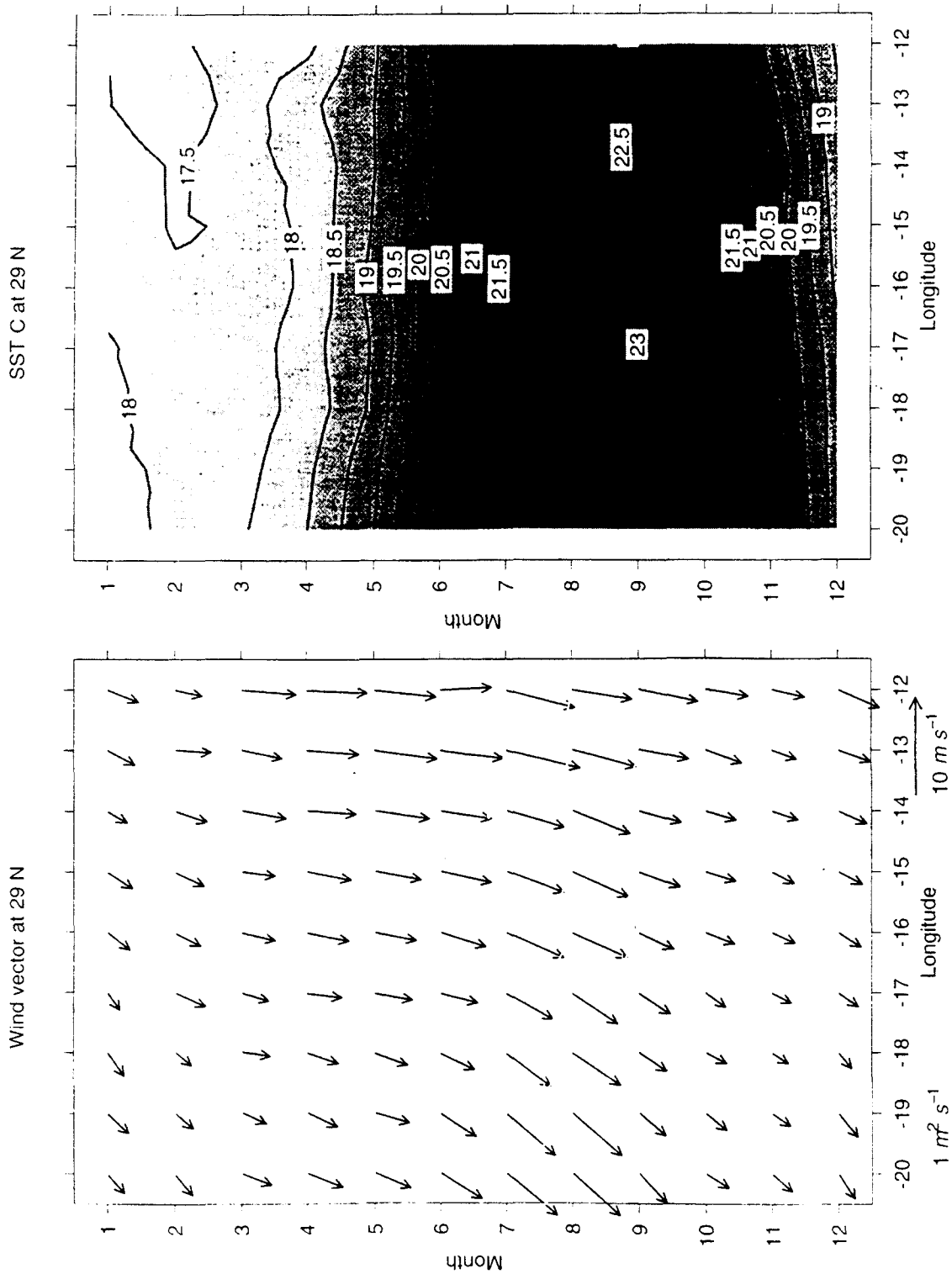


Fig. 3. Annual cycle of monthly mean sea surface temperature ($^{\circ}\text{C}$) and wind vectors at 29°N . Lighter arrows indicate the Ekman transport vector calculated from the mean monthly wind stress.

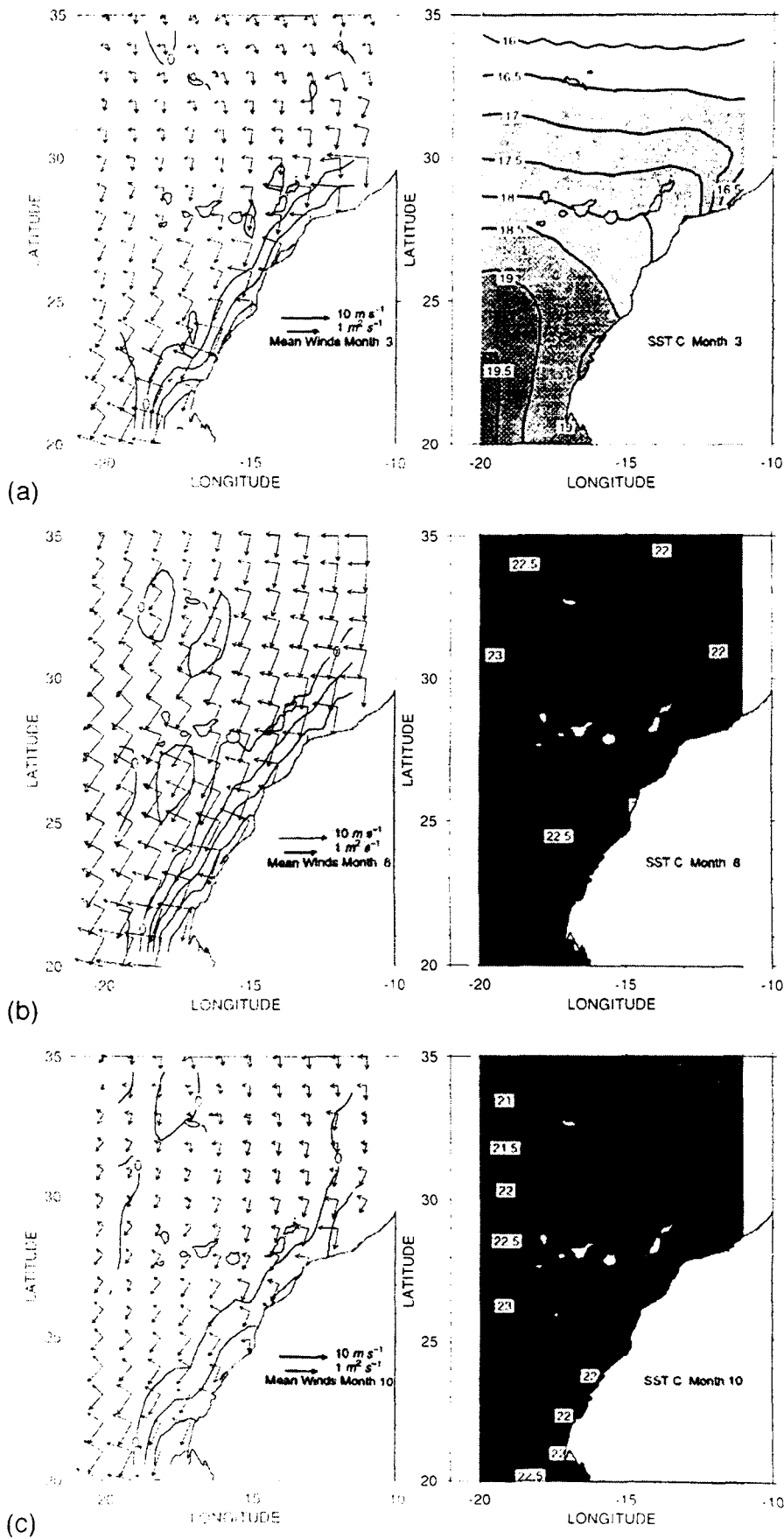


Fig. 4. Maps of monthly mean surface wind velocity, Ekman transport and upwelling velocity (left) and sea surface temperature (right) for (a) March (b) August (c) October. Contours of vertical velocity are at 0.1 m d^{-1} intervals; negative values (downwelling) are shaded.

gence is under-estimated at the coast because of the 1° spacing of the observation grid. In the offshore area the field is weakly convergent. The position of the zero vertical velocity contour varies with season, but provides a basis for locating the hypothetical boundary between upwelling affected areas (1) and (3) and oceanic conditions of areas (2) and (4) indicated in Fig. 2.

The mean annual cycle of temperature in waters to the north-west of the Canaries archipelago is shown in Fig. 5. This exemplifies the seasonal and depth variation of hydrographic structure in the undisturbed and oligotrophic oceanic waters of the Canary Current. The data are monthly averaged values for the area 4 ($29\text{--}31^\circ\text{N}$, $17\text{--}19^\circ\text{W}$) calculated from the National Oceanic Data Center archive. The period of strongest near surface stratification occurs in June to October when not only insolation, but also wind forcing, are strongest. The situation differs from the temperate seas where winter cooling coincides with strong winds. Nevertheless, convection resulting from surface cooling and aided by wind stirring during winter, is sufficient

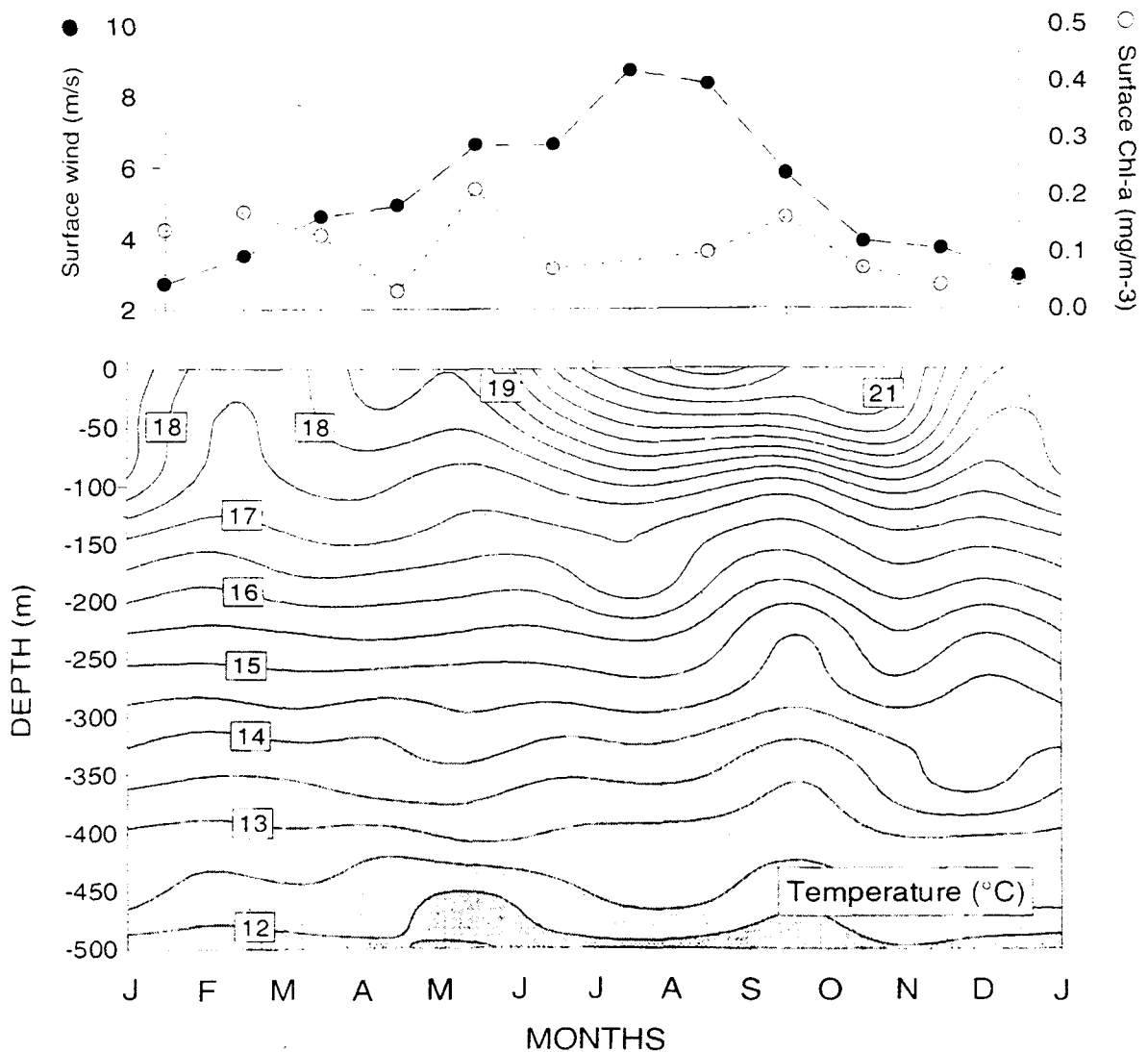


Fig. 5. Annual cycle of temperature, integrated chlorophyll and surface wind in the oceanic region unperturbed by island or upwelling.

to weaken the seasonal stratification from November on. The time of maximum penetration of the surface mixed layer (~100 m) is February to April. The seasonal thermocline begins to reform in April–May and reaches its greatest intensity, when surface temperatures are highest in August–September, despite the maximum winds occurring in August.

Detailed seasonal biological studies of the Canaries region are few but it is reported that mean chlorophyll concentrations are low ($< 0.5 \text{ mg Chl m}^{-3}$) for most of the year (Aristegui, Hernández-León, Gómez, Medina, Ojeda, & Torres, 1989; Aristegui, Tett, Hernández-Guerra, Basterretxea, Montero, Wild, Sangrá, Hernández-León, Cantón, García Braun, Pacheco, & Barton, 1997). Mean monthly surface values compiled from these sources, shown in Fig. 5 for the area northwest of the islands, indicate only slight enhancement at the end of winter. Chlorophyll values up to 1 mg m^{-3} have been reported close to the islands (Braun, Orzaiz, Armas, & Real, 1985), although these concentrations were probably enhanced by local oceanographic processes.

The annual production cycle in Canaries waters unaffected by the NW African coastal upwelling can be broadly divided into three periods: (1) the late winter bloom, when the seasonal thermocline is eroded and nutrients from deeper layers are mixed up into the previously depleted surface waters; (2) the summer season, which corresponds with the period of highest trade winds intensity, and therefore of high coastal upwelling activity; and (3) the autumn season, when wind intensity decreases, the seasonal stratification is at its most intense and plankton productivity falls to its lowest annual values. The dynamics of the winter bloom are more similar to those of the autumn (nutrient-limited) rather than the spring (light-limited) bloom of temperate seas.

From late spring to early winter, the period of superficial stratification, most chlorophyll is found in a deep maximum (DCM) within the seasonal thermocline. Picophytoplankton ($< 2 \mu\text{m}$) are the most typical photosynthetic organisms, contributing to chlorophyll and production with $> 75\%$ in autumn and up to 50% in spring (Montero, 1993). Smaller phytoflagellates dominate the DCM, whereas cyanobacteria are most abundant in the surface mixed layer or SML (Ballesteros, 1994). Phytoplankton larger than $2 \mu\text{m}$ are scarce during most of the year, except in the African coastal upwelling zone, where diatoms are abundant.

The relatively small year round variation in chlorophyll concentrations integrated over the water column (approximately between $15\text{--}60 \text{ mg Chl m}^{-2}$) contrasts with the much larger variability in primary production values. During the autumn, primary production is as low as in the most oligotrophic regions of the world ($25\text{--}30 \text{ mg C m}^{-2} \text{ d}^{-1}$; Li, 1994; Basterretxea, 1994). In late winter and early spring, however, productivity values increase more than an order of magnitude (up to $1000 \text{ mg C m}^{-2} \text{ d}^{-1}$). Even values higher may occur associated with distinct mesoscale features (like eddies and fronts) which produce upwelling of deep nutrient-rich water into the surface waters.

The seasonal increase in primary productivity is not accompanied by a similar increase in chlorophyll accumulation. The study of the available in situ chlorophyll data together with the complete archive of CZCS images in the Canaries region,

indicates that at the start of the mixing period (January–February) only a weak bloom is produced. It appears that grazers take advantage of the phytoplankton bloom rapidly to prevent any surface accumulation (Aristegui, 1990), so that the bloom never has time to build up and then weakens into spring and summer (Braun, Orzaiz, Armas, & Real, 1985). Zooplankton biomass reaches its maximum a few weeks after the phytoplankton peak, and drops sharply as the algal standing crop falls (Hernández-León, 1988). Additional zooplankton peaks have been described during late spring and summer in the wakes of the islands coinciding with strong wind pulses (Hernández-León, 1991). CZCS images show that highest chlorophyll concentrations occurring at the sea surface in the northwest African upwelling region in July–August (Hill, Hickey, Shillington, Strub, Brink, Barton, & Thomas, 1997); highest primary production values we observed were in the upwelling region near Cabo Bojador during the August 1993 cruise.

3.2. Regional variation

Conditions upstream (sub-regions 1 and 2 of Fig. 2) and downstream of the islands (sub-regions 3 and 4) were compared during the cruise carried out in October–November 1991 on board the R/V *Ignat Pavlyuchenkov*. A major goal of the cruise was to look for evidence of increased biological productivity in the wake downstream of the island. Calm seas and strong surface heating typified this period, and winds were even weaker than expected at this time of year. The surface heating reduced sea surface temperature gradients across the area of interest, and the persistent cloudiness prevented acquisition of very many useful satellite images.

Although the sampling period corresponded to the season of lower productivity, lower influence of the African upwelling and higher stratification of the water column, the four Canary region sub-divisions (Fig. 2) were still distinguishable by both their physical and biological properties. The long zonal section made north of the islands was quite uniform in temperature, salinity and chlorophyll-a, typical of the far field, except in the upwelling region near to the African coast (Fig. 6). Whereas a parallel section to the south presented significant perturbations and eddy-like structures, presumably caused by the islands. Comparisons between the sections showed that the southern section was significantly more variable in terms of isotherm excursions and presented a shallower DCM. Chlorophyll integrated over the 0–200m layer was higher in the southern section (Fig. 7), where the nutricline was shallower (Fig. 8). In both sections chlorophyll concentrations (Figs. 6 and 7) and abundances of cyanobacteria and phytoflagellate cells (Fig. 8) were higher in the eastern stations, providing evidence of the upwelling influence. The boundary between the coastal upwelling zone and offshore waters was strongly demarcated between stations 17 and 18, southeast of Gran Canaria (Fig. 6). The mean primary production values in the mixed layer in the southern section (Fig. 7) show a clear influence of a cyclonic eddy at stations 19 and 20 (presumably originating from Gran Canaria). This influence is not so clearly visible in the integrated chlorophyll field. In all instances average chlorophyll concentrations were very low at this time of the year, as was to be expected from the strong stratification.

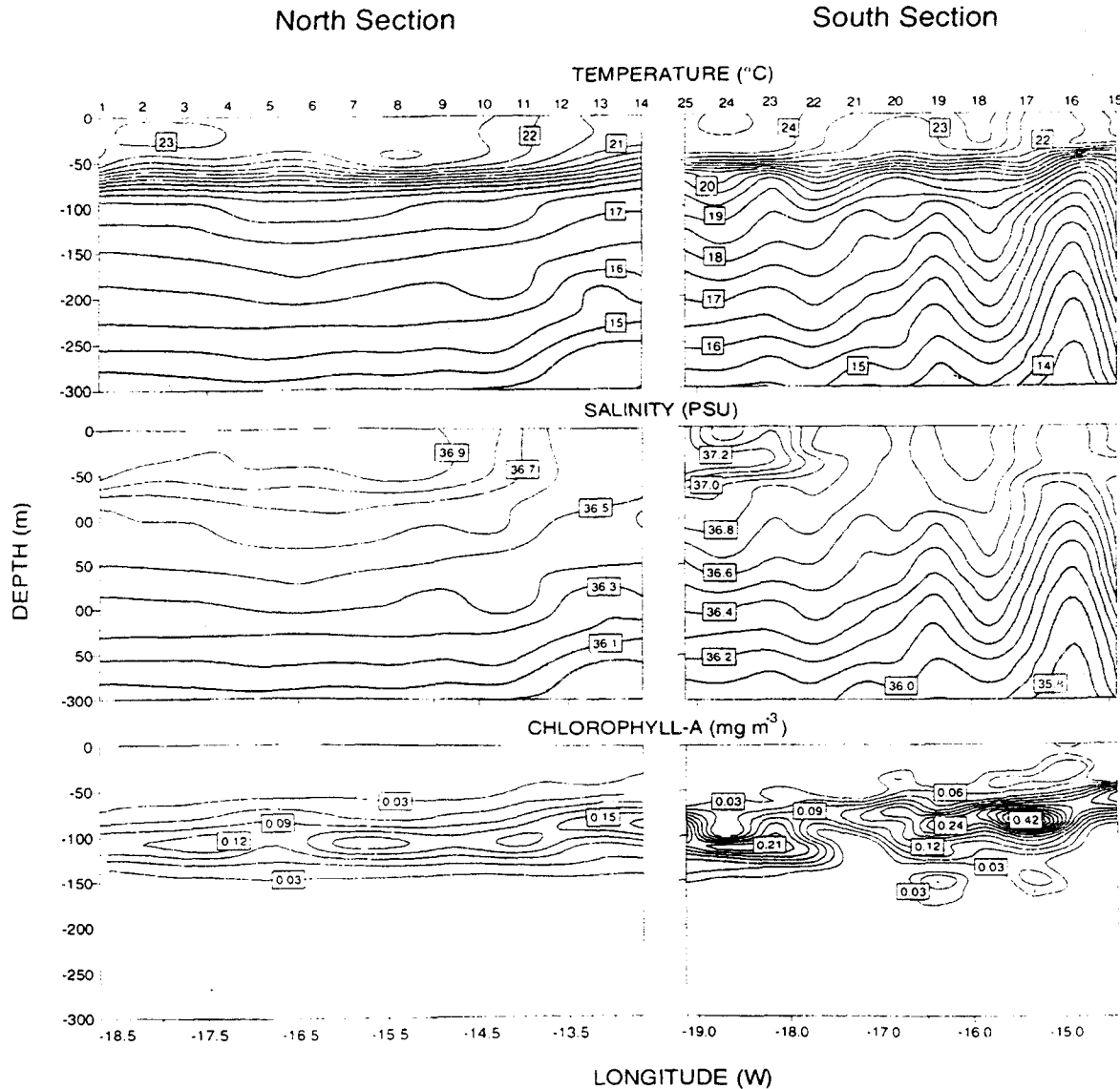


Fig. 6. Sections of temperature, salinity and chlorophyll-a north and south of Canary Islands in October 1991 (Lines N and S in Fig. 2) show the effects of the African upwelling in the east and island perturbations on the southern section.

Evidence of upstream–downstream differences across the archipelago was supported by comparisons of two 24-hour time series made north and south of Gran Canaria in October 1991. At the southern station, close to a cyclonic eddy, the DCM was shallower and more intense although the pycnocline on this occasion was only slightly shallower (Fig. 9). The mean depth of the nutricline was about 30 m shallower and the mean water-column integrated chlorophyll about double that in the far field, at the northern station (Fig. 10). Furthermore, microbial respiration (expressed as ETS activity) was significantly higher in the southern station. While variability between individual stations can occur as a result of patchiness of open ocean phytoplankton on scales of kilometers, the persistent difference between the time series stations and more generally between the northern and southern lines indi-

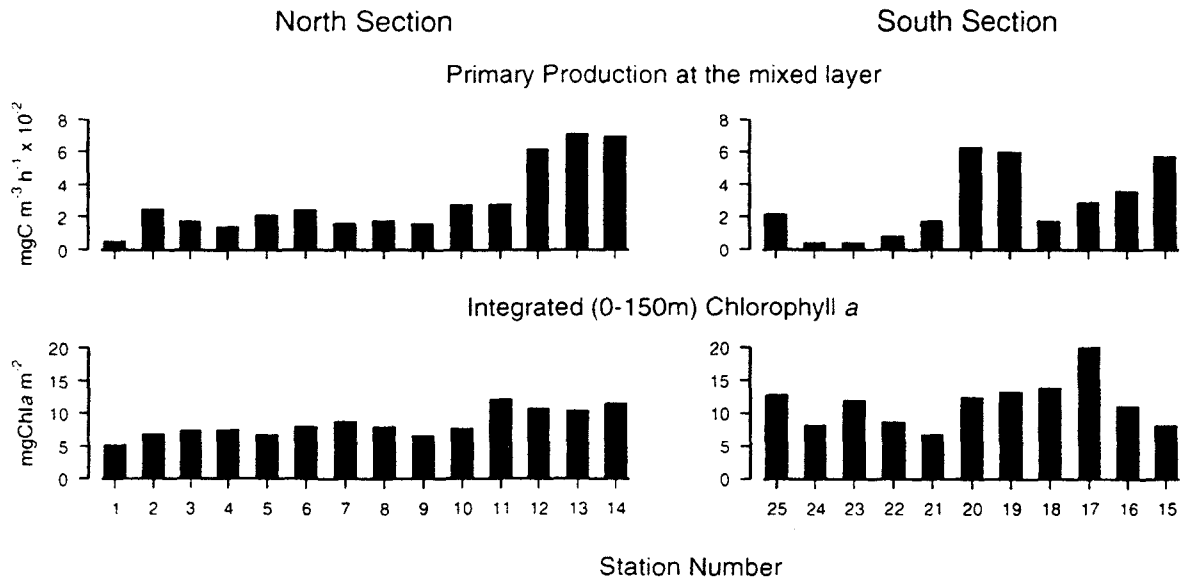


Fig. 7. Horizontal profiles of primary production in the mixed layer and chlorophyll integrated from 0–150 m along the sections north and south of the Canary Islands in October 1991.

cate variability at somewhat larger scales. These results are evidence that there was an island mass effect caused by the archipelago perturbing the mean flow.

4. Mesoscale variability

Recent satellite and field observations have revealed that there is strong year-round mesoscale variability in both temperature and chlorophyll distributions in the waters of the archipelago that is superimposed on the background seasonal and regional variation (Aristegui, Sangrá, Hernández-León, Cantón, Hernández-Guerra, & Kerling, 1994; Aristegui, Tett, Hernández-Guerra, Basterretxea, Montero, Wild, Sangrá, Hernández-León, Cantón, García Braun, Pacheco, & Barton, 1997). By mesoscale, we refer to the range of phenomena whose dominant spatial scale lies between approximately one and ten times the baroclinic Rossby radius, with a concomitant temporal scale of one to ten inertial periods. This encompasses the approximate ranges of 10 to several hundred kilometres and time periods of one day to several weeks. Much of this variation is associated with eddies and other island effects, and with the intrusion of cold, chlorophyll-rich coastal upwelling waters westward into the area of the eastern islands. Substantial mesoscale variability was evident during all three cruises. The variability included both cold-core, cyclonic, eddies, as seen during all cruises, and also warm-core, anticyclonic, eddies, as seen during the March 1991 cruise. The eddies sampled during the cruises lay to the south and south-west of Gran Canaria, as would be expected if they resulted from flow perturbations by the island. Regions of colder and less saline water, evidence of the offshore limits of a filament, were seen to the southeast of Gran Canaria during the cruises in March and October 1991, while in August 1993, a clearly defined upwelling filament, which ended in a cyclonic eddy southeast of Gran Canaria was thoroughly studied.

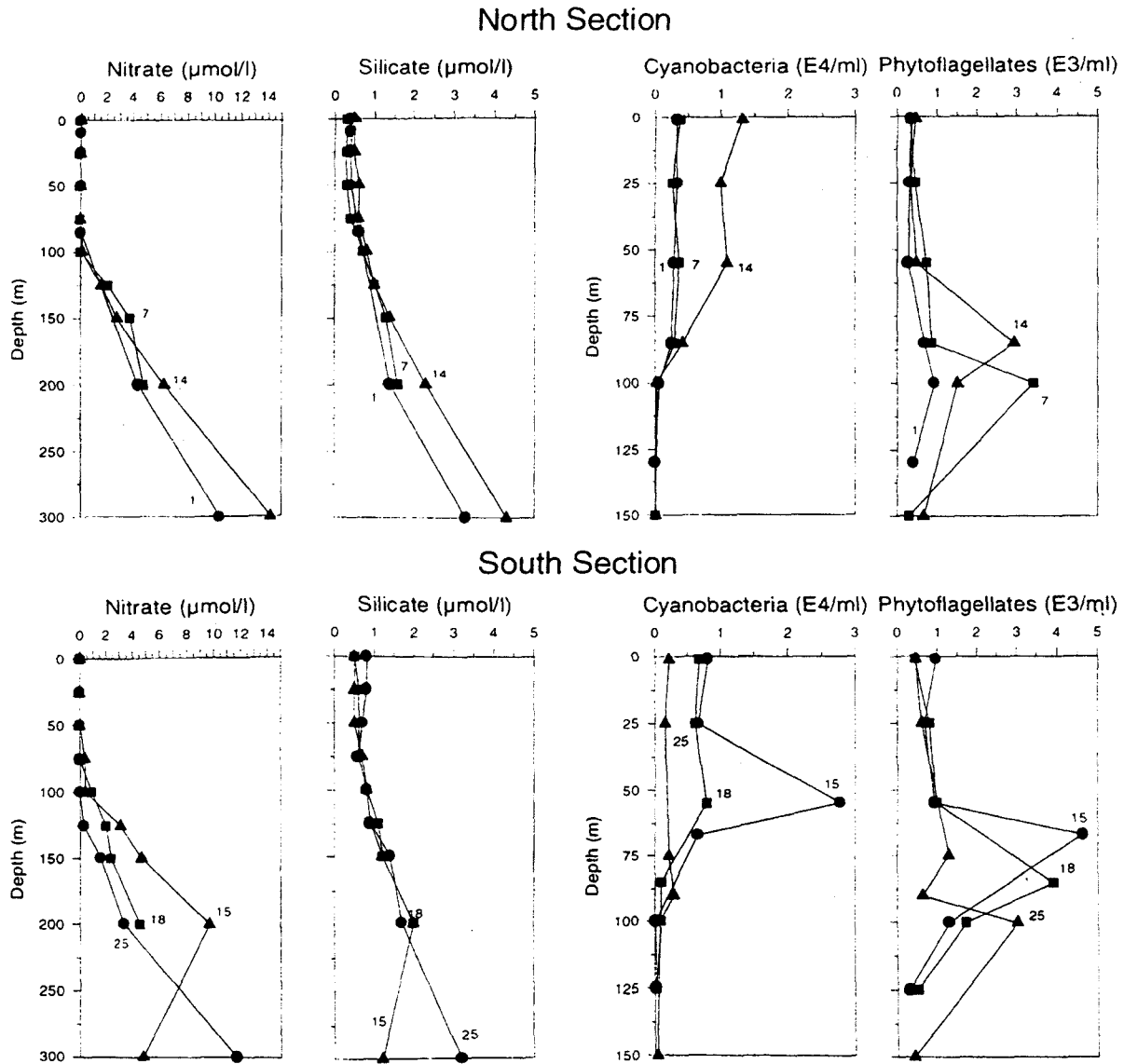


Fig. 8. Vertical profiles of nitrate, silicate, cyanobacteria and phytoplankton at selected stations in the sections north and south of the Canary Islands in October 1991.

4.1. Upwelling filaments

As shown by AVHRR and CZCS (Coastal Zone Color Scanner) imagery, the southeastern Canary region is frequently invaded by upwelling waters arriving in the form of narrow cold chlorophyll-rich filaments extending some hundred kilometres offshore. A detailed study of one of these recurrent features was carried out in August 1993, during the season when, according to the climatic average data, upwelling was strongest. Winds were so strong during the cruise that sampling had to be abandoned for a time because of the sea state. However, as the result of this strong forcing, many well-developed mesoscale features were evident in the area, and were well-sampled.

Atmospheric conditions were clear on a number of days during the cruise and wind mixing prevented significant surface heating from obscuring near-surface temperature patterns. Five images reveal that the filament persisted between 2 and 29

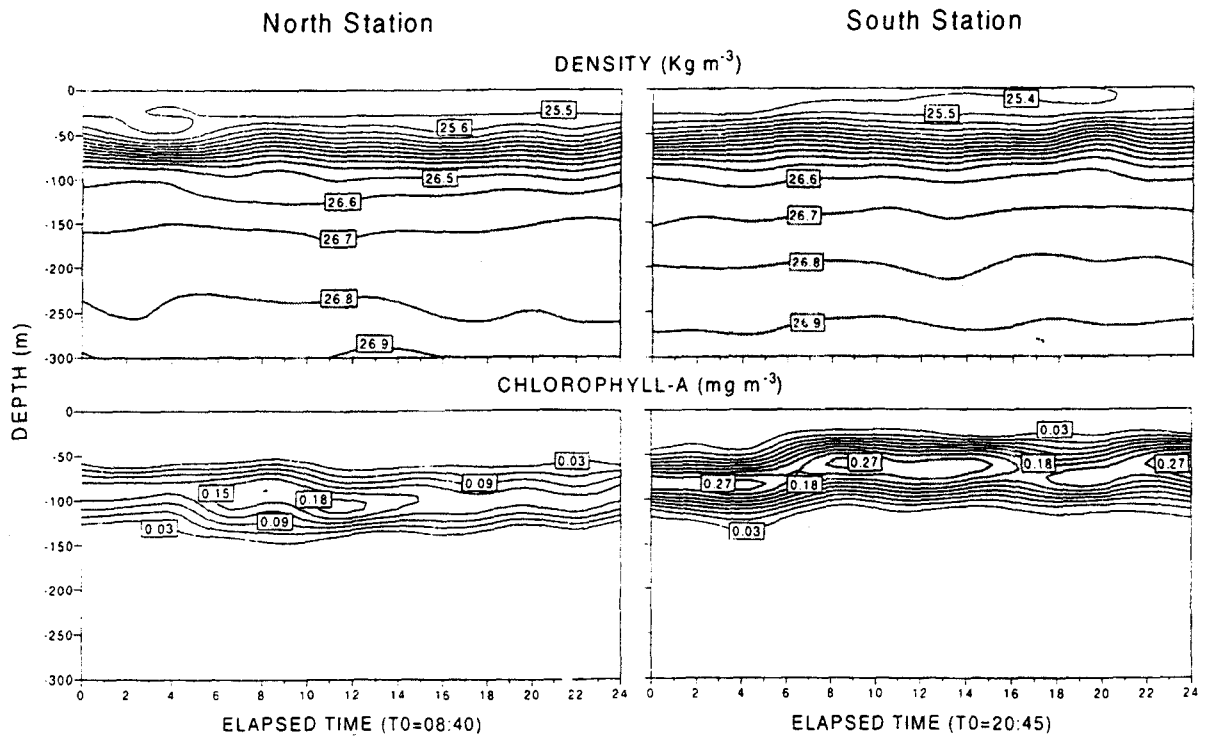


Fig. 9. Time series from two stations north and south of the Canary Islands showing profiles of density anomaly and phytoplankton in October 1991.

August 1993 (Fig. 11a to e). The filament appeared to arise on the continental shelf near 27°N , just north of Cabo Bojador. It extended over 150 km northwest towards Gran Canaria but appeared to be diverted cyclonically to the south in the early images of 2 and 4 August. The development of the filament was related to the winds (Fig. 11f). Following the start of the cruise on 4 August there was a period of strong winds which briefly exceeded 25 m s^{-1} on 7 August. (In the record apparent wind reversals occur where the ship passed through the lee of the islands.) By 10 August the cyclonic formation appeared more clearly and the filament itself was more sharply delineated as an extended narrow tongue of cooler water of $21.5\text{--}22^{\circ}\text{C}$ wrapped around a slightly warmer core. The structure was still present through 18 August, though on that day its detailed configuration was obscured by cloud. After 18 August the winds relaxed considerably and by 29 August, after the end of the cruise, the filament was still clearly visible but less strongly defined. Generally the coastal upwelling seemed to be constrained well within the width of the continental shelf, as defined by the 200 m contour. However, on 10 and 18 August it had expanded to the shelf limit almost everywhere in the region as a result of the wind strength. The filament's width was generally about 20 km or less and it was bounded by strong temperature gradients to both north and south. Coastal upwelling, and the filament temperature contrast, appeared weaker on 4 and 29 August.

The position of the filament's base near to the shore varied little (Fig. 11) except in the image of 18 August, which may have been affected by cloud contamination. Statistical studies of filaments off the western coast of Iberia shows that they frequently arise slightly downstream of particular coastal features such as capes

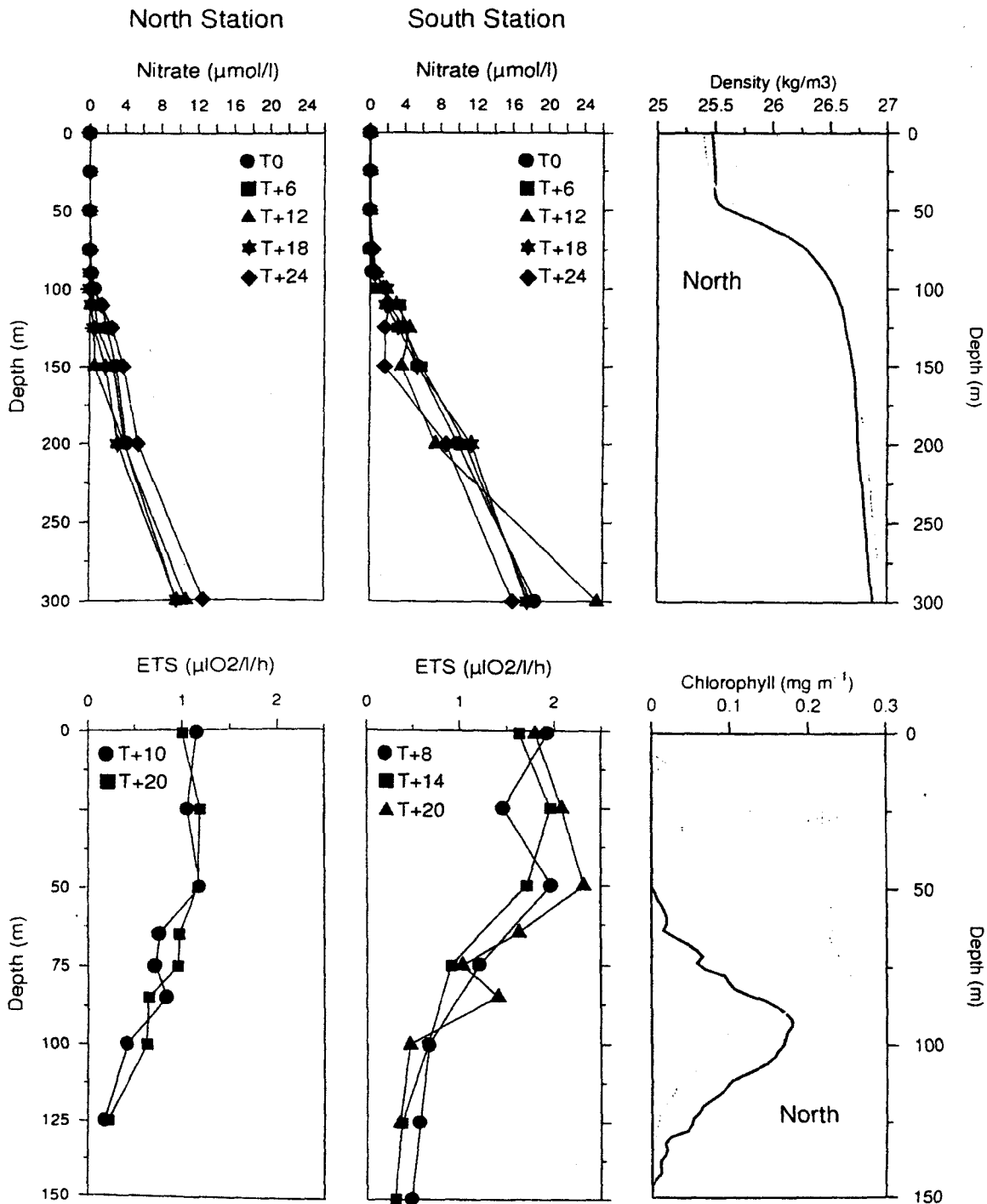


Fig. 10. Vertical profiles of nitrate, ETS activity in microplankton, density and chlorophyll at the 24 hour time series stations north and south of the Canary Islands in October 1991. Times of individual profiles shown are given as T + 6 hours after the start time. [$1.43 \mu\text{l O}_2 \text{l}^{-1} \text{h}^{-1} = 1 \mu\text{g O}_2 \text{dm}^{-3} \text{h}^{-1}$].

(Haynes, Barton, & Pilling, 1993), so the present feature seems anomalous in that it arises upstream rather than downstream of Cabo Bojador. It has been observed though, that in the California Current system, the position of filaments may be quite variable (Huyer, Kosro, Fleischbein, Ramp, Stanton, Washburn, Chavez, Cowles, Pierce, & Smith, 1991; Ramp, Jessen, Brink, Niiler, Daggett, & Best, 1991).

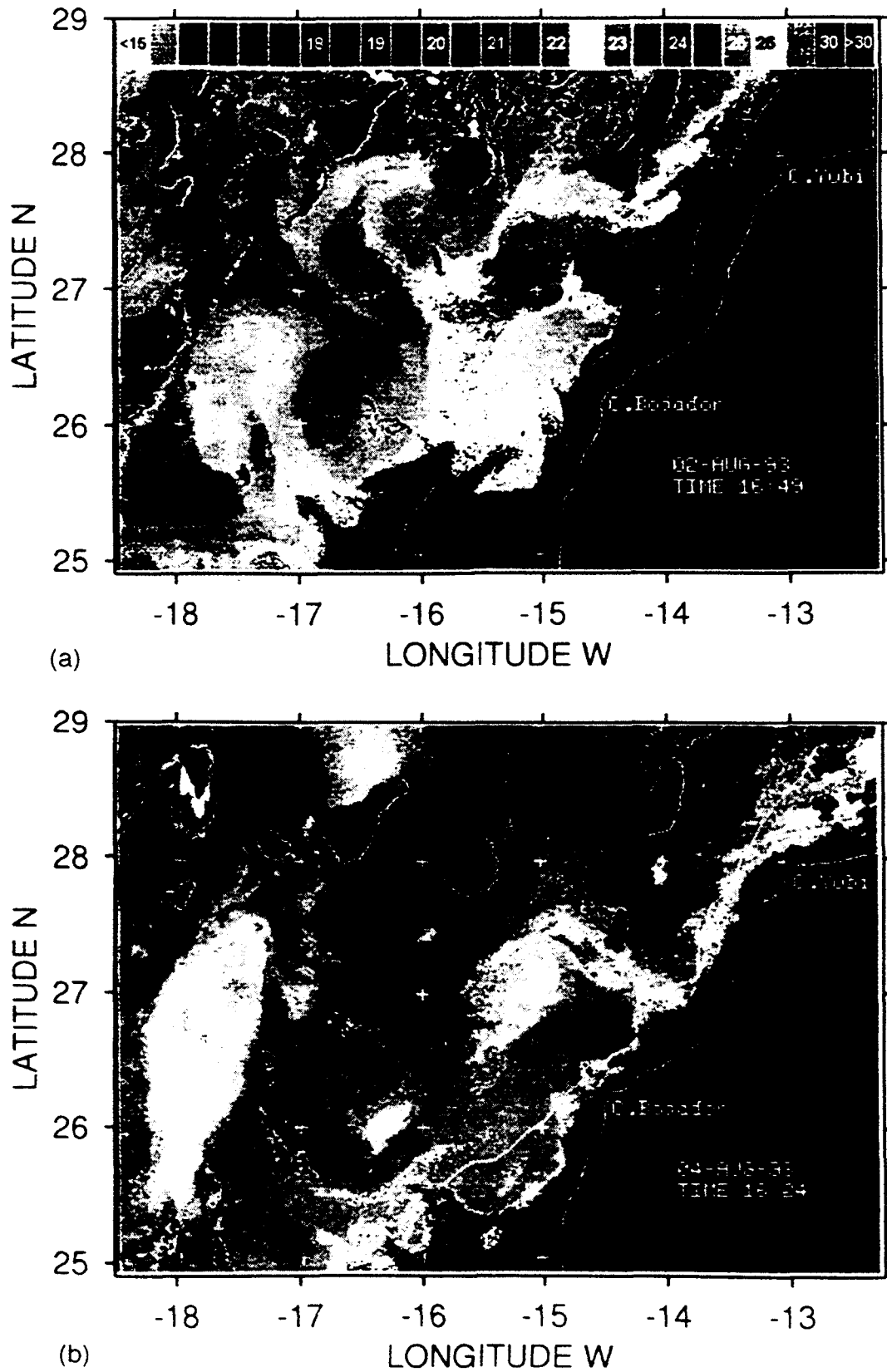


Fig. 11. Series of AVHRR SST images on (a) 2 August (b) 4 August (c) 10 August (d) 18 August (e) 29 August 1993 and (f) wind observed on board *Hespérides* during the period.

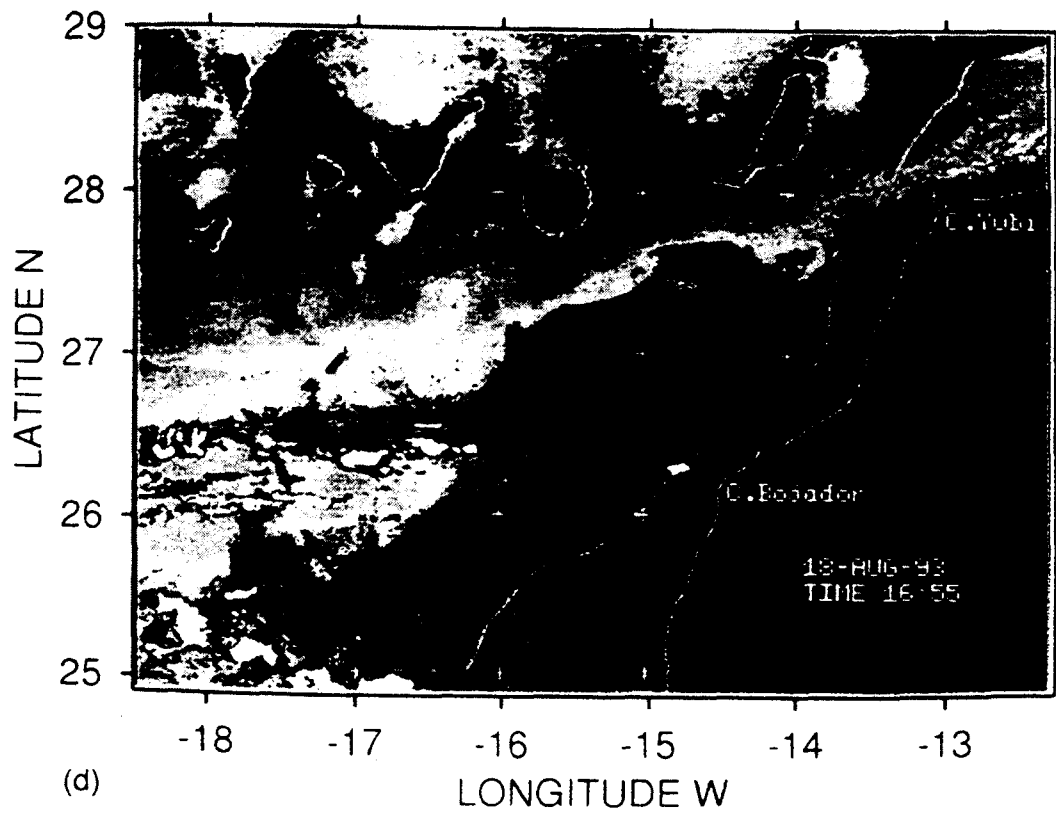
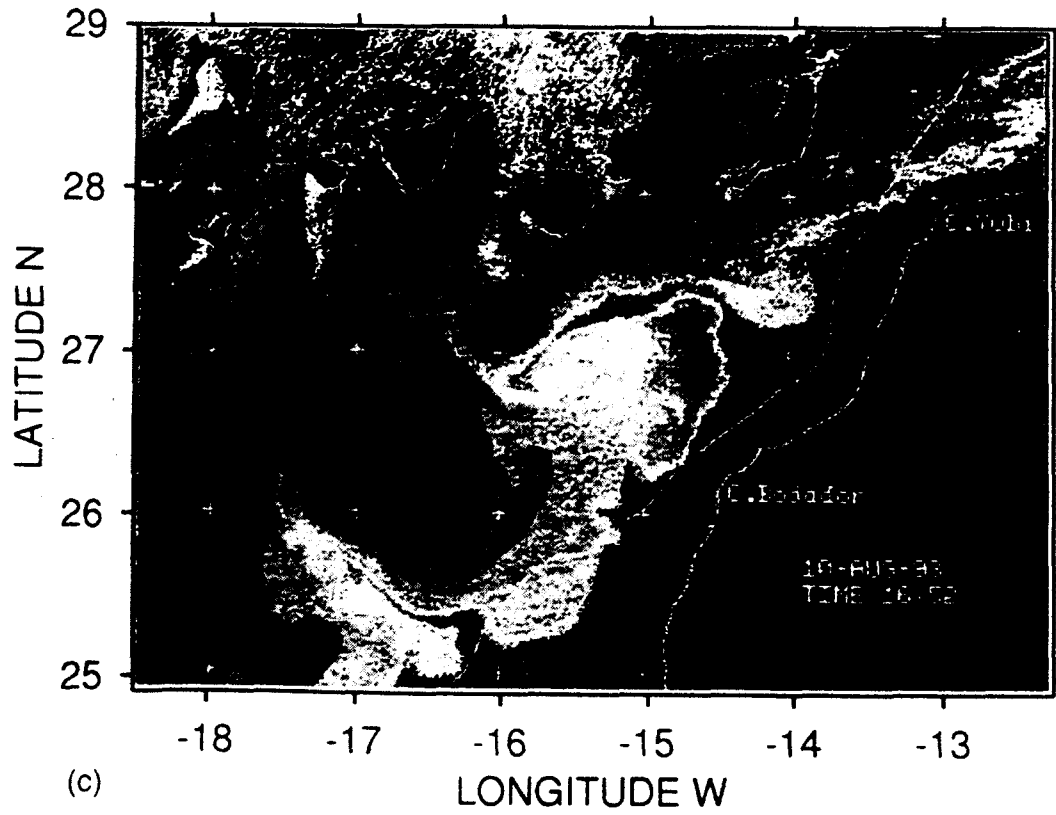


Fig. 11. Continued.

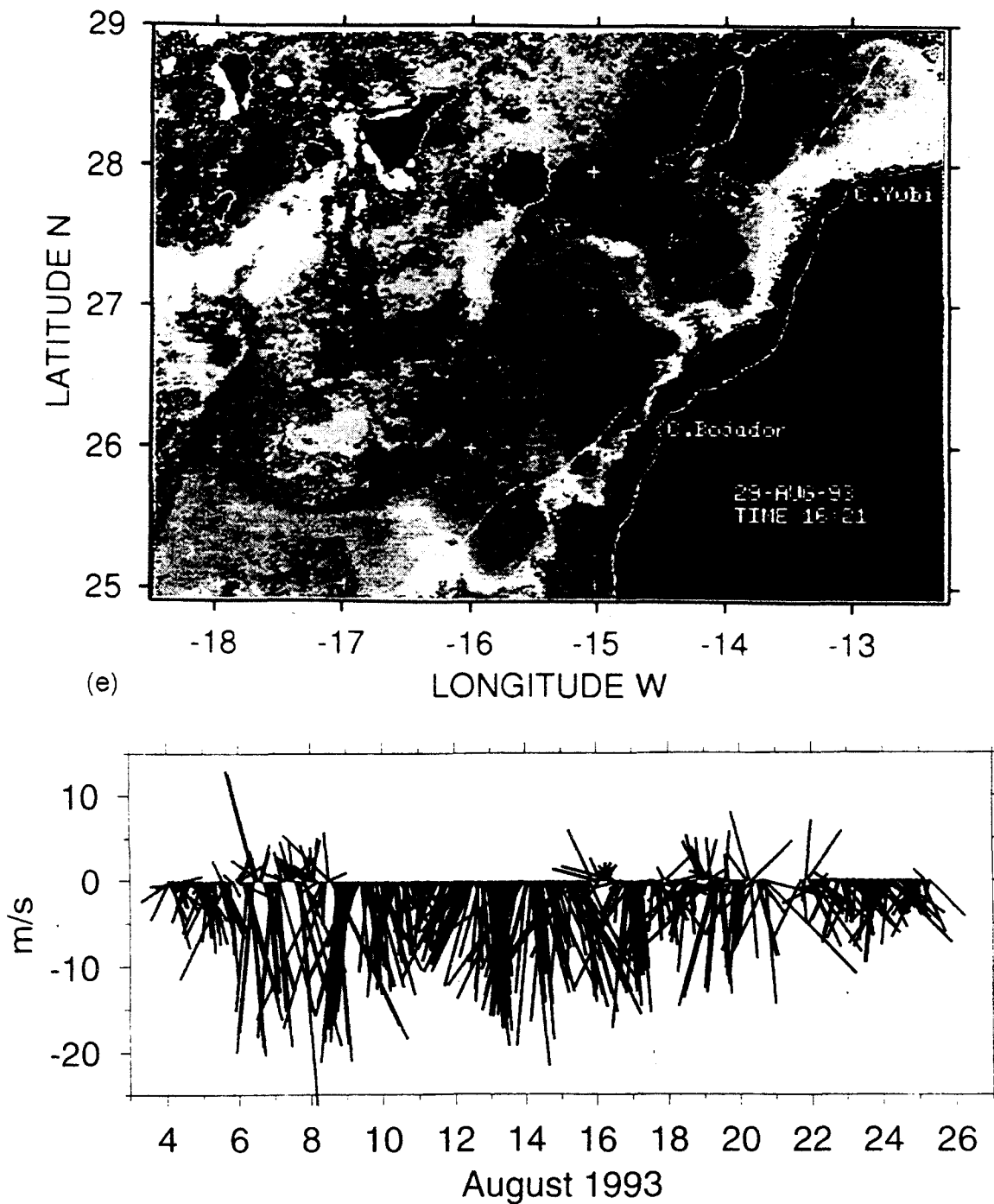


Fig. 11. Continued.

Throughout the image sequence a second filament could be seen extending northwestwards from the shelf about 200 km further south. The offshore limit of the coolest waters in both filaments was at about 150 km from the coast. In several images weakly defined streamers of slightly cooler water extended almost twice as far, but they were probably not directly connected to the filaments.

With the help of the remote sensing imagery, a filament sampling grid was laid out with a standard station spacing of 20 km and closer spacing (of 10, 5 and in

some cases 2 km) in areas of interest like the frontal boundaries. Horizontal distributions reveal that the subsurface structure related to the surface features seen in the SST imagery in a way that changed with increasing depth. At 25 m the temperature distribution (Fig. 12a) retained the form of the filament extending offshore as a well defined tongue of temperatures between 18.5 and 20°C and curving cyclonically towards the south at its offshore limit. The pattern of salinity (Fig. 12b), however, showed only a weak semblance to the near-surface temperature signal and was relatively homogeneous across the area. Highest salinities coincided with higher temperatures in the southwestern offshore waters. The current field measured by shipborne ADCP, overlaid on the 25 m density distribution (Fig. 12c), showed strong structure in relation to the filament. The main feature seen is the large cyclonic eddy around which the filament is entrained. In the near-surface layer (16–25m) flow paralleled the upwelling front and filament structure. Southward flow entering the area over the continental slope in the northeast, turned sharply offshore around the eddy, and eventually returned shoreward. On approaching the slope some of the flow turned southward to continue along the shelf edge whereas the rest re-circulated about the eddy. Nitrate distributions (Fig. 12d) were sampled only at every second

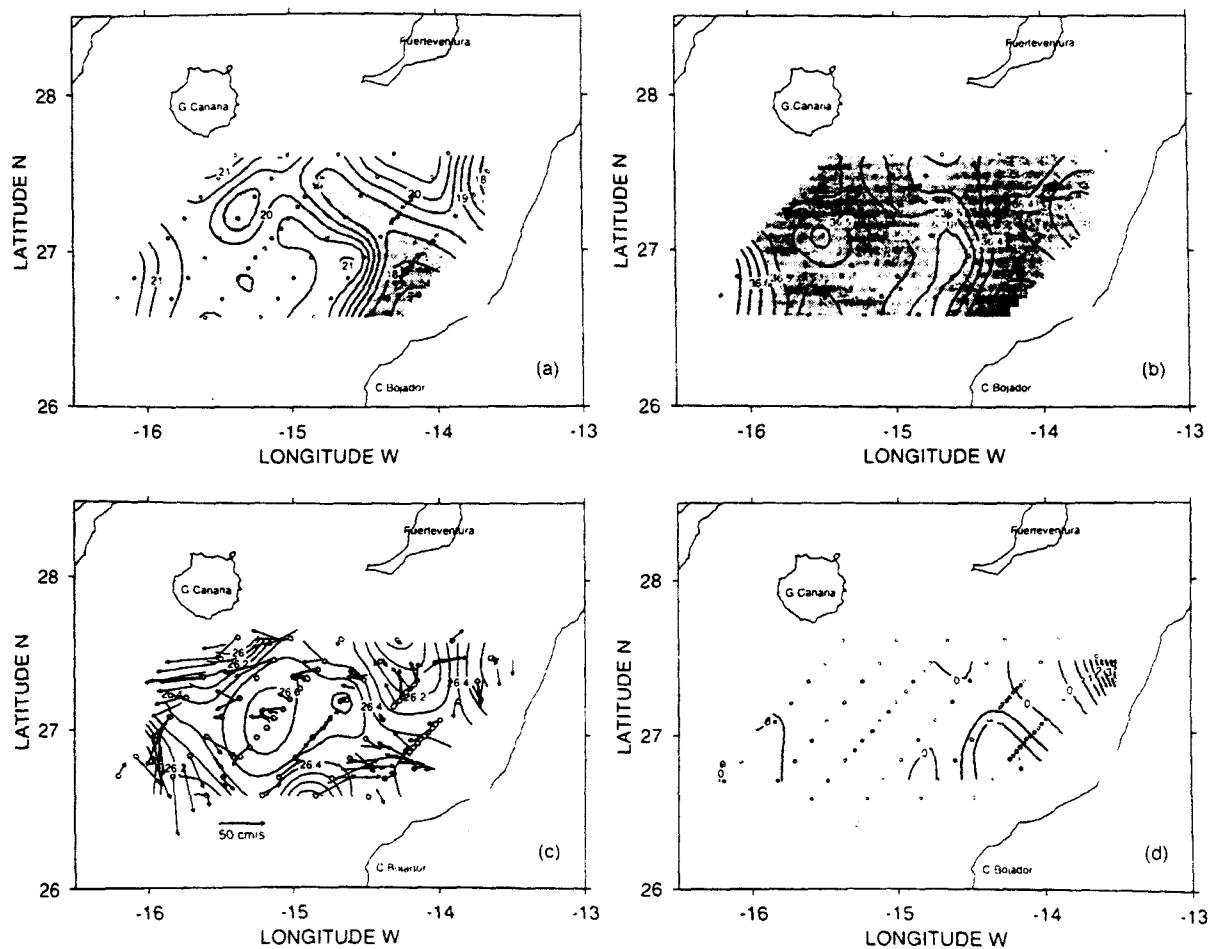


Fig. 12. Maps at 25 m of (a) temperature, (b) salinity, (c) density anomaly and ADCP velocity vectors and (d) nitrate in August 1993.

station but show maximum concentrations in the near surface layer near the African coast. Higher values extended only a short distance offshore in the filament. In offshore waters values were almost zero everywhere.

The distributions at 75 m no longer showed the filament of colder water, but rather a generalised cool area in the centre of the eddy, resulting from the general doming of iso-surfaces in its centre, connected to the near-shore waters affected by upwelling (Fig. 13a). At this sub-thermocline level, salinity and density (Fig. 13b and c) showed strong similarity to temperature. The structure of the currents was similar to that at shallower levels, though flows were generally weaker. At 70 m the nitrate was high over the continental shelf in the areas of coolest near-surface waters (and strongest upwelling), but at this level higher values were also found offshore in the centre of the sample area (Fig. 13d). The cause of the higher nutrient values seemed not to be advection in the filament but more probably upwelling or doming in the centre of the cyclonic eddy.

The map of chlorophyll integrated over the upper 200 m layer (Fig. 14a) also shows highest values near the African coast inside the temperature front marking the offshore edge of the upwelling zone, and a tongue of higher chlorophyll is observed extending northwestwards along the path of the filament. Values generally

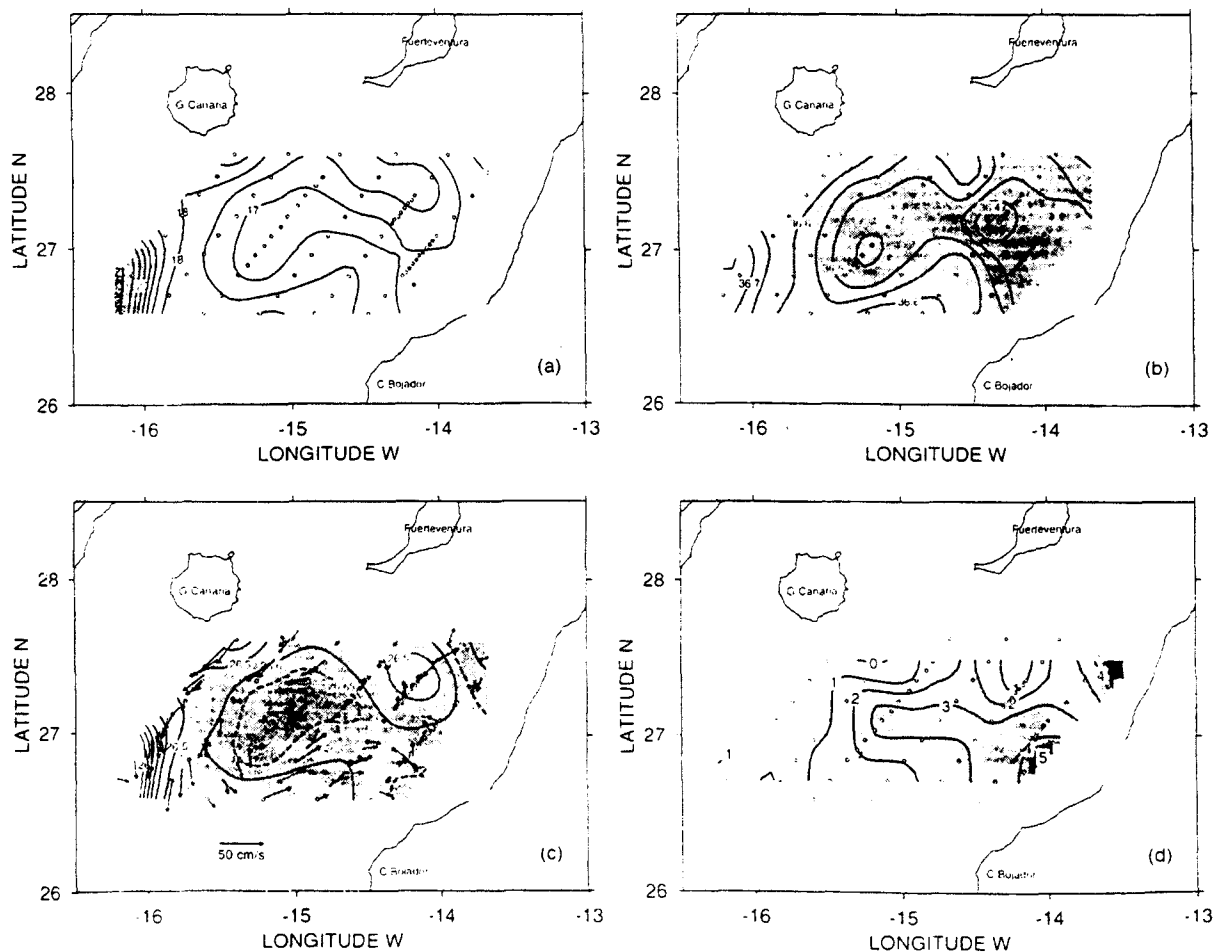


Fig. 13. As Fig. 12 at 75 m depth.

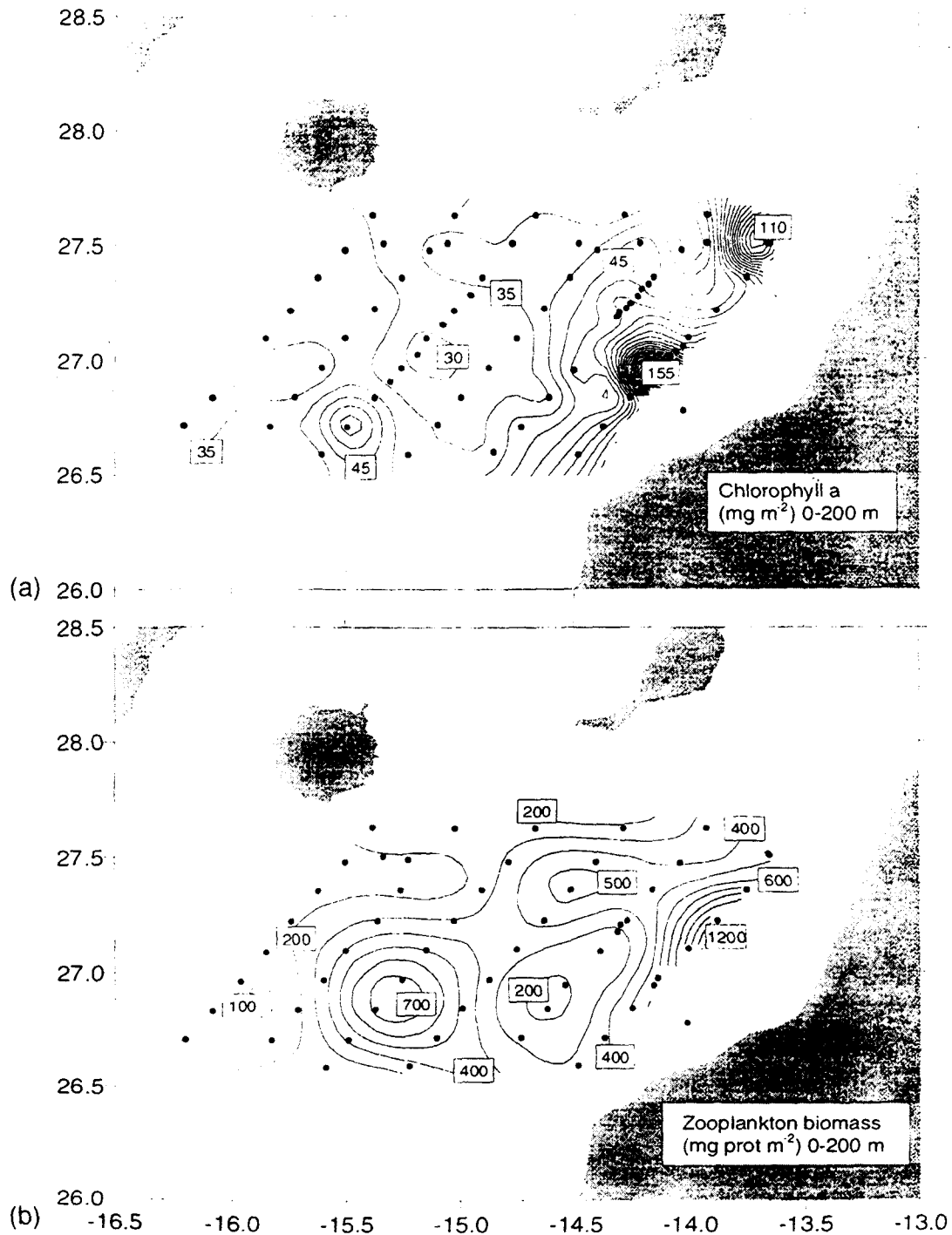


Fig. 14. Maps of (a) chlorophyll, (b) zooplankton biomass, and (c) larval concentration (/10 m²) integrated over the upper 200 m.

decreased along the filament and were low in the offshore part of the eddy, but a localised maximum was located in the return flow in its southern part. This coincided with an area of anomalously low salinity at the depth of the pycnocline at 50 m (not shown). The lowest chlorophyll values were observed in the centre of the cyclonic eddy. This distribution might have resulted partly from zooplankton grazing, since the maxima of total zooplankton biomass tend to coincide with chlorophyll minima

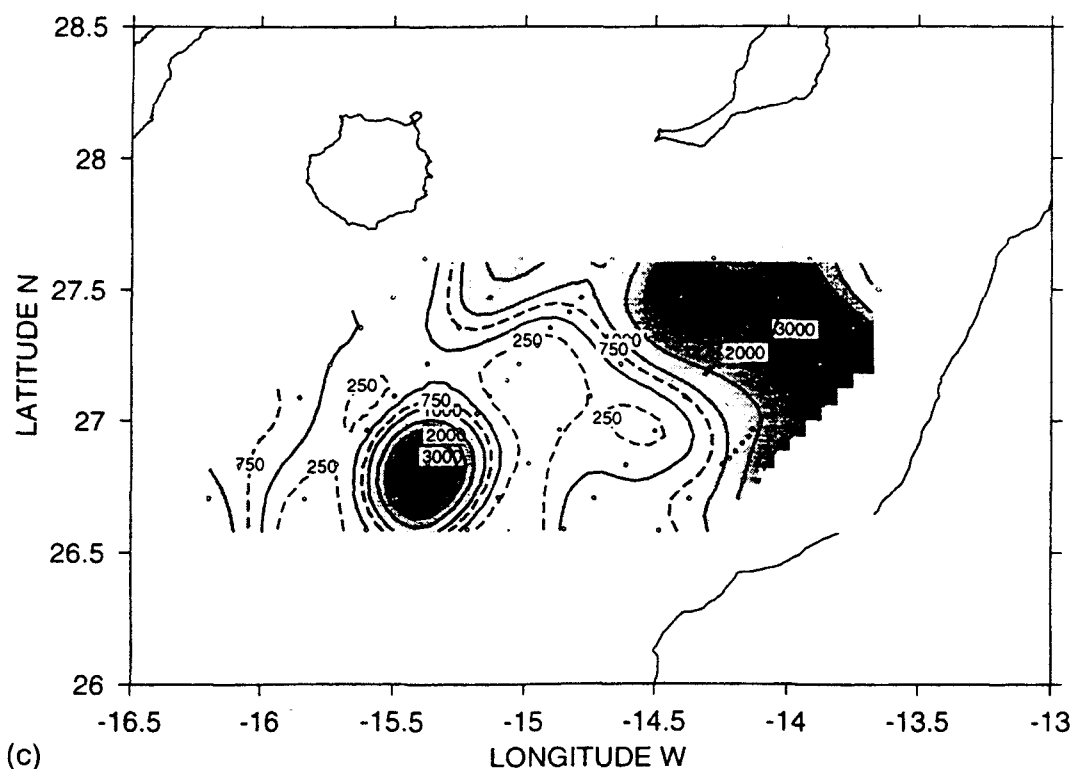


Fig. 14. Continued.

(Fig. 14b). However, it could also be that in the eddy centre phytoplankton had not had sufficient time for significant growth.

The distribution of fish larvae (Rodríguez, 1996) showed a strong dependence on the physical situation (Fig. 14c) as might be expected for organisms that are mainly passive drifters. The larval distributions showed high concentrations occurring on the shelf and reducing along the filament, but with an isolated maximum on the southern flank of the eddy coincident with high zooplankton standing crop. The largest component of the larvae was the sardine *Sardina pilchardus* (28% of all larvae), which are known to be spawned on the continental shelf. These sardine larvae were found only on the shelf and in the filament, including the isolated nucleus indicated by the chlorophyll maximum. In contrast, some oceanic larvae were absent from both the filament and shelf waters. Other neritic species were found only on the shelf and extending a short distance along filament. The higher larval concentrations observed to the north of the filament reflect distributions of anchovy, spawned well to the north off Morocco and spread southwards by the general alongshore flow.

A section parallel to the coast some 20 km offshore of the shelf edge reveals the structure of the filament (Fig. 15). Its width from the surface thermosalinograph trace was about 28 km. Minimum temperature in the filament was 2.5°C lower than in surrounding waters. Surface salinity increased by about 0.2 from north to south across the filament. Near-surface isotherms and isopycnals sloped steeply up from about 50 m depth on either side of the structure, while subsurface isohalines were strongly perturbed down to 150 m. The isosurface slopes weakened at greater depths, becoming undetectable below about 250 m. The deep chlorophyll maximum present

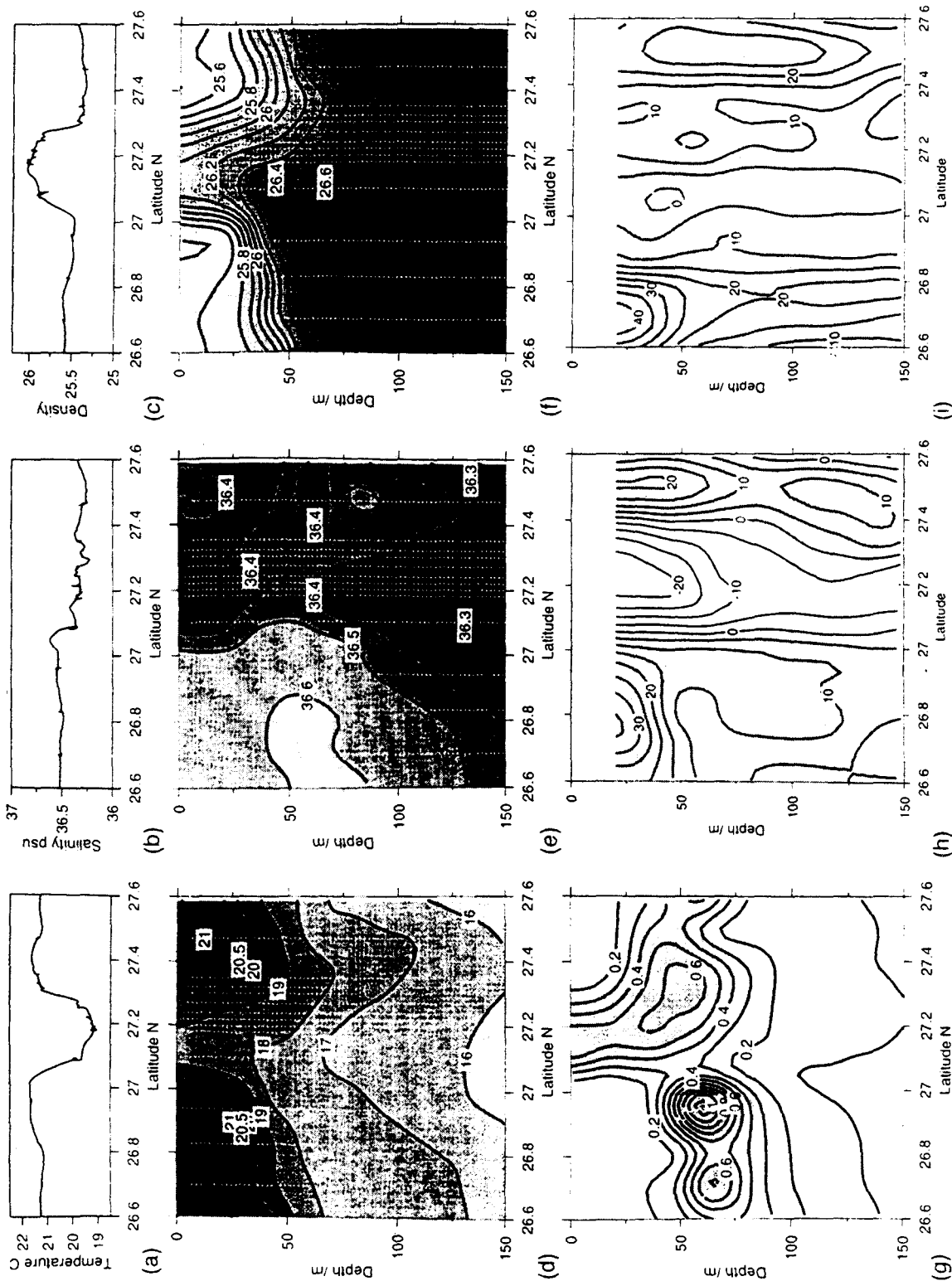


Fig. 15. Section across the filament 30 km beyond the shelf edge showing (a) surface temperature, (b) surface salinity, (c) surface density anomaly, (d) temperature, (e) salinity, (f) density anomaly, (g) fluorescence chlorophyll, (h) onshore and (i) alongshore velocity components in August 1993. Velocity component are rotated so that positive onshore (alongshore) components are normal (parallel) to the section towards 134 (44) degrees.

at the base of the pycnocline was interrupted by the filament where maximum chlorophyll values occurred at the sea surface. The ADCP currents showed a core of offshore (normal to the section) flow up to 0.25 m s^{-1} associated with the northern edge of the cold filament and extending to over 200 m depth. To the south of the filament, the layers above 50 m were flowing shoreward with speeds over 0.35 m s^{-1} but at greater depths the flow weakened to about 10 m s^{-1} . To the north of the filament onshore flow with a near-surface maximum of 0.20 m s^{-1} extended down to 175 m depth. Almost everywhere the alongshore component of flow (parallel to the sections) was poleward with strongest flow of 0.45 m s^{-1} occurring near-surface at the southern end of the transect and a weaker maximum at its northern end. The lack of any clear indication of convergence or divergence in the cross-filament flow in association with the high surface chlorophyll and low temperature suggests that they are the results of advection along the filament rather than local vertical processes.

The filament signal weakened with distance offshore and was barely detectable in the furthest offshore CTD sections. A transect at about 150 km offshore with 10 km station spacing (Fig. 16) failed to detect the subsurface structure of the filament. It was still evident in the surface thermosalinograph trace as an 8 km wide temperature minimum (1°C cooler than surrounding waters) and salinity step of 0.2 centred near 27.38°N . A wider, weak near-surface temperature minimum of $<20.5^\circ\text{C}$ near 27°N seen in the temperature section represents a weak continuation of the filament being entrained around the eddy as seen in the satellite image of Fig. 11c. Below 50 m depth all variables indicated a smoothly domed structure, indicative of the cyclonic circulation around the eddy. The general deep chlorophyll maximum was strongest beneath the two surface temperature minima in the filament. The separation into two maxima reveals entrainment of the deep chlorophyll maximum around the cyclonic eddy. This is consistent with the flow field, which is offshore north of 27°N and onshore to the south. Everywhere along this section the alongshore component of flow was equatorward with a minimum near 27°N close to the eddy centre. Volume transport, estimated from the ADCP observations, was about $10^6 \text{ m}^3 \text{ s}^{-1}$ in the filament where it crossed the nearer-to-shore transect. Further offshore, the broader flow around the eddy, including the entrained filament, had more than twice this transport (Navarro-Pérez, 1996).

Chlorophyll generated in the African upwelling system may be spread into the eastern Canary region or transported by filaments some hundreds of kilometres offshore, extending out as far as south of Gran Canaria (Hernández-Guerra, Arístegui, Cantón, & Nykjaer, 1993; Arístegui, Tett, Hernández-Guerra, Basterretxea, Montero, Wild, Sangrá, Hernández-León, Cantón, García Braun, Pacheco, & Barton, 1997). Previous observations on the offshore boundaries of filaments at the southeastern Canaries (Montero, 1993; Basterretxea, 1994; Arístegui, Tett, Hernández-Guerra, Basterretxea, Montero, Wild, Sangrá, Hernández-León, Cantón, García Braun, Pacheco, & Barton, 1997) coincided in that filaments were always transporting higher concentrations of chlorophyll to open ocean waters. However, the phytoplanktonic community composition is not always the same. In the October 1991 cruise, the filament was transporting relatively large amounts of cyanobacteria. In March 1991 and August 1993 the trend was the opposite: the upwelled waters contained lower

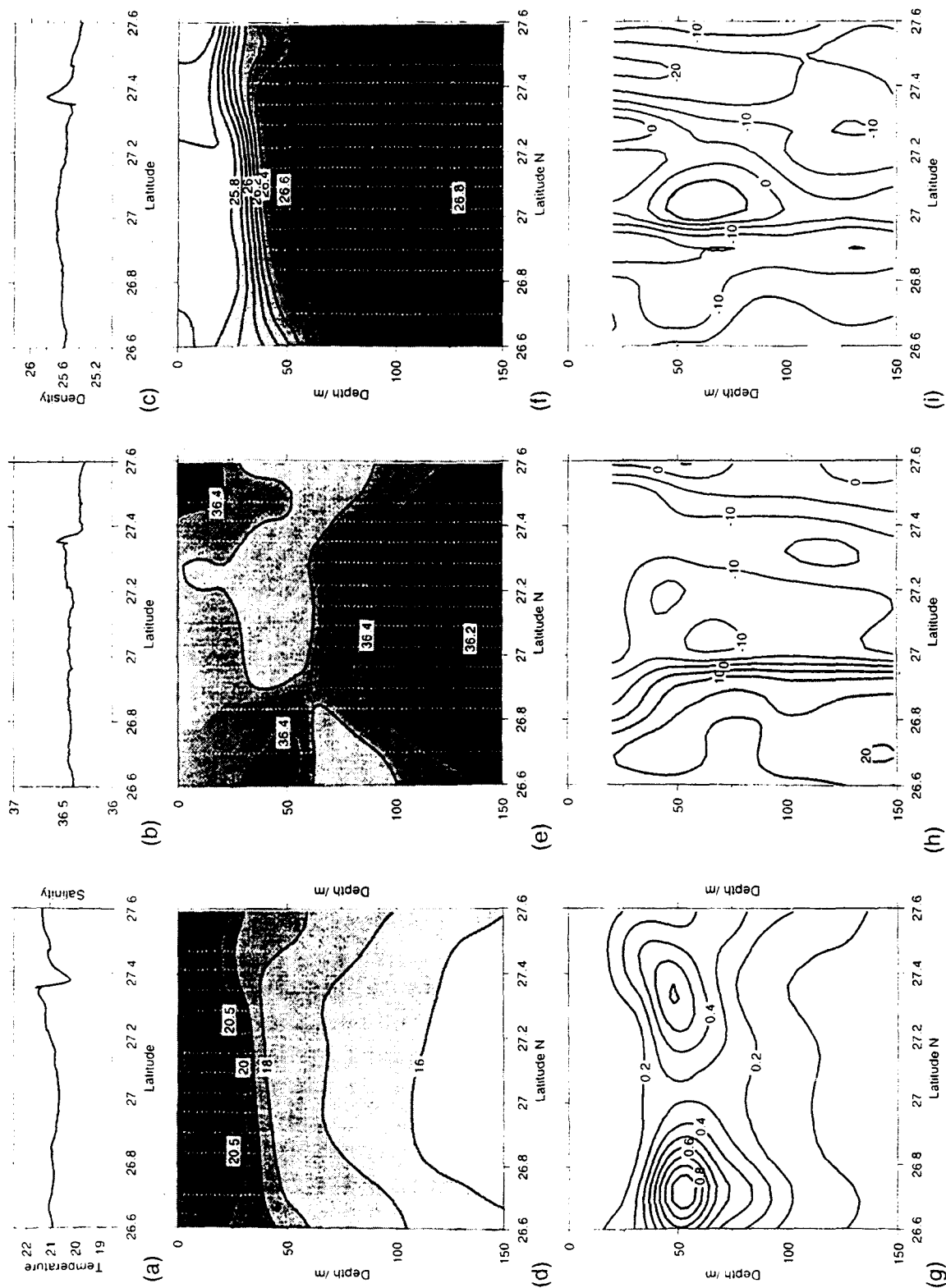


Fig. 16. Section 150 km offshore as Fig. 15.

abundances of cyanobacteria but relatively higher numbers of eukaryotic cells (Ballesteros, 1994; Barton, 1994b). This may indicate a different source and age of the offshore advected water. It is possible that diatoms, when strongly flourishing in the upwelling on the shelf, sink as they are transported offshore in the filament, or are grazed, leaving some new or recycled nutrients to stimulate the growth of small-celled phytoplankton entrained into the filament from the ocean water.

The role of upwelling filaments in transporting nutrients into the Canary region is not as evident as with chlorophyll. Whilst little information is available (e.g. Basterretxea, 1994) indicates that dissolved inorganic nutrients like nitrate are already exhausted in surface waters of upwelling filaments arriving to the south of Gran Canaria, as seen in Fig. 12d. Nevertheless, deep waters upwelling in the core of cyclonic features associated with filaments may be important local sources of nutrients in the offshore regions (e.g. Hayward, & Mantyla, 1990), as seen in the August cruise (Fig. 13d). It is however plausible that under certain situations a net horizontal transport of nutrient-rich coastal upwelled waters could be produced, enhancing productivity in open ocean waters. Intense newly formed upwelling filaments may transport nutrient-enriched waters out into the open ocean before the nutrients become exhausted by phytoplankton (Jones, Mooers, Rienecker, Stanton, & Washburn, 1991). Conversely, if the advection of upwelled water is slower, there will be almost complete utilization of the nutrients by phytoplankton close to the African coast. In either situation both particulate and dissolved organic matter are exported into the eastern Canary region enhancing microbial respiration (Montero, 1993).

In all instances the transport of organic material seems to be a more important process than the dissolved nutrient transport. The representation of nutrients, chlorophyll concentrations and ETS activity along a vertical section extending from upwelled waters to open ocean waters during the August cruise shows that gradients in chlorophyll and ETS activity extend farther offshore than nutrients (Fig. 17). Chlorophyll and ETS activity maxima coincide at stations closest to the African coast, indicating that in the upwelling near to shore respiration is mainly by phytoplankton. However further offshore, the maximum in ETS activity occurs at a shallower level than the DCM suggesting that here the activity is more likely to be the result of bacterial respiration utilising the dissolved organic material produced inshore by photosynthesis in the upwelled water and then advected offshore by the filament. In this long section, south of the islands chain, two cyclonic eddies and one anticyclonic eddy are evident. One of the cyclonic features, located in otherwise oligotrophic waters at distance of 120 km (south of the island of La Palma), showed a significant upward displacement of isopleths. This doming, especially visible in the nitrate section, was apparently producing an increase in chlorophyll concentration and respiratory activity similar to the situation in the coastal upwelling zone.

4.2. Island eddies

Eddies generated by islands in the Canary region were first identified by remote sensing (Hernández-Guerra, Arístegui, Cantón, & Nykjaer, 1993) and their structures later observed by AXBTs and CTD surveys (Arístegui, Sangrá, Hernández-León,

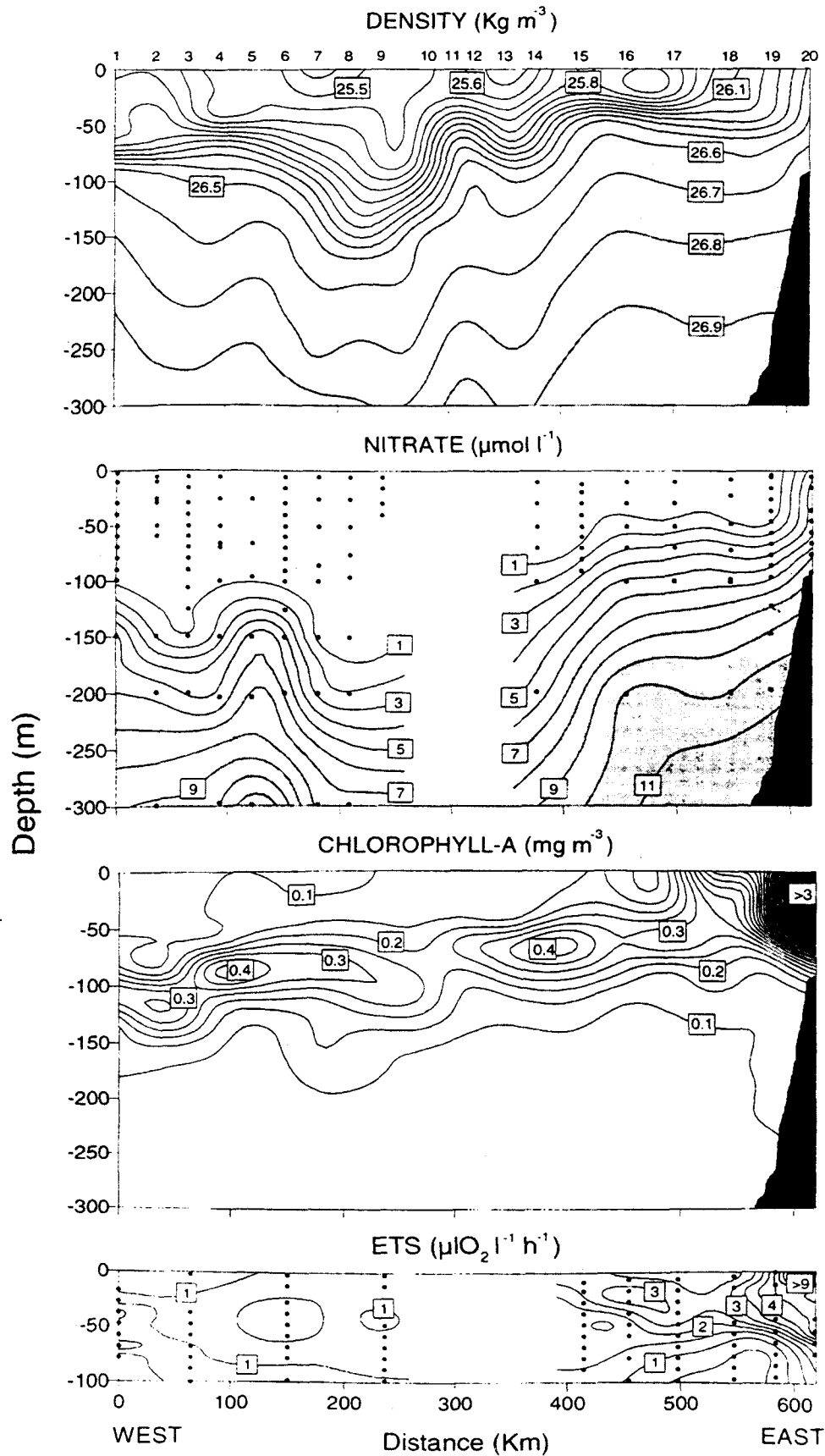


Fig. 17. Long section (H in Fig. 2) south of the archipelago showing density anomaly, nitrate, chlorophyll and ETS activity in microplankton in August 1993. Sampling was interrupted in mid-section by strong winds. [$1.43 \mu\text{l O}_2 \text{l}^{-1} \text{h}^{-1} = 1 \mu\text{g O}_2 \text{dm}^{-3} \text{h}^{-1}$].

Cantón, Hernández-Guerra, & Kerling, 1994). Eddies downstream of Gran Canaria have been studied thoroughly by both satellite and in situ observations (Barton, 1994a; Arístegui, Tett, Hernández-Guerra, Basterretxea, Montero, Wild, Sangrá, Hernández-León, Cantón, García Braun, Pacheco, & Barton, 1997); satellite observations indicate that eddies are also produced downstream of the other islands like Tenerife, Gomera or La Palma. The long section south of the Archipelago depicted in Fig. 17 illustrates the presence of cyclonic and anticyclonic structures in the vicinity of several of the islands. Typically, a cold-core cyclonic eddy is found to the southwest of Gran Canaria. On certain occasions a second warm-core anticyclonic eddy has been also observed to the southeast giving rise to a structure like a von Karman vortex street. However, the extension of the Cape Bojador upwelling filament towards the south of Gran Canaria presumably inhibits the development of the anticyclonic feature in most situations. Another factor which favours cyclogenesis is potential vorticity conservation as the flow encounters deeper waters on leaving the channels between the islands. Eddies have been observed even during the lowest wind intensity periods. This led Arístegui, Sangrá, Hernández-León, Cantón, Hernández-Guerra, & Kerling (1994) to suggest that they are produced as result of the flow past the island, as modelled by Sangrá (1995).

In October 1991 during and after a very low wind period there was clear evidence of a cyclonic eddy to the southwest of the island (Fig. 18), which could be seen at subsurface levels to at least 200 m depth. The surface expression of this cold core eddy was barely apparent because of the strong near surface stratification; isopycnal doming was most pronounced at around 150 m. Nevertheless, the intensity of the eddy (calculated from the ratio between the elevation and eddy radius on the 16°C isotherm) was of the same magnitude as other eddies found during stronger wind periods. Evidence of chlorophyll enhancement around the periphery of the eddy (Fig. 19) was compatible with active pumping of sub thermocline water into the euphotic zone and the uplifting of the DCM to better illuminated depths. Lower chlorophyll values in the eddy centre may reflect the direct effect of strong upwelling of low chlorophyll, nutrient-rich waters coupled with a relatively slow rate of phytoplankton growth.

In March 1991 an anticyclonic and two cyclonic eddies forming a vortex street were studied (Fig. 18). A vertical section crossing one cyclonic and the anticyclonic eddy from west to east shows higher chlorophyll near the upper dome of the cyclone and in the eastern waters of African origin (Fig. 19). Although the March and October cruises were limited in the extent of sampling and areal coverage, during both there was evidence of the influence of water originating in the African coastal upwelling reaching almost to the island of Gran Canaria. A strong boundary was seen to the south and southeast of the island, clearly separating oceanic waters from those transported offshore in the filament from the coastal upwelling. Apart from their contrasting T-S properties, these waters were clearly differentiated by their biological and chemical properties. In particular the coastal upwelled waters always contained higher concentrations of chlorophyll.

In August 1993, an intense cyclonic eddy was once again observed to the southwest of Gran Canaria in the satellite imagery and in situ observations (Figs. 20 and

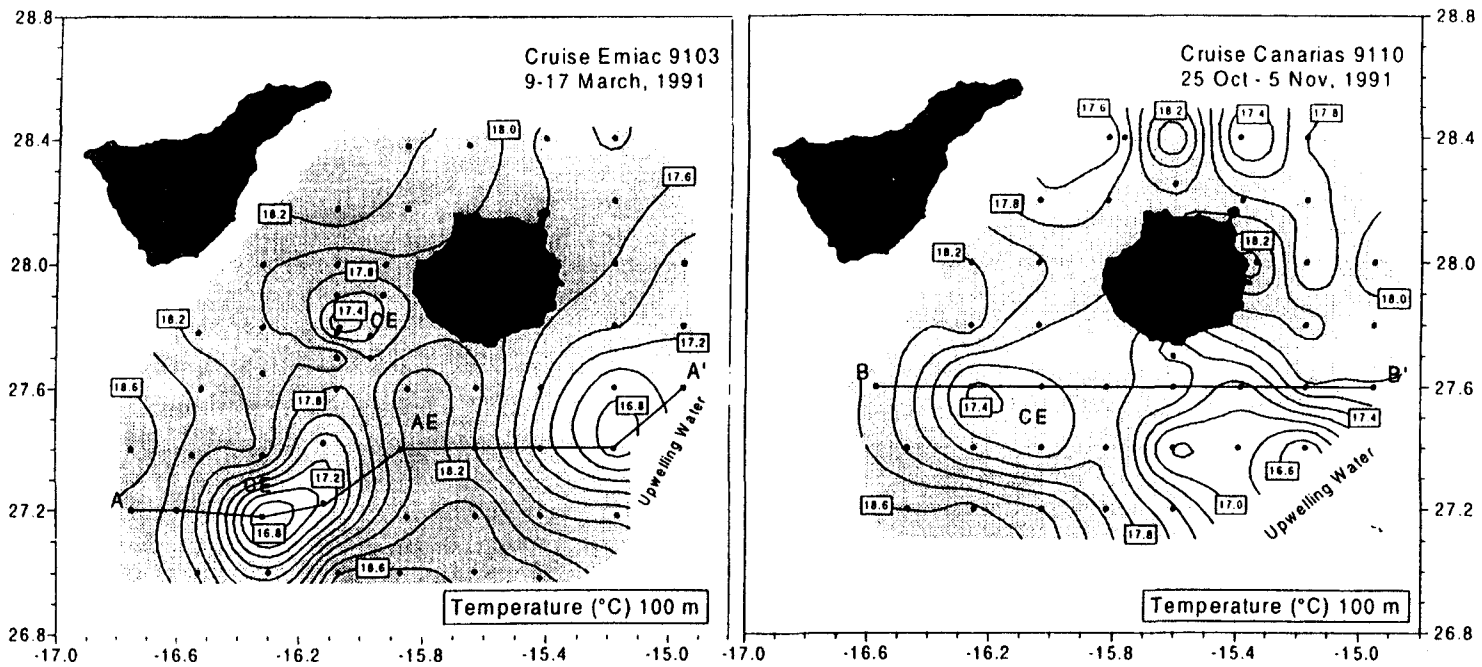


Fig. 18. Maps of temperature at 100 m depth during eddy surveys in March and October 1991 (Box E in Fig. 2).

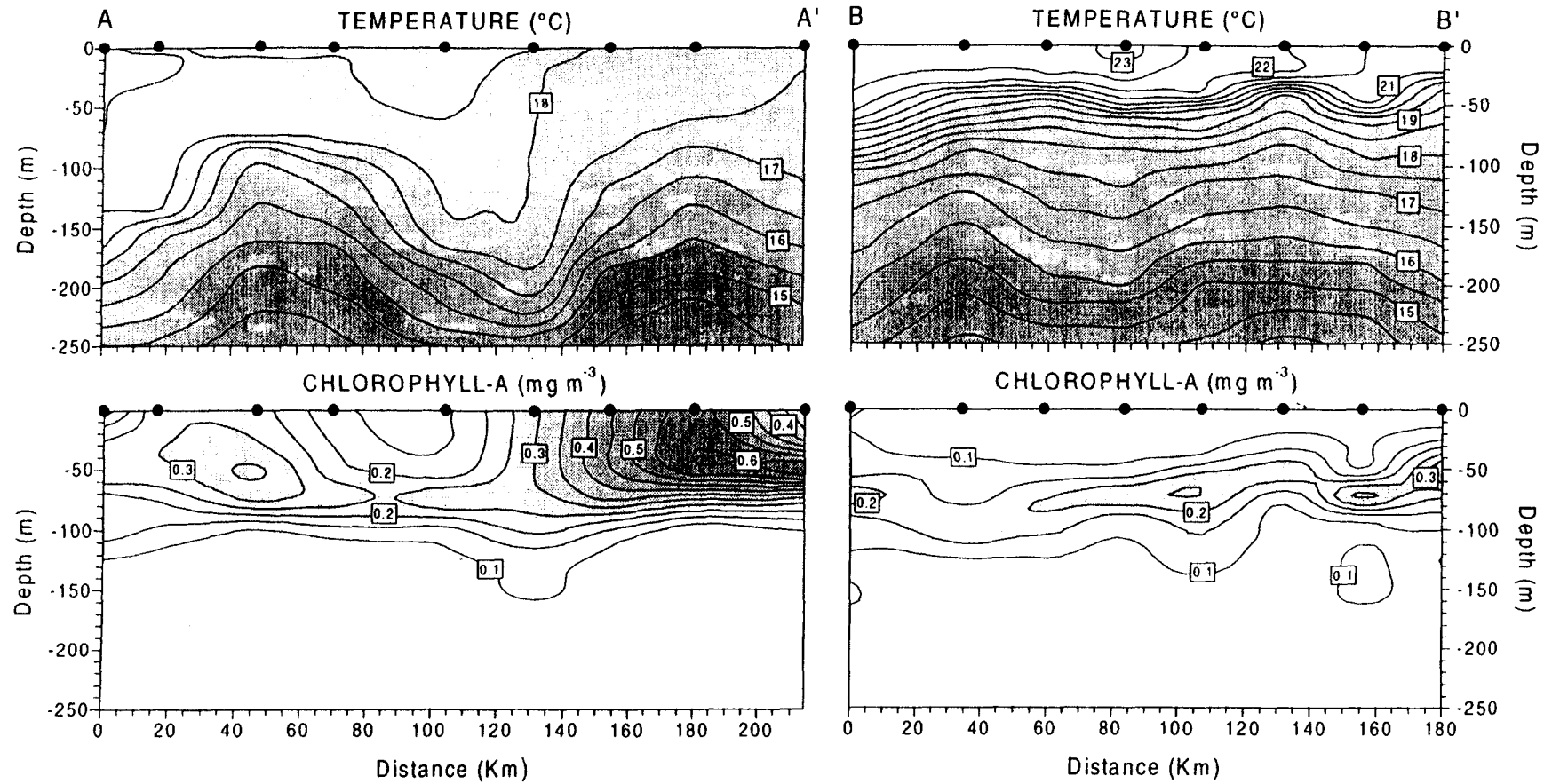


Fig. 19. Sections of temperature and chlorophyll across the transects AA' and BB' marked in Fig. 19.

11c). It was located in a similar position to those sampled during earlier cruises and observed on other occasions by remote sensing. Two eddy surveys (Fig. 21) were made during the *Hespérides* cruise with a separation of three days, during which time the eddy drifted southwards at a speed of about 0.15 m s^{-1} . An Argos drifter dropped close to the estimated centre after the first survey drifted with and around the cyclonic eddy (Fig. 22). Azimuthal velocities with respect to the centre (position linearly interpolated between surveys) were around 0.5 m s^{-1} . The drifter made one almost complete circuit in three days, but also moved out from the centre at an average speed between 0.15 and 0.2 m s^{-1} after the first day of apparent oscillation. Poor knowledge of the precise position of the eddy centre makes the velocity estimates subject to uncertainty at the start. If the later, steadier velocity represents a true radial motion, then it implies a high upwelling speed in the eddy centre. If the outward velocity was occurring over an upper layer depth of 50 m at a radius of 25 km , this implies that the upward velocity was more than 50 m d^{-1} . Since it was possible that there was imperfect coupling between drifter and water column and other factors such as changing background shear (Shapiro, Barton, & Meschanov, 1997) may have influenced the drifter trajectory, the upwelling estimate must be taken as an upper limit.

Despite these reservations, sections across the eddy during the two surveys show

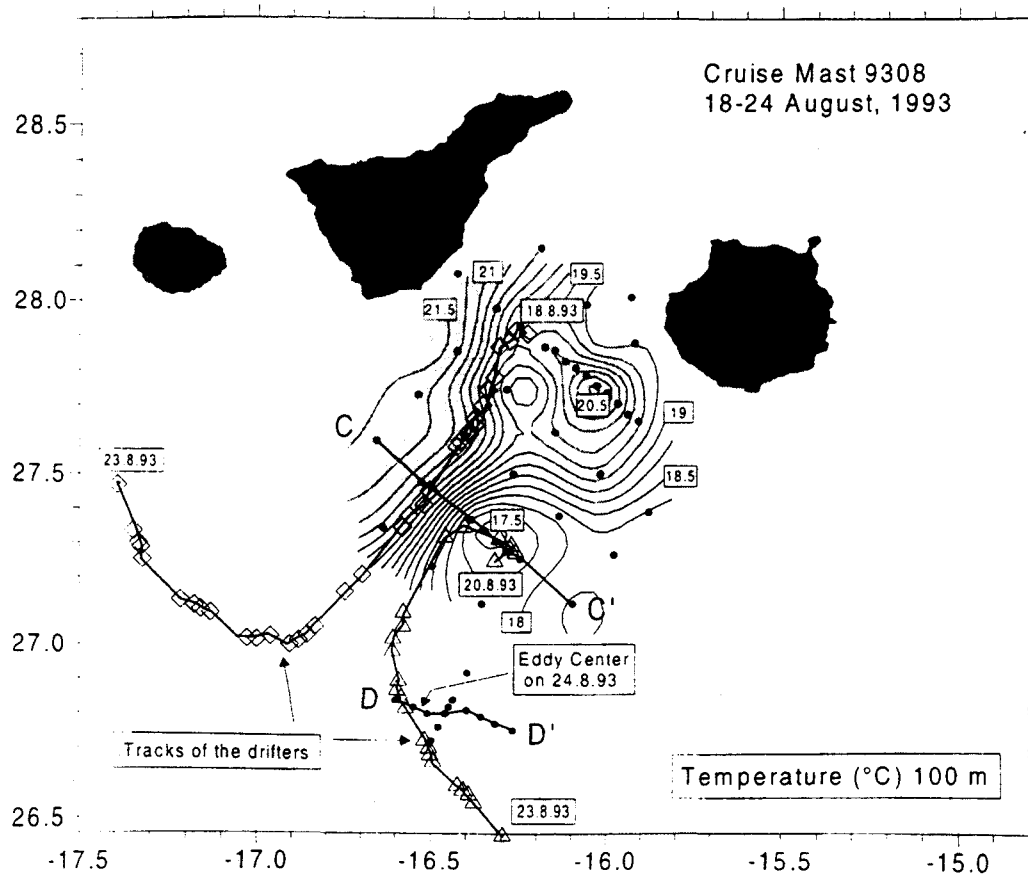


Fig. 20. Maps of temperature at 100 m during August 1993 with drifter tracks superimposed. Open triangles and diamonds indicate drifter Argos fixes. Start and end dates are shown.

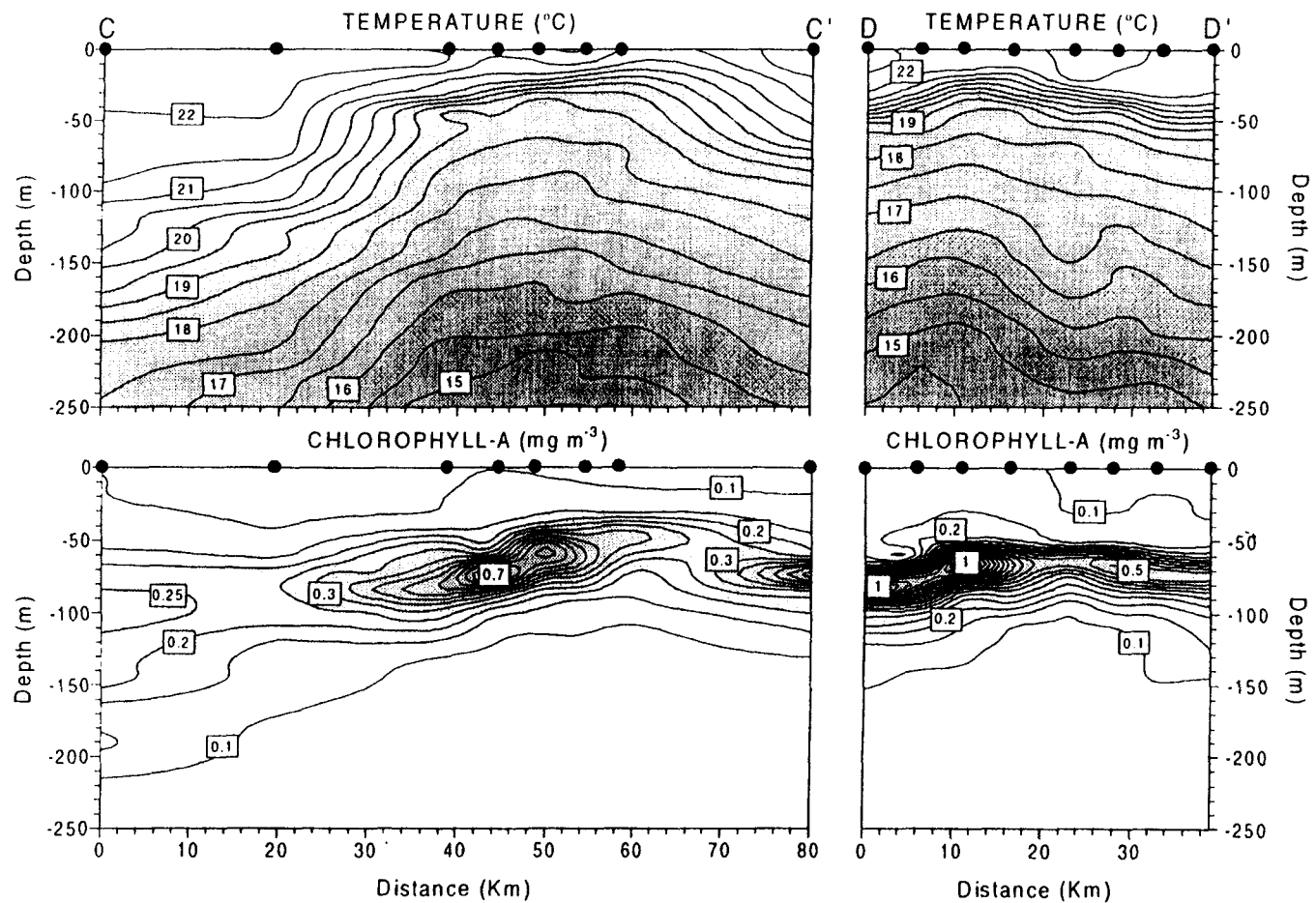


Fig. 21. Sections of temperature and chlorophyll across the transects CC' and DD' marked in Fig. 21.

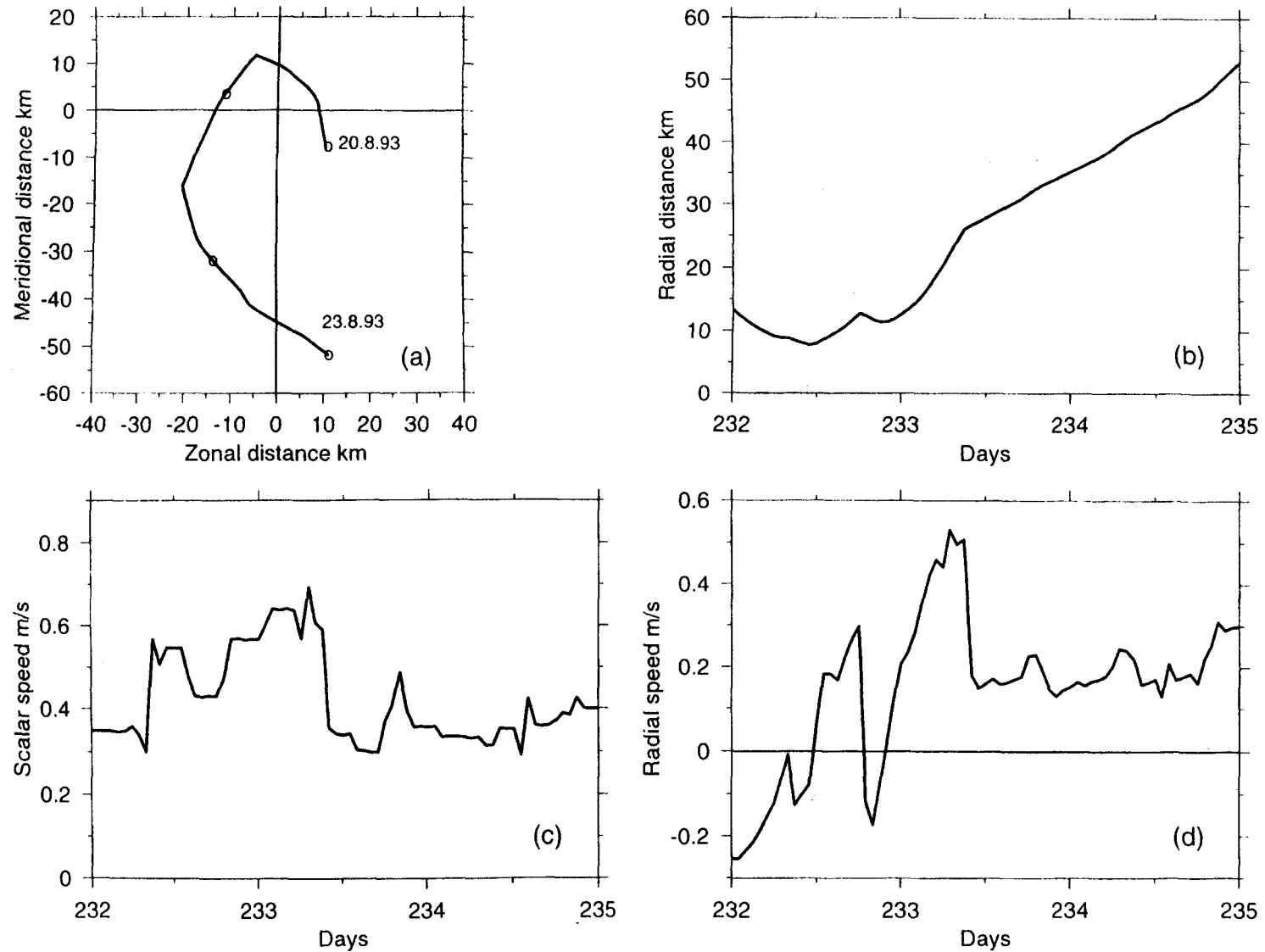


Fig. 22. (a) Drifter trajectory relative to centre of cold-core eddy. Positions interpolated to midnight are marked by a circle (b) Separation distance of drifter from eddy centre estimated by interpolation between positions during two surveys (c) Scalar drifter speed along trajectory (d) rate of increase of separation from estimated eddy centre. Year Day 232 is 20 August 1993.

large vertical excursions of the isosurfaces of up to 150 m in the centre (Fig. 21). Although the later survey was less extensive, and did not show the structure so clearly, the isotherms were just as shallow in the centre as initially. A marked increase in the intensity of the DCM at the top of the eddy dome was evident between the two eddy surveys. This contrasts with the observed chlorophyll enhancements at the periphery of eddies closer to the island (e.g. in the March cruise). Several mechanisms have been proposed to explain chlorophyll distributions in island eddies (Arístegui, Tett, Hernández-Guerra, Basterretxea, Montero, Wild, Sangrá, Hernández-León, Cantón, García Braun, Pacheco, & Barton, 1997). In particular, eddies closer to islands are thought to be at earlier developmental stages than those that have already spun off. The former would have higher upward transport of deep nutrient-rich water in their cores and hence a low chlorophyll content, whereas in older eddies there would have been more time for the growth of phytoplankton to have become apparent.

A second drifter deployed in the channel between Gran Canaria and Tenerife moved rapidly southwestwards and then turned anticyclonically with a radius of about 50 km back towards La Gomera and Tenerife (Fig. 20). Although no detailed survey was carried out at the time, the earlier long section across the south of the islands clearly shows a strong downbowing of isopycnals and other surfaces associated with an anticyclonic eddy to the south of Tenerife (Fig. 17). Whether this is a recurring feature like the cyclonic eddies is not known.

4.3. *Island lee*

Warm lee regions occur downwind of the elevated topography of many of the Canary Islands (Fig. 11). During the August 1993 cruise, sampling was carried out across the warm lee region southwest of Gran Canaria from the exposed waters to the east almost to those on the west. An impression of the lee is given by Fig. 23 which shows wind vectors and the associated density section on 8–9 August when the research vessel was sheltering from particularly strong Trades. Stations were spaced at about 2 km along the sampling line, which was oriented perpendicular to the predominant Trade wind direction. Wind conditions at the time prevented working in the fully exposed ocean, and so one additional station made several days later is included to show conditions further southeast. At the anticyclonic wind shear boundary wind dropped from $> 15 \text{ m s}^{-1}$ to virtually zero over three stations. The shear line was visibly evident from the abrupt contrast in sea state, which changed over a short distance from rough breakers in the exposed area to calm in the lee.

The effect of the wind structure is seen in the vertical distributions across the boundary (Fig. 23). In the density section a strong downward slope from northwest to southeast is seen in all the isopycnals across most of the section, but at the eastern end they slope upwards again to shallow levels. In the centre of the lee region a pool of low density surface water corresponds to the 'warm wake' evident in satellite images. Here daytime heating in the absence of strong wind mixing leads to the formation of a thin warm stratified surface layer. In the exposed regions the effect of surface heating is masked by the strong wind-induced mixing to produce a uniform

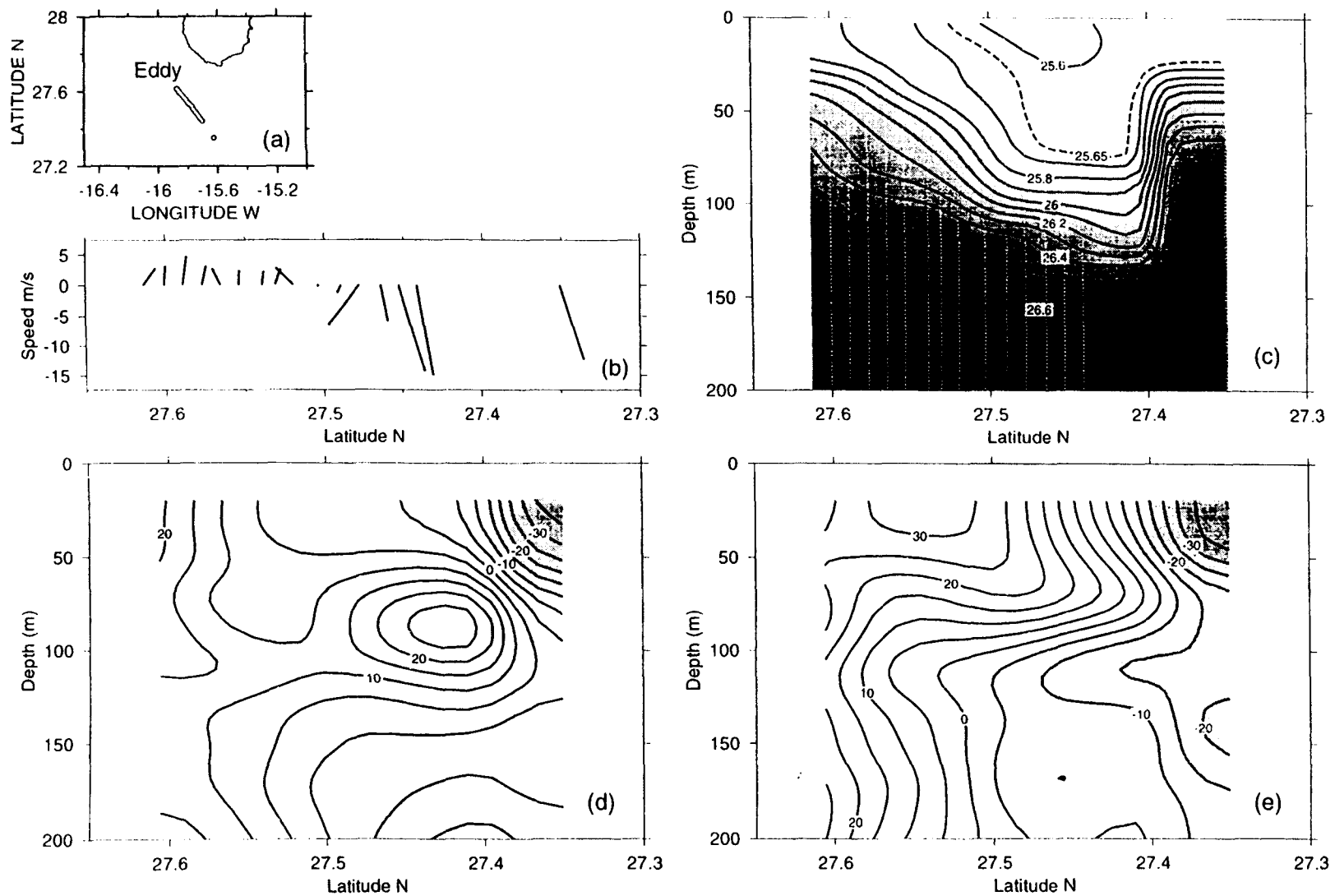


Fig. 23. Section across the lee region of Gran Canaria in August 1993 (a) station positions (b) wind vectors rotated into direction of principal axes of winds during the cruise (up the page represents direction towards 64.5 degrees) (c) Vertical section of density anomaly (d) along-section (positive to southeast) and (e) across-section (positive towards northeast) components of ADCP velocity.

surface layer. The pycnocline across the lee region is elevated at the cyclonic wind shear end and depressed at the anticyclonic end. These distortions of the pycnocline could well be the result of Ekman pumping, which will cause vertical velocities of the same magnitude as in the coastal upwelling. The observed wind speeds of around 15 m s^{-1} would produce vertical motion of $5\text{--}10 \text{ m d}^{-1}$ over a typical Rossby radius of about 15 km.

The ADCP velocity components, rotated parallel and perpendicular to the section (Fig. 23d and e), show strong shear and convergence of currents across the wind shear zone. A component of flow towards the boundary from the southeast is indicated at the easternmost stations, where significant southwestward flow is also seen. In the lee region itself flow above 100 m is mainly northeastward, normal to the line, with small component along the section. Since the easternmost station is on the outer edge of the filament and large cyclonic eddy system the flow in that location is probably more representative of the filament than of any particular dynamics associated with the lee region. The importance of possibly transient effects such as the maximum of cross boundary flow at 100 m (amplified in the interpolation between the two most eastern ADCP profiles) can only be determined with more extended sampling.

Any vertical velocities would be maximal on the boundary between the well-mixed surface waters exposed to the wind and the sheltered waters, subject to strong diurnal surface heating, in the lee. Strong wind events provide upward and downward impulses to the pycnocline on either side of the island. The resultant perturbations have a downstream scale on the order of an island diameter, and so represent a possible mechanism for the production of the eddies observed in the wake of the islands, additional to the conventional one of eddy shedding by flow past an obstacle. Indeed, a cyclonic eddy was observed in the satellite image of 10 August (Fig. 11c) one and a half days after the in situ sampling, centred just the western end of the section shown in Fig. 23. This was the same eddy that was sampled later in the cruise after having drifted to the southwest. The Ekman pumping velocities estimated at the boundaries of the lee are smaller than the eddy upwelling rate estimated from the drifter deployed in the cyclonic eddy, which may indicate over-estimation of the latter. The relative contributions of wind-induced Ekman pumping and island eddy shedding to production of both cyclonic and anticyclonic eddies require further investigation, but these results show that the two phenomena are linked.

5. Discussion

The interaction between the northwest African coastal upwelling and offshore waters is seen to be governed by mesoscale activity in the form of filaments, eddies and island wakes. A major focus of this study, the filament, was sampled at the time of strongest wind forcing when the strongest upwelling signal was present. In the cruises made at other times of year, the offshore boundary of the filament was present in much the same location south east of Gran Canaria. Although remote sensing imagery has shown its presence at various times of year (Hernández-Guerra,

Arístegui, Cantón, & Nykjaer, 1993; Van Camp, Nykjaer, Mittelstaedt, & Schlittenhardt, 1991) there is still no clear idea of its persistence or evolution over the yearly cycle and no information is available on its subsurface structure. The work reported here provides many details of its physical structure and extent, the related velocity field, and its biology and chemistry. These allow estimates of transports and fluxes to be made, and their importance to coastal—open ocean exchanges to be assessed.

Filament structures have been documented in the coastal upwelling regimes off California (Brink, & Cowles, 1991), Portugal (Haynes, Barton, & Pilling, 1993) and southwestern Africa (Lutjeharms, & Stockton, 1987) during their respective coastal upwelling seasons. Though their occurrence seems ubiquitous, their development has been attributed to a variety of different causes, and investigated in numerous modeling and laboratory rotating tank studies. Strub, Kosro, & Huyer (1991) summarized the principal ideas of filament formation in terms of three simplified conceptual models.

The first model is that of 'squirts' or one-way jets, transporting coastally upwelled water into the deep ocean, sometimes terminating in a counter-rotating vortex pair. Frequently occurring patterns of sea surface temperature and pigment fields, denoted as 'mushroom,' 'hammerhead,' or 'T' by Ikeda, & Emery (1984), have been considered to be squirt-like. The idealized squirt is generated by near-shore convergence, caused by local wind relaxation around capes (Huyer, & Kosro, 1987) or blockage of the current by a cape or offshore extending ridge.

The second conceptual model consists of a field of mesoscale eddies imbedded in a slow southward current (Mooers, & Robinson, 1984). Where the eddies draw recently upwelled water away from the coast, they create a surface temperature structure similar to a squirt.

The third conceptual model is based on a continuous, meandering southward jet, which entrains coastally upwelled water near-shore and creates filaments of cold, rich water, extending along the next offshore meander. Closed eddies may be created on either side of the jet by instabilities of the flow, but water in the core of the meandering jet may originate from far upstream, which would not be the case for a squirt and would occur only haphazardly in a mesoscale eddy field.

The filament described here does not correspond neatly with any of the three filament production mechanisms of Strub, Kosro, & Huyer (1991). It seems to be a quasi-permanent feature, which has been noted in satellite images of the region over many years. La Violette (1974) reported Airborne Expendable Bathythermograph observations and early remote sensing of sea surface temperature in the area, which can now be recognised as indicating structure similar to that discussed here. Observations south of Gran Canaria have indicated the influence of an upwelling filament close to the island on several occasions apart from our March and October 1991 cruises (Arístegui, Sangrá, Hernández-León, Cantón, Hernández-Guerra, & Kerling, 1994; Arístegui, Tett, Hernández-Guerra, Basterretxea, Montero, Wild, Sangrá, Hernández-León, Cantón, García Braun, Pacheco, & Barton, 1997). The filament in this location is strongly related to the existence of a, seemingly, permanent cyclonic eddy situated in the trough between Gran Canaria and the African coast. The close relation of the flow field with bottom topography indicates that the origin of this eddy is

most likely vortex stretching of the flow exiting the shallower (< 1500 m) channel between the archipelago and Africa. Whenever upwelling is well developed over the continental shelf, the outer boundary of the cold water and associated alongshore current jet may extend far enough offshore to become entrained around the eddy, so producing the filament. The recurrence of the filament at the same site is indicated by a distinct long term mean temperature minimum extending from north of Cabo Bojador towards Gran Canaria in the average SST image of Fig. 1. With only one realisation of the filament's in situ structure, the variability of the system, which may be significant, remains undetermined. Possible indications of short term variability are the isolated extrema of salinity, chlorophyll and larval density observed on the southern flank of the eddy (Fig. 14). Such features might be produced by intermittent periods of more intense coastal upwelling so that temporal variability at the coast results in spatial variability along the filament.

Another recurrent filament occurs off Cape Ghir some 200 km north of the Canaries. Hagen, Zülicke, & Feistel (1996) have reported that it arises from interaction of the alongshore flow with a local plateau in bottom topography. The filament was formed as one branch of a coastal upwelling jet, the other branch of which continued alongshore through a weak cyclonic meander. The tongue of cold water extended offshore some 200 km between cyclonic and anticyclonic eddies, downstream and upstream, respectively, of the Cape Ghir Plateau. Unlike the present case, there was no indication of a return path to the coast for waters transported offshore in the filament. Transport estimates indicated that upwelling as strong as in the near-shore zone, must occur in the filament itself.

The offshore transport in filaments is often large compared to the Ekman transport. Near to the shelf edge the measured offshore transport in the Cabo Bojador filament was close to $10^6 \text{ m}^3 \text{ s}^{-1}$. Integrating the Ekman transport over the alongshore separation between filaments (200 km) provides a value of $0.4 \times 10^6 \text{ m}^3 \text{ s}^{-1}$, therefore the filament does not simply represent an integration of the wind forcing. The net effect of filament transport may be estimated for the area from the strength, number and temporal occurrence of filaments. The offshore flow in any filament contributes to the net water exchange if water parcels lose their integrity in the offshore region and are not returned intact to the coastal upwelling zone. If the width of the upwelling frontal zone is much less than the offshore extension of the filaments then U_c the net cross-frontal water exchange velocity is given by

$$U_c = n u d t_p,$$

where n is the number of filaments per unit distance alongshore, u is the offshore velocity in the filament, d is the filament width and t_p is the relative duration of the filament as a proportion of days per year when the filament is present. Kostianoy, & Zatsepin (1996) estimated, from satellite sea surface temperature images, the number and frequency of occurrence of cold filaments off north west Africa. In their case, with 60 filaments in an alongshore distance of 1000 km, occurring for a duration of 5 days per year, with a typical velocity of 0.4 m s^{-1} and width 30 km (estimated from one filament), they found $U_c = 0.01 \text{ m s}^{-1}$ within a 50% uncertainty. The equivalent horizontal exchange coefficient is given by $K = U_c D = 500 \text{ m}^2 \text{ s}^{-1}$, where

D is the frontal width. They also made estimates of these values for the southwest African region, with similar results.

In the present case, filaments occur at separations of about 200 km to both south and north (off Cape Ghir) of the one studied. The width of this filament is about 25 km and it persists for most of the year. Taking a typical near-surface offshore velocity as 0.4 m s^{-1} , a value for the net exchange velocity is $U_c = 0.05 \text{ m s}^{-1}$, and $K = 2500 \text{ m}^2 \text{ s}^{-1}$. These derived values would be reduced proportionately if the mean offshore velocity were smaller or the filament duration were less. They are higher than those of Kostianoy, & Zatsepin (1996) principally because of the estimated lifetime of the filament. In their case, the duration seems short compared to filament lifetimes reported for even the strongly seasonal Portugal (Haynes, Barton, & Pilling, 1993) and California Current (Brink, & Cowles, 1991) regions, where durations of months are common. A second important factor which would reduce the present values is the proportion of water which is returned to the coastal zone by recirculation around the eddy with little effective mixing with oceanic waters. Additionally there is little information to indicate the variability of the filament and eddy system in response to changing winds and currents.

The anomalous combination of low salinity and high zooplankton and fish larvae counts along the southern limb of the cyclonic eddy probably reflects variability in forcing. The time taken for a complete circuit of the eddy (diameter 100 km, tangential speed 0.4 m s^{-1}) is about 7 days. This is comparable to the time taken to sample in situ the entire filament station grid, during which time the wind forcing will have varied significantly. The distributions mapped are, therefore, not truly synoptic though the relative persistence of the principal features of the filament and eddy system seen in the AVHRR images indicates that there had been no gross change in the situation. It is clear, however, that conditions along the filament trajectory are not uniform and, moreover, that anomalous concentrations of tracers of coastal origin (low salinity, many sardine larvae) can persist in the filament for more than half a circuit of the eddy. Whether the anomalous region would have become reintegrated into the coastal upwelling regime remains open to speculation, but the possibility exists that a significant proportion of the offshore flow in the filament is returned intact to the coastal zone. If so then both the net exchange velocity and the horizontal mixing coefficient would be reduced.

As well as horizontal exchanges, there may be vertical ones additional to coastal and eddy upwelling. Evidence has been found in the California Current region that subduction is a feature of filaments (Flament, Armi, & Washburn, 1985; Abbot, Brink, Booth, Blasco, Codispoti, Niiler, & Ramp, 1990). Drifters moving along a filament approached the temperature front defining its southern boundary at a rate that indicated a downwelling velocity of 10 m d^{-1} (Brink, & Cowles, 1991). Chlorophyll and Radon distributions also indicated that waters originating from the near-shore euphotic zone were found at depth offshore, implying similar downwelling rates (Kadko, Washburn, & Jones, 1991; Washburn, Kadko, Jones, Hayward, Kosro, Stanton, Ramp, & Cowles, 1991). However, conflicting conclusions on the location of downwelling emphasise the difficulty in generalising the nature, causes and permanency of subduction. In the present case of the Canaries region, although chlorophyll

structure across the filament was reconcilable with sinking of surface waters, it could equally have arisen from horizontal advection. There is no clear evidence in the present data set to suggest that subduction is a significant feature of the Cabo Bojador filament.

The physical structure of the eddy and filament system exerts a major influence on the strong chemical and biological contrasts between the subtropical oligotrophic waters of the oceanic gyre and the fertile upwelling zone of the eastern boundary. Table 1 summarises this contrast as documented by the work reported in this paper. The most basic biological effects of the northwest African upwelling appear in a number of ways. Isopycnals, and nutrient isopleths, are elevated over a distance of several hundred kilometres from the coast (e.g. Figs. 6 and 17). The result of this tilt, and of weak shoreward flows along the isopycnals, is to bring into the euphotic zone water richer in nutrients than at corresponding depths in the far field, and hence to sustain a greater primary production in a shallower DCM than in the far field. The increased production results in the accumulation of extra phytoplankton, and thus of high concentrations of chlorophyll (e.g. Fig. 6). The increased nutrient fluxes do not, however, seem to perturb the structure of the phytoplankton community, which remains dominated by small organisms, especially phytoflagellates (Kennaway, & Tett, 1994) and prochlorophytes (van Lenning et al., personal communication).

Upwelling takes place in a coastal zone about 50 km wide, corresponding roughly to the continental shelf north of Cabo Bojador. Here there are substantial vertical velocities, averaging 3 m d^{-1} and a maximum of 6 m d^{-1} according to calculated Ekman transport. The mean velocity implies a nitrate flux of $\sim 15 \text{ mmol N m}^{-2} \text{ d}^{-1}$

Table 1

Comparison of typical conditions in oligotrophic waters northwest of the archipelago with those in the African coastal upwelling at 27°N . SML is surface mixed layer. DCM is deep chlorophyll maximum

	Oligotrophic	Coastal upwelling
Nutrients	SML strongly depleted in nitrate; nitrocline deep.	SML up to $4 \mu\text{M}$ nitrate; nitrocline shallow.
Chlorophyll	$< 0.05 \text{ mg chl m}^{-3}$ in SML. DCM of $O(0.1) \text{ mg chl m}^{-3}$ at C. 100m.	$2\text{--}4 \text{ mg chl m}^{-3}$ in SML, no DCM
Production and respiration	Production low, $0.1 \text{ g C m}^{-2} \text{ d}^{-1}$; respiration high relative to production	Mean production high, up to $1 \text{ g C m}^{-2} \text{ d}^{-1}$; respiration low relative to production
Phytoplankton	Typically dominated by cyanobacteria in SML, prochlorophytes and small ($< 5 \mu\text{m}$) phytoflagellates in DCM.	Typically dominated by diatoms and larger ($> 5 \mu\text{m}$) phytoflagellates
Zooplankton and fish larvae	Zooplankton scarce ($0.1 \text{ g protein m}^{-2}$ or less); fish larvae uncommon.	Zooplankton patchily abundant (can exceed $1 \text{ g protein m}^{-2}$); patchily abundant sardine larvae.

into the euphotic zone, explaining surface concentrations up to $4 \mu\text{M}$ seen close to shore and potentially supporting new production of $1 \text{ g C m}^{-2} \text{ d}^{-1}$, similar to the maximum rates measured by ^{14}C assimilation during August 1993. Despite the relatively low ratio (about 2:5) of dissolved silica to nitrate, the flux gave rise to large populations of diatoms as well as large ($> 5 \mu\text{m}$) phytoflagellates, which rapidly assimilated the upwelled nutrients. The result is that superficial concentrations of nutrients fall rapidly with distance from the upwelling centre. Data for HPLC-analysed photosynthetic pigments (van Lenning et al., personal communication), as well as some microscopical observations (Kennaway, & Tett, 1994), suggest that the diatoms rapidly vanish as water enters a filament, although it is unclear whether this is the result of grazing or of sedimentation. The phytoflagellate component (which included cryptomonads) appeared more persistent in August 1993, but it seems gradually to give way to the 'oligotrophic' association of small phytoflagellates and cyanobacteria.

The mean flow of the upwelled water has an offshore component in the surface Ekman layer, roughly balanced by a mean shoreward transport at depths below the pycnocline. Given the mean winds during the August cruise of 10 m s^{-1} , the calculated Ekman transport was around $1.8 \text{ m}^2 \text{ s}^{-1}$. However, the actual form of the offshore transport is dominated by the meandering flow around the eddy and by mesoscale mixing processes along its boundaries with oceanic waters (Fig. 23a). As seen in Figs. 11, 12 and 15 the offshore flowing part of the circulation is characterised by a clearly-defined filament of cold water, while the return flow is less evident in sea surface temperature distributions because the surface water has been warmed by insolation to much the same temperature as its surroundings. The horizontal shear between the filament current jet and the surrounding waters results in eddying on a scale of 20 km and smaller (eddy like structures on these scales are seen in Figs. 11 and 12); in this way, an exchange of water parcels between the coastally upwelled water advected in the filament and oceanic waters is effected. Upwelled water is thus entrained into the flow of the Canary Current and therefore the ocean gyre. As documented earlier, the mesoscale stirring action of the islands of the Canary archipelago increases the entrainment rate, diverting some of the water from the filament into island-generated eddies which are themselves carried away by the flow of the Canary Current.

In addition to these horizontal mixing processes, which increase the exchange between oceanic and shelf waters, the Canary region is also responsible for an increase in the vertical exchange between the nutrient-depleted surface zone and the waters of the upper part of the permanent thermocline, which are moderately rich in nutrients (Fig. 24). The increased vertical exchange is the result of pumping by cold-core eddies as well as upwelling (Table 2). Although the values in this table are preliminary and approximate estimates, they suggest that high vertical velocities in the eddies give rise to nutrient fluxes, which are more important than implied by the area of the eddies themselves. Two estimates are included for the cold-core eddy. One, based on the vertical velocity estimated from the drifter separation from the eddy centre, indicates that potentially the eddy could be as important as the coastal upwelling, whereas a more conservative estimate, assuming a vertical velocity similar

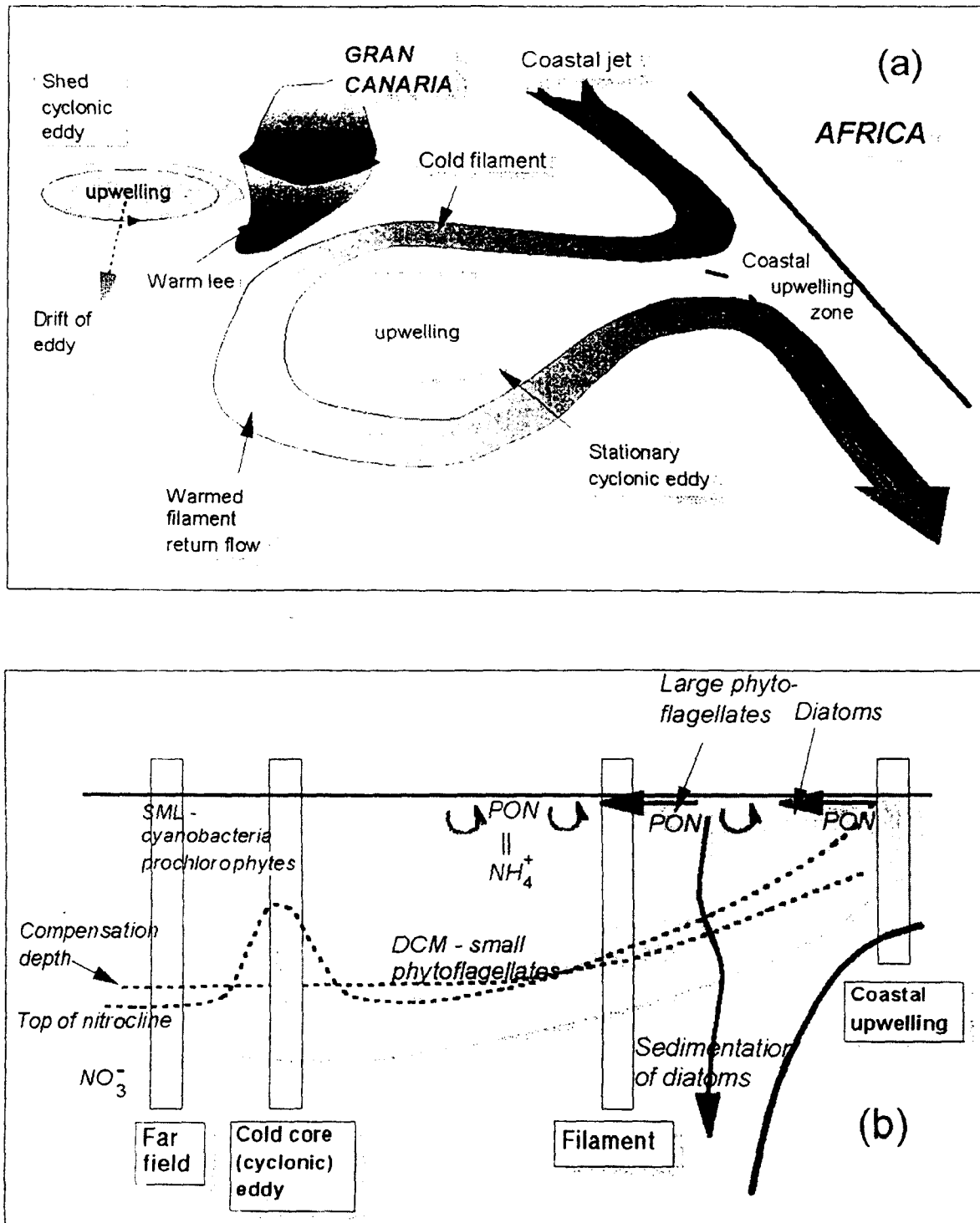


Fig. 24. (a) Schematic of upwelling filament and eddy and (b) associated vertical processes in the filament eddy system. Vertical rectangles indicate typical situations. The *Far-field* nitrocline lies below the compensation depth for phytoplankton growth, and so production is low, carried out by pico- or nano-plankton and likely sustained by recycled ammonium. *Cyclonic Eddies* lift isopycnals and nitrocline relative to the compensation depth, so locally stimulating new production. The DCM intensifies toward the coast and higher nitrate concentrations are exposed above the compensation depth (which itself shallows by shading by more abundant phytoplankton). In the *Upwelling* region, the nitrocline reaches the surface mixed layer, resulting in high production of diatoms, converting nitrate into Particulate Organic Nitrogen. These diatoms sediment or are eaten as upwelled water moves offshore in the *Filament*, leaving large phytoplankton as the dominant producers, supported by recycled ammonia.

Table 2
Nutrient fluxes related to upwelling filaments and eddies

Category	% Area	Upwelling				Vertical Mixing		Total	
		m d ⁻¹	S μM NO ₃	N flux mol m ² yr ⁻¹	Kz m ² d ⁻¹	ΔS/ΔZ mol m ⁻⁴	N flux mol m ² yr ⁻¹	N flux 10 ⁶ kmol yr ⁻¹	
	[0]		[1]			[2]			
Land (Africa)	4%	x	x	x	x	x	x	x	
Land (Canaries)	2%	x	x	x	x	x	x	x	
NW African coastal upwelling	4%	[3]	3	5	5.5	100	0.01	0.37	67
Filaments	3%	[4]	0	2	0	10	0.08	0.29	2
Permanent cyclonic eddy in coastal trough	4%	[5]	1	3	1.1	10	0.07	0.26	15
Island generated wakes and cyclonic eddies	1%	[6]	40(7.5)	22	29.27.3	10	0.08	0.29	8422)
Unperturbed oceanic waters and anticyclonic eddies	81%	[7]	0	0	0	1	0.05	0.02	4

Total area 100% = 285,000 km² Total N flux 173 (111)

[0] Fluxes calculated for 26–30°N, 13–19°W. Area of each feature is its typical extent during cruises and as seen in remote sensing.

[1] Nitrate concentrations observed at base of euphotic zone in August 1993.

[2] Nitrate gradients observed in upper thermocline, or at bases of euphotic zone, in August 1993.

[3] Upwelling velocity from estimated Ekman transport (wind stress divergence) averaged over year.

[4] Vertical mixing enhanced by current shear, value estimated.

[5] Upwelling assumed in balance with vertical mixing of heat over upper 50 m (mixing estimated).

[6] Upwelling velocity from radial velocities in eddy observed in August 1993 and from Ekman pumping in lee.

[7] Typical value of eddy diffusion in upper ocean thermocline.

to that caused by the Ekman pumping on the wake boundaries, still shows eddies may be providing a major contribution to the nitrogen flux. The significant result is that the island induced eddies may constitute major components of the flux. Questions of intermittency and intensity of the eddies during the annual cycle remain to be resolved before reliable conclusions may be drawn (Fig. 24).

What is the fate of the nutrients in these enhanced vertical fluxes? The rapid disappearance of diatoms from filaments suggests that some rapidly sink into deeper waters. However, the enhanced chlorophyll concentrations observed in filaments and cyclonic eddies suggests that some of the nutrient is recycled within the euphotic layer, supporting the small-celled phytoplankton seen in these regions. Furthermore, there is evidence from our measurements of ETS activity and ^{14}C uptake in August 1993 (Fig. 25), that respiration was, proportionally, more important in warmer waters. We thus conclude that the regions of strong vertical nutrient flux support enhanced new production of organic matter which is then spread into surrounding, more oligotrophic, waters. As this happens, the enhanced organic carbon (OC) supply supports additional microbial respiration, and the nitrogen in the extra particulate organic nitrogen (PON) may be recycled several times through ammonium. The balance between observed ETS activity and radiocarbon uptake at a given site will

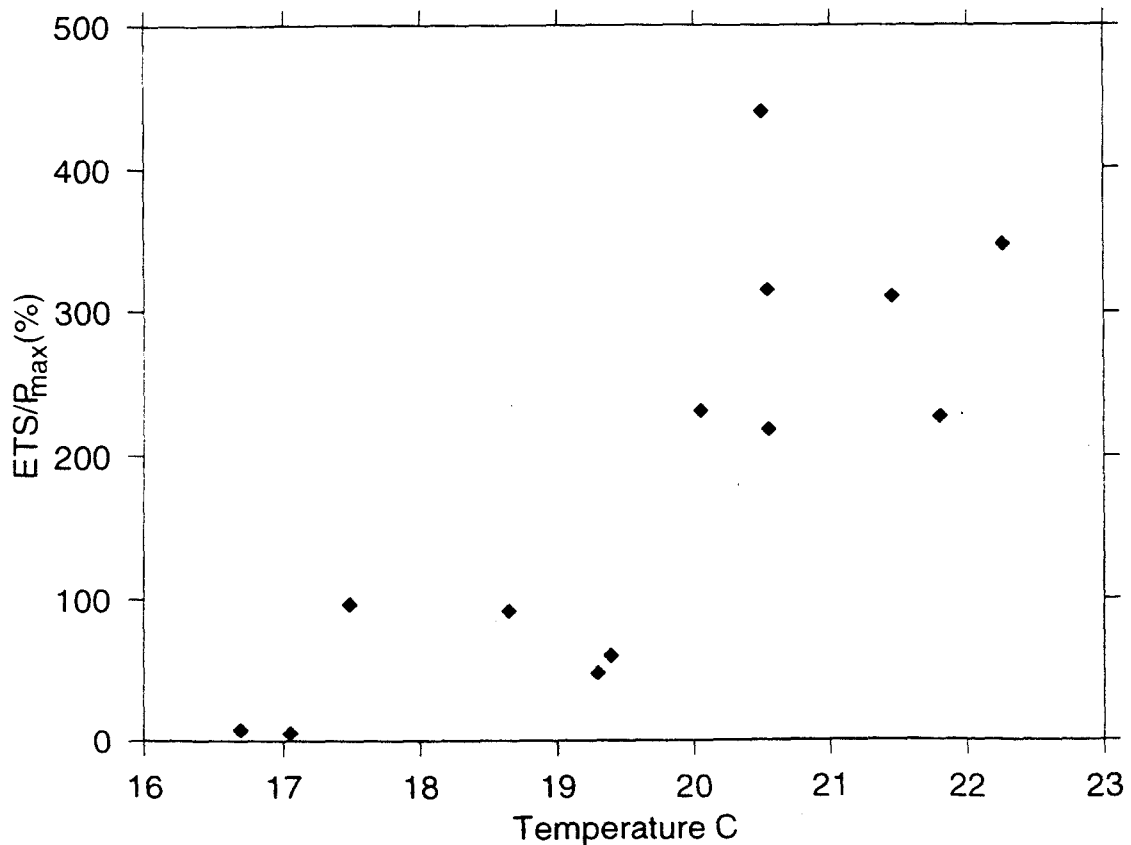


Fig. 25. Relative respiration increase with water temperature at stations in the filament region. Warmer, oligotrophic waters may be net consumers of organic matter produced in upwelling waters. ETS activity represents potential microplankton respiration and was converted to carbon units using a respiratory quotient. Maximum photosynthetic rates (P_{max}) were taken from Photosynthesis-Irradiance curves determined from ^{14}C experiments in subsamples of the same water as ETS activity.

depend on (a) the supply of OC relative to ammonium and nitrate (DIN), and (b) the effect of these OC and DIN supplies on the relationship between respiration and ETS activity, and between photosynthesis and radiocarbon uptake. It is because these are complex matters that the data in Fig. 24 should not be literally interpreted as showing a shift from an absolute excess of photosynthesis over respiration in upwelling waters, to an absolute excess of consumption over production in warmer waters. Nevertheless, we do suggest that filament transport of organic matter may be more important than their transport of inorganic nutrients.

Finally, we can put the vertical fluxes in Table 2 into a larger perspective. The global input of new nitrogen to the upper ocean from deeper waters is currently estimated as about 85×10^9 kmol y^{-1} (Schlesinger, 1997). We estimate that the total vertical flux in the Canaries region is 0.17×10^9 kmol y^{-1} , or 0.2% of the global total from a sea area which is 0.07% of the world ocean. The Canaries region is thus three times as active in vertical transport of nitrogen as the mean of the global ocean. Most impressive of all, a large part of the vertical flux in the Canaries region occurs in the island-generated eddies, which occupy only about 1% of the area of the region. Their vertical flux, estimated by us at $29 \text{ mol N m}^{-2} y^{-1}$, is more than a hundred times the oceanic mean of $0.24 \text{ mol N m}^{-2} y^{-1}$.

The Canary islands are efficient suppliers of nutrient to the euphotic zone for a combination of reasons. First, they lie in oligotrophic waters, so the upper-ocean nutrient gradient is relatively large. Second, they are situated in a region of strong atmospheric and oceanic flows, which encourage the formation of energetic eddies with high core upwelling speeds. Third, the eddies can tap relatively high nutrient concentrations because of the regional uplift of the oceanic nitrocline which is associated with the NW African upwelling.

6. Acknowledgements

This work was supported by the MAST programme of the European Commission through Projects 0031 and CANIGO and by the Spanish Consejo Interministerial de Ciencia y Tecnología with provision of ship time and through the FRENTE project (CICYT, AMB 95-0731). We express our gratitude to our many colleagues who participated in the field work and data processing.

7. References

- Abbot, M.R., Brink, K.H., Booth, C.R., Blasco, D., Codispoti, L.A., Niiler, P.P., & Ramp, S.R. (1990). Observations of phytoplankton and nutrients from a Lagrangian drifter off northern California. *Journal of Geophysical Research*, 95, 9393–9409.
- Aristegui, J. (1990). La distribución de la clorofila *a* en aguas de Canarias. *Boletín del Instituto Español de Oceanografía*, 6(2), 61–72.
- Aristegui, J., Hernández-León, S., Gómez, M., Medina, L., Ojeda, A., & Torres, S. (1989). Influence of the north Trade winds on the biomass and production of neritic plankton in Gran Canaria. In *Topics in Marine Biology*, J.D. Ros, editor. *Scientia Marina*, 53, 223–229.

- Aristegui, J., Sangrá, P., Hernández-León, S., Cantón, M., Hernández-Guerra, A., & Kerling, J.L. (1994). Island-induced eddies in the Canary Islands. *Deep-Sea Research I*, *41*, 1509–1525.
- Aristegui, J., Tett, P., Hernández-Guerra, A., Basterretxea, G., Montero, M.F., Wild, K., Sangrá, P., Hernández-León, S., Cantón, M., García Braun, J.A., Pacheco, M., & Barton, E.D. (1997). The influence of island generated eddies on chlorophyll distribution: a study of mesoscale variation around Gran Canaria. *Deep-Sea Research I*, *44*, 71–96.
- Bakun, A., & Nelson, C.S. (1991). The seasonal cycle of wind-stress curl in subtropical eastern boundary current regions. *Journal of Physical Oceanography*, *21*(12), 1815–1834.
- Ballesteros, S. (1992). *Ignat Pavlyuchenkov cruise report: micro-organisms abundance and distribution*. Data Report 0031-10, School of Ocean Sciences, University of Wales, Bangor, UK.
- Ballesteros, S. (1994). *Influencia de las estructuras mesoescales sobre la distribución y abundancia de bacterias y cianobacterias en aguas de Canarias*. Doctoral thesis. University de Las Palmas de Gran Canaria, 153 pp.
- Barton, E.D. (1994a). Frontal structures downwind and downstream of Gran Canaria. *Annales Geophysicae*, *12*, Suppl. II, C267.
- Barton, E.D. (1994b). *European Coastal Transition Zone: Islas Canarias*. Final Report, MAST Project 0031, School of Ocean Sciences, University of Wales, Bangor, UK, 90 pp.
- Basterretxea, G. (1994). *Influencia de las estructuras oceanográficas mesoescales sobre la producción primaria en la región Canaria*. Doctoral thesis, University of Las Palmas de Gran Canaria, 113 pp.
- Braun, J.G. (1980). Estudios de producción en aguas de las Islas Canarias. I, hidrografía, nutrientes y producción primaria. *Boletín del Instituto Español de Oceanografía*, *285*, 149–154.
- Braun, J.G., & Escánez, J.E. (1996). *Distribution of nutrients and dissolved oxygen during the Ignat Pavlyuchenkov cruise (October 1991)*. Data Report 0031-18, School of Ocean Sciences, University of Wales, Bangor, UK.
- Braun, J.G., Orzaiz, I., Armas, J.D., & Real, F. (1985). Productividad y biomasa del ultraplanton, nanoplanton y fitoplanton de red en aguas de las Islas Canarias. *Boletín del Instituto Español de Oceanografía*, *2*(1), 192–204.
- Brink, K.H., & Cowles, T.J. (1991). The Coastal Transition Zone Experiment. *Journal of Geophysical Research*, *96*, 14637–14647.
- Castagné, N., Le Borgne, P., Le Vourch, J., & Olry, J.P. (1986). Operation measurement of sea surface temperatures at CMS Lannion from NOAA-7 AVHRR data. *International Journal of Remote Sensing*, *7*, 953–984.
- De León, A.R., & Braun, J.G. (1973). Ciclo anual de la producción primaria y su relación con los nutrientes en aguas Canarias. *Boletín del Instituto Español de Oceanografía*, *167*, 1–24.
- Flament, P., Armi, L., & Washburn, L. (1985). The evolving structure of an upwelling filament. *Journal of Geophysical Research*, *90*, 11765–11778.
- Hagen, E., Züllicke, C., & Feistel, R. (1996). Near-surface structures in the Cape Ghir filament off Morocco. *Oceanologica Acta*, *19*(6), 577–598.
- Haynes, R., Barton, E.D., & Pilling, I. (1993). Development, persistence, and variability of upwelling filaments off the Atlantic coast of the Iberian Peninsula. *Journal of Geophysical Research*, *98*, 22681–22692.
- Hayward, T.L., & Mantyla, A.W. (1990). Physical, chemical and biological structure of a coastal eddy near Cape Mendocino. *Journal of Marine Research*, *48*, 825–850.
- Hernández-Guerra, A., Aristegui, J., Cantón, M., & Nykjaer, L. (1993). Phytoplankton pigment patterns in the Canary Islands as determined using Coastal Zone Colour Scanner data. *International Journal of Remote Sensing*, *14*, 1431–1437.
- Hernández-León, S. (1988). Gradients of mesozooplankton biomass and ETS activity in the wind shear area as evidence of an island mass effect. *Marine Biology*, *10*, 1141–1437.
- Hernández-León, S. (1991). Accumulation of mesozooplankton in a wake area as a causative mechanism of the 'island mass effect'. *Marine Biology*, *109*, 141–147.
- Hill, A.E., Hickey, B.M., Shillington, F.A., Strub, P.T., Brink, K.H., Barton, E.D., & Thomas, A.C. (1997). Eastern Ocean Boundaries. In: *The Sea*, A.R. Robinson and K.H. Brink (editors), *10*.
- Huyer, A., Kosro, P.M., Fleischbein, J., Ramp, S.R., Stanton, T., Washburn, L., Chavez, F.P., Cowles,

- T.J., Pierce, S., & Smith, R.L. (1991). Currents and water masses of the Coastal Transition Zone off Northern California, June to August 1988. *Journal of Geophysical Research*, 96, 14809–14832.
- Huyer, A., & Kosro, P.M. (1987). Mesoscale surveys over the shelf and slope in the upwelling region near Point Arena. *California Journal of Geophysical Research*, 92, 1655–1681.
- Ikeda, M., & Emery, W.J. (1984). Satellite observations and modelling of meanders in the California Current System off Oregon and northern California. *Journal of Physical Oceanography*, 14, 3–12.
- Jones, B.D., Mooers, C.N.K., Rienecker, M.M., Stanton, T., & Washburn, L. (1991). Chemical and biological structure and transport of a cool filament associated with a jet-eddy system off northern California in July 1986 (OPTOMA 21). *Journal of Geophysical Research*, 96, 22207–22225.
- Kadko, D.C., Washburn, L., & Jones, B. (1991). Evidence of subduction within cold filaments of the northern Californian coastal transition zone. *Journal of Geophysical Research*, 96, 14909–14926.
- Kennaway, G.M., & Tett, P. (1994). *A scanning electron microscope study of flagellate assemblies from the Hespérides Cruise 9308*. Data Report 0031-17, School of Ocean Sciences, University of Wales, Bangor, UK.
- Kostianoy, A.G., & Zatsepin, A.G. (1996). The West African coastal upwelling filaments and cross-frontal water exchange conditioned by them. *Journal of Marine Systems*, 7, 349–359.
- La Violette, P.E. (1974). A satellite-aircraft thermal study of the upwelled waters off Spanish Sahara. *Journal of Physical Oceanography*, 4, 676–685.
- Le Borgne, P., Le Vourch, J., & Marsouin, A. (1988). Sea surface temperature parameters inferred from meteorological satellite data at CMS Lannion. *International Journal of Remote Sensing*, 9, 1819–1834.
- Li, W.K.W. (1994). Primary production of prochlorophytes, cyanobacteria, and eukaryotic ultraphytoplankton—measurements from flow cytometric sorting. *Limnology and Oceanography*, 39, 169–175.
- Lutjeharms, J.R.E., & Stockton, P.L. (1987). Kinematics of the upwelling front off southern Africa. *South African Journal of Marine Science*, 5, 35–50.
- Montero, M.F. (1992). *Ignat Pavlyuchenkov cruise report: Electron Transport System Activity (ETS) in microplankton around the Canary Islands*. Data Report 0031-11, School of Ocean Sciences, University of Wales, Bangor, UK.
- Montero, M.F. (1993). *Respiración y actividad ETS en microplancton marino. Variabilidad del ETS en aguas de Canarias*. Doctoral thesis, University of Las Palmas de Gran Canaria, 194 pp.
- Mooers, C.N.K., & Robinson, A.R. (1984). Turbulent jets and eddies in the California Current and inferred cross-shore transports. *Science*, 223, 51–53.
- Navarro-Pérez, E. (1996). *Physical oceanography of the Canary Current: short term, seasonal and interannual variability*. Doctoral Thesis, Univ. of Wales, Bangor, 160 pp.
- Navarro-Pérez, E., Vélez-Muñoz, H.S., & Wild, K.A. (1994). *BIO Hespérides Cruise 9308 Cruise Report: Hydrographic Fields*. Data Report 0031-16, School of Ocean Sciences, University of Wales, Bangor, UK.
- Navarro-Pérez, E., & Barton, E.D. (1995). *BIO Hespérides Cruise 9308 Cruise Report: Acoustic Doppler Current Fields*. Data Report 0031-19, School of Ocean Sciences, University of Wales, Bangor, UK.
- Nykjaer, L., & Van Camp, L. (1994). Seasonal and interannual variability of coastal upwelling along northwest Africa and Portugal from 1981 to 1991. *Journal of Geophysical Research*, 99, 14197–14208.
- Ramp, S.R., Jessen, P.F., Brink, K.H., Niiler, P.P., Daggett, F.L., & Best, J.S. (1991). The physical structure of cold filaments near Point Arena, California, during June 1987. *Journal of Geophysical Research*, 96, 14859–14884.
- Rodríguez, J.M. (1996). *El ictioplancton en la Región Canaria: abundancia, distribución y composición taxonómica larvaria*. Doctoral thesis, University of La Laguna, Tenerife, 209 pp.
- Roy, C. and Mendelsohn R. (1995). *Comprehensive Ocean Dataset Extraction users guide*. Climate and Eastern Ocean Systems project report, 62 pp.
- Sangrá, P. (1995). *Perturbación de un flujo geofísico por un obstáculo: aplicación a la isla de Gran Canaria*. Doctoral thesis, University of Las Palmas de Gran Canaria, 200 pp.
- Schlesinger, W.H. (1997). *Biogeochemistry. Analysis of global change (2nd Edition)*. Harcourt Brace Jovanovich, San Diego, 433 pp.
- Shapiro, G., Barton, E.D., & Meschanov, S.L. (1997). Capture and release of Lagrangian floats by eddies in shear flow. *Journal of Geophysical Research*, 102, 27887–27902.

- Speth, P., Detlefsen, H., & Sierts, H.W. (1978). Meteorological influence on upwelling off Northwest Africa. *Deutsches Hydrografisches Zeitschrift*, 31, 95–104.
- Stramma, L., & Siedler, G. (1988). Seasonal changes in the North Atlantic Suptropical Gyre. *Journal of Geophysical Research*, 93, 8111–8118.
- Strub, P.T., Kosro, P.M., & Huyer, A. (1991). The nature of the cold filaments in the California Current System. *Journal of Geophysical Research*, 96, 14743–14768.
- Traganza, E.D., Nestor, D.A., & McDonald, A.K. (1980). Satellite observations of a nutrient upwelling off the coast of California. *Journal of Geophysical Research*, 85, 4101–4106.
- Van Camp, L., Nykjaer, L., Mittelstaedt, E., & Schlittenhardt, P. (1991). Upwelling and boundary circulation off Northwest Africa as depicted by infrared and visible satellite observations. *Progress in Oceanography*, 26, 357–402.
- Vélez-Muñoz, H.S. (1992). *Ignat Pavlyuchenkov cruise report: Hydrographic fields*. Data Report 0031-09, School of Ocean Sciences, University of Wales, Bangor, UK.
- Washburn, L., Kadko, D.C., Jones, B.H., Hayward, T., Kosro, P.M., Stanton, T.P., Ramp, S., & Cowles, T. (1991). Water mass subduction and the transport of phytoplankton in a coastal upwelling system. *Journal of Geophysical Research*, 96, 14927–14945.
- Wild, K.A. (1992). *Ignat Pavlyuchenkov cruise report: general and phytoplankton biomass*. Data Report 0031-08, School of Ocean Sciences, University of Wales, Bangor, UK.
- Wild, K.A. (1995). *The dynamics of the deep chlorophyll maximum in the vicinity of the Canary Islands (Spain)*. Doctoral Thesis, Univ. of Wales, Bangor, 254 pp.
- Wooster, W.S., Bakun, A., & McLain, D.R. (1976). The seasonal upwelling cycle along the eastern boundary of the North Atlantic. *Journal of Marine Research*, 34, 131–141.

DEGRADATIVE DISEASE IN *ULVA RIGIDA* (CHLOROPHYCEAE) ASSOCIATED WITH *ACROCHAETE GENICULATA* (CHLOROPHYCEAE)¹

Elena del Campo,² Guillermo García-Reina

Instituto de Algología Aplicada, Universidad de Las Palmas de Gran Canaria, Muelle de Taliarte s/n. 35214 Telde, Las Palmas, Canary Islands, Spain

and

Juan A. Correa

Departamento de Ecología, Facultad de Ciencias Biológicas, Pontificia Universidad Católica de Chile, Box 114-D, Santiago, Chile

ABSTRACT

A destructive disease affecting tank-cultivated *Ulva rigida* C. Agardh. was characterized by green spots, initially located at the base of the thalli, that spread through the host thallus and gradually caused perforations of the frond. The endophytic filamentous green alga *Acrochaete geniculata* (Gardner) O'Kelly was identified as the causative agent of the disease. The effects of this infection on the host varied from minor injuries to gross frond destruction. Advanced stages of infection resulted in frond wrinkling and severe tissue loss. These symptoms were caused by a primary compaction of the host cells due to a direct effect of the endophyte followed by secondary bacterial infections that became part of the degradative process initiated by the algal pathogen. Co-cultivation of healthy and diseased fronds resulted in transfer of the infection within 2 weeks; however, attempts to infect the host in the laboratory with actively reproducing suspensions of the endophyte were unsuccessful.

Key index words: *Acrochaete geniculata*; disease; endophyte; infection; *Ulva rigida*

Numerous species of pigmented algal endophytes are associated with seaweeds (Goff 1983). They are generally small, filamentous algae that inhabit mainly the intercellular spaces of their hosts. Some of these endophytes cause only minor changes in their hosts, whereas others are known to produce either degradative losses or tumoral lesions. The endophytic phaeophycean *Streblonema aecidioides* causes tissue thickening in the commercially valuable alga *Undaria* sp. (Yoshida and Akiyama 1979), and *Streblonema*-like endophytes are known to produce galls in some algal hosts (Andrews 1977, Apt 1988). In *Chondrus crispus*, another economically important alga, severe degradative lesions and cellular damage were reported during infections by the green algae *Acrochaete operculata* and *A. heteroclada* (Correa et al. 1988, Correa and McLachlan 1991, Correa and McLachlan 1992). Similar degradative lesions have been described in *Mazzaella laminarioides* infected by *Endophyton ramosum* (Correa et al. 1994). None of

the green, red, or brown algal endophytes reported from numerous hosts (Andrews 1977, Garbary 1979, Yoshida and Akiyama 1979, O'Kelly and Yarish 1981, O'Kelly 1982, Nielsen and McLachlan 1986a, b, Peters 1991) have been found in *Ulva*.

Species of *Ulva* have been used as biofilters to remove ammonium and phosphates, the main dissolved pollutants in residual waters from fishpond aquaculture (Neori et al. 1989, 1991, Cohen and Neori 1991, Jimenez del Rio et al. 1994, 1996). *Ulva rigida* was being used for this purpose in a pilot plant for fish (*Sparus aurata*, sea bream) cultivation in Gran Canaria (Canary Islands, Spain). A major problem arose when rapid frond perforations, followed by fragmentation, developed in the algal tanks; most of the algal biomass was lost in a few weeks. Preliminary observations suggested the involvement of a green algal endophyte that was associated consistently with the *Ulva* terminal lesions (i.e. perforations of the lamina).

Thallus integrity is required for an optimal biofiltration by *U. rigida*; therefore, it is important to know the causes of both physiological and structural impairments. This study was designed to 1) characterize the symptoms in the host and 2) identify the causative agent and elucidate the interactions between host and pathogen at the cellular level.

MATERIALS AND METHODS

Ulva rigida was collected at Taliarte harbor, on the east coast of Gran Canaria Island, Canary Islands, and cultivated under greenhouse conditions in 750-L tanks with continuous flow of NH₄-enriched seawater. Sampling was carried out periodically for microscopic observations and isolation of the infecting organism. Thick sections of tissue were used to characterize the disease by light microscopy (BHS, Olympus, Hamburg, Germany). Material used for transmission electron microscopy (TEM) was fixed in 3% glutaraldehyde in 0.45 µm filtered seawater for at least 24 h at 4°C following the procedure outlined by Correa and McLachlan (1994). Samples were infiltrated in Epon 812 and then polymerized for 24 h at 65°C. Thin sections were post-stained with uranyl acetate and/or lead citrate and examined and photographed with a Philips 301 transmission electron microscope operated at 60 kV.

Isolation of the infecting organism. The algal endophyte was isolated using previously described procedures (Correa et al. 1988, Correa and McLachlan 1991). Briefly, crude cultures were initiated by inoculating fragments of clean, infected fronds in 15 × 60-mm sterile plastic petri dishes containing enriched natural seawater (SFC, Correa et al. 1988). Cultures were maintained at 20

¹ Received 28 July 1997. Accepted 11 November 1997.

² Author for reprint requests; e-mail martel@amiq1.ext.ulpgc.es.

C and illuminated with white fluorescent lamps at a photon flux density of 50–60 $\mu\text{mol}\cdot\text{m}^{-2}\cdot\text{s}^{-1}$ and a light regime of 16:8 h LD (standard conditions). Endophytic filaments growing from the host, or germlings grown from swimmers released by the sporangia of the endophyte, were removed from crude cultures with Pasteur pipettes and transferred into 15 × 60-mm plastic sterile petri dishes with fresh medium. Unialgal cultures were maintained under standard conditions with weekly changes of medium.

Infection experiments. For *in vitro* infections, unialgal *Ulva rigida* was obtained from spores released by mature fronds collected at Taliarte. Each infection trial ($n = 10$) was performed by adding 2 mL of an actively reproducing suspension of the endophyte to 100-mL aerated sterile Erlenmeyer flasks containing *U. rigida* plants, 10–15 mg, and 50 mL of SFC medium. The endophyte was induced to sporulate by changing the culture medium 1 week prior to host inoculation. After 2–3 weeks of being in contact with the endophyte, host thalli were brushed and transferred into clean flasks with fresh medium and incubated for 5 weeks under standard culture conditions.

For tank infections, fronds of healthy *Ulva rigida* were transferred to 15-L tanks under greenhouse conditions with continuously flowing NH_4 -enriched seawater. Heavily infected algae (3% of the total number of algae, $n = 35$) were cocultivated with healthy algae. Uninfected fronds from the field and without cocultivation with infected fronds were used as controls. The experiments were carried out in triplicate and conducted during a 3-week period. Plants of *U. rigida* were harvested weekly, spun down at 2800 rpm in a domestic centrifuge (Miele WZ 268, Gütersloh, Germany) for 30 s, and restocked to the initial density, maintaining the proportion of infected to healthy plants.

RESULTS

Symptoms. Macroscopically, healthy fronds of *Ulva rigida* were characterized by a smooth, bright green surface. Infection first appeared in the form of discrete, dark green spots that were restricted to the base of the fronds (Fig. 1) and later spread to other portions of the thallus (Fig. 2). Infected fronds exhibited a rough texture caused by the lesions, although no gall-like structures were observed. Fronds with severe infections were recognized by fragmentation of the lamina, which appeared wrinkled and perforated (Fig. 3) and was accompanied by severe necrosis.

Normal fronds of *Ulva rigida* are distromatic. These cells were elongate and perpendicular to the thallus surface, and their walls were confluent with one another to form a gelatinous matrix. Each cell contained a single peripheral chloroplast oriented toward the outer face of the cell. In infected fronds, cross sections through the lesions first showed the existence of green filaments embedded in the outer cell wall (Fig. 4) that later formed a network of invasive thalli ramifying extensively into the host (Fig. 5).

Endophytic thalli were heterotrichous and consisted of a vegetative system of uniseriate, irregularly branched filaments that, although they frequently crossed the host cell walls, did not penetrate the host plasmalemma. Cells of the endophytic filaments were 5–8 μm wide and one to ten times as long. Each cell contained a single parietal chloroplast, usually with one pyrenoid. In advanced infections, disruption and disorganization of the host tis-

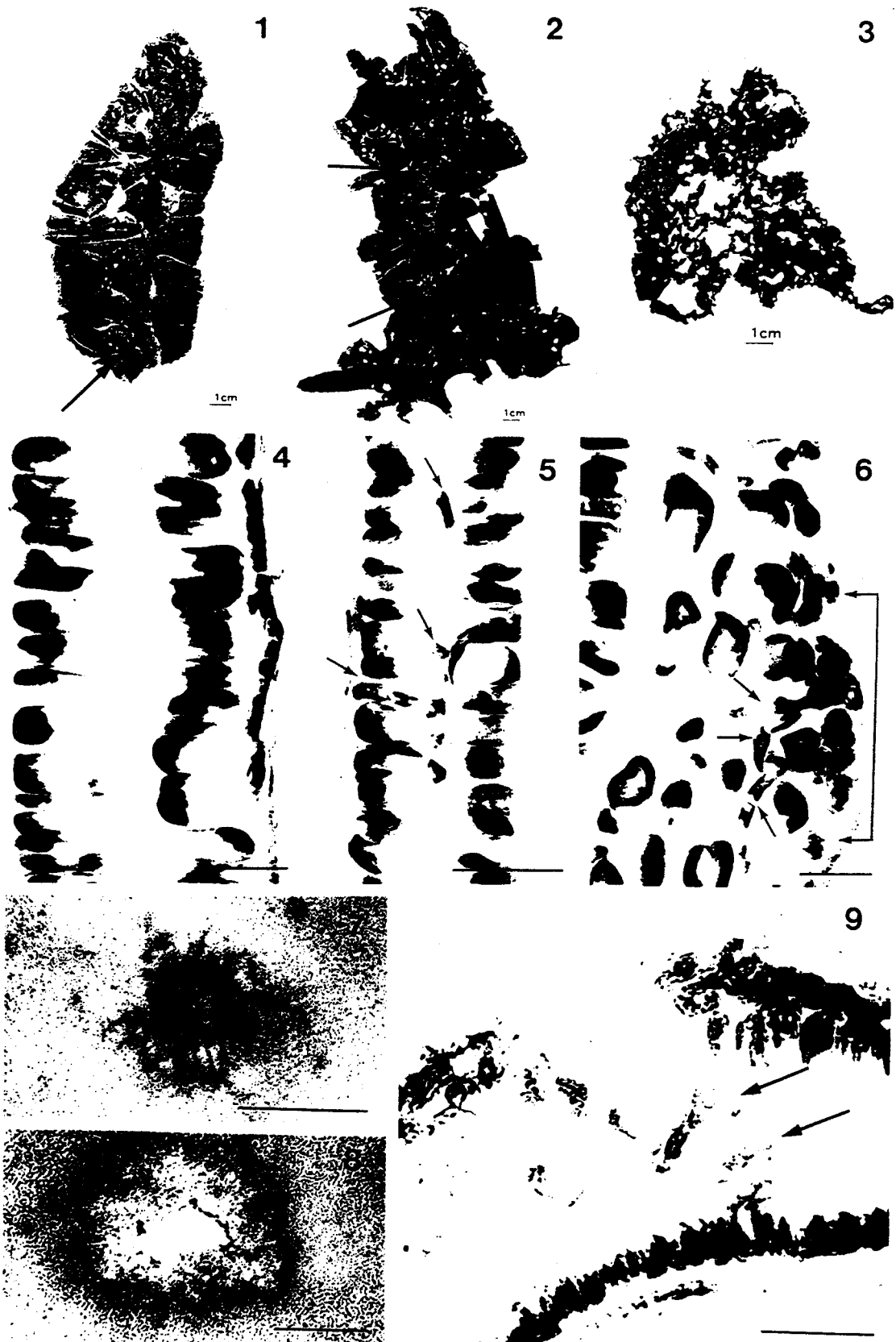
sues by the endophyte resulted in a local thickening of four to six host cells (Fig. 6). These thickenings were caused by host cell hyperplasia and hypertrophy and resulted in abnormal, unorganized cell proliferations.

In surface view, endophytic individuals displayed a radiating, branched profile (Fig. 7) with diameters of the initial infection ranging from 0.5 to 5 mm. In well-developed endophytes, the central part of the thallus appeared, at times, several cells thick. In older infections, a loss of host tissue that resulted in a central perforation of the lesions was observed (Figs. 8, 9). Filaments were still present at the edge of such lesions. This infection stage was also characterized by secondary epiphytism by members of the Ectocarpaceae, which colonized the edge of the perforations. Cross sections through the perforated lesions showed a disintegration of the host cell wall and the presence of endophytic flask-shaped cells (Fig. 9).

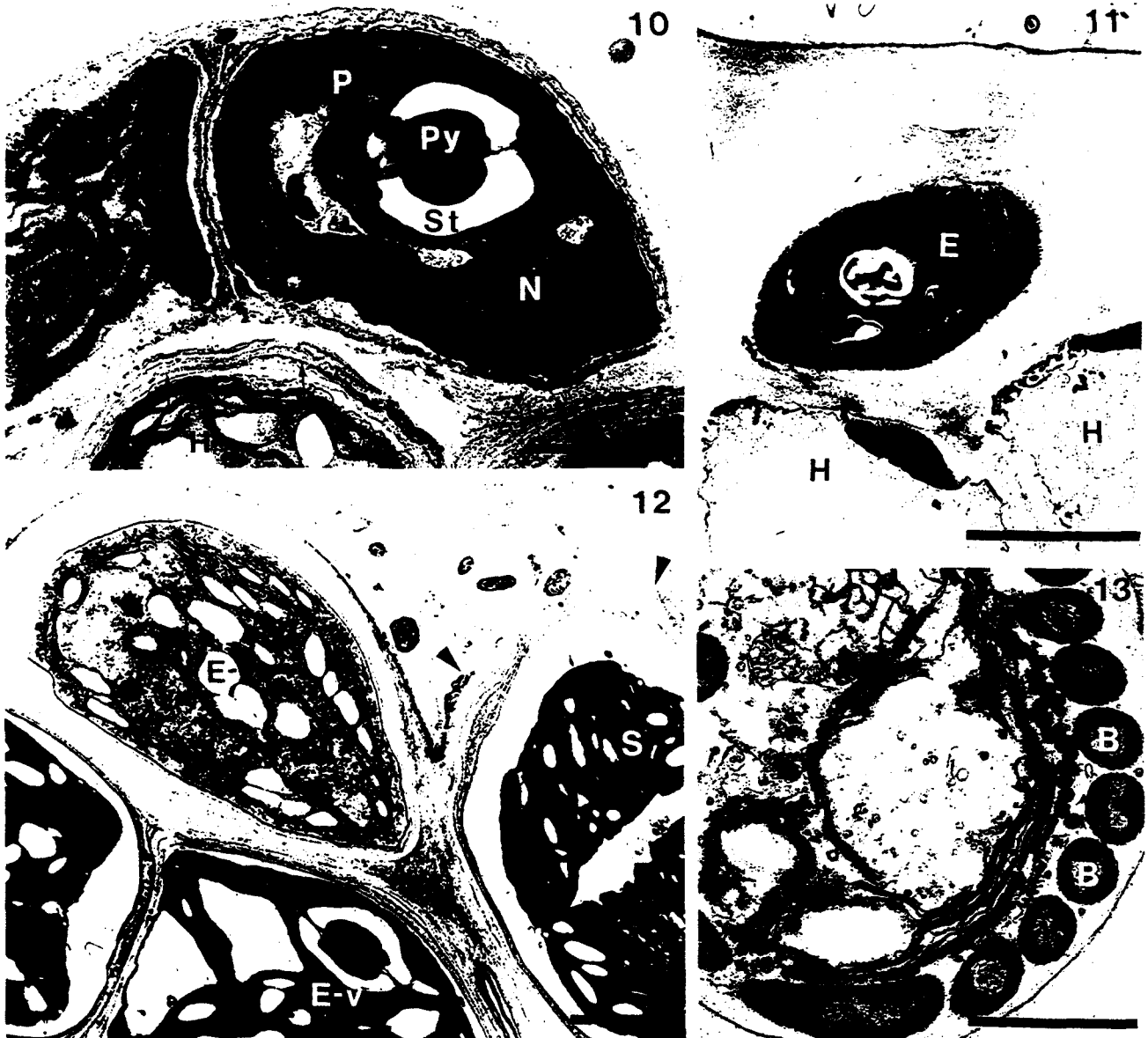
At the ultrastructural level, irregularly shaped vegetative cells of the endophyte were uninucleate and contained a single parietal chloroplast, usually with a single bilenticular pyrenoid. The pyrenoid was surrounded by two starch plates (Fig. 10) and transversed by thylakoids connected to the stroma. When growing on the surface of the host, vegetative cells did not appear to induce structural changes in the host cells at the contact area. Conversely, when endophytic cells became embedded in the tissues of the host, cellular interactions became apparent. An engrossment of the cell wall fibrillar matrix was observed accompanying a compression of the host cells, which displayed a highly reduced chloroplast (Fig. 11), and a pale area was observed at the host–endophyte interface. In older infections, cells of the endophyte growing beneath the outer host cell wall enlarged, especially during sporangium differentiation (Fig. 12). This enlargement resulted in the disruption of the host outer cell wall and the protrusion of endophytic cells from the surface of the host at the center of the lesions. Disruption of the outer cell wall of the host facilitated the penetration of bacteria, which invaded and digested host cells (Fig. 13) and became an active part of the process of tissue decay and lamina fragmentation.

Attempts to infect *Ulva rigida* under laboratory conditions with an actively reproducing suspension of the endophyte were unsuccessful. Even after 2 months of contact with *Ulva* plants, progeny of the endophyte grew only epiphytically on the host. In field trials (tank cultures), however, transmission of the disease was easily achieved by cocultivation of healthy *U. rigida* with diseased thalli. Symptoms in the originally healthy *U. rigida* appeared within 2 weeks of contact with diseased hosts, whereas thalli in the control tanks never developed equivalent symptoms. After 3 weeks, 35% of the plants in the cocultivation tanks were infected (Fig. 14).

Development of the endophyte in unialgal cul-



FIGS. 1-3. Macroscopic signs of the degradative disease of *Ulva ngala*. FIG. 1. Early infection. Spot-like lesions present at the base of the frond (arrow). Most of the thallus surface is normal. Scale bar = 1 cm. FIG. 2. Intermediate infection. Spot-like lesions affect most of the frond (arrows). Scale bar = 1 cm. FIG. 3. Advanced infection with a frond at the fragmentation stage. Scale bar = 1 cm. FIGS. 4-6. Hand sections through the lesions. FIG. 4. Border of an early lesion with an endophytic filament embedded in the host



FIGS. 10-13. Transmission electron microscopy of infected tissue. FIG. 10. Endophytic cell growing on the surface of *Ulva rigida* (H). No distortion of the host outer cell wall (arrows) is evident. Vegetative cell of the endophyte presents a single nucleus (N) and a parietal chloroplast (P) containing one pyrenoid (Py). The pyrenoid appears surrounded by two starch plates (St) and transversed by thylakoids connected to the stroma. Scale bar = 2 μ m. FIG. 11. Endophytic cell (E) embedded in the fibrillar matrix of the outer cell wall of *Ulva rigida*. Adjacent, compressed host cells (H) show highly reduced chloroplasts. Scale bar = 4 μ m. FIG. 12. Old infection, with enlarged endophytic vegetative cells (E-V) and a sporangium initial, after the first cell division (S). The host outer cell wall appears interrupted (arrowheads) as the sporangium grows. Scale bar = 2 μ m. FIG. 13. Bacteria (B) within a damaged host cell. The plastid appears disintegrated, with separated thylakoids and membranous subcellular debris. Scale bar = 1 μ m.

outer cell wall. Scale bar = 20 μ m. FIG. 5. Invasive, endophytic filaments (arrows) breaking through host cells and reaching the center of the lamina. Scale bar = 50 μ m. FIG. 6. Massive colonization (arrows) of the inner region of the host accompanied by disorganization of the palisade structure of the cells resulting in a local thickening of four to six cells (between arrows). Scale bar = 20 μ m.

FIG. 7. Surface view of an early infection in *Ulva rigida*. Scale bar = 500 μ m.

FIG. 8. Surface view of a terminal lesion, with destruction and loss of host tissue. Scale bar = 500 μ m.

FIG. 9. Cross section through a terminal lesion, perforated only at one side of the lamina. Endophytic, flask-shaped cells are present in the inner region (arrows). Scale bar = 50 μ m.

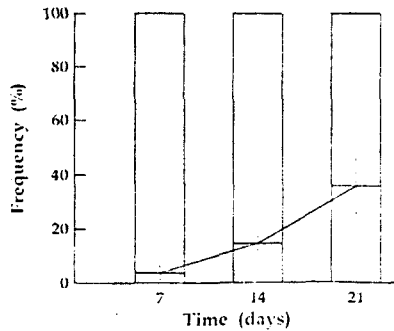
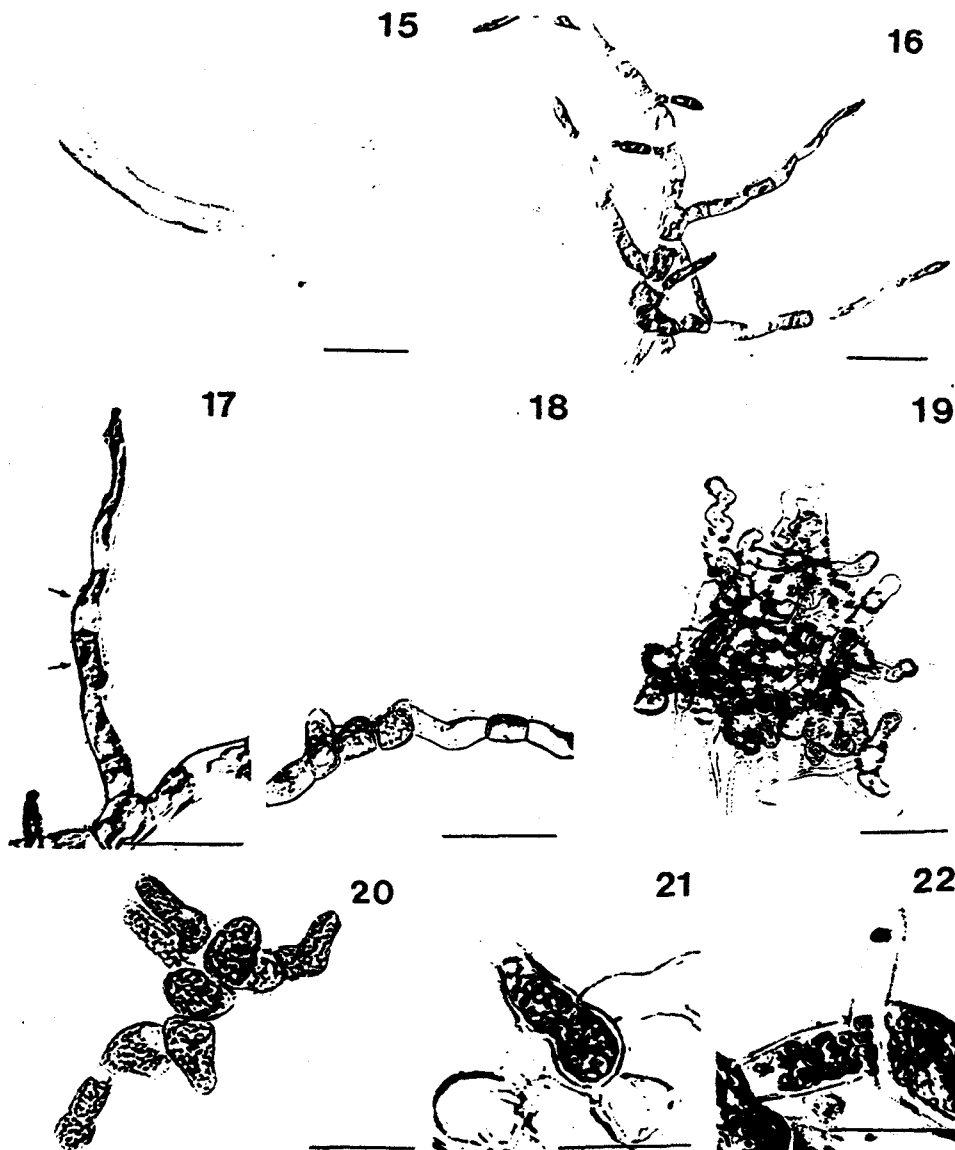


FIG. 14. Frequency (mean \pm SD) of plants infected in coin-cubation experiments. Hatched bars: healthy plants; clear bars: infected plants.

tures began with the settlement of spores. Spore germination was unipolar, and the content of the spore migrated into a well-defined germination tube (Fig. 15). After 1–2 weeks, germlings appeared as sparsely branched filaments (Fig. 16). Vegetative cells of the isolated endophyte were cylindrical and measured $4\text{--}7 \times 7\text{--}90 \mu\text{m}$. In apical cells, the chloroplast filled the entire cytoplasm. Intercalary cells showed a well-defined parietal chloroplast with one pyrenoid (Fig. 17). *Acrochaete*-type hairs, $60\text{--}150 \mu\text{m}$ in length, were observed in plants that were not transferred regularly to fresh culture medium (Fig. 18). In older cultures, filaments became densely aggregated, displaying a pseudoparenchymatous organization (Fig. 19).



FIGS. 15–22. Unialgal cultures of the isolate selected as typical material. FIG. 15. Unipolar germination. Scale bar = $10 \mu\text{m}$. FIG. 16. Two-week-old germling. Scale bar = $20 \mu\text{m}$. FIG. 17. Vegetative filament with intercalary, cylindrical cells containing a parietal chloroplast and a single pyrenoid (arrows). Scale bar = $20 \mu\text{m}$. FIG. 18. Uniseriate filament with *Acrochaete*-type hairs. Scale bar = $20 \mu\text{m}$. FIG. 19. Free-living, old pseudoparenchymatous individual. Numerous *Acrochaete*-type hairs are present. Scale bar = $20 \mu\text{m}$. FIG. 20. Sporangium mother cells. Scale bar = $20 \mu\text{m}$. FIG. 21. Intercalary flask-shaped sporangium. Scale bar = $20 \mu\text{m}$. FIG. 22. Intercalary L-shaped sporangium. Scale bar = $20 \mu\text{m}$.

Sexual maturity of the isolated endophyte was reached when vegetative cells enlarged and formed lateral protuberances. Formation of sporangia was often massive, and nearly all cells became sexual simultaneously (Fig. 20). Mature sporangia were flask or L shaped (Figs. 21, 22) and contained 8 to 16 cells. Swimmers were ovoid to pyriform and measured $4-8 \times 5-9 \mu\text{m}$ with a cup-shaped chloroplast and a red eyespot. Smaller swimmers measuring $3-4 \times 3.5-5 \mu\text{m}$ and with a pale appearance were also observed. Fusion between the two types of swimmers was not observed.

DISCUSSION

This study demonstrates that the lesions affecting tank-cultivated *Ulva rigida* are caused by a green algal endophyte and represents the first report of a destructive infectious disease involving this algal host. The only other study reporting perforation of *Ulva* thalli concluded that the symptoms were not associated with any pathogen; this disease was not transmitted by cocultivation, leading the author to conclude that perforation disease of *Ulva* sp. was triggered by traumatic events during cultivation (Colorni 1989). In our experiments, the endophytic alga was always found associated with the lesions. It was isolated in unialgal cultures, and it infected the host in cocultivation experiments with infected fronds in the field. The endophytic organism reisolated from cocultivated newly infected thalli was morphologically identical to the original isolate.

The presence of *Acrochaete*-type hairs (Nielsen 1979, 1983), the heterotrichous habit, and the pseudoparenchymatous development of algae in older cultures indicate that the causative agent of *Ulva* degradative disease belongs to the chlorophycean genus *Acrochaete* (South 1968, Nielsen 1979). The reproductive features, characteristically flask- or L-shaped sporangia and 8 to 16 swimmers per sporangia, coincide with the description of this species by O'Kelly (1983) for *A. geniculata*.

Other species of *Acrochaete* have been reported previously to be associated with numerous algal hosts as epi- or endophytic organisms (South 1968, Nielsen 1979, 1983, Nielsen and McLachlan 1986a, b, Correa et al. 1988). However, in only one case has it been recognized as the cause of a degradative lesion to the hosts. *Acrochaete operculata* causes direct cellular damage to *Chondrus crispus* and facilitates secondary bacterial infections (Correa et al. 1988, Correa and McLachlan 1994). Another degradative disease affecting a red algal host has been reported recently as the result of the invasion of *Mazzaella laminarioides* by the green algal endophyte *Endophyton ramosum* (Correa et al. 1994).

A pattern of pathogenesis is evident, considering the similarities of the lesions in *C. crispus* (Correa and McLachlan 1994), *M. laminarioides* (Correa et al. 1994), and *Ulva rigida* (this study): 1) an initial phase, with little macroscopic damage of the host

but involving cellular damage, usually by mechanical means; 2) a rupture of the host surface, a symptom detected microscopically; and 3) a secondary bacterial invasion, concluding with massive host destruction. At this point, the symptoms are clearly visible macroscopically and involve thallus fractures, perforations, and softening.

An ecologically important feature of the association between *Ulva rigida* and *Acrochaete geniculata* is the apparent coincidence of the infection with certain seasons when the host displays a lower growth rate. This may be related to a lower rate of cuticle removal (Correa et al. 1994), a phenomenon that permits a longer period of time for the infecting spores to settle, germinate, and penetrate the outermost layers of the host cell wall. Species of *Ulva* are known to have a multilamellar outer cell wall (McArthur and Moss 1977) that, when the host is growing fast, sheds the outermost layers together with all epiphytic and potentially invasive settled organisms. The red algae *Chondrus crispus* and *Mazzaella laminarioides* also have multilamellar, disposable outer cell walls that are especially well developed at the fast-growing regions of the fronds and that have been suggested to be the main mechanism for epiphyte/endophyte removal (Correa and McLachlan 1994, Correa et al. 1994). In fact, the highest incidence of endophytic infections reported for the two host species occur in older areas of the thalli, characterized by slow growth and the absence of a multilamellar outer cell wall (Correa and McLachlan 1994, Correa et al. 1994).

In vitro infections showed that vegetative filaments grew on the surface of *U. rigida* but never penetrated the host. At present, we do not have an explanation for the failure of the *in vitro* infections. However, different laboratory-associated factors, such as changes in morphology, texture, and toughness of *U. rigida* growing in laboratory culture, have been observed and could be involved.

With the gradual accumulation of information, the importance of infectious diseases in either cultivated or algal natural populations is becoming recognized. Such information consistently indicates the involvement of algal endophytes as both primary pathogens and facilitators of secondary bacterial invasions. The result of these complex interactions is usually loss of the diseased individual from the population, a phenomenon demonstrated in cultivated populations of *Chondrus crispus* in Nova Scotia (Craigie and Correa 1996) and *Ulva rigida* (this study) as well as in wild populations of *Mazzaella laminarioides* (Correa and Sánchez 1996, Buschmann et al. 1997, Correa et al. 1997). Mortality due to pathogens is a poorly understood subject in marine ecosystems, but theoretical implications of such mortality at population and community levels have been reviewed (Correa 1997).

In conclusion, a new disease of an algal host caused by an algal endophyte is reported. Our re-

port supports the pathogenic role of algal endophytes, even in associations when both host and pathogen belong to the same family (O'Kelly 1983). Host-specificity experiments ongoing in our laboratory will, we hope, provide new insights into the mechanisms involved in the invasion of *Ulva rigida* by *A. geniculata*.

Gobierno de Canarias is gratefully acknowledged for financial support to Elena del Campo. We also thank the editor and two anonymous reviewers for their helpful suggestions and comments. This research was supported by EC research contract (CT1*CT92-0072).

- Andrews, J. H. 1977. Observations on the pathology of seaweeds on the Pacific Northwest. *Can. J. Bot.* 55:1019-27.
- Apt, K. E. 1988. Etiology and development of hyperplasia induced by *Streblonema* sp. (Phaeophyta) on members of the Laminariales (Phaeophyta). *J. Phycol.* 24:28-34.
- Buschmann, A., Correa, J. A., Beltrán, J. & Retamales, C. 1997. Determinants of disease expression and survival of infected individual ponds in wild populations of *Mazella laminarioides* (Rhodophyta) in central and southern Chile. *Mar. Ecol. Prog. Ser.* 154:269-80.
- Cohen, I. & Neori, A. 1991. *Ulva lactuca* biofilters for marine fishponds effluents. *Bot. Mar.* 34:475-82.
- Colomi, A. 1989. Perforation disease affecting *Ulva* sp. cultured in Israel on the Red Sea. *Dis. Aquat. Org.* 7:71-3.
- Correa, J. A. 1997. Algal diseases. In Round, F. & Chapman, D. J. [Eds.] *Progress in Phycological Research*, Vol. 12. Biopress, Bristol, United Kingdom, pp. 149-80.
- Correa, J. A., Buschmann, A., Retamales, C. & Beltrán, J. 1997. Infectious diseases of *Mazella laminarioides* (Rhodophyta): changes in infection prevalence and disease expression associated with season, locality and within-site location. *J. Phycol.* 33:344-52.
- Correa, J. A., Flores, V. & Garrido, J. 1994. Green patch disease in *Iridaea laminarioides* (Rhodophyta) caused by *Endophyton* sp. (Chlorophyta). *Dis. Aquat. Org.* 19:203-13.
- Correa, J. A. & McLachlan, J. L. 1991. Endophytic algae of *C. crispus* (Rhodophyta). III. Host specificity. *J. Phycol.* 27:448-59.
- 1992. Endophytic algae of *C. crispus* (Rhodophyta). IV. Detrimental effects on the host following infections by *Acrochaete operculata* and *Acrochaete heteroclada* (Chlorophyta). *Mar. Ecol. Prog. Ser.* 81:73-87.
- 1994. Endophytic algae of *C. crispus* (Rhodophyta). V. Fine structure of the infection by *Acrochaete operculata* (Chlorophyta). *Eur. J. Phycol.* 29:33-47.
- Correa, J. A., Nielsen, R. & Grund, D. W. 1988. Endophytic algae of *Chondrus crispus* Stackhouse II. *Acrochaete heteroclada* sp. nov., *Acrochaete operculata* sp. nov., and *Phaeophila dendroides* (Crouan frat.) Batters (Chlorophyta). *J. Phycol.* 24:528-39.
- Correa, J. A. & Sánchez, P. A. 1996. Ecological aspects of algal infectious diseases. *Hydrobiologia* 326/327:89-95.
- Craige, J. S. & Correa, J. A. 1996. Etiology of infectious diseases in cultivated *Chondrus crispus* (Gigartinales, Rhodophyta). *Hydrobiologia* 326/327:97-104.
- Garbary, D. 1979. A revised species concept for endophytic and endozoic members of the Acrochaetiaceae (Rhodophyta). *Bot. Not.* 132:451-55.
- Goff, L. J. 1983. Marine algal interactions: epibiosis, endobiosis, parasitism and disease. In Tseng, C. K. [Ed.] *Proceedings of the Joint China-U.S. Phycology Symposium*. Science Press, Beijing, pp. 221-74.
- Jimenez del Rio, M., Ramazanov, Z. & Garcia-Reina, G. 1994. Optimization of yield and biofiltering efficiencies of *Ulva rigida* C. Ag. cultivated with *Spargus aurata* L. waste waters. *Sci. Mar.* 58:329-35.
- 1996. *Ulva rigida* (Ulvales, Chlorophyta) tank culture as biofilters for dissolved inorganic nitrogen from fishpond effluents. *Hydrobiologia* 326/327:61-6.
- McArthur, D. M. & Moss, B. L. 1977. The ultrastructure of cell walls in *Enteromorpha intestinalis* (L.) Link. *Br. Phycol. J.* 12: 359-68.
- Neori, A., Cohen, I. & Gordin, H. 1991. *Ulva lactuca* biofilters for marine fishpond effluents. II. Growth rate, yield and C:N ratio. *Bot. Mar.* 34:483-9.
- Neori, A., Krom, M. D., Cohen, I. & Gordin, H. 1989. Water quality conditions and particulate chlorophyll *a* of new intensive seawater fishponds in Eliat, Israel: Daily and die variations. *Aquaculture* 80:63-78.
- Nielsen, R. 1979. Culture studies on the type species of *Acrochaete*, *Bolbocoleon* and *Entocladia* (Chaetophoraceae, Chlorophyceae). *Bot. Not.* 132:441-9.
- 1983. Culture studies of *Acrochaete leptochaete* comb. nov. and *A. wittrockii* comb. nov. (Chaetophoraceae, Chlorophyceae). *Nord. J. Bot.* 3:689-94.
- Nielsen, R. & McLachlan, J. 1986a. Investigations of the marine algae of Nova Scotia. XVI. The occurrence of small green algae. *Can. J. Bot.* 64:808-14.
- 1986b. *Acrochaete marchantiae* comb. nov. and *Trichothyrira irregularis* gen. et sp. nov. with notes on other species of small filamentous green algae from St. Lucia (West Indies). *Nord. J. Bot.* 6:515-24.
- O'Kelly, C. J. 1982. Observations in marine Chaetophoraceae (Chlorophyta). III. The structure, reproduction and life history of *Endophyton vamosum*. *Phycologia* 21:247-57.
- 1983. Observations in marine Chaetophoraceae (Chlorophyta). IV. The structure, reproduction and life history of *Acrochaete geniculata*. *Phycologia* 22:13-21.
- O'Kelly, C. J. & Yarish, C. 1981. Observations on marine Chaetophoraceae (Chlorophyta). II. On the circumscription of the genus *Entocladia* Reinke. *Phycologia* 20:32-45.
- Peters, A. K. 1991. Field and culture studies of *Streblonema macrocystis* sp. nov. (Ectocarpales, Phaeophyceae) from Chile, a sexual endophyte of giant kelp. *J. Phycol.* 30:365-77.
- South, G. R. 1968. Aspects of the development and reproduction of *Acrochaete repens* and *Bolbocoleon piliferum*. *Can. J. Bot.* 46: 101-13.
- Yoshida, T. & Akiyama, K. 1979. *Streblonema* (Phaeophyceae) infection in the frond of cultivated *Undaria* (Phaeophyceae). *Proc. Int. Seaweed Symp.* 9:219-23.

***Floriceps saccatus* Plerocerci (Trypanorhyncha, Lacistorhynchidae) as Parasites of Dolphin Fish (*Coryphaena hippurus* L.) and Pompano Dolphin (*Coryphaena equiselis* L.) in Western Mediterranean and Eastern Atlantic Waters. Ecological and Biological Aspects**

E. Carbonell, J. J. Castro*, and E. Massutí†. Facultad de Biología, C/ Dr. Moliner, 50, 46100 Burjassot, Valencia, Spain; *Departamento de Biología, Universidad de Las Palmas de Gran Canaria, Apto. 550, Las Palmas de Gran Canaria, Spain; and †IEO-Centre Oceanográfico de les Balears, Moll de Ponent s/n, Apto. 291, 07080 Palma de Mallorca, Spain

ABSTRACT: A study of the plerocerci of *Floriceps saccatus* from the abdominal cavity of dolphin fish (*Coryphaena hippurus*) and pompano dolphin (*Coryphaena equiselis*) was conducted. In all, 565 dolphin fish-

es were collected from Majorcan waters (Balearic Islands, western Mediterranean) during 3 summer and autumn seasons (1990, 1991, and 1995). From the Canary Islands (eastern Atlantic), 41 specimens of



TABLE 1. Infection parameters of *Floriceps saccatus* cysts in the 3 size groups of *Coryphaena hippurus* and *Coryphaena equiselis*.

Size group (fork length)	Eastern Mediterranean			Western Atlantic	
	<i>C. hippurus</i>			<i>C. hippurus</i>	<i>C. equiselis</i>
	1990	1991	1995	1994	1995
<30 cm					
n	62	31	12	0	0
Prevalence	0	0	0	—	—
Mean intensity	—	—	—	—	—
Abundance	—	—	—	—	—
Range	—	—	—	—	—
30–60					
n	89	83	222	11	49
Prevalence	6.76	3.60	0	0	0
Mean intensity	1.66 ± 0.8	1.33 ± 0.57	—	—	—
Abundance	0.11 ± 0.46	0.05 ± 0.26	—	—	—
Range	1–3	1–2	—	—	—
>60 cm					
n	20	21	25	30	0
Prevalence	60	28.57	28	30	—
Mean intensity	3 ± 1.53	1.5 ± 0.54	2.85 ± 1.34	1.66 ± 0.5	—
Abundance	1.8 ± 1.9	0.42 ± 0.74	0.8 ± 1.47	0.5 ± 0.82	—
Range	1–5	1–2	1–5	1–2	—

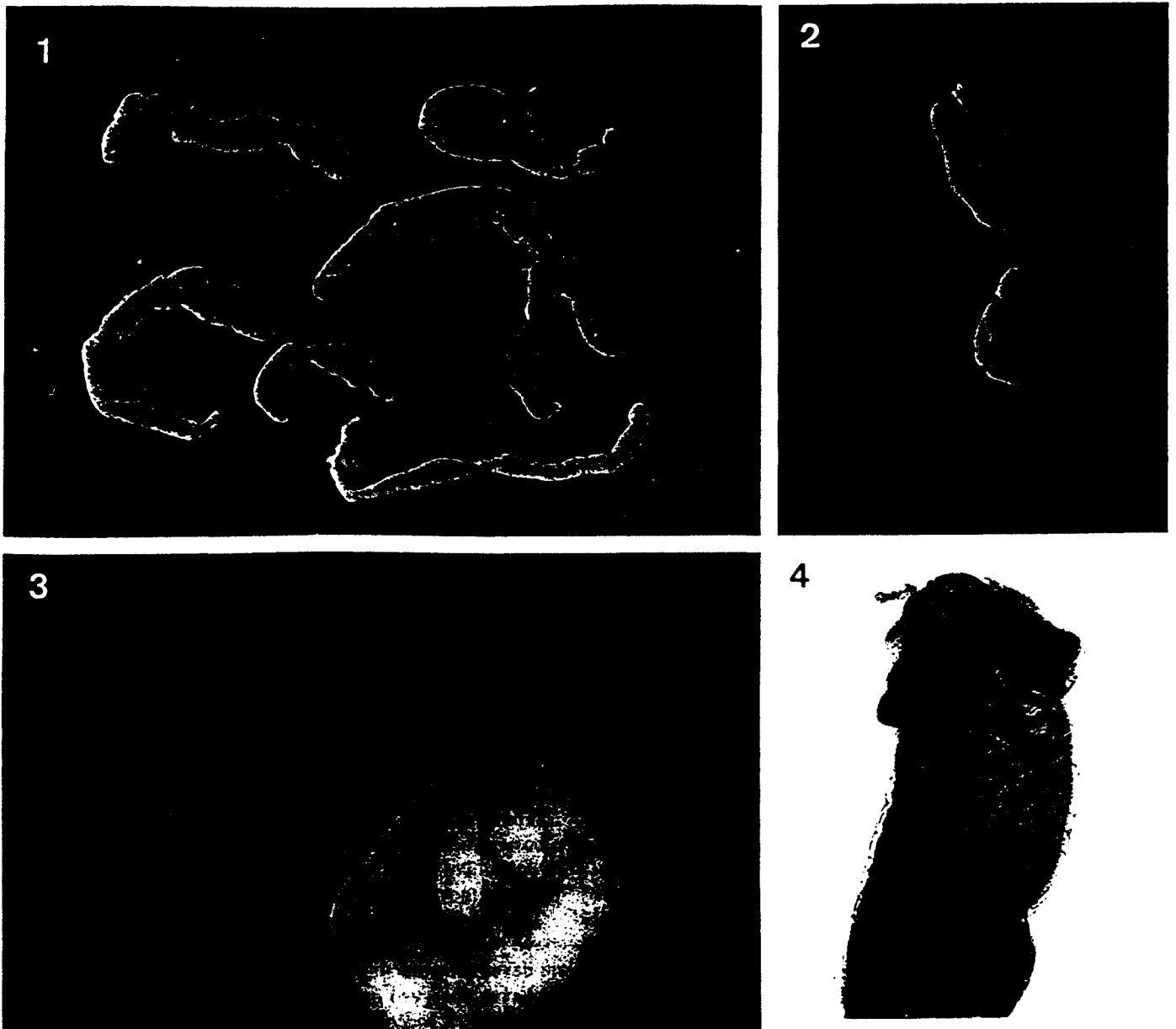
dolphin fish were caught during 1994 and 49 specimens of pompano dolphin during 1995. Cysts of different shapes and sizes appeared in the conjunctive tissues of the abdomen and viscera, mainly in the liver, gonads, and pancreas. A larva was found inside every cyst examined. Small, medium size, and large larvae were found. The largest larvae correspond to *Floriceps saccatus* plerocercoids. Stomach contents indicated that crustaceans and fish larvae were the main prey items of juvenile *C. hippurus*, whereas teleosts and cephalopods were the only food found in adult dolphin fishes. Infection of *F. saccatus* plerocercoids takes place in preadult dolphin fishes. Prevalence increases as fishes grow and change to a diet of teleosts. *Coryphaena equiselis* was not infected.

Floriceps saccatus Cuvier, 1817 is a trypanorhynch cestode of sharks whose plerocercoids have been reported in the abdominal cavity of teleost fishes, such as *Mola mola* (Linnaeus, 1758), *Xiphias gladius* (Linnaeus, 1758), and *Zeus faber* (Linnaeus, 1758), whereas adult cestodes are parasites of elasmobranchs (*Isurus oxyrinchus* Rafinesque, 1810, *Carcharodon carcharias* Linnaeus, 1758, and *Oxynotus centrina* Linnaeus, 1758) (Joyeux and Baer, 1936). The only reference for the plerocercoids of *F. saccatus* in Coryphaenidae is from fishes caught in French Atlantic waters (Dollfus, 1946). Little is known about the larval stages of trypanorhynch life cycles. It seems that proceroids develop in planktonic copepods, whereas plerocercoids do so in teleost fishes (Mudry and Dailey, 1971; Sakanari and Moser, 1985, 1989). A 4-host cycle has been described for *Callitetrarhynchus nipponica* Nakajima and Egusa, 1973, which is a species very closely related to *F. saccatus*. In this cycle, the proceroids require 2 hosts, e. g., planktonic copepods and clupeid fishes, for maturation, whereas the plerocercoids develop in the body cavity of the yellow-tail (*Seriola quinqueradiata* Temminck and Schlegel), and the definitive host is the shark (*Triakis scyllium* Müller and Henle, 1839) (Nakajima and Egusa, 1992).

The dolphin fish (*Coryphaena hippurus* Linnaeus, 1758) and

the pompano dolphin (*Coryphaena equiselis* Linnaeus, 1758) (Pisces: Coryphaenidae) are both epipelagic species distributed throughout tropical and subtropical waters of the world (Palko et al., 1982). *Coryphaena hippurus* makes an annual reproductive migration from the eastern Atlantic to the Mediterranean Sea that is thought to be triggered by seasonal changes in surface water temperature. Adult and mature dolphins first arrive in the Mediterranean in May–June, when water temperatures are higher than 16–18 C. Then, juvenile fishes are found in the Mediterranean Sea from August to early December. When temperatures fall below 16 C, both adult and juvenile fishes migrate to warmer waters in the Atlantic Ocean (Massutí and Morales-Nin, 1995). *Coryphaena equiselis* is rarely captured in Mediterranean waters. Although their presence has occasionally been reported in this area, it is not known if pompano dolphins reproduce in this sea (Shcherbachev, 1973). In the warm waters of the Atlantic Ocean, both species apparently spawn all year round, whereas in the Mediterranean Sea, it seems that only *C. hippurus* reproduces every summer. This behavior allowed us to study 2 well-differentiated populations or stocks of dolphin fish, e.g., adults from the Atlantic Ocean and juveniles born in the Mediterranean Sea.

Coryphaena hippurus is a top-level predator that shows low prey selectivity, feeding on a wide range of pelagic organisms. In the Mediterranean Sea, Massutí et al. (1998) indicated 2 feeding size classes: a juvenile class (14–55 cm fork length) in the Mediterranean Sea whose main prey items included crustacean larvae, fishes, and amphipods and an adult class (55–117 cm fork length) whose main food items included teleost fishes and cephalopods. Decapod larvae and amphipods represented more than 50% of the prey in the <30-cm length class, whereas stomatopod larvae were present in fishes up to 55–60 cm in fork length.



FIGURES 1–4. 1. Different forms of cysts (real size) taken from the abdominal cavities of *Coryphaena hippurus* and *Coryphaena equiselis*. 2. Enlarged scolex without bothridia (above) and hoodlike scolex (below) of *Floriceps saccatus* larvae ($\times 10$). 3. A *Floriceps saccatus* larva with two leaflike bothridia ($\times 15$). 4. Anterior region of a *Floriceps saccatus* larva resembling 4 bothridia and showing tentacles and pars vaginalis ($\times 25$).

The objectives of this study were to determine when parasite recruitment occurred in both species and areas, the morphology and structure of cysts and larvae, and the relationships between both fish species and the parasite in order to establish the possible life cycle of *F. saccatus*.

Samples came from the commercial landings of 2 fisheries in Majorcan waters (Balearic Islands, western Mediterranean) and in the Canary Islands (eastern Atlantic). In all, 565 specimens of *C. hippurus* were collected from Mediterranean waters during 3 summer and autumn seasons (1990, 1991, and 1995). From Atlantic waters, 41 specimens of *C. hippurus* during 1994 and 49 specimens of *C. equiselis* during 1995 were caught throughout the summer and autumn seasons. Juvenile fishes

were obtained from the small-scale fleet landings with nets around aggregation devices, whereas adult specimens were caught with drifting surface long-lines (Massutí and Morales-Nin, 1995).

In the laboratory, the fishes were sexed, weighed, and measured to the nearest centimeter fork length; gonadal development was also noted. The abdominal cavity and viscera were examined and the location of the cysts was noted prior to their removal. Wet mounts were prepared to verify cyst morphology and consistency, and they were subsequently preserved in 10% buffered formalin. Each cyst was opened in order to examine its contents. Gut contents were also removed and examined. Prey items found were identified and classified to the order level

TABLE II. Index of numerical importance (NII) for the main crustacean and teleost prey of *Coryphaena hippurus* in the Mediterranean Sea.

Prey	NII*
Crustaceans	
Amphipods	10.02
Isopods	1.52
Decapod larvae	19.23
Stomatopod larvae	6.05
Total crustaceans	44.79
Cephalopods	8.96
Teleosts	
Fish larvae	22.00
Clupeids	18.67
Exocoetids	5.86
Scombrids	10.06
Carangids	4.41
Sparids	3.51
Gadids	3.15
Unidentified fishes	7.91
Total teleosts	65.89

* $NII = \sqrt{N} \times F$. N (numerical composition): number of specimens of the same prey \times 100/total number of prey items. F (frequency of occurrence): number of stomachs with a prey \times 100/total number of stomachs containing food.

for crustaceans and to the family level for fishes. The numerical importance index was determined.

To investigate differences in parasitism as a function of size, the fishes examined were assigned to 1 of 3 classes in order to obtain a sufficient number of specimens per length class. The parasite infestation level by size class was analyzed according to standard methods (Margolis et al., 1982) in order to establish the prevalence, mean intensity, mean abundance, and range of the parasite.

The 565 specimens of *C. hippurus* from the Mediterranean Sea ranged in size between 14 and 117 cm. From the Atlantic Ocean, the 41 specimens of *C. hippurus* ranged in size from 42 to 124 cm and the 49 specimens of *C. equiselis* from 30 to 50 cm. Juvenile fishes were between 14 and 50 cm in length, and mature individuals were between 50 and 124 cm. Only dolphin fishes larger than 50 cm were parasitized. Intensity, abundance, and particularly prevalence were higher in the mature fishes, increasing as the fishes became older. The same pattern was observed in *C. hippurus* from the Mediterranean Sea and from the Atlantic Ocean. Pompano dolphin were not infected. The infection parameters of cysts by class intervals are given in Table I.

Ninety-one cysts were collected from the abdominal cavity and viscera. Cyst size was variable and ranged between 20 and 50 mm. The shape of the cysts also showed a great variety of forms (Fig. 1), but cysts always had a terminal globular region, where the larva was accommodated, and a tail-like structure. All cysts contained a plerocercoid. The smallest larvae measured 4–7 mm in length and showed an enlarged scolex with a terminal tail (Fig. 1, above) or a hoodlike head with 2 rounded extensions and a terminal tail (Fig. 2, below). The medium-sized larvae measured 10–12 mm and had tentacles and 2 leaflike bothridia that were not indented and were without cordiform margins (Fig. 3). The largest larvae were 15–25 mm in length and had 2 deeply indented bothridia, which superficially resembled 4 bothridia (Fig. 4). The morphology and measurements of these larvae

agree with the description of Dollfus (1946) for the trypanorhynch *F. saccatus*. There was no apparent relationship between the size of the cyst and the size of the larva.

Most cysts were attached to the parietal peritoneum and mesenteries (80%), with 10% fixed to the gonadal parenchyma, 7% to the hepatic serosa, and 3% to the pancreatic serosa. Cysts fixed to the peritoneal serosa did not cause any lesions. Apparently, the peritoneal connective tissue covers the larva, producing the cyst. However, in the hepatic and gonadal tissues as well as in the pancreas, the cysts produced some local damage, which was represented by a necrotic area probably as a result of local ischemia.

The stomach contents indicated a wide variety of prey. Crustaceans (copepods, amphipods, stomatopod larvae, and decapod larvae) were the main prey items (60%) found in small *C. hippurus* (<30 cm fork length), whereas fish larvae completed the diet. From 30 to 60 cm fork length, crustaceans disappeared progressively, with teleosts and cephalopods making up the total food content (83% and 17%, respectively). The highest Index of Numerical Importance of the teleosts belonged to clupeids and scombrids (Table II). In the case of *C. equiselis*, the stomach contents were somewhat different because crustaceans and exocoetids were the main prey items, whereas clupeids were not present and the only representative of vertical migratory fishes was *Scomber japonicus* (L., 1758).

Flriceps saccatus plerocerci have been recorded in teleosts, whereas the adult cestodes are gut parasites of several elasmobranchs from the Atlantic and Pacific Oceans (Campbell and Beveridge, 1994). In the Mediterranean Sea, larvae of *F. saccatus* have been found mainly in the peritoneum and on the liver surfaces of *M. mola* (Schmidt, 1986). Guiart (1935) reported that the plerocercoid of *F. saccatus* is a small larva contained in peritoneal cysts of *M. mola* and is morphologically different from the larva found in the liver of this fish and other teleosts. The only reference to these larvae in *C. hippurus* was given by Dollfus (1946), who examined 4 plerocercoids from 4 cysts removed from walls of the visceral cavity.

The available evidence suggests that all the larvae described above belong to the same species, possibly representing different developmental stages of *F. saccatus*. Alternatively, some of the larvae observed in this report may belong to cestode species other than *F. saccatus*. However, Nakajima and Egusa (1992) experimentally showed that *C. nipponica* requires a copepod and a teleost fish for proceroid maturation and other teleosts (*S. quinqueradiata*) for plerocercoid development.

Infection by *F. saccatus* plerocerci takes place when *C. hippurus* are 50 cm in length or larger, and the prevalence increases as dolphins grow and change to a diet of fishes and cephalopods. Juveniles, on the other hand, prey mainly on crustaceans and were not infected. The simplest explanation for our observations is that the parasite recruitment takes place when *C. hippurus* feeds on plankton feeder fishes, mainly clupeids, that are infected with cestode larvae. Therefore, the late infection of dolphins suggests a 4-host cycle with crustaceans and plankton feeder fishes for proceroids, dolphins for plerocercoids, and sharks for adult cestodes. The observation that clupeid fishes are an important prey of dolphin adds further support to this hypothesis. One of the most important prey items of adult dolphin is *Sardinella aurita* Valenciennes, 1847, which, together with other clupeids, is the main representative of plankton feeders and vertical migratory fishes in the Mediterranean Sea. Sev-

eral sharks such as the shortfin mako (*I. oxyrinchus*), the porbeagle (*Lamna nasus* Bonaterre, 1788), and the blue shark (*Prionace glauca* Linnaeus, 1758), which are 3 elasmobranchs widely distributed in the Mediterranean area (Bauchot, 1987), could represent the final hosts where plerocercoids reach the adult stage. The presence of *F. saccatus* plerocercoids in Mediterranean as well as in Atlantic stocks of *C. hippurus* indicates that parasite recruitment in both areas is possible. The absence of parasitism in *C. equiselis* may be due to the small size of the specimens in the sample, which included individuals in the range 30–52 cm fork length. Alternatively, the diet composition of pompano dolphin may explain the lack of parasites in this species.

We thank B. Morales-Nin (CSIC-Institut Mediterrani d'Estudis Avancats) and the Centre Oceanogràfic de Balears for the facilities provided. Special thanks to Ian Beveridge (School of Veterinary Science, Australia), who determined the cestode species *F. saccatus* and revised this paper. Chris Rodgers revised the English version of the manuscript.

LITERATURE CITED

- BAUCHOT, M. L. 1987. Requins. In Fiches FAO d'identification des espèces pour les besoins de la pêche. Méditerranée et mer Noire. Zone de Pêche 37, Vol. II. Vertébrés. W. Fischer, M. L. Bauchot, and M. Schneider, (eds.). FAO, Roma, Italy, p. 767–885.
- CAMPBELL, R. A., AND I. BEVERIDGE. 1994. Order Trypanorhyncha Diesing, 1863. In Keys to the cestode parasites of vertebrates, L. F. Khalil, A. Jones, and R. A. Bray (eds.). CAB International, Wallingford, U.K., p. 51–148.
- DOLLFUS, R. PH. 1946. Notes diverses sur les tetrarhynques. Mémoires du Muséum d'Histoire Naturelle (Paris) France 22: 179–219.
- GUIART, J. 1935. Le véritable *Floriceps saccatus* Cuvier n'est pas la larve géant de Tetrarhynque vivant dans le foie du môle (*Mola mola*). Bulletin Institut Oceanographique de Monaco 666: 1–15.
- JOYEUX, CH., AND S. G. BAER. 1936. Faune de France. Cestodes. Lechevalier et Fils, Paris, France, 613 p.
- MARGOLIS, L., G. W. ESCH, J. C. HOLMES, A. M. KURIS, AND G. A. SCHAD. 1982. The use of ecological terms in parasitology (report of an ad hoc committee of the American Society of Parasitologists). Journal of Parasitology 68: 131–133.
- MASSUTI, E., S. DEUDERO, P. SÁNCHEZ, AND B. MORALES-NIN. 1998. Diet and feeding of dolphin (*Coryphaena hippurus* L.) in western Mediterranean waters. Bulletin of Marine Science 62: (in press).
- , AND B. MORALES-NIN. 1995. Seasonality and reproduction of dolphin fish (*Coryphaena hippurus*) in the western Mediterranean. Scientia Marina 59: 357–364.
- MUDRY, D. R., AND M. D. DAILEY. 1971. Postembryonic development of certain tetraphyllidean and trypanorhynchan cestodes with a possible alternative life-cycle for the order Trypanorhyncha. In Parasitic worms of fish, H. Williams and A. Jones (eds.). Taylor and Francis, London, U.K., p. 73–85.
- NAKAJIMA, K., AND S. EGUSA. 1992. Tapeworm Infection. In Infectious diseases of fish, S. Egusa (ed.). A. A. Balkema Publishers, Rotterdam, The Netherlands, p. 630–642.
- PALKO, B. J., G. L. BEARDSLEY, AND W. J. RICHARDS. 1982. Synopsis of the biological data of dolphin fishes, *Coryphaena hippurus* Linnaeus and *Coryphaena equiselis* Linnaeus. FAO Fisheries Synopsis 130: 1–28.
- SAKANARI, J., AND M. MOSER. 1985. Infectivity of, and laboratory infection with, an elasmobranch cestode, *Lacistorhynchus tenuis* (Van Beneden, 1858). Journal of Parasitology 71: 788–791.
- , AND ———. 1989. Complete life-cycle of the elasmobranch cestode *Lacistorhynchus dollfusi* Beveridge and Sakanari, 1987 (Trypanorhyncha). Journal of Parasitology 71: 806–808.
- SCHMIDT, G. D. 1986. Handbook of tapeworm identification. CRC Press, Boca Raton, Florida, 675 p.
- SHCHERBACHEV, N. YU. 1973. The biology and distribution of dolphins (Pisces: Coryphaenidae). Journal of Ichthyology 13: 182–191.

Hotspot volcanism close to a passive continental margin: the Canary Islands

J. C. CARRACEDO*†, S. DAY†, H. GUILLOU‡, E. RODRÍGUEZ BADIOLA§,
J. A. CANAS¶ & F. J. PÉREZ TORRADO#

* Estación Volcanológica de Canarias, IPNA, CSIC, La Laguna, Tenerife, Canary Islands, Spain

† Benfield Greig Centre for Hazard Research, University College London, UK

‡ Centre des Faibles Radioactivités, CEA-CNRS, Gif sur Yvette, France

§ Museo Nacional de Ciencias Naturales, CSIC, Madrid, Spain

¶ ETSICC, Universidad Politécnica de Cataluña, Spain

Facultad de Ciencias del Mar, ULPGC, Las Palmas, Gran Canaria, Canary Islands, Spain

(Received 8 January 1998; accepted 27 April 1998)

Abstract – The Canarian Archipelago is a group of volcanic islands on a slow-moving oceanic plate, close to a continental margin. The origins of the archipelago are controversial: a hotspot or mantle plume, a zone of lithospheric deformation, a region of compressional block-faulting or a rupture propagating westwards from the active Atlas Mountains fold belt have been proposed by different authors. However, comparison of the Canarian Archipelago with the prototypical hotspot-related island group, the Hawaiian Archipelago, reveals that the differences between the two are not as great as had previously been supposed on the basis of older data. Quaternary igneous activity in the Canaries is concentrated at the western end of the archipelago, close to the present-day location of the inferred hotspot. This is the same relationship as seen in the Hawaiian and Cape Verde islands. The latter archipelago, associated with a well-defined but slow-moving mantle plume, shows anomalies in a plot of island age against distance which are comparable to those seen in the Canary Islands: these anomalies cannot therefore be used to argue against a hotspot origin for the Canaries. Individual islands in both archipelagoes are characterized by initial rapid growth (the ‘shield-building’ stages of activity), followed by a period of quiescence and deep erosion (erosion gap) which in turn is followed by a ‘post-erosional’ stage of activity. The absence of post-shield stage subsidence in the Canaries is in marked contrast with the major subsidence experienced by the Hawaiian Islands, but is comparable with the lack of subsidence evident in other island groups at slow-moving hotspots, such as the Cape Verdes. Comparison of the structure and structural evolution of the Canary Islands with other oceanic islands such as Hawaii and Réunion reveals many similarities. These include the development of triple (‘Mercedes Star’) rift zones and the occurrence of giant lateral collapses on the flanks of these rift zones. The apparent absence of these features in the post-erosional islands may in part be a result of their greater age and deeper erosion, which has removed much of the evidence for their early volcanic architecture. We conclude that the many similarities between the Canary Islands and island groups whose hotspot origins are undisputed show that the Canaries have been produced in the same way.

1. Previous interpretations of the Canary Islands

The Canarian Archipelago is, apart perhaps from the Hawaiian Islands, the most extensively studied group of oceanic islands in the world. However, although these issues have been the subject of a long debate, the origin and evolution of the Canarian Archipelago are far from being as well explained and modelled as those of the Hawaiian Islands. Several circumstances may account for the difficulty in defining a model for the genesis and evolution of the Canary Islands. The complexities of the geology of the Canaries, in the east of the archipelago in particular, are such that it may not be possible to reach a conclusive solution in favour of one of the various possible alternatives on the basis of the limited data available.

Definitive evidence for the relative roles of regional tectonics and mantle plumes in the genesis of the islands may come from large-scale seismological and structural studies of the deep structure of the surrounding oceanic crust and lithosphere and from constraints provided by geochemical and isotopic features of the magmas involved. Nevertheless, it may be interesting to analyse, as we do in this work, the existing geological information from the islands themselves, especially the timing of eruptive activity in the islands and their morphological and structural features. This may help to establish some clear constraints that narrow down the range of acceptable models for the genesis and development of the Canary Islands.

Comparison of the geology and evolution of these islands with more typical hotspot-induced groups like the Hawaiian, Cape Verde and Réunion islands provides insights into factors controlling the geology of

* Author for correspondence: jcarracedo@ipna.csic.es

oceanic islands and helps in the understanding of the processes involved in the genesis and development of the Canarian Archipelago. In this paper we will compare the Canary Islands with the Hawaiian Islands in particular, because of the wealth of data available for the latter group and because they have come to be regarded as paradigmatic hotspot-related islands. The Hawaiian Islands are located in the middle of an oceanic plate (the Pacific plate) which is moving rapidly with respect to the underlying mantle hotspot. Many aspects of the geology and geological history of the Hawaiian Islands are related to these features and their highly productive hotspot, which are by no means applicable to all oceanic island groups. In the future it may be more appropriate to compare the geology of the Canary Islands with those of other island groups on a slow-moving plate, such as the Cape Verde islands: unfortunately the geology and geochronology of these islands are relatively little-known at present.

The Canary Islands are located in a very different geodynamic setting from that of the Hawaiian Islands: in the case of the Canary Islands, on old (Jurassic) oceanic lithosphere, close to a continental margin, and on a tectonic plate which is moving very slowly in relation to an underlying mantle hotspot. The absolute motion of the African plate over fixed hotspots has been estimated (O'Connor & Duncan, 1990) for the Walvis Ridge at about 7° in latitude and 34° in longitude for the last 60 Ma. In the region of the Canaries these values may be as low as 2.4° and 5°, respectively, for the same period. The active life of most oceanic volcanoes is generally limited by the displacement of the corresponding plate to a few million years. In contrast, the Canary Islands, the Cape Verde Islands (Mitchell *et al.* 1983) and the oceanic sector of the Cameroon line (Lee *et al.* 1994), all of which lie on the slow-moving African plate, are rare examples of long-lived oceanic volcanic islands.

The Cape Verde islands, located 500 km off the west African continental margin, exhibit all the characteristic geophysical features of a mantle plume-induced volcanic archipelago, including a prominent lithospheric swell estimated at between 400 km (Grunau *et al.* 1975) and 1500 km (Courtney & White, 1986) across and as much as 1500 m high at its centre (Courtney & White, 1986). In contrast, the eastern Canary Islands are as little as 100 km from the edge of the African continental shelf and the archipelago as a whole is not associated with a comparable lithospheric swell. This apparent lack of a swell was used by Filmer & McNutt (1988) as an argument against the presence of a hotspot in the Canaries and has also been noted by other authors (Hoernle & Schmincke, 1993; Watts, 1994). However, Canales & Dañobeitia (1998) analysed a number of seismic lines in the vicinity of the archipelago and demonstrated the existence of a subdued (*c.* 500 m maximum elevation) lithospheric

depth anomaly around the Canary Islands. These authors proposed that this anomaly could be related to a swell that was otherwise obscured by the weight (and perhaps also mechanical effects (Watts & Marr, 1995)) of the thick sedimentary cover along the north-west African continental margin and by the weight of the volcanic rocks of the islands themselves.

Morgan (1971) and McDougall (1971) simultaneously presented the hotspot and membrane tectonics ideas to explain the origin of oceanic volcanic island chains. Accordingly, the models proposed for the origin of the Canary Islands were immediately polarized into these two apparently self-excluding categories. However, the early models proposed have two important limitations: (1) they were too dependent on limited radiometric data, later substantially revised, and (2) these models were based upon information from the eastern and central islands (see Fig. 1a). The western islands of La Palma and El Hierro, which we considered to be crucial to the understanding of the archipelago, were very poorly known at that time.

Geological (structural and geochronological) work carried out in the western Canaries has revealed the presence of development patterns and structural features which are in apparent contrast to those of the eastern islands. We examine these studies in a subsequent section and show that these apparently contrasting features, previously interpreted as reflecting variations in the nature and rigidity of the lithosphere (Carracedo, 1996a), may be related to the different stages of evolution of the Canaries.

2. Age of the Canary Islands volcanism

The extensive K/Ar dating carried out in the Canaries, with about 450 K/Ar ages published from lava flows, gives a remarkable control of the subaerial volcanic history of this archipelago. The age of the earliest exposed volcanic rocks as well as the periods of volcanic activity and alternating gaps are clearly delineated (Fig. 1a).

Detailed geochronological work using accurate dating techniques and cross-checking against palaeomagnetic reversals has proved that some of the previous age determinations in these islands have substantial errors, sometimes of several million years (McDougall & Schmincke, 1976). Such errors are especially significant in the islands of La Palma and El Hierro, where most of the subaerial lavas are of Quaternary age (Guillou *et al.* 1996). Recent studies have shown that ages from stratigraphic sequences, consistent with the general volcanic stratigraphy and the corresponding polarities of the standard geomagnetic polarity time-scale, are the most reliable (Carracedo, 1979; Guillou *et al.* 1996).

Figure 1a shows a plot of published radiometric ages from lavas of the Canary Islands. Two groups are clearly defined: (1) the islands of Lanzarote,

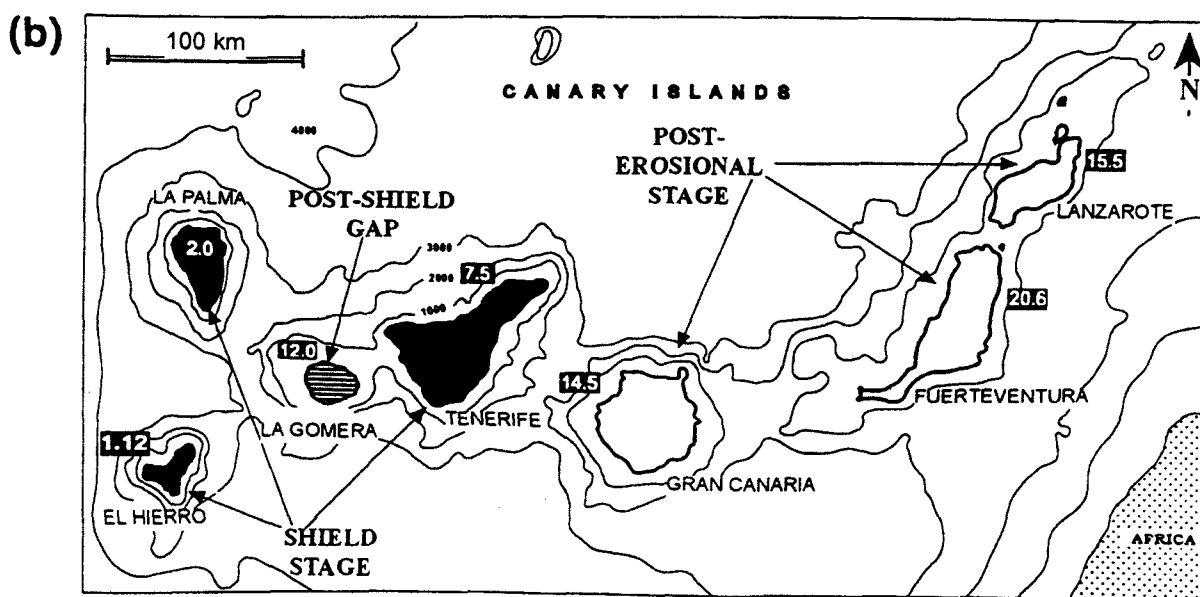
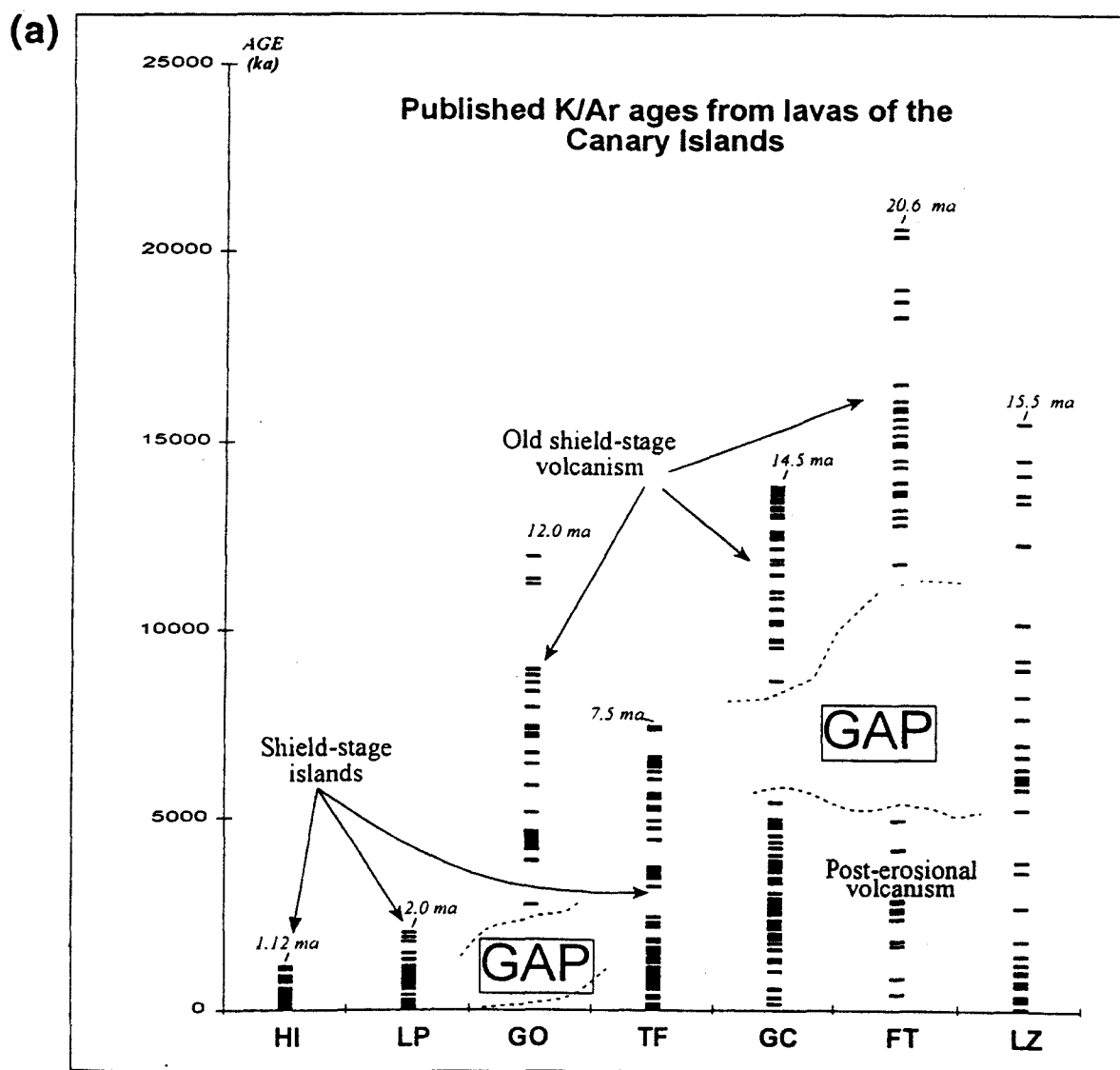


Figure 1. (a) Published K–Ar ages from volcanic rocks of the Canary Islands. (b) Oldest published K–Ar ages of the subaerial volcanism of the Canary Islands. As observed in the Hawaiian Islands, the Canaries can be separated into three groups: islands in the shield-stage of development, in the gap stage and in the post-erosional stage.

Fuerteventura, Gran Canaria and La Gomera, with subaerial volcanism 12 Ma or older and well-defined hiatuses in the volcanic activity, and (2) the islands of Tenerife, La Palma and El Hierro, with exposed volcanic rocks 7.5 Ma old or younger and essentially uninterrupted volcanic histories.

The oldest subaerial volcanic rocks of Tenerife consistently yield ages under 7.5 Ma (Ancochea *et al.* 1990; Carracedo, 1979; Abdel-Monem, Watkins & Gast, 1971; Feraud *et al.* 1985). This age can therefore be estimated, with all probability, as the oldest limit for the emergence of the island of Tenerife.

2.a. Gaps in volcanic activity

Detailed radiometric dating of previously defined magneto-stratigraphic units in the Canaries (Watkins, 1974; Carracedo, 1979; Carracedo & Soler, 1995; Guillou *et al.* 1996; Carracedo *et al.* 1997a) have shown the presence of gaps or hiatuses in the eruptive activity in several of the Canaries that can be excluded as related to sampling. It appears that these eruptive gaps occur only in the early (Middle–Lower Miocene)-emerged islands of Lanzarote, Fuerteventura, Gran Canaria and La Gomera (Fig. 1a). In contrast, volcanic activity has continued uninterrupted from the time of subaerial emergence to the present day in the late (uppermost Miocene–Quaternary)-emerged islands of Tenerife, La Palma and El Hierro.

Similar interruptions are observed in the prototypical hotspot islands of the Hawaiian Archipelago, where they constitute a key stratigraphic feature separating the shield-stage volcanism from the post-erosional or rejuvenated-stage volcanism (Langenheim & Clague, 1987; Walker, 1990). We may conclude that, as in the Hawaiian Islands, the periods of volcanic quiescence allow the separation of the Canaries into different categories (Fig. 1b): (a) the islands of Lanzarote, Fuerteventura and Gran Canaria, at present with post-erosional rejuvenated-stage volcanism; (b) the island of La Gomera, presently in the gap stage, and (c) the islands of Tenerife, El Hierro and La Palma, in the pre-gap shield stage. Tenerife is probably approaching the period of volcanic quiescence, while La Palma and El Hierro are in the most active phase of shield-stage volcanism.

Much of the previous mapping of the Canary Islands has involved the definition of numbered Volcanic Series. In the older islands (Fuerteventura, Lanzarote, Gran Canaria), 'Series I' corresponds to the shield-building stage subaerial volcanic rocks (Füster *et al.* 1968; Füster, Fernández Santín & Sagredo, 1968). These are followed after a long erosional interval by relatively small-volume 'Series II', and in some cases 'Series III' and 'Series IV', which correspond to our 'post-erosional volcanism'. In contrast, in the younger islands such as El Hierro (Füster *et al.* 1993), the same authors define as many as four

'Series' which are not separated by long erosional intervals and which all lie within the early phases of the 'shield-building' stage (Guillou *et al.* 1996). Thus, the use of 'Series' as a stratigraphic unit is inconsistent between islands and likely to lead to confusion. We therefore propose discarding numerically based 'Series' and use instead the 'shield-building' and 'post-erosional' stratigraphic distinction developed in the Hawaiian Islands (see MacDonald & Abbott, 1970, for a review of stratigraphic units and concepts in the Hawaiian Islands). We also propose discarding the generally used distinction between 'eastern' and 'western' groups in the Canarian Archipelago in favour of an age-based criterion, to recognize the location of the older island of La Gomera in the middle of the younger ('western') Canaries group.

2.b. Pre-shield stage rocks

The subaerial shield-stage volcanic rocks are the oldest rocks exposed above sea level in the Hawaiian Islands. It has, however, long been recognized that these must be preceded by a 'seamount stage' of submarine volcanism, represented in the present by Loihi Seamount to the southeast of Hawaii (Fornari *et al.* 1988). In the Canarian islands of Fuerteventura, La Gomera and La Palma the shield volcanism rests upon variably deformed and uplifted sequences of submarine sediments, volcanic rocks (mainly pillow basalts), dyke swarms and plutonic intrusions which form the cores of these islands. These have been interpreted as uplifted blocks of 'oceanic basement' in the pre-Plate Tectonic sense (Hausen, 1958; Füster *et al.* 1968). However, this interpretation is inconsistent with the observation that the igneous rocks are younger than the oceanic sedimentary sequences (Robertson & Stillman, 1979). The hypothesis was then modified to suggest that the 'basal complex' of Fuerteventura developed in an off-axis spreading centre analogous to the southeast Iceland rift zone (Stillman *et al.* 1975; Stillman, 1987). However, more recent studies in Fuerteventura (Stillman, 1997) have demonstrated that the submarine volcanic rocks pass up through littoral volcanic rocks into the oldest subaerial shield-building rocks, although unconformities break up the sequence in many places. This therefore implies that the 'basal complex' of Fuerteventura represents the seamount stage of the growth of this island. A similar conclusion had previously been reached for the 'basal complex' of La Palma by Staudigel (Staudigel & Schmincke, 1984). We therefore propose that the previously used term 'basal complex' for these pre-shield submarine igneous sequences be discarded and replaced by the general term 'seamount series'. The presence of these rocks above sea level is in strong contrast to the Hawaiian Islands (although similar rocks are to be found in the Cape Verde islands, notably on Maio (Stillman *et al.* 1982)). We relate this to the dif-

ferent uplift and subsidence histories of the islands (see below).

2.c. Alternation of activity between islands: are age–distance plots useful at low plate velocities?

It is customary to plot the ages of islands in hotspot-related archipelagoes against the distance from the present-day location of the mantle plume generating them. Such plots show a good age–distance correlation for archipelagoes such as the Hawaiian Islands, located on lithosphere that is moving rapidly relative to the underlying mantle plume (see Langenheim & Clague, 1987, for a recent version of the age–distance plot of the Hawaiian Islands–Emperor Seamount chain). Kauai, the oldest island still to have a significant part of its bulk above sea level, is less than 6 Ma old but lies 580 km from the hotspot at which it initially formed and on the periphery of the hotspot topographic swell. In contrast, the oldest rocks on Fuerteventura are just over 400 km from the youngest island, El Hierro (Figs 1b, 2). We note here, however, that these lateral motions together with the small movement of even the oldest islands in the Canaries relative to the possible dimensions of a plume source mean that neither a perfect age–distance correlation nor single, well-defined episodes of shield and post-erosional activity are to be expected. Thus, the occurrence of anomalies in the age–distance plot of the Canary Islands, such as those represented by the pair La Gomera–Tenerife and the pair Fuerteventura–

Lanzarote (Fig. 2), is not a strong argument against generation of the Canary Islands by a mantle plume. Neither are these time–distance anomalies in themselves a strong argument in favour of a ‘blob-type’ heterogeneous plume (Hoernle & Schmincke, 1993), although of course there may be strong geochemical arguments in favour of such a model.

Similar anomalies in age–distance plots to those found in the Canary Islands also exist in other volcanic archipelagoes located on slow-moving plates. In the Cape Verde islands, although a general southward and westward trend in age exists in the eastern and southern islands of the archipelago (Sal, Boa Vista, Maio, Santiago, Fogo, Brava, with Sal being the morphologically oldest island and Quaternary volcanism concentrated in Fogo and Brava), the focus of late Quaternary volcanism has shifted back from Brava to Fogo in a manner possibly analogous to the late Miocene switch in activity from La Gomera to Tenerife in the Canaries. Furthermore, the northwestern group of islands in the Cape Verdes, from Sao Nicolau to Santo Antao, appears to define a separate, northwest directed age trend. All of these islands are, however, located within 500 km of one another, and all are located on the top of the broad lithospheric swell which is the primary signature of the Cape Verde mantle plume (Courtney & White, 1986). It may therefore be inappropriate to expect perfect age–distance correlations within hotspot-related island groups in slow-moving plates, where the distances between islands are such that all lie close to the mantle plume involved.

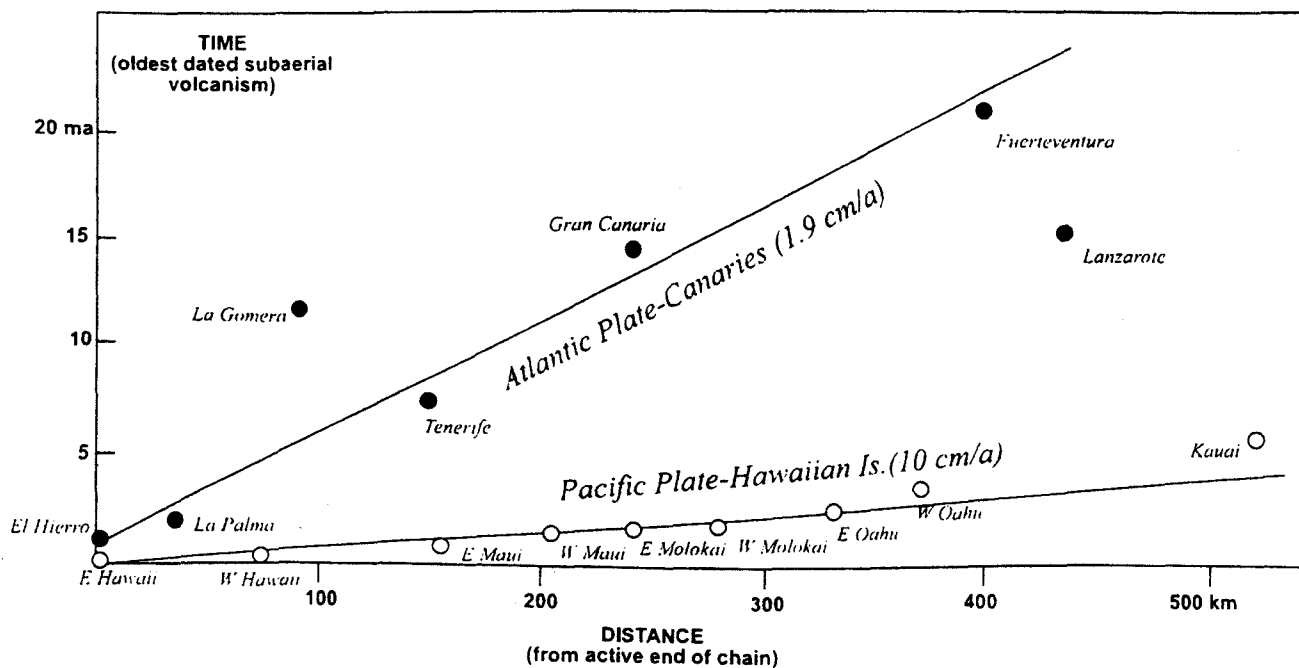


Figure 2. Distances of the successive islands in the Canarian and Hawaiian archipelagoes from their respective active end of chain plotted against the oldest subaerial published ages of the different volcanoes. The Hawaiian volcanoes fit in a straight distance vs. time line corresponding to a plate velocity of about 10 cm/a. The Canaries fit in a similar line corresponding to a plate velocity of about 1.9 cm/a, with the exception of La Gomera and Lanzarote, as explained in the text.

3. Production rates and evolution of magmas in the Canary Islands

Although the Canaries and the Hawaiian islands share a common trend of two-stage subaerial evolution – high effusion rate, shield-stage volcanism, followed by multiple, intermittent and essentially asynchronous post-erosional eruptive episodes – they differ greatly in the type of magmas involved. In the Hawaiian Islands the pre-gap volcanism is characterized by tholeiitic basalts, with late minor volumes of alkali basalts and associated differentiated magmas. During the rejuvenated stage, silica-poor magmas (alkali basalts, basanites and nephelinites) predominate. In the Canaries, no such contrast is evident and magma compositions are much more varied in both stages. The rocks of the pre-gap shield volcanism are predominantly basaltic (picrites, tholeiites and basanites) but with associated differentiated lavas (phonolites and trachytes). Highly differentiated felsic rocks occur in large volumes in the shield-stage volcanism of both Tenerife and Gran Canaria, and to a lesser extent in the other islands. Post-erosional rejuvenated volcanism repeats a similar trend but with much smaller volumes of rock involved in most cases, although the Pliocene Roque Nublo stratovolcano in Gran Canaria (Pérez Torrado, Carracedo & Mangas, 1995) represents perhaps the most voluminous episode of post-erosional volcanism in any island in the world. Wide variations in alkalinity occur in the post-erosional stage volcanism, sometimes within individual eruptions. The variation from basanites to alkali basalts seems to be a common feature in Holocene volcanic eruptions in the Canaries but exceptional variations from basanites to alkali basalts and tholeiites in a single eruption have been observed in the 1730–36 eruption of Lanzarote (Carracedo, Rodríguez Badiola & Soler, 1992). The latter is one of only two historic eruptions to have occurred in a post-erosional stage island in the Canaries (the other is the small eruption of 1824, also on Lanzarote).

A similar lack of contrast between shield-stage and post-erosional magma compositions may also be evident in other island groups on slow-moving plates. In the Cape Verde islands, magma compositions in all stages of activity are alkaline and, commonly, extremely so. The only systematic trend identified by Davies *et al.* (1989) was spatial: they found that rocks in the northwestern islands (Sao Vicente, Santo Antao) were systematically more silica-undersaturated than those from the islands (Sal, Brava) which in their shield stage of activity were located above the inferred mantle plume head. The spatial and temporal patterns of compositional variation in hotspot-related island groups on slow-moving plates may therefore, in general, be more complex than in island groups on fast-moving plates such as the Hawaiian Islands.

A second well-documented distinction between the

shield-building and post-erosional stages in the Hawaiian Islands is the much greater rate of magma supply in the former. This is clearly reflected both in the far greater volumes of the Hawaiian shields as compared to the products of the post-erosional magmatism in each island and in the much higher frequency of eruptions during the shield-building stage of each volcano. Moore & Clague (1992) estimated average magma supply rates during the entire (shield-building) history of the island of Hawaii to be of the order of 0.02 km³/year.

This includes the hiatuses between growth of individual shield volcanoes, and peak magma production rates may be much higher. However, magma production rates may be difficult or impossible to evaluate in the Canary Islands. Two main reasons for this are: (1) the discontinuous character of volcanism, in which eruptive gaps, inherently difficult to date, may predominate over periods of activity, making true evaluation of magma production rates untrustworthy unless large time intervals are compared, and (2) the occurrence of giant lateral collapses which may repeatedly remove large fractions of the mass of an island, especially during the shield-building stage, and redistribute it over distances of hundreds or even thousands of kilometres. Several megaturbidites deposited in the Madeira abyssal plain within the past 1 Ma have been shown to have originated in the Canarian Archipelago (Weaver *et al.* 1992).

The former problem is exemplified by the case of Lanzarote, where the 1730–36 eruption is perhaps the largest to have occurred in the archipelago in historic time by as much as an order of magnitude in volume. However, the previous eruption of note in Lanzarote is that of Montaña Corona, dated at 53 ka (Guillou, unpub. data) using the high-precision Cassinot technique (Guillou *et al.* 1996). In the same period, as many as 100–1000 eruptions may have taken place in the shield-building stage islands of El Hierro, La Palma and Tenerife. Some of these eruptions, such as those of Tanganasoga on El Hierro (Füster *et al.* 1993, Carracedo *et al.* 1997a) and the Volcán Fuego on La Palma (Carracedo *et al.* 1997b) were of comparable or greater volume than the 1730–36 Lanzarote eruption.

Eruption rates during the subaerial shield-building stage which are two to three orders of magnitude greater than those during the post-erosional stage are therefore implied by considering a period of the order of tens of thousands of years. But even this may not be a sufficient averaging period because of the switching of activity between shield-stage islands on timescales of the order of hundreds of thousands of years and the occurrence of episodes of relatively intense post-erosional volcanism such as that which produced the Roque Nublo volcano on Gran Canaria (Pérez Torrado, Carracedo & Mangas, 1995).

The island of El Hierro probably presents the best geochronological control in the Canary Islands. The

uncomplicated development of the island, which is still in its juvenile stage of shield growth, and the abundant and accurate K/Ar ages combined with magnetic stratigraphy (Guillou *et al.* 1996), allow the closest possible approach to the reconstruction of the entire emerged volcanic history of any of the Canaries. The present emerged volume of the island, of about 140–150 km³, has been produced in the last 1.12 Ma, giving an apparent average magma production rate of 0.12–0.13 km³/ka. However, if we take into consideration the three consecutive giant lateral collapses that affected the island, each clearly exceeding 100 km³, the magma production rate for this juvenile stage of growth of El Hierro increases to > 0.4 km³/ka.

A similar evaluation of shield-stage magma production rates in the presently post-erosional islands is highly problematic. This is because it is impossible to evaluate the volume removed by lateral collapses (Canals *et al.* 1997; Stillman, 1997); it is difficult to determine even the number of collapses in these deeply eroded islands, let alone the volumes of individual collapses.

4. Contrasting structural features in the older and younger islands?

Recent onshore and offshore studies of the younger islands of Tenerife, La Palma and El Hierro (Holcomb & Searle, 1991; Canals *et al.* 1997; Carracedo, 1994, 1996a; Carracedo *et al.* 1997a; Watts & Masson, 1995; Guillou *et al.* 1996; Day, Carracedo & Guillou, 1997) have revealed the existence of volcanological, structural and geomorphological features (triple-armed active rifts and giant landslides) typical of hotspot islands. These features, are difficult to identify in the older islands of the archipelago.

Among the most distinctive of these features are triple-armed active rifts, described in detail in previous works (Carracedo, 1994, 1996a), and clearly observable in the islands of Tenerife and El Hierro and in the Mauna Kea Volcano (Fig. 3). While these are easily related to the radially symmetric stress patterns associated with hotspots (Walker, 1992; Carracedo, 1994), triple-armed rifts are difficult to relate to regional fractures, as recently discussed (Carracedo, 1996b). Giant slope collapses, another characteristic feature of hotspot-induced oceanic islands (Hawaii, Réunion, etc.), have recently been identified in the western islands (Fig. 4), and their onshore and offshore features described (Holcomb & Searle, 1991; Carracedo, 1994, 1996a,b; Watts & Masson, 1995; Guillou *et al.* 1996). In the younger Canaries, the link between giant collapses and the volcanic rifts is clear (Carracedo, 1994, 1996a,b).

The apparent contrast in structural features observable in the younger and older Canaries may, however, reflect only different stages of development of the islands. Recent studies in Fuerteventura in particular

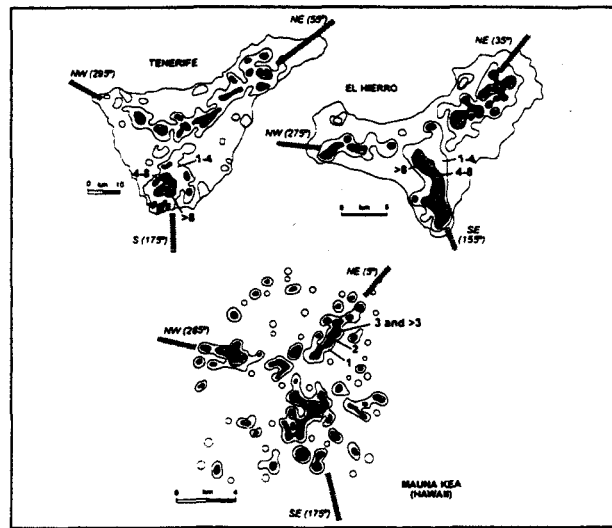


Figure 3. Distribution of emission vents in island-volcanoes. Numbers indicate concentration of eruptive vents (vents/km²). The islands of Tenerife and El Hierro, and the Mauna Kea Volcano evolved unbuttressed, and the rifts have preserved the regular, three-armed geometry. Many other Hawaiian volcanoes and the Cumbre Vieja Volcano in La Palma have evolved to asymmetric configurations as the rifts were constrained in their progress. The distribution of Mauna Kea vents is from Porter (1972).

(Ancochea *et al.* 1996; Stillman, 1997) have identified triple-rift geometries in the shield volcanoes making up the subaerial stage of growth of the island, and west-directed lateral collapse structures. At similar stages of evolution the islands appear to have similar structural features. We consider the multiple rifts and giant landslides to be characteristic features of the shield-stage of development, both in the Canaries and other intraplate oceanic islands of a hotspot-related origin. At this time of active volcanism and frequent eruptions, high aspect ratio, rift-growth-controlled, unstable volcanoes develop. Modifications during the erosional gaps, that in the Canaries are considerably longer than in most of the other archipelagoes of similar origin, hinder recognition of these features in the older islands. Onshore erosion obscures landslide scars, and offshore sedimentation from the nearby continent and younger islands covers the corresponding debris avalanche and debris flow deposits. The characteristic triple rifts may evolve and lose their symmetrical configuration due to buttressing of successive nearby volcanoes even within the shield stage. Intense erosion of the predominantly pyroclastic facies present in the rift zones may erode these features during eruptive quiescence in the erosional gaps.

Furthermore, as has been observed in the Hawaiian Islands, eruptions occur during the rejuvenated or post-erosional stage at vents whose distribution is unrelated to the pre-existing rifts (Langenheim & Clague, 1987). The deep, densely intruded core of the old, thermally aged and eroded rifts may in fact act as effective barriers rather than preferential paths for new

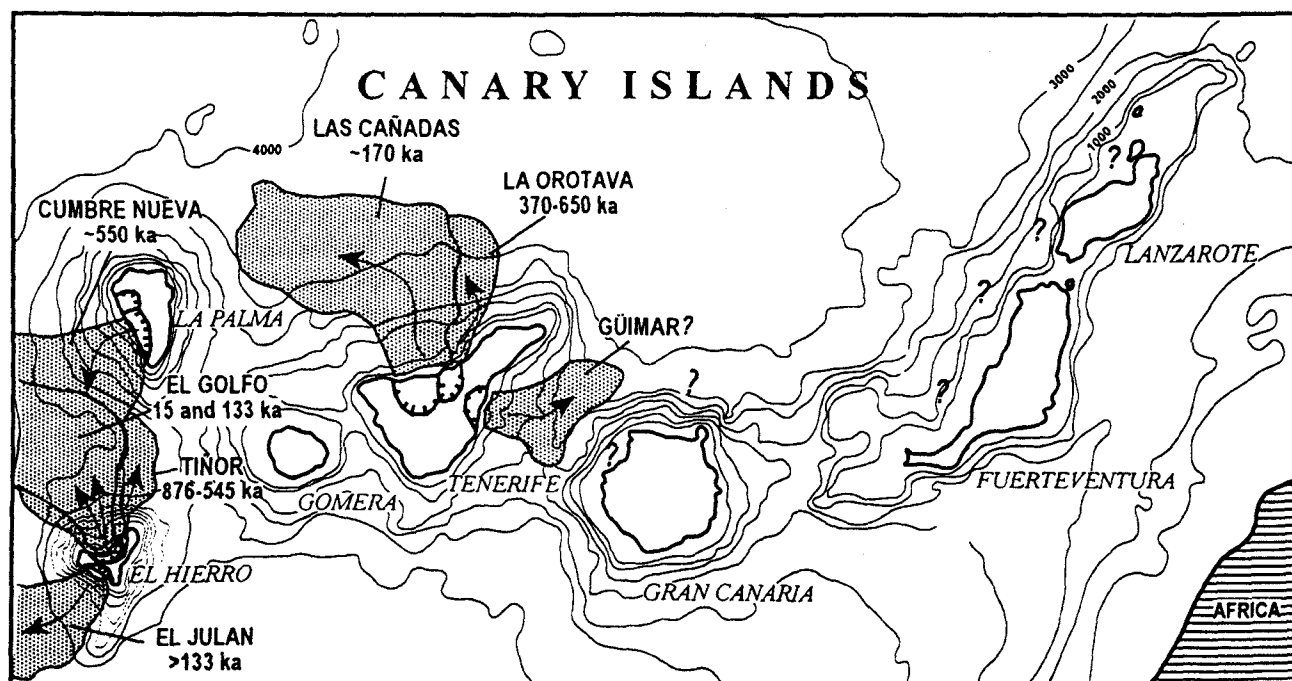


Figure 4. Giant landslides and associated submarine deposits in the Canary Islands. The ages of the landslides in La Palma and El Hierro are estimated from on-shore geological and geochronological data. The giant landslides of Tenerife are from Watts & Masson (1995).

eruptive conduits, explaining this decoupling of rejuvenated volcanism from the shield-stage rifts. Therefore, rejuvenated-stage volcanism may have helped erosion in largely obscuring the structural features of the shield stage in the older Canaries, accounting for the present apparent contrast in the structure of the older and younger islands.

5. Subsidence history of the Canarian islands

The most striking movements relative to sea level in the Canarian islands are recorded by the early seamount series rocks which are now uplifted to up to 1.5 km above sea level (Staudigel & Schmincke, 1984) and furthermore have been deeply incised by syn- and post-uplift erosion. In all the islands where seamount series rocks are exposed, this uplift is accompanied by tilting and/or thrusting away from centres of continued intrusion. It is therefore likely that the uplift is accomplished by large-scale endogenous growth of the volcanic edifices due to emplacement of intense dyke swarms and larger plutons within them. In contrast, the bulk of the subaerial shield-building stage and the subsequent periods are in general characterized by much evidence for a high degree of stability.

Evidence for the position of contemporary sea levels, in the form of marine abrasion platforms, littoral and beach sedimentary deposits, coastal volcanic deposits such as hyaloclastite-based lava deltas and Surtseyan tuff rings, and erosional palaeocliffs, is widespread in the Canary Islands. These markers occur close to present sea level, within the range of

eustatic sea level change. Marine abrasion platforms up to several million years old are present in the oldest islands of Fuerteventura and Lanzarote. Schmincke, Sumita & Funck (1997) argue for the stability of Gran Canaria with respect to sea level over the whole of the last 14 Ma on land and marine evidence. These authors describe late Miocene to Recent age nearly horizontal seismic reflectors north of Gran Canaria, extending to northern Tenerife. Even in the very young island of La Palma, still in the shield-building stage, a beach shoreface sand deposit between about 0.5 Ma and 0.2 Ma old is to be found close to present sea level at El Time. Surtseyan tuff rings occur at present sea level in the Taburiente volcanic edifice at Santa Cruz de La Palma and in the cliff-forming series of the Cumbre Vieja volcano: likely ages for these are about 1 Ma and 100 ka, respectively. It appears that, in common with the other islands, La Palma is extremely stable and has undergone neither subsidence nor uplift since the end of the seamount series uplift.

The lack of post-emergence subsidence in the Canary Islands is in very strong contrast to the rapid subsidence seen during the shield stage and later in the Hawaiian Islands (Moore, 1987). However, islands in the Cape Verde archipelago such as Maio (Stillman *et al.* 1982) also show evidence for no post-emergence subsidence in the form of uplifted seamount-stage rocks. Littoral volcanic landforms and well-developed old marine abrasion platforms crop out close to and above the present sea level. A lack of post-emergence subsidence may be a general feature of islands associated with slow-moving hotspots.

6. Constraints upon proposed models for the origin of the Canary Islands

6.a. The Canary Islands and the Alpine Orogenic Belt

A potentially very important difference between the Canarian Archipelago and most other hotspot-related island groups is that the Canaries are located adjacent to a region of intense active deformation, comprising the Atlas Mountains, Rif Mountains, Alboran Sea and Betic Cordillera provinces of the Alpine orogenic belt. A number of models have been proposed in the past which relate the magmatism which produced the islands to deformation of the oceanic lithosphere to the west and southwest of these continental deformation provinces, and consequent decompression melting of the underlying asthenosphere (Anguita & Hernán, 1975; Araña & Ortiz, 1991). These models explicitly sought to provide an alternative to hotspot-type models for the Canarian Archipelago. Thus the proposal that magmatism in the Canarian Archipelago may be related to the tectonic evolution of the western end of the Alpine chain acquired general significance in the years following the first enunciation of contrasting hypotheses to explain the origin of oceanic volcanic island chains (Morgan, 1971; McDougall, 1971).

Anguita & Hernán (1975) proposed that NNW–SSE directed extension, perpendicular to the overall 080 trend of the archipelago, was responsible for decompression melting of the asthenosphere, and correlated periods of intense magmatic activity in the islands with preceding periods of compression-related uplift in the High Atlas mountains. They postulated that extension in the region of the archipelago occurred as the Atlantic Ocean lithosphere deformed to accommodate membrane–tectonic stresses set up by the preceding phases of compressional deformation to the east. The model is therefore based on a fracture or fractures propagating from the Atlas to the Canaries. It proposes that this fracture is sufficient to tap melts from the asthenosphere and trigger volcanism as it propagates westwards. The timing of the lithospheric fracturing would be related, as mentioned earlier, to orogenic pulses associated to the Atlas tectonism (Fig. 5).

This model, however, was based on age determinations that were subsequently substantially revised. The island of Fuerteventura is a lineation of volcanic complexes with similar oldest subaerial ages of about 20 Ma (Ancochea *et al.* 1996). The island of Lanzarote is the prolongation of Fuerteventura to the northeast (parallel to the continental edge), separated by a narrow stretch less than 100 m deep. The age of the volcanic complexes that form Lanzarote decreases towards the northeast (Abdel-Monem, Watkins & Gast, 1972; Coello *et al.* 1992). Therefore, the initial spread of volcanism in the Canaries would be opposite in direction to a fracture propagating from the Atlas. The other aspect to note is the age relationship of La

Gomera and Tenerife. As already mentioned, the island of Tenerife probably started to grow east of La Gomera when this island was already fully developed and approaching the gap stage. This ‘anomaly’ is difficult to relate to a fracture propagating from the Atlas, but is conceivable in the context of a very slow-moving mantle plume, where a blob may have been decoupled from plumbing La Gomera and diverted by this island edifice against the general spreading trend.

The Anguita & Hernán (1975) propagating fracture model has some points of resemblance to the ‘hot line’ model originally proposed for the Cameroon Line by Fitton & Dunlop (1985). It is noteworthy, however, that re-analysis of the age data for the initial stages of growth of islands in the oceanic part of the Cameroon Line (Lee *et al.* 1994) has led to a revised model in which the development of these islands is related to a mantle plume.

The long periods of quiescence or gaps (see Fig. 1a) have been repeatedly asserted by Anguita & Hernán (1975) to be one of the main pieces of evidence against a hotspot model for the Canaries. These authors assert in a later paper that in a hotspot model all the Canaries, with the exception of La Palma and El Hierro, should be long inactive (Anguita & Hernán, 1986). They do not take into account the fact that the presence of long periods of interruption of the volcanic activity is precisely a characteristic of hotspot-related island chains, otherwise, the shield/post-erosional stratigraphic distinction could not be made in island groups such as the Hawaiian Islands. The comparatively longer duration of gaps in the Canarian Archipelago is probably a consequence of the slow rate of motion of the Canarian hotspot and the properties of the oceanic lithosphere on which the islands have formed.

A strong objection to this model is related to the production of magma required to build the Canary Islands by lithospheric extension in the absence of an asthenospheric anomaly. Quaternary basanites and alkali basalts occur in the Middle Atlas of Morocco (Harmand & Cantagrel, 1984). However, if the extension–melt production relationships proposed in decompression melting models, such as that of McKenzie & Bickle (1988), are only even approximately applicable to the Canary Islands, the small degrees of lithospheric extension associated with the Atlas tectonics, although perhaps sufficient to produce the small-volume volcanic sequences in the Atlas mountain basins, will be insufficient in the absence of elevated (plume-generated) asthenospheric temperatures to produce the very large volumes of igneous rocks within the archipelago itself.

A further important objection to propagating-fracture models for the Canaries is related to the propagation of tectonic stresses from continental to oceanic lithosphere. In the simplest hypothesis of Anguita & Hernán (1975) the Canary Islands would be originated

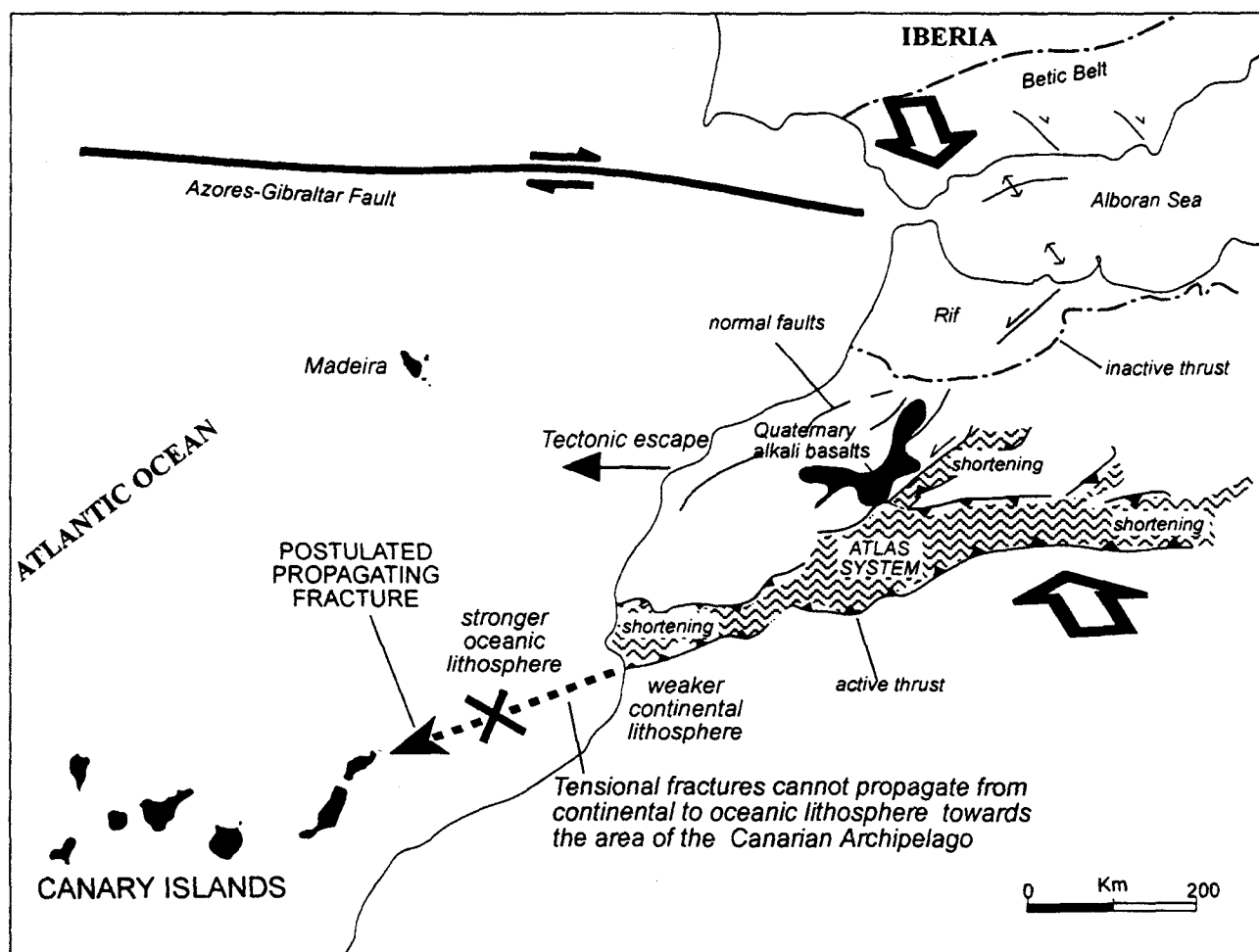


Figure 5. Geodynamic setting of the Canary Islands. The figure shows some of the main objections to relating the origin of the Canary Islands to the Atlas tectonism, as explained in the text.

by an offshore extension of the Trans-Agadir Fault. Seismic, magnetic and geological studies carried out off the coast of Morocco (Dillon & Sougy, 1974) concluded that the Anti-Atlas feature abruptly terminated along the coast, without any evidence of an offshore continuation of this structure. Furthermore, the propagation of such a feature from continental into oceanic lithosphere may be mechanically impossible. Analysis of strength differences between continents and oceans has been an important issue in the study of the development of plate boundaries. Vink, Morgan & Zhao (1984) considered strength differences between continents and oceans and reached the conclusion that continents are always weaker. Steckler & ten Brink (1986) and ten Brink (1991) analysed the total integrated strength of continental and oceanic lithosphere. Applying their conclusions to the African margin in the Atlas region it is evident that the > 150 Ma old oceanic lithosphere is considerably stronger than the continent, precluding any fracture propagating from the Atlas towards the Canaries.

Araña & Ortiz (1991) proposed an alternative model in which shortening of the lithosphere, on high-angle reverse faults, produces decompression melting

of the asthenosphere beneath the rising blocks. Evidence is present for localized uplift by up to perhaps 5 km on some islands, notably in the seamount series of La Palma (Staudigel & Schmincke, 1984) and in the Basal Complex of Fuerteventura (Ancochea *et al.* 1996). However, the model of Araña & Ortiz (1991) requires the systematic and continuous uplift of all the islands by distances of the order of tens of kilometres to produce decompression melting on the scale and degree of partial melting needed to account for the volume and composition of the Canarian magmas (McKenzie & Bickle, 1988), most especially those which characterize the early stage of subaerial magmatism in the older islands. There is no evidence to suggest the occurrence of uplift on this scale in the Canaries. Finally, in this model the initiation of volcanism should be nearly synchronous along the entire archipelago, instead of the observed general progression oceanwards of the oldest subaerial volcanism.

6.b. The hotspot model

The association of the Canarian Archipelago with an asthenospheric hotspot was originally proposed by

Burke & Wilson (1972) and has since been proposed repeatedly (Schmincke, 1973; Carracedo, 1979; Feraud *et al.* 1985; Holik, Rabinowitz & Austin, 1991; Hoernle & Schmincke, 1993; Watts, 1994; Carracedo, 1994, 1996a). However, the applicability of the hotspot model to the Canaries has commonly been questioned on the grounds that the archipelago lacks some of the geophysical features associated with the prototypical hotspot-related island groups.

The hotspot model was first defined in the Hawaiian Islands, where a very productive and vigorous mantle plume and a fast-moving plate combined to generate the prototypical hotspot-induced island chain. However, as in the case of the Canaries, these prototypical circumstances cannot always be expected to be present, making the identification of the hotspot signature more difficult. The wide variation in the characteristics of mid-plate oceanic islands has been noted by Watts (1994), who related these variations to absolute plate motions and the long-term thermal and mechanical properties of the lithosphere. These circumstances may play a role in precluding a simple relationship between the elastic thickness of the lithosphere and the characteristic regional anomalies (topographic swells, gravity/geoid highs).

The Canary and Cape Verde Islands seem to be the only regions of convection-generated tensional stress fields in northwest Africa, as shown by global scale models derived from convection-generated stresses in the lithosphere inferred from satellite and surface gravity data (Liu, 1980). Recent work compiling intraplate seismicity in the Atlantic in the period 1918–1990 (Wyssession *et al.* 1995) shows that seismicity within the African plate offshore from the Atlantic coast is also concentrated in two areas: within the Cape Verde swell and in a region of similar extent around the Canaries. The authors interpret this seismicity as being related to plume-generated magmatic activity.

Seismic studies carried out off the coast of Morocco (Holik, Rabinowitz & Austin, 1991) identified a velocity inversion between a body of 4.7 km/s seismic velocity and the underlying 3.1 km/s sediments and a deep crustal layer with anomalous velocities of 7.1–7.4 km/s. They interpreted this sequence as being igneous in origin, with a group of shallow intrusive and volcanic rocks being emplaced within and above sediments (to produce the velocity inversion) and being fed from deep crustal intrusions (to produce the anomalous deep layer). They proposed that the development of this igneous province was due to passage of a hotspot that rejuvenated the ancient crust off Morocco from approximately 60 Ma (1 in Fig. 6) onwards. They trace the underplated igneous body to the north of the Canary Islands following a broad bathymetric arch across the continental rise west of the Fuerteventura–Lanzarote ridge that connects with the western part of the Canarian Archipelago. The

arrival of the hotspot at this end of the island chain would have taken place, according to Holik, Rabinowitz & Austin (1991), at about 10 Ma.

In a different model of the same general ‘hot spot’ type, Watts (1994) postulated a narrow asthenospheric feature encircling the Canaries and probably extending below the African continent (2 in Fig. 6).

7. Conclusions

We conclude that, in contrast to the propagating fracture model, not only do hotspot-type models not conflict with available geological information, but in fact they explain many of the apparent inconsistencies pointed out in the development of the Canaries.

In our model, we postulate that the Canaries originated by an asthenospheric plume (Canas *et al.* 1994). The first volcanic manifestations of this hotspot would have been localized at the continental–oceanic boundary west of Fuerteventura (see Fig. 6). Sediment thickness at continental margins exceeding 10 km should be a major factor in modifying the strength of the lithosphere. Lower overburden and conductivity of the sediments are associated with significant weakening of the lithosphere (Vink, Morgan & Zhao, 1984). The gravity anomaly study of Watts & Marr (1995) provides independent evidence for the weakness of the continent–ocean transition zone at the eastern end of the Canary Islands.

The thick sedimentary sequence in the continental margin off Cape Juby may have thus provided a favourable location for the first Canarian volcanism, defining the volcanic complex lineation parallel to the coast described by Ancochea *et al.* (1996). In this initial stage – the earlier non-folded submarine volcanism of Fuerteventura dated at about 36 Ma (Abdel-Monem, Watkins & Gast, 1972) and 39 Ma (Coello *et al.* 1992) and of Eocene–Oligocene age according to palaeontological evidence (Robertson & Stillman, 1979) – volcanism may have been spreading to the northeast and southwest along the weak continental–ocean crust transition zone, producing the Fuerteventura–Lanzarote ridge (A in Fig. 6). As described by Dillon & Sougy (1974), interaction between the Canary Islands volcanism and the African continental margin is apparent off Cape Juby, where strongly magnetic volcanic seamounts extend in the lower continental slope along lines continuous with the Canary trend.

As discussed above, the assertion that the volcanic activity progresses from Lanzarote to Fuerteventura and oceanwards is inconsistent with the presently accepted geochronological and geological information, and reflects an unfounded link between the Canaries and the Atlas tectonism. After this initial stage, slow motion of the hotspot may have initiated the general westward trend followed by the Canaries (B in Fig. 6). The succession of the islands is broadly

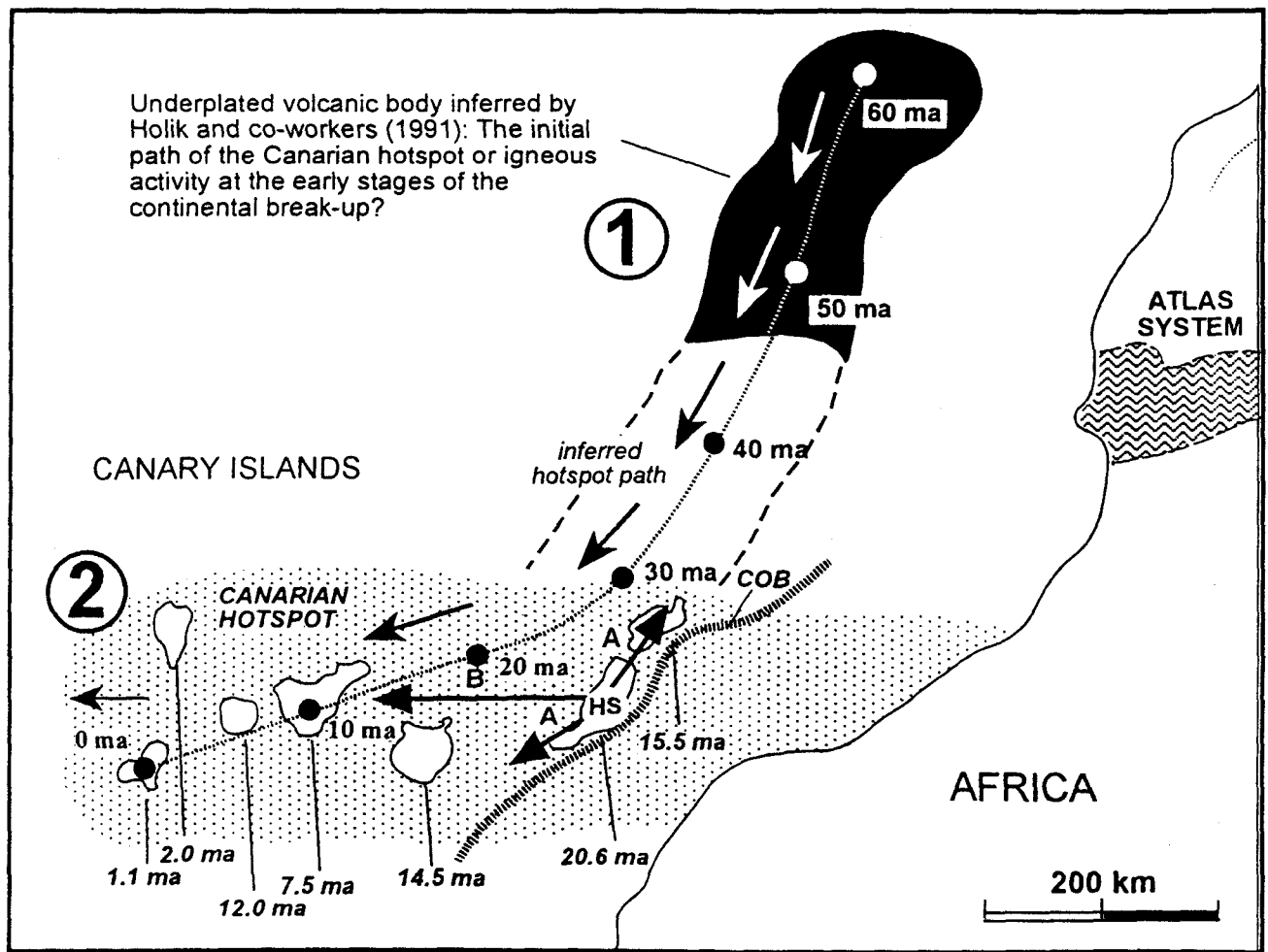


Figure 6. Figure illustrating the origin of the Canaries in relation to a hotspot. HS: initial activity of the CHS, close to the continental–oceanic boundary. A: initial progression of volcanism along the continental–oceanic boundary (COB). B: general progression of volcanism induced by the displacement of the African plate. Ages in italics: the oldest dated subaerial volcanism of each island. The two scenarios (1 and 2) are explained in the text.

congruent with the westward progression of the hotspot; for reasons discussed above a perfect age–distance correlation is not to be expected because of the very low velocity of the African plate relative to the plume reference frame.

Acknowledgements. The ideas presented in this paper have been greatly clarified and developed through our discussions with Uri ten Brink, Tony Watts, Tim Minshull, Robin Holcomb, Bruce Nelson and Hubert Staudigel. Stimulating comments from Hans Schmincke also helped us to focus our arguments. We thank all of them for their assistance in various stages of the preparation of this paper.

References

- ABDEL-MONEM, A., WATKINS, N. D. & GAST, P. W. 1971. Potassium–argon ages, volcanic stratigraphy, and geomagnetic polarity history of the Canary Islands: Lanzarote, Fuerteventura, Gran Canaria and La Gomera. *American Journal of Science* **271**, 490–521.
- ABDEL-MONEM, A., WATKINS, N. D. & GAST, P. W. 1972. Potassium–argon ages, volcanic stratigraphy, and geomagnetic polarity history of the Canary Islands: Tenerife, La Palma, and Hierro. *American Journal of Science* **272**, 805–25.
- ANCOCHEA, E., BRÄNDLE, J. L., CUBAS, C. R., HERNÁN, F. & HUERTAS, M. J. 1996. Volcanic complexes in the eastern ridge of the Canary Islands: the Miocene activity of the island of Fuerteventura. *Journal of Volcanology and Geothermal Research* **70**, 183–204.
- ANCOCHEA, E., FÜSTER, J. M., IBARROLA, E., CENDRERO, A., COELLO, J., HERNÁN, F., CANTAGREL, J. M. & JAMOND, C. 1990. Volcanic evolution of the Island of Tenerife (Canary Islands) in the light of new K–Ar data. *Journal of Volcanology and Geothermal Research* **4**, 231–49.
- ANGUITA, F. & HERNÁN, F. 1975. A propagating fracture model versus a hotspot origin for the Canary Islands. *Earth and Planetary Science Letters* **27**, 11–19.
- ANGUITA, F. & HERNÁN, F. 1986. Geochronology of some Canarian dike swarms: contribution to the volcano-tectonic evolution of the Archipelago. *Journal of Volcanology and Geothermal Research* **30**, 155–62.
- ARAÑA, V. & ORTIZ, R. 1991. The Canary Islands: Tectonics, magmatism and geodynamic framework. In *Magmatism in extensional structural settings (The Phanerozoic African plate)* (eds A. B. Kampunzu and R. T. Lubala), pp. 209–563. Barcelona, Spain: Springer-Verlag.

- BURKE, K. & WILSON, J. T. 1972. Is the African plate stationary? *Nature* **239**, 387–90.
- CANALES, J. P. & DAÑOBEITIA, J. 1998. The Canary Islands swell: a coherence analysis of bathymetry and gravity. *Geophysical Journal International* **132**, 479–88.
- CANALS, M., ALIBES, B., URGELES, R. & ALONSO, B. 1997. Landsliding on the Canary islands. The missing submarine sediment record. *International Workshop, Volcanism & Volcanic Hazards in Immature Intraplate Oceanic Islands. La Palma, Canary Islands. Abstract Volume*, 106–9.
- CANAS, J. A., PUJADES, L. G., BLANCO, M. J., SOLER, V. & CARRACEDO, J. C. 1994. Coda-Q distribution in the Canary Islands. *Tectonophysics* **246**, 245–61.
- CARRACEDO, J. C. 1979. *Paleomagnetismo e historia volcánica de Tenerife*. Aula de Cultura, Cabildo Insular de Tenerife, 82 pp.
- CARRACEDO, J. C. 1994. The Canary Islands: An example of structural control on the growth of large oceanic-island volcanoes. *Journal of Volcanology and Geothermal Research* **60**, 225–41.
- CARRACEDO, J. C. 1996a. A simple model for the genesis of large gravitational landslide hazards in the Canary Islands. In *Volcano Instability on the Earth and other Planets* (eds X. McGuiere, X. Jones and X. Neuberg), pp. 125–35. Geological Society Special Publication no. 110.
- CARRACEDO, J. C. 1996b. Morphological and structural evolution of the western Canary Islands: Hotspot-induced three-armed rifts or regional tectonic trends? *Journal of Volcanology and Geothermal Research* **72**, 151–62.
- CARRACEDO, J. C. & SOLER, V. 1995. Anomalous shallow palaeomagnetic inclinations and the question of the age of the Canarian Archipelago. *Geophysical Journal International* **122**, 393–406.
- CARRACEDO, J. C., DAY, S., GUILLOU, H. & PÉREZ TORRADO, J. F. 1997a. El Hierro Geological Excursion Guidebook. *International Workshop, Volcanism & Volcanic Hazards in Immature Intraplate Oceanic Islands. La Palma, Canary Islands, September 1997*.
- CARRACEDO, J. C., DAY, S., GUILLOU, H. & GRAVESTOCK, P. 1997b. *Geological colour map (1:33 000) of the Cumbre Vieja Volcano, La Palma, Canary Islands*. Pub. CSIC & Cons. Política Territorial, Gobierno Canarias.
- CARRACEDO, J. C., RODRIGUEZ BADIOLA, E. & SOLER, V. 1992. The 1730–1736 eruption of Lanzarote: an unusually long, high magnitude fissural basaltic eruption in the recent volcanism of the Canary Islands. *Journal of Volcanology and Geothermal Research* **53**, 239–50.
- COELLO, J., CANTAGREL, J. M., HERNÁN, F., FÜSTER, J. M., IBARROLA, E., ANCOCHEA, E., CASQUET, C., JAMOND, C., DÍAZ DE TERÁN, J. R. & CENDRERO, A. 1992. Evolution of the eastern volcanic ridge of the Canary Islands based on new K–Ar data. *Journal of Volcanology and Geothermal Research* **53**, 251–74.
- COURTNEY, R. C. & WHITE, R. S. 1986. Anomalous heat flow and geoid across the Cape Verde Rise: evidence for dynamic support from a thermal plume in the mantle. *Geophysical Journal of the Royal Astronomical Society: Volcanology and Geothermal Research* **87**, 815–67.
- DAVIES, G. R., NORRY, M. J., GERLACH, D. C. & CLIFF, R. A. 1989. A combined chemical and Pb–Sr–Nd isotope study of the Azores and Cape Verde hotspots: the geodynamic implications. In *Migmatism in the Ocean Basins* (eds A. D. Saunders and M. J. Norry), pp. 231–55. Geological Society Special Publication no. 42.
- DAY, S. J., CARRACEDO, J. C. & GUILLOU, H. 1997. Age and geometry of an aborted rift flank collapse: the San Andrés fault system, El Hierro, Canary Islands. *Geological Magazine* **134**, 523–37.
- DILLON, W. P. & SOUGY, J. M. A. 1974. Geology of West Africa and Canary and Cape Verde Islands. In *The Ocean Basins and Margins* (eds A. E. M. Nairn and F. G. Stehli), pp. 315–90. New York: Plenum Press.
- FERAUD, G., GIANNERINI, G., CAMPREDON, R. & STILLMAN, C. J. 1985. Geochronology of some Canarian dike swarms: Contribution to the volcano-tectonic evolution of the Archipelago. *Journal of Volcanology and Geothermal Research* **25**, 29–52.
- FILMER, P. E. & MCNUTT, M. K. 1988. Geoid anomalies over the Canary Islands group. *Marine Geophysical Research* **11**, 77–87.
- FITTON, J. G. & DUNLOP, H. M. 1985. The Cameroon line, West Africa, and its bearing on the origin of oceanic and continental alkaline basalts. *Earth and Planetary Science Letters* **72**, 23–38.
- FORNARI, D. J., GARCIA, M. O., TYCE, R. C. & GALLO, D. G. 1988. Morphology and structure of Loihi Seamount based on Seabeam sonar mapping. *Journal of Geophysical Research* **93**, 15227–38.
- FÜSTER, J. M., CENDRERO, A., GASTESI, P., IBARROLA, E. & LOPEZ RUIZ, J. 1968. Geología y Volcanología de las Islas Canarias: Fuerteventura. Instituto “Lucas Mallada”, C.S.I.C., Madrid, 239 pp.
- FÜSTER, J. M., FERNÁNDEZ SANTÍN, S. & SAGREDO, J. 1968. *Geología y Volcanología de las Islas Canarias: Lanzarote*. Instituto “Lucas Mallada”, C.S.I.C., Madrid, 177 pp.
- FÜSTER, J. M., HERNÁN, F., CENDRERO, A., COELLO, J., CANTAGREL, J. M., ANCOCHEA, E. & IBARROLA, E. 1993. Geocronología de la isla de El Hierro (Islas Canarias). *Boletín de la Real Sociedad Española de Historia Natural (Sección Geología)* **88**, 85–97.
- GRUNAU, H. R., LEHNER, P., CLEINTUAR, M. R., ALLENBACH, P. & BAKKER, G. 1975. New radiometric ages and seismic data from Fuerteventura (Canary Islands), Maio (Cape Verde Islands), and Sao Tomé (Gulf of Guinea). *Progress in Geodynamics. Royal Netherlands Academy of Arts and Science*, 90–118.
- GUILLOU, H., CARRACEDO, J. C., PÉREZ TORRADO, F. & RODRIGUEZ BADIOLA, E. 1996. K–Ar ages and magnetic stratigraphy of a hotspot-induced, fast grown oceanic island: El Hierro, Canary Islands. *Journal of Volcanology and Geothermal Research* **73**, 141–55.
- HARMAND, C. & CANTAGREL, J. M. 1984. Le volcanisme alcaline Tertiaire et Quaternaire du Moyen Atlas (Maroc): chronologie K/Ar et cadre géodynamique. *Journal of African Earth Sciences* **2**, 51–5.
- HAUSEN, H. 1958. On the geology of Fuerteventura (Canary Islands). *Societas Scientiarum Fennica, Commentationes Physico-Mathematicae* **22-1**, 1–211.
- HOERNLE, K. & SCHMINCKE, H. U. 1993. The role of partial melting in the 15-Ma geochemical evolution of Gran Canaria: a blob model for the Canarian hotspot. *Geotechnology* **10**, 19–32.
- HOLCOMB, R. T. & SEARLE, R. C. 1991. Large landslides from oceanic volcanoes. *Marine Geotechnology* **10**, 19–32.
- HOLIK, J. S., RABINOWITZ, P. D. & AUSTIN, J. A. 1991. Effects of Canary hotspot volcanism on structure of oceanic crust off Morocco. *Journal of Geophysical Research* **96**, 12039–67.
- LANGENHEIM, V. A. M. & CLAGUE, D. A. 1987. The Hawaiian–Emperor volcanic chain. Part II:

- Stratigraphic framework of volcanic rocks of the Hawaiian Islands. In *Volcanism in Hawaii* (eds W. Decker, T. L. Wright and P. H. Stauffer), pp. 55–84. U.S. Geological Survey Professional Paper 1350, vol. 1.
- LEE, D. C., HALLIDAY, A. N., FITTON, J. G. & POLI, G. 1994. Isotopic variations with distance and time in the volcanic islands of the Cameroon line: evidence for a mantle plume origin. *Earth and Planetary Science Letters* **123**, 119–38.
- LIU, H. S. 1980. Convection generated stress field and intraplate volcanism. *Tectonophysics* **65**, 225–44.
- MACDONALD, G. A. & ABBOT, A. T. 1970. *Volcanoes in the sea – The geology of Hawaii*. Honolulu: University of Hawaii Press, 441 pp.
- MCDUGALL, I. 1971. Volcanic island chains and seafloor spreading. *Nature* **231**, 141–4.
- MCDUGALL, I. & SCHMINCKE, H. U. 1976. Geochronology of Gran Canaria, Canary Islands: Age of shield building volcanism and other magmatic phases. *Bulletin of Volcanology* **40**, 57–77.
- MCKENZIE, D. & BICKLE, M. J. 1988. The volume and composition of melt generated by extension of the lithosphere. *Journal of Petrology* **29**, 625–79.
- MITCHELL, J. G., LE BAS, M. J., ZIELONKA, J. & FURNES, H. 1983. On dating the magmatism of Maio, Cape Verde islands. *Earth and Planetary Science Letters* **64**, 61–76.
- MOORE, J. G. 1987. Subsidence of the Hawaiian Ridge. In *Volcanism in Hawaii* (eds W. Decker, T. L. Wright and P. H. Stauffer), pp. 85–107. U. S. Geological Survey Professional Paper 1350, vol. 1.
- MOORE, J. G. & CLAGUE, D. A. 1992. Volcano growth and evolution of the island of Hawaii. *Geological Society of America Bulletin* **104**, 1471–84.
- MORGAN, W. J. 1971. Convection plumes in the lower mantle. *Nature* **230**, 42–43.
- O'CONNOR, J. M. & DUNCAN, R. A. 1990. Evolution of the Walvis Ridge-Rio Grande Rise hotspot system: implications for African and South American plate motions over plumes. *Journal of Geophysical Research* **95**, 17475–502.
- PÉREZ TORRADO, F., CARRACEDO, J. C. & MANGAS, J. 1995. Geochronology and stratigraphy of the Roque Nublo Cycle, Gran Canaria, Canary Islands. *Journal of the Geological Society, London* **152**, 807–18.
- PORTER, S. C. 1972. Distribution, morphology and size frequency of cinder cones on Mauna Kea. *Geological Society of America Bulletin* **84**, 607–12.
- ROBERTSON, A. H. F. & STILLMAN, C. J. 1979. Submarine volcanic and associated sedimentary rocks of the Fuerteventura Basal Complex, Canary Islands. *Geological Magazine* **116**, 203–14.
- SCHMINCKE, H. U. 1973. Magmatic evolution and tectonic regime in the Canary, Madeira, and Azores Island groups. *Geological Society of America Bulletin* **84**, 633–48.
- SCHMINCKE, H. U., SUMITA, M. & FUNCK, T. 1997. Growth and destruction of Gran Canaria: Evidence from land studies, bathymetry, offshore seismic studies and drilling during ODP Leg 157. *International Workshop, Volcanism & Volcanic Hazards in Immature Intraplate Oceanic Islands. La Palma, Canary Islands, Abstract Volume*, 10–12.
- STAUDIGEL, H. & SCHMINCKE, H. U. 1984. The Pliocene seamount series of La Palma/Canary Islands. *Journal of Geophysical Research* **89**, 11190–215.
- STECKLER, M. S. & TEN BRINK, U. S. 1986. Lithospheric strength variations as a control on new plate boundaries: examples from the northern Red Sea region. *Earth and Planetary Science Letters* **79**, 120–32.
- STILLMAN, C. J. 1987. A Canary island dyke swarm: implications for the formation of oceanic islands by extensional fissural volcanism. In *Mafic dyke swarms* (eds H. C. Hallis and W. F. Fahrig), pp. 243–55. Geological Association of Canada Special Paper no. 34.
- STILLMAN, C. J. 1997. The episodic growth and partial destruction of pre-shield-lava Fuerteventura. *International Workshop, Volcanism & Volcanic Hazards in Immature Intraplate Oceanic Islands. La Palma, Canary Islands, Abstract Volume*, 56–8.
- STILLMAN, C. J., FURNES, H., LE BAS, M. J., ROBERTSON, A. H. F. & ZIELONKA, J. 1982. The geological history of Maio, Cape Verde Islands. *Journal of the Geological Society, London* **139**, 347–61.
- STILLMAN, C. J., FÜSTER, J. M., BENNELL BARKER, M. J., MUÑOZ, M., SWEWING, J. D. & SAGREDO, J. 1975. Basal Complex of Fuerteventura is an oceanic intrusive complex with rift-system affinities. *Nature* **257**, 469–70.
- TEN BRINK, U. S. 1991. Volcano spacing and plate rigidity. *Geology* **19**, 397–400.
- VINK, G. E., MORGAN, W. J. & ZHAO, W. L. 1984. Preferential rifting of continents: a source of displaced terranes. *Journal of Geophysical Research* **89**, 10072–6.
- WALKER, G. P. L. 1990. Geology and volcanology of the Hawaiian Islands. *Pacific Science* **44**, 315–47.
- WALKER, G. P. L. 1992. Coherent intrusion complexes in large basaltic volcanoes – a new structural model. *Journal of Volcanology and Geothermal Research* **50**, 41–54.
- WATKINS, N. D. 1974. Paleomagnetism of the Canary Islands and Madeira. *Geophysical Journal of the Royal Astronomical Society* **32**, 249–67.
- WATTS, A. B. 1994. Crustal structure, gravity anomalies and flexure of the lithosphere in the vicinity of the Canary Islands. *Geophysical Journal International* **119**, 648–66.
- WATTS, A. B. & MARR, C. 1995. Gravity anomalies and the thermal and mechanical structure of rifted continental margins. In *Rifted Ocean-Continent Boundaries* (eds E. Banda *et al.*), pp. 65–94. Kluwer Publishing.
- WATTS, A. B. & MASSON, D. G. 1995. A giant landslide on the north flank of Tenerife, Canary Islands. *Journal of Geophysical Research* **100**, 24487–98.
- WEAVER, P. P. E., ROTHWELL, R. G., EBBING, J., GUNN, D. E. & HUNTER, P. M. 1992. Correlation, frequency of emplacement and source directions of megaturbidites on the Madeira Abyssal Plain. *Marine Geology* **109**, 1–20.
- WYSESSION, M. E., WILSON, J., BARTKÓ, L. & SAKATA, R. 1995. Intraplate seismicity in the Atlantic Ocean Basin: A teleseismic catalog. *Bulletin of the Seismological Society of America* **85**, 755–74.

groups (usually with a sparse number of individuals) of animals are linear [Andries and Nelissen, 1990].

The process of individual recognition and learning plays an important role in the establishment of linear dominance hierarchy in small groups of fish because the dominant fish is able to differentiate and rank subordinate fish into different categories based on previous encounters among individuals [Drickamer et al., 1996]. In the case of resource defense, conspecifics manifest differences in fighting ability, and, thus, the energy invested by the owner specimens to keep all the competitors at bay from the resource will not be equally distributed (i.e., either the degree of agonistic interactions with each competitor or the duration of the contests).

Inside the group, the fish establishes priorities with respect to which conspecific is to be the first from which to defend its food and with most intensity. We expect that the dominant specimens will invest more energy (measured as the proportion of agonistic interactions) in defending their resource from the conspecifics which may possess greater ability to contend for the resource and will attack these more frequently and with greater intensity [Maynard-Smith, 1982; Senar, 1990]. As a consequence of the differences in ability to exploit the resource and size [Enquist et al., 1987], aggressiveness [Huntingford et al., 1990], and/or standard metabolic rate [Metcalf et al., 1995] as possible indicators together with the differentials in aggressive behavior, dominance hierarchies are established [Milinski, 1984; Drickamer et al., 1996].

The aim of this study is to test the assumption that most agonistic interactions are directed at the conspecific with the most competitive abilities (but of lower hierarchical rank) and to measure the consequence that this has on the growth rate of each component of the group. White-seabream were selected for this study since juveniles of this species naturally form small groups of 10 to 30 individuals.

METHODS

Twenty-four juvenile white-seabream (*Diplodus sargus cadenati*) of the same shoal were collected from a pool in the north coast of the island of Gran Canaria, Spain (28°10' N, 15°40' W) in July 1995. The fish were transported to the laboratory and housed in groups of 4 individuals in six 90 litre aquariums with recirculating seawater at 20–22°C, for 1 month (the aquariums were lettered from A to F). Fish were measured and weighed individually at the beginning and end of the trial and then returned to their natural environment ($\bar{L}_{10} = 3.37$; SD = 0.74 cm and $W_{10} = 0.60$; SD = 0.38 g at the beginning of the experiment, and $\bar{L}_{11} = 3.96$; SD = 0.70 cm and $W_{11} = 1.05$; SD = 0.53 g at the end). Each tank had 3 opaque sides and a glass front used for observation.

The fish were fed fast-sinking pelletized food once a day delivered always at the same location via a plastic tube.

The fish were originally identified by a random code number which bore no relation to the rank number later bestowed upon them. All fish could be recognized by their natural body marks (e.g., the size and shape of the saddle-like dark blotch on the caudal peduncle). We allowed a dominant-subordinate relationship to be established between 4 juvenile fish and monitored the number of agonistic interactions (nips, chases, and lateral displays) between each fish during 3 periods of 20 min each day.

Statistical data analysis was carried out to establish differences in the number of aggressive interactions between fish. The Kruskal-Wallis ANOVA and Friedman ANOVA

tests (nonparametric statistical methods) were used. In order to establish differential aggression (non-random aggression), we analyzed 24 data files, 1 per fish, pertaining to the number of aggressive acts, expected and observed, of each fish toward its 3 corresponding conspecifics over the whole period using the nonparametric observed vs. expected chi-square test.

RESULTS

There were no differences in the length and weight of fish over the 6 aquariums (Kruskal-Wallis ANOVA, $P = 0.80$ at the beginning and $P = 0.83$ at the end of the trial).

The α -fish in each aquarium was identified as the individual which initiated and subsequently (after winning) displaced the other fish in most social interaction events (e.g., lateral displays, chases, etc.). The α -fish attempted to defend their feeding places and generally expelled conspecifics. Subordinate fish (β , γ , and ω) were defined as those that normally were attacked and displaced by the dominant (α -fish) and/or other subordinates. The α -fish were always larger than subordinates.

The α -fish generally directed the largest number of aggressive acts at the β -fish (Friedman ANOVA, $P = 0.001$) [Siegel, 1986] which was usually the second largest fish in each aquarium (Table I). The attacks of α -fish on β -fish did not appear to be made by chance (observed vs. expected chi-square, $P = 0.001$) [Siegel, 1986]. The attacks of β -fish were mainly on the γ -fish, which followed them in size (Friedman ANOVA, $P = 0.0016$) (Table II). The attacks carried out by the γ -fish were mainly directed at the smallest fish (ω -fish) (Friedman ANOVA, $P = 0.001$) (Table III). Although these ω -fish were the least aggressive specimens in all the aquariums, their few aggressive incursions were mainly directed at the γ -fish, which were nearest in size (Friedman ANOVA, $P = 0.001$) (Table IV).

In aquarium E, the second fish in size was sick during part of the experiment due to a skin infection produced by *Oodinium* sp. [Schubert, 1987], and during this period the attacks of the α -fish on this individual were less frequent and were mainly directed at the specimens which were closest in size (Friedman ANOVA, $P < 0.014$). After treating the aquarium with copper sulphate, the sick fish recovered its vitality and social status and consequently received a large number of aggressive interactions with the α -fish. From then on (the last week of the experiment), there were no significant differences between the number of attacks received by both subordinates from the α -fish (Friedman ANOVA, $P < 0.09$).

The weight increase experienced by each fish at the end of the experiment showed a

TABLE I. Percentage of Aggressive Interactions Initiated by the α -Fish Toward Other Fish in Each Aquarium

Aquarium	Conspecific			N
	β	γ	ω	
A	49.82	39.12	11.06	823
B	43.79	31.99	24.22	822
C	57.88	25.12	17.00	1,047
D	64.22	20.51	15.27	1,146
E	35.51	48.21	16.28	1,118
F	84.30	10.21	5.49	911

TABLE II. Percentage of Aggressive Interactions Initiated by the β -Fish Toward Other Fish in Each Aquarium

Aquarium	Conspecific			N
	α	γ	ω	
A	19.33	66.39	14.28	119
B	1.84	79.75	34.97	489
C	5.61	80.14	14.18	141
D	4.06	50.40	45.53	123
E	0.97	57.28	41.75	206
F	3.49	73.72	22.79	860

significant correlation ($F = 12.367$; $P = 0.002$) to the number of aggressive interactions initiated by them ($R = 0.5999$), indicating, with few exceptions, that more aggressive fish grow faster (Fig. 1).

DISCUSSION

Generally, in a group of animals with a dominance structure [Senar et al., 1990; Wilson, 1992], not all the opponents are equal and they do not have the same submissive status [Tinbergen, 1965; Nelissen, 1985; Andries and Nelissen, 1990; Carranza, 1994; Ridley, 1995]. This makes it necessary for the dominant individual to be more aggressive in order to reinforce its supremacy on the subordinate conspecific which is next in line within the dominance hierarchy.

From our results, we can deduce that the dominant juvenile white-seabream carry out aggressive attacks selectively on fish whose subordination level is immediately inferior to their own. Attacks are more frequently directed at the following individual in the hierarchical order, establishing a peck-dominance hierarchy. In peck-dominance hierarchies, the majority of agonistic acts range from dominant (highest) to subordinate [Tinbergen, 1965; Drickamer et al., 1996]. We could perhaps conclude that the observed results of differential aggression reflect variation in the opponents' willingness to challenge others. That is to say, the "boldest" subordinate would always be expected to challenge the dominant fish more than the other subordinates. Thus, this trend would be an automatic outcome of variation in willingness to take risks. We could also deduce that once the dominant fish relinquished the resource (because it was satiated) to the second fish in line, the entire process would begin again with the "boldest" of the remaining subordinates challenging the third fish in line more than the others (and so on).

TABLE III. Percentage of Aggressive Interactions Initiated by the γ -Fish Toward Other Fish in Each Aquarium

Aquarium	Conspecific			N
	α	β	ω	
A	2.38	17.69	79.93	294
B	0.70	4.53	94.77	287
C	0.00	1.22	98.78	82
D	5.68	22.16	72.16	176
E	0.31	2.46	97.23	325
F	0.65	0.44	98.91	458

TABLE IV. Percentage of Aggressive Interactions Initiated by the ω -Fish Toward Other Fish in Each Aquarium

Aquarium	Conspecific			N
	α	β	ω	
A	0.00	0.00	100.00	4
B	1.23	12.34	86.42	81
C	0.00	0.00	100.00	2
D	0.00	7.69	92.30	52
E	0.00	35.71	64.28	14
F	25.00	8.30	66.66	12

However, this latter explanation is highly unsatisfactory because the dominant white-seabream normally attacked the fish second in line even when they were quiet and relatively distant (at the other extreme of the aquarium) and even when there was no resource to defend (e.g., before feeding or when food had been totally depleted 1 to 2 hr previous). Nevertheless, the highest proportions (51.7%; SD = 8.01) of aggressive interaction measured during the trial were initiated during feeding. The fish second in line manifest a similar pattern of attack to the third in line even when they had no possibility of access to food.

Dominant white-seabream also interact aggressively with individuals of a much lower hierarchical order and sometimes aggressions on the lower order individuals by the higher range specimens, although such cases are less frequent.

Although agonistic behavior in groups may include aggressions from any individual and in any direction (however, they are less frequent from lower order to higher order), the linear hierarchy presents a higher predictability with respect to the outcome of future competitive interaction [Rowell, 1974]. This dominance hierarchy allows energy saving [McFarland, 1993] in combats where there was a high probability of losing to all the members of the group [Andries and Nelissen, 1990]. As the dominant individual may save energy in intermediate fights, it submits the subordinate fish of highest range and hence indirectly dominates all the remaining individuals. In the same way, the ascending attacks, although furtive, represent a possibility of ascending in status if they are successful [Senar et al., 1990; Wilson, 1992].

Being the dominant fish has costs and benefits [Gotceitas and Godin, 1992; Hannes et al., 1984; Jakobsson et al., 1995; Metcalfe et al., 1989; Ryer and Olla, 1995]. In accordance with the observations of Grant [1990], Metcalfe and Thorpe [1992], and Metcalfe et al. [1992] in salmonid species, more aggressive fish grow faster (and this could be said of individuals C1, E1, and B1 in Fig. 1). However, in some environments (i.e., under high levels of agonistic interactions and competition for food [Ryer and Olla, 1995]), the energy spent keeping opponents at bay may weigh more than the benefits acquired due to previous and prior access to food (see individuals A1, D1, and C1 in Fig. 1). Usually larger fish initiate aggressive encounters (except when the smaller individual is the owner of the territory and the larger is an intruder) and are more likely to win in a shorter fight, but as pointed out by Miklósi et al. [1995], similarity in size will increase the duration of a contest (increasing the energetic cost).

Moderately aggressive fish may have advantages in some circumstances (see individuals A3 and F3 in Fig. 1 and Table V). The continuing fight between opponents of similar abilities (i.e., dominant and subordinate of the highest range) in order to rein-

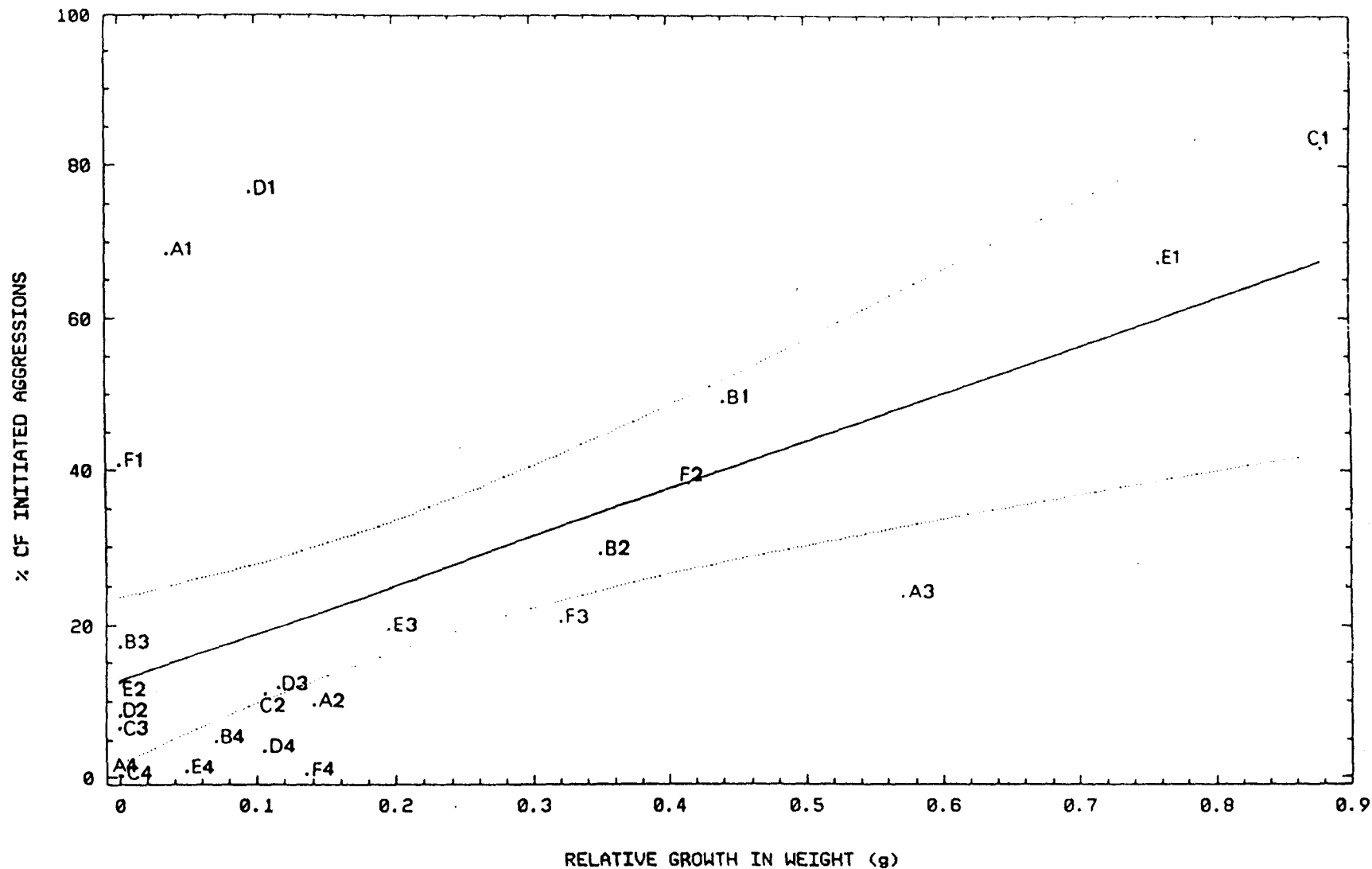


Fig. 1. Relative growth in weight of individual fish in relation to the percentage of their initiated aggressive interactions in each aquarium ($\% \text{ of Initiated Aggressions} = 12.73127 + 61.99825 * \text{Relative Growth in Weight}$; $R = 0.5999$). Each fish is represented by a capital letter indicating the aquarium (A-F) and a number indicating the fish hierarchical range (1 = α -fish, 2 = β -fish, 3 = γ -fish, 4 = ω -fish).

TABLE V. Percentage of Aggressive Interactions Initiated by Each Fish in Each Aquarium During the Trial

Conspecific	Aquarium					
	A	B	C	D	E	F
α	68.37	48.96	82.31	76.55	67.27	40.65
β	9.60	29.12	11.08	8.22	12.39	38.37
γ	23.71	17.09	6.45	11.76	19.54	20.44
ω	0.32	4.82	0.16	3.47	0.84	0.53
N	1,240	1,679	1,272	1,497	1,663	2,241

force the hierarchy may favor lesser-able individuals with effective strategies evolved to avoid attacks or to pass by unassailed the fish of higher ranges. Therefore, the social environment will determine which strategy will be most effective and profitable.

ACKNOWLEDGMENTS

Our thanks to Dr. Vicente Hernández, Mr. J.A. Santiago, and Mrs. A. Santana Ortega for their help in housing fish and collecting data.

REFERENCES

Andries S, Nelissen MHJ (1990): A study of the dominance hierarchy in four Mbuna-species: *Melanochromis johanni*, *M. auratus*, *Pseudotropheus ornatus*, and *P. lombardoi* (Teleostei: Cichlidae). *Belgian Journal of Zoology* 120:165-193.

Carranza J (1994): "Etología: Introducción a la ciencia del comportamiento." Cáceres: Universidad de Extremadura.

Drickamer LC, Vessey SH, Meikle D (1996): "Animal Behaviour." 4th ed. Dubuque, IA: Wm. C. Brown Publishers.

Enquist M, Lungberg T, Zandor A (1987): Visual assessment of fighting ability in the cichlid fish *Nannacara anomala*. *Animal Behavior* 35(4): 1262-1263.

Grant JWA (1990): Aggressiveness and the foraging behaviour of young-of-the-year brook charr (*Salvelinus fontinalis*). *Canadian Journal of Fisheries and Aquatic Sciences* 47:915-920.

Gotceitas V, Godin J-GJ (1992): Effects of location of food delivery and social status on foraging-site selection by juvenile Atlantic salmon. *Environmental Biology of Fishes* 35:291-300.

Hannes R-P, Franck D, Liemann F (1984): Effects of rank order fights on whole body and blood concentrations of androgens and corticosteroids in the male swordtail (*Xiphophorus helleri*). *Z. Tierpsychol.* 65:53-65.

Huntingford FA, Metcalfe NB, Thorpe SE, Graham WD, Adams CE (1990): Social dominance and body size in Atlantic salmon parr, *Salmo salar*. *L. Journal of Fish Biology* 36:877-881.

Jakobsson S, Brick O, Kullberg C (1995): Escalated fighting behaviour incurs increased predation risk. *Animal Behavior* 49:235-239.

Maynard-Smith J (1982): "Evolution and the Theory of Games." Cambridge, MA: Cambridge University Press.

McFarland D (1993): "Animal Behaviour: Psychology, Ethology, and Evolution." 2nd. ed. Singapore: Longman Scientific & Technical.

Metcalfe NB, Thorpe JE (1992): Early predictors of life-history events: The link between first feeding date, dominance and seaward migration in Atlantic salmon, *Salmo salar*. *L. Journal of Fish Biology* 41(Supplement B):93-99.

Metcalfe NB, Huntingford FA, Graham WD, Thorpe JE (1989). Early social status and the development of life-history strategies in Atlantic salmon. *Proceedings of the Royal Society of London B* 236:7-19.

Metcalfe NB, Wright PJ, Thorpe JE (1992): Relationships between social status, otolith size at first feeding and subsequent growth in Atlantic salmon (*Salmo salar*). *Journal of Animal Ecology* 61:585-589.

Metcalfe NB, Taylor AC, Thorpe JE (1995): Metabolic rate, social status and life-history strategies in Atlantic salmon. *Animal Behavior* 49:431-436.

Milinski M (1984): Competitive resource sharing: An experimental test of learning rule of EESs. *Animal Behavior* 32:233-242.

- Miklósi A, Haller J, Csányi V (1995): The influence of opponent-related and outcome-related memory on repeated aggressive encounters in the paradise fish (*Macropodus opercularis*). *Biological Bulletin* 188:83-88.
- Nelissen M (1985): Structure of the dominance hierarchy and dominance determining "group factors" in *Melanochromis auratus* (Pisces, Cichlidae). *Behaviour* 94:85-107.
- Ridley M (1995): "Animal Behaviour". 2nd ed. Boston: Blackwell Scientific Publications.
- Rowell TE (1974): The concept of social dominance. *Behavioral Biology* 11:131-154.
- Ryer CH, Olla BL (1995): The influence of food distribution upon the development of aggressive and competitive behaviour in juvenile chum salmon, *Oncorhynchus keta*. *Journal of Fish Biology* 46:264-272.
- Schubert G (1987): "A Complete Guide to Fish Diseases." New Jersey: T.F.H. Publications, Inc.
- Senar JC (1990): Agonistic communication in social species: What is communicated? *Behaviour* 112:270-283.
- Senar JC, Copete JL, NB Metcalfe (1990): Dominance relationships between resident and transient wintering sisking. *Ornis Scandinavica* 21:129-132.
- Siegel S (1986): "Estadística No Paramétrica Aplicada a las Ciencias de la Conducta." 2nd ed. México D.F.: Editorial Trillas.
- Tinbergen N (1965): "Social Behaviour in Animals, with Special References to Vertebrates." 3rd ed. London: Chapman & Hall.
- Wilson JD (1992): A re-assessment of the significance of status signalling in wild populations of great tits (*Parus major*). *Animal Behavior* 43:999-1009.

The Influence of Food Distribution on the Aggressive Behaviour of Juvenile White-Seabream (*Diplodus sargus cadenati* de la Paz, Bauchot and Daget, 1974)

José J. Castro* and José A. Santiago

Departamento de Biología, Universidad de Las Palmas de Gran Canaria, Las Palmas de Gran Canaria, Canary Islands, Spain

Experiments were conducted to investigate the effect of differences in the spatial distribution of food on the aggressive behaviour of juvenile white-seabream, *Diplodus sargus cadenati*, both in the presence and in the absence of food. The groups of fish receiving spatially fixed food displayed less aggression than those receiving spatially variable food. The period (before, during, or after feeding) during which aggressiveness is measured also has influence in the results. During the prefeeding and postfeeding periods (absence of food), groups that were fed with food spatially fixed displayed less aggression than those that received spatially variable food. However, when food was present there were no differences in the number of aggressive acts carried out by fish groups in both environments. The aggressiveness shown by the groups of fish was always more pronounced during the postfeeding period than during the prefeeding period. The dominant fish was more aggressive when food was spatially fixed, and especially when food was present. Therefore, the subordinates were more aggressive when food was spatially variable and particularly when food was present and during the postfeeding period. *Aggr. Behav.* 24:379–384, 1998. © 1998 Wiley-Liss, Inc.

Key words: agonistic behaviour; *Diplodus sargus cadenati*; resource defence; resource monopolization; foraging; intraspecific competition

INTRODUCTION

Current theory suggests that the spatial and temporal distribution of resources plays an important role in influencing how individuals within a social group interact [Davies and Houston, 1984; Grand and Grant, 1994; Grant, 1993]. The potential for monopolization and defence of resources is predicted to increase as resources become more clumped in space or dispersed in time or when spatial predictability increases [Grant, 1993; Grant and Kramer, 1992; Monaghan and Metcalfe, 1985; Ryer and Olla, 1995].

*Correspondence to: José J. Castro, Departamento de Biología, Universidad de Las Palmas de Gran Canaria, Apdo. 550, Las Palmas de Gran Canaria, Canary Islands, Spain. E-mail: josejuan.castro@biologia.ulpgc.es
Received 17 June 1997; amended version accepted 15 July 1997

In many species, aggression is closely associated with competition for defensible feeding sites [Huntingford and Turner, 1987] but is less frequent or less intense in the same species when food is indefensible [Grant and Kramer, 1992; Ryer and Olla, 1991]. However, given that food distribution affects aggression during feeding, it is less clear how food distribution influences aggression when food is not present because it is not available or because it has already been totally consumed. We are not aware of what happens when food location is spatially variable, and several individuals have had the opportunity of initiating the monopolisation of a defensible area.

In this work, our aim was to test the hypothesis that when food localisation is spatially variable, fish groups are more aggressive than when food location is spatially fixed, and if this premise could be extended when food is absent (before and after feeding) and for all fish rank. The resolution of these questions could be of application of resource defence theory to methods of feeding fish in the aquaculture industry.

METHODS

Sixty juvenile white-seabream (*Diplodus sargus cadenati*) were collected from pools in the north coast of the island of Gran Canaria, Spain (28°10' N, 15°40' W), in July 1994. The fish were transported to the laboratory at Las Palmas de Gran Canaria University, where they were randomly housed in groups of five individuals in 180-L aquaria with recirculating seawater at 20 to 24°C. Fish were individually measured at the beginning of the trial (L = 3.96; SD = 0.44 cm); after a trial of 6 days, they were returned to the wild. Each tank had three opaque sides and a glass front used for observation.

The fish were fed fast-sinking pelletised food once a day, always delivered all at once via plastic tubes. Six groups of fish were fed with pellets always dropped at the same location (food spatially fixed); six other groups were fed with pellets dropped at two different locations placed at opposite sides of the aquaria, where on one day food was introduced in one location, the following day in the other location, and the third day in both locations simultaneously (half of the food in each one), and so on, alternating the location of food (food spatially variable).

The fish were originally identified by a random code number that bore no relation to the rank number later bestowed on them. All fish could be recognized by their natural body marks (e.g., the size and shape of the saddlelike dark blotch on the caudal peduncle). We allowed a dominant-subordinate relationship to be established between five juvenile fish and monitored the number of agonistic interactions (nips, chases, and lateral displays) between each fish during three 20-minute periods each day (before, during, and after feeding). All the aggressive interactions were identically scored.

Statistical analysis of data was performed in two steps: the first step was conducted to find differences in aggressiveness between groups with different food distribution and the second to find differences in aggressiveness between individual fish in each aquarium to test the suitability of our hypothesis (and indirectly the current theory) to groups or individuals. Nonparametric statistical methods were used [Siegel, 1990].

RESULTS

Aggressiveness, Dominance, and Relative Body Size

The dominant fish in each aquarium was identified as the individual that initiated and subsequently (after winning) displaced the other fish in most social interaction events

(e.g., lateral displays, chases, etc.). The dominant fish attempted to defend their feeding sites and generally expelled conspecifics. Subordinate fish were defined as those that normally were attacked and displaced by the dominant (a-fish) and/or other subordinates. The dominant fish were always larger than subordinates (Mann-Whitney U test; $U = 85.5$, $P = .004$). We classified 13 individuals as dominant and 47 as subordinate. There was typically a single dominant fish in each tank, but in one group, where the location of food was alternated between two sites, two dominant fish were present, each dominating one side of the tank.

Qualitative Aggressive Behaviour

Chases were the most frequent expressions of aggressiveness exhibited by juvenile white-seabream. Attacks were initiated with a quick burst of swimming speed by the aggressor in the direction of the opponent. Generally, attacks were directed toward fish of a lower or similar rank, and rarely toward fish of a higher rank. The agonistic interactions between juvenile white-seabream in small groups originated a linear dominance hierarchy [Castro and Caballero, 1998].

Lateral displays were generally displayed by fish of similar rank. During lateral displays, both fish swam in circles with the dorsal fins extended, and as fish swam around each other in this manner, they also shook their bodies. Normally, the display lasted until one of the contenders retreated, generally chased by the other, or as a result of interference by a third fish (normally the dominant fish of the group), which put an end to the interaction in that it launched an attack on one of the original opponents.

Apparently, the spatial position of the fish's body is important and must be included in the attack pattern. Sometimes during an attack, the opponent fish responded by swimming along the transversal plane, with the dorsal fin withdrawn. This posture of the body was always observed when one fish was repelling attacks by another (submission posture).

Influence of Food Distribution on the Aggressive Behaviour

Aggressiveness was significantly greater in those groups in which food was spatially variable compared with those in which food was spatially fixed (Mann-Whitney U test; $U = 57332.0$, $P = .004$). The number of aggressive interactions increased significantly from the beginning (first day) to the end (sixth day) of the trial (Kruskal-Wallis ANOVA; $P < .0001$) independent of how food was introduced into the experimental tank.

Although the agonistic interactions were more frequent in those groups in which food location was spatially variable, there were not significant differences in the level of aggressiveness between both environments, before (Mann-Whitney U test; $U = 5358.0$, $P = .14$) and during (Mann-Whitney U test; $U = 9900.0$, $P = .79$) feeding periods. However, 1 hour after that food was totally depleted, the number of agonistic interactions was significantly greater (Mann-Whitney U test; $U = 4243.0$, $P < .0001$) in those groups where fish were fed with food location spatially variable.

Groups were more aggressive after feeding than before (Wilcoxon Matched Pairs Test; $P < .0001$) and during (Wilcoxon Matched Pairs Test; $P < .0001$) feeding, independent of the form of food delivery.

AGGRESSIVENESS BY FISH HIERARCHICAL RANK

The dominant fish were significantly more aggressive in groups in which food location was spatially fixed than in groups in which food location was spatially variable

(Mann-Whitney U test; $U = 54407.0$, $P = .0002$). Subordinate fish showed a lower level of aggressiveness in those groups in which location of food was fixed than when it was distributed alternatively between two places (Mann-Whitney U test; $U = 45483.0$, $P < .0001$) (Table I). The number of aggressive acts initiated by the dominant fish or by the subordinates increased significantly day to day (Kruskal-Wallis ANOVA; $P < .0001$), independent of the form of food delivery. Moreover, the dominant fish were significantly more aggressive during the postfeeding period than during the prefeeding period (Friedman ANOVA; $\chi^2 = 9.22$, $P < .002$ when food location was fixed and $\chi^2 = 17.31$, $P < .0001$ when food location was variable). Table I shows that the dominant fish were more aggressive when food was present (Friedman ANOVA; $P < .0001$).

The dominant fish, when location of food was fixed, was always more aggressive than all its subordinates together (Friedman ANOVA; $\chi^2 = 76.12$, $P = .0001$); however, this difference in aggressiveness was not significant during the prefeeding period (Friedman ANOVA; $\chi^2 = 1.15$, $P = .28$). On the other hand, when location of food was spatially variable, the dominant fish was only more aggressive (although not significant, Friedman ANOVA; $\chi^2 = 2.84$, $P < .09$) than all its subordinates together when food was present. In this last environment, before feeding (Friedman ANOVA; $\chi^2 = 6.32$, $P < .01$) and after feeding (Friedman ANOVA; $\chi^2 = 6.26$, $P < .01$) the group of subordinates developed a larger number of aggressive acts than the dominant fish, although rarely against it.

DISCUSSION

Monopolisation and defence of food resources have consequences in the social environment of groups of juvenile white-seabream, generating the establishment of dominance hierarchies [Castro and Caballero, 1998] as a consequence of agonistic interactions and asymmetry in fighting ability [Maynard Smith and Parker, 1976]. This has significant effects on biological aspects (i.e., it generates differential growth rates between individuals [Blanckenhorn, 1992; Jobling, 1995; Lutnesky and Szyper, 1991; Ruzzante and Doyle, 1993]) that at the same time influence the social environment, intensifying the asymmetries [Huntingford and Turner, 1987; Metcalfe et al., 1989]. The literature on aggressive behaviour in fish suggests that resource distribution exerts a strong influence on whether fish defend a resource [Gotceitas and Godin, 1992; Grant, 1993; Magnuson, 1962; Ryer and Olla, 1995], which is generally consistent with predictions of the theory of economic defensibility [Brown, 1964; Davies and Houston, 1984; Wyman and Hotaling, 1988]. However, there is comparatively little information on how food

TABLE I. Average Number of Aggressive Interactions per Minute Initiated by the Dominant Fish and Its Subordinates in Relation to the Pattern of Food Distribution (Fixed or Variable)

Period	Food location fixed				Food location variable			
	Dominant		Subordinates		Dominant		Subordinates	
	x	SD	x	SD	x	SD	x	SD
Total	3.26	2.74	1.44	1.31	2.57	2.33	2.43	2.05
Prefeeding	1.54	1.18	1.38	1.26	1.43	1.49	1.83	1.63
During Feeding	5.23	3.12	1.66	1.32	3.54	2.78	2.70	2.40
Postfeeding	2.41	1.44	1.70	1.31	2.46	1.77	2.66	1.81

distribution influences resource defence and aggression when food is not actually present, in prefeeding and postfeeding.

When we analyse the aggressiveness developed by the dominant fish, our results are consistent with the current theory that suggests that its agonistic behaviour increases as resources become more clumped in space [Monaghan and Metcalfe, 1985; Ryer and Olla, 1995], probably because the individual can occupy a progressively smaller home range that is easier to defend [Grant, 1993]. The owner of the resource becomes more aggressive when food is more defensible [Grant, 1993; Monaghan and Metcalfe, 1985], but will it also be reflected in the group's total aggressiveness? Lutnesky and Szypper [1991] and Ryer and Olla [1995] observed that agonistic behaviour increases when the distribution of food is spatially clumped; however, our results indicate that the levels of aggression were greater in groups of juvenile white-seabream given spatially variable food than in groups given spatially fixed food.

In the postfeeding period, 1 hour after food had been totally consumed, the level of aggressiveness was greater in those groups of juvenile white-seabream in which the location of food was spatially variable. This could be a consequence of two factors: (1) the effect of the aggressiveness that has been developed during feeding, "the inertial response" [Rand and Rand, 1978; Sevenster, 1961; Wilz, 1970]. This effect is mitigated in proportion to the increase in time from feeding [Chase et al., 1994]. (2) The effect of recent experiences of positive success in acquiring food aggressively during feeding [Franck and Ribowski, 1989; Wright and Shanks, 1993]. This last effect will be more notable when the location of food is variable in space because several individuals have had the opportunity to initiate the monopolisation of a defensible area without a previous owner.

Experiments with regard to food monopolisation could explain why, after feeding, those groups in which the location of food was spatially variable showed greater aggressiveness. Previous and recent positive experiences in acquiring food could predispose fish to act anti-economically [Wyman and Hotaling, 1988] being more aggressive, but probably this behaviour is not extended for a long time if no profit is obtained to reinforce it (no food was obtained after food was totally depleted).

Agonistic behavior potentially produces disproportionate food acquisition and generates differential growth rates [Lutnesky and Szypper, 1991]; therefore, the influence of food distribution on agonistic behaviour is important for efficient aquaculture of any fish species. It is a prerequisite for achievement of a homogeneous rate of growth, and uniform size at harvest, that feed supply be evenly distributed among the fish making up the rearing group. Disparate feed acquisition may arise because of behavioural interactions that result from high levels of competition for spatially limited food resources (an environment characterized by high levels of agonistic interactions). If spatial predictability of food distribution is possible, fish will attempt its monopolisation [Grand and Grant, 1994; Grant, 1993], and the aggressive interactions between competitors will increase. The results obtained are a potential application of resource defence theory to methods of feeding fish in the aquaculture industry.

ACKNOWLEDGMENTS

We thank the staff of the Department of Biology of Las Palmas de Gran Canaria University, Canary Islands, Spain, who provided experimental facilities and lodging.

REFERENCES

- Blanckenhorn WU (1992): Group size and the cost of agonistic behavior in pumpkinseed sunfish. *Ethology Ecology, and Evolution* 4:255-271.
- Brown JL (1964): The evolution of diversity in avian territorial systems. *Wilson Bulletin* 76:160-169.
- Castro JJ, Caballero C (1998): Dominance structure in small groups of juvenile white-seabream (*Diplodus sargus cadenati* de la Paz, Bauchot and Daget 1974). *Aggressive Behavior* 24:197-204.
- Chase ID, Bartolomeo C, Dugatkin LA (1994): Aggressive interactions and inter-content interval: How long do winners keep winning? *Animal Behaviour* 48:393-400.
- Davies NB, Houston AI (1984): Territory economics. In Krebs JR, Davies NB (eds): "Behavioural Ecology: An Evolutionary Approach, 2nd ed." Oxford: Blackwell Scientific Publications, pp 263-299.
- Franck D, Ribowski A (1989): Escalating fights for rank-order position between male swordtails (*Xiphophorus helleri*): Effects of prior rank-order experience and information transfer. *Behavioral Ecology and Sociobiology* 24:133-143.
- Gotceitas V, Godin J-G J (1992): Effects of location of food delivery and social status on foraging-site selection by juvenile Atlantic salmon. *Environmental Biology of Fishes* 35:291-300.
- Grand TC, Grant JWA (1994): Spatial predictability of food influence its monopolization and defence by juvenile convict cichlids. *Animal Behaviour* 47:91-100.
- Grant, JWA (1993): Whether or not to defend? The influence of resource distribution. *Marine Behavior and Physiology* 23:137-153.
- Grant JWA, Kramer DL (1992): Temporal clumping of food arrival reduces its monopolization and defence by zebrafish. *Brachydanio rerio*. *Animal Behaviour* 44:101-110.
- Huntingford FA, Turner A (1987). "Animal Conflict" London: Chapman and Hall.
- Jobling M (1995): Feeding of charr in relation to aquaculture. In Klemetsen A, Jonsson B, Elliott JM (eds): "Proceeding of the Third International Charr Symposium, June 13-18, 1994, Trondheim, Norway." *Nordic Journal of Freshwater Research* 71:102-112.
- Lutesky MME, Szyper JP (1991): The influence of spatial food distribution on agonistic behavior in juvenile mahimahi, *Coryphaena hippurus*. *Journal of Applied Ichthyology* 7:253-256.
- Magnuson JJ (1962): An analysis of aggressive behaviour, growth and competition for food and space in medaka (*Oryzias latipes* [Pisces, Cyprinodontidae]). *Canadian Journal of Zoology* 40:214-234.
- Maynard Smith J, Parker GA (1976): The logic of asymmetric contests. *Animal Behaviour* 24:159-175.
- Metcalfe NB, Huntingford FA, Graham WD, Thorpe JE (1989): Early social status and the development of life-history strategies in Atlantic salmon. *Proceedings of the Royal Society of London Series B* 236:7-19.
- Monaghan P, Metcalfe NB (1985): Group foraging in wild brown hares: Effects of resource distribution and social status. *Animal Behaviour* 33:993-999.
- Rand AS, Rand WM (1978): Display and dispute settlement in nesting iguanas. In Greenberg N, Maclean PO (eds): "Behaviour and Neurology of Lizards." Rockville, MD: National Institute of Mental Health, pp 245-252.
- Ruzzante DE, Doyle RW (1993): Evolution of social behavior in a resource-rich, structured environment: Selection experiments with medaka (*Oryzias latipes*). *Evolution* 47:456-470.
- Ryer CH, Olla BL (1991): Agonistic behaviour in a schooling fish: Form, function and ontogeny. *Environmental Biology of Fishes* 31:355-363.
- Ryer CH, Olla BL (1995): The influence of food distribution upon the development of aggressive and competitive behaviour in juvenile chum salmon, *Oncorhynchus keta*. *Journal of Fish Biology* 46:264-272.
- Sevenster P (1961): A causal analysis of displacement activity (fanning in *Gasterosteus aculeatus* L.). *Behaviour Suppl* 9:1-170.
- Siegel S (1990): Estadística no paramétrica aplicada a las ciencias de la conducta. Editorial Trillas, México D.F.
- Wilz KJ (1970): Causal and functional analysis of dorsal pricking and nest activity in the courtship of the three-spined stickleback *Gasterosteus aculeatus*. *Animal Behaviour* 18:115-124.
- Wright WG, Shanks AI. (1993): Previous experience determines territorial behaviour in an archaeogastropod limpet. *Journal of Experimental Marine Biology and Ecology* 166:217-229.
- Wyman RL, Hotaling I. (1988): A test of the economic defendability of a resource and territoriality using young *Etioplos maculatus* and *Pelmatochromis subocellatus knibensis*. *Environmental Biology of Fishes* 21:69-76.

Determination of polychlorinated biphenyls by liquid chromatography following cloud-point extraction

A. Eiguren Fernández, Z. Sosa Ferrera, J.J. Santana Rodríguez*

Department of Chemistry, Faculty of Marine Sciences, University of Las Palmas de Gran Canaria, 35017 Las Palmas de Gran Canaria, Spain

Received 22 July 1997; received in revised form 3 October 1997; accepted 22 October 1997

Abstract

In this study, a new methodology, based on the 'cloud-point phenomenon' of non-ionic surfactants, is applied for the extraction and preconcentration of polychlorinated biphenyls (PCBs). Once the PCBs are extracted from the solution, they are determined by liquid chromatography. The non-ionic surfactants used are polyoxyethylene 4-lauryl ether (Brij 30) and polyoxyethylene-10-oleyl ether (Brij 97). In this study, the optimum conditions for the preconcentration and determination of PCBs have been established and the method has been applied to determine PCBs in sea-water samples. © 1998 Elsevier Science B.V.

Keywords: Cloud-point; Preconcentration; Brij 30; Brij 97; Polychlorinated biphenyls; Liquid chromatography

1. Introduction

Polychlorinated biphenyls (PCBs) are organic compounds which have some characteristics, such as chemical and thermal stability, that make them useful in industrial applications and products. These compounds were commonly used without taking into account their persistent presence in the environment as a contaminant. Various analytical techniques designed at isolating and determining non-ortho-substituted PCBs have been described [1,2].

The PCBs are present in various media, but always at low concentrations, which makes it very difficult to determine them using normal methodologies. Usually,

an extraction with an organic solvent is used for PCBs preconcentration. A new methodology, known as cloud-point extraction (CPE), offers a possibility of combining extraction and preconcentration in one step. In CPE the solution separates into two isotropic phases, a surfactant-rich phase with a small amount of water (surfactant phase), and a bulk aqueous solution (aqueous phase) [3–7]. The surfactant-rich phase allows us to preconcentrate and extract the PCBs in small volume, so the preconcentration factors are very high. Moreover, the surfactant-rich phase is compatible with the micellar and aqueous-organic mobile phase in LC, so it facilitates the application of this analytical method for subsequent studies for determination of PCBs.

Cloud-point extraction (CPE) has been applied to the preconcentration of different compounds in various media [8–14]. This methodology has the

*Corresponding author. Fax: +34 28 452 922; e-mail: josejuan.santana@quimica.ulpgc.es

benefits of safety, cost and no toxicological effects. Although the use of CPE is now quite general, there are not many works that explain the most important parameters which affect this phenomenon. It is known that the effect of temperature and the pH can alter the cloud-point considerably, but there are other parameters such as ionic strength, equilibration temperature and time, and analyte concentration that can influence the efficiency of the process [15–17].

In this work, we report the results of a study carried out to determine the effect of these parameters on the application of CPE for PCBs, using two non-ionic surfactants, polyoxyethylene-4-lauryl ether (Brij 30) and polyoxyethylene-10-oleyl ether (Brij 97). This CPE methodology has been applied for the analysis of mixtures of PCBs in sea-water samples.

2. Experimental

2.1. Reagents

Stock solutions of 1.0×10^{-4} mol l⁻¹ PCBs (Accu-Standard, 99% purity) were prepared by dissolving appropriate amounts of each PCB in ethanol (Merck). Stock solutions of the surfactants, polyoxyethylene-4-lauryl ether (Brij 30) (Sigma), and polyoxyethylene-10-oleyl ether (Brij 97) (Sigma) were prepared in deionized water. HPLC-grade methanol and KNO₃ were obtained from Panreac.

All solvents and analytes were filtered through a 0.45 μm nylon membrane filter, and an ultra-high quality water was used throughout.

2.2. Apparatus

The LC system consisted of a Waters pump (model 510) fitted with a Rheodyne injector valve (model 7725i) with a 20 μl sample loop and a Waters 474 scanning fluorescence detector. The system and the data management were controlled by Millennium software from Waters. The stationary-phase column was a Waters Nova-Pack C₁₈ 3.9 × 150 mm i.d., 4 μm particle diameter.

The excitation λ_{ex} and emission λ_{em} maxima of each PCB, in the presence of surfactant, were determined

using a Perkin–Elmer luminescence spectrophotometer, model LS-50 (photomultipliers L2251300 and L2251301, sample and reference, respectively). Excitation and emission slits of 5 nm were used.

A thermostatted bath (model Tectron 200) and a centrifuge (model Mixtasel) from Selecta, were also used.

2.3. Procedure

2.3.1. Cloud-point determination

The cloud-point of different solutions of surfactant, in a range of concentrations 0.05–3% (w/v) for Brij 30 and 0.05–5% (w/v) for Brij 97, was determined by heating in a thermostatted bath and increasing the temperature up to 5°C after every 15 min until turbidity and the consequent phase separation were observed.

2.3.2. Ratio of phases

The ratio between the volume of the aqueous phase (V_w) and the volume of the surfactant-rich phase (V_s), i.e. (V_w/V_s), was determined for several solutions containing different surfactant concentrations.

2.3.3. Preconcentration

Aliquots of 10 ml, with the analyte in the presence of 2% (w/v) aqueous surfactant solutions, were kept in a thermostatically controlled bath for 15 min at 100°C for both surfactants. Separation of the two phases was achieved by centrifuging for 5 min at 1921 g. The initial concentration of the analyte was 30–360 ng ml⁻¹ and after preconcentration and extraction, the concentration was in the range 0.3–3.6 μg ml⁻¹.

2.3.4. Liquid chromatographic analysis with fluorescent detection

Once an adequate volume of surfactant-rich phase was extracted with a microsyringe, the separation and determination of PCBs were carried out by directly injecting 20 μl of this phase into the liquid chromatograph and monitoring the relative intensity of fluorescence at the maximum λ_{em} and λ_{ex} for each PCB under study. λ_{em} and λ_{ex} were previously determined, using solutions containing a known concentration of

Table 1
Fluorescent wavelength maxima (nm) of PCBs in 2% (w/v) aqueous solutions of Brij 30 and Brij 97

No.	Name	A ^a	Brij 30		Brij 97	
			λ_{ex}	λ_{em}	λ_{ex}	λ_{em}
1	Biphenyl	BP	247	315	246	315
2	4-Chlorobiphenyl	MonoBP	254	321	254	321
3	4,4'-Dichlorobiphenyl	DiBP	258	326	258	324
4	3,4,4'-Trichlorobiphenyl	TriBP	259	328	264	328
5	3,3',4,4'-Tetrachlorobiphenyl	TetraBP	262	330	261	330
6	3,3',4,4',5-Pentachlorobiphenyl	PentaBP	258	360	264	329
7	3,3',4,4',5,5'-Hexachlorobiphenyl	HexaBP	265	338	256	353

^a Abreviation.

PCB in the presence of 2% (w/v) aqueous solutions of the chosen surfactant (Table 1.)

The chromatographic conditions were established in a methanol : water (85 : 15, v/v) mobile phase and 1 ml min⁻¹ flow rate, which allowed efficient separation of seven PCBs.

2.3.5. Determination of PCBs in sea water

Prior to the determination, sea water was passed successively through filters of different porosity (0.45 and 0.22 μ m) and ultraviolet radiation to avoid the possible interference of marine microorganisms. Solutions of 10 ml containing 5 ml of sea water

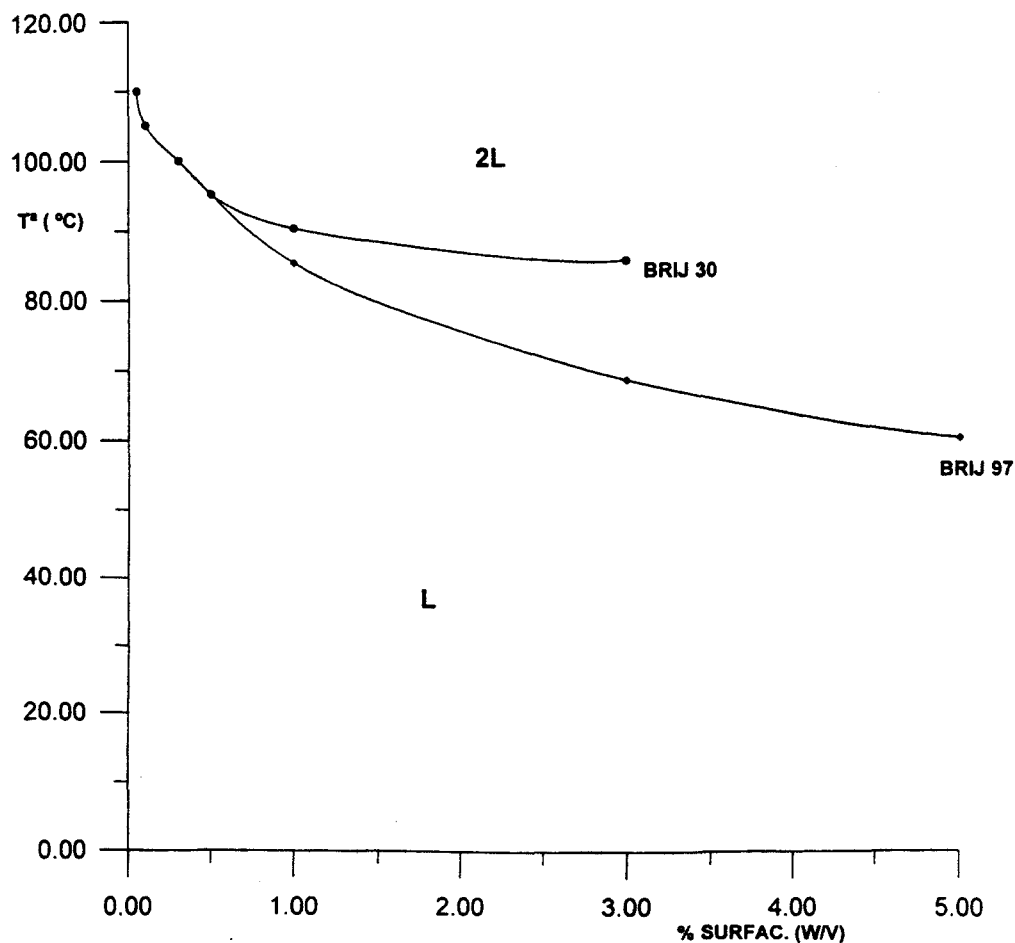


Fig. 1. Phase diagram for Brij 30 (1) and Brij 97 (2). The region above the cosolution curve is a two phase region (2L).

and 2% (w/v) surfactant were spiked with suitable amounts of PCBs and analysed according to the established CPE method.

3. Results and discussion

3.1. Phase diagram

When non-ionic surfactant solutions are heated above the cloud-point temperature, the micellar solution separates in two phases. When we plot cloud-point values against the percentage (w/v) of surfactant in solution, the figure shows a co-solution curve, above which the two phases appear. Fig. 1. shows the phase diagram for Brij 30 and Brij 97. The co-solution curves are similar for both surfactants under study, first showing a sharp drop in the temperature up to a concentration of 2% (w/v) above which the cloud-point temperature is fairly constant. These diagrams are quite similar to the phase diagrams, expected for non-ionic surfactant [16,18].

According to the results obtained, the critical temperature of the cloud-point for Brij 30 is $95 \pm 1^\circ\text{C}$ and $85 \pm 1^\circ\text{C}$ for Brij 97.

3.2. Optimization of the preconcentration factor

The theoretical preconcentration factor depends on the volume of the surfactant-rich phase, which at the same time varies with the surfactant concentration in solution.

Table 2
Relationship between volume ratio (V_w/V_s) for different concentrations of Brij 30 and Brij 97

Surface conc. (% w/v)	V_w/V_s Brij 30	V_w/V_s Brij 97
0.05	^a	65.7
0.10	^a	49.0
0.30	99.0	27.6
0.50	65.7	24.0
1.00	39.0	9.0
3.00	32.3	8.1
5.00	^b	7.4

^a The surfactant-rich phase has a volume too small to be measured.

^b This concentration was too high to be obtained for this surfactant.

There are different parameters that can alter the extraction process, and, due to this, the preconcentration factor too. To obtain the relationship between the preconcentration factor and these parameters, a study of the factors that may have an influence on the extraction process for PCBs was carried out.

3.2.1. Effect of the concentration and volume of surfactant

The study was carried out to determine the influence of these two variables: one keeping the added volume of surfactant constant but varying the final concentra-

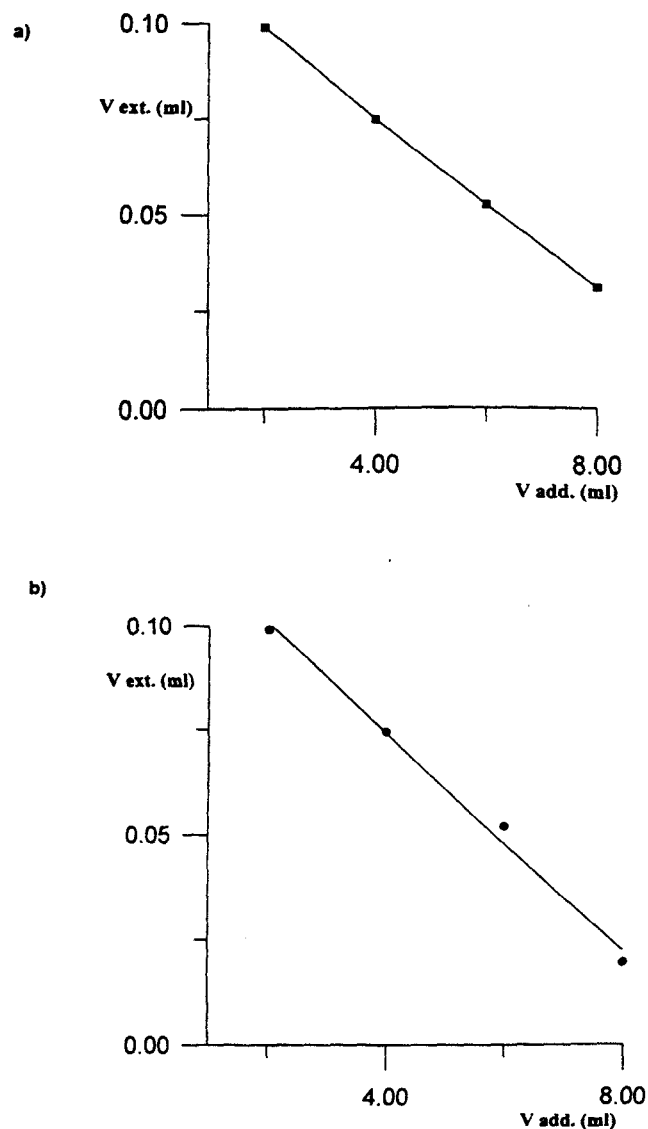


Fig. 2. Influence of the added volume of surfactant to the solution in the extracted volume of surfactant-rich phase. (a) Brij 30, (b) Brij 97.

tion in solution, and another varying the added volume of surfactant in solution and keeping the final concentration constant.

When the concentration of surfactant in solution varies in the range 0.05–5% (w/v), a decrease in the volume ratio (V_w/V_s) for both surfactants can be observed, it being more important for Brij 30. Once

the concentration is above 1%, the ratio decreases more slowly (Table 2). This shows that the smaller the concentration of surfactant, the higher are the pre-concentration factors; but when the volume of surfactant-rich phase is small, the extraction process becomes more difficult, and the accuracy and reproducibility probably suffer. To establish an adequate

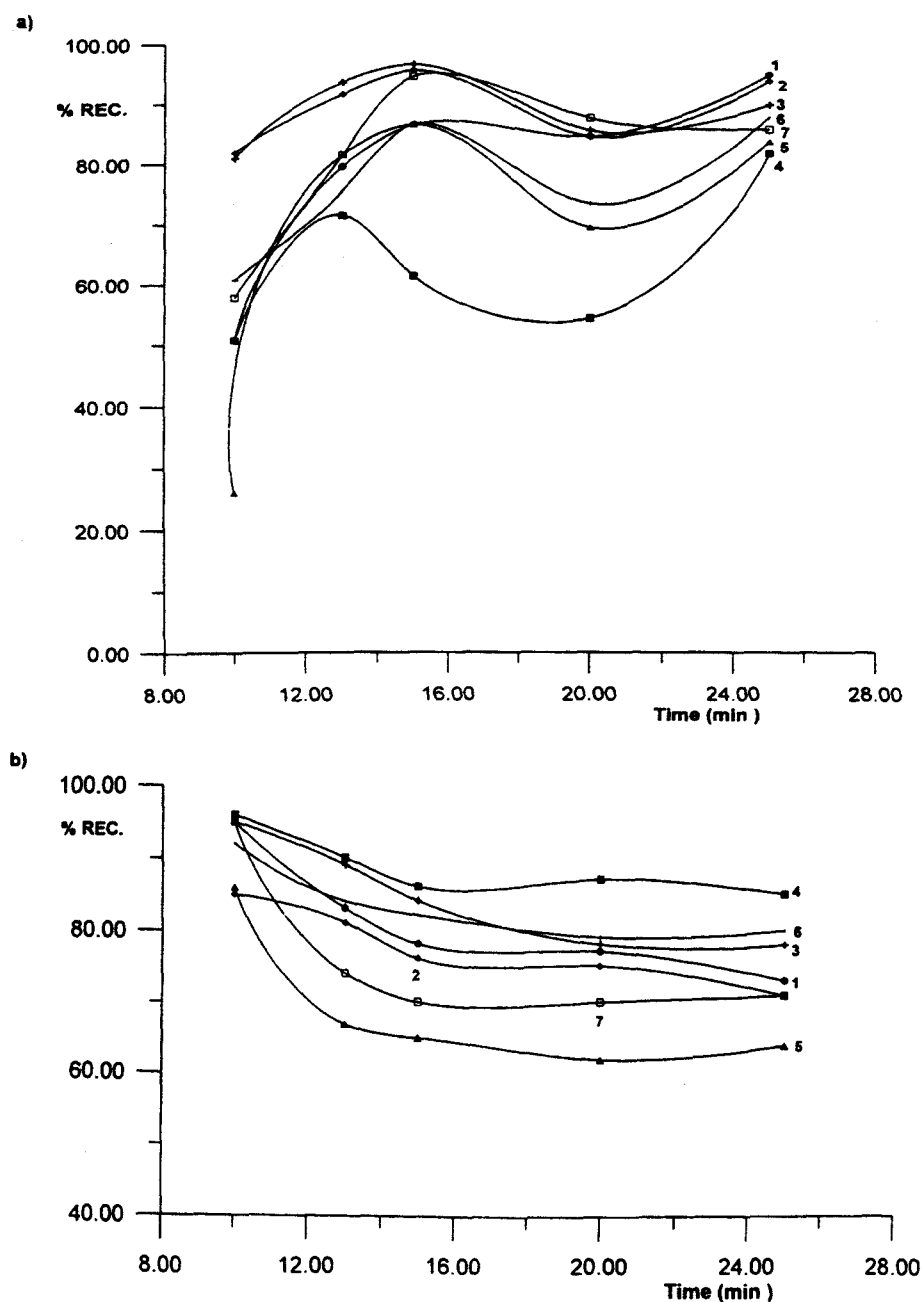


Fig. 3. Influence of equilibration time on recovery of PCBs using: (a) Brij 30 and (b) Brij 97. 1, BP; 2, MonoBP; 3, DiBP; 4, TriBP; 5, TetraBP; 6, PentaBP; 7, HexaBP.

relation between the concentration of surfactant in solution and the extracted surfactant-rich phase, a concentration of 2% (w/v) was chosen.

When we vary the volume of added surfactant to the solution, keeping the final concentration of surfactant constant, the extracted surfactant-rich phase volume decreases linearly as the added volume increases. Fig. 2 shows this linearity, similar for both surfactants. A volume of 4 ml of surfactant was considered as the most adequate to add to the solution.

3.2.2. Effect of the equilibration time

Surfactants can exhibit different behaviours when the equilibration time varies. To obtain appropriate recovery percentages for the analytes, a study to determine the optimum equilibration time was carried out.

For Brij 30, the surfactant exhibits a similar behaviour for all the PCBs for the concentration range

Table 3

Variation of the extracted volume (ml) of surfactant-rich phase with the addition of different concentration of KNO_3

KNO_3 (% w/v)	Brij 30	Brij 97
1	0.3	0.8
3	0.3	0.8
5	0.3	0.8
7	0.3	0.8
10	0.2	0.7

studied. Fig. 3(a) shows an increase in the recovery percentage with time up to a maximum of 15 min decreasing for 20 min and going up again at 25 min.

In the case of Brij 97 (Fig. 3(b)), the best recovery percentage is obtained at 10 min, decreasing slightly up to 15 min, and being practically constant for longer

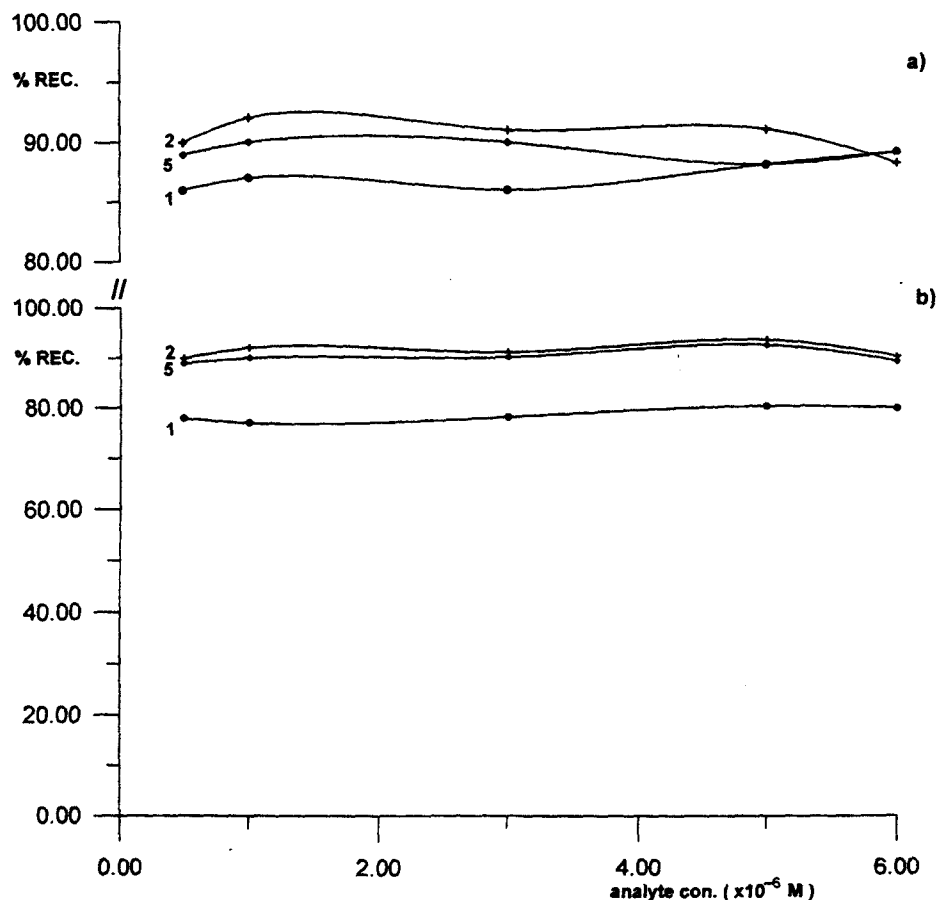


Fig. 4. Influence of the initial concentration of analyte in solution on the recovery. (a) Brij 30, (b) Brij 97. 1. BP; 2. MonoBP; 5. TetraBP.

duration. All the PCBs studied exhibited the same behaviour for the concentration range studied.

3.2.3. Effect of the ionic strength

It is known that the addition of salt to the solution can influence the extraction process. To study the influence of the ionic strength, different percentages of KNO_3 (1–10% w/v) were added to the solution. The extracted volumes of the surfactant-rich phase for the different solutions containing different percentages of KNO_3 are listed in Table 3 for individual surfactant.

These results are in concordance with similar studies carried out by other authors. The results indicate that an increase in the ionic strength does not have an appreciable influence on the final volume of the extracted surfactant-rich phase. Nevertheless, the addition of this inert salt facilitates the separation

of the two phases, because it increases the density of the bulk aqueous phase [19,20].

3.2.4. Effect of the analyte concentration

To determine the effect of the initial concentration of analyte in solution, solutions containing different concentrations of PCBs were subjected to the CPE procedure. The results indicate that the recovery percentages do not vary to a great extent for Brij 30 (Fig. 4(a)) and Brij 97 (Fig. 4(b)) when the analyte concentration varies between $0.46\text{--}175\text{ ng ml}^{-1}$ ($0.3\text{--}6.0 \times 10^{-6}\text{ M}$). This characteristic allows one to use this methodology without taking into account the initial concentration of the analyte in solution. Thus, CPE can be applied to solutions in which the initial concentration of PCBs is unknown.

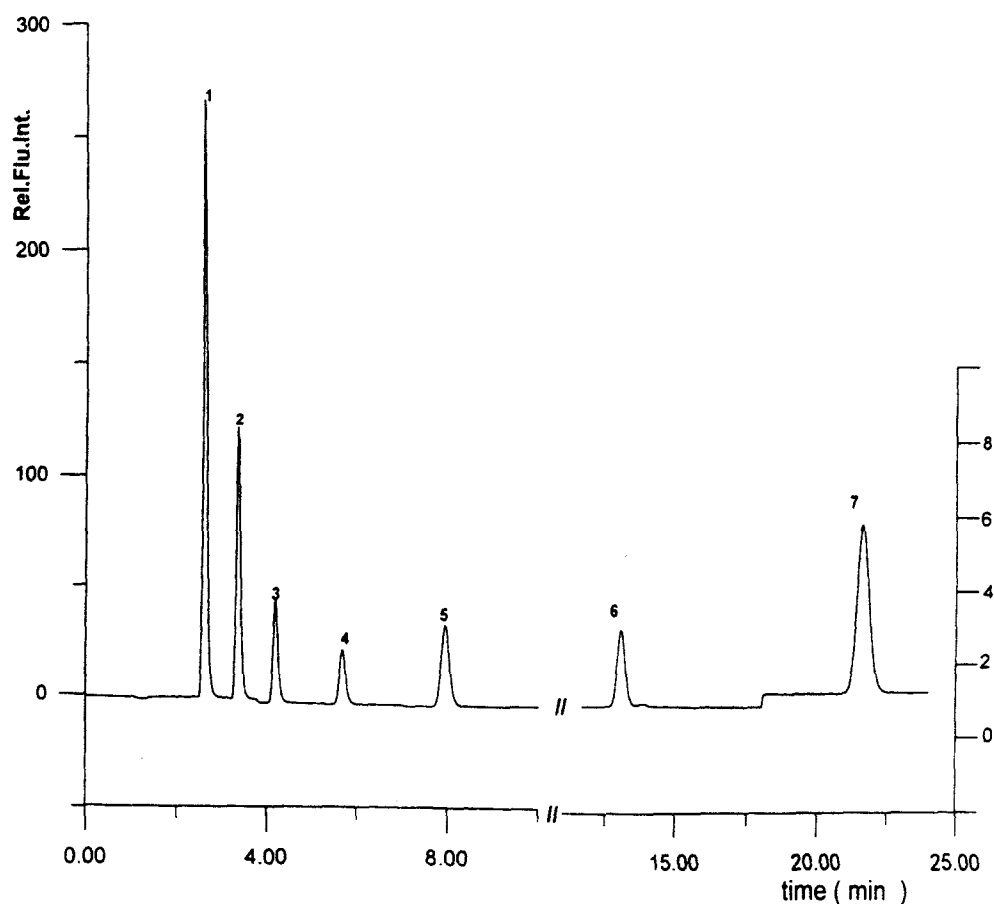


Fig. 5. Elution of a mixture of seven PCBs using 2% (w/v) Brij 30. 1, BP; 2, MonoBP; 3, DiBP; 4, TriBP; 5, TetraBP; 6, PentaBP; 7, HexaBP. Concentration of each PCB: 500 ng ml^{-1} ; Eluent: methanol : water (85 : 15, v/v); Flow rate: 1.0 ml min^{-1} .

Table 4
Linear calibration parameters for the determination of PCBs by CPE
(a)

PCB	Conc. (ng ml ⁻¹)	Brij 30		Brij 97	
		a ^a (×10 ⁻⁵)	b ^b (×10 ⁻⁴)	a ^a (×10 ⁻⁵)	b ^b (×10 ⁻⁴)
BP	308.0–1542.0	2.520	2.200	2.260	4.850
MonoBP	377.4–1887.0	1.270	4.270	1.390	4.300
DiBP	446.2–2231.0	0.569	1.120	1.440	0.158
TriBP	515.2–2576.0	0.380	1.050	0.278	2.010
TetraBP	584.2–2920.0	0.771	0.383	0.154	0.198
PentaBP	652.8–3264.0	0.068	0.290	0.243	0.852
HexaBP	720.8–3604.0	0.224	0.371	0.088	0.012

(b)

PCB	Conc. (µg ml ⁻¹)	Brij 30		Brij 97	
		a ^a (×10 ⁻⁴)	b ^b (×10 ⁻⁴)	a ^a (×10 ⁻⁴)	b ^b (×10 ⁻⁴)
BP	3.1–12.3	1.830	8.940	1.830	5.080
MonoBP	3.8–15.1	0.797	7.010	0.815	4.900
DiBP	4.5–17.8	0.418	1.540	0.486	2.270
TriBP	5.1–20.6	0.282	2.880	0.210	-0.081
TetraBP	5.8–23.4	0.651	-0.378	0.579	3.900
PentaBP	6.5–26.1	0.062	-0.031	0.197	0.411
HexaBP	7.2–28.8	0.154	1.070	0.126	-0.103

^a Slope, arbitrary units.^b Intercept, arbitrary units.

Table 5
Recovery obtained for each PCB after CPE and chromatographic determination

PCB	Conc. 3.1–28.8 µg ml ⁻¹		Conc. 308–3604 ng ml ⁻¹	
	Brij 30 Recovery (%) ^a	Brij 97 Recovery (%) ^a	Brij 30 Recovery (%) ^a	Brij 97 Recovery (%) ^a
BP	95	95	92	78
MonoBP	96	85	92	93
DiBP	97	95	93	83
TriBP	82	96	96	87
TetraBP	87	86	88	92
PentaBP	88	92	98	85
HexaBP	95	95	97	76

^a Referred to the initial concentration of PCB in solution.

Table 6
Relative standard deviation and detection limit for PCBs

PCB	Brij 30		Brij 97	
	RSD ^a (%)	LOD ^b (ng ml ⁻¹)	RSD ^a (%)	LOD ^b (ng ml ⁻¹)
BP	0.54	1.54	0.16	0.70
MonoBP	0.37	1.89	0.45	0.94
DiBP	0.27	2.23	0.52	1.10
TriBP	0.42	7.71	0.27	2.57
TetraBP	0.49	2.92	0.66	2.92
PentaBP	0.36	16.30	0.58	16.30
HexaBP	0.61	10.82	0.56	18.04

^a Relative standard deviation, in the range of Table 4(a), n=6.^b Limit of detection.

Table 7
Determination of PCBs in sea water

PCB	Added (ng ml ⁻¹)	Found ^a (ng ml ⁻¹)	Recov. (%)	Added (ng ml ⁻¹)	Found ^a (ng ml ⁻¹)	Recov. (%)	Added (μg ml ⁻¹)	Found ^a (μg ml ⁻¹)	Recov. (%)	Added (μg ml ⁻¹)	Found ^a (μg ml ⁻¹)	Recov. (%)
<i>(a) Arinaga-SE</i>												
<i>Brij 30</i>												
BP	46.0	40.0	86.0	92.0	81.0	88.0	0.46	0.40	87.0	0.92	0.84	91.0
MonoBP	57.0	57.5	101.0	113.0	105.1	93.0	0.57	0.53	92.0	1.13	0.99	88.0
DiBP	67.0	62.3	93.0	134.0	111.2	83.0	0.67	0.61	91.0	1.34	1.38	103.0
TriBP	77.0	76.0	99.0	145.0	131.9	91.0	0.77	0.60	78.0	1.45	1.30	90.0
Tetra	88.0	73.0	83.0	175.0	157.5	90.0	0.88	0.90	102.0	1.75	1.70	97.0
PentaBP	98.0	93.0	95.0	196.0	184.2	94.0	0.98	0.89	91.0	1.96	1.57	80.0
HexaBP	108.0	94.0	87.0	216.0	179.3	83.0	1.08	1.06	98.0	2.16	2.03	94.0
<i>Brij 97</i>												
BP	46.0	42.3	92.0	92	75.4	82.0	0.46	0.37	82.0	0.92	0.85	92.0
MonoBP	57.0	53.6	94.0	113	108.5	96.0	0.57	0.52	91.0	1.13	0.93	82.0
DiBP	67.0	55.6	83.0	134	123.3	92.0	0.67	0.54	81.0	1.34	1.41	105.0
TriBP	77.0	64.7	84.0	145	119.0	82.0	0.77	0.61	79.0	1.45	1.30	90.0
Tetra	88.0	82.0	93.0	175	166.2	95.0	0.88	0.74	84.0	1.75	1.50	86.0
PentaBP	98.0	93.1	95.0	196	205.8	105.0	0.98	1.02	104.0	1.96	1.80	92.0
HexaBP	108.0	94.0	87.0	216	218.2	101.0	1.08	1.10	102.0	2.16	1.88	87.0
<i>(b) Agaete-NW</i>												
<i>Brij 30</i>												
BP	46.0	41.1	90.0	92.0	73.6	80	0.46	0.38	83.0	0.92	0.85	92.0
MonoBP	57.0	51.9	91.0	113.0	106.2	94	0.57	0.60	106.0	1.13	1.20	106.0
DiBP	67.0	61.6	92.0	134.0	130.0	97	0.67	0.69	103.0	1.34	1.37	102.0
TriBP	77.0	64.0	83.0	145.0	114.5	79	0.77	0.75	97.0	1.45	1.38	95.0
Tetra	88.0	93.3	106.0	175.0	159.2	91	0.88	0.82	93.0	1.75	1.68	96.0
PentaBP	98.0	94.1	96.0	196.0	174.4	89	0.98	0.90	92.0	1.96	1.92	98.0
HexaBP	108.0	86.4	80.0	216.0	220.3	102	1.08	0.90	83.0	2.16	1.94	90.0
<i>Brij 97</i>												
BP	46.0	46.9	102.0	92.0	82.8	90.0	0.46	0.38	83.0	0.92	0.87	95.0
MonoBP	57.0	51.3	90.0	113.0	105.1	93.0	0.57	0.51	90.0	1.13	1.16	103.0
DiBP	67.0	71.0	106.0	134.0	116.6	87.0	0.67	0.70	104.0	1.34	1.15	86.0
TriBP	77.0	77.0	100.0	145.0	130.5	90.0	0.77	0.79	103.0	1.45	1.39	96.0
Tetra	88.0	70.4	80.0	175.0	145.2	83.0	0.88	0.79	90.0	1.75	1.71	98.0
PentaBP	98.0	87.2	89.0	196.0	151.0	77.0	0.98	0.81	83.0	1.96	1.84	94.0
HexaBP	108.0	102.6	95.0	216.0	200.9	93.0	1.08	0.94	87.0	2.16	1.94	90.0

^a Mean of three determinations, referred to the initial concentration of PCB in solution.

3.3. Cloud-point preconcentration and liquid chromatographic analysis

Once the parameters for the optimum extraction and preconcentration were established, the appropriate conditions for the separation of PCBs by liquid chromatography (LC) and their subsequent determination with fluorescence detection were studied.

There are two important factors to be taken into account in LC separations: the time of analysis, and a good separation of analytes. The results show that a methanol : water (85 : 15, v/v) mobile phase is the most adequate for this study. The chromatogram obtained for the mixture of selected PCBs in Brij 30, using this mobile phase can be observed in Fig. 5.

The corresponding calibration graphs for each PCB were obtained by duplicate injection of the sample containing 2% (w/v) of surfactant and the corresponding PCB concentration. Two different ranges were studied: 1308–3600 ng ml⁻¹ and 3.0–29.0 µg ml⁻¹. In each calibration, a linear relationship between fluorescence signal and concentration of analyte was found for all the analytes with high correlation coefficients (0.999). Table 4 lists the calibration characteristics of the method.

In order to check the recoveries obtained by the CPE method, different mixtures of PCBs were prepared in 10 ml of 2% (w/v) aqueous solutions of Brij 30 and Brij 97. After the CPE, 20 µl of the extracted surfactant-rich phase was injected directly into the chromatographic system. The data obtained, listed in Table 5, show excellent recoveries for the analytes studied: 82–98% for Brij 30 and 76–96% for Brij 97.

Although the recovery percentages obtained for Brij 30 are little higher than for Brij 97, the use of the former surfactant presents a disadvantage: when the CPE methodology is carried out using Brij 30, a great preconcentration factor can be obtained, but the surfactant-rich phase has a small volume which can make the separation of the two phases and the manipulation of the sample difficult.

The limits of detection [21] calculated for the different PCBs in both surfactants, using CPE methodology, are listed in Table 6, together with the relative standard deviation for six samples to which the complete procedure (cloud-point preconcentration

and extraction and chromatographic separation) was applied for all the compounds studied in 2% (w/v) Brij 30 and Brij 97 solutions.

3.4. Analytical applications

Once optimized, the proposed method was applied to the determination of PCBs in sea water from different areas around the Canary Islands (Arinaga-SE and Agaete-NW), previously spiked with suitable amounts of PCBs. The results shown in Table 7 indicate satisfactory recovery data. The recovery percentages obtained for sea water are similar to those obtained by other authors in different matrices [14].

Acknowledgements

This work was supported by funds provided by D.G.I.C.Y.T. (Spain). Research Project No. PB94-0431.

References

- [1] C.S. Creaser, F. Krokos, J.R. Startin, *Chemosphere* 25 (1992) 1981.
- [2] J. Hernández García, Z. Sosa Ferrera, A. Bermejo Martín-Lázaro, J.J. Santana Rodríguez, *Anal. Letters* 27(7) (1994) 1355.
- [3] D.W. Armstrong, *Separation and Purification Method* 14(2) (1985) 213.
- [4] J.G. Dorsey, *Advances in Chromatography*, 27 (1987).
- [5] W.L. Hinze, E. Pramauro, *Critical Reviews in Analytical Chemistry* 24(2) (1993) 133.
- [6] W.L. Hinze, *Annali di Chimica* 77 (1987) 167.
- [7] R.G. Laughrin, *Advances in Liquid Crystals*, G.H. Brown, Ed., Academic Press: New York 3 (1978) 99.
- [8] T. Saitoh, W.L. Hinze, *Talanta* 42(1) (1995) 119.
- [9] H. Watanabe, H. Tanaka, *Talanta* 25 (1978) 585.
- [10] C. García Pinto, J.L. Pérez Pavón, B. Moreno Coedero, *Analytical Chemistry* 67 (1995) 2606.
- [11] Y. Gotlieb, J.W. Bozzelli, E. Gotlieb, *Separation Science and Technology* 28(1)–3 (1993) 793.
- [12] C. García Pinto, J.L. Pérez Pavón, B. Moreno Cordero, *Journal of Analytical Atomic Spectrometry* 11 (1996) 37.
- [13] E. Pramauro, *Annali di Chimica* 80 (1990) 101.
- [14] B. Fröschl, G. Stangl, R. Niessner, *Fresenius J. Anal. Chem.* 257 (1997) 743.
- [15] R.P. Frankewich, W.L. Hinze, *Anal. Chem.* 66 (1994) 944.

- [16] A. Eiguren Fernández, Z. Sosa Ferrera, J.J. Santana Rodríguez, *Química Analítica* in press.
- [17] W.N. Maclay, *Journal of Colloid Science* 11 (1956) 272.
- [18] E. Pramauro, E. Pelizzetti, *Trends in Analytical Chemistry* 7(7) (1988) 260.
- [19] W.J. Horvath, C.W. Huie, *Talanta* 39 (1992) 487.
- [20] G. Alcaraz, J.P. Kivet, N. Kumai, S.A. Wark, H. Metzger, *J. Biol. Chem.* 259 (1984) 14922.
- [21] S. Lindsay, *High Performance Liquid Chromatography*, John Wiley and Sons, New York (1992) 71, 72.

Influence of plant growth regulators, polyamines and glycerol interaction on growth and morphogenesis of carposporelings of *Grateloupia* cultured *in vitro*

Pilar Garcia-Jimenez, Marta Rodrigo & Rafael R. Robaina*

Departamento de Biología, Universidad de Las Palmas G.C., Campus de Tafira, 35017 Las Palmas G.C., Canary Islands, Spain

Received 6 June 1997; revised 16 February 1998; accepted 16 February 1998

Key words: carposporeling, cell and tissue culture, glycerol, *Grateloupia doryphora*, macroalga, plant growth regulators, polyamines, Rhodophyta

Abstract

The influence of the plant growth regulators 2,4-D, GA₃, BA and kinetin, and the polyamines putrescine, spermidine and spermine were tested on axenic *in vitro* cultures of carposporelings of *Grateloupia doryphora*. The auxin 2,4-D (10⁻³ M) and the polyamine spermine (10⁻⁶ M and 10⁻³ M) induced a callus (disorganised cell mass that arose from the organised tissue of the carposporeling, as demonstrated by microscopic monitoring of the tissue). Putrescine and spermidine (10⁻³ M) transformed the carposporelings into cell masses that produced shoots. BA (10⁻³ M) and kinetin (10⁻⁶ M and 10⁻³ M) were inhibitory. In 10⁻¹ M glycerol-containing culture medium, which is known to induce the formation of morphogenic cell masses, the addition of GA₃ (10⁻³ M) resulted in the inhibition of the morphogenesis (i.e. shoot emission) in the cell mass. The kinetin at 10⁻⁶ M inhibited morphogenesis, whilst at 10⁻³ M inhibited even the formation of the cell masses. The combination of glycerol (10⁻¹ M) and the auxin 2,4-D (10⁻⁶ and 10⁻³ M) or the polyamines putrescine, spermidine and spermine (10⁻⁶ and 10⁻³ M) resulted in a bigger size of the cell masses that led to a higher amount of shoots per cell mass than in glycerol alone.

Abbreviations: 2,4-D – 2,4 dichlorophenoxyacetic acid; GA₃ – gibberellic acid; BA – benzylaminopurine; kin – kinetin; put – putrescine; spd – spermidine; spm – spermine

Introduction

Organic carbon sources and plant growth regulators are basic tools for the *in vitro* propagation of macroalgae. It is normally understood that the organic carbon source supports carbon requirements for plant growth and development, and that the plant growth regulators may allow direction of the pattern of growth and development of the cells and tissues.

The carbon source by itself may alter the pattern of growth and development. In the red alga *Grateloupia doryphora*, we reported (Robaina et al., 1990b) that glycerol stimulated morphogenesis (shoot emission) in thallus explants. Glycerol also promoted growth (elongation and high cell division rate) and morphogenesis that transforms carposporelings of *G. doryphora*

into morphogenic cell masses (Garcia-Jimenez et al., 1996).

Auxins, cytokinins and gibberellins have been reported to occur endogenously in algae (Bradley, 1991; Evans & Trewavas, 1991). Polyamines, like putrescine, spermidine and spermine, are ubiquitous substances that can be found in algae, animals and plants. In plants they have an effect resembling that of the plant growth regulators (Galston & Kaur-Sawhney, 1982; Smith, 1982 and references therein, 1985; Tiburcio et al., 1993), being associated with cell division in tissue (Evans & Malmberg, 1989).

The aim of this work was to study the influence of the addition of plant growth regulators (auxin, cytokinins, gibberellins) and the polyamines putrescine, spermidine and spermine on the growth

and morphogenesis of carposporelings cultured in glycerol-containing media.

Materials and methods

Thalli of *Grateloupia doryphora* (Sheet 129 of the LPA herbarium) were collected in the upper and middle part of the coastal zone of Gran Canaria (Canary Islands). Fertile material bearing cystocarps were cut to 3 mm diameter, disinfected and tested for sterility following methods which ensured that explants and the carpospores subsequently released were axenic. Sterile and fertile disc fragments were then cultured in agarised Provasoli Enriched Seawater (PES, Provasoli, 1968) for 1 month until carpospores were liberated (Garcia-Jimenez et al., 1996). Culture conditions were $30 \mu\text{mol photon m}^{-2} \text{s}^{-1}$ light intensity from cool white fluorescent lamps (Sylvania grolux), a 18:6 h light: dark cycle, $18 \pm 2^\circ\text{C}$.

All experiments were carried out with 1-month old carposporelings (12 to 20 per Petri dish, ca. 45 per treatment) which were recultured every 15 d (3 recultures). Glycerol-containing media were prepared with an enriched seawater medium based on PES which was supplemented with 10^{-1} M of glycerol + 0.8% agar in water made by dilution of the seawater with distilled water (90% seawater, PES90- glycerol: Robaina et al., 1990b). The osmolality of the medium was 1 osmol kg^{-1} as checked in an AutostatTM osmometer (Dai-ichi kogaku Co. Ltd, Tokyo, Japan).

To examine the effects of plant growth regulators, we used cytokinins, benzylaminopurine (BA) and kinetin (kin); gibberellins and gibberellic acid (GA_3); auxins as 2,4 dichlorophenoxyacetic acid (2,4-D) and polyamines putrescine (put), spermine (spm) and spermidine (spd) at final concentrations of 10^{-3} and 10^{-6} M. They were added individually to autoclaved cultured medium as filter-sterilised stock solutions. All chemicals were from the Sigma Chemical Company. To ensure that results were caused by the addition of plant growth regulators, control assays with PES, PES + plant growth regulators (or plus polyamines) and PES90-glycerol without growth regulators (or polyamines) were run simultaneously.

Three specimens from each treatment were fixed with 2.5% glutaraldehyde in 10^{-1} M sodium cacodylate buffer containing 0.3 M NaCl (pH 7.4) for 4 h at room temperature. This was followed by washing in the same buffer containing 0.3 M NaCl (2×30 min) and embedded in glycol methacrylate (GMA, Historesin

TM, Reichert-Jung, Gerrids & Smid, 1983). Serial sections $5\text{-}\mu\text{m}$ thick were cut on a Reichert-Jung 2050 microtome and stained for the observation of general morphology with toluidine blue and haematoxylin-eosin (Tsekos, 1983).

The experiments were repeated twice with three replicates of each treatment. Two quantitative indices were used: i) mass growth index as diameter of the cell mass in mm, determined by using an electronic caliper (Mitutoyo Digimatic Caliper, Mitutoyo Co.); and ii) morphogenic index as the number of protrusions or shoots regenerated per carposporeling (Robaina et al., 1990a, b; Robaina et al., 1992). Mean values of the index in the different treatments were compared to the control (PES90-glycerol) using student's t-test.

Results

The addition of the plant growth regulators or polyamines to the PES medium influenced the growth and development of the carposporelings: calli were observed in 10^{-3} M 2,4-D and in 10^{-6} M and 10^{-3} M spermine. Calli extended from the surface of the carposporeling as a disorganised mass of tissue to cover it almost entirely. Microscopy showed that a disorganised dense cellular mass formed the calli (Figure 1). Mass growth index reached 0.50 mm in callus in 10^{-3} M 2,4-D as the maximum value observed. 10^{-3} M BA and 10^{-6} and 10^{-3} M kinetin were inhibitory as the carposporeling did not develop further (even months after the experiments had finished). The carposporelings grew and transformed into small morphogenic cell masses (Figure 2) in the treatments with putrescine and spermidine alone at both concentrations tested. The morphogenic index ranged from 1.70 to 6.83 shoots per morphogenic carposporeling observed in media with polyamines. The cell masses resembled these typical of carposporelings grown in glycerol. In treatments with GA_3 the carposporelings formed new shoots (morphogenic index 3.5 ± 0.53 in 10^{-3} M). In PES, the carposporelings emitted 1–2 shoots (actually just the protrusion on the surface of the carposporeling, morphogenic index = 0–2 and mass growth index was 0.20 ± 0.1).

Table 1 shows the results as values of mass growth and morphogenic indices obtained from the combination of the carbon source (glycerol) and the plant growth regulators tested. When carposporelings of *G. doryphyora* were cultured in a glycerol-containing medium, glycerol first increased cell division, produc-

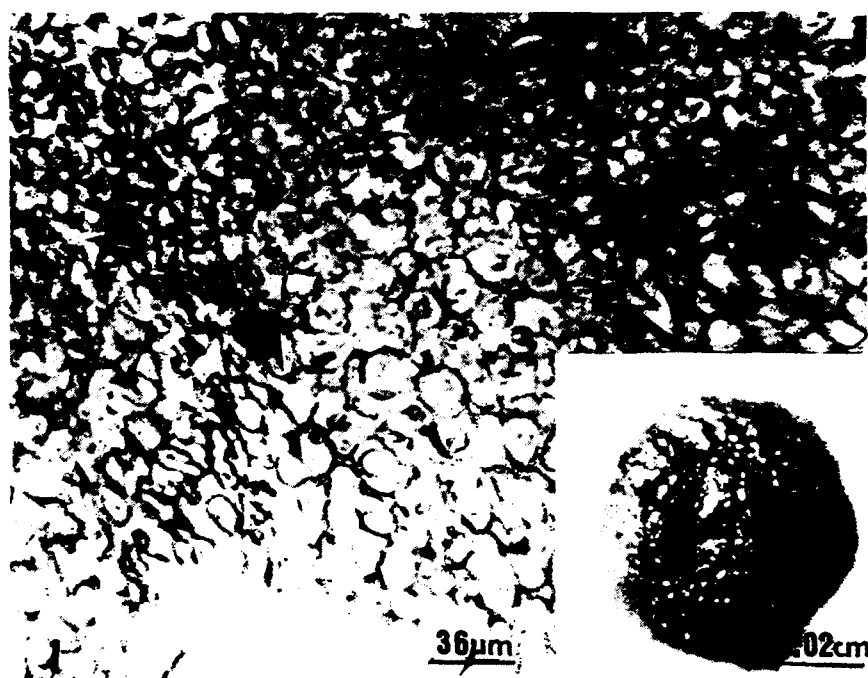


Figure 1. Callus formed by the carposporeling of *G. doryphora* cultivated in 10^{-3} M 2,4-D (lower right corner). Note the disorganised mass (arrow). Semithin sections ($5 \mu\text{m}$) stained with toluidine blue.

Table 1. Effect of plant growth regulators on carposporelings of *Grateloupia doryphora* when combined with glycerol. Data are the mean (\pm SD) from two experiments, each with three replicates.

Treatment	Diameter of the cell mass (mm)	Shoots per morphogenic carposporeling
10^{-1} M Glycerol	0.72 ± 0.08	9.83 ± 1.25
10^{-1} M Glycerol + 10^{-6} M 2,4-D	$0.90 \pm 0.15^*$	9.50 ± 4.34
10^{-1} M Glycerol + 10^{-6} M 2,4-D	$1.36 \pm 0.31^*$	$23.50 \pm 4.68^*$
10^{-1} M Glycerol + 10^{-6} M BA	0.75 ± 0.13	10 ± 4.9
10^{-1} M Glycerol + 10^{-3} M BA	Inhibitory	Inhibitory
10^{-1} M Glycerol + 10^{-6} M kin	0.72 ± 0.09	Non-morphogenic
10^{-1} M Glycerol + 10^{-3} M kin	Inhibitory	Inhibitory
10^{-1} M Glycerol + 10^{-6} M GA ₃	0.74 ± 0.07	Non-morphogenic
10^{-1} M Glycerol + 10^{-3} M GA ₃	0.64 ± 0.05	Non-morphogenic

* $P < 0.001$ as compared to control. Inhibitory = carposporeling appeared as they were at the beginning of the experiment.

ing the cell masses, and then the shoots were formed. The values of mass growth and morphogenic index in the glycerol-containing medium are higher than those obtained in plain PES or PES + plant growth regulators. The highest value for mass growth and morphogenic indices was observed in glycerol + 10^{-3} M 2,4-D among all treatments tested, included those of polyamines described below. The cell masses produced by this treatment were fully covered by sprouting shoots. The addition of 10^{-6} M kinetin or 10^{-6} and

10^{-3} M GA₃ to glycerol-containing media inhibited morphogenesis. The 10^{-3} M kinetin and 10^{-3} M BA inhibited both growth and morphogenesis.

Table 2 shows results obtained with glycerol plus polyamines. Except for 10^{-6} M putrescine and the slight increase in mass growth observed in 10^{-3} M spermidine, all the treatments with polyamines significantly increased cell growth and morphogenesis over the control with glycerol, as seen in the values of mass growth and morphogenic indices in Table 2. The effect

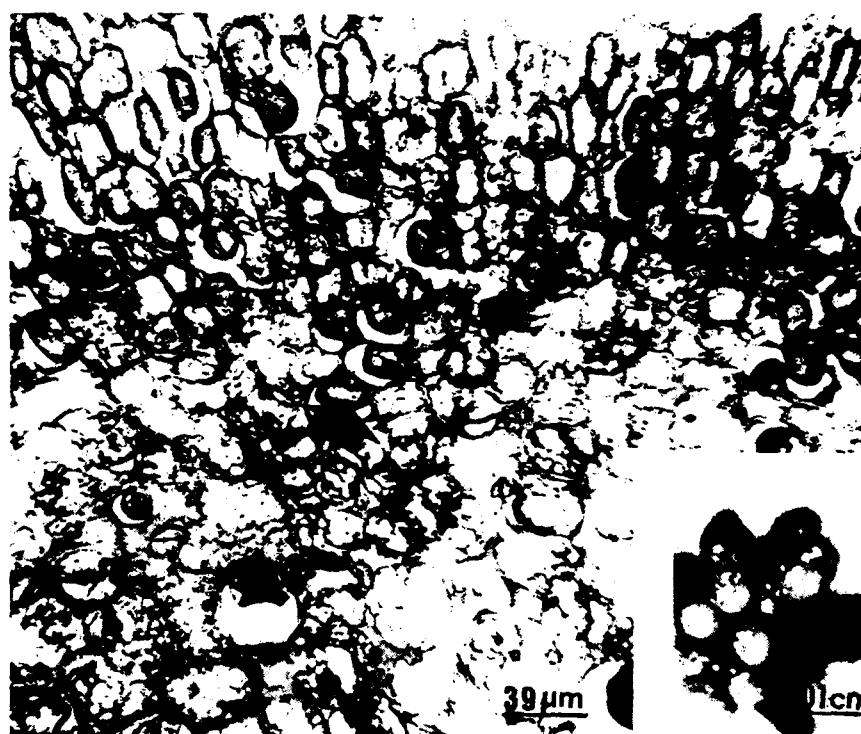


Figure 2. Cell mass formed by the carposporeling of *G. doryphora* in media with the polyamines, glycerol (10^{-1} M) and in glycerol + plant growth regulators or plus polyamines. Example shown is that observed in PES + 10^{-3} M put. Note the cells in organised arrangement (arrow). Semithin section ($5 \mu\text{m}$) stained with haematoxylin-eosin.

Table 2. Effects of polyamines on carposporelings of *Grateloupia doryphora* when combined with glycerol. Data are the mean (\pm SD) from two experiments each with three replicates.

Treatment	Diameter of cell mass (mm)	Shoots per morphogenic carposporeling
10^{-1} Glycerol	0.72 ± 0.08	9.83 ± 1.25
10^{-1} M Glycerol + 10^{-6} M put	0.63 ± 0.10	Non-morphogenic
10^{-1} M Glycerol + 10^{-3} M put	$0.91 \pm 0.15^*$	$14.7 \pm 4.65^*$
10^{-1} M Glycerol + 10^{-6} M spd	1.05 ± 0.32	$16 \pm 3.51^*$
10^{-1} M Glycerol + 10^{-3} M spd	0.83 ± 0.13	$12 \pm 1.86^*$
10^{-1} M Glycerol + 10^{-6} M spd	1.21 ± 0.17	$18 \pm 4.14^*$
10^{-1} M Glycerol + 10^{-3} M spd	$1.18 \pm 0.21^*$	$18.5 \pm 2.20^*$

* $P < 0.001$ as compared to control.

of the combination of polyamines and glycerol on growth and morphogenesis increased from the lowest concentration of putrescine to spermine. In addition, the calli observed when spermine was tested alone was not observed when combined with glycerol.

Discussion

The 2,4-D is a synthetic auxin able to induce cell division and growth even in the more recalcitrant plant

tissues (Evans et al., 1983). It has been reported to induce filament growth in *Ascophyllum* (Fries, 1991) and the growth of callus-like structures in *Grateloupia dichotoma* (Yokoya & Handro, 1996). In the present study, a callus sprouting from the carposporelings of *G. doryphora* was observed as a result of treatment with 10^{-3} M 2,4-D (Figure 1). The 2,4-D combined with glycerol increased growth and morphogenesis over glycerol and glycerol and the other plant regulators tested (Table 1). It should be mentioned that calli induced by 2,4-D and cell masses obtained in 2,4-

D + glycerol were further propagated in PES, where they regenerated shoots and apparently normal thalli in PES (26 calli of about 20 mg fresh weight produced up to 200 mg fresh weight thalli in 4 months). A combination of glycerol and plant growth regulators was reported to induce growth of the callus in *Gracilaria verrucosa* (Kaczyna & Megnet, 1993) although the auxin 2,4-D had no significant effect.

Result on Table 1 also show that cytokinins and gibberellins influenced on the effects of glycerol on growth and morphogenesis of the carposporelings. The 10^{-6} M kinetin and 10^{-6} and 10^{-3} M GA₃ tested inhibited the morphogenic effect of glycerol. At higher concentration (10^{-3} M), BA and kinetin inhibited both growth and morphogenesis.

Glycerol also influenced the effects of the plant growth regulators as compared when they were tested alone. Thus, callus was not observed when 2,4-D was combined with glycerol since the carposporelings became organised cell masses (compare Figure 1 to Figure 2), and the presence of glycerol relieved the inhibitory effect of the lowest (10^{-6} M) concentration of kinetin.

The causes of the interaction of glycerol and plant growth regulators (and polyamines, discussed below) remain to be explored. Nevertheless, it is interesting to note that when algae are supplied with organic substrates, the latter altered basic metabolic features and redirected them towards different end-products (Antia, 1980; Robaina et al., 1995). Carposporelings of *G. doryphora* accumulate floridean starch, phenolic and other unknown compounds in large electron-dense vesicles when cultured in glycerol (Garcia-Jimenez et al., 1996). Metabolic differences as the algae are grown with or without glycerol may result in different endogenous concentrations of plant growth regulators in the carposporelings, hence the exogenous addition of the same amount of a particular plant growth regulator would produce different effects in each case. Mooney and Van Staden (1986) argued explicitly that exogenous applied kinetin inhibited growth in algae due to the fact that supraoptimal concentrations were achieved.

There are few reports on the occurrence of polyamines in algae. Uptake and transport within the thallus were reported in *Ulva rigida* (Badini et al., 1994). The unicellular *Porphyridium* absorbed polyamines with the polysaccharides in the cell wall (Scoccianti et al., 1989; Scoccianti & Bagni, 1992). Cohen et al. (1984) found evidence that the polyamines promoted cell division in *Chlorella*. In the present

paper, carposporelings cultured in the presence of putrescine and spermidine grew and became cell masses (Figure 2) similar to those reported for glycerol (though smaller, see Figure 14 in Garcia-Jimenez et al., 1996). The polyamines combined to glycerol interacted to significantly increase growth and morphogenesis of the carposporelings in a concentration-dependent manner (Table 2). The strongest effect was obtained with the polyamine spermine, with which we have found the highest increase in mass growth and morphogenic indices. In fact, the results obtained with spermine were closed to those of the auxin 2,4-D, considering that both substances induced callus or enhanced cell growth and morphogenesis when combined with glycerol (Tables 1 and 2).

Several authors (Seraffini-Fracassini, 1991; Kotzabasis, 1996) have related the effects of polyamines to their contribution to cellular carbon and nitrogen. Although this possibility cannot be discarded as an explanation for our results, it is unlikely that the sole addition of 10^{-3} or 10^{-6} M of polyamines to 10^{-1} M glycerol would increase by itself the amount of organic carbon available for growth and morphogenesis. Our previous experiences have proved that carbon sources were ineffective below 10^{-1} M (Robaina et al., 1990b).

In conclusion, the cytokinins kinetin and BA and gibberellins GA₃ were inhibitory for growth and/or morphogenesis induced by glycerol in carposporeling cultured *in vitro*. The auxin 2,4-D (10^{-6} and 10^{-3} M) or the polyamines putrescine, spermidine and spermine (10^{-6} and 10^{-3} M) resulted in bigger cell masses that emitted higher amount of shoots per cell mass than in glycerol alone.

References

- Antia NJ (1980) Nutritional physiology and biochemistry of marine cryptomonads and chrysomonads. In Levandowsky M, Hunter SH (eds), *Biochemistry and Physiology of Protozoa*. Academic Press, New York: 67-115.
- Badini L, Pitocchi R, Bagni N (1994) Polyamine transport in the seaweed *Ulva rigida* (Chlorophyta). *J. Phycol.* 30: 599-605.
- Bradley PM (1991) Plant hormones do have a role in controlling growth and development of algae. *J. Phycol.* 27: 317-321.
- Cohen E, Shoshana A, Heimer YH, Mizrahi Y (1984) Polyamine biosynthetic enzymes in the cell cycle of *Chlorella*. *Plant Physiol.* 74: 385-388.
- Evans DA, Sharp WR, Ammirato PV, Yamada Y (1983) *Handbook of Plant Cell Cultures*. McMillan Publications, New York.
- Evans LV, Trewavas AJ (1991) Is algal development controlled by plant growth substances? *J. Phycol.* 27: 322-326.
- Evans PT, Malmberg RL (1989) Do polyamines have a role in plant development? *Ann. Rev. Plan. Physiol. Plant Mol. Biol.* 40: 235-269.

- Fries L (1991) Formation of filaments and single cells by the activity of meristoderm of axenic *Ascophyllum nodosum* (Fucaceae, Phaeophyta). *Phycologia* 30: 310–313.
- Galston AW, Kaur-Sawhney R (1982) Polyamines: are they a new class of plant growth regulators? In Wareing PF (ed), *Plant Growth Regulators*. Academic Press, New York: 451–461.
- Garcia-Jimenez P, Robaina RR, Luque A, Tsekos I (1996) Glycerol activated cellular division and biosynthetic activity during growth and morphogenesis of carpospore seedlings of *Grateloupia doryphora* (Cryptonemiales, Rhodophyta). *Phycologia* 35: 261–269.
- Gerrids PO, Smid L (1983) A new less toxic polymerization system for the embedding of soft tissue in glycol methacrylate and subsequent preparing of serial sections. *J. Microscopy* 132: 81–85.
- Kaczyna F, Megnet R (1993) The effects of glycerol and plant growth regulators on *Gracilaria verrucosa* (Gigartinales, Rhodophyta). *Hydrobiologia* 268: 57–64.
- Kotzabasis K (1996) A role for chloroplast-associated polyamines? *Bot. Acta* 109: 5–7.
- Mooney PA, Van Staden J (1986) Algae and cytokinins. *J. Plant Physiol.* 123: 1–21.
- Provasoli L (1968) Media and prospects for the cultivation of marine algae. In Watanabe A, Hattori A (eds), *Cultures and Collection of Algae*. Japanese Society of Plant Physiologist, Tokyo: 63–67.
- Robaina RR, Garcia-Jimenez P, Luque A (1992) The growth pattern and structure of callus from the red alga *Laurencia* sp. (Rhodophyta, Ceramiales) compared to shoot regeneration. *Bot. mar.* 35: 267–272.
- Robaina RR, Garcia-Jimenez P, Luque A (1996) Light and glycerol driven development of *Grateloupia doryphora* (Rhodophyta) *in vitro*. *Sci. mar.* 60: 283–289.
- Robaina RR, Garcia-Reina G, Luque A (1990a) The effects of the physical characteristics of the culture medium on the development of red seaweeds in tissue culture. *Hydrobiologia* 204/205: 137–142.
- Robaina RR, Garcia-Jimenez P, Brito I, Luque A (1995) Light control of the respiration of exogenous glycerol by the red macroalga *Grateloupia doryphora*. *Eur. J. Phycol.* 30: 81–86.
- Robaina RR, Garcia-Jimenez P, Garcia-Reina G, Luque A (1990b) Morphogenetic effect of glycerol on tissue cultures of the red seaweed *Grateloupia doryphora*. *J. Appl. Phycol.* 2: 137–143.
- Rodrigo M, Robaina RR (1997) Stress tolerance of photosynthesis in sporelings of the red alga *Grateloupia doryphora* as compared to that of stage III thalli. *Mar. Biol.* 128: 689–694.
- Scoccianti V, Bagni N (1992) *In vitro* interactions between polyamines and isolated *Porphyridium* sp. polysaccharides. *Plant. Physiol. Biochem.* 30: 135–138.
- Scoccianti V, Bagni N, Dubinsky O, Arad S (1989) Interaction between polyamines and cells of the marine unicellular red alga *Porphyridium* sp. *Plant Physiol. Biochem* 27: 899–904.
- Seraffini-Fracassini, D (1991) Polyamine biosynthesis and conjugation to macromolecules during the cell cycle of *Helianthus tuberosum* tuber. In Galston AW, Tiburcio A (eds), *Lecture Course on Polyamines as Modulators of Plant Development*. Fundación Juan March, Madrid, vol. 257: 40–45.
- Smith TA (1982) The function and metabolism of polyamines in higher plants. In Wareing PF (ed), *Plant Growth Regulators*. Academic Press, New York: 463–472.
- Smith TA (1985) Polyamines. *Ann. Rev. Plant Physiol.* 36: 117–143.
- Tiburcio AF, Campos JL, Figueras X, Besford RT (1993) Recent advances in the understanding of polyamine functions during plant development. *Plant Growth Regulation* 12: 331–340.
- Tsekos I (1983) The ultrastructure of carposporogenesis in *Gigartina teedii* (Gigartinales, Rhodophyceae): gonimoblast cells and carpospores. *Flora* 174: 191–211.
- Yokoya NS, Handro W (1996) Effects of auxins and cytokinins on tissue culture of *Grateloupia dichotoma* (Gigartinales, Rhodophyta). *Hydrobiologia* 326/327: 393–400.

ANALISIS GRAFICO DEL COMPORTAMIENTO DINAMICO DE PAUTAS ESPACIALES EN SISTEMAS DE REACCION-DIFUSION

J.L. GARCIA, I. FERNANDEZ y J.M. PACHECO

Univ. de las Palmas de Gran Canaria, Depto. de Matemáticas,, Campus de Tafira Baja, E-35017 Las Palmas - España

RESUMEN

En este artículo se presenta un estudio y análisis sobre el comportamiento dinámico de pautas espaciales generadas por sistemas de ecuaciones de reacción-difusión. Se estudió un modelo general de dos ecuaciones en dimensión espacial 1 y se consideró dos expresiones cinéticas para la reacción. Se propone un método gráfico para decidir acerca del movimiento espacial de las pautas obtenidas. Se encontró que el método propuesto describe adecuadamente el movimiento espacial.

GRAPHICAL ANALYSIS OF THE DYNAMIC BEHAVIOR OF SPATIAL PATTERNS IN REACTION-DIFFUSION SYSTEMS

ABSTRACT

The dynamic behavior of spatial patterns generated by reaction-diffusion systems has been analyzed and is presented in this article. A general model for the one-dimensional case was studied considering two kinetic expressions for the reaction. A graphical method is proposed in order to decide about the spatial translation of the obtained patterns. It was found that the proposed method is accurate for the description of the patterns movement.

Keywords: reaction-diffusion, spatial patterns, graphical methods, kinetics

MODELO CON PAUTAS ESPACIALES

Se trata de modelizar la evolución espacio-temporal de las concentraciones $X_1(x, t)$ y $X_2(x, t)$ de dos especies que interaccionan entre sí en presencia de una tercera, que actúa como catalizador. Esta última no reacciona con las otras. Restringimos aquí el problema al caso espacialmente unidimensional, considerándose que la difusión del catalizador está regida por un coeficiente constante, mientras que los coeficientes de difusión D_1 y D_2 dependen de la concentración del catalizador. Así el modelo puede escribirse (Murray, 1989):

$$\frac{\partial X_1}{\partial t} = \gamma f_1(X_1, X_2) + \frac{\partial}{\partial x} (D_1(X_3) \frac{\partial X_1}{\partial x}), \quad (1)$$

$$\frac{\partial X_2}{\partial t} = \gamma f_2(X_1, X_2) + \frac{\partial}{\partial x} (D_2(X_3) \frac{\partial X_2}{\partial x}), \quad (2)$$

$$\frac{\partial X_3}{\partial t} = -dX_3 + k \frac{\partial^2 X_3}{\partial x^2}. \quad (3)$$

El dominio espacio-temporal es $[0, 1] \times [0, \infty)$ y las condiciones de contorno son flujo cero para X_1 y X_2 en los extremos del intervalo, mientras que X_3 está sujeto a flujo cero en $x = 0$ y toma un valor constante en $x = 1$, esto es $X_3(1, t) = c$. X_3 alcanza un equilibrio estable en un periodo corto de tiempo en el cual las concentraciones X_1 y X_2 no cambian significativamente, por lo que la ecuación (3) puede ser reemplazada por la concentración de equilibrio de X_3 :

$$X_3(x) = c \frac{\text{Cosh}(x\sqrt{\frac{d}{k}})}{\text{Cosh}(\sqrt{\frac{d}{k}})}, \quad (4)$$

y el modelo se reduce a:

$$\frac{\partial X_1}{\partial t} = \gamma f_1(X_1, X_2) + \frac{\partial}{\partial x} (D_1(X_3(x)) \frac{\partial X_1}{\partial x}), \quad (5)$$

$$\frac{\partial X_2}{\partial t} = \gamma f_2(X_1, X_2) + \frac{\partial}{\partial x} (D_2(X_3(x)) \frac{\partial X_2}{\partial x}). \quad (6)$$

Una condición para la aparición de pautas desarrolladas espacialmente es que los coeficientes de difusión sean diferentes (Turing, 1952). En la práctica D_2 se toma como algún múltiplo mD_1 de D_1 , y aquí vamos a considerar que $D_1(X_3)$ es una función afín de X_3 , esto es:

$$D_1(X_3) = \alpha X_3 + \beta, \quad D_2 = mD_1, \quad (\alpha < 0, \beta > 0, m > 0). \quad (7)$$

Este modelo se ha estudiado anteriormente por los autores (García-Cortí *et al.*, 1996) mostrando que cumple las condiciones bajo las que se producen pautas espaciales. En el presente trabajo se analizará la existencia de bifurcaciones para el modelo con cinéticas de retroalimentación positiva y de activación-inhibición, siendo $\sqrt{d/k}$ el parámetro de bifurcación. El proceso de resolución consiste en linealizar en torno a un punto singular del sistema sin difusión y resolver el sistema así obtenido bajo la hipótesis de que posee soluciones de la forma:

$$X_1 = X_{10} + e^{\lambda t} Y_1(x), \quad (8)$$

$$X_2 = X_{20} + e^{\lambda t} Y_2(x). \quad (9)$$

Todos los cálculos, simbólicos y numéricos, de este trabajo han sido efectuados con Mathematica.

Se presentan dos versiones del sistema (1)(2)(3) con diferentes términos de reacción. El primero corresponde a la llamada cinética de Schnackenberg:

$$f_1 = w_1 - X_1 + X_1^2 X_2 \quad (10)$$

$$f_2 = w_2 - X_1^2 X_2 \quad (11)$$

En los experimentos numéricos realizados los parámetros elegidos son:

$\alpha = -1, \beta = 20, \gamma = 1000, c = 15, m = 10, w_1 = 0.1, w_2 = 0.9$ y $\sqrt{d/k} = 1$ para las figuras 1.a y 1.b, mientras $\sqrt{d/k} = 2$ para las figuras 1.c y 1.d.

El segundo es el sistema activador-inhibidor donde:

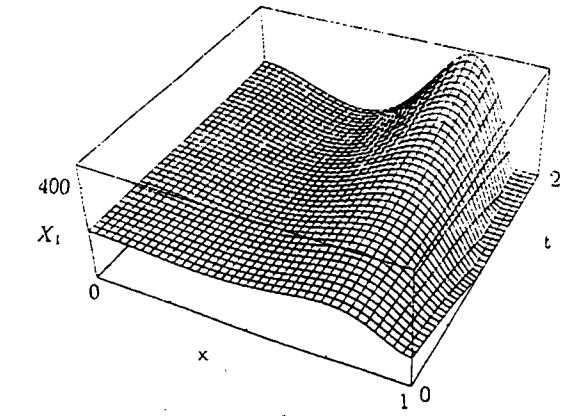
$$f_1 = w_1 - w_2 X_1 + \frac{X_1^2}{X_2(1 + \theta X_1^2)} \quad (12)$$

$$f_2 = X_1^2 - X_2 \quad (13)$$

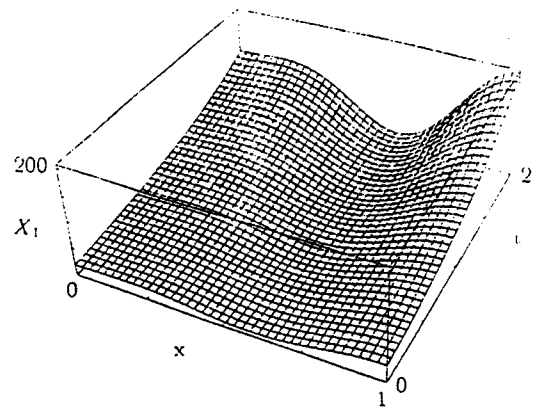
Los parámetros elegidos son:

$\alpha = -1, \beta = 20, \gamma = 1000, c = 15, m = 12, w_1 = 0.1, w_2 = 1, \theta = 0.05$, con $\sqrt{d/k} = 0.1$ para las figuras 2.a y 2.b, mientras $\sqrt{d/k} = 2$ para las figuras 2.c y 2.d.

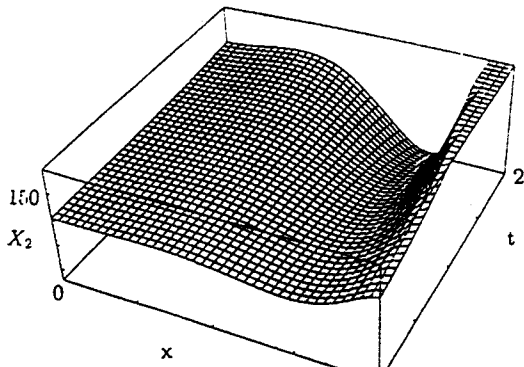
Estos experimentos muestran que la raíz cuadrada $\sqrt{d/k}$ del cociente entre los elementos característicos de la cinética del catalizador actúa como parámetro de bifurcación, en la formación de pautas espaciales para las concentraciones X_1 y X_2 .



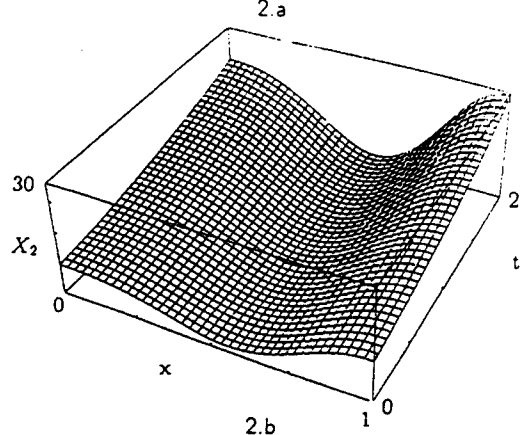
1.a



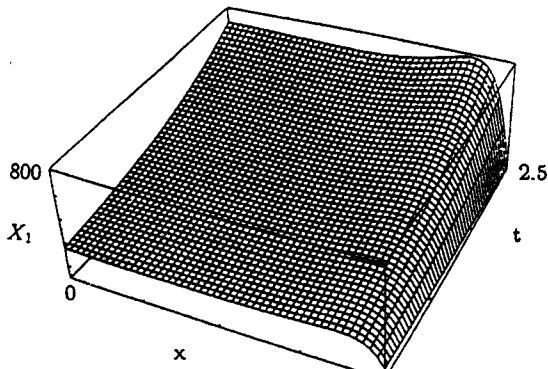
2.a



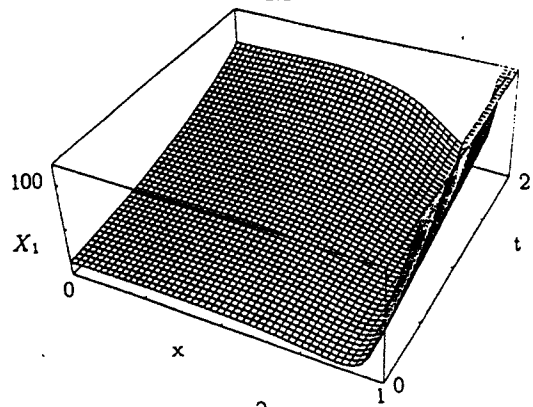
1.b



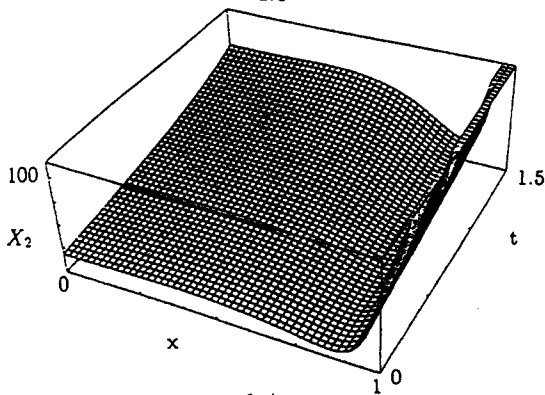
2.b



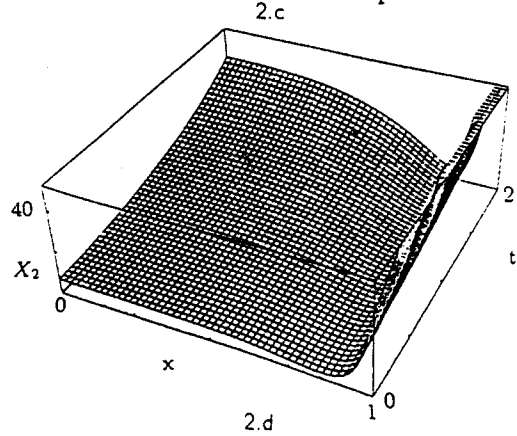
1.c



2.c



1.d



2.d

Fig. 1: Cinética de Schnackenberg: (a) y (b) Concentraciones X_1 y X_2 , con parámetro de bifurcación igual a 1. (c) y (d) con parámetro de bifurcación igual a 2.

Fig. 2: Activador-inhibidor: (a) y (b) Concentraciones X_1 y X_2 , con parámetro de bifurcación igual a 0.1. (c) y (d) con parámetro de bifurcación igual a 2.

ANÁLISIS GRÁFICO

Una observación cuidadosa de las gráficas correspondientes a los modelos analizados indica que la solución obtenida para cada una de las variables $X_i(x, t)$, para t fijo, es una función de x que difiere "poco" de una constante, presentando un único extremo en el intervalo de trabajo $[0, 1]$. Por otra parte, al variar t se constata que este extremo se desplaza sobre el intervalo $[0, 1]$. De este modo se plantea de manera natural el estudio del siguiente problema: ¿Cómo formular matemáticamente el movimiento o desplazamiento de las pautas en el espacio?

En trabajos experimentales, se ha comprobado la existencia de tales desplazamientos en reacciones químicas con difusión dependiente del espacio. Los modelos con catalizador estudiados anteriormente desembocan en modelos de reacción-difusión con difusividades dependientes del espacio, lo cual justifica emprender este análisis.

Existen trabajos teóricos que demuestran tal movilidad para un cierto tipo de cinéticas (Panfilov y Keener, 1995).

En otros de los casos analizados se observa un tipo de movimiento acompañado de evolución, esto es, crecimiento o decrecimiento de la concentración, en uno de los extremos del intervalo $[0, 1]$. Para obtener una relación que nos dé información tanto acerca de la dirección, como de la velocidad en que se produce la acumulación, se considera la función:

$$F(\mu) = n\Lambda, \quad n \in (0, 1), \quad (14)$$

que representa una parte fijada del área bajo la curva trazada en el plano $t = t_k$, que se obtiene al cortar la superficie:

$$X = X(x, t), \quad (15)$$

por el plano $t = t_k$. Por tanto μ es un punto variable del intervalo $[0, 1]$, que depende del tiempo. Esto es: $\mu = \mu(t)$.

Lo anterior conduce a definir (para un t fijo):

$$F(\mu_i(t)) = \int_{\mu_i}^1 X_i(x, t) dx = n\Lambda_i, \quad (16)$$

o bien:

$$F(\mu_i(t)) = \int_0^{\mu_i} X_i(x, t) dx = (1-n)\Lambda_i, \quad (17)$$

con:

$$\Lambda_i = \int_0^1 X_i(x, t) dx \quad y \quad n \in (0, 1). \quad (18)$$

A la curva que describe un punto interior del intervalo $[0, \mu_i(t)]$ (o bien $[\mu_i(t), 1]$), que se denota $\nu(t)$, se le llama "variedad guía". De esta manera $\nu(t)$ describe la dirección en que aumenta o disminuye la concentración, y su derivada da la velocidad con que esto ocurre.

En el caso de la figura 3.a se ha considerado el sistema activador-inhibidor, con:

$$f_1(X_1, X_2) = X_1 + 5 - X_2, \quad (19)$$

$$f_2(X_1, X_2) = \eta X_1 - 3X_2. \quad (20)$$

Los valores de los parámetros elegidos son:

$\alpha = -1, \beta = 20, \gamma = 1000, \eta = 4, c = 15, m = 20, \sqrt{d/k} = 2$. Con esto, los resultados obtenidos (mediante un ajuste no lineal) son:

$$\nu_1(t) = a + b e^{-t} \quad (21)$$

en donde en el caso de X_1 :

$$a = 4.719 \cdot 10^{-5}, b = 0.448 \text{ y } c = 998.604$$

La figura 3.b representa a la "variedad guía" correspondiente.

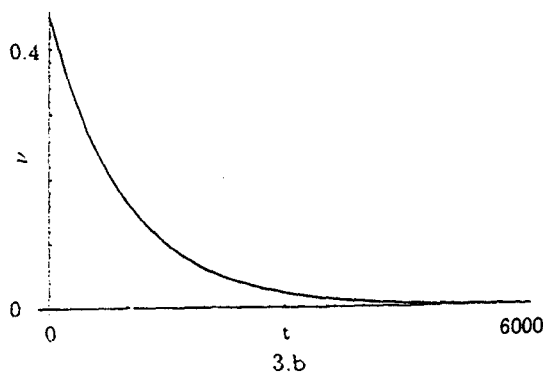
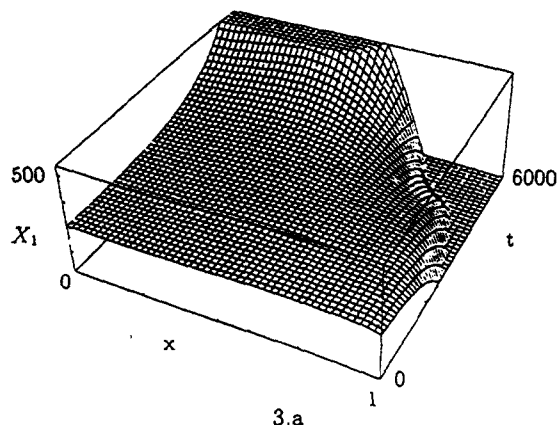


Fig. 3: Activador-inhibidor: (a) La acumulación de concentración X_1 se produce en torno a $x = 0$. (b) Variedad guía correspondiente.

En otros casos la acumulación de concentración no se produce únicamente en los alrededores de uno de los extremos del intervalo. Así, en la figura 4 el fenómeno se produce tanto en un extremo como en el interior del intervalo, mientras que en la figura 5 la acumulación tiene lugar en ambos extremos.

Para tales casos (y para otros más generales), se define una partición $P = \{p_0, p_1, \dots, p_x\}$ del intervalo $[0, 1]$, y en cada subintervalo $[p_{j-1}, p_j]$ se consideran las funciones:

$$F_{j1}(\mu_{1j}(t)) = \int_{\mu_{1j}}^{p_j} X_i(x, t) dx = n\Lambda_{ij}, \quad (22)$$

$$F_{j2}(\mu_{2j}(t)) = \int_{p_{j-1}}^{\mu_{2j}} X_i(x, t) dx = m\Lambda_{ij}, \quad (23)$$

con:

$$\Lambda_{ij} = \int_{p_{j-1}}^{p_j} X_i(x) dx \quad y \quad n, m \in (0, 1). \quad (24)$$

Los signos de $\mu_{1j} - p_{j-1}$ y de $\mu_{2j} - p_j$ nos ofrecen una interpretación cualitativa de lo que ocurre con respecto al crecimiento y decrecimiento de acumulación en $[p_{j-1}, p_j]$. Aquí, definimos la función:

$$\nu_j(t) = \frac{\mu_{1j} + \mu_{2j}}{2}, \quad (25)$$

a cuya gráfica llamamos también "variedad guía", y que nos ofrece una aproximación del movimiento de la pauta.

En los casos de las figuras 4 y 5, se ha considerado el sistema de reacción-difusión con cinética de Schnackenberg.

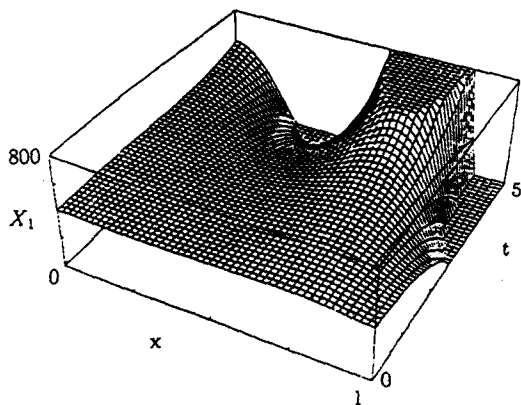


Fig. 4: La acumulación de concentración se produce en torno a un extremo y a un punto interior del intervalo $[0, 1]$.

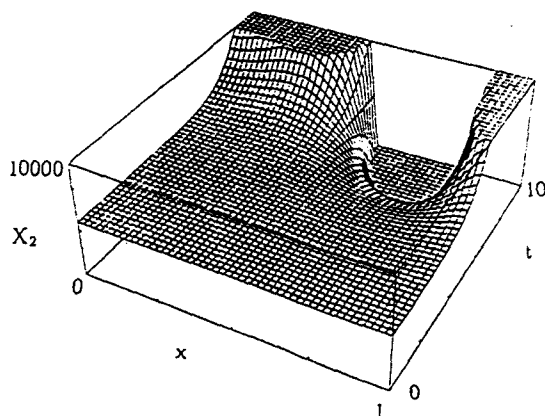


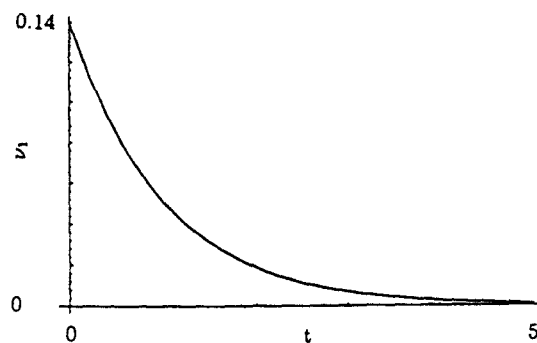
Fig. 5: La acumulación de concentración se produce en torno a los extremos del intervalo $[0, 1]$.

La gráfica 4 representa el comportamiento de X_1 . Aquí la partición considerada ha sido $P = \{0, 0.35, 1\}$, obteniendo para el intervalo $[0, 0.35]$ los siguientes resultados:

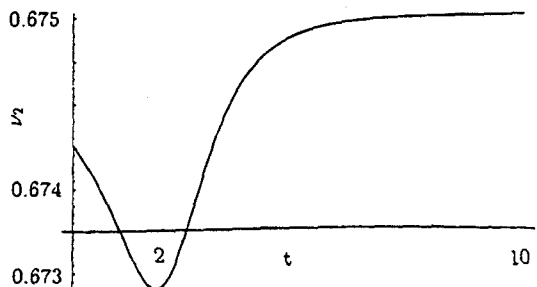
$$\nu_1(t) = a + b e^{-t}, \quad (26)$$

en donde:

$$a=2.214 \cdot 10^{-5}, \quad b=0.139 \quad y \quad c=0.997$$



6.a



6.b

Fig. 6. Variedades guías para la concentración X_1 con cinética de Schnackenberg. (a) En el intervalo $[0, 0.35]$. (b) En el intervalo $[0.35, 1]$.

La figura 6.a representa a la "variedad guía" en el intervalo $[0, 0.35]$, y puede observarse el crecimiento exponencial de la acumulación hacia las proximidades de $x = 0$.

En el intervalo $[0.35, 1]$ los resultados son:

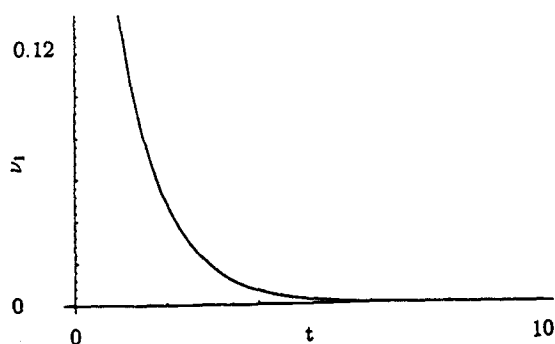
$$\nu_2(t) = \frac{a + ct + et^2}{1 + bt + dt^2}, \quad (27)$$

con:

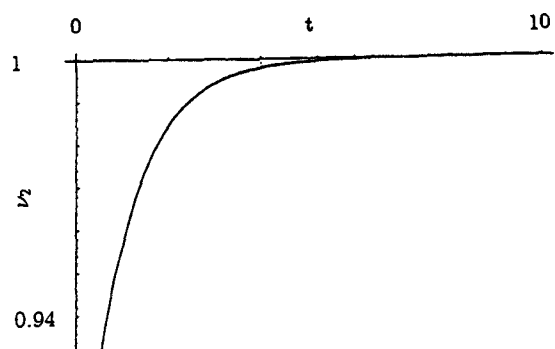
$$a=0.674, b=-0.680, c=-0.459, d=0.161 \text{ y } e=0.108.$$

La figura 6.b representa a la "variedad guía" en este intervalo, y como puede verse, el crecimiento de acumulación tiende a producirse en los alrededores de $x = 0.675$.

La figura 5 representa el comportamiento espacio-temporal de X_2 . La partición considerada es: $P = \{0, 0.75, 1\}$, obteniendo para el intervalo $[0, 0.75]$ los



7.a



7.b

Fig. 7: Variedades guías para la concentración X_2 con cinética de Schnackenberg. (a) En el intervalo $[0, 0.75]$. (b) En el intervalo $[0.75, 1]$.

resultados:

$$\nu_1(t) = a + be^{-\frac{t}{c}}, \quad (28)$$

con:

$$a=3.560 \cdot 10^{-5}, b=0.355, c=0.997.$$

La figura 7.a representa a la "variedad guía" en el intervalo $[0, 0.75]$.

En el intervalo $[0.75, 1]$ los resultados son:

$$\nu_2(t) = a + bt + ct\sqrt{t} + de^{-t} \quad (29)$$

con:

$$a=1.001, b=-0.0008, c=0.0002, d=-0.119.$$

La figura 7.b representa a la "variedad guía" en este intervalo, y como puede verse, el crecimiento de acumulación tiende a producirse en los alrededores de $x = 1$.

CONCLUSIONES

Se muestra gráficamente que para cinéticas, tanto de activación-inhibición como de retroalimentación positiva, se producen movimientos acompañados de evolución de las pautas espaciales. Todo ello, en un modelo de reacción-difusión unidimensional donde la interacción entre dos especies está regida por otra especie, que actúa como catalizador. Este modelo se ha estudiado anteriormente por los autores, mostrando que cumple las condiciones bajo las que se producen pautas espaciales.

REFERENCIAS

- García-Cortí, J.L., Fernández, I., Pacheco, J.M.: An analysis of morphogenesis in reaction-diffusion systems with a catalyst, *Journal of Institute of Mathematics and Computer Sciences (Mathematics Series)*, Vol.9, No.1, 11-18 (1996)
- Murray, J. : *Mathematical Biology*, Springer Verlag (1989)
- Panfilov, A., Keener, J. : Dynamics of dissipative structures in reaction-diffusion equations, *SIAM J. App. Math* 55-1, 205-219 (1995)
- Turing, A.M.: The chemical basis of morphogenesis, *Phil. Trans. R. Soc. Lond.*, B237, pp.37-72 (1952)



Nitrogen availability influences the biochemical composition and photosynthesis of tank-cultivated *Ulva rigida* (Chlorophyta)

Juan Luis Gómez Pinchetti*, Elena del Campo Fernández, Paula Moreno Díez & Guillermo García Reina

Instituto de Algología Aplicada, Universidad de Las Palmas de G.C., Muelle de Taliarte s/n, 35214 Telde, Las Palmas, Canary Islands, Spain

(* Author for correspondence; fax: +34 928 132830; e-mail: pinchetti@infovia.ulpgc.es)

Received 13 March 1998; revised 25 May; accepted 25 May 1998

Key words: ammonium, C:N ratio, tank culture, dietary fibre, fatty acids, nitrogen, photosynthesis, *Ulva rigida*

Abstract

Physiological and biochemical changes in relation to inorganic nitrogen availability were studied for tank-cultivated *Ulva rigida* grown under nitrogen-enriched and nitrogen-depleted seawater. *U. rigida* was initially cultivated in nitrogen-enriched seawater (daily concentrations of NH_4^+ and $\text{NO}_3^- + \text{NO}_2^-$ ranged between 0.5–1.7 and 0.06–0.15 mg L^{-1} , respectively), then transferred to nitrogen-depleted seawater where photosynthetic capacity decreased to zero after 23 d. At the time (14 d) when photosynthetic rates were lower than $2.0 \mu\text{mol O}_2 \text{g}^{-1} \text{FW min}^{-1}$ and strong bleaching had occurred, some algae were returned to the initial nitrogen-enriched seawater to study recovery from N-limited growth. Data on biochemical composition (chlorophylls, ash, caloric content, fatty acids and dietary fibres) and colouration varied significantly depending on the nitrogen conditions. C:N ratios correlated significantly with biochemical parameters. Fatty acid (FA) synthesis continued during the N-starvation period; saturated and mono-unsaturated FA increased to a maximum of 72.2%, while poly-unsaturated fatty acids (PUFA) decreased to 27.7%. During the N-enriched recovery period, the reverse was found. C:N ratios above 10 correlated with carbohydrate synthesis as shown by the dietary fibre level. Under nitrogen enriched conditions, C:N ratios decreased along with a decrease in fibre level. Under controlled conditions, nitrogen represents a major influence on the development of intensive tank cultivation of *Ulva rigida*, not only by affecting parameters closely related to nitrogen metabolism but also some clearly influenced by carbon uptake.

Introduction

Interest in seaweeds as novel foods with potential nutritional benefits (Darcy-Vrillon, 1993), fodder (recently for fish culture purposes; Davies et al., 1997), fertilizers and sources of fine chemicals for the pharmaceutical, food and chemical industries is expanding in Western countries. In fact, cultivation techniques are being improved with the main objective of obtaining higher algal biomass that exhibit specific qualities (Lobban & Harrison, 1994).

Physical and chemical factors such as temperature, salinity and light (Lobban & Harrison, 1994), aera-

tion (Chen & Johns, 1991) or nutrient concentrations (Björnsäter & Wheeler, 1990; Floreto et al., 1996; García-Ferris et al., 1996) influence the biochemical composition, physiological status and ultrastructure of micro- and macroalgae. Nitrogen is one of the most important limiting nutrients in the marine environment (Hanisak, 1983) and nitrogen control is critical for the intensive cultivation of algae due to its role in growth, and regulation of metabolism (Smit et al. 1997).

The green macroalga *Ulva* has been widely used as a biofilter because of its high efficiency to remove nitrogenous inorganic compounds (up to 90%

in the form of ammonium) from wastewaters (Neri et al., 1991; Jiménez del Río et al., 1996). *Ulva* species show the capacity to utilize, quickly absorb and metabolize different forms of inorganic nitrogen, mainly nitrate and ammonium, depending on their availability. However, ammonium (NH_4^+), which can be toxic or inhibitory for some seaweeds at concentrations higher than 30–50 μm , is the preferred nitrogen form for *Ulva* and other species of macroalgae (Lobban & Harrison, 1994). Moreover, Jiménez del Río et al. (1995) demonstrated that NH_4^+ availability controls ribulose-1,5-bisphosphate carboxylase/oxygenase (Rubisco) and carbonic anhydrase (CA) activities in *Ulva rigida*, confirming that there is a close relationship between inorganic nitrogen, photosynthesis and carbon metabolism (see review by Turpin, 1991).

Excess and depletion of nitrogen sources in the culture medium causes important cellular responses in algae. Excess nitrogen, as well as other nutrients, can be stored and used for growth during nutrient limited periods by a number of macroalgae including *Ulva fenestrata* and *Enteromorpha intestinalis* (Björnsäter & Wheeler, 1990), *Codium fragile* (Hanisak, 1979), *Chaetomorpha linum* (McGlathery et al., 1996) or *Gracilaria* spp. (Jones et al., 1996; Smit et al., 1997). Storage occurs as inorganic nitrogen (NO_3^- and NH_4^+) (Chapman & Craigie, 1977) and organic compounds, amino acids and proteins (Jones et al., 1996; McGlathery et al., 1996). When nitrogen limits growth, carbohydrate synthesis predominates and accounts for the increase in polysaccharide levels and related high C:N ratio values (Vergara et al., 1993; Lahaye et al., 1995).

Few reports have specifically considered the effects of nitrogen resupply on photosynthesis, algal recovery and biochemical transformation of seaweeds. The study of these effects can clarify processes by which nutrient resupply enhances growth and nutrient utilization. The present study investigates the influence of N-limitation and N-enrichment on growth and a number of physiological and biochemical characteristics of tank-cultivated *Ulva rigida*, and in particular, evaluates how nitrogen supply can alter and/or modify specific properties of interest in the composition and physical properties of the biomass.

Materials and methods

Algal material and cultivation conditions

Ulva rigida C. Agardh was collected from Taliarte harbour, east coast of Gran Canaria (Canary Islands) and cultivated in 750 L aerated tanks at a density of 2.5 g L^{-1} . Nitrogen enriched seawater at turnover rates of 8 vol d^{-1} was pumped from a 2000- m^3 tank with approximately 40 t of gilthead seabream (*Sparus aurata*). Daily concentrations of NH_4^+ and $\text{NO}_3^- + \text{NO}_2^-$ ranged between 0.5–1.7 and 0.06–0.15 mg L^{-1} , respectively. Maximum irradiance levels were $1975 \pm 98 \mu\text{mol photon m}^{-2} \text{s}^{-1}$ and the water temperature ranged between 20 and 24 °C. Relative growth rates μ ($\% \text{d}^{-1}$) were calculated according to the equation $\mu = 100 \ln (W_t/W_0)/t$ (D'Elia & Deboer, 1978), where W_0 = initial fresh weight (FW), W_t = final fresh weight, and t = time in days.

After one month, algae were transferred (under the same physical conditions) to running seawater without any nitrogen addition ($\text{NH}_4^+ + \text{NO}_3^- + \text{NO}_2^-$ concentrations $\leq 3 \mu\text{m}$). After 14 d, when photosynthetic rates reached values lower than 2.0 $\mu\text{mol O}_2 \text{g}^{-1} \text{FW min}^{-1}$ and strong bleaching was observed, algae were returned (early in the morning) to the initial nitrogen enriched seawater to study recovery.

Prior to analysis samples were washed with distilled water and freeze dried. Determination of C:N ratios was performed with a Perkin Elmer Elemental Analyzer Model 2400 CHN. Caloric content values were determined by combustion in an Ika-calorimeter C700 (Janke & Kunkel). Percent ash was determined by combusting dried samples at 450 °C to a constant weight. Determinations were carried out in triplicate. Where not indicated, variability did not exceed 10% of the mean.

Photosynthesis and chlorophyll measurements

Oxygen exchange was measured with a Clark-type oxygen electrode fitted with a water jacketed chamber (Hansatech Instruments Ltd., UK) at 20 °C. Thallus fragments (10 mg FW) were transferred to the chamber containing 2 mL filtered (through 0.2 μm filters) seawater buffered at pH 8.2 with 30 mM TRIS. Light was provided by a slide projector (Reflecta, Germany) and irradiance measured with a LI-1000 data logger and a spherical quantum sensor LI-193SA (Li-Cor, USA). Oxygen evolution at a Photon Flux Density (PFD) of 750 $\mu\text{mol photon m}^{-2} \text{s}^{-1}$ was recorded.

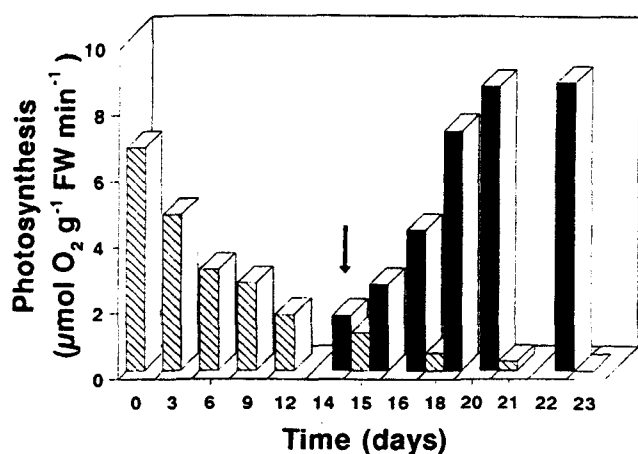


Figure 1. Maximum photosynthetic rates of nitrogen-starved (crossed bars) and nitrogen-enriched (black bars) *Ulva rigida*. Arrow shows the day of change of nitrogen-starved algae to nitrogen-enriched seawater. Measurements were taken at $750 \mu\text{mol photon m}^{-2} \text{s}^{-1}$ and 20°C .

Table 1. Effect of N-starvation and N-enrichment (indicated as -N and +N, respectively) on the chlorophyll *a* and *b* concentrations of tank-cultivated *Ulva rigida*. The starting day of the nitrogen starvation period is indicated as day 0. Algal recovery in N-enriched seawater started on day 14, independent of tanks where N-starved *U. rigida* was maintained to day 23 (as indicated in Figure 1). Mean \pm SD; $n=5$.

Time (day)	Chl <i>a</i> ($\mu\text{g g}^{-1}$ FW)	Chl <i>b</i> ($\mu\text{g g}^{-1}$ FW)	Chl <i>a</i> /Chl <i>b</i> ratio
-N 0	1162.5 ± 26.2	604.9 ± 29.9	1.92
15	54.6 ± 6.7	29.9 ± 4.2	1.83
21	40.0 ± 7.1	20.3 ± 3.2	1.97
+N 14	65.4 ± 7.0	43.9 ± 4.6	1.49
16	381.7 ± 54.3	281.5 ± 28.3	1.35
20	672.2 ± 70.2	418.3 ± 60.1	1.61

Chlorophylls *a* and *b* were extracted in 90% acetone and determined according to Jeffrey and Humphrey (1975).

Fatty acids and dietary fibre analysis

Lipid extraction and trans-esterification of freeze dried and ground samples (particle size $< 200 \mu\text{m}$) were carried out as described by Cohen et al. (1987). Fatty acid methyl esters (FAME) were separated by capillary gas chromatography using a Shimadzu GC-15A equipped with FID and a Shimadzu Chromatopac C-R5A integrator. Samples ($1.0 \mu\text{L}$) were injected in a Supelcowax 10 fused silica capillary column ($30 \text{ m} \times 0.32 \text{ mm}$) using helium as the carrier gas

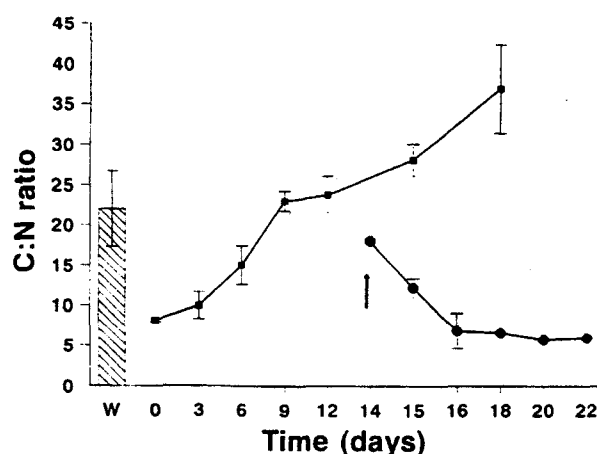


Figure 2. Effect of nitrogen starvation (■) and enrichment (●) on the C:N ratio of *Ulva rigida*. Arrow shows the day of change of nitrogen-starved algae to nitrogen-enriched seawater. Bar shows the C:N value of wild collected *U. rigida*.

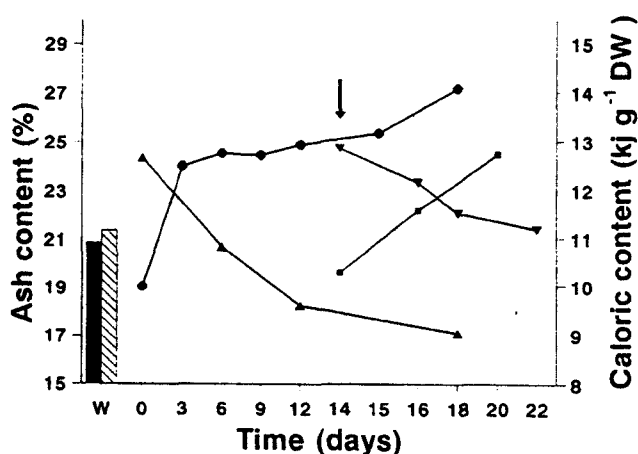


Figure 3. Effect of nitrogen starvation (● ash; ▲ caloric content) and enrichment (▼ ash; ■ caloric content) on the ash and caloric contents of *Ulva rigida*. Arrow shows the day of change of nitrogen-starved algae to nitrogen-enriched seawater. Bars show ash (black bar) and caloric contents (crossed bar) of wild collected *U. rigida*.

and operated at 180°C during 10 min and then at 215°C after an increase rate of $2.5^\circ\text{C min}^{-1}$. Both the injector and detector temperature was 250°C . For quantitative analysis, nonadecanoic acid (19:0) methyl ester was added as an internal standard. Peaks were identified by comparison with known standards (Sigma and Supelco).

Soluble and insoluble dietary fibre content of freeze dried samples were determined as described by Lahaye (1991). Percent of soluble and insoluble dietary fibre was obtained by subtracting total residual proteins and ash contents from the respective yield of the liquid and solid fractions. Proteins were

Table 2. Effect of N-starvation and N-enrichment (indicated as -N and +N, respectively) on the fatty acid composition (% total fatty acids) of tank-cultivated *Ulva rigida*. The starting day of the nitrogen starvation period is indicated as day 0. Algal recovery in N-enriched seawater started on day 14. Wild: fatty acids composition from wild collected *U. rigida*.

	Wild	-N		+N				
		Day						
		0	6	12	18	14	16	22
Saturated								
14:0	3.3	3.3	2.9	1.5	-	3.1	1.8	1.7
16:0	47.3	31.7	38.7	49.9	58.1	47.5	48.1	31.3
18:0	1.2	0.4	0.4	-	-	-	0.7	0.6
Mono-unsaturated								
16:1w9	2.9	0.3	-	-	-	-	-	0.2
16:1w7	1.9	0.5	0.5	2.9	-	1.7	1.1	0.6
16:1w5	-	3.5	1.5	2.5	-	-	2.7	3.1
18:1w9	2.3	0.6	0.6	1.8	-	2.5	1.6	1.0
18:1w7	16.8	8.1	9.7	10.7	14.2	12.1	10.9	5.5
Di-unsaturated								
18:2w6	5.0	7.1	4.7	4.9	4.9	5.4	5.8	5.4
Tri-unsaturated								
18:3w6	-	-	-	-	-	-	-	1.0
18:3w3	7.5	13.3	14.1	10.9	11.8	11.5	11.3	16.5
20:3w6	-	-	-	-	-	-	-	0.2
22:3w6	-	-	-	-	-	-	-	0.8
Tetra-unsaturated								
16:4w1	2.7	10.6	9.0	4.5	-	4.3	2.8	11.1
18:4w3	3.1	14.3	12.3	6.9	6.7	6.6	6.2	13.9
18:4w1	0.2	-	-	-	-	-	0.7	0.9
20:4w6	-	0.3	-	-	-	-	-	0.3
20:4w3	-	0.6	0.5	-	-	-	0.8	0.8
Penta-unsaturated								
20:5w6	-	0.3	-	-	-	-	0.5	0.5
20:5w3	4.4	2.4	3.1	3.5	4.3	5.4	2.5	1.7
22:5w3	1.5	2.7	2.1	-	-	-	2.6	3.1
Total S & M	75.4	48.4	54.3	69.3	72.3	66.9	66.9	44.0
Total PUFA	24.4	51.6	45.8	30.7	27.7	33.2	33.2	56.2

determined as nitrogen using the Kjeldahl method ($N \times 6.25$).

Results

Photosynthesis and pigment composition

In the initial nitrogen enriched condition, *Ulva rigida* growth rates ranged between 12 and 16% d^{-1} , chlorophyll concentration reached maximum levels (Table 1) and algae became a deeply pigmented green. Maximum photosynthetic rates reached 6.8 $\mu\text{mol O}_2 \text{ g}^{-1} \text{ FW min}^{-1}$ (Figure 1).

When transferred to nitrogen depleted seawater, growth rates decreased to less than 2% d^{-1} and material ceased growing after 5 d. Algae became bleaching and photosynthetic rates decreased significantly to zero on day 23 (Figure 1). With N-enrichment renewal for some algae on day 14, there was a recovery of chlorophyll, resulting in greater pigmentation, and photosynthesis (Table 1, Figure 1). Following N-enrichment, algae reached maximum photosynthetic levels that were higher than the initial material within 6 d. Chlorophyll levels paralleled the variations in photosynthetic rates and chlorophyll *a/b* ratios were

constant, independently of the nitrogen conditions (Table 1).

C:N ratios

Lower C:N values were observed in algae grown in nitrogen enriched seawater and increased until day 18 when values approached 35, indicating nitrogen limitation (Figure 2). Freshly collected algae showed intermediate values suggesting that they were nitrogen limited. Maximum and minimum carbon tissue composition ranged from 36.4% measured on the starting day of nitrogen starvation period (indicated as day 0) to 15.7% on day 16 of the nitrogen enrichment period. Nitrogen tissue values varied from 5.7% on day 20 of the nitrogen enrichment period, to 0.6%, on day 18 of nitrogen starvation. In wild algae, the percent of tissue carbon and nitrogen were 28.7 and 1.3, respectively.

Ash and caloric content values

Ash and caloric contents in algae varied inversely with N conditions (Figure 3); nitrogen limited algae had greater ash content and less caloric content. Wild algae showed intermediate values for both variables.

Fatty acids and dietary fibre contents

Total saturated and mono-unsaturated FA increased and total poly-unsaturated FAs decreased during nitrogen starvation to reach values close to those found in wild algae (Table 2). During the acute N-limitation period, fatty acids were represented mainly by six FAs (16:0; 18:1w7; 18:2w6; 18:3w3; 18:4w3 and 20:5w3). When returned to nitrogen enriched conditions the FA composition was reversed; total saturated and mono-unsaturated FA decreased and PUFA increased. During this recovery period, PUFA not found in wild algae appeared (18.3w6, 20.3w6, 22.3w6, 20.4w6, 20.4w3, 20.5w6), but were not major constituents.

Major FAs were palmitic (16.0) and vaccenic (18.1w7) acids. Both increased, from 31.8 to 58.0% and 8.1 to 14.2% of total FA, respectively, during starvation. The remaining FAs disappeared at the peak of nitrogen starvation and reappeared under nitrogen enriched conditions. In general, PUFA decreased in algae grown in nitrogen starved conditions except for eicosapentaenoic acid (20.5w3) which showed a transitory increase. Major PUFAs were linolenic (18.3w3), parinaric (18.4w3) and hexadecatetraenoic (16.4w1) acids.

A general increase in dietary fibre was observed in nitrogen starved algae, with a decrease during the recovery period (Table 3). The soluble fibre fraction was higher compared to the insoluble fraction.

Discussion

The biochemical and physiological characterization of nitrogen enrichment and starvation in previous studies has demonstrated how macroalgae may respond to a temporal imbalance of N availability (McGlathery et al., 1996). Further, the N requirements for growth, storage and use during subsequent periods of low external nutrient supply have been described (Lapointe & Ryther, 1979; Björnsäter & Wheeler, 1990; McGlathery et al., 1996).

In tank-cultivated *Ulva rigida*, decrease in growth and bleaching occurred during the nitrogen starvation period. Nitrogen previously stored in algae is used in growth when N becomes limiting or when light or temperature increase (Duke et al., 1986; Coutinho & Zingmark, 1993). Bleaching, a result of pigments being metabolized as a source of protein, has also been described for *Gracilaria* (Smit et al., 1997). A change in the ratio of Chl *a* to accessory chlorophyll was evident for Chl *a/b* ratios during N-enrichment and starvation in *Ulva*, and is a common phenomenon (Turpin, 1991). Shifts in chlorophylls content were important even though daily irradiance values reached high maximum levels (up to 1900 $\mu\text{mol photon m}^{-2} \text{s}^{-1}$) suggesting that pigment content was controlled by dissolved nitrogen and not by light.

The photosynthetic capacity during nitrogen starvation progressively declined to zero after 23 d, while algae showing photosynthetic rates of 2.0 $\mu\text{mol O}_2 \text{g}^{-1} \text{FW min}^{-1}$ and transferred to nitrogen enriched conditions recovered rapidly. Nitrogen-deficiency clearly affects the light harvesting system and the activity of the enzymes of inorganic carbon metabolism (Turpin, 1991; Jiménez del Rio et al., 1995), in addition to growth. It appears that soluble proteins decrease under low nitrogen levels in relation to the internal nitrogen pool (Turpin, 1991).

The C:N ratio is a strong index of the physiological status of micro- and macroalgae (Chen & Johns, 1991; Vergara et al., 1993). The ratio shows low values when N was abundant and increased when N supply was limited. C:N values close to 10 have been described as optimal or normal for the nitrogen status of algae and a ratio greater than 10 indicates N-limitation in

Table 3. Effect of N-starvation and N-enrichment (indicated as - N and + N, respectively) on the soluble, insoluble and total dietary fibres composition (%) of tank-cultivated *Ulva rigida*. The starting day of the nitrogen starvation period is indicated as day 0. Algal recovery in N-enriched seawater started on day 14. Wild: digestive fibres composition from wild collected *U. rigida*.

	Wild	- N		+N		
		Days				
		0	6	18	14	20
Soluble	30.6	34.6	35.1	37.1	37.0	36.2
Insoluble	6.3	8.8	13.9	12.3	9.7	7.7
Total	36.9	43.4	49.0	49.4	46.7	43.9

Gracilaria (Lapointe & Ryther, 1979). In the present study, freshly collected *Ulva rigida* was nitrogen deficient as indicated by its C:N value close to 22. During the experiments, stored N was used to maintain algae at least for 23 d under N-depleted seawater conditions.

Ash content correlates with C:N ratio suggesting control by nitrogen uptake and influencing the organic and caloric content of *Gracilaria* (Lapointe & Ryther, 1979). In our study, N-starved *Ulva rigida* (higher C:N ratios) showed a higher ash content and lower caloric values than N-enriched algae (lower C:N values). These findings contrast with those of Lapointe & Ryther (1979) who found that N-limited *Gracilaria* contained less ash and a higher caloric content per unit dry weight; however, caloric content of the ash-free organic matter was higher in N-enriched algae. Also, on an ash-free basis, low caloric value and high ash content coincided with maximal growth of several freshly collected red and brown algae (Himmelman & Carefoot, 1975).

During the experiments, nitrogen availability also affected levels of protein, amino acids, (both decreasing in nitrogen limited conditions; Betancort, 1997) and carbohydrate. The dietary fibre content found was similar to that obtained previously by Lahaye et al. (1995). In *U. rigida*, when nitrogen limits growth, carbohydrate synthesis predominates as shown by the dietary fibres content whereas, in nitrogen enriched conditions, a decrease in fibres composition is observed.

Fatty acids synthesis continued during N-starvation with saturated and mono-unsaturated FAs increasing to a maximum, while PUFA decreased. The increase in specific FAs might be related to the formation of

lipid layers which play a role as light filters preventing photooxidative damage and in reducing water losses, as for *Chlorella zofingiensis* (Bar et al., 1995).

FA composition reversed during the N-enriched recovery period suggesting that PUFAs are used to create storage compounds in optimum conditions which can then be used as energy sources during periods of stress. During recovery, FAs which were not present in wild algae or were minority components in N-starved *Ulva*, may be used by intermediary precursors for the group of major fatty acids.

All results correlate with changes in the C:N ratio. Chen and Johns (1991) indicated that the proportion of unsaturated FAs (especially trienoic acids) increased significantly when C:N ratios were low in *Chlorella sorokiniana*. At higher C:N ratios, carbon is supplied in excess, nitrogen becomes limiting, and the increase of the cell lipid content may be explained as a carbon storage mechanism. Similar results were described for *Gracilaria verrucosa* by Pohl and Zurheide (1979).

Our results suggest that, under controlled conditions, nitrogen (mainly in the form of NH_4^+) presents a strong influence on the development and composition of intensive tank-cultivated *Ulva rigida*, not only by affecting parameters closely related to nitrogen metabolism but also to carbon uptake. Data on nitrogen requirements for growth, storage and use during limitation and resupply periods agree with those previously described for macroalgae. However, it is demonstrated that nitrogen availability clearly affected the specific composition of important biochemical parameters such as chlorophylls, saturated and unsaturated fatty acids, dietary fibres, ash and caloric content, which were directly correlated with C:N ratio dynamic.

Acknowledgements

The authors are indebted to Lidia Robaina, María Salhi and H. Fernández-Palacios (GIA, Instituto Canario de Ciencias Marinas, ICCM) for helpful advice during the experiments. We thank Dr B.A. Whitton, Dr M.T. Brown (Department of Biological Sciences, University of Plymouth) and an anonymous reviewer for helpful comments on the manuscript.

References

- Bar E, Rise M, Vishkautsan M, Arad SM (1995) Pigment and structural changes in *Chlorella zofingiensis* upon light and nitrogen stress. *J. Plant Physiol.* 146: 527–534.
- Betancort JR (1997) Determinación de aminoácidos por HPLC. Estudio cualitativo y cuantitativo de aminoácidos libres en algas y su variación por condiciones de cultivo. Ph.D. Thesis. Univ. de Las Palmas de G.C. 135 pp.
- Björnsäter BR, Wheeler PA (1990) Effect of nitrogen and phosphorus supply on growth and tissue composition of *Ulva fenestrata* and *Enteromorpha intestinalis* (Ulvales, Chlorophyta). *J. Phycol.* 26: 603–611.
- Chapman AR, Craigie JS (1977) Seasonal growth in *Laminaria longicruris*: relations with dissolved inorganic nutrients and internal reserves of nitrogen. *Mar. Biol.* 40: 197–205.
- Chen F, Johns MR (1991) Effect of C/N ratio and aeration on the fatty acid composition of heterotrophic *Chlorella sorokiniana*. *J. appl. Phycol.* 3: 203–209.
- Cohen Z, Vonshak A, Richmond A (1987) Fatty acid composition of *Spirulina* strains grown under various environmental conditions. *Phytochemistry* 26: 2255–2258.
- Coutinho R, Zingmark R (1993) Interactions of light and nitrogen on photosynthesis and growth of the marine macroalga *Ulva curvata* (Kützting) De Toni. *J. exp. mar. Biol. Ecol.* 167: 11–19.
- Darcy-Vrillon B (1993) Nutritional aspects of the developing use of marine macroalgae for the human food industry. *Int. J. Food Sci. Nutr.* 44: S23–S35.
- Davies SJ, Brown MT, Camilleri M (1997) Preliminary assessment of the seaweed *Porphyra purpurea* in artificial diets for thick-lipped grey mullet (*Chelon labrosus*). *Aquaculture* 152: 249–258.
- D'Elia CF, DeBoer JA (1978) Nutritional studies of two red algae. II. Kinetics of ammonium and nitrate uptake. *J. Phycol.* 14: 266–272.
- Duke CS, Lapointe BE, Ramus J (1986) Effects of light on growth, RuBPCase activity and chemical composition of *Ulva* species (Chlorophyta). *J. Phycol.* 22: 362–370.
- Floreto EAT, Teshima S, Ishikawa M (1996) Effects of nitrogen and phosphorus on the growth and fatty acid composition of *Ulva pertusa* Kjellman (Chlorophyta). *Bot. mar.* 39: 69–74.
- García-Ferris C, de los Ríos A, Ascaso C, Moreno J (1996) Correlated biochemical and ultrastructural changes in nitrogen-starved *Euglena gracilis*. *J. Phycol.* 32: 953–963.
- Hanisak MD (1979) Nitrogen limitation of *Codium fragile* ssp. *tomentosoides* as determined by tissue analysis. *Mar. Biol.* 50: 333–337.
- Hanisak MD (1983) The nitrogen relationships of marine macroalgae. In: Carpenter EJ, Capone DG (eds), *Nitrogen in the Marine Environment*. Academic Press, New York: 699–730.
- Himmelman JH, Carefoot TH (1975) Seasonal changes in calorific value of three Pacific coast seaweeds, and their significance to some marine invertebrate herbivores. *J. exp. mar. Biol. Ecol.* 18: 139–151.
- Jeffrey SW, Humphrey GF (1975) New spectrophotometric equations for determining chlorophyll *a*, *b*, *c1*, *c2* in higher plants, algae and natural phytoplankton. *Biochem. Physiol. Pflanz.* 167: 191–194.
- Jiménez del Río M, Ramazanov Z, García Reina G (1995) Effect of nitrogen supply on photosynthesis and carbonic anhydrase activity in the green seaweed *Ulva rigida* (Chlorophyta). *Mar. Biol.* 123: 687–691.
- Jiménez del Río M, Ramazanov Z, García Reina G (1996) *Ulva rigida* (Ulvales: Chlorophyta) tank culture as biofilters for dissolved inorganic nitrogen from fishpond effluents. *Hydrobiologia* 326/327: 61–66.
- Jones AB, Dennison WC, Stewart GR (1996) Macroalgal responses to nitrogen source and availability: amino acid metabolic profiling as a bioindicator using *Gracilaria edulis* (Rhodophyta). *J. Phycol.* 32: 757–766.
- Lahaye M (1991) Marine algae as sources of fibres: determination of soluble and insoluble dietary fibre contents in some sea vegetables. *J. Sci. Food Agric.* 54: 587–594.
- Lahaye M, Gómez-Pinchetti JL, Jiménez del Río M, García-Reina G (1995) Natural decoloration, composition and increase in dietary fibre content of an edible marine algae, *Ulva rigida* (Chlorophyta), grown under different nitrogen conditions. *J. Sci. Food Agric.* 68: 99–104.
- Lapointe BE, Ryther JH (1979) The effects of nitrogen and seawater flow rate on the growth and biochemical composition of *Gracilaria foliifera* var. *angustissima* in mass outdoor cultures. *Bot. mar.* 22: 529–537.
- Lobban CS, Harrison PJ (1994) *Seaweed Ecology and Physiology*. Cambridge University Press, New York. 366 pp.
- McGlathery KJ, Pedersen MF, Borum J (1996) Changes in intracellular nitrogen pools and feedback controls on nitrogen uptake in *Chaetomorpha linum* (Chlorophyta). *J. Phycol.* 32: 393–401.
- Neori A, Cohen I, Gordin H (1991) *Ulva lactuca* biofilters for marine fishpond effluents. II. Growth rate, yield and C:N ratio. *Bot. mar.* 34: 483–489.
- Pohl P, Zurheide F (1979) Fatty acids and lipids of marine algae and the control of their biosynthesis by environmental factors. In: Hoppe HA, Levring T, Tanaka Y (eds), *Marine Algae in Pharmaceutical Science*. Walter de Gruyter, Berlin: 473–523.
- Smit AJ, Robertson BL, du Preez DR (1997) Influence of ammonium-N pulse concentrations and frequency, tank condition and nitrogen starvation on growth rate and biochemical composition of *Gracilaria gracilis*. *J. appl. Phycol.* 8: 473–481.
- Turpin DH (1991) Effects of inorganic N availability on algal photosynthesis and carbon metabolism. *J. Phycol.* 27: 14–20.
- Vergara JJ, Niell FX, Torres M (1993) Culture of *Gelidium sesquipedale* (Clem.) Born. et Thur. in a chemostat system. Biomass production and metabolic responses affected by N flow. *J. appl. Phycol.* 5: 405–415.

Estudio de la comunidad mesozooplancónica en relación a un efecto de isla en aguas de Gran Canaria

MAY GÓMEZ y SANTIAGO HERNÁNDEZ-LEÓN

*Facultad de Ciencias del Mar, Apartado 550,
Las Palmas de Gran Canaria. Islas Canarias, España.*

GÓMEZ, M. & S. HERNÁNDEZ-LEÓN (1998). Mesozooplankton community structure in relation to an island effect in the waters around Gran Canaria island. *VIERAEA* 26 (1997): 11-21.

ABSTRACT: The structure of the mesozooplankton community was studied in two stations southwest of Gran Canaria. One station (E-1) was located in the calm area on the leeward of the island while the other (E-3) was located in an area characterized by the turbulence produced by the north trade winds. Both stations were studied from autumn to spring. The highest abundance of organisms ($1208 \text{ ind}\cdot\text{m}^{-3}$) was recorded in the turbulent area, where the community was composed by small individuals ($3,64 \mu\text{g protein}\cdot\text{ind}^{-1}$). This area was characterized by an increased primary production. In the calm station, zooplankton abundance was lower ($964 \text{ ind}\cdot\text{m}^{-3}$), although organisms were larger ($4,50 \mu\text{g protein}\cdot\text{ind}^{-1}$). The average biomass for both areas ($3,89 \text{ mg protein}\cdot\text{m}^{-3}$) was in the range observed in the literature for this area. Taxonomic composition showed the higher abundance for copepods (75%). Appendicularians represented 20% and chaetognaths 1,5%, while the remaining groups accounted for less than 4%.

Key words: Mesozooplankton, abundance, structure, Canary Islands.

RESUMEN: Se realizó un estudio descriptivo de la comunidad mesozooplancónica en dos estaciones situadas al suroeste de Gran Canaria, una en la zona de calma al abrigo de la isla (E-1) y la otra en una zona influenciada por los vientos alisios (E-3). Ambas estaciones fueron muestreadas desde otoño hasta primavera. El mayor número de organismos ($1208 \text{ ind}\cdot\text{m}^{-3}$) se observó en la estación E-3 conformada por individuos con una biomasa individual de $3,64 \mu\text{g proteina}\cdot\text{ind}^{-1}$. Esta zona se caracterizó por la presencia de una mayor producción primaria debido a la mezcla vertical sobre la plataforma. En la zona de calma la densidad fue menor ($964 \text{ ind}\cdot\text{m}^{-3}$), siendo la biomasa individual más alta ($4,50 \mu\text{g proteina}\cdot\text{ind}^{-1}$). La biomasa proteica media observada ($3,89 \text{ mg proteina}\cdot\text{m}^{-3}$) es del rango de la encontrada en la literatura. En composición porcentual por grupos taxonómicos, destacó la dominancia de copépodos con un 75%, seguido de apendiculariáceos (20%) y quetognatos (1,5%), mientras que el resto de los grupos no superó el 4%. Palabras clave: Mesozooplankton, abundancia, estructura, Islas Canarias.

INTRODUCCIÓN

La influencia de la isla de Gran Canaria en la productividad y biomasa zooplanctónica de sus aguas circundantes fue descrita por Hernández-León (1986, 1988 a y b, 1991) como un «efecto de masa de isla». Como consecuencia, se observa un incremento de la biomasa zooplanctónica alrededor de dichas islas, a sotavento e íntimamente ligadas al contorno físico de las mismas. Asimismo, Hernández-León (1987, 1988a) describe la aparición de gradientes de biomasa e índices de actividad respiratoria del zooplancton en las zonas de cizallamiento del campo de vientos. Estas áreas de frentes limítrofes entre las zonas turbulenta y de calma, a ambos lados de la estela producida por la isla, se encuentran asociadas a procesos productivos originados por mezcla vertical sobre la plataforma insular. Con posterioridad, Hernández-León (1988b) observa que los organismos mesozooplanctónicos tienen una actividad respiratoria alta en las zonas de turbulencia y se acumulan en las zonas de cizallamiento del campo de viento; de esta forma el mesozooplancton se mantendría en contacto con las aguas turbulentas potencialmente más productivas. Arístegui *et al.* (1989) exponen los resultados de un muestreo simultáneo al que aquí presentamos, realizando un estudio hidrológico y de la biomasa y producción fitoplanctónica, así como de la actividad metabólica del mesozooplancton. Observan valores más altos del número de asimilación del fitoplancton en las zonas turbulentas, asociadas a una mayor abundancia de mesozooplancton.

El objetivo del presente trabajo comprende el estudio de la influencia de la acción del viento sobre los fenómenos de acumulación del mesozooplancton, comparando las variaciones en la biomasa y la composición taxonómica en las áreas batidas por el viento y en las áreas de calma.

MATERIAL Y MÉTODOS

Se estudiaron dos estaciones costeras situadas sobre la isobata de 50 metros, al suroeste de la isla de Gran Canaria, caracterizadas por estar una a sotavento de la isla en una zona de calma (E-1) y la otra por estar en una zona influenciada por la presencia de los vientos alisios y por tanto con una importante turbulencia (E-3, figura 1). Se realizaron cinco muestreos entre los meses de noviembre de 1986 y mayo de 1987. Las muestras de zooplancton se recolectaron con una red WP-2 doble, versión de la red WP-2 estándar (Unesco, 1968), equipada con malla de 200 μm , mediante arrastres verticales desde 50 m hasta la superficie. El contenido de uno de los colectores fue utilizado para la determinación de la biomasa proteica según el método de Lowry *et al.* (1951), utilizando albumina bovina (BSA) como referencia. La muestra del segundo colector fue fijada en formol al 4% para posteriormente ser subdividida en un aparato Folsom. Las cuatro alicuotas representantes de la 1/16 partes del total de la muestra fueron contadas y clasificadas bajo un microscopio estereoscópico. Los datos obtenidos fueron sometidos al cálculo propuesto por Horwood & Driver (1976), expresando los resultados como número de animales por metro cúbico y como porcentaje con respecto al total de la muestra. Para facilitar la interpretación de los resultados, los organismos fueron agrupados y clasificados en los siguientes grupos: grupo 1, copépodos; grupo 2, quetognatos;

grupo 3, apendicularios; grupo 4, ostrácodos; grupo 5, cladóceros; grupo 6, huevos (mayoritariamente de invertebrados bentónicos). En el grupo 7 (otros) se agruparon todos aquellos organismos con escaso porcentaje de representación y cuya aparición en las muestras fue ocasional. En él se incluyeron pequeños hervíboros (pterópodos, larvas de moluscos, larvas de equinodermos), poliquetos y larvas de peces. En el grupo 8 otros crustáceos, se incluyeron misidáceos, isópodos y fases larvianas de decápodos y eufausiáceos, y en el grupo 9 componentes del denominado «plancton gelatinoso», formado por taliáceos (sálpidos y doliólidos), sifonóforos e hidromedusas.

RESULTADOS

La temperatura del agua se mantuvo más alta en la estación 1, situada en la estela de la isla, aún en los meses de invierno. En la estación 3, sin embargo, se produjo un enfriamiento en la columna de agua desde diciembre (figura 2). Así pues, en febrero se alcanzó hasta 1°C de diferencia en la temperatura superficial del agua entre las estaciones 1 y 3.

El número medio de individuos por metro cúbico (Tabla I) fue superior en la estación 3 (1208 ind·m⁻³) que en la estación 1 (964 ind·m⁻³). En cuanto a la biomasa proteica, también fue ligeramente superior la encontrada en la estación 3 (4,09 ± 1,64 µg prot·m⁻³) frente a la estación 1 (3,64 ± 1,46 µg prot·m⁻³). Asimismo, observamos que los organismos de la estación 1 presentaban mayor contenido de proteínas por individuo (4,50 ± 2,73 µg prot·ind⁻¹) que los de la estación 3 (3,64 ± 0,95 µg prot·ind⁻¹).

El máximo valor para la biomasa (5,74 µg prot·m⁻³) y la abundancia (2149 ind·m⁻³) se encontró en la estación 3 en el mes de noviembre (figura 3), presentando valores muy superiores a los observados en la estación 1. Es de destacar el importante papel que mostraron los apendiculáriaceos, representando un 36% del total y alcanzando un valor máximo de 770 ind·m⁻³ en la estación 3, mientras que en la estación 1 fue ligeramente inferior pero con el mismo porcentaje. En la estación 1 los valores máximos de biomasa y abundancia se obtuvieron en febrero, coincidiendo con el máximo en el número de células de fitoplancton para esta estación.

El contenido en proteínas por individuo fue menor en los meses de noviembre a febrero, donde se encontraron los valores máximos en el número de individuos, mientras que en los meses de marzo y mayo, dicho contenido proteico por individuo aumentó considerablemente (figura 3 b), observándose la presencia de un mayor número de copépodos calanoides de gran tamaño. Por otra parte, en el mes de diciembre se detectan los valores mínimos tanto para la biomasa como para la abundancia.

Las variaciones en la abundancia de copépodos, en las dos estaciones muestreadas y para todo el periodo de estudio siguió la misma pauta que el número total de organismos (figura 4). Este grupo representó hasta un 90% de la comunidad, con un valor medio del 75%. Es de destacar que el porcentaje máximo de copépodos ocurre en mayo cuando disminuyen los valores de biomasa proteica y la abundancia de organismos (figura 5). Por el contrario, el mínimo porcentaje de representación de este grupo fue en noviembre (60%), debido a un aumento en la abundancia de los apendiculáriaceos, que representaron el 35%. El valor mínimo para este grupo se observó en mayo, en la estación 1 (26 ind·m⁻³). El resto de los grupos no superó el 4%, aunque la importancia relativa de cada uno de ellos fue distinta en función de la época del año.

En general y para todos los grupos, los valores más altos se encontraron en la estación 3 (Tabla I). Los valores máximos en el número de huevos ($47 \text{ huevos} \cdot \text{m}^{-3}$, 2,2%, en la estación 3 y $22 \text{ huevos} \cdot \text{m}^{-3}$, 1,84%, en la estación 1, ver figura 4) se observaron en noviembre. Por el contrario, el grupo de organismos gelatinosos presentó en este mes sus valores máximos en la estación 1, aunque su abundancia en el periodo de muestreo no superó el 0,5%.

El máximo para quetognatos se observó en febrero para ambas estaciones, siendo más abundantes en la estación 3. Los cladóceros tuvieron una escasa abundancia, apareciendo únicamente en marzo. Por otra parte hay que destacar que al contrario de lo ocurrido con los otros grupos, para cladóceros y ostrácodos se observan valores más altos en la estación 1. Otros grupos, constituidos por misidáceos, isópodos, eufausiáceos, pteropodos, poliquetos, larvas de peces y de invertebrados, mostraron sus mayores valores en diciembre y marzo si bien su porcentaje fue muy bajo oscilando entre 0,06% y 1,63%.

DISCUSIÓN

Los valores medios de biomasa observados en ambas estaciones se encuentran en el rango de los observados por Hernández-León (1988a). Los máximos valores para la biomasa y la abundancia se registraron en noviembre en la estación 3. La aparición de un máximo en la biomasa en esta época del ciclo en aguas del archipiélago Canario fue descrito por Fernández de Puelles (1987) para una estación al NE de la isla de Tenerife. Por otra parte, los valores mínimos para ambos parámetros se observaron en diciembre, lo que coincide con lo ya descrito por Fernández de Puelles (1987) y Hernández-León (1988c). Como era de esperar, las variaciones en el número total de individuos se vieron influenciadas por los cambios en la población de copépodos, que alcanzó hasta un 90% de representación en los meses donde la biomasa proteica y el número de individuos disminuyeron. El valor medio observado en el número de copépodos fue del 75% estando en el rango de los citados para el área de Canarias que oscilan entre un 64% (Mingorance, 1983) y un 85% (Hernández-León, 1988c). Los apendiculariáceos representaron más del 35% del total en noviembre. Este aumento en el número de apendiculariáceos, organismos que se alimentan de nano y ultraplanton, coincidió con un pequeño pico de clorofila *a* observado en el área (Aristegui *et al.*, 1989). Los quetognatos presentaron durante todo el periodo de muestreo porcentajes inferiores al 2%, valores similares a los observados por Hernández-León (1988c). El resto de los grupos no mostraron una representación importante. Es de destacar que la densidad media de organismos fue superior a la encontrada por otros autores en el archipiélago canario (Tabla II), si exceptuamos los resultados de Santamaría *et al.* (1989). Estos valores en la abundancia media pudieran estar influenciados por los procesos de mezcla vertical sobre la plataforma en las zonas turbulentas, potencialmente más productivas. A este respecto debemos considerar que el periodo de este muestreo tuvo lugar en cinco meses que incluyeron la época más productiva dentro del ciclo anual en aguas de Canarias.

En general, se observó un mayor número de individuos en la estación 3 en relación a la estación 1. Por otra parte, los individuos de la estación 3 fueron de menor biomasa individual, mientras que en la estación 1 la biomasa individual fue superior.

Este resultado se sustenta con lo postulado por Rodríguez y Mullin (1986), quienes encuentran que una perturbación en el ecosistema se traduce en un incremento de la biomasa del zooplancton de pequeña talla y con altas tasas de renovación, de forma que estas variaciones son más importantes que las fluctuaciones registradas en el número de especies o de individuos. Esta apreciación podría ser la causa de las diferencias observadas entre la biomasa expresada como proteínas y como número de individuos. Asimismo, Hernández-León (1988b) encuentra en las zonas de turbulencia mayor actividad del sistema de transporte de electrones como índice de la actividad respiratoria del zooplancton. Dicho fenómeno pudiera estar relacionado con la presencia de estos organismos de menor tamaño y con una mayor actividad metabólica.

Ambas estaciones mostraron características distintas. En la estación 1 se registraron para el fitoplancton valores bajos de clorofila *a* \cdot cel^{-1} (Aristegui *et al.*, 1989) mientras que el zooplancton mostró, entre febrero y mayo, pequeñas variaciones en su biomasa, registrándose un aumento en la talla individual hacia el mes de mayo. La estación 3 estuvo influenciada por una fuerte advección y un régimen más turbulento debido a la continua acción de los vientos alisios. Como resultado, los nutrientes se repartieron rápidamente en la columna de agua. El fitoplancton de esta estación presentó mayores valores de clorofila *a* \cdot cel^{-1} y números de asimilación más altos, lo que indica la presencia de fitoplancton más activo (Aristegui *et al.*, 1989). La producción primaria, relativamente alta en esta estación (Tabla II), permitió mantener una mayor biomasa de mesozooplancton de pequeño tamaño así como una gran actividad metabólica. Estos resultados redundan en la idea de que los ecosistemas costeros con plataformas más o menos extensas al sur de Gran Canaria son más productivos que los ecosistemas oceánicos, siendo capaces de mantener una producción secundaria de relativa importancia.

El presente trabajo representa una contribución a la descripción de los procesos productivos debidos al mesozooplancton, que ocurren en la zona de plataforma al sur de Gran Canaria.

AGRADECIMIENTOS

Deseamos expresar nuestro agradecimiento al Dr. Santiago Torres Curbelo por su colaboración en el presente trabajo. Este trabajo fue subvencionado en parte por el proyecto 82/22.04.85 del Gobierno Autónomo de Canarias.

BIBLIOGRAFÍA

- ARÍSTEGUI, J., S. HERNÁNDEZ-LEÓN, M. GÓMEZ, L. MEDINA, A. OJEDA & S. TORRES. (1989). Influence of the north trade winds on the biomass and production of neritic plankton in Gran Canaria. In: Topics in Marine Biology. Ros, J.D. (Ed.). *Scient. Mar.*, 53 (2-3):223-229.
- BRAUN, J.G. (1981) Estudios de producción de las Islas Canarias. II Producción del zooplancton. *Bol. Inst. Esp. Oceanogr.*, 290:89-96.

- FERNÁNDEZ DE PUELLES, M.L. (1986). Ciclo anual de la comunidad de meso y microzooplancton; su biomasa, estructura, relaciones tróficas y producción en aguas de las Islas Canarias. *Tesis Doctoral*, Univ. Autónoma de Madrid, 275pp.
- FERNÁNDEZ DE PUELLES, M.L. (1987). Evolución anual del microzooplancton en aguas de las Islas Canarias. *Bol. Inst. Esp. Oceanogr.*, 4(2):79-90.
- GARCÍA-RAMOS, C, J.G. BRAUM, J.M. RODRÍGUEZ & J.E. ESCÁMEZ (1990). Seasonal distribution of zooplankton in Canary islands waters in the upper 200 meters. *ICES. Biological Oceanogr. Committee*, N1 199.
- HERNÁNDEZ-LEÓN, S. (1986). Efecto de masa de isla en aguas del Archipiélago Canario según estudios de biomasa y actividad del Sistema de Transporte de Electrones en el mesozooplancton. *Tesis Doctoral*. Univ. La Laguna. 402 pp.
- HERNÁNDEZ-LEÓN, S. (1987). Actividad del Sistema de Transporte de Electrones en el mesozooplancton durante un máximo primaveral en aguas del Archipiélago Canario. *Inv. Pesq.*, 51(4): 491-499.
- HERNÁNDEZ-LEÓN, S. (1988a). Ciclo anual de la biomasa del mesozooplancton sobre un área de plataforma en aguas del Archipiélago Canario. *Inv. Pesq.*, 52(1):3-16.
- HERNÁNDEZ-LEÓN, S. (1988b). Gradients of mesozooplancton biomass and ETS activity in the wind shear area as evidence of an Island Mass Effect in the Canary Island waters. *J. Plankton Res.*, 10(6):1141-1154.
- HERNÁNDEZ-LEÓN, S. (1988c). Algunas observaciones sobre la abundancia y estructura del mesozooplancton en aguas del Archipiélago Canario. *Bol. Inst. Esp. Oceanogr.*, 5(1):109-118.
- HERNÁNDEZ-LEÓN, S. (1991). Accumulation of mesozooplancton in a wake area as a causative mechanism of the «island-mass effect». *Mar. Biol.*, 109: 141-147.
- HORWOOD, J.W. & R. M. DRIVER (1976). A note on a theoretical subsampling distribution of macroplankton. *J. Cons. explor. Mer*, 36(3):274-276.
- LOWRY, P.H., N.J. ROSENBOUGH, A.L. FARR & R.J. RANDALL (1951). Protein measurement with a Folin phenol reagent. *J. Biol. Chem.*, 193:265-275.
- MINGORANCE, M.C. (1983). Introducción al estudio del ciclo anual del zooplancton de la isla de Tenerife, con especial atención al grupo de los cladóceros. *Tesina*. Univ. La Laguna, 109 pp.
- RODRÍGUEZ, J. & M.M. MULLIN (1986). Diel and interannual variation of size distribution of oceanic zooplankton biomass. *Ecology*, 67:215-222.
- SANTAMARÍA, M.T. (1984). Estudio comparativo de las comunidades zooplanctónicas en San Andrés y Los Cristianos (Tenerife). *Tesina*. Univ. La Laguna, 97 pp.
- SANTAMARÍA, M.T.G, J.G. BRAUM, J.D. DE ARMAS, F.C. REAL, J.E. ESCAMEZ y J.E. VILLAMANDOS (1989). Estudio comparativo de las comunidades zooplanctónicas en San Andrés y los Cristianos. (Tenerife). *Bol. Inst. Esp. Oceanogr.*, 5(2): 57-70.
- UNESCO (1968). Zooplankton sampling. *Monography of Oceanographical Methods*. 2:1-174.

	E-1	E-3	Total
Biomasa mg prot·m ⁻³	3,64 ± 1,46	4,09 ± 1,64	3,89 ± 1,48
Abundancia ind·m ⁻³	964 ± 364	1208 ± 662	1087 ± 520
Peso ind.(µg prot·ind ⁻¹)	4,50 ± 2,73	3,64 ± 0,95	4,02 ± 1,86
Copépodos	700 ± 209 (75%)	858 ± 394 (74%)	779 ± 309 (75%)
Apendicularios	219 ± 175 (20%)	292 ± 290 (20%)	242 ± 240 (20%)
Quetognatos	12 ± 4 (1%)	18 ± 8 (2%)	15 ± 7 (1,5%)
Ostrácodos	6 ± 7 (0,7%)	5 ± 5 (0,5%)	6 ± 5 (0,6%)
Cladóceros	2 ± 3 (0,1%)	0,8 ± 1 (0,05%)	1 ± 2 (0,1%)
Huevos	16 ± 7 (2%)	21 ± 16 (2%)	18 ± 12 (2%)
Otros Crustáceos	3 ± 3 (0,3%)	6 ± 2 (0,7%)	5 ± 3 (0,5%)
Gelatinosos	2 ± 2 (0,3%)	2 ± 1 (0,2%)	2 ± 2 (0,3%)
Otros	5 ± 2 (0,5%)	6 ± 3 (0,6%)	5 ± 3 (0,6%)
Clorofila \underline{a} (µg·l ⁻¹) *	0,19 ±	0,18 ±	
Células·ml ⁻¹ *	1 ±	0,3 ±	
Producción Primaria. (mg C·m ⁻³ ·h ⁻¹)*	0,46 ±	0,77 ±	
Número de Asimilación (mg C·mg Cl a ⁻¹ ·h ⁻¹)*	2,55 ±	5 ±	

Tabla I.- Valores comparativos entre ambas estaciones y la media para el área. E-1, estación situada en la calma. E-3, estación situada en la zona turbulenta. (*) Datos tomados de Arístegui *et al.*, (1989).

Referencia	Abundancia (No. ind/m ³)	Área
Braun (1981)	253	NE Tenerife
Mingorance (1983)	420	Sur Tenerife
Fernández De Puelles (1986)	282	NE Tenerife
Hernández-León (1988c)	553	Sur G.Canaria
Santamaría <i>et al.</i> (1989)	1314	NE Tenerife
« «	760	Sur Tenerife
García Ramos <i>et al.</i> (1990)	444	NE Tenerife
« «	616	SW Tenerife
Presente trabajo	1284	E-3, SW G.Canaria.
« «	964	E-1, SW G.Canaria.

Tabla II.- Densidad media de organismos mesozooplancónicos en el área de Canarias.

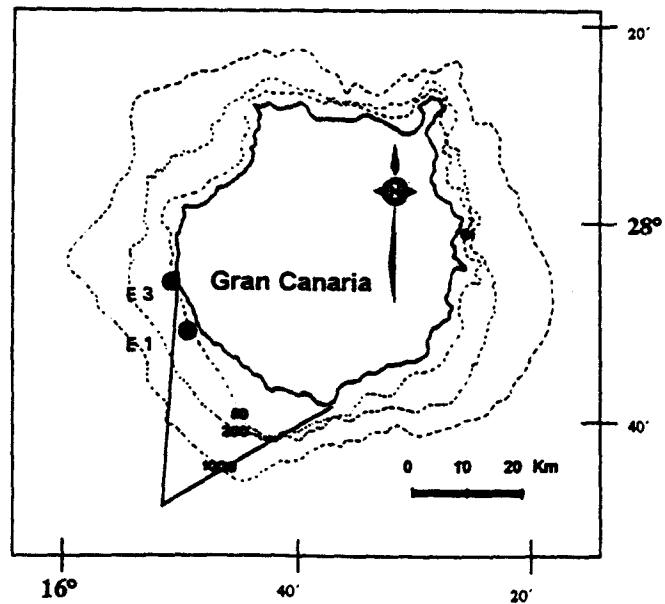


Fig. 1.- Posición de las estaciones muestreadas, en relación a la estela formada a sotavento de la isla por los vientos alisios dominantes en el área.

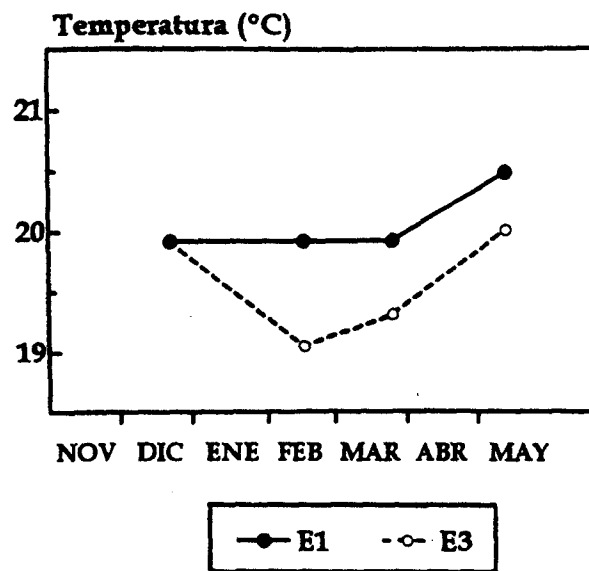


Fig. 2.- Cambios en la temperatura superficial del agua, durante el período de estudio para ambas estaciones. Tomado de Aristegui *et al.* (1989).

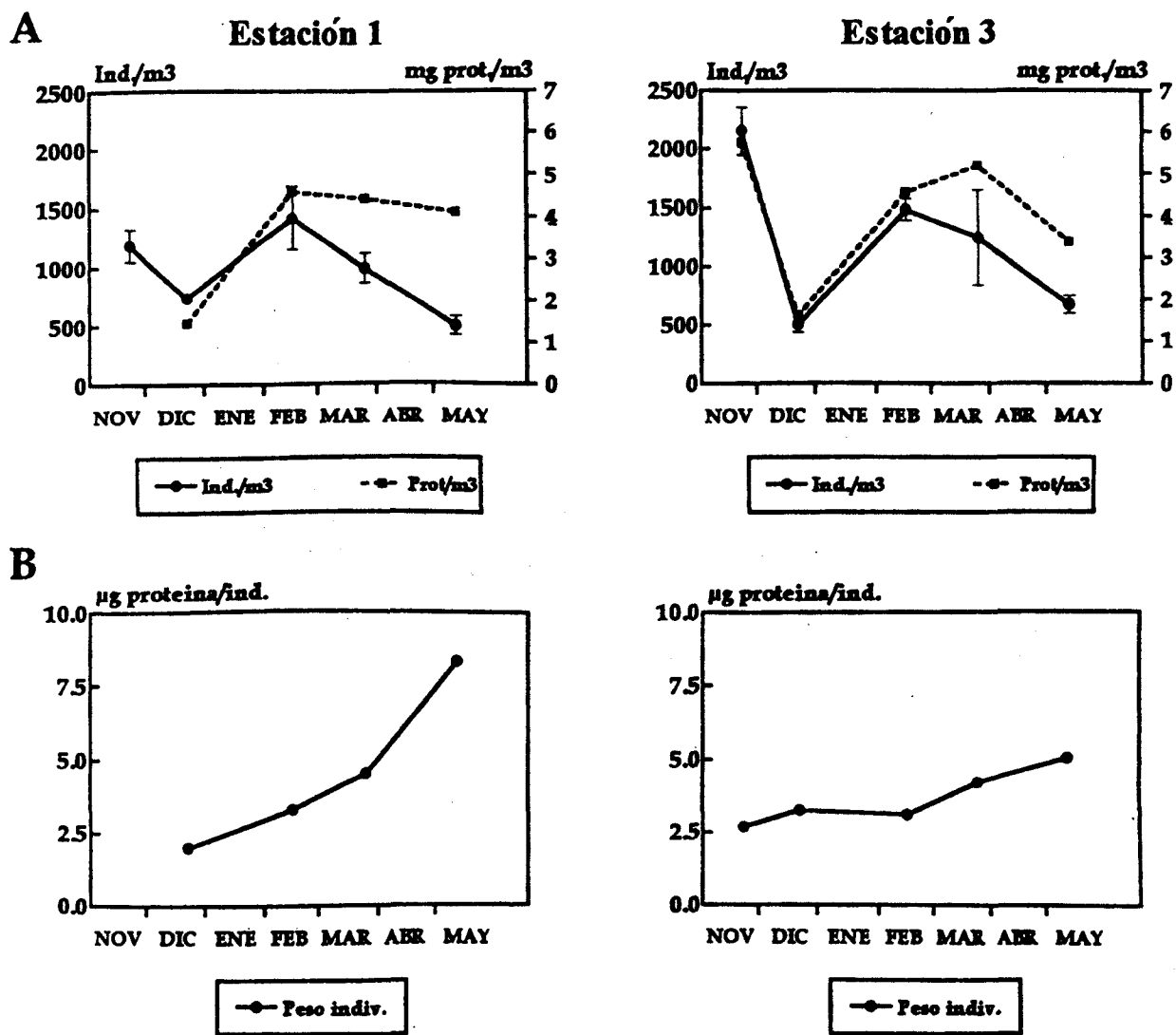


Fig. 3.- A) Evolución de la biomasa proteica y de la abundancia de organismos en las dos estaciones. B) Peso individual de los organismos (cociente entre la biomasa proteica y el número total de individuos) para ambas comunidades.

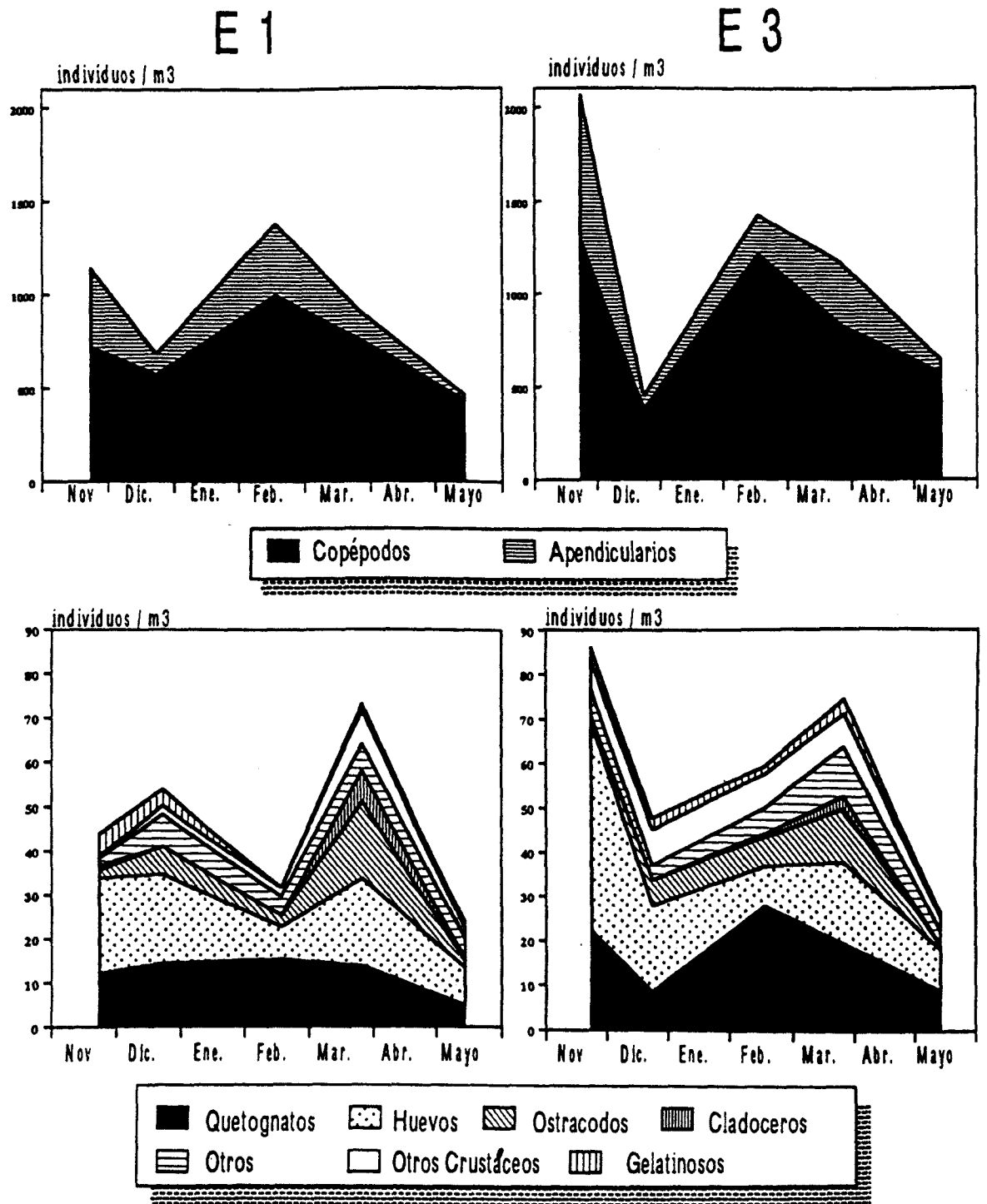


Fig. 4.- Densidad de organismos dentro de los distintos grupos considerados (copépodos y apendiculario se ha separado del resto por su mayor abundancia).

The octopus (*Octopus vulgaris*) in the small-scale trap fishery off the Canary Islands (Central-East Atlantic)

V. Hernández-García¹, J.L. Hernández-López, J.J. Castro^{*}

Departamento de Biología, Universidad de Las Palmas de Gran Canaria, Apdo. 550, 35017 Las Palmas de Gran Canaria, Canary Islands, Spain

Received 3 June 1997; accepted 21 December 1997

Abstract

A small-scale trap fishery for many benthic species is carried out along the coastal shelves of the Canary Islands (Central-East Atlantic) by small boats (7.5 to 12.4 m in length). The target species of the fishery are seabreams (Sparidae), but substantial numbers of octopus (*Octopus vulgaris*) are also landed. In this paper, we report fishing data for octopus landed at the port of Mogán (Southwest of Gran Canaria) from 1989 to 1996. The landing of *O. vulgaris* increased steadily from 1989 to 1994, from 7 t to 25 t. However, in 1995, the catch fell to the level of 1989 (7 t), and in 1996 was only 6 t, the lowest figure for the decade. The CPUE shows two seasonal peaks of maximal abundance, one in April–May and the other in September–November, both coinciding with reproductive periods, while the lowest figure is in summer (July–August). We describe the fishing methods and the seasonal variations of the catch records and fishing effort in relation to years and market strategies. © 1998 Elsevier Science B.V. All rights reserved.

Keywords: *Octopus vulgaris*; Cephalopods; Artisanal fishery; Trap fishing; The Canary Islands

1. Introduction

In the Canary Islands, there are no accurate landing statistics which reflect the evolution of the small artisanal fisheries over the entire coastal area. Due to the complex morphology of the coastlines of these islands, the artisanal fleet lands the catches at a great variety of ports and beaches, making it difficult to obtain the total catch data for the whole of the archipelago. However, in some ports, thanks to the

trading network, there are catch data for the most recent two decades.

The cephalopods caught in the Canary Islands are mostly *Octopus vulgaris* and to a lesser extent, *Sepia officinalis*. There are also seasonal fisheries of pelagic species like *Loligo* spp. in the winter and *Sthenoteuthis pteropus* and *Ommastrephes bartramii* in the summer (Hernández-García, 1995). Catches of squid, via hand-jigging, are sparse and poorly documented.

O. vulgaris is also the target species of a fishery developed on the neighbouring African shelf (García-Cabrera, 1968; Guerra and Pérez-Gándaras, 1983; Hernández-García and Bas, 1993) with annual catches which have regularly reached over 100 000 t

^{*} Corresponding author. Tel.: +34 28 454549; fax: +34 28 452922; e-mail: josejuan.castro@biologia.ulpgc.es

¹ Also corresponding author. E-mail: vicente.hernandez@biologia.ulpgc.es

(Guerra and Pérez-Gándaras, 1983; Bravo de Laguna, 1985; FAO, 1988, 1991; Bravo de Laguna and Balguerías, 1993). *O. vulgaris* and *S. officinalis* are caught in the Canary Islands trap fishery which is designed for demersal fish. There is no direct demersal cephalopod fishery. Thus, the seasonal variations in catch are related not only to the life cycle of the species but also to the fishing objectives and gear used at any time. This latter aspect is especially relevant when the fishery for demersal species becomes secondary to tuna fishing by the same fleet (Bas et al., 1995).

This paper describes, for the first time, catch levels and the fluctuations in the abundance of *O. vulgaris* recorded over the last two decades from the small-scale trap fishery off the coastline of the Canary Islands, based on catch data from 1980 to 1996 and effort data, as fishing days, from 1989 to 1996.

2. Methods

In order to describe the level of exploitation of the octopus in the Canary Islands, we used the port of Mogán as the main basis of the study (Fig. 1). This port is considered representative of the fishing activ-

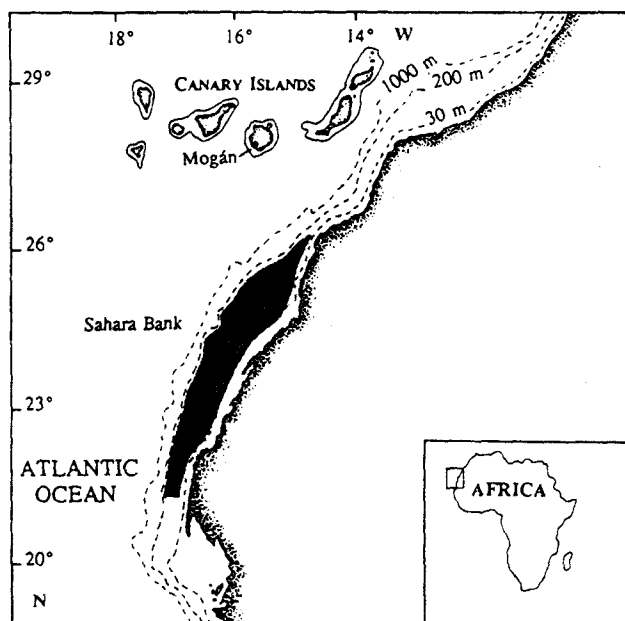


Fig. 1. Location map of the Canary Islands, the insular and continental shelves and the octopus fishery area in the Sahara Bank (around the islands, the 1000-m deep isobath is shown).

ity in Gran Canaria and we estimated that, together with the port of Arguineguín, both represent over 80% of the catch landed by the artisanal fleet on the island. Mogán is located to the southwest of Gran Canaria and is one of the most important ports in the archipelago both in fishing potential and level of catches landed. However, the choice of this port was made not only on account of these characteristics, but also because all the catches over the last two decades have been recorded by one fishmonger, thus providing landing statistics for this port. The fishing data from 1980 to 1988 were obtained from the literature (González et al., 1991), but there is a lack of information on the fishing effort deployed. We were able to obtain the daily catch data (in kilograms) by species and the days devoted to benthic and tuna fisheries by boats from 1989 to 1996. However, we could not verify the exact number of traps deployed monthly per boat each year.

The CPUE was estimated monthly from the total weight in kilograms of octopus caught per month from 1989 to 1996 divided by the monthly effort deployed. We used, as an effort unit, the average number of days devoted to trap fishery by boat. However, the unit of effort (f) should be calculated in the following way:

$$f = B_y F_j \bar{T}_d \bar{i} \bar{T}_h,$$

where B_y is the average number of boats per month throughout the year, F_j is the average number of fishing days per boat per month, \bar{T}_d is the average number of traps deployed per boat, \bar{i} is the average soak time in days, and \bar{T}_h is the average number of traps lifted every fishing day. However, due to the complexity of calculating \bar{T}_d , \bar{i} and \bar{T}_h , we obtained these information by interviewing some fishermen personally on site (the crews of seven boats which represented about 25% of the fleet) and determined that these parameters were almost constant for all the fishery. So, in the calculation of the monthly CPUE, we used only the number of fishing days per boat per month as the unit of effort.

The statistical analysis of data was conducted to find differences in the effort deployed from 1989 to 1996 and the implications of these on the variations of the CPUE. The evolution of catches was also analysed to determine significant variations in abun-

dance. Given the fact that the catch data series did not show a normal distribution, the Kruskal–Wallis ANOVA test by Ranks and Friedman (nonparametric statistical methods) was used.

3. Results

3.1. Description of the fishery

Cephalopods are caught in the Canary Islands in two types of fisheries. Benthic species (*O. vulgaris* and *S. officinalis*) are caught in a trap fishery while the pelagic species are caught in winter (*Loligo* spp.) and summer (*S. pteropus* and *O. bartramii*) via hand-jig fishery. The benthic species support higher catch levels than the pelagic.

The artisanal fishing fleet based in the port of Mogán is made up of 31 wooden crafts ranging in length from 7.5 to 12.4 ms ($\bar{x} = 9.4$, $SD = 1.2$) which are equipped with 18–150 hp ($\bar{x} = 52.7$, $SD = 44.2$) engines. Most of these boats catch demersal fish over almost the whole year using traps, line or longline (26 boats). A great number of these boats (23 boats) gave up this type of fishing to fish tuna in the summer and fall, although some operate both fisheries simultaneously (5–13 boats according to the years). The crew of this artisanal fleet was made up of 94 men in December 1994. The small boats are manned by two fishermen and the larger ones by three to four fishermen. Fishing is carried out at depths ranging from between 18 m and 200 m.

O. vulgaris is caught by traps, which are made of iron, are circular in shape and covered with metallic mesh (Fig. 2). There are two types of traps: small ones (the mesh size is 31.6 mm) used for fishing in shallow waters and larger traps with wider mesh size (over 60 mm) used for deep waters. These gears are used the whole year round, although during the tuna season, only two to four boats are devoted exclusively to fishing with traps.

The information obtained from the interviews of fishermen was that the average number of traps deployed per boat was 275 (between 150 and 400), the average soak time was five days (between 3 days and a week, sometimes 15 days) and the average number of traps hauled every fishing day was 50 (between 8 and 10 lines of five–six traps each).

3.2. The catches from 1980 to 1996

The catch of octopus during this period showed strong fluctuations (Table 1). In 1982, a catch of 21.5 t was obtained, but this decreased by about 40% in 1983 and reached an all-time low of 3 t in 1985 (15% of the 1982 catch). After the maximum landing of the two decades reached in 1994, the 1995 catch dropped to 28%, falling to the level of 1989. In 1996, the catch fell to the lowest level of the decade (24% of the catch obtained in 1994).

The fishing effort exerted by the fleet increased gradually, although not significantly (Kruskal–Wallis ANOVA, $H(7, N = 96) = 12.25$, $P < 0.09$), from 1989 to 1994 with a slight decrease in 1995 and an

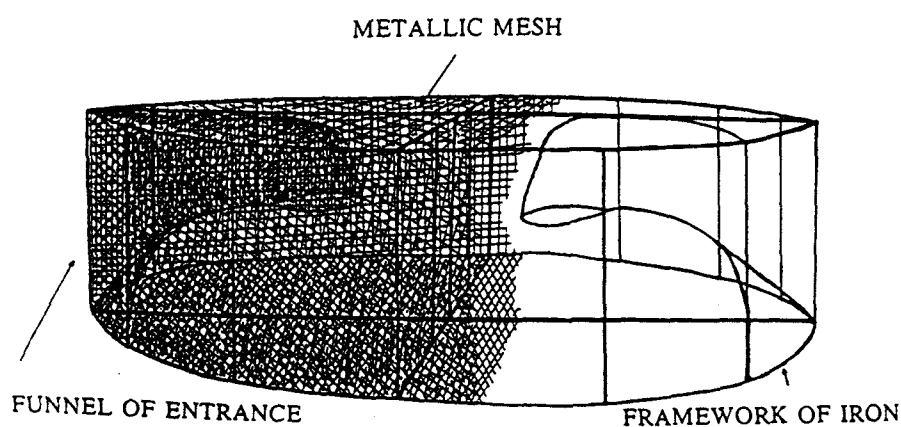


Fig. 2. Detailed diagram of the trap used for benthic fish species (especially, *O. vulgaris* and *S. officinalis*).

Table 1

Fishing days and total catch (in kg) of octopus and skipjack tuna landed at the port of Mogán (Gran Canaria Island) from 1980 to 1996

Year	Catches of octopus	Catches of skipjack	Days devoted to trap fishery	CPUE of octopus	Days devoted to skipjack fishery
1980	2181	148 811			
1981	9884	186 735			
1982	21 472	319 465			
1983	8340	67 511			
1984	5217	145 146			
1985	3136	267 635			
1986	3541	142 646			
1987	6045	238 854			
1988	4936	113 279			
1989	7006	334 336	1209	5.79	
1990	7096	431 457	1544	4.59	1080
1991	11 412	627 441	1742	6.55	919
1992	15 561	1056 925	1145	13.59	1235
1993	19 507	230 577	1638	11.91	834
1994	25 209	569 072	2931	8.60	842
1995	7409	981 534	1645	4.50	1867
1996	6007	616 657	1693	3.55	1586

increase again in 1996. The CPUE of the trap fishery from 1989 to 1996 shows significant variations from year to year (Friedman ANOVA, $P < 0.001$). The

main fluctuation was originated in the CPUE values from 1992 to 1994, a period during which they were maximal and did not show significant differences

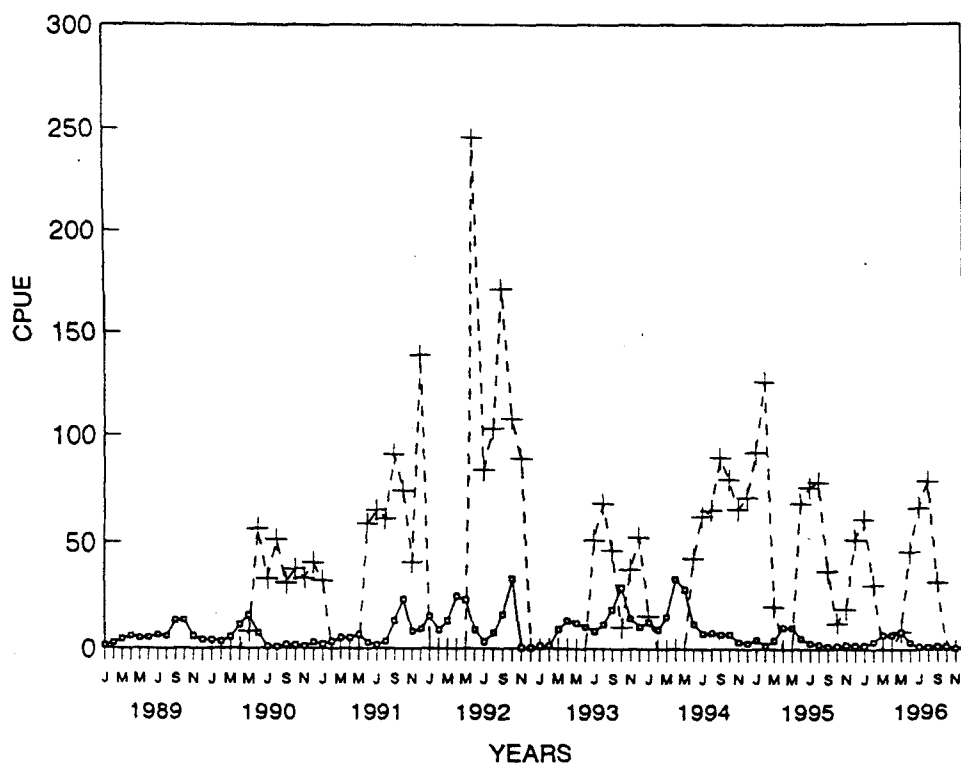


Fig. 3. Monthly CPUE of *O. vulgaris* (unbroken line) and *K. pelamis* (dashes) landed at the port of Mogán (Gran Canaria Island) from 1989 to 1996. Values of the CPUE of skipjack tuna plotted are divided by 10.

(Friedman ANOVA, $P < 0.47$). The CPUE figures before and after this latter period (1992–1994) were lower and not significantly different the one from the other (Friedman ANOVA, $P < 0.49$).

3.3. Monthly evolution of catches

The octopus CPUE reveals two seasonal peaks of maximum abundance, one between April and May and the other from September to November (Kruskal–Wallis ANOVA, $H(3, N = 32) = 1.568$, $P = 0.67$). The lowest CPUE is in July and August and is coincidental with the maximum in tuna CPUE (Fig. 3). The highest peak varies in time between spring and autumn, fluctuating from year to year.

The effort deployed by the fleet in the trap fishery was clearly seasonal, with significantly lower effort during the summer (Kruskal–Wallis ANOVA: $H(3, N = 32) = 16.65$, $P < 0.001$). The mean number of fishing days per month in the trap fishery ranged from 95 in 1992 to 244 in 1994 (Table 1).

The monthly CPUE of the trap fishery decreased during the period of the tuna season when most of the fleet were devoted to fishing tuna. The summer captures of tuna fluctuate from year to year, due to variations in the price of skipjack (*Katsuwonus pelamis*), the most common tuna species caught in the Canary Islands. When the price of skipjack in the fish market was high, the catches of benthic species (especially fish) during the summer were low and vice versa. However, the most frequent pattern in the trap fishery is a significant decrease in the CPUE figures during the months between July and September (Kruskal–Wallis ANOVA, $H(3, N = 96) = 12.308$, $P = 0.006$).

4. Discussion

Although octopus is not the target species of the trap fishery off the Canary Islands, it is important in the catches landed by the artisanal fleet. Octopus ranked first in catches in 1992 and 1993, falling progressively to fourth in the three following years, to be later replaced in catches by the common seabream (*Sparus pagrus pagrus*), common pandora (*Pagellus erythrinus*), and red mullet (*Mullus surmuletus*).

The variations in the catch figures throughout the year for the fishery of octopus are a consequence of the combination of the fishing strategy and the species' life cycle. We have observed two peaks of maximum catch of octopus, one in April–May and the other in September–November, coinciding with the reproductive periods (Fig. 4). The concentration of individuals for spawning would probably give local and high catches of this species (Mangold, 1983). During spawning, individuals are concentrated in shallow waters, a fact which fishermen take advantage of. The lowest catch rates of octopus are obtained in the summer.

We think that the monthly changes in the CPUE indicate that the most important factor for the seasonal fluctuations is the life cycle of the species. On the Sahara Bank, the most important fishing grounds close to the Islands, the reproductive cycle of the octopus features a spawning maximum in spring, generating a peak of recruitment of immature individuals in autumn. Hatanaka (quoted in FAO, 1982) pointed out the existence of a second spawning in autumn, weaker than in the spring, which generates individuals to form part of the reproductive stock the next autumn. Similar results were obtained by Nigmatullin and Ostapenko (1977) and Nigmatullin and Barkovsky (1990) in the Cape Blank area. In support of these studies, we have found that the catches in Mogán in June and July 1996 were made up of large specimens (800–2500 g), and included spent speci-

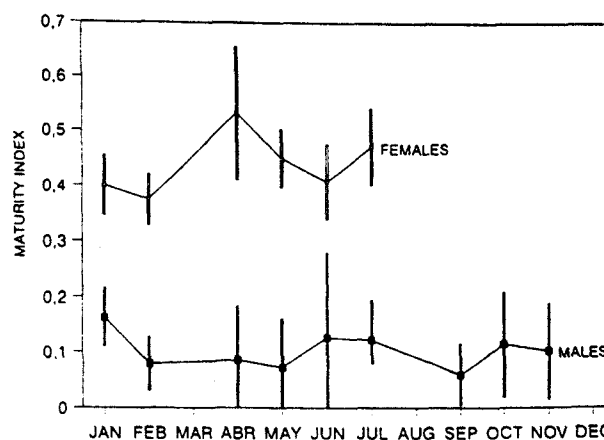


Fig. 4. Monthly evolution of the maturity index of *O. vulgaris* caught off the Canary Islands (the maturity index was calculated sensus Guerra, 1975).

mens. The decline of the CPUE of octopus in the summer, despite reduced fishing effort, indicates a decline in abundance of octopus in the fishing area during this period, probably as a result of the withdrawal of the population to deeper areas (outside the grounds of the trap fishery) as suggested by Mangold (1983).

As Table 1 illustrates, there was a gradual increase in the catches of *O. vulgaris* from 1985 to 1994 (from 3 to 25 t). In 1995 and 1996, the catch dropped below the level of 1989, although the CPUE values were not different from those obtained before 1992. It is of great concern to find a decline in the CPUEs in 1995 and 1996 below those of 1992–1994, despite similar fishing effort levels. We have serious doubts as to whether the fishing effort was constant over the period studied. Although the number of fishing days did not vary significantly, we know that the number of traps deployed by boat has increased, but we were not able to quantify it. This increase in the number of traps deployed by boat has generated a decline in the abundance of the octopus population during recent years, and is also reflected in the catches of other fish species which were caught in the trap fishery. The total CPUE (including all the demersal species caught) has been relatively stable, with highest levels in 1994 and lowest levels in 1990 and 1995. In 1996, the total CPUE went back to 'normal' figures.

Nonetheless, the catch of octopus in 1982 was of the same order as that of 1994 (Table 1), and after this first peak, catches declined to 40% and remained at lower values over the following years. These two peaks (1982 and 1994) and their successive decline periods could be related to warm and cold episodes of similar characteristics, that of 'El Niño' (NOAA Climate Prediction Center). This sudden decline in abundance may imply that the fishery resources are being heavily exploited, not only for the cephalopod species but also for several benthic fish species which are targets of the artisanal fleet (Pajuelo and Lorenzo, 1995, 1996). Basing our judgments on the analysed data, we cannot rule out the idea that the evolution of catches could indicate a cyclical variation in the abundance of octopus. The lack of fishing effort data previous to 1989 does not allow us to reach any definite conclusions with respect to the true nature of this fishery. We need to continue to

compare these results against the catches of the next few years.

Acknowledgements

Our thanks to Mrs. Leo Hernández and the staff of La Moganera and the Fishermen Association of Mogán for making available the information for this paper. Thanks are also given to Mrs. Ana Santana-Ortega, Eva Gómez and Catalina Caballero for their assistance in data collection. Special words of thanks to Prof. Carlos Bas for his helpful suggestions.

References

- Bas, C., Castro, J.J., Hernández-García, V., Lorenzo, J.M., Moreno, T., Pajuelo, J.G., Ramos, A.G., 1995. La Pesca en Canarias y Áreas de Influencia. Ediciones del Cabildo Insular de Gran Canaria, Madrid, 300 pp.
- Bravo de Laguna, J., 1985. Los recursos pesqueros del área de afloramiento del NO africano. In: Bas, C., Margalef, R., Rubies, P. (Eds.), Simposio Internacional Sobre las Áreas de Afloramiento más Importantes del Oeste Africano (Cabo Blanco y Benguela), Vol. 2. Instituto de Investigaciones Pesqueras, Barcelona, pp. 761–778.
- Bravo de Laguna, J., Balguerías, E., 1993. La pesquería sahariana del cefalópodos: una breve revisión. Bol. Inst. Esp. Oceanogr. 9 (1), 203–213.
- FAO, 1982. Rapport du groupe de travail special sur les stocks de céphalopodes de la région nord du COPACE. COPACE/PACE SERIES 82/24 (Fr.), Rome, 180 pp.
- FAO, 1988. Fishery information, data and statistics service. Statistical Bulletin for the Fishery Committee for the Eastern Central Atlantic (CECAF), No. 5. Nominal Catches, 1974–1986. Fishery Committee for the Eastern Central Atlantic, FAO, Rome.
- FAO, 1991. Fishery information, data and statistics service. Statistical Bulletin for the Fishery Committee for the Eastern Central Atlantic (CECAF), No. 6. Nominal Catches, 1977–1989. Fishery Committee for the Eastern Central Atlantic, FAO, Rome.
- García-Cabrera, C., 1968. Biología y pesca del pulpo (*Octopus vulgaris*) y choco (*Sepia officinalis hierredda*) en aguas del Sahara español. Publ. Téc. Jun. Est. Pesc. 7, 141–198.
- Guerra, A., 1975. Determinación de las diferentes fases del desarrollo sexual de *Octopus vulgaris* Lamarck, mediante un índice de madurez. Inv. Pesq. 39 (2), 397–416.
- Guerra, A., Pérez-Gándaras, G., 1983. Las pesquerías mundiales de cefalópodos: situación actual y perspectivas. Inf. Téc. Inst. Inv. Pesq. 102–104, 139 pp.
- González, J.A., Santana, J.I., Carrillo, J., 1991. La Pesca en el puerto de Mogán (Islas Canarias): flota, artes y análisis de las capturas entre 1980 y 1990. In: Cabildo Insular de Gran

- Canaria (Ed.), Informe Técnico del Centro de Tecnología Pesquera (Pesquerías), Telde, Las Palmas, 32 pp.
- Hernández-García, V., 1995. Contribución al conocimiento bioecológico de la Familia Ommastrephidae (Steenstrup, 1857) en el Atlántico Centro-Oriental. PhD Thesis, Universidad de Las Palmas de Gran Canaria, Canary Islands, Spain, 307 pp.
- Hernández-García, V., Bas, C., 1991. Análisis de la evolución de las tallas de los cefalópodos explotados en la Costa del Sahara (División 34.1.3 de CEECAF) entre los períodos 1967–70 y 1989–90. Bol. Inst. Español Oceanogr. 9 (1), 215–225.
- Mangold, K., 1983. *Octopus vulgaris*. In: Boyle, P.R. (Ed.), Cephalopod Life Cycles, Vol. 1. Academic Press, London, pp. 335–364.
- Nigmatullin, Ch.M., Barkovsky, A.E., 1990. Seasonal grouping of *Octopus vulgaris* off Cap Blanc (Mauritania). In: 5th All-Union Conference on the Comm. Invertebrates, Minsk (Naroch), 9–13 Octubre 1990, Thesis Reports. VNIRO, Moscow, pp. 87–89.
- Nigmatullin, Ch.M., Ostapenko, A.A., 1977. Several features of the ecology of the common octopus (*Octopus vulgaris*) off the coast of Northwest Africa. In: All USSR Sci. Conference on Util. Comm. Invertebrates. Abstr. Report, pp. 56–57.
- Pajuelo, J.G., Lorenzo, J.M., 1995. Biological parameters reflecting the current state of the exploited pink dentex, *Dentex gibbosus* (Pisces: Sparidae), population off the Canary Islands. S. Afr. J. Mar. Sci. 16, 311–319.
- Pajuelo, J.G., Lorenzo, J.M., 1996. Life history of the red porgy, *Pagrus pagrus* (Teleostei: Sparidae), off the Canary Islands, Central-East Atlantic. Fish. Res. 28, 163–177.

MORPHOLOGICAL VARIABILITY IN *ILLEX COINDETII* (CEPHALOPODA: OMMASTREPHIDAE) ALONG THE NORTH-WEST COAST OF AFRICA

V. HERNÁNDEZ-GARCÍA AND J.J. CASTRO

Departamento de Biología, Universidad de Las Palmas de Gran Canaria, Apartado 550, Las Palmas de Gran Canaria, Canary Islands, Spain. E-mail: vicente.hernandez@biologia.ulpgc.es, josejuan.castro@biologia.ulpgc.es

This paper gives morphometric variations and dorsal mantle length–total weight (DML–TW) relationships for *Illex coindetii* in the eastern Central Atlantic area. Positive allometry was observed in males and negative in females of the species. The most variable body measurements between males and females were width and perimeter of the head. In the study area, divergence of morphometric measurement starts at 95 mm. The point of divergence, however, varies with latitude; fluctuating from 104 mm in the north (Morocco and Sahara) to 76 mm in the central area (Mauritania and north of Senegal) and 73 mm in the south (Gulf of Guinea).

The relationships between DML and TW showed that sexual dimorphism due to differential growth between males and females starts to occur at 56 mm ML. The starting point of sexual dimorphism (56 mm) varies according to the zone; the higher the latitude, the later it occurs. Thus, sexual dimorphism occurs at 49 mm in the south (Gulf of Guinea), at 54 mm in the central area (Mauritania and north of Senegal) and at 74 mm in the north (Morocco and Sahara). Females grow larger than males, but males were heavier at any given length. As latitude decreased, a slow down in the increase in weight-at-length was observed in both sexes.

INTRODUCTION

Length and weight are two basic variables in the biological study of any species at an individual or a population level. Thus information about the length and weight distribution of any population will provide more information on important aspects of how that population functions (Gulland, 1985). These distributions are the result of interactions between growth, reproduction and mortality, and may also be influenced by another totally independent component – the environment – which increases biological variability (Boyle, 1987). Furthermore, this provides other valuable information by combining the two variables (length and weight), along with the interrelation between the two and other specific biological parameters: e.g. mantle length and the weight of the nidamental glands in relation to reproduction.

Illex coindetii is a neritic species that inhabits inshore waters of the continental shelf, with a vertical range from the surface down to 1100 m, although it is most frequently found between 100 and 400 m. It is distributed throughout the eastern Atlantic, from the North Sea south along the coast of Europe, into the Mediterranean Sea and along the African coast to Angola. It is of great commercial

interest and the main fishing grounds of north-west Africa are located off Spanish Sahara, between 50 and 500 m, with maximum catches between 90 and 250 m, over mud and sandy bottoms (there are no separate statistics for the species) (Roper & Sweeney, 1981). Specimens of this species can reach a dorsal mantle length of 370 mm; 260 mm is common in females and 220 mm in males (Guerra, 1992).

The aim of this paper is to provide morphological relationships for *I. coindetii* and the geographical variations along the north-west coast of Africa. Geographical areas were selected in accordance with previous analyses (Hernández-García, 1995) which indicated significant differences in the maximum lengths attained by both sexes of *I. coindetii* as a function of latitude. This information will enhance our knowledge of the population structure of the species along the north-west coast of Africa, especially concerning the use of the data in evaluation models (Beverton & Holt, 1957).

MATERIALS AND METHODS

Illex coindetii is caught by trawlers along the north-west coast of Africa (Figure 1). A total of 1430 specimens were examined between 1990 and 1991. The dorsal length of the mantle (DML) was measured in mm, the total weight (TW) in grams and the sex

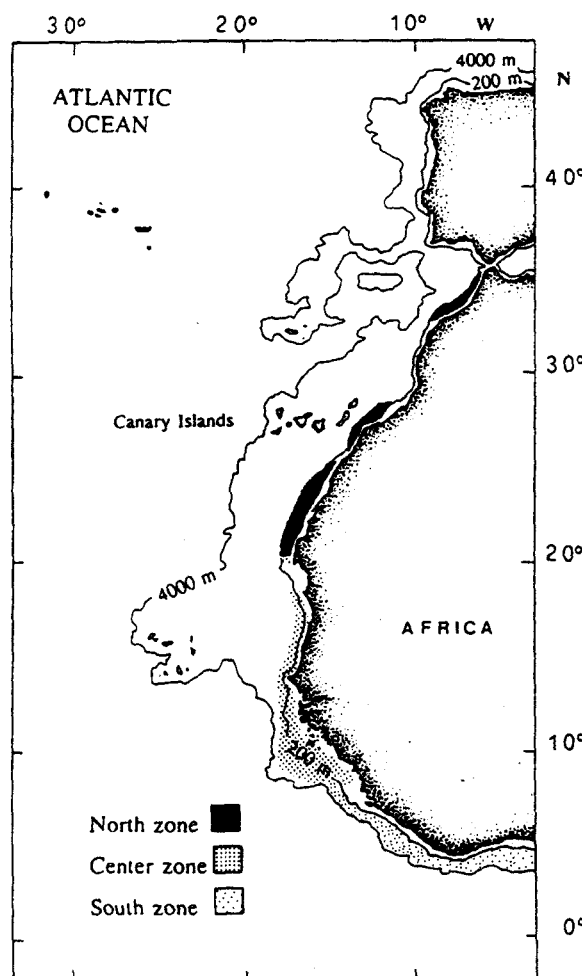


Figure 1. Map of north-west Africa subdivided into the three areas studied: north (Morocco and Sahara), central area (Mauritania and north of Senegal) and south (Gulf of Guinea).

determined for each specimen. The maximum width (Mw) and the maximum perimeter of the mantle (Mp), the maximum width and perimeter of the head (Hw and Hp respectively), fin height (F1), the width of the fins (Fw) and the length of the gladius (G1) were measured. Figure 2 shows these measurements organized in accordance with the definition of Roper & Voss (1983).

Huxley's model (Bas, 1959; Rodríguez-Roda, 1983) was used for processing and analysing the data. According to the model, the relationship between each of these body measurements and DML is a potential one that can be expressed by the following equation:

$$y = a \times x^b \quad (1)$$

where (x), the independent variable, represents DML and (y), the dependent variable, is any one of the aforementioned parameters; *a* and *b* are the coefficients that relate the two variables. The coefficients were obtained with linear regression after decimal logarithmic transformation of the data series, using the minimum squares method to minimize the sum of the squares of the vertical distances between the points and the line (Ricker, 1973). The relationship between DML and TW was calculated for each sex. The relationship between mantle weight (d1W) and eviscerated weight (d2W) with DML in a similar manner were also calculated.

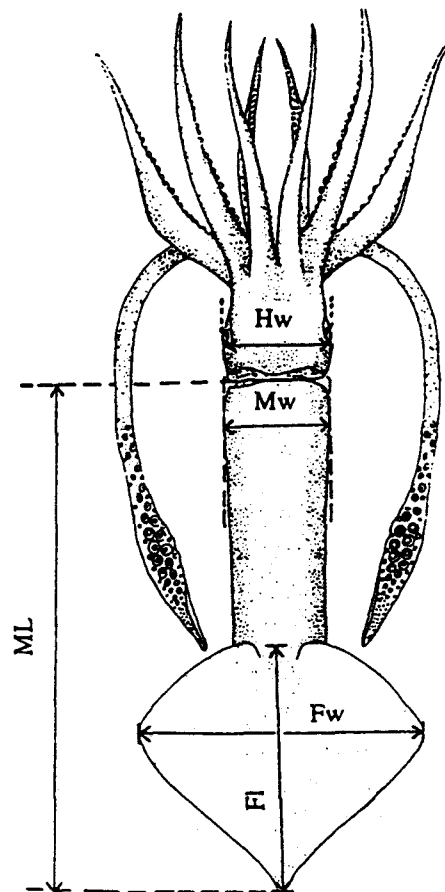


Figure 2. Diagram of an omastrephid cephalopod with the morphometric measurements taken in this study: DML, dorsal mantle length; Mw, maximum mantle width; Hw, maximum head width; F1, fin height; Fw, fin width.

Statistical analysis of the data was done with CSS: statistica software (StatSoft, Inc.). To find out whether the aforementioned morphometric parameters differed in their growth pattern between zones, the slope contrast test (Martín-Andrés & Luna del Castillo, 1990) was applied to the previously calculated linear regressions ($P < 0.05$ was considered significant).

RESULTS

Morphometric analysis

The measurements of DML and G1 provided a potential relationship between the two ($G1 = 1.002305 \times DML^{0.997}$, $\beta = 0.99895$). This value for β , approaching 1, indicates an isometric growth of the gladius with respect to DML.

Relationships between body measurements and DML show negative allometry, or are slightly isometric in females, whereas in males, the relationship is generally positive (Table 1A&B). There are notable differences between males and females in the growth pattern of the head (Hw and Hp). Females present an almost isometric pattern in head growth (Table 1A), whereas in males, head growth shows positive allometry in relation to DML (Table 1B). Divergence in head growth pattern between the sexes starts around 95 mm. When DML was around 120–150 mm, the ranges of Hw and Hp for the two sexes did not overlap. Nonetheless, size divergence varies according to latitude, with the point of divergence oscillating from 104 mm in the north (Morocco and Sahara), 76 mm in the central area (Mauritania and north of Senegal) to 73 mm in the south (Gulf of Guinea). The relationships DML–TW in both sexes did not show different slopes between the north and central zones, but they were significantly different with the south zone (Table 2).

Regressions for Mw and Mp with DML show lesser sexual dimorphism. This is due to the dispersion of the data, which, in turn, is because of the variability found among the different degrees of maturity. The F1–DML relationship showed significantly different slopes between sexes and they were allometrically positive, whereas the growth pattern for Fw was isometric in females and allometric positive in males (Table 1A&B).

Size–weight relationships

Weight in females varied between 11.83 and 750.68 g. In males, weight oscillated between 3.94 and 378.3 g. Sexual dimorphism due to differential growth rates between males and females started to occur around 56 mm DML. The starting point for sexual dimorphism varies according to the area and happens later as latitude increases. Starting points for sexual dimorphism were: 49 mm in the south, 54 mm in the central area and 74 mm in the north. Males were heavier than females at any given weight.

Table 1. Regression results for different body measurements compared to dorsal mantle length (DML) for specimens of *Illex coindetii* in each zone. The Student t-test was used.

A. Female specimens.

Zone	N	Morphometric relationships	β	r^2	F	P
North	218	Hw=0.186117×DML ^{1.002}	0.95393	0.9099	2183.7	<0.000001
Centre	86	Hw=0.156704×DML ^{1.023}	0.95583	0.9136	888.3	<0.000001
South	31	Hw=0.211940×DML ^{0.974}	0.96268	0.9267	366.9	<0.000001
North	218	Hp=0.583714×DML ^{0.969}	0.95819	0.9181	2421.9	<0.000001
Centre	86	Hp=0.402707×DML ^{1.033}	0.97465	0.9499	1594.3	<0.000001
South	31	Hp=0.664117×DML ^{0.940}	0.96635	0.9338	409.2	<0.000001
North	221	Mw=0.452622×DML ^{0.908}	0.93894	0.8816	1630.7	<0.000001
Centre	86	Mw=0.328511×DML ^{0.952}	0.91127	0.8304	411.3	<0.000001
South	31	Mw=0.401802×DML ^{0.896}	0.93138	0.8674	189.8	<0.000001
North	221	Mp=0.797204×DML ^{0.961}	0.95555	0.9130	2300.6	<0.000001
Centre	86	Mp=0.613835×DML ^{0.997}	0.94777	0.8982	741.6	<0.000001
South	31	Mp=1.028729×DML ^{0.886}	0.95705	0.9159	316.0	<0.000001
North	218	Fl=0.235683×DML ^{1.099}	0.98508	0.9703	7078.6	<0.000001
Centre	85	Fl=0.170945×DML ^{1.159}	0.99086	0.9817	4476.0	<0.000001
South	31	Fl=0.176732×DML ^{1.155}	0.99051	0.9811	1506.6	<0.000001
North	218	Fw=0.610558×DML ^{0.992}	0.97705	0.9546	4545.4	<0.000001
Centre	85	Fw=0.445108×DML ^{1.046}	0.98140	0.9631	2168.7	<0.000001
South	31	Fw=0.561644×DML ^{0.997}	0.98488	0.9699	936.9	<0.000001

B. Male specimens.

Zone	N	Morphometric relationships	β	r^2	F	P
North	201	Hw=0.027903×DML ^{1.409}	0.93028	0.8654	1279.6	<0.000001
Centre	89	Hw=0.041152×DML ^{1.319}	0.92844	0.8620	543.4	<0.000001
South	28	Hw=0.113817×DML ^{1.135}	0.95704	0.9159	283.2	<0.000001
North	196	Hp=0.075524×DML ^{1.410}	0.94129	0.8860	1508.0	<0.000001
Centre	88	Hp=0.148668×DML ^{1.264}	0.93158	0.8678	564.7	<0.000001
South	28	Hp=0.209279×DML ^{1.210}	0.94126	0.8859	201.9	<0.000001
North	205	Mw=0.193344×DML ^{1.093}	0.94315	0.8895	1634.7	<0.000001
Centre	90	Mw=0.157880×DML ^{1.117}	0.92185	0.8498	497.8	<0.000001
South	29	Mw=0.518991×DML ^{0.858}	0.88683	0.7864	99.4	<0.000001
North	201	Mp=0.374305×DML ^{1.127}	0.95815	0.9180	2229.2	<0.000001
Centre	89	Mp=0.364646×DML ^{1.117}	0.94039	0.8843	665.2	<0.000001
South	29	Mp=1.148655×DML ^{0.877}	0.93488	0.8740	187.2	<0.000001
North	203	Fl=0.127954×DML ^{1.217}	0.98253	0.9653	5602.6	<0.000001
Centre	91	Fl=0.103613×DML ^{1.262}	0.97403	0.9487	1646.7	<0.000001
South	27	Fl=0.192629×DML ^{1.137}	0.95468	0.9114	257.2	<0.000001
North	203	Fw=0.240978×DML ^{1.184}	0.97219	0.9451	3463.8	<0.000001
Centre	91	Fw=0.345082×DML ^{1.109}	0.97665	0.9538	1818.6	<0.000001
South	27	Fw=0.521878×DML ^{1.025}	0.98782	0.9757	1007.2	<0.000001

Mw, maximum mantle width; Mp, maximum mantle perimeter; Hw, maximum head width; Hp, maximum head perimeter; Fl; fin height; Fw; fin width; N, number of cases.

Table 2. Relation of linear regression that show significantly different slopes by sex and zone (slope contrast test; $P < 0.05$).

	North/Centre	Centre/South	North/South
Males	DML-Fw	DML-TW DML-Mp DML-Mw DML-Hw	DML-TW DML-Mp DML-Mw DML-Hw DML-Hp
Females	DML-F1 DML-Fw	DML-TW	DML-TW

DML, Dorsal mantle length; TW, total weight; Mw, maximum mantle width; Mp, maximum mantle perimeter; Hw, maximum head width; Hp, maximum head perimeter; F1, fin height; Fw, fin width.

Maximum size in both sexes diminishes with latitude. The decrease in the b coefficient from north to south is around 0.5 units for males and 0.3 units for females (Table 3).

The parameters for the regression equations DML-d1W are similar for both sexes. Regressions between DML and d2W, however, show completely different curve values for males and females (Figure 3, Table 3).

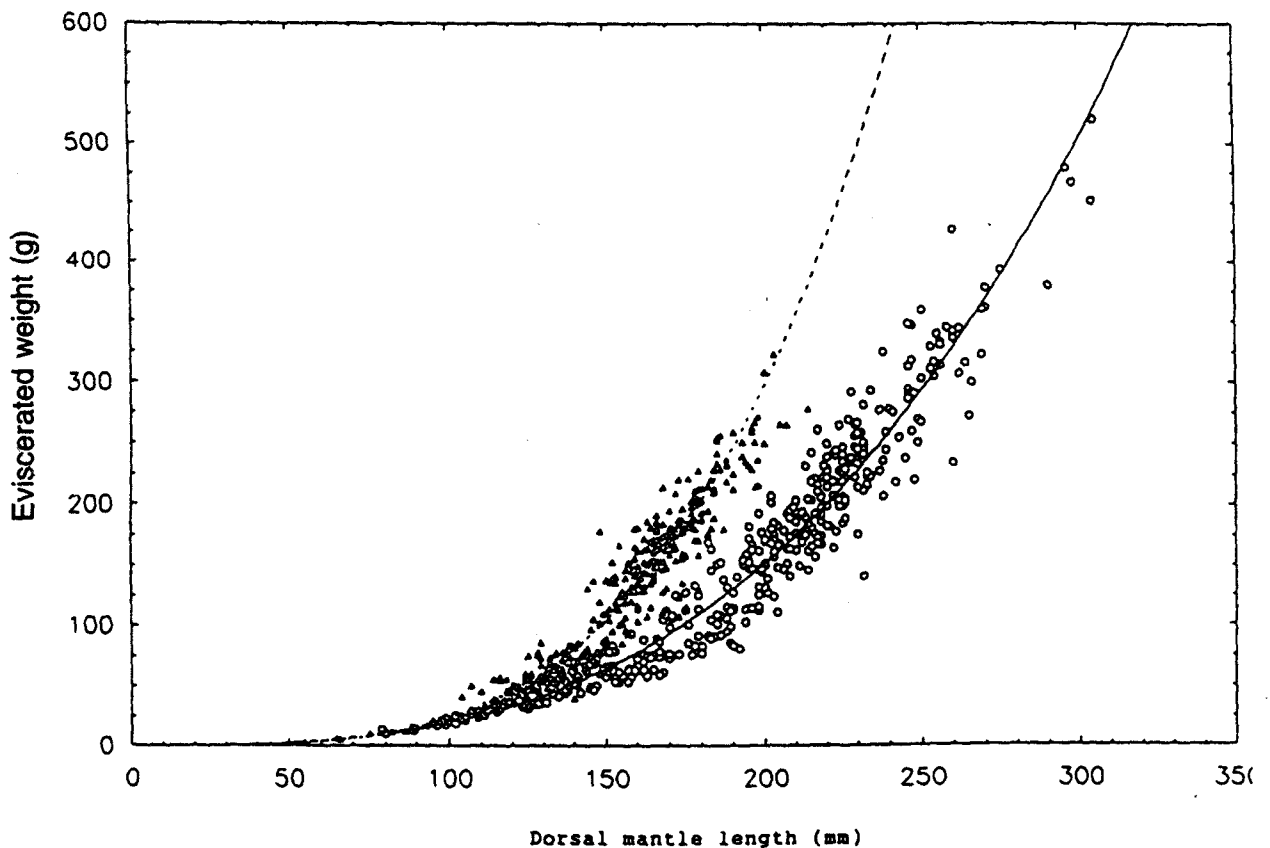


Figure 3. Relationship between dorsal mantle length (DML) and eviscerated weight (d2W) for male (Δ) and female (\circ) *Illex coindetii* in the central east Atlantic.

Table 3. Results of the regression between *Illex coindetii* total weight (TW), mantle weight (d1W) and eviscerated weight (d2W) and dorsal mantle length (DML) for each sex and in each area studied.

Zone	Sex	N	DML-TW relationships	β	r^2	F	df	P
CECAF Area	♀	721	TW=0.0000109×DML ^{3.152}	0.9784	0.9572	16116.9	719	<0.000001
CECAF Area	♂	708	TW=0.0000023×DML ^{3.548}	0.9708	0.9424	11572.1	706	<0.000001
North	♀	429	TW=0.0000187×DML ^{3.063}	0.9780	0.9565	9403.6	427	<0.000001
Centre	♀	105	TW=0.0000104×DML ^{3.153}	0.9861	0.9724	3634.9	103	<0.000001
South	♀	187	TW=0.0000708×DML ^{2.771}	0.9742	0.9491	3455.4	185	<0.000001
North	♂	446	TW=0.0000025×DML ^{3.536}	0.9659	0.9331	6193.6	444	<0.000001
Centre	♂	124	TW=0.0000029×DML ^{3.478}	0.9736	0.9479	2220.9	122	<0.000001
South	♂	138	TW=0.0000217×DML ^{3.081}	0.9535	0.9092	1362.8	136	<0.000001
CECAF Area	♀	412	d1W=0.0000275×DML ^{2.816}	0.9745	0.9497	7755.7	410	<0.000001
CECAF Area	♂	377	d1W=0.0000072×DML ^{3.119}	0.9818	0.9625	9625.4	375	<0.000001
CECAF Area	♀	414	d2W=0.0000224×DML ^{2.968}	0.9774	0.9554	8833.6	412	<0.000001
CECAF Area	♂	383	d2W=0.0000013×DML ^{3.632}	0.9723	0.9453	6596.2	381	<0.000001

DISCUSSION

The central-eastern Atlantic can be divided by oceanographic features, into three main areas, especially the fluctuations of the frontal zone between Cape Blanc and Cape Verga (Wauthy, 1983). The fisheries in the CECAF area (Committee for the Eastern Central Atlantic Fishery) (Figure 1) are also dependent on the enormous variability of the area's oceanographic characteristics (Mittelstaedt, 1991; Müller & Siedler, 1992). The environmental differences are reflected in the bioecological characteristics of some of the species that are distributed throughout the area, such as *Illex coindetii*. The latitude dependent morphometric variations found in this species are a consequence of environmental influence on its development.

Specimens that live at the colder limits of their geographic range tend to grow larger (Frank, 1975; Ricker, 1979; Hixon et al., 1981), and the mean size of *I. coindetii* decreases with latitude, fitting the hypothesis. This is concordant with Arkhipkin's observations (1996) on size-age relationships. In the eastern Atlantic, *I. coindetii* has an extensive geographic distribution, from the North Sea down to Angola (Roper & Sweeney, 1981). Variability of environmental factors (e.g. water mass temperature) does not only affect squid distribution (Dawe & Warren, 1993; Beck et al., 1994), it also influences the metabolic rates (Reynolds & Casterlin, 1980), maturity (Mangold, 1987; Zolotnitskij & Monin, 1990; González et al., 1992) and growth rates (Brett, 1979; Van Heukelem, 1979; Calderón, 1989) of specimens. The influence of the environment on the development of *I. coindetii* is clearly reflected at the moment when sexual dimorphism starts to occur, as sexual dimorphism and sexual maturity occur earlier in warmer areas (Gulf of Guinea) than it is in the colder waters of higher latitudes (Morocco and Sahara), which is in concordance with the observations of González et al. (1992) on the Galician shelf.

The external structure of *I. coindetii* presents no sexual dimorphism until sexual development starts (Sánchez, 1981; Hernández-García, 1995; Belcari, 1996). At that moment, when growth rates change for males and females (Arkhipkin, 1996), there is an obvious difference in the growth rate of male heads and the size that these attain. In mature specimens, the size of the head clearly indicates the sex of the individual, as Zuev & Nesis (1971) observed. This can be seen when the size-weight equations for the two sexes are compared, as males show a positive allometric regression coefficient that is clearly greater than the coefficient of females. The faster weight increase in males is due to the differential growth of the head between the two sexes. The greater positive allometry in males has been reported by several authors in studies done both on this species in other areas (Sánchez, 1981; Ragonese & Jereb, 1990; González, 1994; Belcari, 1996) and in other related species (i.e. *Illex illecebrosus* (Dawe, 1988)).

The weight of the visceral mass in females, however, accounts for a high percentage of total weight (Hernández-García, 1995). The reproductive apparatus can represent 20% of total weight. Females seem to invest more energy in reproduction, whereas males tend to minimize this effort, concerning the formation of the reproductive apparatus (Forsythe & Van Heukelem, 1987). Males, on the other hand, show a high percentage of somatic growth in the head and arms, which play a more important role in reproduction. Males have to deposit their spermatophores at the base of the female's gills (Mangold, 1987).

The positive allometric growth of the head in males is closely related to reproductive behaviour and development in males. This positive allometry is reflected in the need for strong arms to be able to transfer spermatophores to the female. The maximum size in males is always less than maximum size in females (Hernández-García, 1995; Arkhipkin, 1996), although males are heavier than females at any given size because of the large somatic mass in the head and arms.

Our thanks to Dr Carlos Bas, who encouraged us so strongly to work on this subject. Thanks are also given to Dr Angelo Santana del Pino.

REFERENCES

- Arkhipkin, A., 1996. Geographical variation in growth and maturation of the squid *Illex coindetii* (Oegopsida, Ommastrephidae) off the north-west African coast. *Journal of the Marine Biological Association of the United Kingdom*, **76**, 1091–1106.
- Bas, C., 1959. Consideraciones acerca del crecimiento de la caballa (*Scomber scombrus* L.) en el Mediterráneo Español. Parte I. *Investigación Pesquera*, **14**, 65–113.
- Beck, P.C., Dawe, E.G. & Drew, J., 1994. An update of the fishery for short-finned squid (*Illex illecebrosus*) in the Newfoundland area during 1989–1993 with descriptions of some biological characteristics and temperature trends. *Northwest Atlantic Fisheries Organization, Scientific Council Research Document*, no. 94–37, 1–14.
- Belcari, P., 1996. Length-weight relationships in relation to sexual maturation of *Illex coindetii* (Cephalopoda: Ommastrephidae) in the northern Tyrrhenian Sea (western Mediterranean). *Scientia Marina*, **60**, 379–384.
- Beverton, R.J.H. & Holt, S.S., 1957. On the dynamic of exploited fish populations. *Fishery Investigations, Series 2. MAFF, London*, **19**, 1–533.
- Boyle, P.R., 1987. *Cephalopod life-cycles*, vol. 2. London: Academic Press.

- Brett, J.R., 1979. Environmental factors and growth. In *Fish physiology*, vol. 8 (ed. W.J. Hoar et al.), pp. 599–675. New York: Academic Press.
- Calderon, L.E., 1989. *Modelo de las variaciones del crecimiento de la bacaladilla Micromesistius poutassou del Mediterráneo occidental y su relación con el ambiente*. Tesis doctoral, Universidad Politécnica de Cataluña, Spain.
- Dawe, E.G., 1988. Length–weight relationships for short-finned squid in Newfoundland and the effect of diet on condition and growth. *Transactions of the American Fishery Society*, **117**, 591–599.
- Dawe, E.G. & Warren, W.G., 1993. Recruitment of short-finned squid in the northwest Atlantic Ocean and some environmental relationships. *Journal of Cephalopod Biology*, **2**, 1–21.
- Forsythe, J.W. & Van Heukelem, W.F., 1987. Growth. In *Cephalopod life cycles*, vol. 2 (ed. P.R. Boyle), pp. 135–156. London: Academic Press.
- Frank, P.W., 1975. Latitudinal variation in the life history features of the black turban snail *Tegula funebris* (Prosobranchia: Trochidae). *Marine Biology*, **31**, 181–192.
- González, A.F., 1994. *Bioecología de Illex coindetii (Verany, 1839) (Cephalopoda, Ommastrephidae) de las Aguas de Galicia*. Tesis doctoral, Universidad de Vigo, Spain.
- González, A.F., Rasero, M. & Guerra, A., 1992. *Illex coindetii* and *Todaropsis eblanae* (Cephalopoda, Ommastrephidae): their present status in Galician fisheries. *International Council for the Exploration of the Sea (CM Papers and Reports)*, CM 1992/K:5, 1–14.
- Guerra, A., 1992. Mollusca, Cephalopoda. In *Fauna Ibérica*, vol. 1 (ed. M.A. Ramos et al.), pp. 1–327. Madrid: Museo Nacional de Ciencias Naturales.
- Gulland, J.A., 1985. *Fish stock assessment. A manual of basic methods*. Chichester: John Wiley & Sons.
- Hernández-García, V., 1995. *Contribución al conocimiento bioecológico de la familia Ommastrephidae Steenstrup, 1857 en el Atlántico Centro Oriental*. Tesis doctoral, Universidad de Las Palmas de Gran Canaria, Spain.
- Hixon, R.F., Hanlon, R.T. & Hulet, W.H., 1981. Growth and maximal size of the long-finned squid *Loligo pealei* in the northwestern Gulf of Mexico. *Journal of Shellfish Research*, **1**, 182–185.
- Mangold, K., 1987. Reproduction. In *Cephalopod life cycles*, vol. 2 (ed. P.R. Boyle), pp. 135–156. London: Academic Press.
- Martín-Andrés, A. & Luna del Castillo, J.D., 1990. *Bioestadística para las ciencias de la salud*. Madrid: Ediciones Norma S.A.
- Mittelstaedt, E., 1991. The ocean boundary along the northwest African coast: circulation and oceanographic properties at the sea surface. *Progress in Oceanography*, **26**, 307–355.
- Müller, J.T. & Siedler, G., 1992. Multi-year current time series in the eastern North Atlantic Ocean. *Journal of Marine Research*, **50**, 62–98.
- Ragonese, S. & Jereb, P., 1990. Length-weight relationships of *Illex coindetii* Verany, 1839 (Mollusca: Cephalopoda) in the Sicilian channel. *N.T.R. Istituto di Tecnologia della Pesca e del Pescato*, **21**, 1–18.
- Reynolds, W.W. & Casterlin, M.E., 1980. Role of temperature in the environmental physiology of fishes. In *Environmental physiology of fishes* (ed. M.A. Ali), pp. 497–518. New York: Plenum Press.
- Ricker, W.E., 1973. Linear regressions in fishery research. *Journal of the Fisheries Research Board of Canada*, **30**, 409–434.
- Ricker, W.E., 1979. Growth rates and models. In *Fish physiology*, vol. 8 (ed. W.S. Hoar et al.), pp. 677–743. New York: Academic Press.
- Rodríguez-Roda, J., 1983. La función alométrica aplicada al crecimiento diferencial en el atún, *Thunnus thynnus* (L.). Estudio de las poblaciones de atunes de ambas orillas del Atlántico Norte y del Mediterráneo. *Investigación Pesquera*, **47**, 171–202.
- Roper, C.F. & Sweeney, M.J., 1981. Ommastrephidae. In *FAO Species identification sheets for fishery purposes. Eastern Central Atlantic; Fishing areas 34, 47 (in part)*, vol. VI (ed. W. Fischer et al.), pp. 1–18. Canada Funds-in-Trust. Ottawa, Department of Fisheries and Oceans Canada, by arrangement with the Food and Agriculture Organization of the United Nations.
- Roper, C.F.E. & Voss, G.L., 1983. Guidelines for taxonomic descriptions of cephalopod species. *Memoirs of the National Museum Victoria*, **44**, 48–63.

- Sánchez, P., 1981. *Características bioecológicas de Illex coindetii (Vérany, 1837) en el mar Catalán*. Tesis doctoral. Universidad de Barcelona, Spain.
- Van Heukelem, W.F., 1979. Environmental control of reproduction and life span in *Octopus*: an hypothesis. In *Reproductive ecology of marine invertebrates* (ed. S.E. Stancyk), pp. 123–133. Columbia: University of South Carolina Press. [The Belle W. Baruch Library in Marine Science, no. 9.]
- Wauthy, B., 1983. Introduction à la climatologie du Golfe de Guinée. *Océanographie Tropicale*, **18**, 103–138.
- Zolotnitskij, A.P. & Monin, V.L., 1990. Individual fecundity and generative production in the mussel *Mytilus galloprovincialis* from the Black Sea. *Biologia Morya*, **6**, 24–30. [In Russian.]
- Zuev, G.V. & Nesis, K.N., 1971. *Squids (biology and fisheries)*. Moscow: Pishcherya Promyshlenost.

Submitted 23 June 1997. Accepted 10 October 1997.

Annual cycle of epiplanktonic copepods in Canary Island waters

SANTIAGO HERNÁNDEZ-LEÓN

Facultad de Ciencias del Mar, Universidad de Las Palmas de Gran Canaria, Campus Universitario de Tafira, 35017 Las Palmas de GC, Canary Islands (e-mail: santiago.hernandez-leon@biologia.ulpgc.es)

ABSTRACT

The species composition of epiplanktonic (0–20 m depth) copepods was studied over an annual cycle at a sampling interval of approximately 10 days at an oceanic station off Tenerife Island (Canary Islands). A taxonomic list of 110 species was obtained but only species represented by more than 300 individuals in the collection of 35 samples were studied. These comprised 23 species from which only 7 species were represented by more than 1000 individuals from all samples combined. *Oithona plumifera* was the most abundant species; *Oithona setigera*, *Temora stylifera* and *Clausocalanus arcuicornis* were also well represented. *Acartia negligens* was only observed after the temperature minimum in late winter. By contrast, *Lucicutia flavicornis* was observed before this temperature minimum. *Nannocalanus minor*, although numerically important, was represented only by copepodite stages during the period of study. There was great variability in the abundance of the above-named species, with some indications of higher abundance at about a 28–30 day period, possibly coinciding with the full moon phase. These fluctuations are discussed in relation to the vertical distribution of copepods, lunar phase, the impact of deep scattering layers on epizooplankton and the importance of these fluctuations in the energy flux through planktonic communities in subtropical waters.

Key words: annual cycle, Canary Islands, copepods, lunar cycle

Received for publication 5 April 1998

Accepted for publication 3 June 1998

INTRODUCTION

One of the aims of the Global Ecosystem Dynamics (GLOBEC) initiative is the study of the dynamics of zooplankton populations in relation to phytoplankton and to their major predators, and their influence on the structure of marine communities (GLOBEC Science Plan, 1997). In relation to this objective, the strategy is to acquire a knowledge of the alteration of species composition as a predictor of changes in the ocean, rather than quantification of flows of carbon in food-web networks. Thus, the selection of the 'target species' which represent the evolution of ecosystems is a key factor in understanding the plankton dynamics. In warm oceanic waters, characterized by a high diversity, the identification of such species representative of the ecosystem dynamics is a challenge.

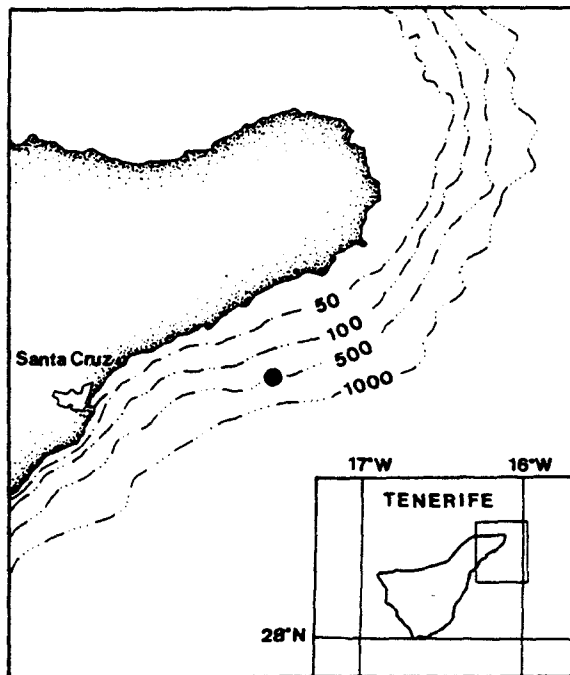
Around the Canary Islands, information about zooplankton species composition is sparse and is mostly published in older monographs. A total of 275 species of copepods have been described for the Canary Island region (Vives, 1982). The composition of epipelagic copepods has been described by Corral (1970, 1974), Roe (1972), Corral and Pereiro (1974), Fernández de Puelles (1987a,b) and Fernández de Puelles and García-Braun (1996), among others. From these contributions to the knowledge of marine copepods of this area of the subtropical gyre, we centred our attention on sampling over an annual cycle during 1968–69 (Corral, 1970), so as to gain information on species composition and to identify representative species of the annual cycle in these waters.

METHODS

Data from Corral (1970) were entered into a computer database as counts for 110 species of copepods from 35 samples corresponding to an annual cycle. From a total of 47 839 copepods, analysis was carried out only for those species with >300 individuals in total from the 35 samples combined.

The sampling was carried out between October 1968 and September 1969 at dawn at an oceanic station (500 m depth) north of Tenerife Island (Fig. 1). Sampling took place at intervals of about 10 days and

Figure 1. Location of the oceanographic station north of Tenerife Island.

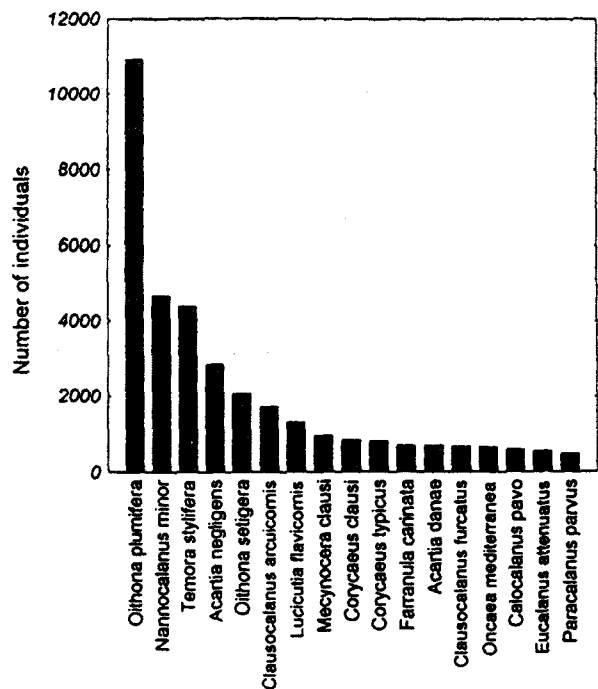


consisted of subsurface and horizontal hauls over 30 min at a velocity of about 1 knot (0.5 ms^{-1}) using a 100 m length of towing rope and a 50 cm diameter net equipped with $475 \mu\text{m}$ mesh net. Because all tows were taken over the same sampling duration, the total count of copepods in each sample was used in this comparative study. Sampling depth was between 0 and 20 m, calculated from the wire angle. Temperature was measured at the surface using a reversing thermometer (Negretti-Zambra). Identification and counting of the copepods was carried out under a binocular microscope. Copepods were measured, dissected and identified by sex and developmental stage.

The use of a large mesh ($475 \mu\text{m}$) in subtropical waters is not a recommended procedure due to the small size of zooplanktonic organisms in these waters. The effect of this net would have been to underestimate smaller species such as those of the genera *Calocalanus*, *Paracalanus* and *Clausocalanus*. The species described in the present paper should be considered as mid- to large-sized species of these waters. Because of the large mesh size used in this work, the adult stage of the different species was best represented in all samples (67.2% of all specimens identified). Therefore, we based our study on the adult stages, although very abundant copepodite stages were also considered if they represented a significant number of individuals.

© 1998 Blackwell Science Ltd., *Fish. Oceanogr.*, 7:3/4, 252–257.

Figure 2. Ranked count of copepods in all the 35 samples combined. Only species with more than 300 individuals in all samples combined are represented.



RESULTS

The ranked total number of copepods in all samples combined is shown in Fig. 2. These can be separated into two groups: the first group includes the most abundant copepods such as *Oithona plumifera*, *Nannocalanus minor*, *Temora stylifera*, *Acartia negligens*, *Oithona setigera*, *Clausocalanus arcuicornis* and *Lucicutia flavicornis*. These species were represented by more than 1000 individuals in all samples combined. The

Figure 3. Seasonal changes in sea surface temperature at the sampling station.

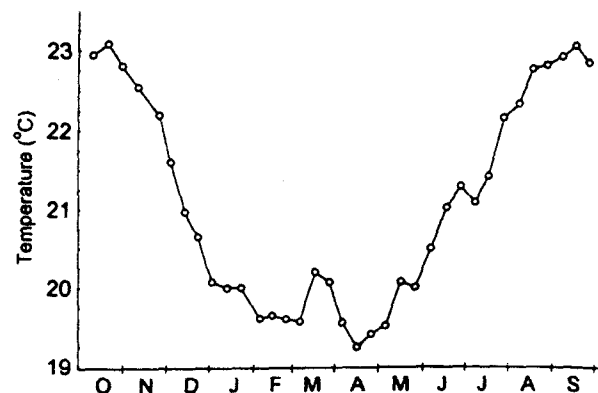
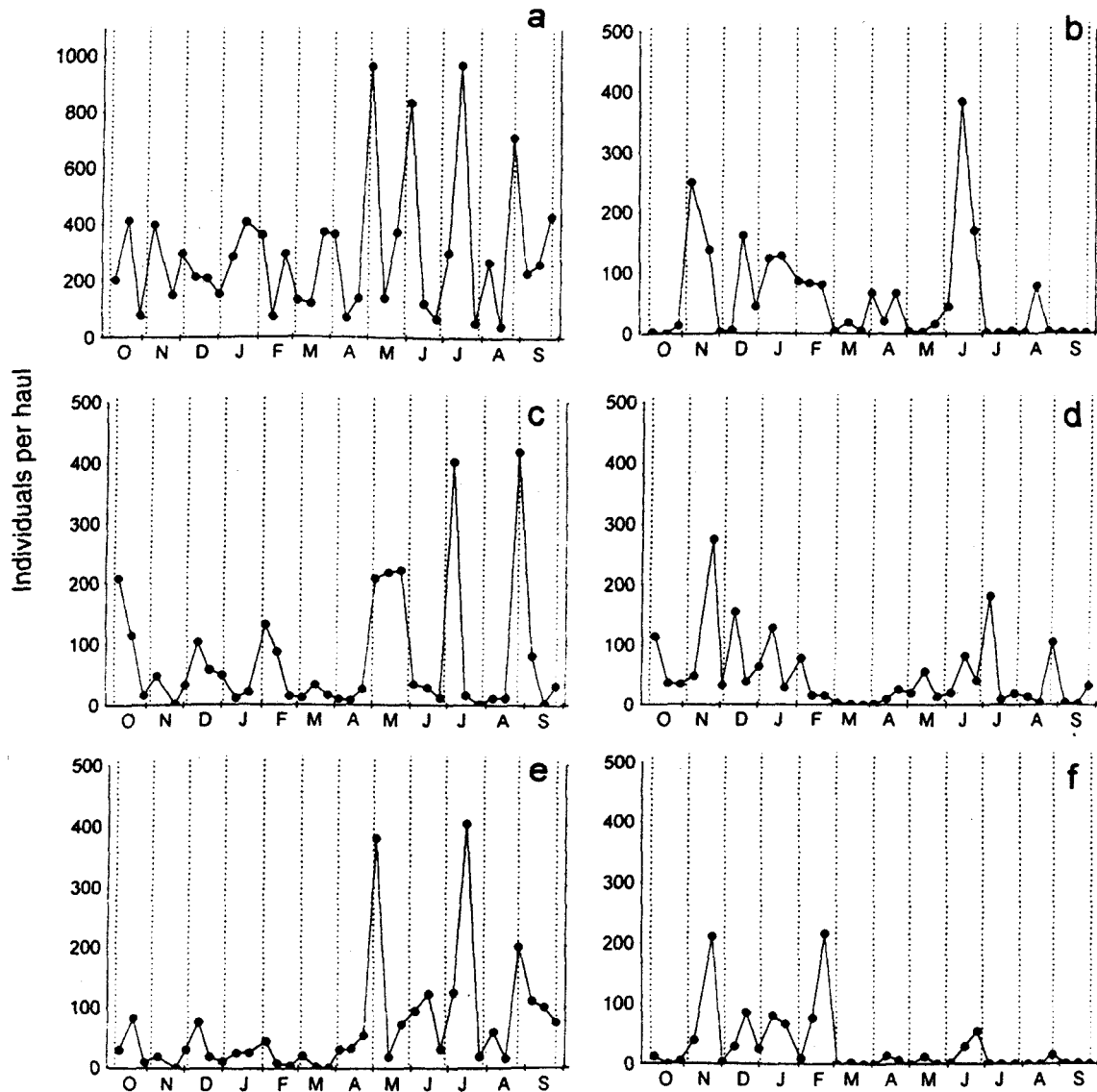


Figure 4. Seasonal changes in the number of adult copepods collected on each zooplankton haul of (a) *Oithona plumifera*, (b) *Oithona setigera*, (c) *Temora stylifera*, (d) *Clausocalanus arcuicornis*, (e) *Acartia negligens* and (f) *Lucicutia flavicornis*. The dates of the full moon are indicated by vertical dashed lines. Note the different scale in Fig. 4(a).

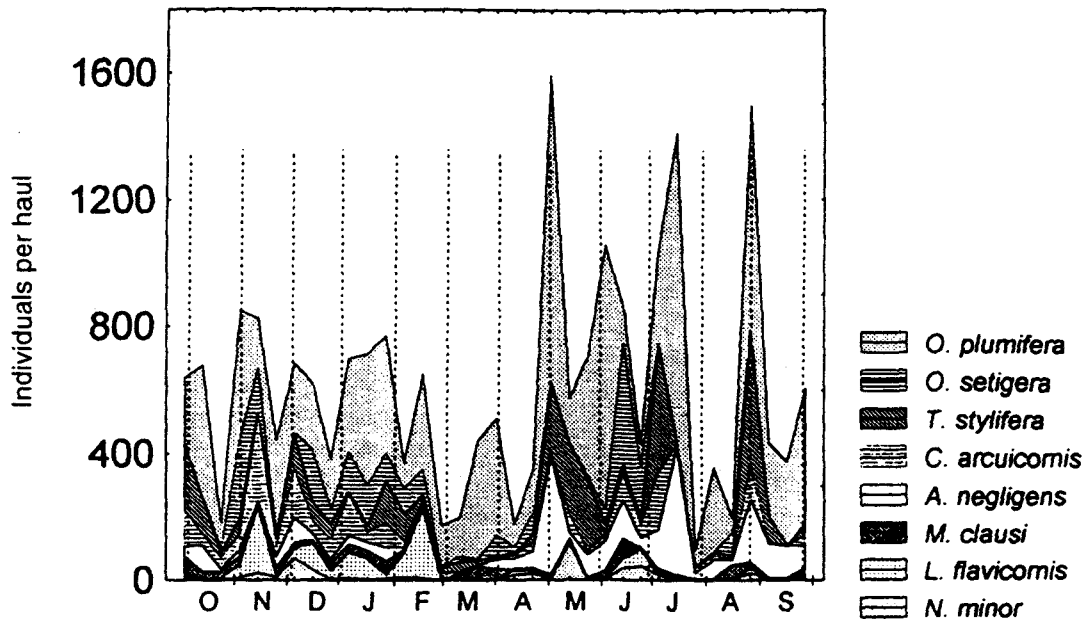


second group is formed by 16 species which were represented by >300 but <1000 copepods. In the first group, 88.7% of *Nannocalanus minor* consisted of copepodite stages.

Over the annual sampling cycle, surface temperature decreased from October to April and thereafter increased through the spring to reach maximum values during the period from August to September (Fig. 3). This is a typical feature of the annual cycle in Canary Island waters (De León and Braun, 1973; Braun, 1980, 1981; Hernández-León *et al.*, 1984; Hernández-León, 1988). Briefly, at the end of winter, cooling of surface

waters erodes the seasonal thermocline, producing an ephemeral increase in nutrients in the euphotic zone and producing a 'late winter bloom'. During the spring, the seasonal thermocline is re-established, as is the characteristic oligotrophy of these waters. During the period of minimum temperature, Braun (1981), Hernández-León *et al.* (1984), Hernández-León (1988), and Fernández de Puelles and García-Braun (1996) all observed the greatest zooplankton biomass during the months in which the late winter bloom is produced. This is contrary to the results in the present study (Figs 4 and 5).

Figure 5. Cumulative abundance of adult copepods of the eight most abundant species (Fig. 2). The dates of the full moon are indicated by vertical dashed lines.



Oithona plumifera was the dominant species in terms of numerical abundance (Figs 2 and 4a). Other specimens such as *Oithona setigera*, *Temora stylifera* and *Clausocalanus arcuicornis* were also well represented during the year (Fig. 4b, c, d). In relation to the annual temperature cycle, *Acartia negligens* was most abundant after the temperature minimum (Fig. 4e), whereas *Lucicutia flavicornis* was most abundant before the winter minimum (Fig. 4f).

Figure 5 shows the abundance of the adult population of the eight most abundant copepod species. A high variability was observed for all species throughout the annual cycle, this being most pronounced during the spring and summer months. During those months, a higher abundance of most species was observed coinciding with longer light periods during the day. These changes in abundance represented a two-to-fourfold variability in the number of copepods. Moreover, those increments in the number of copepods were often evident at roughly 28–30 day intervals, coinciding with or being proximate to the lunar cycle. However, synchronism between species abundance and the lunar phase was not always consistent. For example, *O. plumifera* (the most abundant species) showed out-of-phase peaks in October and July. Other less abundant species also showed no clear correspondence with the lunar cycle.

DISCUSSION

A few species showed an important presence in these waters despite the high diversity observed in this study (110 species) as well as in the Canary Island region (275 species). *Oithona plumifera* was the best represented, being twice as numerous as the second and third most abundant species (*Nannocalanus minor* and *Temora stylifera*). Fernández de Puelles and García-Braun (1996), sampling in the same area, observed that four genera [*Oncaea* (18%), *Clausocalanus* (18%), *Oithona* (17%) and *Paracalanus* (7%)] accounted for 60% of copepods during the annual cycle. The difference between their samples and the present data is related to the sampling procedure. They sampled the 0–200 m water column with a 250 μm mesh net, being able to capture smaller organisms throughout the euphotic zone. Although those genera were observed in our set of data, it seems clear that at least *Oncaea* and *Paracalanus* were not found to be abundant because of the large-mesh net used or because of a deeper distribution of these species.

However, the most interesting feature observed was the high variability of the numerically most important species. Despite the oceanographic conditions remaining rather stable during the annual cycle – or at least we did not observe drastic changes between the 28–30 day period in abundance repeatedly observed during the cycle studied – the number of copepods fluctuates drastically (two-to-fourfold). The shifts

observed were in phase with the moon cycle in most of the peaks observed. To our knowledge, there is only one study dealing with the effect of the moon on planktonic communities. Gliwicz (1986) found fresh-water zooplankton of different reservoirs in south-eastern Africa to fluctuate in phase with the moon. He observed an exponential increase in population density from the last quarter of the moon through the new moon and the first quarter, until the full moon, then a sudden decrease resulting in lowest numbers during the moon's last quarter. This cycle was shown to be induced by predation from fish. Moreover, the sudden decrease in zooplankton after the full moon was observed to be related to the effect of a combination of vertical migration of zooplankton at dusk and the moonrise during the first hours of the night. This phenomenon produced the so-called 'plankton trap' by which those zooplankters in surface waters were visually located by fish during the moonrise. Considering the data presented in this study, the fluctuation of adult stages of epipelagic copepods (Fig. 5) resembles the pattern of variability observed by Gliwicz (1986). Analysing the abundance of *O. plumifera*, it could be observed that only a few peaks were clearly out of phase with the moon: a first one in October and a second in July, while no increase was observed at the end of December. The mismatch observed in July can be explained by the presence of other species. As observed in Fig. 5, *T. stylifera* peaked before the increase of *O. plumifera*. If predation was the causative mechanism of those shifts in the abundance of these species, the predator should feed on this relatively large copepod, reducing the predatory pressure on *O. plumifera*. When the abundance of *T. stylifera* decreased, then the number of *O. plumifera* decreased. The interplay between the growth of different species can give some insight to explain the uncoupling with the lunar phase. Reviewing historical data in these islands, Fernández de Puelles (1987a) observed a strong decrease in the number of copepods over only 3–6 days during a detailed study of the late winter bloom in these waters. In that work, the highest number of copepods coincided with the full moon phase, which is the repeated finding of the present work. Such a sharp decrease suggests that the decreases observed should occur rather rapidly as was also described by Gliwicz (1986). The data of Fernández de Puelles (1987a) also suggest that the phenomenon that we observed for epipelagic copepods seems to be produced at the level, at least, of the euphotic zone (most of the biomass being concentrated in this layer), as her sampling took place over a depth range of 0–200 m.

It is known that diel vertical migrants increase the number of predators in the epiplankton by about 70% (Longhurst and Williams, 1979). In oceanic areas, those organisms have shown a different behaviour in their vertical movements related to moonlight. Boden and Kampa (1967) showed the response of deep scattering layers to small variations of light at dusk and dawn, to clouds and to moon illumination. Roger (1974) observed that moonrise during the full moon induced a deepening of all species of euphausiids in the tropical Pacific Ocean, resulting in an impoverishment in the upper 120–165 m depth range. This is a behaviour normally observed in echosounder data: during full moon the scattering layers remain below 150 m depth, at which the light intensity is similar to that observed at 500 m during the day. Therefore, we can propose the effect of migrants to explain the fluctuation in copepod numbers observed. Euphausiids are important components of the diel vertical migrants and are known to feed on mesozooplankton when large phytoplanktonic cells are scarce (Stuart and Huggett, 1992), and this is the scenario in 'blue-water' environments. If they avoid the surface waters during the full moon phase, the epipelagic copepods are free of the predatory pressure imposed by those organisms (or others that behave in similar way), allowing their growth. The new moon phase will produce the opposite effect. An argument in favour of this effect of lunar illumination on the observed fluctuation in numbers of copepods is that these shifts in abundance were higher during spring and summer months, when daylight time is longer, than during autumn and winter months. During longer days, moonrise during full moon coincides with daylight during more days than in winter in a moon cycle. This effect will prevent diel vertical migrants from reaching the surface during the first hours of the night, at least during more days than in autumn and winter months, reducing in this way the effect of this 'oceanic plankton trap'.

Whether or not the mechanisms discussed above are significant explanations of the observed shifts in zooplankton, the impact of this phenomenon in the structure and energy flow of pelagic ecosystems should be considered in the study of warm-water environments. Sediment-trap studies have shown the importance of large faecal pellets at mesopelagic depths (900 m) in subtropical waters (Fischer *et al.*, 1996) and their data also show changes in the flux of sedimented material at about a 28–30 day periodicity. Moreover, the highest values of total sedimented flux were observed during the new moon phase, coinciding with the presence of diel vertical migrants in the

epipelagic zone during night and consistent with findings of decreasing copepod abundance during that time. Finally, the short-period fluctuation of epipelagic copepods could promote an appreciable source of error in biomass estimations in open waters, and emphasizes the role of predation in determining pelagic structure, energy flow and dynamics (Verity and Smetacek, 1996).

ACKNOWLEDGEMENTS

The author is indebted to Dr J. Corral for support, helpful comments on this manuscript and for provision of the data. This study was funded, in part, by the MAST project CANIGO of the European Union and project MESOPELAGIC (MAR97-1036, CICYT, Spanish Ministry of Education).

REFERENCES

- Boden, B.P. and Kampa, E.M. (1967) The influence of natural light on the vertical migrations of an animal community in the sea. *Symp. Zool. Soc. London* 19:15-26.
- Braun, J.G. (1980) Estudios de producción en aguas de las Islas Canarias. I. Hidrografía, nutrientes y producción primaria. *Bol. Inst. Esp. Oceanogr.* 285:147-154.
- Braun, J.G. (1981) Estudios de producción en aguas de las Islas Canarias. II. Producción del zooplancton. *Bol. Inst. Esp. Oceanogr.* 290:89-96.
- Corral, J. (1970) *Contribución al conocimiento del plancton de Canarias*. PhD thesis, Universidad de Madrid, 343 pp.
- Corral, J. (1974) Ciclo anual de la diversidad específica en comunidades superficiales de copépodos de las Islas Canarias. *Vieraea* 3:95-99.
- Corral, J. and Pereiro, J.A. (1974) Estudio de las asociaciones de copépodos planctónicos en una zona de las Islas Canarias. *Bol. Inst. Esp. Oceanogr.* 175:1-32.
- De León, A.R. and Braun, J.G. (1973) Ciclo anual de la producción primaria y su relación con los nutrientes en aguas Canarias. *Bol. Inst. Esp. Oceanogr.* 167:3-24.
- Fernández de Puelles, M.L. (1987a) *Ciclo anual de la comunidad de meso y microzooplancton; su biomasa, estructura, relaciones tróficas y producción en aguas de las Islas Canarias*. PhD thesis, Universidad Autónoma de Madrid, 275 pp.
- Fernández de Puelles, M.L. (1987b) Evolución anual de microzooplancton en aguas de las Islas Canarias. *Bol. Inst. Esp. Oceanogr.* 4:79-90.
- Fernández de Puelles, M.L. and García-Braun, J. (1996) Micro and mesozooplankton in Canarian waters (28°30'N, 16°06'W). In: *Oceanography and Marine Resources in the Eastern Central Atlantic*. O. Llinás, J.A. González and M.J. Rueda (eds). Las Palmas, Gran Canaria: DGUI Gobierno de Canarias-Cabildo Insular de Gran Canaria, pp. 69-89.
- Fischer, G., Neuer, S., Wefer, G. and Krause, G. (1996) Short-term sedimentation pulses recorded with a fluorescence sensor and sediment traps at 900 m depth in the Canary basin. *Limnol. Oceanogr.* 41:1354-1359.
- Gliwicz, Z.M. (1986) A lunar cycle in zooplankton. *Ecology* 67:883-897.
- GLOBEC Science Plan (1997) *Global Ocean Ecosystem Dynamics. Science Plan*. R. Harris and members of GLOBEC Scientific Steering Committee (SSC). Stockholm: IGBP Secretariat, 83 pp.
- Hernández-León, S. (1988) Ciclo anual de la biomasa del mesozooplankton sobre un área de plataforma en aguas del Archipiélago Canario. *Invest. Pesquera* 52:3-16.
- Hernández-León, S., Llinás, O. and Braun, J.G. (1984) Nota sobre la variación de la biomasa mesozooplanktonica en aguas del Archipiélago Canario. *Invest. Pesquera* 48:495-508.
- Longhurst, A.R. and Williams, R. (1979) Materials for plankton modelling: vertical distribution of Atlantic zooplankton in summer. *J. Plankton Res.* 1:1-28.
- Roe, H.S. (1972) The vertical distribution and diurnal migrations of calanoid copepods collected on the SOND Cruise 1965. I. The total population and general discussion. *J. Mar. Biol. Ass. U.K.* 52:277-314.
- Roger, C. (1974) Influence de la phase et de l'éclairement lunaire sur les répartitions verticales nocturnes superficielles de crustacés macroplanctoniques (*Euphausiacea*). *Cah. ORSTOM, Sér. Océanogr.* 12:159-171.
- Stuart, V. and Huggett, J.A. (1992) Prey selection by *Euphausia lucens* (Hansen) and feeding behaviour in response to a mixed algal and animal diet. *J. Exp. Mar. Biol. Ecol.* 164:117-133.
- Verity, P.G. and Smetacek, V. (1996) Organism life cycles, predation, and the structure of marine pelagic ecosystems. *Mar. Ecol. Progr. Ser.* 130:277-293.
- Vives, F. (1982) Sur les copépodes de la région CINECA (parties nord et centrale). *Rapp. P.-v. Réun. Cons. Int. Explor. Mer* 180:289-296.

INTERNATIONAL UNION OF PURE
AND APPLIED CHEMISTRY
MACROMOLECULAR DIVISION
COMMISSION ON MACROMOLECULAR NOMENCLATURE*

DEFINITION OF TERMS RELATING TO THE
NON-ULTIMATE MECHANICAL PROPERTIES
OF POLYMERS

(IUPAC Recommendations 1998)

Prepared by a Working Group consisting of
A. Kaye (UK), R. F. T. Stepto (UK), W. J. Work (USA),
J. V. Alemán (Spain), A. Ya. Malkin (Russia)

*Membership of the Commission during the preparation of this report (1993–97) was as follows:

Titular Members: R. E. Bareiss (Germany, to 1993); M. Barón (Argentina, Associate Member to 1995, Titular Member from 1996); K. Hatada (Japan); J. Kahovec (Czech Republic); E. Maréchal (France); W. V. Metanomski (USA); C. Noël (France, to 1993); V. P. Shibaev (Russia, to 1995, Associate Member from 1996); R. F. T. Stepto (UK, *Chairman*); W. J. Work (USA, *Secretary*).

Associate Members contributing to this report: J. V. Alemán (Spain, to 1995); M. Hess (Germany, from 1996); K. Horie (Japan, from 1996); J.-I. Jin (Korea, National Representative to 1993, Associate Member from 1994); O. Kramer (Denmark, from 1996); P. Kubisa (Poland, from 1996); S. Penczek (Poland, from 1994); U. W. Suter (Switzerland, to 1993).

Others contributing to this report: H. A. Barnes (UK); R. B. Bird (USA); C. B. Bucknall (UK); J. M. Dealy (USA); J. D. Ferry (USA); R. B. Fox (USA); W. W. Graessley (USA); A. D. Jenkins (UK); A. Kaye (UK); P. Kratochvíl (Czech Republic); T. Masuda (Japan); I. Mita (Japan); D. R. Moore (UK) and Commission IV.2; K. Osaki (Japan); N. A. Platé (Russia, National Representative); J. C. Rigg (The Netherlands); R. Simha (USA); A. Sirigu (Italy, National Representative); R. I. Tanner (Australia); K. Walters (UK).

Republication or reproduction of this report or its storage and/or dissemination by electronic means is permitted without the need for formal IUPAC permission on condition that an acknowledgement, with full reference to the source along with use of the copyright symbol ©, the name IUPAC and the year of publication are prominently visible. Publication of a translation into another language is subject to the additional condition of prior approval from the relevant IUPAC National Adhering Organization.

Definition of terms relating to the non-ultimate mechanical properties of polymers (IUPAC Recommendations 1998)

DEFINITION OF TERMS RELATING TO THE NON-ULTIMATE MECHANICAL PROPERTIES OF POLYMERS

SUMMARY

The document gives definitions of terms related to the non-ultimate mechanical behaviour of polymeric materials, in particular bulk polymers and concentrated solutions and their elastic and viscoelastic properties.

The terms which have been selected are those met in the conventional mechanical characterization of isotropic polymeric materials. They have additionally been limited to those which can be defined precisely and with mathematical rigour. They are arranged in sections dealing with basic definitions of stress and strain, deformations used experimentally, stresses observed experimentally, quantities relating stress and deformation, linear viscoelastic behaviour, and oscillatory deformations and stresses used experimentally for solids.

An index, an alphabetical list of terms and a glossary of symbols are included for ease of reference.

INTRODUCTION

This document gives definitions of terms related to the non-ultimate mechanical behaviour or mechanical behaviour prior to failure of polymeric materials, in particular bulk polymers and concentrated solutions and their elastic and viscoelastic properties.

The terms are arranged into sections dealing with basic definitions of stress and strain, deformations used experimentally, stresses observed experimentally, quantities relating stress and deformation, linear viscoelastic behaviour, and oscillatory deformations and stresses used experimentally for solids. The terms which have been selected are those met in the conventional mechanical characterization of polymeric materials.

To compile the definitions, a number of sources have been used. A number of the definitions were adapted from an International Standards Organization (ISO) manuscript on *Plastics Vocabulary*¹. Where possible, the names for properties, their definitions and the symbols for linear viscoelastic properties were checked against past compilations of terminology²⁻⁶. Other documents consulted include ASTM publications⁷⁻¹³.

The document does not deal with the properties of anisotropic materials. This is an extensive subject in its own right and the reader is referred to specialized texts^{14,15} for information.

In the list of contents, main terms separated by / are alternative names, and terms in parentheses give those which are defined in the context of main terms, usually as notes to the definitions of main terms, with their names printed in bold type in the main text. Multicomponent quantities (vectors, tensors, matrices) are printed in bold type. Names printed in italics are defined elsewhere in the document and their definitions can be found by reference to the alphabetical list of terms.

CONTENTS**1. BASIC DEFINITIONS**

	<u>Page</u>
1.1 traction/stress vector	707
1.2 stress/stress tensor (true stress, plane stress)	707
1.3 deformation of an elastic solid (homogeneous deformation, inhomogeneous deformation, deformation gradients)	708
1.4 deformation gradient tensor for an elastic solid	708
1.5 deformation of a viscoelastic liquid or solid (homogeneous deformation)	708
1.6 deformation gradients in a viscoelastic liquid or solid	709
1.7 deformation gradient tensor for a viscoelastic liquid or solid	709
1.8 strain tensor (C , B , C^{-1} , B^{-1} , plane strain)	710
1.9 Cauchy tensor (C) for a viscoelastic liquid or solid	710
1.10 Green tensor (B) for an elastic solid (small-strain tensor)	710
1.11 Finger tensor (C^{-1}) for a viscoelastic liquid or solid	711
1.12 rate-of-strain tensor for a viscoelastic liquid or solid in homogeneous deformation	711
1.13 vorticity tensor for a viscoelastic liquid or solid in homogeneous deformation	712
1.14 Rivlin-Ericksen tensors for a viscoelastic liquid or solid in homogeneous deformation.	712

2. DEFORMATIONS USED EXPERIMENTALLY

2.1 general orthogonal homogeneous deformation of an elastic solid (deformation gradient, deformation ratio)	712
2.2 uniaxial deformation of an elastic solid	713
2.3 uniaxial deformation ratio/deformation ratio (extension ratio)	713
2.4 uniaxial strain/engineering strain (tensile strain, compressive strain)	714
2.5 Hencky strain	714
2.6 Poisson's ratio (lateral strain/lateral contraction ratio)	714

	<u>Page</u>
2.7 pure shear of an elastic solid	715
2.8 simple shear of an elastic solid (shear/shear strain)	715
2.9 bulk compression/volume compression/isotropic compression/bulk compressive strain	716
2.10 general homogeneous deformation or flow of a viscoelastic liquid or solid	716
2.11 homogeneous orthogonal deformation or flow of an incompressible viscoelastic liquid or solid (uniaxial deformation or flow)	716
2.12 steady uniaxial homogeneous elongational deformation or flow of an incompressible viscoelastic liquid or solid (elongational/extensional strain rate)	717
2.13 homogeneous simple shear deformation or flow of an incompressible viscoelastic liquid or solid (shear, shear rate, steady (simple) shear flow, oscillatory (simple) shear flow)	717

3. STRESSES OBSERVED EXPERIMENTALLY

3.1 stress tensor resulting from an orthogonal deformation or flow (uniaxial orthogonal deformation or flow, pure shear deformation or flow, pure shear stress)	718
3.2 tensile stress	719
3.3 compressive stress	719
3.4 engineering stress/nominal stress	719
3.5 stress tensor resulting from a simple shear deformation or flow (normal stresses, shear stress)	719
3.6 first normal-stress difference/first normal-stress function	720
3.7 second normal-stress difference/second normal-stress function	720

4. QUANTITIES RELATING STRESS AND DEFORMATION

4.1 constitutive equation for an elastic solid (stored energy function)	721
4.2 constitutive equation for an incompressible viscoelastic liquid or solid (Newtonian liquid, non-Newtonian liquid)	721
4.3 modulus (elastic modulus/modulus of elasticity)	722
4.4 compliance	723

	<u>Page</u>
4.5 bulk modulus/bulk compressive modulus	723
4.6 bulk compliance/bulk compressive compliance	723
4.7 Young's modulus (tensile modulus, secant modulus, tangent modulus)	724
4.8 uniaxial compliance (tensile compliance)	724
4.9 extensional viscosity/elongational viscosity	725
4.10 shear modulus	725
4.11 shear compliance	725
4.12 shear viscosity/coefficient of viscosity/viscosity (apparent viscosity, zero-shear viscosity, infinite-shear viscosity)	726
4.13 first normal-stress coefficient	726
4.14 second normal-stress coefficient	727

5. LINEAR VISCOELASTIC BEHAVIOUR

5.1 viscoelasticity (dynamic stress or strain)	727
5.2 linear viscoelastic behaviour (liquid, solid)	727
5.3 Maxwell model/Maxwell element (spring constant, dashpot constant)	728
5.4 Voigt-Kelvin model/Voigt-Kelvin element (Voigt model/Voigt element, spring constant, dashpot constant)	729
5.5 standard linear viscoelastic solid	729
5.6 relaxation time (relaxation spectrum)	730
5.7 stress relaxation (relaxation function)	730
5.8 retardation time (retardation spectrum)	731
5.9 creep (creep function, creep compliance)	731
5.10 forced oscillation (strain amplitude, angular velocity, stress amplitude, phase angle, loss angle)	732
5.11 loss factor/loss tangent (loss curve)	733
5.12 storage modulus	733

	<u>Page</u>
5.13 loss modulus	733
5.14 absolute modulus	734
5.15 complex modulus (complex strain, complex stress)	734
5.16 storage compliance	735
5.17 loss compliance	735
5.18 absolute compliance	735
5.19 complex compliance (complex strain, complex stress)	736
5.20 dynamic viscosity	737
5.21 out-of-phase viscosity	737
5.22 complex viscosity (complex rate of strain, complex stress)	737

6. OSCILLATORY DEFORMATIONS AND STRESSES USED EXPERIMENTALLY FOR SOLIDS

6.1 free oscillation	738
6.2 damping curve (torsion pendulum)	738
6.3 decay constant	739
6.4 decay frequency	739
6.5 logarithmic decrement	740
6.6 forced uniaxial extensional oscillation (resonance frequency)	741
6.7 forced flexural oscillation (three-point bending/flexure, second moment of area, neutral axis/plane, resonance frequency, angular velocity of resonance frequency)	742
6.8 flexural force (flexural stress)	744
6.9 flexural deflection	744
6.10 flexural modulus	744
6.11 resonance curve	745
6.12 resonance frequency	745
6.13 half-width of resonance curve	746

	<u>Page</u>
<u>7. REFERENCES</u>	747
<u>8. ALPHABETICAL INDEX OF TERMS</u>	748
<u>9. GLOSSARY OF SYMBOLS</u>	752

1. BASIC DEFINITIONS

In this section, quantities are expressed with respect to rectangular Cartesian co-ordinate axes, Ox_1 , Ox_2 , Ox_3 , except where otherwise stated. The components of a vector V are denoted V_1 , V_2 , and V_3 with respect to these axes.

1.1 traction stress vector

Recommended symbol: t

A vector force per unit area on an infinitesimal element of area that has a given normal and is at a given point in a body.

Unit: Pa

Note

1. The components of t are written as t_1 , t_2 , t_3 .
2. t is sometimes called true stress. The term *traction* (or *stress vector*) is preferred to avoid confusion with *stress tensor* (see 1.2 note 5)

1.2 stress tensor stress

Recommended symbol: σ

The tensor with components σ_{ij} which are the components of the traction in the Ox_i direction on an element of area whose normal is in the Ox_j direction.

Unit: Pa

Notes

1. A unit vector area with normal n can be resolved into three smaller areas equal to n_1 , n_2 , and n_3 with normals in the directions of the respective co-ordinate axes. Accordingly, each component of the traction on the original area can be considered as the sum of components in the same direction on the smaller areas to give

$$t_i = \sum_{j=1}^3 \sigma_{ij} n_j, \quad i = 1, 2, 3.$$

2. In usual circumstances, in the absence of body couples, $\sigma_{ij} = \sigma_{ji}$.
3. For a homogeneous stress σ is the same at all points in a body.

4. For an inhomogeneous stress $\sigma_{ij} = \sigma_{ij}(x_1, x_2, x_3)$.
5. σ is a **true stress** because its components are forces per unit current area (cf. 3,4).
6. If $\sigma_{13} (= \sigma_{31}) = \sigma_{23} (= \sigma_{32}) = \sigma_{33} = 0$ then the stress is called a **plane stress**. Plane stresses are associated with the deformation of a sheet of material in the plane of the sheet.

1.3 deformation of an elastic solid

A deformation of an elastic solid through which a mass point of the solid with co-ordinates X_1, X_2, X_3 in the undeformed state moves to a point with co-ordinates x_1, x_2, x_3 in the deformed state and the deformation is defined by

$$x_i = x_i(X_1, X_2, X_3), \quad i = 1, 2, 3$$

Notes

1. A **homogeneous deformation** is one in which the relationships between the co-ordinates in the undeformed and deformed states reduce to

$$x_i = \sum_{j=1}^3 f_{ij} X_j, \quad i = 1, 2, 3$$

where the f_{ij} are constants.

2. An **inhomogeneous deformation** is one in which the incremental changes in the undeformed and deformed co-ordinates are related by

$$dx_i = \sum_{j=1}^3 f_{ij} dX_j, \quad i = 1, 2, 3$$

where $f_{ij} = \partial x_i / \partial X_j$, $i, j = 1, 2, 3$, and where the f_{ij} are the functions of the coordinates x_j .

3. The f_{ij} in notes 1 and 2 are **deformation gradients**.

1.4 deformation gradient tensor for an elastic solid

Recommended symbol: F

The tensor whose components are deformation gradients in an elastic solid.

Notes

1. The components of F are denoted f_{ij} .
2. See 1.3 for the definitions of f_{ij} .

1.5 deformation of a viscoelastic liquid or solid

A deformation of a viscoelastic liquid or solid through which a mass point of the viscoelastic liquid or solid with co-ordinates x'_1, x'_2, x'_3 at time t' moves to a point with co-ordinates x_1, x_2, x_3 at time t such that there are functions g_i , $i = 1, 2, 3$, where

$$g_i(x'_1, x'_2, x'_3, t') = g_i(x_1, x_2, x_3, t).$$

Notes

1. t' often refers to some past time and t to the present time.
2. The relationships between the total differentials of the functions g_i define how particles of the material move relative to each other. Thus, if two particles are at small distances dx'_1, dx'_2, dx'_3 apart at time t' and dx_1, dx_2, dx_3 at time t then

$$\sum_{j=1}^3 g'_{ij} dx'_j = \sum_{j=1}^3 g_{ij} dx_j$$

$$\text{where } g'_{ij}(x'_1, x'_2, x'_3, t') = \frac{\partial g_i(x'_1, x'_2, x'_3, t')}{\partial x'_j}$$

$$\text{and } g_{ij}(x_1, x_2, x_3, t) = \frac{\partial g_i(x_1, x_2, x_3, t)}{\partial x_j}$$

$$i, j = 1, 2, 3.$$

3. The matrix with elements g_{ij} is denoted G and the matrix with elements g'_{ij} is denoted G' .
4. A **homogeneous deformation** is one in which the functions g_i are linear functions of the x_j , $i, j = 1, 2, 3$. As a result, the g_{ij} and G are functions of t only and the equations which define the deformation become

$$\sum_{j=1}^3 g'_{ij}(t') x'_j = \sum_{j=1}^3 g_{ij}(t) x_j$$

5. **Homogeneous deformations** are commonly used or assumed in the methods employed for characterising the mechanical properties of viscoelastic polymeric liquids and solids.

1.6 deformation gradients in a viscoelastic liquid or solid

Recommended symbol: f_{ij}

If two mass points of a liquid are at a small distance dx'_1, dx'_2, dx'_3 apart at time t' then the deformation gradients are the rates of change of dx'_i with respect to dx_j , $i, j = 1, 2, 3$.

Note

$$f_{ij} = \partial x'_i / \partial x_j, \quad i, j = 1, 2, 3$$

1.7 deformation gradient tensor for a viscoelastic liquid or solid

Recommended symbol: F

The tensor whose components are deformation gradients in a viscoelastic liquid or solid.

Notes

1. The components of F are denoted f_{ij}
2. See 1.6 for the definition of f_{ij} .
3. By matrix multiplication, $F = (G')^{-1}G$ where the matrices G and G' are those defined in 1.5.

1.8 strain tensor

A symmetric tensor that results when a deformation gradient tensor is factorised into a rotation tensor followed or preceded by a symmetric tensor

Notes

1. A strain tensor is a measure of the relative displacement of the mass points of a body.
2. The deformation gradient tensor F may be factorised as

$$F = R U = V R,$$
 where R is an orthogonal matrix representing a rotation and U and V are strain tensors which are symmetric.
3. Alternative strain tensors are often more useful.
 For example:
 the Cauchy tensor, $C = U^2 = F^T F$
 the Green tensor, $B = V^2 = F F^T$
 the Finger tensor, C^{-1}
 the Piola tensor, B^{-1}
 'T' denotes transpose and '1' denotes inverse. B is most useful for solids and C and C^{-1} for viscoelastic liquids and solids.
4. If the 1,3; 3,1; 2,3; 3,2; 3,3 elements of a strain tensor are equal to zero then the strain is termed **plane strain**

1.9 Cauchy tensor

Recommended symbol: C

The strain tensor for a viscoelastic liquid or solid, whose elements are

$$c_{ij} = \sum_{k=1}^3 \frac{\partial x'_k}{\partial x_i} \cdot \frac{\partial x'_k}{\partial x_j},$$

where x'_i and x_i are co-ordinates of a particle at times t' and t , respectively.

Notes

1. See 1.5 for the definition of x'_i and x_i
2. See 1.8 for the definition of a *strain tensor*.

1.10 Green tensor

Recommended symbol: B

The strain tensor for an elastic solid, whose elements are

$$b_{ij} = \sum_{k=1}^3 \frac{\partial x_i}{\partial X_k} \cdot \frac{\partial x_j}{\partial X_k},$$

where X_i and x_i are co-ordinates in the undeformed and deformed states, respectively.

Notes

1. See 1.3 for the definition of X_i and x_i .
2. See 1.8 for the definition of a *strain tensor*
3. For small strains, B may be expressed by the equation

$$B = I + 2\varepsilon ,$$

where I is the unit matrix of order three and ε is the **small-strain tensor**. The components of ε are

$$\varepsilon_{ij} = \frac{1}{2} \left(\frac{\partial u_i}{\partial x_j} + \frac{\partial u_j}{\partial x_i} \right) ,$$

with $u_k = x_k - X_k$, $k = 1,2,3$, the displacements due to the deformation.

1.11 Finger tensor

Recommended symbol: C^{-1}

The strain tensor, for a viscoelastic liquid or solid, whose elements are

$$c_{ij}^{-1} = \sum_{k=1}^3 \frac{\partial x_i}{\partial x'_k} \cdot \frac{\partial x_j}{\partial x'_k} .$$

where x'_i and x_i are co-ordinates of a particle at times t' and t , respectively.

Notes

1. See 1.5 for the definition of x'_i and x_i .
2. See 1.8 for the definition of a *strain tensor*.

1.12 rate-of-strain tensor

Recommended symbol: D

The time derivative of a strain tensor for a viscoelastic liquid or solid in homogeneous deformation at reference time, t .

Unit: s^{-1}

Notes

1. For an *inhomogeneous deformation*, the material derivative has to be used to find time derivatives of strain.
2. $D = \lim_{t' \rightarrow t} \left(\frac{\partial U}{\partial t'} \right) = \lim_{t' \rightarrow t} \left(\frac{\partial V}{\partial t'} \right)$, where U and V are defined in 1.8, note 2.
3. The elements of D are

$$d_{ij} = \frac{1}{2} \left(\frac{\partial v_i}{\partial x_j} + \frac{\partial v_j}{\partial x_i} \right) ,$$

where the v_k are the components of the velocity \mathbf{v} at \mathbf{x} and time, t .

1.13 vorticity tensor

Recommended symbol: \mathbf{W}

The derivative, for a viscoelastic liquid or solid in homogeneous deformation, of the rotational part of the deformation-gradient tensor at reference time, t .

Unit: s^{-1}

Notes

1. For an *inhomogeneous deformation* the material derivative has to be used.
2. $\mathbf{W} = \lim_{t' \rightarrow t} \left(\frac{\partial \mathbf{R}}{\partial t'} \right)$, where \mathbf{R} is defined in 1.8, note 2.
3. The elements of \mathbf{W} are

$$w_{ij} = \frac{1}{2} \left(\frac{\partial v_i}{\partial x_j} - \frac{\partial v_j}{\partial x_i} \right),$$

where the v_k are the components of the velocity \mathbf{v} at \mathbf{x} and time t .

1.14 Rivlin-Ericksen tensors

Recommended symbol: \mathbf{A}_n

The Rivlin-Ericksen tensor of order n , for a viscoelastic liquid or solid in homogeneous deformation, is the n th time derivative of the Cauchy strain tensor at reference time, t .

Unit: s^{-n}

Notes

1. For an *inhomogeneous deformation* the material derivatives have to be used.
2. $\mathbf{A}_n = \lim_{t' \rightarrow t} \left(\frac{\partial^n \mathbf{C}}{\partial t'^n} \right)$, where \mathbf{C} is defined in 1.9.
3. $\mathbf{A}_0 = \mathbf{I}$, where \mathbf{I} is the unit matrix of order three.
4. $\mathbf{A}_1 = \dot{\mathbf{F}}^T + \dot{\mathbf{F}} = 2\mathbf{D}$, where \mathbf{F} is the *deformation-gradient tensor* (see 1.7),
 $\dot{\mathbf{F}} = \lim_{t' \rightarrow t} \left(\frac{\partial \mathbf{F}}{\partial t'} \right)$, 'T' denotes transpose and \mathbf{D} is the *rate-of-strain tensor* (see 1.12).
5. In general, $\mathbf{A}_{n+1} = \dot{\mathbf{A}}_n + \dot{\mathbf{F}}^T \mathbf{A}_n + \mathbf{A}_n \dot{\mathbf{F}}$, $n = 0, 1, 2, \dots$

2. DEFORMATIONS USED EXPERIMENTALLY

All deformations used in conventional measurements of mechanical properties are interpreted in terms of *homogeneous deformations*.

2.1 general orthogonal homogeneous deformation of an elastic solid

A deformation, such that a mass point of the solid with co-ordinates X_1, X_2, X_3 in the undeformed

state moves to a point with co-ordinates x_1, x_2, x_3 in the deformed state, with

$$x_i = \lambda_i X_i, \quad i = 1, 2, 3,$$

where the λ_i are constants.

Notes

1. The relationships between the x_i and X_i for orthogonal homogeneous deformations are a particular case of the general relationships given in 1.3, provided the deformation does not include a rotation and the co-ordinate axes are chosen as the principal directions of the deformation.
2. The λ_i are effectively **deformation gradients**, or, for finite deformations, the **deformation ratios** characterising the deformation.
3. For an incompressible material

$$\lambda_1 \lambda_2 \lambda_3 = 1.$$

4. The λ_i are elements of the deformation gradient tensor F (see 1.4) and the resulting *Cauchy* and *Green tensors* C and B (see 1.9 and 1.10) are

$$C = B = \begin{bmatrix} \lambda_1^2 & 0 & 0 \\ 0 & \lambda_2^2 & 0 \\ 0 & 0 & \lambda_3^2 \end{bmatrix}$$

2.2 uniaxial deformation of an elastic solid

An orthogonal, homogeneous deformation in which, say,

$$\text{and} \quad \begin{aligned} \lambda_1 &= \lambda \\ \lambda_2 &= \lambda_3 \end{aligned}$$

Notes

1. See 2.1 for the definition of λ_i , $i = 1, 2, 3$.
2. For an incompressible material

$$\lambda_2 = \lambda_3 = 1/\lambda^{1/2}$$

2.3 uniaxial deformation ratio deformation ratio

Recommended symbol: λ

The quotient of the length (l) of a sample under uniaxial tension or compression and its original length (l_0)

$$\lambda = l/l_0$$

Notes

1. In tension $\lambda (>1)$ may be termed the **extension ratio**.

2. In compression λ (<1) may be termed the **compression ratio**.

3. λ is equivalent to λ_1 in 2.1 and 2.2.

2.4 uniaxial strain engineering strain

Recommended symbol: ε

The change in length of a sample in uniaxial tensile or compressive deformation divided by its initial length

$$\varepsilon = (l_1 - l_0) / l_0$$

where l_0 and l_1 are, respectively, the initial and final lengths.

Notes

1. $\varepsilon = \lambda - 1$, where λ is the *uniaxial deformation ratio* (see 2.3).

2. $\varepsilon > 0$ is referred to as **(uniaxial) tensile strain**.

3. $\varepsilon < 0$ is referred to as **(uniaxial) compressive strain**.

2.5 Hencky strain

Recommended symbol: ε_H

The integral over the total change in length of a sample of the incremental strain in uniaxial tensile deformation

$$\varepsilon_H = \int_{l_0}^{l_1} dl / l = \ln(l_1 / l_0)$$

l_0 , l_1 and l are, respectively, the initial, final and instantaneous lengths.

Notes

1. See *uniaxial strain* (2.4).

2. The same equation can be used to define a quantity ε_H (< 0) in compression.

2.6 Poisson's ratio

Recommended symbol: μ

In a sample under small uniaxial deformation, the negative quotient of the lateral strain (ε_{lat}) and the longitudinal strain (ε_{long}) in the direction of the uniaxial force

$$\mu = - \left(\frac{\varepsilon_{lat}}{\varepsilon_{long}} \right)$$

Notes

1. **Lateral strain** ε_{lat} is the strain normal to the uniaxial deformation.

$\varepsilon_{lat} = \lambda_2 - 1 = \lambda_3 - 1$ (see 2.2 and 2.4).

2. For an isotropic, incompressible material, $\mu = 0.5$. It should be noted that, in materials referred to as incompressible, volume changes do in fact occur in deformation, but they may be neglected.
3. For an anisotropic material, μ varies with the direction of the uniaxial deformation.
4. *Poisson's ratio* is also sometimes called the **lateral contraction ratio** and is sometimes used in cases of non-linear deformation. The present definition will not apply in such cases.

2.7 pure shear of an elastic solid

An orthogonal, homogeneous deformation in which

$$\begin{aligned}\lambda_1 &= \lambda \\ \lambda_2 &= 1/\lambda \\ \lambda_3 &= 1\end{aligned}$$

Note

See 2.1 for the definition of λ_i , $i = 1, 2, 3$.

2.8 simple shear of an elastic solid

A homogeneous deformation, such that a mass point of the solid with co-ordinates X_1, X_2, X_3 in the undeformed state moves to a point with co-ordinate x_1, x_2, x_3 in the deformed state, with

$$\begin{aligned}x_1 &= X_1 + \gamma X_2 \\ x_2 &= X_2 \\ x_3 &= X_3\end{aligned}$$

where γ is constant.

Notes

1. The relationships between the x_i and X_i , $i = 1, 2, 3$, in simple shear are a particular case of the general relationships given in 1.3.
2. γ is known as the **shear** or **shear strain**.
3. The *deformation gradient tensor* for the simple shear of an elastic solid (see 1.4) is

$$F = \begin{pmatrix} 1 & \gamma & 0 \\ 0 & 1 & 0 \\ 0 & 0 & 1 \end{pmatrix}$$

and the *Cauchy* (C) and *Green* (B) strain tensors (see 1.9 and 1.10) are

$$C = \begin{pmatrix} 1 & \gamma & 0 \\ \gamma & 1+\gamma^2 & 0 \\ 0 & 0 & 1 \end{pmatrix} \quad \text{and} \quad B = \begin{pmatrix} 1+\gamma^2 & \gamma & 0 \\ \gamma & 1 & 0 \\ 0 & 0 & 1 \end{pmatrix}.$$

2.9 bulk compression

Recommended symbol: χ

The fractional decrease in volume (V) caused by a hydrostatic pressure

$$\chi = - \Delta V/V.$$

Note

Also referred to as **volume compression, isotropic compression and bulk compressive strain.**

2.10 general homogeneous deformation or flow of a viscoelastic liquid or solid

A flow or deformation such that a particle of the viscoelastic liquid or solid with co-ordinate vector X' at time t' moves to a point with co-ordinate vector X at time t with

$$GX' = GX$$

where G' and G are tensors defining the type of deformation or flow and are functions of time only.

Notes

1. The definition is equivalent to that given in 1.5 note 4. Accordingly, the elements of G' and G are denoted $g'_{ij}(t')$ and $g_{ij}(t)$ and those of X' and X , (x'_1, x'_2, x'_3) and (x_1, x_2, x_3) .
2. For an incompressible material
 $\det G = 1$
 where $\det G$ is the determinant of G .
3. Deformations and flows used in conventional measurements of properties of viscoelastic liquids and solids are usually interpreted assuming incompressibility.

2.11 homogeneous orthogonal deformation or flow of an incompressible viscoelastic liquid or solid

A deformation or flow, as defined in 2.10, such that

$$G = \begin{pmatrix} g_{11}(t) & 0 & 0 \\ 0 & g_{22}(t) & 0 \\ 0 & 0 & g_{33}(t) \end{pmatrix}.$$

Notes

1. The g_{ii} are defined in 1.5, notes 2 to 4.
2. If $g_{22} = g_{33} = 1/g_{11}^{1/2}$ the elongational deformation or flow is **uniaxial**.
3. The *Finger strain tensor* for an homogeneous orthogonal deformation or flow of incompressible, viscoelastic liquid or solid (see 1.11) is

$$C^{-1} = \begin{pmatrix} \left(\frac{g'_{11}(t')}{g_{11}(t)}\right)^2 & 0 & 0 \\ 0 & \left(\frac{g'_{22}(t')}{g_{22}(t)}\right)^2 & 0 \\ 0 & 0 & \left(\frac{g'_{33}(t')}{g_{33}(t)}\right)^2 \end{pmatrix}$$

2.12 steady uniaxial homogeneous elongational deformation or flow of an incompressible viscoelastic liquid or solid

Uniaxial homogeneous elongational flow in which

$$g_{11}(t) = \exp(-\dot{\gamma}_E t)$$

where $\dot{\gamma}_E$ is a constant, and $g_{22} = g_{33} = 1/g_{11}^{1/2}$.

Notes

1. $g_{11}(t)$, $g_{22}(t)$ and $g_{33}(t)$ are elements of the tensor \mathbf{G} defined in 1.5.
2. From the definition of general homogeneous flow (1.5) ($\mathbf{G}'\mathbf{X}' = \mathbf{G}\mathbf{X} = \text{constant}$) in the particular case of *steady uniaxial elongation flow*

$$x_1 g_{11}(t) = x_1 \exp(-\dot{\gamma}_E t) = \text{constant}$$

and differentiation with respect to time gives

$$\dot{\gamma}_E = (1/x_1)(dx_1/dt)$$

Hence, $\dot{\gamma}_E$ is the **elongational or extensional strain rate**.

3. The *Finger strain tensor* for a steady uniaxial homogeneous elongation deformation or flow of an incompressible viscoelastic liquid or solid (see 1.11) is

$$C^{-1} = \begin{pmatrix} \exp(2\dot{\gamma}_E(t-t')) & 0 & 0 \\ 0 & \exp(-\dot{\gamma}_E(t-t')) & 0 \\ 0 & 0 & \exp(-\dot{\gamma}_E(t-t')) \end{pmatrix}$$

2.13 homogeneous simple shear deformation or flow of an incompressible viscoelastic liquid or solid

A flow or deformation such that

$$\mathbf{G} = \begin{pmatrix} 1 & -\gamma(t) & 0 \\ 0 & 1 & 0 \\ 0 & 0 & 1 \end{pmatrix}$$

where $\gamma(t)$ is the shear.

Notes

1. The general tensor G is defined in 1.5.
2. $\dot{\gamma} = d\gamma(t)/dt$ is the **shear rate**. The unit of $\dot{\gamma}$ is s^{-1} .
3. If $\gamma(t) = \dot{\gamma}t$, where $\dot{\gamma}$ is a constant, then the flow has a constant shear rate and is known as **steady (simple) shear flow**.
4. If $\gamma(t) = \gamma_0 \sin 2\pi\nu t$ then the flow is **oscillatory (simple) shear flow** of frequency ν and amplitude γ_0 . The unit of ν is Hz.
5. The *Finger strain tensor* for simple shear flow (see 1.11) is

$$C^{-1} = \begin{pmatrix} 1 + (\gamma(t) - \gamma(t'))^2 & \gamma(t) - \gamma(t') & 0 \\ \gamma(t) - \gamma(t') & 1 & 0 \\ 0 & 0 & 1 \end{pmatrix}$$

where $\gamma(t) - \gamma(t')$ is the amount of shear given to the liquid between the times t' and t . For steady simple shear flow C^{-1} becomes

$$C^{-1} = \begin{pmatrix} 1 + \dot{\gamma}^2(t-t') & \dot{\gamma}(t-t') & 0 \\ \dot{\gamma}(t-t') & 1 & 0 \\ 0 & 0 & 1 \end{pmatrix}$$

3. STRESSES OBSERVED EXPERIMENTALLY

For a given deformation or flow, the resulting stress depends on the material. However, the *stress tensor* (see 1.2) does take particular general forms for experimentally used deformations (see section 2). The definitions apply to elastic solids, and viscoelastic liquids and solids.

3.1 stress tensor resulting from an orthogonal deformation or flow

Recommended symbol: σ

For an orthogonal deformation or flow the stress tensor is diagonal with

$$\sigma = \begin{pmatrix} \sigma_{11} & 0 & 0 \\ 0 & \sigma_{22} & 0 \\ 0 & 0 & \sigma_{33} \end{pmatrix}$$

Unit: Pa

Notes

1. See 1.2 for the general definition of σ .
2. If the *strain tensor* is diagonal for all time then the *stress tensor* is diagonal for all time for isotropic materials.

3. For a **uniaxial (orthogonal) deformation or flow** $\sigma_{22} = \sigma_{33}$.
4. For a **pure shear deformation or flow** the stresses (σ_{11} , σ_{22} , σ_{33}) are usually all different from each other.
5. The *stress tensor* resulting from a *pure shear deformation or flow* is called a **pure shear stress**.

3.2 tensile stress

Recommended symbol: σ

The component σ_{11} of the stress tensor resulting from a tensile uniaxial deformation.

Unit: Pa

Notes

1. The *stress tensor* for a *uniaxial deformation* is given in 3.1.
2. The $0x_1$ direction is chosen as the direction of the *uniaxial deformation*.

3.3 compressive stress

Recommended symbol: σ

The component σ_{11} of the stress tensor resulting from a compressive uniaxial deformation.

Unit: Pa

Note

See notes 1 and 2 of 3.2.

3.4 nominal stress engineering stress

Recommended symbol: σ

The force resulting from an applied tensile or compressive uniaxial deformation divided by the initial cross-sectional area of the sample normal to the applied deformation.

Unit: Pa

Note

The term *engineering* or *nominal stress* is often used in circumstances when the deformation of the body is not infinitesimal and its cross-sectional area changes.

3.5 stress tensor resulting from a simple shear deformation or flow

Recommended symbol: σ

For a simple shear deformation or flow the stress tensor takes the form

$$\boldsymbol{\sigma} = \begin{pmatrix} \sigma_{11} & \sigma_{12} & 0 \\ \sigma_{21} & \sigma_{22} & 0 \\ 0 & 0 & \sigma_{33} \end{pmatrix}$$

where σ_{21} is numerically equal to σ_{12} .

Unit: Pa

Notes

1. See 1.2 for the general definition of $\boldsymbol{\sigma}$
2. σ_{ii} , $i = 1, 2, 3$ are denoted **normal stresses**.
3. σ_{12} is called the **shear stress**.

3.6 first normal-stress difference first normal-stress function

Recommended symbol: N_1

The difference between the first two normal stresses σ_{11} and σ_{22} in simple shear flow

$$N_1 = \sigma_{11} - \sigma_{22} .$$

Unit: Pa

Notes

1. See 3.5 for the definition of σ_{11} and σ_{22} .
2. For Newtonian liquids (see 4.2 note 3) $N_1 = 0$.

3.7 second normal-stress difference second normal-stress function

Recommended symbol: N_2

The difference between the second and third normal-stresses ($\sigma_{22} - \sigma_{33}$) in simple shear flow

$$N_2 = \sigma_{22} - \sigma_{33} .$$

Unit: Pa

Notes

1. See 3.5 for the definition of σ_{22} and σ_{33}
2. For *Newtonian liquids* (see 4.2 note 3), $N_2 = 0$.

4. QUANTITIES RELATING STRESS AND DEFORMATION

4.1 constitutive equation for an elastic solid

An equation relating stress and strain in an elastic solid.

Notes

1. For an elastic solid, the constitutive equation may be written

$$\boldsymbol{\sigma} = \frac{2}{I_3^{1/2}} \left(\frac{\partial W}{\partial I_1} \mathbf{B} + \frac{\partial W}{\partial I_2} (I_1 \mathbf{B} - \mathbf{B}^2) + I_3 \frac{\partial W}{\partial I_3} \mathbf{I} \right),$$

where \mathbf{B} is the *Green strain tensor* (see 1.10).

I_1, I_2, I_3 are invariants of \mathbf{B} ,

with $I_1 = \text{Tr}(\mathbf{B})$

$$I_2 = 1/2 ((\text{Tr}(\mathbf{B}))^2 - \text{Tr}(\mathbf{B}^2))$$

$$I_3 = \det(\mathbf{B}),$$

where 'Tr' denotes trace and 'det' denotes determinant. (Invariants are independent of the co-ordinate axes used and for symmetric tensors there are three independent invariants.)

W is a function of I_1, I_2 , and I_3 and is known as the **stored energy function** and is the increase in energy (stored energy) per unit initial volume due to the deformation.

2. For small deformations, the constitutive equation may be written

$$\boldsymbol{\sigma} = 2G\boldsymbol{\varepsilon} + lI\text{Tr}(\boldsymbol{\varepsilon}),$$

where G is the shear modulus (see 4.10), $\boldsymbol{\varepsilon}$ is the *small-strain tensor* (see 1.10, note 3) and l is a **Lamé constant**

3. The *Lamé constant*, (l), is related to the shear modulus (G) and Young's modulus (E) (see 4.7) by the equation

$$l = G(2G - E)/(E - 3G),$$

4. For an incompressible elastic solid, the constitutive equation may be written

$$\boldsymbol{\sigma} + P\mathbf{I} = 2 \frac{\partial W}{\partial I_1} \mathbf{B} - 2 \frac{\partial W}{\partial I_2} \mathbf{B}^{-1},$$

where P is the hydrostatic (or isotropic) pressure, $I_3 = 1$ and W is a function of I_1 and I_2 , only.

5. For small deformations of an incompressible, inelastic solid, the constitutive equation may be written

$$\boldsymbol{\sigma} + P\mathbf{I} = 2G\boldsymbol{\varepsilon}$$

4.2 constitutive equation for an incompressible viscoelastic liquid or solid

An equation relating stress and deformation in an incompressible viscoelastic liquid or solid.

Notes

1. A possible general form of constitutive equation when there is no dependence of stress on amount of strain is

$$\sigma + PI = f(A_1, A_2, \dots, A_n),$$

where A_1, A_2, \dots are the Rivlin-Ericksen tensors (see 1.14)

2. For a *non-Newtonian liquid* (see note 3), a form of the general constitutive equation which may be used is

$$\sigma + PI = \eta A_1^2 + \alpha A_1 + \beta A_2,$$

where η is the *viscosity* (see 4.12) and α and β are constants.

3. A **Newtonian liquid** is a liquid for which the constitutive equation may be written

$$\sigma + PI = \eta A_1 = 2\eta D,$$

where D is the *rate-of-strain tensor* (see 1.12). Liquids which do not obey this constitutive equation are termed **non-Newtonian liquids**.

4. For cases where there is a dependence of stress on strain history the following constitutive equation may be used, namely

$$\sigma + PI = 2 \int_{-\infty}^t \left(\frac{\partial \Omega}{\partial I_1} C^{-1} - \frac{\partial \Omega}{\partial I_2} C \right) dt',$$

where C is the *Cauchy strain tensor* (see 1.9) and Ω is a function of the invariants I_1, I_2 and I_3 of C^t and the time interval $t-t'$. Ω is formally equivalent to the stored-energy function, W , of a solid (see 4.1, note 4).

4.3 modulus

Recommended symbols: general M
 in bulk compressive deformation K
 in uniaxial deformation E
 in shear deformation G

The quotient of stress and strain where the type of stress and strain is defined by the type of deformation employed.

Unit: Pa

Notes

- The detailed definitions of K, E and G are given in 4.5, 4.7 and 4.10.
- An **elastic modulus** or **modulus of elasticity** is a modulus of a body which obeys Hooke's law (stress \propto strain).

4.4 compliance

Recommended symbols: general C
 in bulk compressive deformation B
 in uniaxial deformation D
 in shear deformation J

The quotient of strain and stress where the type of strain and stress is defined by the type of deformation employed.

Unit: Pa^{-1}

Notes

1. $C = 1/M$, where M is modulus (see 4.3).
2. The detailed definitions of B , D and J are given in 4.6, 4.8 and 4.11.

4.5 bulk modulus

Recommended symbol: K

The quotient of hydrostatic pressure (P) and bulk compression (χ)

$$K = P/\chi .$$

Unit: Pa

Notes

1. Also known as **bulk compressive modulus**.
2. For the definition of χ , see 2.9.
3. At small deformations, the bulk modulus is related to *Young's modulus* (E) (see 4.7) by

$$K = E/(3(1 - 2\mu))$$

where μ is *Poisson's ratio* (see 2.6).

4.6 bulk compliance

Recommended symbol: B

The quotient of bulk compression (χ) and hydrostatic pressure (P)

$$B = \chi/P .$$

Unit: Pa^{-1}

Notes

1. Also known as **bulk compressive compliance**.

2. For the definition of χ , see 2.9.

3. $B = 1/K$, where K is the *bulk modulus* (see 4.5)

4.7 Young's modulus

Recommended symbol: E

The quotient of uniaxial stress (σ) and strain (ϵ) in the limit of zero strain

$$E = \lim_{\epsilon \rightarrow 0} (\sigma/\epsilon) .$$

Unit: Pa

Notes

1. The stress is a *true stress*, as in 3.2 and 3.3, and not a *nominal stress*, as in 3.4.
2. ϵ is defined in 2.4.
3. *Young's modulus* may be evaluated using *tensile or compressive uniaxial deformation* (see 2.4). If determined using tensile deformation it may be termed **tensile modulus**.
4. For non-Hookean materials (see 4.3), the *Young's modulus* is sometimes evaluated as:

(i) the **secant modulus** - the quotient of *stress* (σ) and strain at some nominal *strain* (ϵ) in which case

$$E = \sigma/\epsilon$$

(ii) the **tangent modulus** - the slope of the stress-strain curve at some nominal *strain* (ϵ'), in which case

$$E = (d\sigma/d\epsilon)_{\epsilon=\epsilon'}$$

4.8 uniaxial compliance

Recommended symbol: D

The quotient of uniaxial strain (ϵ) and uniaxial stress (σ) in the limit of zero strain

$$D = \lim_{\sigma \rightarrow 0} (\epsilon / \sigma) .$$

Unit: Pa⁻¹

Notes

1. The stress is a *true stress* as in 3.2 and 3.3, and not a *nominal stress*, as in 3.4.
2. ϵ is defined in 2.4.
3. Uniaxial compliance may be evaluated using *tensile or compressive uniaxial deformation* (see 2.4). If determined using tensile deformation it may be termed **tensile compliance**.
4. $D = 1/E$, where E is *Young's modulus* (see 4.7).

4.9 extensional viscosity elongational viscosity

Recommended symbol: η_E

The quotient of the difference between the longitudinal stress (σ_{11}) and the lateral stress (σ_{22}) and the elongational strain rate ($\dot{\gamma}_E$) in steady uniaxial flow

$$\eta_E = (\sigma_{11} - \sigma_{22}) / \dot{\gamma}_E$$

Unit: Pa s

Note

See 3.1 and 2.12 for the definitions of σ_{11} , σ_{22} and $\dot{\gamma}_E$

4.10 shear modulus

Recommended symbol: G

The quotient of shear stress (σ_{12}) and shear strain (γ)

$$G = \sigma_{12} / \gamma$$

Unit: Pa

Notes

1. See 2.8 for the definitions of γ for an elastic solid and 3.5 for the definition of σ_{12} .
2. The *shear modulus* is related to *Young's modulus* (E) (see 4.7) by the equation

$$G = E / (2(1 + \mu))$$

where μ is *Poisson's ratio* (see 2.6).

3. For elastomers, which are assumed incompressible, the modulus is often evaluated in *uniaxial tensile* or *compressive deformation* using $\lambda - \lambda^{-2}$ as the strain function (where λ is the *uniaxial deformation ratio* (see 2.3)). In the limit of zero deformation the *shear modulus* is evaluated as

$$\frac{d\sigma}{d(\lambda - \lambda^{-2})} = \frac{E}{3} = G \text{ (for } \mu = 0.5 \text{) ,}$$

where σ is the *tensile* or *compressive stress* (see 3.2 and 3.3).

4.11 shear compliance

Recommended symbol: J

The quotient of shear strain (γ) and shear stress (σ_{12})

$$J = \gamma / \sigma_{12}$$

Unit: Pa⁻¹

Notes

1. See 2.8 for the definition of γ for an elastic solid and 3.5 for the definition of σ_{12} .
2. $J = 1/G$, where G is the *shear modulus* (see 4.10).

4.12 shear viscosity coefficient of viscosity viscosity

Recommended symbol: η

The quotient of shear stress (σ_{12}) and shear rate ($\dot{\gamma}$) in steady, simple shear flow

$$\eta = \sigma_{12} / \dot{\gamma}$$

Unit: Pa s

Notes

1. See 3.5 and 2.13 for the definitions of σ_{12} and $\dot{\gamma}$
2. For *Newtonian liquids* (see 4.2 note 3), σ_{12} is directly proportional to $\dot{\gamma}$ and η is constant.
3. For *non-Newtonian liquids* (see 4.2 note 3), when σ_{12} is not directly proportional to $\dot{\gamma}$, η varies with $\dot{\gamma}$. The value of η evaluated at a given value of $\dot{\gamma}$ is termed the **non-Newtonian viscosity**.
4. Some experimental methods, such as capillary flow and flow between parallel plates, employ a range of shear rates. The value of η evaluated at some nominal average value of $\dot{\gamma}$ is termed the **apparent viscosity** and given the symbol η_{app} . It should be noted that *apparent viscosity* is an imprecisely defined quantity.
5. Extrapolation of η or η_{app} for *non-Newtonian liquids* to zero $\dot{\gamma}$ gives the **zero-shear viscosity**, which is given the symbol η_0 .
6. Extrapolation of η and η_{app} for *non-Newtonian liquids* to infinite $\dot{\gamma}$ gives the **infinite-shear viscosity**, which is given the symbol η_∞ .

4.13 first normal-stress coefficient

Recommended symbol: ψ_1

The quotient of the first normal stress difference (N_1) and the square of the shear rate ($\dot{\gamma}$) in the limit of zero shear rate

$$\psi_1 = \lim_{\dot{\gamma} \rightarrow 0} (N_1 / \dot{\gamma}^2) .$$

Unit: Pa s²

Note

See 3.6 and 2.13 for the definitions of N_1 and $\dot{\gamma}$

4.14 second normal-stress coefficient

Recommended symbol: ψ_2

The quotient of the second normal stress difference (N_2) and the square of the shear rate ($\dot{\gamma}$) in the limit of zero shear rate

$$\psi_2 = \lim_{\dot{\gamma} \rightarrow 0} (N_2 / \dot{\gamma}^2)$$

Unit: Pa s²

Note

See 3.7 and 2.13 for the definitions of N_2 and $\dot{\gamma}$.

5. LINEAR VISCOELASTIC BEHAVIOUR

5.1 viscoelasticity

The time-dependent response of a liquid or solid subjected to stress or strain.

Notes

1. Both viscous and elastic responses to stress or strain are required for the description of viscoelastic behaviour.
2. Viscoelastic properties are usually measured as responses to an instantaneously applied or removed constant stress or strain or a **dynamic stress or strain**. The latter is defined as a sinusoidal stress or strain of small amplitude, which may or may not decrease with time.

5.2 linear viscoelastic behaviour

The interpretation of the viscoelastic behaviour of a liquid or solid in *simple shear* or *uniaxial deformation* such that

$$P(D)\sigma = Q(D)\gamma$$

where σ is the shear stress or uniaxial stress, γ is the shear strain or uniaxial strain, and $P(D)$ and $Q(D)$ are polynomials in D , where D is the differential coefficient operator d/dr .

Notes

1. In *linear viscoelastic behaviour*, stress and strain are assumed to be small so that the squares and higher powers of σ and γ may be neglected.

2. See 3.5 and 2.13 for the definitions of σ and γ in *simple shear*.
3. See 3.2 and 2.12 for definitions of σ and γ ($\equiv \gamma_E$) in *uniaxial deformations*.
4. The polynomials $Q(D)$ and $P(D)$ have the forms:

$$Q(D) = a(D + q_0) \dots (D + q_n)$$

(a polynomial of degree $n + 1$)

$$P(D) = (D + p_0) (D + p_1) \dots (D + p_n)$$

(a polynomial of degree $n + 1$)

and

$$P(D) = (D + p_0) (D + p_1) \dots (D + p_{n-1})$$

(a polynomial of degree n)

where

(i) a is a constant

(ii) $q_0 \geq 0, p_0 > 0$ and $p_s, q_s > 0, s = 1, \dots, n$.

(iii) $q_i < p_i < q_{i+1}$ and $q_n < p_n$ (if p_n exists)

p_i and q_i are related to *relaxation* and *retardation times*, respectively (see 5.6 - 5.9).

5. If $q_0 = 0$, the material is a **liquid**, otherwise it is a **solid**.
6. Given that $Q(D)$ is a polynomial of degree $n + 1$; if $P(D)$ is also of degree $n + 1$ the material shows instantaneous elasticity; if $P(D)$ is of degree n , the material does not show instantaneous elasticity (i.e. elasticity immediately the deformation is applied.)
7. There are definitions of linear viscoelasticity which use integral equations instead of the differential equation in definition 5.2. (See, for example, ref. 11.) Such definitions have certain advantages regarding their mathematical generality. However, the approach in the present document, in terms of differential equations, has the advantage that the definitions and descriptions of various viscoelastic properties can be made in terms of commonly used mechano-mathematical models (e.g. the Maxwell and Voigt-Kelvin models).

5.3 Maxwell model

Maxwell element

A model of the linear viscoelastic behaviour of a liquid in which

$$(\alpha D + \beta)\sigma = D\gamma$$

where α and β are positive constants, D is the differential coefficient operator d/dt , and σ and γ are the stress and strain in *simple shear* or *uniaxial deformation*.

Notes

1. See 5.2 for a discussion of σ and γ .
2. The relationship defining the *Maxwell model* may be written

$$d\sigma/dt + (\beta/\alpha)\sigma = (1/\alpha)d\gamma/dt$$

- Comparison with the general definition of *linear viscoelastic behaviour* (5.2) shows that the polynomials $P(D)$ and $Q(D)$ are of order one, $q_0=0$, $p_0=\beta/\alpha$ and $a=1/\alpha$. Hence, a material described by a *Maxwell model* is a *liquid* ($q_0 = 0$) having instantaneous elasticity ($P(D)$ and $Q(D)$ are of the same order).
- The *Maxwell model* may be represented by a spring and a dashpot filled with a *Newtonian liquid* in series, in which case $1/\alpha$ is the **spring constant** (force = $1/\alpha$ ·extension) and $1/\beta$ is the **dashpot constant** (force = $(1/\beta)$ ·rate of extension).

5.4 Voigt-Kelvin model Voigt-Kelvin element

A model of the *linear viscoelastic behaviour* of a solid in which

$$\sigma = (\alpha + \beta D)\gamma$$

where α and β are positive constants, D is the differential coefficient operator d/dt , and σ and γ are the stresses and strain in *simple shear* or *uniaxial deformation*.

Notes

- The Voigt-Kelvin model is also known as the **Voigt model** or **Voigt element**.
- See 5.2 for a discussion of σ and γ .
- The relationship defining the *Voigt-Kelvin model* may be written

$$\sigma = \alpha\gamma + \alpha\beta(dy/dt).$$

- Comparison with the general definition of *linear viscoelastic behaviour* (5.2) shows that the polynomial $P(D)$ is of order zero, $Q(D)$ is of order one, $aq_0 = \alpha$, and $a = \beta$. Hence, a material described by the *Voigt-Kelvin model* is a *solid* ($q_0 > 0$) without instantaneous elasticity ($P(D)$ is a polynomial of order one less than $Q(D)$).
- The **Voigt-Kelvin model** may be represented by a spring and a dashpot filled with a *Newtonian liquid* in parallel, in which case α is the **spring constant** (force = α ·extension) and β is the **dashpot constant** (force = β ·rate of extension).

5.5 standard linear viscoelastic solid

A model of the *linear viscoelastic behaviour* of a solid in which

$$(\alpha_1 + \beta_1 D)\sigma = (\alpha_2 + \beta_2 D)\gamma$$

where α_1 , β_1 , α_2 and β_2 are positive constants, D is the differential coefficient operator d/dt , and σ and γ are the stress and strain in *simple shear* or *uniaxial deformation*.

Notes

- See 5.2 for a discussion of σ and γ .
- The relationship defining the *standard linear viscoelastic solid* may be written

$$\alpha_1\sigma + \beta_1(d\sigma/dt) = \alpha_2\gamma + \beta_2(d\gamma/dt)$$
- Comparison with the general definition of a *linear viscoelastic behaviour* (5.2) shows that the polynomial $P(D)$ and $Q(D)$ are of order one, $q_0 = \alpha_2/\beta_2$, $a = \beta_2/\beta_1$ and $p_0 =$

α_1/α_2 . Hence, the *standard linear viscoelastic solid* is a solid ($aq_0 > 0$) having instantaneous elasticity ($P(D)$ and $Q(D)$ are of the same order).

4. The *standard linear viscoelastic solid* may be represented by:

(i) a *Maxwell model* (of spring constant h_2 and dashpot constant k_2) in parallel with a spring (of spring constant h_1) in which case $\alpha_1 = h_2$, $\beta_1 = k_2$, $\alpha_2 = h_1 h_2$ and $\beta_2 = h_1 k_2 + h_2 k_2$.

(ii) a *Voigt-Kelvin model* (of spring constant h_2 and dashpot constant k_2) in series with a spring (of spring constant h_1) in which case $\alpha_1 = h_1 + h_2$, $\beta_1 = k_2$, $\alpha_2 = h_1 h_2$ and $\beta_2 = h_1 k_2$.

5. The *standard linear viscoelastic solid* can be used to represent both *creep* (see 5.9) and *stress relaxation* (see 5.7) in materials in terms of single retardation and relaxation times, respectively.

5.6 relaxation time

Recommended symbol: τ

A time characterising the response of a viscoelastic liquid or solid to the instantaneous application of a constant strain.

Unit: s

Notes

1. The response of a material to the instantaneous application of a constant strain is termed *stress relaxation* (see 5.7).
2. The relaxation time of a *Maxwell element* (5.3) is $\tau = 1/p_0 = \alpha/\beta$.
3. The *relaxation time* of a *standard linear viscoelastic solid* (5.5) is $\tau = 1/p_0 = \beta_1/\alpha_1$.
4. Generally, a *linear viscoelastic material* has a spectrum of relaxation times, which are the reciprocals of p_i , $i = 0, 1, \dots, n$ in the polynomial $P(D)$ (see 5.2).
5. The **relaxation spectrum** (spectrum of relaxation times) describing *stress relaxation* in polymers may be considered as arising from a group of *Maxwell elements* in parallel (see 5.7).

5.7 stress relaxation

The change in stress with time after the instantaneous application of a constant strain.

Notes

1. The applied strain is of the form $\gamma = 0$ for $t < 0$ and $\gamma = \gamma_0$ for $t > 0$ and is usually a *uniaxial extension* or a *simple shear* (see 5.2).
2. For *linear viscoelastic behaviour*, the stress takes the form

$$\sigma(t) = (c + \bar{\psi}(t))\gamma_0$$

c is a constant that is non-zero if the material has instantaneous elasticity and $\bar{\psi}(t)$ is the **relaxation function**.

3. $\bar{\psi}(t)$ has the form

$$\bar{\psi}(t) = \sum_{i=0}^n \beta_i e^{-p_i t}$$

where the β_i are functions of the p_i and q_i of the polynomials $P(D)$ and $Q(D)$ defining the *linear viscoelastic material* (see 5.1).

4. The relaxation times of the material are $1/p_i$ (see 5.6).

5.8 retardation time

Recommended symbol: τ

A time characterising the response of a viscoelastic material to the instantaneous application of a constant stress.

Unit: s

Notes:

1. The response of a material to the instantaneous application of a constant stress is termed *creep* (see 5.9).
2. The *retardation time* of a *Voigt-Kelvin element* is $\tau = 1/q_0 = \beta/\alpha = (\text{dashpot constant})/(\text{spring constant})$.
3. The *retardation time* of a *standard linear viscoelastic solid* (5.5) is $\tau = 1/q_0 = \beta_2/\alpha_2$.
4. Generally, a *linear viscoelastic material* has a spectrum of *retardation times*, which are reciprocals of q_i , $i = 0, 1, \dots, n$ in the polynomial $Q(D)$ (see 5.2).
5. The **retardation spectrum** (spectrum of retardation times) describing *creep* in polymers may be considered as arising from a group of *Voigt-Kelvin elements* in series (see 5.9).

5.9 creep

The change in strain with time after the instantaneous application of a constant stress.

Notes

1. The applied stress is of the form $\sigma = 0$ for $t < 0$ and $\sigma = \sigma_0$ for $t > 0$ and is usually a *uniaxial stress* or a *simple shear stress* (see 5.2).
2. For *linear viscoelastic behaviour*, the *strain* usually takes the form

$$\gamma(t) = (a + bt + \psi(t))\sigma_0$$

a is a constant that is non-zero if the material has instantaneous elasticity and b is a

constant that is non-zero if the material is a liquid. $\psi(t)$ is the **creep function**. In addition,

$$J(t) = \gamma(t)/\sigma_0$$

is sometimes called the **creep compliance**.

3. The **creep function** has the form

$$\psi(t) = \sum_i A_i e^{-q_i t}$$

where the summation runs from $i = 0$ to n for a *solid* and 1 to n for a *liquid*. The A_i are functions of the p_i and q_i of the polynomials $P(D)$ and $Q(D)$ defining the *linear viscoelastic material* and the q_i are the q_i of the polynomial $Q(D)$ (see 5.1).

4. The *retardation times* of the material are $1/q_i$ (see 5.8).

5. Creep is sometimes described in terms of non-linear viscoelastic behaviour, leading, for example, to evaluation of recoverable shear and steady-state recoverable shear compliance. The definitions of such terms are outside the scope of this document.

5.10 forced oscillation

The deformation of a material by the application of a small sinusoidal strain (γ) such that

$$\gamma = \gamma_0 \cos \omega t$$

where γ_0 and ω are positive constants.

Notes

1. γ may be in *simple shear* (see 2.8 and 2.13) or *uniaxial deformation* (often denoted ϵ , see 2.4).
2. γ_0 is the **strain amplitude**.
3. ω is the **angular velocity** of the circular motion equivalent to a sinusoidal frequency ν , with $\omega = 2\pi\nu$. The unit of ω is rad s^{-1} .
4. For *linear viscoelastic behaviour*, a sinusoidal stress (σ) results from the sinusoidal strain with

$$\sigma = \sigma_0 \cos(\omega t + \delta) = \sigma_0 \cos \delta \cdot \cos \omega t - \sigma_0 \sin \delta \cdot \sin \omega t.$$

σ_0 is the **stress amplitude**. δ is the **phase angle** or **loss angle** between stress and strain.

5. Alternative descriptions of the sinusoidal stress and strain in a viscoelastic material under forced oscillations are:

$$(i) \gamma = \gamma_0 \sin \omega t$$

$$\begin{aligned} \sigma &= \sigma_0 \sin(\omega t + \delta) \\ &= \sigma_0 \sin \delta \cdot \cos \omega t + \\ &\quad \sigma_0 \cos \delta \cdot \sin \omega t \end{aligned}$$

$$(ii) \begin{aligned} \gamma &= \gamma_0 \cos(\omega t - \delta) & \sigma &= \sigma_0 \cos \omega t \\ &= \gamma_0 \cos \delta \cdot \cos \omega t + & & \\ & \quad \gamma_0 \sin \delta \cdot \sin \omega t & & \end{aligned}$$

5.11 loss factor loss tangent

Recommended symbol: $\tan \delta$

The tangent of the phase angle difference (δ) between stress and strain during forced oscillations.

Notes

1. $\tan \delta$ is calculated using
 $\gamma = \gamma_0 \cos \omega t$ and $\sigma = \sigma_0 \cos(\omega t + \delta)$. (see 5.10).
2. $\tan \delta$ is also equal to the ratio of *loss* to *storage modulus* (see 5.12 and 5.13).
3. A plot of $\tan \delta$ versus temperature or frequency is known as a **loss curve**.

5.12 storage modulus

Recommended symbol: general M'
 in simple shear deformation G'
 in uniaxial deformation E'

The ratio of the amplitude of the stress in phase with the strain ($\sigma_0 \cos \delta$) to the amplitude of the strain (γ_0) in the forced oscillation of a material

$$M' = (\sigma_0 \cos \delta) / \gamma_0.$$

Unit: Pa

Note

See 5.10 for the definition of a *forced oscillation* in which $\gamma = \gamma_0 \cos \omega t$ and $\sigma = \sigma_0 \cos(\omega t + \delta)$.

5.13 loss modulus

Recommended symbols: General M''
 in simple shear deformation G''
 in uniaxial deformation in E''

The ratio of the amplitude of the stress 90° out of phase with the strain ($\sigma_0 \sin \delta$) to the amplitude of the strain (γ_0) in the forced oscillation of a material

$$M'' = (\sigma_0 \sin \delta) / \gamma_0$$

Unit: Pa

Note

See 5.10 for the definition of a *forced oscillation* in which $\gamma = \gamma_0 \cos \omega t$ and $\sigma = \sigma_0 \cos (\omega t + \delta)$.

5.14 absolute modulus

Recommended symbols: general $|M^*|$
 in simple shear deformation $|G^*|$
 in uniaxial deformation $|E^*|$

The ratio of the amplitude of the stress (σ_0) to the amplitude of the strain (γ_0) in the forced oscillation of a material

$$|M^*| = \sigma_0 / \gamma_0 .$$

Unit: Pa

Notes

1. See 5.10 for the definition of a *forced oscillation* in which $\gamma = \gamma_0 \cos \omega t$ and $\sigma = \sigma_0 \cos (\omega t + \delta)$.
2. The absolute modulus is related to the *storage modulus* (5.12) and the *loss modulus* (5.13) by the relationship

$$|M^*| = \left(\frac{\sigma_0^2 \cos^2 \delta}{\gamma_0^2} + \frac{\sigma_0^2 \sin^2 \delta}{\gamma_0^2} \right)^{1/2} = (M'^2 + M''^2)^{1/2} .$$

5.15 complex modulus

Recommended symbols: general M^*
 in simple shear deformation G^*
 in uniaxial deformation E^*

The ratio of complex stress (σ^*) to complex strain (γ^*) in the forced oscillation of material

$$M^* = \sigma^* / \gamma^* .$$

Unit: Pa

Notes

1. See 5.10 for the definition of a *forced oscillation* in which $\gamma = \gamma_0 \cos \omega t$ and $\sigma = \sigma_0 \cos (\omega t + \delta)$.
2. The **complex strain** $\gamma^* = \gamma_0 e^{i\omega t} = \gamma_0 (\cos \omega t + i \sin \omega t)$, where $i = \sqrt{-1}$, so that the real part of the complex strain is that actually applied to the material.
3. The **complex stress** $\sigma^* = \sigma_0 e^{i(\omega t + \delta)} = \sigma_0 (\cos(\omega t + \delta) + i \sin(\omega t + \delta))$, so that the real part of the complex stress is that actually experienced by the material.

4. The *complex modulus* is related to the *storage* and *loss moduli* through the relationships

$$M^* = \sigma^* / \gamma^* = \sigma_0 e^{i\delta} / \gamma_0 = (\sigma_0 / \gamma_0) (\cos \delta + i \sin \delta) = M' + iM''.$$

5. For linear viscoelastic behaviour interpreted in terms of *complex stress* and *strain* (see notes 2, 3)

$$P(D)\sigma^* = Q(D)\gamma^*$$

(see 5.2). Further as $D\sigma^* = d\sigma^*/dt = i\omega\sigma^*$ and $D\gamma^* = i\omega\gamma^*$

$$M^* = \sigma^* / \gamma^* = Q(i\omega) / P(i\omega)$$

5.16 storage compliance

Recommended symbols: general C'
 in simple shear deformation J'
 in uniaxial deformation D'

The ratio of the amplitude of the strain in phase with the stress ($\gamma_0 \cos \delta$) to the amplitude of the stress (σ_0) in the forced oscillation of a material

$$C' = (\gamma_0 \cos \delta) / \sigma_0.$$

Unit: Pa^{-1}

Note

See 5.10, note 5 for the definition of a *forced oscillation* in which $\gamma = \gamma_0 \cos(\omega t - \delta)$ and $\sigma = \sigma_0 \cos \omega t$.

5.17 loss compliance

Recommended symbols: general C''
 in simple shear deformation J''
 in uniaxial deformation D''

The ratio of the amplitude of the strain 90° out of phase with the stress ($\gamma_0 \sin \delta$) to the amplitude of the stress (σ_0) in the forced oscillation of a material

$$C'' = (\gamma_0 \sin \delta) / \sigma_0.$$

Unit: Pa^{-1}

Note

See 5.10 for the definition of a *forced oscillation* in which $\gamma = \gamma_0 \cos(\omega t - \delta)$ and $\sigma = \sigma_0 \cos \omega t$.

5.18 absolute compliance

Recommended symbols: general $|C^*|$
 in simple shear deformation $|J^*|$
 in uniaxial deformation $|D^*|$

The ratio of the amplitude of the strain (γ_0) to the amplitude of the stress (σ_0) in the forced oscillation of a material

$$|C^*| = \gamma_0/\sigma_0.$$

Unit: Pa⁻¹

Notes

1. See 5.10 note 5 for the definition of a *forced oscillation* in which $\gamma = \gamma_0 \cos(\omega t - \delta)$ and $\sigma = \sigma_0 \cos \omega t$.
2. The absolute compliance is related to the *storage compliance* (5.16) and the *loss compliance* (5.17) by the relationship

$$|C^*| = \left(\frac{\gamma_0^2 \cos^2 \delta}{\sigma_0^2} + \frac{\gamma_0^2 \sin^2 \delta}{\sigma_0^2} \right)^{1/2} = (C'^2 + C''^2)^{1/2}.$$

3. The absolute compliance is the reciprocal of the *absolute modulus* (5.14).

$$|C^*| = 1/|M^*|.$$

5.19 complex compliance

Recommended symbols: general C^*
 in simple shear deformation J^*
 in shear deformation D^*

The ratio of complex strain (γ^*) to complex stress (σ^*) in the forced oscillation of a material

$$C^* = \gamma^*/\sigma^*.$$

Unit: Pa⁻¹

Notes

1. See 5.10 for the definition of a *forced oscillation* in which $\gamma = \gamma_0 \cos(\omega t - \delta)$ and $\sigma = \sigma_0 \cos \omega t$.
2. The **complex strain** $\gamma^* = \gamma_0 e^{i(\omega t - \delta)} = \gamma_0 (\cos(\omega t - \delta) + i \sin(\omega t - \delta))$, where $i = \sqrt{-1}$, so that the real part of the complex strain is that actually experienced by the material.
3. The **complex stress** $\sigma^* = \sigma_0 e^{i\omega t} = \sigma_0 (\cos \omega t + i \sin \omega t)$, so that the real part of the complex stress is that actually applied to the material.
4. The complex compliance is related to the *storage* and *loss compliances* (5.16 and 5.17) through the relationships

$$C^* = \gamma^*/\sigma^* = \gamma_0 e^{-i\delta} / \sigma_0 = (\gamma_0/\sigma_0)(\cos \delta - i \sin \delta) = C' - iC''$$

5. The complex compliance is the reciprocal of the *complex modulus*

$$C^* = 1/M^*.$$

5.20 dynamic viscosityRecommended symbol: η'

The ratio of the stress in phase with the rate of strain ($\sigma_0 \sin \delta$) to the amplitude of the rate of strain ($\omega \gamma_0$) in the forced oscillation of a material

$$\eta' = (\sigma_0 \sin \delta) / (\omega \gamma_0) .$$

Unit: Pa s

Notes

1. See 5.10, note 5 for the definition of a *forced oscillation* in which $\gamma = \gamma_0 \sin \omega t$ and $\sigma = \sigma_0 \sin(\omega t + \delta)$, so that $\dot{\gamma} = \omega \gamma_0 \cos \omega t$ and $\sigma = \sigma_0 \sin \delta \cdot \cos \omega t + \sigma_0 \cos \delta \cdot \sin \omega t$.
2. See 5.2, note 6: $\eta' = M''/\omega$ may be used for evaluating the *dynamic viscosity*. The same expression is often used to evaluate the *shear viscosity*. The latter use of this expression is not recommended.

5.21 out-of-phase viscosityRecommended symbol: η''

The ratio of the stress 90° out of phase with the rate of strain ($\sigma_0 \cos \delta$) to the amplitude of the rate of strain ($\omega \gamma_0$) in the forced oscillation of a material

$$\eta'' = (\sigma_0 \cos \delta) / (\omega \gamma_0) .$$

Unit: Pa s

Notes

1. See 5.10, note 5 for the definition of a *forced oscillation* in which $\gamma = \gamma_0 \sin \omega t$ and $\sigma = \sigma_0 \sin(\omega t + \delta)$, so that $\dot{\gamma} = \omega \gamma_0 \cos \omega t$ and $\sigma = \sigma_0 \sin \delta \cdot \cos \omega t + \sigma_0 \cos \delta \cdot \sin \omega t$.
2. See 5.22, note 6: $\eta'' = M'/\omega$ may be used to evaluate the *out-of-phase viscosity*.

5.22 complex viscosityRecommended symbol: η^*

The ratio of complex stress (σ^*) to complex rate of strain ($\dot{\gamma}^*$) in the forced oscillation of a material

$$\eta^* = \sigma^* / \dot{\gamma}^* .$$

Unit: Pa s

Notes

1. See 5.10, note 5 for the definition of a *forced oscillation* in which $\gamma = \gamma_0 \sin \omega t$ and $\sigma = \sigma_0 \cos(\omega t + \delta)$ and the rate of strain $\dot{\gamma} = \omega_0 \cos \omega t$.

2. The **complex rate of strain** $\dot{\gamma}^* = i \omega \gamma_0 e^{i\omega t} = i \omega \gamma_0 (\cos \omega t + i \sin \omega t)$, where $i = \sqrt{-1}$.

3. The **complex stress** $\sigma^* = \sigma_0 e^{i(\omega t + \delta)} = \sigma_0 (\cos(\omega t + \delta) + i \sin(\omega t + \delta))$

4. The *complex viscosity* may alternatively be expressed as

$$\eta^* = \sigma^* / \dot{\gamma}^* = (\sigma_0 e^{i\delta}) / (i \omega \gamma_0) = M^* / i \omega$$

where M^* is the *complex modulus* (see 5.15).

5. The *complex viscosity* is related to the *dynamic* and *out-of-phase viscosities* through the relationships

$$\eta^* = \sigma^* / \dot{\gamma}^* = \sigma_0 (\cos \delta + i \sin \delta) / (i \omega \gamma_0) = \eta' - i \eta''.$$

6. The *dynamic* and *out-of-phase viscosities* are related to the *storage* and *loss moduli* (5.11 and 5.13) by the relationships $\eta^* = \eta' - i \eta'' = M^* / i \omega = (M' + i M'') / i \omega$, so that $\eta' = M' / \omega$ and $\eta'' = M'' / \omega$.

6. OSCILLATORY DEFORMATIONS AND STRESSES USED EXPERIMENTALLY

There are three modes of **free** and **forced** oscillatory deformations which are commonly used experimentally, **torsional oscillations**, **uniaxial extensional oscillations** and **flexural oscillations**.

The oscillatory deformations and stresses can be used for solids and liquids. However, the apparatuses employed to measure them are usually designed for solid materials. In principle, they can be modified for use with liquids.

Analyses of the results obtained depend on the shape of the specimen, whether or not the distribution of mass in the specimen is accounted for and the assumed model used to represent the linear viscoelastic properties of the material. The following terms relate to analyses which generally assume small deformations, specimens of uniform cross-section, non-distributed mass and a Voigt-Kelvin solid (see 5.4). These are the conventional assumptions.

6.1 free oscillation

The oscillatory deformation of a material specimen with the motion generated without the continuous application of an external force.

Note

For any real sample of material the resulting oscillatory deformation is one of decaying amplitude.

6.2 damping curve

The decreased deformation of a material specimen versus time when the specimen is subjected to a free oscillation.

Notes

1. See 6.1 for the definition of a *free oscillation*.
2. The term 'damping curve' is sometimes used to describe a *loss curve* (see 5.11).
3. A *damping curve* is usually obtained using a **torsion pendulum**, involving the measurement of decrease of the axial, torsional displacement of a specimen of uniform cross-section of known shape, with the torsional displacement initiated using a torsion bar of known moment of inertia.
4. *Damping curves* are conventionally analysed in terms of the *Voigt-Kelvin solid* (see 5.4) giving a decaying amplitude and a single frequency.
5. Given the properties of a *Voigt-Kelvin solid*, a damping curve is described by the equation

$$X = A \exp(-\beta t) \sin(\omega t - \phi),$$

where X is the displacement from equilibrium (for torsion $X = \theta$, the angular displacement), t is time, A is the amplitude, β is the *decay constant* (see 6.3), ω is the *angular velocity* corresponding to the *decay frequency* (see 5.10 and 6.4) and ϕ is the phase angle.

6.3 decay constant

Recommended symbol: β

The exponential coefficient of the time-dependent decay of a damping curve, assuming Voigt-Kelvin behaviour

Unit: s^{-1}

Notes

1. See *damping curve* (6.2) and the equation therefor (6.2, note 5).
2. See *Voigt-Kelvin solid* (5.4).
3. For small damping, β is related to the *loss modulus* (M''), see 5.13, through the equation

$$M'' = 2\beta\omega/H.$$

ω is the angular velocity corresponding to the *decay frequency* (see 5.10 and 6.4). H depends on the cross-sectional shape of the specimen and the type of deformation. (For example, for the axial torsion of a circular rod of radius a and length l using a *torsion pendulum* (see 6.2, note 3) with a torsion bar of moment of inertia I

$$H = \pi a^4 / (2I)$$

and $M'' \cong G''$, the loss modulus in simple shear)

6.4 decay frequency

Recommended symbol: ν

The frequency of a damping curve assuming Voigt-Kelvin behaviour.

Unit: Hz

Notes

1. See *damping curve* (6.2) and the equation therefor (6.2, note 5).
2. See *Voigt-Kelvin solid* (5.4).
3. $\nu = \omega/2\pi$, where ω is the *angular velocity* corresponding to ν (see 5.10).
4. For small damping, the *storage modulus* (M'), see 5.12, may be evaluated from ω through the equation

$$M' = \omega^2/H,$$

where H is discussed in 6.3, note 3. Again, for torsion, $M' \cong G'$, the *storage modulus* in simple shear.

6.5 logarithmic decrement

Recommended symbol: Λ

Natural logarithm of the ratio of the displacement of a damping curve separated by one period of the displacement.

Notes

1. *Voigt-Kelvin* behaviour (see 5.4) is assumed so that the displacement decays with a single period T , where

$$T = \frac{1}{\nu} = \frac{2\pi}{\omega}$$

with ν the frequency and ω is the angular velocity corresponding to ν (see 6.4).

2. The *logarithmic decrement* can be used to evaluate the *decay constant* β (see 6.3). From the equation for the *damping curve* of a *Voigt-Kelvin solid* (see 6.2, note 5).

$$\Lambda = \ln(X_n/X_{n+1}) = \beta(t_{n+1} - t_n) = \beta \cdot T,$$

where X_n and t_n are the displacement and time at a chosen point (usually near a maximum) in the n -th period of the decay, and X_{n+1} and t_{n+1} are the corresponding displacement and time one period later.

3. Λ can also be defined using displacements k periods apart, with

$$\Lambda = (1/k)\ln(X_n/X_{n+k}).$$

4. For small damping, Λ is related to the *loss tangent*, $\tan \delta$ (see 5.11) by

$$\tan \delta = M''/M' = 2\beta/\omega = 2\Lambda/T\omega = \Lambda/\pi$$

(See 6.3 and 6.4 for expressions for M' and M'').

6.6 forced uniaxial extensional oscillations

The uniaxial extensional deformation of a material specimen of uniform cross-sectional area along its long axis by the continuous application of a sinusoidal force of constant amplitude.

Notes

1. For a specimen of negligible mass, the linear-viscoelastic interpretation of the resulting deformation gives

$$(A/L)Q(D)l = P(D)f_0 \cos \omega t$$

where $P(D)$ and $Q(D)$ are the polynomials in $D(=d/dt)$ characterising the *linear-viscoelastic behaviour* (see 5.2), A is the cross-sectional area of the specimen, L its original length, l is here the change in length, f_0 the amplitude of the applied force of *angular velocity* ω (see 5.10, note 3) and t the time.

2. For a *Voigt-Kelvin* solid (see 5.4), with $P(D)=1$ and $Q(D)=\alpha+\beta D$, where α is the spring constant and β the dashpot constant, the equation describing the deformation becomes

$$(A/L)\beta(dl/dt) + (A/L)\alpha l = f_0 \cos \omega t$$

or, in terms of *stress* and *strain*,

$$\alpha \varepsilon + \beta \frac{d\varepsilon}{dt} = \sigma_0 \cos \omega t$$

where $\varepsilon = l/L$ is the *uniaxial strain* (see 2.4 and 5.10) and $\sigma_0 = f_0/A$ is the amplitude of the *stress* (see 5.10). The solution of the equation is

$$\varepsilon = \frac{\sigma_0}{(\alpha^2 + \beta^2 \omega^2)^{1/2}} \cos(\omega t - \delta) = \varepsilon_0 \cos(\omega t - \delta)$$

where δ is the *phase angle* (see 5.10) with $\tan \delta = \beta\omega/\alpha$.

3. From 5.14, the *absolute modulus* in *uniaxial deformation*

$$|E^*| = \sigma_0/\varepsilon_0 = (\alpha^2 + \beta^2 \omega^2)^{1/2}$$

where $\alpha = E'$, $\beta\omega = E''$ and $\tan \delta = E''/E'$ equal to the *loss tangent* (see 5.11).

4. If one end of the specimen is fixed in position and a mass m is attached to the moving end, the *linear-viscoelastic* interpretation of the resulting deformation gives

$$m \cdot P(D)(d^2l/dt^2) + (A/L)Q(D)l = P(D)f_0 \cos \omega t$$

where the symbols have the same meaning as in note 1.

5. For a *Voigt-Kelvin* solid (cf. note 2), the equation in note 4 describing the deformation becomes

$$m(d^2l/dt^2) + (A/L)\beta(dl/dt) + (A/L)\alpha l = f_0 \cos \omega t$$

with the solution



$$\varepsilon = \frac{\sigma_0 \cdot (A/(Lm))}{\left(\left(\frac{A_\infty}{Lm} - \omega^2 \right)^2 + \omega^2 \left(\frac{A\beta}{Lm} \right)^2 \right)^{1/2}} \cos(\omega t - \theta) = \varepsilon_0 \cos(\omega t - \theta)$$

where $\tan \theta = \frac{((A\beta)/(Lm)) \cdot \omega}{((A\alpha)/(Lm)) - \omega^2}$ and symbols have the same meaning as in notes 1 and 2.

6. The amplitude of the strain ε_0 is maximal when

$$\omega^2 = A\alpha/(Lm) = \omega_R^2$$

giving the value of the angular velocity (ω_R) of the *resonance frequency* of the specimen (see 6.12) in forced uniaxial extensional oscillation.

7. Notes 2 and 5 show that application of a sinusoidal uniaxial force to a *Voigt-Kelvin* solid of negligible mass, with or without added mass, results in an out-of-phase sinusoidal uniaxial extensional oscillation of the same frequency.

6.7 forced flexural oscillation

The flexural deformation (bending) of a material specimen of uniform cross-sectional area perpendicular to its long axis by the continuous application of a sinusoidal force of constant amplitude.

Notes

1. There are three modes of flexure in common use.

- (i) Application of the flexural force at one end of the specimen with the other end clamped.
- (ii) Application of the flexural force at the centre of the specimen with the two ends clamped (**three-point bending** or **flexure**).
- (iii) Application of the flexural force at the centre of the specimen with the two ends resting freely on supports (also known as **three-point bending** or **flexure**).

2. For specimens *without mass*, the linear-viscoelastic interpretation of the resulting deformations follows a differential equation of the same form as that for a *uniaxial extensional forced oscillation* (see 6.6, note 1), namely

$$(HJ/L^3)Q(D)y = P(D)f_0 \cos \omega t$$

where $P(D)$, $Q(D)$, f_0 , ω and t have the same meaning as for a *forced uniaxial extensional oscillation* (see 6.6, note 1) and H is a constant. The length of the specimen is $2L$. For mode of flexure (i) $H=3$, for (ii) $H=24$ and for (iii) $H=6$ (see note 1). J is the **second moment of area** of the specimen, defined by

$$J = \int_A q^2 dA$$

where dA is an element of the cross-sectional area (A) of the specimen and q is the distance of that element from the **neutral axis or plane** of the specimen, lying centrally in the specimen and defined by points which experience neither compression nor extension during the flexure. For a specimen of circular cross-section $J=\pi r^2/4$, where r is the radius, and for one of rectangular cross-section $J=4ab^3/3$, where $2a$ and $2b$ are the lateral dimensions with flexure along the b dimension. Finally, y is the *flexural deflection* (see 6.9) of the specimen at the point of application of the force, of either the end (mode of flexure (i)) or the middle (modes of flexure (ii) and (iii)).

3. For a *Voigt-Kelvin solid*, the equation describing the deformation becomes

$$(HJ/L^3)\alpha y + (HJ/L^3)\beta(dy/dt) = f_0 \cos \omega t$$

with solution

$$y = \frac{f_0 L^3}{HJ(\alpha^2 + \beta^2 \omega^2)^{1/2}} \cos(\omega t - \delta)$$

where δ is the *phase angle* with

$$\tan \delta = \beta\omega/\alpha$$

equal to the *loss tangent* (see 5.11).

4. Unlike the strain in *forced uniaxial extensional oscillations*, those in *forced flexural deformations* are not homogeneous. In the latter modes of deformation, the strains vary from point-to-point in the specimen. Hence, the equation defining the displacement y in terms of the amplitude of applied force (f_0) cannot be converted into one defining strain in terms of amplitude of stress.
5. If a mass m is attached to the specimen at the point of application of the force, the linear-viscoelastic interpretation of the resulting deformation gives

$$m \cdot P(D) (d^2y/dt^2) + (HJ/L^3)Q(D)y = P(D)f_0 \cos \omega t$$

(cf. 6.6, note 4).

6. For a *Voigt-Kelvin solid* (cf. note 3 and 6.6, note 5), the equation describing the deformation becomes

$$m(d^2y/dt^2) + (HJ/L^3)\beta(dy/dt) + (HJ/L^3)\alpha y = f_0 \cos \omega t$$

with the solution

$$y = \frac{f_0/m}{\left(\left(\frac{HJ\alpha}{L^3 m} - \omega^2 \right)^2 + \omega^2 \left(\frac{HJ\beta}{L^3 m} \right)^2 \right)^{1/2}} \cos(\omega t - \delta)$$

where $\tan \delta = \frac{(HJ\beta/(L^3 m))\omega}{\left(\frac{HJ\alpha}{L^3 m} - \omega^2 \right)}$

7. The *flexural deflection* y (see 6.9) is maximal when

$$\omega^2 = HJ\alpha/(L^3m) = \omega_R^2$$

giving the value of the **angular velocity** (ω_R) of the **resonance frequency** of the specimen (see 6.6, note 6) in forced flexural oscillations.

8. Notes 3 and 6 show that the application of the defined sinusoidal flexural forces (i), (ii) and (iii) (note 1) to a *Voigt-Kelvin* solid of negligible mass, with or without added mass at the points of application of the forces, results in out-of-plane sinusoidal flexural oscillations of the same frequency.

6.8 flexural force

Recommended symbol: f_0

The amplitude of the force applied to a material specimen to cause a forced flexural oscillation.

Unit: N

Notes

1. See 6.7 for the definition and interpretation of *forced flexural oscillation*.
2. A related quantity is the **flexural stress** which is somewhat arbitrarily defined as the amplitude of the stress in the convex, outer surface of a material specimen in forced flexural oscillation.

6.9 flexural deflection

Recommended symbol: y

The deflection of a specimen subject to a forced flexural oscillation at the point of application of the flexural force.

Unit: m

Notes

1. See 6.7 for the definition and interpretation of *forced flexural oscillations*
2. See 6.8 for the definition of *flexural force*.

6.10 flexural modulus

Recommended symbol: $|E^*|$

The modulus measured using forced flexural oscillations.

Unit: Pa

Notes

1. See 6.7 for the definition and interpretation of *forced flexural oscillations*.

2. For a *Voigt-Kelvin solid* (see 5.4) of negligible mass, the absolute modulus can be evaluated from the ratio of the *flexural force* (f_0) and the amplitude of the *flexural deflection* (y) with

$$f_0/Y_0 = (HJ/L^3)(\alpha^2 + \beta^2\omega^2)^{1/2}$$

where Y_0 is the amplitude of the *flexural deflection* (see 6.7, note 3, 6.8 and 6.9),

$$|E^*| = (\alpha^2 + \beta^2\omega^2)^{1/2}$$

(see 5.14 and 6.6, note 3) and the remaining symbols are as defined in 6.7, note 2.

3. The ratio of the loss to the storage flexural modulus (E''/E') is derived from the *loss tangent* ($\tan \delta$) of the *forced flexural oscillation* with

$$\tan \delta = \beta\omega/\alpha = E''/E'$$

(see 5.11 and 6.7, note 3).

4. The flexural modulus has been given the same symbol as the *absolute modulus* in uniaxial deformation (see 5.14) as it becomes equal to that quantity in the limit of zero amplitudes of applied force and deformation. Under real experimental conditions it is often used as an approximation to $|E^*|$.

6.11 resonance curve

Recommended symbol: $A(\nu)$

The curve of the frequency dependence of the amplitude of the displacement of a material specimen subject to forced oscillations in the region of a resonance frequency.

Unit: that of the amplitude A

Notes

1. See 6.6 and 6.7 for the description of modes of forced oscillation commonly used.
2. See 6.12 for the definition of *resonance frequency*.

6.12 resonance frequency

Recommended symbol: ν_R

The frequency at a maximum of a resonance curve

Unit: Hz

Notes

1. See 6.11 for the definition of a *resonance curve*.
2. Material specimens subject to a *forced oscillations* (see 6.6 and 6.7) in general have a spectrum of resonance frequencies.

3. In cases of a single *resonance frequency*, the *resonance frequency* is proportional to the square root of the *storage modulus* (M') of the material (see 5.12).
4. A material specimen which behaves as a *Voigt-Kelvin solid* under forced oscillations with a mass added at the point of application of the applied oscillatory force has a single resonance frequency.
5. Under a *forced uniaxial extensional oscillation* the resonance frequency

$$\nu_R = \omega_R / 2\pi = \left(\frac{A\alpha}{Lm} \right)^{1/2} / 2\pi = \left(\frac{AE'}{Lm} \right)^{1/2} / 2\pi$$

(see 6.6 for the origin of the equation and definitions of symbols). E' is the *storage modulus in uniaxial extension* (see 5.12).

6. Under a *forced flexural oscillation* the resonance frequency

$$\nu_R = \omega_R / 2\pi = \left(\frac{HJ\alpha}{L^3m} \right)^{1/2} / 2\pi = \left(\frac{HJE'}{L^3m} \right)^{1/2} / 2\pi$$

(see 6.7 for the origin of the equation and the definition of symbols).

6.13 width of the resonance curve

Recommended symbol: $\Delta\nu$

The magnitude of the difference in frequency between two points on a resonance curve on either side of ν_R which have amplitudes equal to $(1/\sqrt{2})A(\nu_R)$.

Unit: Hz

Notes

1. For a material specimen which behaves as a *Voigt-Kelvin solid* under *forced uniaxial extensional oscillation* with mass added at the point of application of the applied oscillatory force, $\Delta\nu$ is proportional to the *loss modulus* (E'') (see 5.13).

$$2\pi\Delta\nu = \frac{A}{Lm} \cdot \beta = \frac{A}{Lm} \cdot \frac{E''}{\omega_R}$$

In addition (6.6, note 6), the *storage modulus* (E') (see 5.12) may be evaluated from

$$\omega_R^2 = \frac{A}{Lm} \cdot \alpha = \frac{A}{Lm} \cdot E'$$

(see 6.6 for the definition of symbols).

2. For a material specimen which behaves as *Voigt-Kelvin solid* under forced flexural oscillations with added mass at the point of application of the applied oscillatory force, $\Delta\nu$ is proportional to the loss modulus (E'') (see 5.13)

$$2\pi\Delta\nu = \frac{HJ}{L^3m} \cdot \beta = \frac{HJ}{L^3m} \cdot \frac{E''}{\omega_R}$$

In addition, the *storage modulus* (E') (see 5.12) may be evaluated from

$$\omega_R^2 = \frac{HJ}{L^3m} \cdot \alpha = \frac{HJ}{L^3m} \cdot E'$$

(see 6.7 for the definition of symbols).

3. For the *Voigt-Kelvin* behaviours specified in notes 1 and 2, the ratio of $\Delta\nu$ and the resonance frequency (ν_R) is equal to the *loss tangent* ($\tan \delta$).

Under *forced uniaxial extensional oscillation*

$$\frac{\Delta\nu}{\nu_R} = \left(\frac{A}{Lm} \right) \beta \omega_R \cdot \frac{Lm}{A\alpha} = \frac{\beta}{\alpha} \omega_R = \frac{E''}{E'} = \tan \delta$$

Under *forced flexural oscillation*

$$\frac{\Delta\nu_R}{\nu_R} = \left(\frac{HJ}{L^3m} \right) \beta \omega_R \cdot \frac{L^3m}{HJ\alpha} = \frac{\beta}{\alpha} \omega_R = \frac{E''}{E'} = \tan \delta$$

(see 5.11 for the definition of $\tan \delta$).

7. REFERENCES

1. ISO 472, ISO TC-61, Dec. 1991 Draft, *Plastics Vocabulary*
2. C.L. Sieglaff, *Trans. Soc. Rheol.* 1976 **20** 311
3. D.W. Hadley, J.D. Weber, *Rheol. Acta* 1975 **14** 1098
4. D.W. Hadley, J.D. Weber, *Bull. Br. Soc. Rheol.* 1979 **22** 4
5. M. Reiner, G.W. Scott Blair, *Rheology*, Vol. 4, ed. F.R. Eirich, Academic Press, New York, 1967
6. J.M. Dealy, *J. Rheol.* 1984 **28** 181; 1995 **39** 253
7. ASTM E 6-88, 'Standard Definitions of Terms Relating to Methods of Mechanical Testing, Annual Book of ASTM Standards, Vol. 8.03, 1989, p. 672
8. ASTM D4092-83a, 'Standard Definitions and Descriptions of Terms Relating to Dynamical Mechanical Measurements on Plastics', Annual Book ASTM Standards, Vol. 8.03, 1989, p. 334
9. ASTM D 883-88, 'Standard Definitions of Terms Relating to Plastics, Annual Book of ASTM Standards, Vol. 8.01, 1989, p. 333.

10. G. Astarita and G. Marucci, 'Principles of Non-Newtonian Fluid Mechanics', McGraw-Hill Book Company (UK) Ltd., Maidenhead, 1974.
11. J.D. Ferry, 'Viscoelastic Properties of Polymers', John Wiley and Sons, New York, third edition, 1980
12. R.I. Tanner, 'Engineering Rheology', Clarendon Press, Oxford, 1985.
13. H.A. Barnes, J.F. Hutton and K. Walters, 'An Introduction to Rheology', Elsevier, Amsterdam, 1989
14. J.F. Nye, 'Physical Properties of Crystals', Oxford University Press, 1969
15. I.M. Ward and D.W. Hadley, 'An Introduction to the Mechanical Properties of Solid Polymers', John Wiley and Sons, Chichester, 1993

8. ALPHABETICAL INDEX OF TERMS

- absolute compliance (5.18)
- absolute modulus (5.14)
- angular velocity (of a forced oscillation) (5.10)
- angular velocity of resonance frequency (6.7)
- apparent viscosity (4.12)

- bulk compliance (4.6)
- bulk compression (2.9)
- bulk compressive compliance (4.6)
- bulk compressive modulus (4.5)
- bulk compressive strain (2.9)
- bulk modulus (4.5)

- Cauchy tensor (1.8, 1.9)
- coefficient of viscosity (4.12)
- complex compliance (5.19)
- complex modulus (5.15)
- complex rate of strain (5.22)
- complex strain (5.15, 5.19)
- complex stress (5.15, 5.19, 5.22)
- complex viscosity (5.22)
- compliance (4.4)
- compressive strain (2.4)
- compressive stress (3.3)
- constitutive equation for an elastic solid (4.1)
- constitutive equation for an incompressible viscoelastic liquid or solid (4.2)
- creep (5.9)
- creep compliance (5.9)
- creep function (5.9)

- damping curve (6.2)
- dashpot constant (5.3, 5.4)
- decay constant (6.3)

- decay frequency (6.4)
- deformation gradients in an elastic solid (1.3)
- deformation gradients in a viscoelastic liquid or solid (1.6)
- deformation gradient in the orthogonal deformation of an elastic solid (2.1)
- deformation gradient tensor for an elastic solid (1.4)
- deformation gradient tensor for a viscoelastic liquid or solid (1.7)
- deformation of an elastic solid (1.3)
- deformation of a viscoelastic liquid or a solid (1.5)
- deformation ratio (2.3)
- deformation ratio in the orthogonal deformation of an elastic solid (2.1)
- dynamic strain (5.1)
- dynamic stress (5.1)
- dynamic viscosity (5.20)

- elastic modulus (4.3)
- elongational strain rate (2.12)
- elongational viscosity (4.9)
- engineering strain (2.4)
- engineering stress (3.4)
- extensional strain rate (2.12)
- extensional viscosity (4.9)
- extension ratio (2.3)

- Finger tensor (1.8, 1.11)
- first normal-stress coefficient (4.13)
- first normal-stress difference (3.6)
- first normal-stress function (3.6)
- flexural deflection (6.9)
- flexural force (6.8)
- flexural modulus (6.10)
- flexural stress (6.8)
- forced flexural oscillation (6.7)
- forced oscillation (5.10)
- forced uniaxial extensional oscillation (6.6)
- free oscillation (6.1)

- general homogenous deformation or flow of a viscoelastic liquid or solid (2.10)
- general orthogonal homogeneous deformation of an elastic solid (2.1)
- Green tensor (1.8, 1.10)

- Hencky strain (2.5)
- homogeneous deformation of elastic solids (1.3)
- homogeneous deformation of viscoelastic liquids and solids (1.5)
- homogeneous orthogonal deformation or flow of an incompressible viscoelastic liquid or solid (2.11)
- homogeneous simple shear deformation or flow of an incompressible viscoelastic liquid or solid (2.13)

- infinite-shear viscosity (4.12)
- inhomogeneous deformation of elastic solids (1.3)
- isotropic compression (2.9)

- lateral contraction ratio (2.6)
- lateral strain (2.6)
- linear viscoelastic behaviour (5.2)

linear viscoelastic behaviour of a liquid (5.2)
linear viscoelastic behaviour of a solid (5.2)
logarithmic decrement (6.5)
loss angle of a forced oscillation (5.10)
loss compliance (5.17)
loss curve (5.11)
loss factor (5.11)
loss modulus (5.13)
loss tangent (5.11)

Maxwell element (5.3)
Maxwell model (5.3)
modulus (4.3)
modulus of elasticity (4.3)

neutral axis (in forced flexural oscillation) (6.7)
neutral plane (in forced flexural oscillation) (6.7)
Newtonian liquid (4.2)
nominal stress (3.4)
non-Newtonian liquid (4.2)
normal stresses (3.5)

oscillatory (simple) shear flow (2.13)
out-of-phase viscosity (5.21)

phase angle (of a forced oscillation) (5.10)
Piola tensor (1.8)
plane strain (1.8)
plane stress (1.2)
Poisson's ratio (2.6)
pure shear deformation or flow (3.1)
pure shear of an elastic solid (2.7)
pure shear stress (3.1)

rate-of-strain tensor (1.12)
relaxation function (5.7)
relaxation spectrum (5.6)
relaxation time (5.6)
resonance curve (6.11)
resonance frequency (6.12)
resonance frequency (in forced flexural oscillation) (6.7)
resonance frequency (in forced uniaxial extensional oscillation) (6.7)
retardation spectrum (5.8)
retardation time (5.8)
Rivlin-Ericksen tensors (1.14)

secant modulus (4.7)
second moment of area (in forced flexural oscillation) (6.7)
second normal-stress coefficient (4.14)
second normal-stress difference (3.7)
second normal-stress function (3.7)
shear (2.8, 2.13)
shear compliance (4.11)
shear modulus (4.10)
shear rate (2.13)
shear strain (2.8)

shear stress (3.5)
shear viscosity (4.12)
simple shear of an elastic solid (2.8)
small-strain tensor (1.10)
spring constant (5.3, 5.4)
standard linear viscoelastic solid (5.5)
steady (simple) shear flow (2.13)
steady uniaxial homogeneous elongational deformation or flow of an incompressible viscoelastic liquid or solid (2.12)
storage compliance (5.16)
storage modulus (5.12)
stored energy function (4.1)
strain amplitude (of a forced oscillation) (5.10)
strain tensor (1.8)
stress (1.2)
stress amplitude (of a forced oscillation) (5.10)
stress relaxation (5.7)
stress tensor (1.2)
stress tensor resulting from an orthogonal deformation or flow (3.1)
stress tensor resulting from a simple shear deformation or flow (3.5)
stress vector (1.1)

tangent modulus (4.7)
tensile compliance (4.8)
tensile modulus (4.7)
tensile strain (2.4)
tensile stress (3.2)
three-point bending (6.7)
three-point flexure (6.7)
torsion pendulum (6.2)
traction (1.1)
true stress (1.2)

uniaxial compliance (4.8)
uniaxial deformation of an elastic solid (2.2)
uniaxial deformation or flow of an incompressible viscoelastic liquid or solid (2.11)
uniaxial deformation ratio (2.3)
uniaxial orthogonal deformation or flow (3.1)
uniaxial strain (2.4)

viscoelasticity (5.1)
viscosity (4.12)
Voigt-Kelvin element (5.4)
Voigt-Kelvin model (5.4)
Voigt element (5.4)
Voigt model (5.4)
volume compression (2.9)
vorticity tensor (1.13)

width of the resonance curve (6.13)

Young's modulus (4.7)

zero-shear viscosity (4.12)

9. GLOSSARY OF SYMBOLS

$A(\nu)$	resonance curve (6.11)
A_n	Rivlin-Ericksen tensors (1.14)
B	compliance in bulk compressive deformation (4.4)/ bulk compliance/bulk compressive compliance (4.6)
B	Green tensor (1.8, 1.10)
B^{-1}	Piola tensor (1.8)
C	compliance (general symbol) (4.4)
C'	storage compliance (general symbol) (5.16)
C''	loss compliance (general symbol) (5.17)
C^*	complex compliance (general symbol) (5.19)
$ C^* $	absolute compliance (general symbol) (5.18)
C	Cauchy tensor (1.8, 1.9)
C^{-1}	Finger tensor (1.8, 1.11)
D	compliance in uniaxial deformation (4.4)/ uniaxial compliance/tensile compliance (4.8)
D'	storage compliance in uniaxial deformation (5.16)
D''	loss compliance in uniaxial deformation (5.17)
D^*	complex compliance in uniaxial deformation (5.19)
$ D^* $	absolute compliance in uniaxial deformation (5.18)
D	rate-of-strain tensor (1.12)
E	modulus in uniaxial deformation (4.3)/Young's modulus/tensile modulus/secant modulus/tangent modulus (4.7)
E'	storage modulus in uniaxial deformation (5.12)
E''	loss modulus in uniaxial deformation (5.13)
E^*	complex modulus in uniaxial deformation (5.15)
$ E^* $	absolute modulus in uniaxial deformation (5.14)
$ E^* $	flexural modulus (6.10)
F	deformation gradient tensor for an elastic solid (1.4) and for a viscoelastic liquid or solid (1.7)
f_0	flexural force (6.8)
G	modulus in shear deformation (4.3)/shear modulus (4.10)
G'	storage modulus in simple shear deformation (5.12)
G''	loss modulus in simple shear deformation (5.13)
G^*	complex modulus in simple shear deformation (5.15)
$ G^* $	absolute modulus in simple shear deformation (5.14)
J	compliance in shear deformation (4.7)/shear compliance (4.11)/ creep compliance (5.9)
J	second moment of area (in a forced flexural oscillation)(6.7)
J'	storage compliance in simple shear deformation (5.16)
J''	loss compliance in simple shear deformation (5.17)
J^*	complex compliance in simple shear deformation (5.19)
$ J^* $	absolute compliance in simple shear deformation (5.18)

K	modulus in bulk compressive deformation (4.3)/bulk modulus/ bulk compressive modulus (4.5)
M	modulus (general symbol) (4.3)
M'	storage modulus (general symbol) (5.12)
M''	loss modulus (general symbol) (5.13)
M^*	complex modulus (general symbol) (5.15)
$ M^* $	absolute modulus (general symbol) (5.14)
N_1	first normal-stress difference/first normal-stress function (3.6)
N_2	second normal-stress difference/second normal-stress function (3.7)
t	traction (1.1)
$\tan \delta$	loss factor/loss tangent (5.11)
W	stored energy function (4.1)
\mathbf{W}	vorticity tensor (1.13)
y	flexural deflection (6.9)
β	decay constant (of a damping curve) (6.2, 6.3)
$\Delta\nu$	width of the resonance curve (6.13)
γ	shear/shear strain (2.8)
$\dot{\gamma}$	shear rate (2.13)
γ_0	strain amplitude (of a forced oscillation)(5.10)
$\dot{\gamma}_E$	elongational strain rate/extension strain rate (2.12)
γ^*	complex strain (of a forced oscillation) (5.15, 5.19)
$\dot{\gamma}^*$	complex rate of strain (of a forced oscillation) (5.22)
δ	phase angle (of a forced oscillation)/loss angle of a forced oscillation (5.10)
ϵ	uniaxial strain/engineering strain/(uniaxial) tensile strain/(uniaxial) compressive strain (2.4)
ϵ	small-strain tensor (1.10)
ϵ_H	Hencky strain (2.5)
ϵ_{lat}	lateral strain (2.6)
η	shear viscosity/coefficient of viscosity/viscosity (4.12)
η'	dynamic viscosity (5.20)
η''	out-of-phase viscosity (5.21)
η_{app}	apparent viscosity (4.12)
η_E	extensional viscosity/elongational viscosity (4.9)
η_0	zero shear viscosity (4.12)
η^*	complex viscosity (5.22)
η_∞	infinite-shear viscosity (4.12)

λ	uniaxial deformation ratio/deformation ratio/ extension ratio/compression ratio (2.3)
λ_i	deformation gradients/deformation ratios; $i = 1,2,3$ (2.1)
Λ	logarithmic decrement (of a decay curve) (6.5)
μ	Poisson's ratio (2.6)
ν	decay frequency (of a damping curve) (6.4)
ν_R	resonance frequency (6.12)
σ	tensile stress (3.2)
σ	compressive stress (3.3)
σ	engineering stress (3.4)
σ_{ii}	normal stresses; $i = 1,2,3$ (3.5)
σ_0	stress amplitude (of a forced oscillation) (5.10)
σ_{12}	shear stress (3.5)
σ	stress/stress tensor (1.2, 3.1, 3.5)
σ^*	complex stress (in a forced oscillation) (5.15, 5.19, 5.22)
τ	relaxation time (5.6)/retardation time (5.8)
χ	bulk compression/volume compression/isotropic compression/ bulk compressive strain (2.9)
ψ_1	first normal-stress coefficient (4.13)
ψ_2	second normal-stress coefficient (4.14)
$\psi(t)$	creep function (5.9)
$\bar{\psi}(t)$	relaxation function (5.7)
ω	angular velocity (of a forced oscillation) (5.10)
ω	angular velocity (of a decay frequency) (6.2)
ω_R	angular velocity of the resonance frequency (of a forced flexural oscillation) (6.7)



Spatial and temporal variation in distribution of *Gelidium canariensis* (Rhodophyta) from natural populations of the Canary Islands

A. Lindgren¹, N. Bouza², P. Åberg¹ & P. A. Sosa^{2*}

¹ Department of Marine Botany, Göteborg University, Box 461, S-405 30, S-413 19 Göteborg, Sweden

² Department of Biology, University of Las Palmas, Campus Universitario Tafira, 35017 Las Palmas de Gran Canaria, Canary Islands, Spain

(* Author for correspondence: E-mail, pedro.sosa@biologia.ulpgc.es)

Received 12 December 1997; revised 5 June 1998; accepted 7 June 1998

Key words: Canary Islands, *Gelidium canariensis*, hierarchical sampling, spatial variation, temporal variation

Abstract

This study was designed to investigate spatial and temporal variation in *Gelidium canariensis* populations at two shores in northern Gran Canaria during two years. Spatial scales ranged from some hundred meters (distance between shores), 10 to 30 m (distance between plots) to less than 3 m (distance between quadrats). *Gelidium* individuals were defined as distinct *Gelidium* clumps. The results show a significant difference in size of clumps between shores, but not on the smaller spatial scales. No significant temporal variation was found. There was no significant temporal or spatial variation in standing crop or density (counts made in quadrats where *Gelidium* was present, rather than counts for the total shore). Sporophytic and gametophytic clumps were also distinguished by identifying reproductive structures in the field. The total proportion of sporophytes was larger than the proportion of gametophytes, but at a smaller scale there could be a shift in dominance. The survival rate of clumps was similar between shores with a mean survival rate of 85%, but there was a significant difference in recruitment between shores. The results indicate a stable population structure.

Introduction

Gelidium canariensis (Grunow) Seoane Camba is an endemic species of the Canary Islands which grows on wave exposed rocky shores in the lower intertidal. At the lower end of its tidal range it may form smaller beds, but higher on the shore it forms clumps mixed with *G. arbuscula* and other algae. The tidal range is about 2 m, the part of the *G. canariensis* population growing higher on the shore being exposed to the air twice a day for about 1 h; wave spray is, however, frequent. Like other *Gelidium* species, *G. canariensis* is a perennial with a modular type of construction where erect fronds develop from a basal system of prostrate axes that are attached to the substratum by rhizoids. It exhibits the triphasic/polysiphonian life cycle with isomorphic generations, but can also expand vegetatively by growth of new fronds from the prostrate

axes. Also like other *Gelidium* species, sporophytes of *G. canariensis* have been reported as more abundant than female gametophytes based on the presence of reproductive structures (Santelices, 1988; Betancort-Villalba & Gonzalez-Henriquez, 1991; Sosa & Garcia-Reina, 1993). The reproductive structure of male gametophytes is impossible to distinguish in the field.

The aim of this study was to investigate patterns of spatial and temporal variation in populations of *G. canariensis*. The general hypothesis was that variation in population characters of *G. canariensis* should differ at different spatial scales and/or in different years. To distinguish genets (genetic individuals, Kays & Harper, 1974) is often a problem when studying the ecology of algae (e.g. Åberg, 1989; Lazo et al., 1989; Santos, 1994; Lindgren & Åberg, 1996). For plants each genet is usually composed of modules which for *Gelidium* are individual fronds. There is thus two lev-

els of population structure in plant communities, the structure of genets and the structure of modules within genets (Harper, 1977). Whether a specific level or both should be studied depends on the hypotheses tested in the experiment. In the present study, which is part of a larger study of the demography and population genetics of algal populations, we ask questions about genets and to study the frond dynamics alone is thus not relevant here. For that reason it was designed to study genets which have been defined as distinct individual clumps. Whether these clumps are genets or not will be tested in future studies. Two indications that clumps could be genets are that we never found cystocarps and tetrasporangial sori on fronds from the same clump and that no difference in isozyme banding patterns has been found among fronds from the same clump (P.A.Sosa, unpublished results). It is known that sporeling coalescence may occur and that separate genets of the same stage may grow together, but our methods so far have been unable to distinguish this. This study is based on an analysis of the structure of clumps which in many cases probably are genets; if not, they can be regarded as distinct patches of fronds.

Materials and methods

Study area

This study was performed during July 1996 and 1997 at two rocky shores separated by a sandy beach about 450 m long, at Bocabarranco, northern Gran Canaria, Canary Islands. The investigation was performed in the upper part of the *G. canariensis* belt.

Experimental design

At the two shores, a total of 168 clumps were distinguished, scraped off and put in separate plastic bags and brought back to the laboratory, where maximum circumference (C) and maximum length (L) were measured. Maximum circumference was achieved by laying all fronds from one clump parallel and the maximum circumference will then be at the thickest part of the bundle (cf Åberg, 1990). Dry weight (DW) was measured after drying the clumps to constant weight at 60 °C. To estimate biomass from clump size a regression between LC^2 and DW was done. If there is a strong positive correlation, measuring L and C in the field can be used to estimate the size of clumps (Åberg, 1990).

The spatial variation in clump size and abundance of *G. canariensis* was investigated on three spatial scales using a hierarchical sampling design. The scales were 2 shores (about 450 m apart), 2 plots within each shore (20–50 m apart) and 5 quadrats within each plot (< 3 m apart). The quadrats (0.25 × 0.25 m) were placed randomly where *G. canariensis* was present to obtain a large number of clumps rather than an examination of its presence over the whole shore. The study was repeated with a set of new quadrats after one year. All clumps within a quadrat were characterized by maximum length and circumference and, if at least one frond within a clump was reproductive, the life cycle stage (i.e. sporophyte, female gametophyte) was noted. Since quadrats were only placed where *G. canariensis* was present, the values for standing crop dry weight and density are a measure of biomass and abundance, respectively, in *G. canariensis* stands, not for a whole shore. To illustrate the size distribution, the clumps were divided into size classes. Since the growth of the genets can be treated as an exponential process (Harper, 1977), the width of the size classes was chosen to be equally large on a logarithmic scale. The survival rate was investigated by monitoring mapped clumps through time and recruitment by noting new clumps within a quadrat.

Statistical analysis

Spatial and temporal variability were analyzed using analysis of variance (ANOVA). The factor Year was chosen and consequently considered as fixed. The factors Shore, Plot and Quadrats were chosen randomly. In the analysis of the life cycle stages, Stages was also considered as fixed factor. The assumption of homogeneity of variances was tested with Cochran's test (Winer et al., 1991). When variances were heterogeneous, the data were \log_e - or $\log_e(x + 1)$ transformed. Post hoc pooling of mean values for quadrats was applied as described in Underwood (1997) and in such cases only the ANOVA table after pooling is given.

Results

A significant relationship was found between DW and LC^2 , ($p < 0.01$), (Figure 1) and LC^2 explained 95% of the variation in dry weight. The predictive equation was $DW = 0.0096LC^2 + 0.45$ (Figure 1).

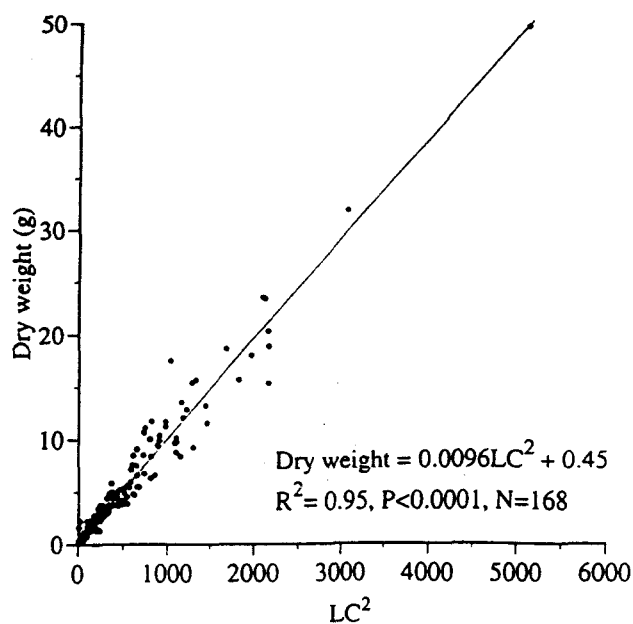


Figure 1. Regression of the relationship between dry weight and LC^2 .

Table 1. ANOVA of clumps dry weight after post hoc pooling the factors Plot (Shore), Year * Plot (Shore) and Year * Quadrat (Plot, Shore). Data \log_e -transformed to meet assumptions of homogeneity of variances

Source	df	MS	F	P
Year	1	4.20	2.29	> 0.35
Shore	1	20.01	18.93	< 0.001
Year * Shore	1	1.83	2.62	> 0.10
Quadrat (Plot, Shore)	28	1.06	1.52	> 0.05
Residual	88	0.70		
Cochran's C-test	40,2	0.10		> 0.05

Dry weight per clump

A significant difference in mean dry weight per clump was found between shores (Table 1), mean clump dry weight being 5.5 g at shore 1 and 2.4 g at shore 2. There was no significant temporal or spatial variation at any of the other scales. Dividing the clumps into size classes showed that a large proportion of the population belonged to size classes 1 and 2 (Figure 2). Within each shore the size distribution is similar in 1996 and 1997.

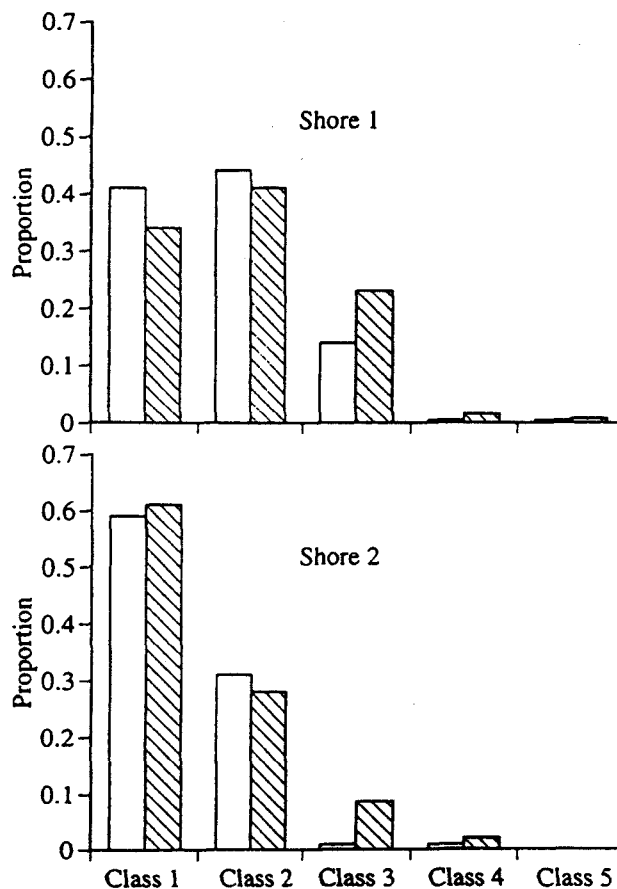


Figure 2. Size frequency distribution of clumps at the two shores in 1996 (white columns) and 1997 (striped columns). Class 1, < 1.16 g; Class 2, < 2.32 g; Class 3, < 3.49 g; Class 4, < 4.66 g; Class 5, > 4.66 g.

Table 2. ANOVA of standing crop dry weight within *G. canariensis* stands. Data \log_e -transformed to meet assumptions of homogeneity of variances

Source	df	MS	F	P
Year	1	1.18	5.76	> 0.25
Shore	1	0.15	1.41	> 0.35
Year * Shore	1	0.20	0.36	> 0.60
Plot (Shore)	2	0.11	0.48	> 0.60
Year * Plot (Shore)	2	0.57	2.63	> 0.05
Residual	32	0.22		
Cochran's C-test	8,4	0.29		> 0.05

Table 3. ANOVA of density (clumps m^{-2}) within *G. canariensis* stands

Source	df	MS	F	P
Year	1	2.5	0.21	> 0.70
Shore	1	220.9	4.42	> 0.15
Year * Shore	1	12.1	2.33	> 0.25
Plot (Shore)	2	50.0	1.60	> 0.20
Year * (Plot, Shore)	2	5.2	0.17	> 0.80
Residual	32	31.2		
Cochran's C-test	8.4	0.27		> 0.05

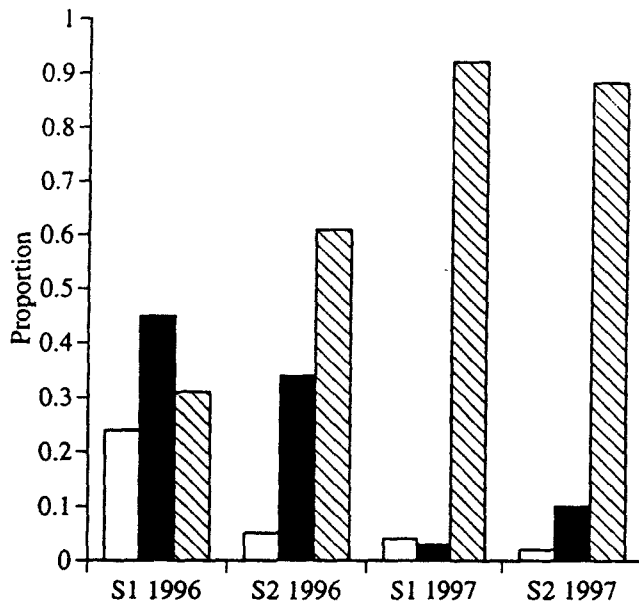


Figure 3. Proportion of gametophytes (white columns), sporophytes (black columns) and vegetative clumps (striped columns) in 1996 and 1997. S = shore.

Standing crop and density

For standing crop dry weight no significant differences were found at any level (Table 2). Mean standing crop at shore 1 was 960 g m^{-2} and 912 g m^{-2} at shore 2. There were no significant differences in densities found at any level (Table 3). The mean number of clumps at shore 1 was $136 \text{ clumps m}^{-2}$ and at shore 2 was $211 \text{ clumps m}^{-2}$.

Life cycle stages

The proportion of vegetative clumps was much higher in 1997 (Figure 3). This is probably due to the difficult sampling circumstances in 1997, which hindered careful examination of the plants. For that reason we

Table 4. ANOVA of the proportion of female gametophytes and sporophytes in 1996. Data $\log_e(x+1)$ -transformed to meet assumptions of homogeneity of variances

Source	df	MS	F	P
Stage	1	0.23	2.7	> 0.30
Shore	1	0.10	0.69	> 0.45
Stage * Shore	1	0.08	0.35	> 0.60
Plot (Shore)	2	0.14	4.35	< 0.05
Stage * Plot (Shore)	2	0.24	7.34	< 0.005
Residual	24	0.03		
Cochran's C-test	8.3	0.42		> 0.05

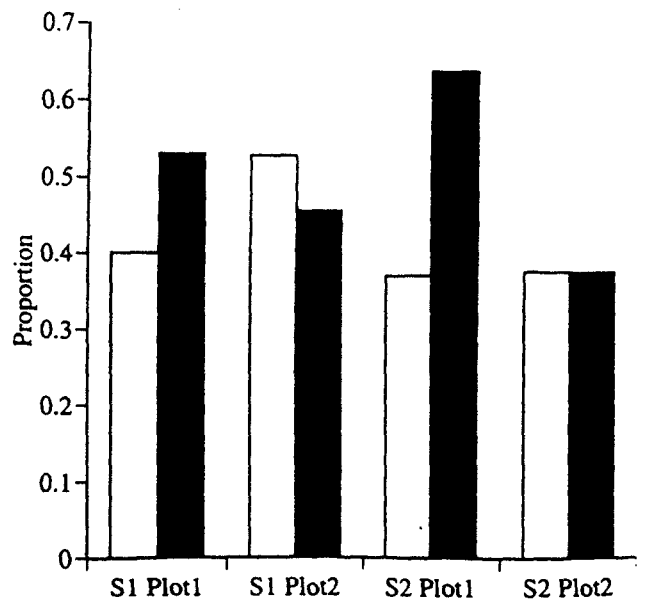


Figure 4. Proportion of gametophytes (white columns) and sporophytes (black columns) in 1996 at plots within shores. S = shore.

only tested the spatial variation in the proportion of life cycle stages for the year 1996. The total proportion of fertile clumps in 1996 was 0.69 at shore 1 and 0.39 at shore 2 (Figure 3). The significant interaction between Stage and Plot within Shores in Table 4 shows that on a small scale there can be either a dominance of sporophytes or female gametophytes (Table 4, Figure 4). The overall mean for both shores was 37% sporophytes and 15% female gametophytes but this difference was not statistically significant (Table 4).

Survival and recruitment

There was no significant difference in the survival rate of clumps between the shores (Table 5), and the mean

Table 5. ANOVA of survival rate of *G. canariensis* clumps

Source	df	MS	F	P
Shore	1	0.10	2.76	> 0.20
Plot (Shore)	2	0.04	1.06	> 0.35
Residual	20	0.04		
Cochran's C-test	4.5	0.47		> 0.05

value was 85%. There was a significant difference in recruitment between the shores (Table 6) and the mean number of new clumps was 1 at shore 1 and 3 at shore 2.

Discussion

The strong positive correlation between DW and LC² shows that this non-destructive method to estimate the size of clumps in the field works well for *G. canariensis*. The results indicate that *G. canariensis* has a stable population structure. There were no significant differences between the years in any of the variables investigated. There was an initial difference between the shores in size structure, the clumps being much larger at shore 1, and this was maintained in the following year. The relatively high survival rate of the clumps also supports this conclusion. However, we do not know anything about the population dynamics within a year, such as the percentage of recruits which fail to survive, frond loss etc. Still, the overall result is that the general population structure remains the same from one year to another. The difference in population structure between the shores could be due to differences in the exposure to wave action. Limpets are harvested at both shores, but to what extent and how often is unknown. Differences in harvesting could give rise to differences in grazing pressure, which in turn could affect the growth of *G. canariensis*. Since we defined individuals as clumps, it is difficult to compare the individual dry mass and density values with other species of *Gelidium*, since most studies have been performed on fronds. The standing crop for *G. canariensis* was about 1000 g m² in this study. Standing stock values normally found in commercial beds are reported to range from a some hundred grams to 1.5 kg m² (Santelices, 1988). Taking these values into

consideration, *G. canariensis* seems to have quite a high standing crop.

Considering the number of tetrasporangial and carposporangial plants there was a low recruitment of new clumps, mean number of recruits being 1 and 3 for the two shores. However, we have so far no data on temporal variation within or between years. That is, new clumps may have appeared and disappeared without our knowledge within the year we studied and the recruitment may be higher another year. Factors affecting the recruitment and survival of juvenile stages could be the same as those suggested for affecting the growth. Both wave action and grazing have been reported as mortality factors for spores and juvenile stages of *Gelidium* species (Santelices, 1988). The large number of spores produced in other *Gelidium* species as well as other perennial red algae seems to be excessive with respect to the amount necessary for maintenance of the population (Bhattacharya, 1985). However, released spores may have a very high mortality. Estimates of the probability of transition from tetraspores to recruits of *Gelidium sesquipedale* are as low as 4.7×10^{-5} (Santos & Duarte, 1996). Better understanding of the recruitment of *G. canariensis* requires studies using both larger and smaller temporal scales.

Investigation of the life cycle stages indicates that a large part of the population consisted of vegetative clumps (as have been reported for many red algae e.g. May, 1986; Santelices, 1990; De Wreede & Green, 1990). In 1996 the proportion fertile clumps varied from 0.69 to 0.39 between shores. In 1997 the proportions was about 0.10. The lower proportion in 1997 is probably due to the much more difficult sampling conditions, with high waves and the lowest tide late in the evening and hence decreasing light. In 1996, at the larger spatial scales (500 m) there was a dominance of sporophytes, but at smaller scales (20–50 m) either gametophytes or sporophytes could be dominant (Figure 4). The proportion of gametophytes was in fact even higher, since male gametophytes were not included. These results indicate the importance of including small scales in studies of life cycle ratios of *G. canariensis*. Factors explaining the pattern may also be ones varying on a small scale; it is known that small-scale variation in light or temperature can be important factors influencing fertility (Santelices, 1988). The relative importance of sexual reproduction could also be different depending on the scale. The opposite situation was found for the other variables, where there was little variation at the smaller spatial scales, which

is usually where the largest variation occurs in marine environments (Lindegardh et al., 1995; Åberg & Pavia, 1997). Additional demographic studies should reveal more about the structure and dynamics of *G. canariensis* populations.

Acknowledgements

We thank Per Nilsson at Tjärnö Marine Biological Laboratory for statistical advice. This study is part of the BIOGAP (Biodiversity and Genetics of Algal Populations) project MAS 3-CT 95-0019. European Union, Brussels.

References

- Åberg P (1989) Distinguishing between genetic individuals in *Ascophyllum nodosum* populations on the Swedish west coast. *Br. phycol. J.* 24: 183–190.
- Åberg P (1990) Measuring size and choosing category size for a transition matrix study of the seaweed *Ascophyllum nodosum*. *Mar. Ecol. Progr. Ser.* 63: 281–287.
- Åberg P, Pavia H (1997) Temporal and multiple scale spatial variation in juvenile and adult abundance of the brown alga *Ascophyllum nodosum*. *Mar. Ecol. Progr. Ser.* 158: 111–119.
- Betancort-Villalba MJ, Gonzalez-Henriquez MN (1991) Estudio preliminar sobre la biología de las poblaciones de *Gelidium canariensis* (Grunow) Seoane en Gran Canaria. *Acta Botanica Malacitana* 16: 51–58.
- Bhattacharya D (1985) The demography of fronds of *Chondrus crispus* Stackhouse. *J. exp. mar. Biol. Ecol.* 91: 217–231.
- De Wreede RE, Green LG (1990) Patterns of gametophyte dominance of *Iridaea splendens* (Rhodophyta) in Vancouver Harbour, Vancouver, British Columbia, Canada. *J. appl. Phycol.* 2: 27–34.
- Harper JL (1977) *Population Biology of Plants*. Academic Press, London: 892 pp.
- Kays S, Harper JL (1974) The regulation of plant and tiller density in a grass sward. *J. Ecol.* 62: 97–105.
- Kays S, Harper JL (1974) The regulation of plant and tiller density in grass sward. *J. Ecol.* 62: 97–105.
- Lazo ML, Greenwell M, McLachlan J (1989) Population structure of *Chondrus crispus* Stackhouse (Gigartinales, Rhodophyta) along the coast of Prince Edward Island, Canada: distribution of gametophytic and sporophytic fronds. *J. exp. mar. Biol. Ecol.* 12: 45–58.
- Lindegardh M, André C, Jonsson PR (1995) Analysis of the spatial variability in abundance and age structure of two infaunal bivalves, *Cerastoderma edule* and *C. lamarcki*, using hierarchical sampling programs. *Mar. Ecol. Progr. Ser.* 116: 85–97.
- Lindgren A, Åberg P (1996) Proportion of life cycle stages of *Chondrus crispus* and its population structure: a comparison between a marine and an estuarine environment. *Bot. mar.* 39: 263–268.
- May G (1986) Life history variations in a predominantly gametophytic population of *Iridaea cordata* (Gigartinales, Rhodophyta). *J. Phycol.* 22: 448–455.
- Santelices B (1988) Synopsis of biological data on the seaweed genera *Gelidium* and *Pterocladia* (Rhodophyta) FAO Fisheries Synopsis 145.
- Santelices B (1990) Patterns of reproduction, dispersal and recruitment in seaweeds. *Oceanogr. Mar. Biol. Annu. Rev.* 28: 177–276.
- Santos R (1994) Frond dynamics of the commercial seaweed *Gelidium sesquipedale*: effects of size and of frond history. *Mar. Ecol. Progr. Ser.* 107: 295–305.
- Santos R, Duarte P (1996) Fecundity, spore recruitment and size in *Gelidium sesquipedale* (Gelidiales, Rhodophyta). *Hydrobiologia* 326/327: 223–228.
- Sosa PA, Garcia-Reina G (1993) Genetic variability of *Gelidium canariensis* (Rhodophyta) determined by isozyme electrophoresis. *J. Phycol.* 29: 118–124.
- Underwood AJ (1997) *Experiments in Ecology: Their Logical Design and Interpretation Using Analysis of Variance*. Cambridge University Press, Cambridge, 504 pp.
- Winer BJ, Brown DR, Michels KM (1991) *Statistical Principles in Experimental Design*. McGraw-Hill, New York, 1057 pp.

Depletion of serum alternative complement pathway activity in gilthead seabream caused by α -tocopherol and n-3 HUFA dietary deficiencies

D. Montero¹, L. Tort², M.S. Izquierdo³, L. Robaina³ and J.M. Vergara³

¹Instituto Canario de ciencias Marinas, Gobierno de Canarias, P.O. Box 56, 35200, Telde, Las Palmas, Canary Islands, Spain; ²Departamento de Biología Celular y Fisiología, Facultad de Ciencias, Universidad Autónoma de Barcelona, 08193 Cerdanyola, Barcelona, Spain; ³Departamento de Biología, Universidad de Las Palmas de Gran Canaria, Campus Universitario de Tafira, 35017, Las Palmas de Gran Canaria, Canary Islands, Spain

Accepted: July 16, 1997

Key words: alternative complement, stress, *Sparus aurata*, cortisol, vitamin E, n-3 HUFA

Abstract

Studies on the alternative complement pathway (ACP) activity in fish have suggested the particular relevance of this pathway as a non-specific immune mechanism being its activation directly related with the availability of certain nutrients. In the present study ACP activity in gilthead seabream fed different dietary levels of α -tocopherol and n-3 HUFA deficiencies was studied under different stress conditions (overcrowding and repetitive chasing).

A reduction in ACP activity was found when diets with deficiencies in α -tocopherol and n-3 HUFA were assayed at any of the experimental conditions assayed. Levels of plasma cortisol were similar to those of fish after crowding stress subjected to dietary deficiencies at low stocking density, suggesting that dietary deficiencies produced a chronic elevation of cortisol. When fish were subjected to repetitive chasing, plasma cortisol from fish fed control diet showed a progressive increase whereas plasma cortisol levels from both dietary deficient groups showed a transitory peak 4 days after the beginning of the repetitive chasing. However, ACP activity levels of fish fed deficient diets remained lower than the control group and constant during chasing period. These results suggest that both α -tocopherol and n-3 HUFA nutritional deficiencies rather than stress are an important determinant of fish complement activity.

Introduction

As one of the main immune responses, the complement system has been described for different fresh water fish species, including salmonids, tilapia (*Tilapia nilotica*), goldfish (*Carassius auratus*) or carp (*Cyprinus carpio*) (Sakai 1981). The classical pathway of complement activation, characterized by the triggering of first component by formation of antigen-antibody compounds, is well described in fish (Sakai 1992), but little is known on the alternative pathway (ACP), characterized by the absence of antigen-antibody compounds and regarded as a non-specific response.

There are several studies on ACP in freshwater fish, such as carp, rainbow trout (*Oncorhynchus mykiss*), tilapia, ayu (*Plecoglossus altivelis*) (Yano et al. 1988a), and catfish (*Ictalurus punctatus*) (Jenkins et al. 1991). However, only few studies have been reported on ACP in seawater fish, like red seabream (*Pagrus major*) (Yano et al. 1987), yellowtail (*Seriola quinqueradiata*), flounder (*Paralichthys olivaceus*) (Yano et al. 1988a) or gilthead seabream (*Sparus aurata*) (Sunyer and Tort 1994). In general, values of ACP activity obtained for fish are considerably higher than those for mammals, suggesting that this activation pathway of the complement system is of

particular relevance for fish as non-specific immune mechanism (Yano et al. 1988a; Sunyer and Tort 1995).

The activity of the complement system in fish is directly related to dietary inclusion level of certain nutrients, such as vitamin E (Blazer and Wolke 1984; Hardie et al. 1990; Obach et al. 1993), choline chloride and calcium pantothenate (Yano et al. 1988b), vitamin A (Thompson et al. 1994) or vitamin C (Li and Lovell 1985; Hardie et al. 1991; Verlhac et al. 1993).

Preliminary results obtained in our laboratory on gilthead seabream showed that fish fed diets without supplementation of α -tocopherol showed lower ACP activity when compared with fish fed a diet supplemented with 150 mg of α -tocopherol per kg of diet (Montero et al. 1996). Similarly, the reduction in the ACP activity was also correlated with dietary deficiencies in n-3 highly unsaturated fatty acid (HUFA).

On the other hand, aquaculture conditions such as overcrowding or frequent handling has been reported to induce a stress response characterized by the release of the stress hormones (catecholamines and cortisol) with a subsequent depletion of the immune system (Pickering and Pottinger 1989; Maule et al. 1989). But at present, only few studies are known about the effect of stress on complement system in fish (Sunyer et al. 1995).

The aim of this work was to study the influence of selected diet components on the alternative complement activity in gilthead seabream. Two experiments were carried out in order to confirm preliminary results and to assess the effect of common aquaculture practices (overcrowding and handling) associated to stress responses in fish, on ACP activity.

Materials and methods

The experiments presented in this study were carried out at the Instituto Canario de Ciencias Marinas of the Autonomous Government of Canary Islands, with gilthead seabream (*Sparus aurata*) juveniles fed the following experimental diets.

Diets

The composition of the experimental diets is shown in Table 1. Different pelleted diets were prepared with the same proximal composition and supplemented respectively with 150 mg α -tocopherol/kg diet (Control diet; C) and 0 mg α -tocopherol per kg diet (NE). A third diet contained 150 mg α -tocopherol/kg diet but it was deficient on n-3 HUFA (NFA) (Ibeas et al. 1994) (Table 2).

Experimental procedures

Experiment I. One thousand and two hundred and sixty gilthead seabream, 22 g mean weight from a local farm (ADSA, San Bartolome de Tirajana, Canary Islands, Spain), were distributed among 18 circular fibre tanks, in order to evaluate the combined effect of both overcrowding and nutritional deficiencies. Each tank contained 250 l open seawater circulation, and were provided with natural light cycle (12h/12h). Nine hundred and ninety fish were randomly stocked in 9 of these tanks, triplicate for each experimental diet, at higher stocking densities (12 and 34 kg per m³ of initial and final density –treatment 1–), and two hundred and seventy fish were randomly distributed in other 9 tanks, triplicate for the three experimental diets, at lower stocking densities (2.64 and 10.04 kg per m³ –treatment 2–). Thus, each experimental diet was evaluated both at high and low stocking density conditions (Tables 3 and 4).

Fish were fed twice daily at a feeding rate of 2.5% fish body weight per day, 6 days a week for 15 weeks. Body weight was measured at the beginning and at the end of the experiment. At the end of the experiment, blood samples were taken from fish for cell counting, haematocrit determination and plasma and serum collection.

Experiment II. At the end of the experiment I all the fish of each tank of treatment 2 were chased with a hand-held net for 5 min every day at the same time for the 14 days in order to evaluate the combined effect of both netting and nutritional deficiencies. Fish were sampled at 2, 4, 8, 10 and 14 days for plasma and serum collection. The

Table 1. Composition of the experimental diets

Ingredients (% dry weight)	Diet		
	C	NE	NFA
Sardine meal	67.91	67.91	19.53
Oil extracted sardine meal	–	–	43.36
Sardine oil	0.96	0.96	–
Beef tallow	3.96	3.96	9.98
Starch	12	12	12
Dextrin	4	4	4
α -Cellulose	6.5	6.5	6.5
CMC ¹	0.5	0.5	0.5
Vitamin mix ²	2	2	2
Mineral mix ³	1.3	1.3	1.3
Choline chloride	0.9	0.9	0.9
α -tocopherol (mg/kg diet)	150	0	150

¹Carboximethylcellulose; ²(mg per kg diet): Vit A: 25; Vit D₃: 5; Vit K: 20; Vit B₁₂: 0.5; Vit H: 1; Folic acid: 10; Vit B₆: 40; Vit B₁: 40; Vit B₂: 50; Pantothenic acid: 117; Nicotinic acid: 200; Myo-inositol: 2000; Ascorbic acid: 5,000; Ethoxyquin: 100; ³(g kg⁻¹ diet): (H₂PO₄)Ca: 1.605; CaCO₃: 4.0; FeSO₄·7H₂O: 1.5; MgSO₄·7H₂O: 1.605; K₂HPO₄: 2.8; Na₂PO₄·AH₂O: 1; Al(SO₄)₃·6H₂O: 0.02; ZnSO₄·7H₂O: 0.24; CuSO₄·5H₂O: 0.12; KI: 0.02; CoSO₄·7H₂O: 0.08; MnSO₄·AH₂O: 0.08.

Table 2. Proximal composition and levels of n-3 HUFA and vitamin E of the experimental diets

Composition (% Dry weight)	Diet		
	C	NE	NFA
Crude proteins	48.08	49.93	49.56
Crude lipids	12.23	12.78	12.74
Moisture	11.16	11.01	10.97
Ash	12.07	11.58	11.55
n-3 HUFA	1.50	1.44	0.42
α -tocopherol (mg kg ⁻¹ diet)	167.5	18.5	160.5

samples were obtained before chasing in order to avoid the capture effects (Pearson and Stevens 1991).

Biochemical analysis of diets

Proximal and fatty acid composition of the experimental diets were measured. Crude protein was determined with Kjeldahl method. Lipids were extracted as described by Folch et al. (1957). Fatty acids were obtained by transmethylolation as described by Christie (1982) and iden-

tified using gas chromatography under the conditions previously described (Izquierdo et al. 1990).

Blood collection and sample preparation

Fish were rapidly captured from the tanks. Blood was obtained by caudal sinus puncture with 1 ml plastic syringe. An aliquot of blood was used for haematological and plasma determination and a second aliquot for serum analysis. Sampled fish were not reused. Fish handling time was less than 1 min per fish to minimize stress effects on analyzed parameters.

Blood samples for plasma determination were immediately transferred to an eppendorf tube coated with lithium heparin as anticoagulant. The plasma was obtained by centrifugation at 3000 rpm for 10 min. Plasma was then separated and stored at -80°C for plasma cortisol and total plasma protein determinations. A second aliquot of blood was transferred to an eppendorf tube without anticoagulant and allowed to clot at 4°C for 2 h. Serum was separated by centrifugation at 3000 rpm for 10 min, and stored at -80°C for serum complement activity determination.

Haematology and plasma analysis

A portion of blood was transferred to an eppendorf tube coated with lithium heparin as anticoagulant for cell counting and haematocrit determination. Haematocrit (Ht) was measured by microcentrifugation (3,000 rpm, 10 min) and red blood cells number (RBC) were obtained using a haematological counter Sysmex 800. The remaining blood was used for plasma determination.

Plasma cortisol was determined by radioimmunoassay using the trypsin-antitrypsin method as described for gilthead seabream (Molinero and Gonzalez 1995). Total plasma protein was determined using a commercial available kit (Boehringer-Mannheim S.A., Barcelona, Spain).

Haemolytic activity of ACP

The following buffers were used: GVB (Isotonic veronal buffered saline), pH 7.3, containing 0.1%

gelatin, EDTA-GVB, as previous one but containing 20 mM EDTA, and Mg-EGTA-GVB, which is GVB with 10 mM Mg^{++} and 10 mM EGTA. Rabbit red blood cells (RaRBC) were used for ACP determination. Blood was withdrawn from ear artery of a rabbit and placed into heparinized tubes. RaRBC were washed four times in GVB and resuspended in GVB to a concentration of 2.5×10^8 cells per ml (Sunyer and Tort 1994).

Alternative complement pathway (ACP) was estimated as described by Sunyer and Tort (1995), using 25 μ l of RaRBC suspension added to 100 microlitres of serially diluted serum in Mg-EGTA-GVB buffer. Samples were incubated at room temperature (22 °C) for 100 min with regular shaking. The reaction was stopped by adding 1 ml of cold EDTA-GVB. Samples were then centrifuged and the extent of hemolysis was estimated by measuring the optical density of the supernatant at 414 nm using a spectrophotometer (Shimadzu Corporation, Kyoto, Japan). The ACH50 units were defined as the concentration of serum giving 50% haemolysis of RaRBC. All analysis were conducted by triplicates.

Statistical analysis

All data were subjected to one-way analysis of variance (ANOVA), and differences between means compared by Tukey test at a 95% interval of confidence ($p < 0.05$). If the variances were not normally distributed (plasma cortisol levels in experiment II), the Kruskal-Wallis non-parametric test was applied to the data (Sokal and Rolf 1979).

Results

All the experimental diets were accepted and thus no significant differences were found in feeding intake among the experimental groups.

Experiment I

Final stocking density was significantly reduced ($p < 0.05$) when fish were fed NFA diet at any of

the stocking densities assayed (Tables 3, 4) due to the reduction in growth.

Tables 3 and 4 show plasma cortisol and total plasma protein values obtained in fish fed different experimental diets under different stocking densities. Values of plasma cortisol at low stocking density were significantly ($p < 0.05$) higher when fish were fed NE diet (Table 3), whereas in the fish groups held at high density, plasma cortisol did not show statistical differences (Table 4). Total plasma protein values were similar for fish cultured at low densities and fed the experimental diets. However, total plasma protein values were statistically ($p < 0.05$) lower in fish kept at high density and fed n-3 HUFA deficient diet when compared with the fish fed the NE diet.

Values of haemolytic activity due to alternative complement pathway obtained showed large variations for the different treatments. At low density, fish fed the deficient diets showed a significant ($p < 0.05$) lower haemolytic activity than those fish fed control diet but no differences were present between deficient diets (Table 3). Fish groups at high density showed significant differences in haemolytic activity between them, both showing a significantly ($p < 0.05$) lower haemolytic activity than those fish fed the control diet (Table 4).

Tables 3 and 4 also show haematological values for experimental fish held at high and low stocking densities. Haematocrit and RBC values of fish held at high density were higher than those from fish held at low density. In addition, fish fed non-supplemented α -tocopherol diet at high stocking density showed significantly higher RBC ($p < 0.05$) than those from fish fed the other experimental diets.

Experiment II

Figure 1 shows values of haemolytic activity due to ACP obtained for fish fed the different experimental diets after chasing stress. ACH50 was statistically ($p < 0.05$) lower along the experimental period for fish fed deficient diets when compared with the control-diet group. Moreover, there was a not statistically significant drop in haemolytic activity of the ACP in fish fed the control diet from the second day. Values were maintained

Table 3. Parameters of fish held at low stocking density*

	Diet		
	C	NE	NFA
Initial density (kg m ⁻³) ⁽¹⁾	3.28 ± 0.03a	3.27 ± 0.05a	3.25 ± 0.04a
Final density (kg m ⁻³) ⁽¹⁾	10.04 ± 0.57a	9.60 ± 0.30ab	8.77 ± 0.17b
Plasma Cortisol (ng ml ⁻¹) ⁽²⁾	3.91 ± 3.52a	21.70 ± 26.04b	13.86 ± 20.43ab
Plasma proteins (mg ml ⁻¹) ⁽²⁾	3.70 ± 0.65a	3.76 ± 0.41a	3.88 ± 0.54a
Ht (%) ⁽²⁾	37.21 ± 6.35a	36.20 ± 5.85a	39.50 ± 7.39a
RBC (×10 ⁶ mm ⁻³) ⁽²⁾	2.82 ± 0.54a	2.72 ± 0.87a	2.61 ± 0.67a
ACH50 (U ml ⁻¹) ⁽²⁾	167.23 ± 21.67a	100.99 ± 12.71b	93.66 ± 9.65b

*Values with different letter within a line are significantly different ($p < 0.05$); (mean ± SD); ¹n = 3; ²n = 5 × 3.

Table 4. Parameters of fish held at high stocking density*

	Diet		
	C	NE	NFA
Initial density (kg m ⁻³) ¹	12.00 ± 0.12a	12.00 ± 0.12a	12.09 ± 0.15a
Final density (kg m ⁻³) ¹	34.01 ± 0.37a	32.40 ± 0.90a	28.73 ± 1.88b
Plasma cortisol (ng ml ⁻¹) ²	16.25 ± 23.62a	16.56 ± 26.70a	16.36 ± 19.73a
Plasma proteins (mg ml ⁻¹) ²	4.22 ± 0.41ab	4.46 ± 0.59a	4.10 ± 0.41b
Ht (%) ²	43.87 ± 4.90a	42.73 ± 4.78a	43.17 ± 4.78a
RBC (×10 ⁶ mm ⁻³) ²	3.36 ± 0.59a	4.35 ± 0.59b	2.90 ± 0.71c
ACH50 (U ml ⁻¹) ²	146.37 ± 9.44a	106.91 ± 6.93b	92.19 ± 20.54c

*Values with different letter within a line are significantly different ($p < 0.05$); (mean ± SD); ¹n = 3; ²n = 10 × 3; ³n = 6 × 3.

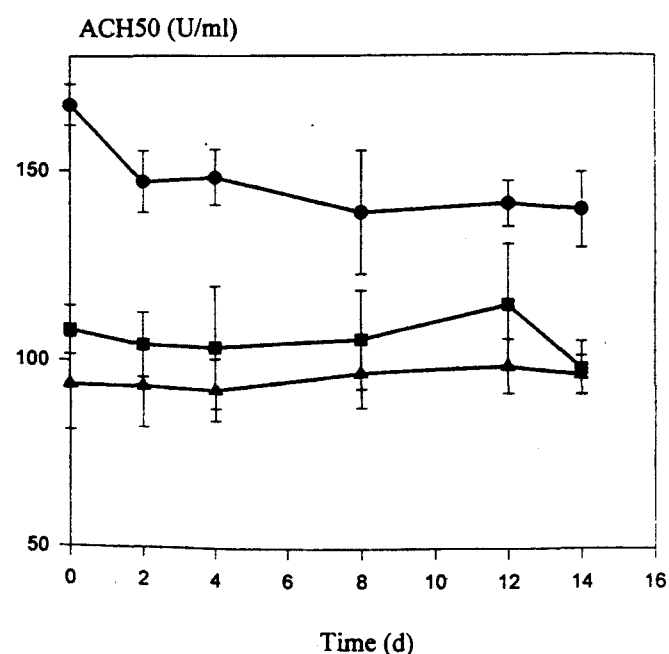


Figure 1. Effect of repetitive chasing on haemolytic activity due to alternative complement pathway in gilthead seabream fed control diet (Diet C) (●), diet without supplementation of α -tocopherol (Diet NE) (■) and diet deficient on n-3 HUFA (Diet NFA) (▲). n = 5 × 3. ACH50 values measured from fish fed both NE and NFA diet were significant ($p < 0.05$) lower than those from control fish along the experimental period.

along the experimental period. Those fish fed deficient diets showed haemolytic activity values not statistically different along the experiment.

Plasma cortisol levels showed different trends between experimental groups. Plasma cortisol levels in fish fed diets NE and NFA increased up to 30–40 ng cortisol ml⁻¹ plasma during the first 4 days followed by a reduction of those levels down to the initial one at day 14th. However, plasma cortisol level in control fish showed a moderate but continuous increase up to 25 ng ml⁻¹ plasma at day 14 (Figure 2).

Discussion

Gilthead seabream requires 0.5 to 2.5% of n-3 HUFA in the diet for optimum growth (Kalogeropoulos et al. 1992; Ibeas et al. 1994; Montero et al. 1996). The requirements of vitamin E have only been established for larval gilthead seabream (González et al. 1995), but there are no available data on the requirements

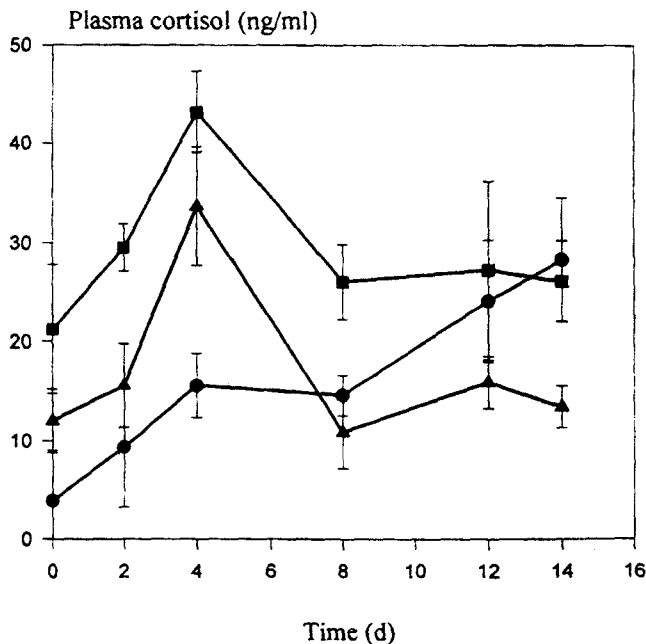


Figure 2. Effect of repetitive chasing on plasma cortisol levels in gilthead seabream fed control diet (Diet C) (●), diet without supplementation of α -tocopherol (Diet NE) (■) and diet deficient on n-3 HUFA (Diet NFA) (▲). $n = 5 \times 3$. Plasma cortisol levels determined from fish fed both NE and NFA diet at day 4th were significant ($p < 0.05$) higher than those from control fish at the same day. Plasma cortisol values determined from fish fed control diet at days 12 and 14 were significant ($p < 0.05$) higher than initial one.

for juveniles of this species. Non vitamin E supplemented sardine meal based diet reduced the immune system of gilthead seabream juveniles without affecting growth (Montero et al. 1996).

In the present study, dietary deficiencies of vitamin E or n-3 HUFA produced an important depletion of ACP in gilthead seabream juveniles. These results confirm previous data for this species (Montero et al. 1996; Tort et al. 1996a). It is known that deficiencies in structural components may produce a range of effects in membrane of immune cells. Thus, fish granulocyte activity is decreased by essential fatty acids dietary deficiencies (Sheldon and Blazer 1991; Kiron et al. 1995) as well as marginal vitamin E dietary deficiencies (Blazer 1982; Blazer and Wolke 1984; Wise et al. 1993). Structural changes caused by component deficiencies in membrane immune cells can alter eicosanoids production, enzymatic kinetics, cytokines receptors, ion transport and membrane permeability. Regarding the complement system, it is possible that this could be affected by alterations in the leukocyte

membrane (Obach et al. 1993) having suggested that cell membrane changes can modulate ACP and malnutrition can produce an inhibition in complement protein synthesis (Mold et al. 1989).

The effect of vitamin E on complement activation is important. Some authors have reported a depletion in haemolytic activity by complement activation due to low dietary vitamin E levels. Blazer and Wolke (1984) showed that non-supplemented α -tocopherol diets reduced serum haemolytic activity in rainbow trout sensitized with intraperitoneally injected sheep red blood cells. Fish fed with non-supplemented α -tocopherol diets had lower haemolytic values than those fed with 250 I.U. of α -tocopherol per kg supplemented diets. Serum from these fish were not heat inactivated, then this haemolytic activity was due to complement activity (Landolt 1989). Hardie et al. (1990) reported a depletion in complement activity in Atlantic salmon fed vitamin E deficient diet (7 mg vitamin E per kg diet), when compared with fish fed diets with higher vitamin E supplementation (326 mg or 800 mg vitamin E per kg diet). These authors suggested that dietary deficient vitamin E-mediated reduction in complement activity is not produced by a general protein depletion, but there is a specific effect of dietary vitamin E deficiency on complement activity. A similar effect of complement depletion, accompanied with high mortality rates, has been described in sea bass (*Dicentrarchus labrax*) subjected to vitamin E dietary deficiency after infection with *Aeromonas salmonicida* (Obach et al. 1993). On the other hand, Waagbo et al. (1995) found a positive correlation between serum polyenes and complement activity in cod (*Gadus morhua*). McClelland et al. (1995) found a positive correlation between dietary fatty acids and plasma fatty acid in gilthead seabream. The above may suggest that, in the present study, the depletion in complement activity could be related with a reduction in the n-3 HUFA levels.

Crowding also induced a reduction in ACP activity. It is known that stress may induce immunosuppressed states through the increase of cortisol levels. Cortisol is the major corticosteroid in teleost (Idler and Truscott 1972) and plasma levels show an increase as a primary stress response (Schreck 1981; Barton 1988; Pickering and Pottinger 1989). Elevated cortisol levels are

related with an immunosuppressive effect in fish (Pickering 1984; Pickering and Pottinger 1985; Barton and Iwama 1991). Some studies relate high plasma cortisol levels with serum haemolytic activity depletion. Thus, Iida et al. (1989) found a depletion in haemolytic activity during spawning season in trout, when plasma cortisol levels are high. Sunyer et al. (1995) described a reduction in complement activities (both the classical and alternative pathways) in gilthead seabream following 16 days of daily acute stress. More recently, it has been shown that crowding stress reduces the agglutinating and complement activity in this species (Tort et al. 1996b).

When fish fed deficient diets were subjected to repeated chasing stress, it should be noted that no differences were produced on ACP levels and these remained constant in time. These results suggest that deficiencies rather than stress could be a more important determinant of fish complement activity, and that fish subjected to an important degree of ACP depletion would be less sensitive to other agents otherwise causing reduction of ACP activity.

Levels of plasma cortisol after crowding stress or dietary deficiencies in n-3 HUFA or vitamin E supported similar results. Thus, crowding increased 4 fold the control cortisol levels and both deficiencies increased 3.5 (NFA) to 5.5 (NE) fold the control values. However, when deficient diets were given to crowded fish, no differences were found between groups, thus suggesting that crowding induces the activation of Hypothalamic-Pituitary-Interrenal (HPI) axis and that marginal dietary deficiencies are not able to affect the activity of the axis, leading to chronically elevated and consistent cortisol figures.

On the other hand, when fish were subjected to repeated stress, plasma cortisol of fish fed control diet showed a different trend when compared with cortisol from fish fed the other diets. Plasma cortisol values raised from 3.95 ng ml⁻¹ at the beginning and increased during all the stress period up to 25 ng ml⁻¹ at day 14. However, fish fed deficient diets showed a clear peak after 4 days and thereafter cortisol levels returned to the values of pre-stress levels. Therefore, a continuous activation of the HPI axis was apparent in the control fish, as far as cortisol levels is concerned. It appears that deficiencies in diet may result in a situation of chronic stress, and fish under this

situation experience a different response to a novel stress, compared to fish not previously HPI-activated. Thus, chronically stressed fish show a transitory elevation of cortisol (day 4) and further recovery (day 8), suggesting an adaptation to the novel stress.

These results differ from those reported by Sunyer et al. (1995), who found a reduction in gilthead seabream ACP activity under similar experimental procedures of repeated stress. A possible reason for this difference could be due to a combined effect of plasma cortisol and temperature during experimental procedure, which was as low as 12 °C (Sunyer et al. 1995) being at the low range of the optimum temperature for this species. Hayman et al. (1992) showed a relationship between decreases in temperature and complement activity in channel catfish, suggesting that relative low temperatures could affect the synthesis of some complement proteins. Nevertheless, the intensity of the stress may well have produced the differences observed, as the cortisol levels reached 80 ng ml⁻¹ in that work compared with 40 ng ml⁻¹ in the present work.

Regarding plasma proteins, fish fed NFA diet showed the lowest total plasma protein levels after crowding when compared with other experimental groups, whereas there were no significant differences in total plasma protein levels among fish fed experimental diets under low stocking density. Under high stocking density, ACP of the fish fed NFA diet were significantly lower than ACP from fish fed NE diet. This difference could be due to haemoconcentration showed by fish fed NE diet, as it has been reported that haemoconcentration produces a total plasma protein rise (Wedemeyer and McLeay 1981; Waring et al. 1996).

The results of the present study showed the negative effect of vitamin E and n-3 HUFA dietary deficiencies on serum haemolytic activity of gilthead seabream juveniles. The importance of this immune response in poikilothermic animals (Sakai 1992) and the degree of ACP reduction indicates that consequences of improper diet may result in a severe immunosuppression. Moreover, the combined effects of dietary deficiencies plus stress conditions related with routine aquaculture practices may lead to a decrease in the resistance potential of fish.

References cited

- Barton, B.A. 1988. Endocrine and metabolic responses of fish to stress. *Int. Assoc. Aquat. Anim. Med. Proc.* 19: 41–55.
- Barton, B.A. and Iwama, G.K. 1991. Physiological changes in fish from stress in aquaculture with emphasis on the response and effects of corticosteroids. *Ann. Rev. Fish Dis.*: 3–26.
- Blazer, V.S. 1982. The effect of marginal deficiencies of ascorbic acid and α -tocopherol on the natural resistance and immune response of rainbow trout (*Salmo gairdneri*). Ph. D. Dissertation. University of Rhode Island, U.S.A.
- Blazer, V.S. and Wolke, R.E. 1984. The effects of α -tocopherol on the immune response and non-specific resistance factors of rainbow trout (*Salmo gairdneri* Richardson). *Aquaculture* 37: 1–9.
- Christie, W.W. 1982. *Lipid Analysis*. Pergamon Press, Oxford.
- Folch, J., Lees, M. and Sloane-Stanley, G.H. 1957. A simple method for the isolation and purification of total lipids from animal tissues. *J. Biol. Biochem.*, 226: 497–509.
- González, M.M., Izquierdo, M.S., Salhi, M., Hernández-Cruz, C.M. and Fernández-Palacios, H. 1995. Dietary vitamin E for *Sparus aurata* larvae. *Europ. Aqua. Soc. Spec. Publ.* 24: 239–242.
- Hardie, L.J., Fletcher, T.C. and Secombes, C.J. 1990. The effect of vitamin E on the immune responses of the Atlantic salmon (*Salmo salar* L.). *Aquaculture* 87: 1–13.
- Hardie, L.J., Fletcher, T.C. and Secombes, C.J. 1991. The effect of dietary vitamin C on the immune responses of the Atlantic salmon (*Salmo salar* L.). *Aquaculture* 95: 201–214.
- Hayman, J.R., Bly, J.E., Levine, R.P. and Lobb, C.J. 1992. Complement deficiencies in channel catfish (*Ictalurus punctatus*) associated with temperature and seasonal mortality. *Fish Shellfish Immunol.* 2: 183–192.
- Ibeas, C., Izquierdo, M.S. and Lorenzo, A. 1994. Effect of different levels of n-3 highly unsaturated fatty acids on growth and fatty acid composition of juvenile gilthead seabream (*Sparus aurata*). *Aquaculture* 127: 177–188.
- Idler, D.R. and Truscott, B. 1972. Corticosteroids in fish. *In Steroids in Non-mammalian Vertebrates* pp. 127–252. Edited by D.R. Idler. Academic Press, London.
- Iida, T., Takahashi, K. and Wakabayashi, H. 1989. Decrease in the bactericidal activity of normal serum during the spawning period of rainbow trout. *Nippon Suisan Gakkaishi* 55: 463–465.
- Izquierdo, M.S., Watanabe, T., Takeuchi, T., Arakawa, T. and Kitajima, C. 1990. Optimum EFA levels in *Artemia* to meet the EFA requirements of red sea bream (*Pagrus major*). *In The Current Status of Fish Nutrition in Aquaculture*, pp. 221–232. Edited by M. Takeda and T. Watanabe. Tokyo Univ. Fisheries, Tokyo.
- Jenkins, J.A., Rosell, R., Ourth, D.D. and Coons, L.B. 1991. Electron microscopy of bactericidal effects produced by the alternative complement pathway of channel catfish. *J. Aquat. Anim. Health* 3: 16–22.
- Kalogeropoulos, N., Alexis, M.N. and Henderson, R.J. 1992. Effects of dietary soybean and cod-liver oil levels on growth and body composition of gilthead seabream (*Sparus aurata*). *Aquaculture* 104: 293–308.
- Kiron, V., Fukuda, H., Takeuchi, T. and Watanabe, T. 1995. Essential fatty acid nutrition and defence mechanisms in rainbow trout *Oncorhynchus mykiss*. *Comp. Biochem. Physiol.* 111A: 361–367.
- Landolt, M. 1989. The relationship between diet and the immune response of fish. *Aquaculture* 79: 193–206.
- Li, Y. and Lovell, R.T. 1985. Elevated levels of dietary ascorbic acid increase immune responses in channel catfish. *J. Nutr.* 115: 123–131.
- Maule, A.G., Tripp, R.A., Kaattari, S.L. and Schreck, C.B. 1989. Stress alters the immune function and disease resistance in chinook salmon *Oncorhynchus tshawytscha*. *J. Endocrinol.* 120: 135–142.
- McClelland, G., Zwingelstein, G., Weber, J.M. and Brichon, G. 1995. Lipid composition of tissue and plasma in two mediterranean fishes, the gilthead sea bream (*Chrysophrys auratus*) and the european seabass (*Dicentrarchus labrax*). *Can. J. Fish. Aquat. Sci.* 52: 161–170.
- Mold, C. 1989. Effect of membrane phospholipids on activation of the alternative complement pathway. *J. Immunol.* 143: 1663–1668.
- Molinero, A. and González, J. 1995. Comparative effects of MS-222 and 2-phenoxyethanol on gilthead sea bream (*Sparus aurata* L.) during confinement. *Comp. Biochem. Physiol.* 111: 405–414.
- Montero, D., Tort, L., Izquierdo, M.S., Socorro, J., Robaina, L., Vergara, J.M. and Fernández-Palacios, H. 1996. Effect of α -tocopherol and n-3 HUFA deficient diets on blood cells, selected immune parameters and proximate body composition of gilthead seabream (*Sparus aurata*) *In Modulators of Immune Response. The Evolutionary Trail*, pp. 251–266. Edited by J.S. Stolen, T.C. Fletcher, C.J. Bayne, C.J. Secombes, J.L. Zelikoff, L. Twerdok and D.P. Anderson. SOS Publications, Fair Haven.
- Obach, A., Quentel, C. and Baudin Laurencin, F. 1993. Effects of alpha-tocopherol and dietary oxidized fish oil on the immune response of sea bass *Dicentrarchus labrax*. *Dis. Aquat. Organ.* 13: 175–185.
- Pearson, M.P. and Stevens, E.D. 1991. Size and hematological impact of the splenic erythrocyte reservoir in rainbow trout, *Oncorhynchus mykiss*. *Fish Physiol. Biochem.* 9: 39–50.
- Pickering, A.D. 1984. Cortisol-induced lymphocytopenia in brown trout, *Salmo trutta* L. *Gen. Comp. Endocrinol.* 53: 252–259.
- Pickering, A.D. and Pottinger, T.G. 1985. Cortisol can increase the susceptibility of brown trout *Salmo trutta* L., to disease without reducing the white blood cell count. *J. Fish Biol.* 27: 611–619.
- Pickering, A.D. and Pottinger, T.G. 1989. Stress responses and disease resistance in salmonid fish: effects of chronic elevation of plasma cortisol. *Fish Physiol. Biochem.* 7: 253–258.
- Sakai, D.K. 1981. Spontaneous and antibody-dependent hemolysis activities of fish sera and inapplicability of mammalian complements to the immune hemolysis reaction of fishes. *Bull. Jap. Soc. Fish.* 47: 979–991.
- Sakai, D.K. 1992. Repertoire of complement in immunological defense mechanisms of fish. *Ann. Rev. Fish. Dis.*: 223–247.
- Schreck, C.B. 1981. Stress and compensation in teleostean fishes: Response to social and physical factors. *In Stress and Fish*, pp. 295–231. Edited by A.D. Pickering. Academic Press, London.
- Sheldon, W.H. and Blazer, V.S. 1991. Influence of dietary lipid and temperature on bactericidal activity of channel

- catfish macrophages. *J. Aquat. An. Health* 3: 87-93.
- Sokal, R.R. and Rolf, J. 1979. *Biometria*. Blume, Madrid.
- Sunyer, J.O. and Tort, L. 1994. The complement system of the teleost fish *Sparus aurata*. *Ann. N.Y. Acad. Sci.* 712: 371-373.
- Sunyer, J.O. and Tort, L. 1995. Natural hemolytic and bactericidal activities of sea bream *Sparus aurata* serum effected by the alternative complement pathway. *Vet. Immunol. Immunopathol.* 45: 333-345.
- Sunyer, J.O., Gómez, E., Navarro, V., Quesada, J. and Tort, L. 1995. Physiological responses and depression of humoral components of the immune system in gilthead seabream (*Sparus aurata*) following daily acute stress. *Can. J. Fish. Aquat. Sci.* 52: 2339-2346.
- Thompson, I., Fletcher, T.C., Houlihan, D.F. and Secombes, C.J. 1994. The effect of dietary vitamin A on the immunocompetence of Atlantic salmon (*Salmo salar* L.). *Fish Physiol. Biochem.* 12: 513-523.
- Tort, L., Gómez, E., Montero, D. and Sunyer, J.O. 1996a. Serum haemolytic and agglutinating activity as indicators of fish immunocompetence: their suitability in stress and dietary studies. *Aquacult. Int.* 4: 31-41.
- Tort, L., Sunyer, J.O., Gómez, E. and Molinero, A. 1996b. Crowding stress induces changes in serum haemolytic and agglutinating activity in gilthead seabream *Sparus aurata*. *Vet. Immunol. Immunopathol.* 51: 179-188.
- Verlhac, V., N'doye, A., Gabaudan, J., Troutaud, D. and Deschaux, P. 1993. Vitamin nutrition and fish immunity: influence of antioxidant vitamins (C and E) on immune responses of rainbow trout. *In Fish Nutrition in Practice*. pp. 167-177. INRA, Paris (Les Colloques, No 61).
- Waagbo, R., Hemre, G.I., Holm, J. CHR. and Lie, O. 1995. Tissue fatty acid composition, haematology and immunity in adult cod, *Gadus morhua* L., fed three dietary lipid sources. *J. Fish Dis.* 18: 615-622.
- Waring, C.P., Stagg, R.M. and Poxton, M.G. 1996. Physiology responses to handling in the turbot. *J. Fish Biol.* 48: 161-173.
- Wedemeyer G.A. and McLeay, D.J. 1981. Methods for determining the tolerance of fishes to environmental stressors. *In Stress and Fish*. pp. 247-275. Edited by A.D. Pickering. Academic Press, London.
- Wise, D.J., Tomasso, J.R., Gatlin, D.M. III, Bai, S.C. and Blazer, V.S. 1993. Effects of dietary selenium and vitamin E on red blood cell peroxidation, glutathione peroxidase activity, and macrophage superoxide anion production in channel catfish. *J. Aquat. Anim. Health* 5: 177-182.
- Yano, T., Matsuyama, H., Tanaka, K. and Nakao, M. 1987. Alternative pathway-hemolytic complement titer (ACH50) of porgy *Pagrus major* serum. *Nippon Suisan Gakkaishi*, 53: 1887-1891.
- Yano, T., Hatayama, Y., Matsuyama, H. and Nakao, M. 1988a. Titration of the alternative complement pathway activity of representative cultured fishes. *Nippon Suisan Gakkaishi* 54: 1049-1054.
- Yano, T., Nakao, M., Furuichi, M. and Yone, Y. 1988b. Effects of dietary choline, pantothenic acid and vitamin C on the serum complement activity of red sea bream. *Bull. Jap. Soc. Sci. Fish.* 54: 141-144.

Lipids, Fatty Acids and Sterols of *Cystoseira abies-marina*

P. Moreno^a, G. Petkov^{b,*}, Z. Ramazanov^a and G. Garsia^a

^a Institute of Applied Algology, E-35214 Muelle de Taliarte, Telde, Las Palmas, Spain

^b Institute of Plant Physiology, Bulgarian Academy of Sciences bl. 21, Sofia 1113, Bulgaria

* Corresponding author

Lipid content, fatty acids and sterol composition of *Cystoseira abies-marina* and total fatty acids of *C. humilis* from Gran Canaria were studied. A high content of polyunsaturated fatty acids 16 : 3 and 16 : 4 was found. Their content in monogalactosyldiacylglycerols is over 90%. Triacylglycerols and phospholipids contain mainly arachidonic and eicosapentaenoic acids. Reasons for the differences in the composition of fatty acids and sterols of various species of *Cystoseira* are discussed. Some technological approaches are recommended.

Introduction

Brown algae of the genus *Cystoseira* are wide spread in the seas and represented by many species (Piattelli 1990, Amico 1995). Some species have been studied for their lipid composition. There are data on the total fatty acids of *Cystoseira barbata* (Good. et Wood.) Ag. (Piatek et al. 1978, Stefanov et al. 1988, 1990). A comparison of the fatty acid composition of *C. fibrosa* (Hudson) C. Ag. = *C. baccata* (S. Gmel.) Silva (Riguera et al. 1984) and *C. compressa* (Esper) Derb. et Sol. (Kanas et al. 1992) shows remarkable differences.

The sterol composition of several species of *Cystoseira* has been studied (Iatrides et al. 1983, Vilalta et al. 1984, Riguera et al. 1985, Milkova et al. 1997), including some seasonal variations (Francisco et al. 1977, Combaut et al. 1984, 1985). Fucosterol is the main sterol in all *Cystoseira* species studied. Its concentration varies between 60 and 96% of the total sterols. Al Easa et al. (1995) have found ergosterol in the sterol mixture of *C. trinodes* (Förssk.) C. Ag. but this result has not been confirmed by other authors.

There are no data about the composition of the lipophylic fraction of *C. abies-marina* (Turner) C. Ag., which is wide spread on the sublittoral rocks of the Canary Islands.

The aim of this paper was to study the lipid content, fatty acids and sterol composition of *Cystoseira abies-marina*. Moreover, there are substantial differences in the data published for the lipid, fatty acid and sterol composition of *Cystoseira* species and, in our opinion, these differences are worth a detailed discussion.

Materials and Methods

The fresh plants of *Cystoseira abies-marina* (Turner) C. Ag. were collected from sublittoral rocks on the coast of Gran Canaria, washed and dried at 60 °C.

The dry material (6.163 g) was extracted with ethanol 3 times for 0.5 h under reflux, the extract was evaporated, the residue was re-extracted with chloroform, and total lipids were estimated gravimetrically (0.591 g).

Further material was obtained after drying in the sun to constant dry weight. Water extracted material was obtained after extraction of sun-dried, milled materials. Lipids of fresh material (without drying) were extracted after the above mentioned method, converted to fatty acid methyl esters in methanol containing 6 wt% anhydrous HCl at 60 °C for 1.5 h, extracted with diethyl ether and purified by thin layer chromatography (TLC) on silica gel with hexan – diethyl ether (10 : 1 v/v).

Another part of the lipid extract from fresh material was saponified with 5% m/v KOH in 96% v/v ethanol for two hours under reflux. Unsaponifiable matter was extracted with diethyl ether. Sterols were separated on TLC and acetylated with a pyridine – acetic anhydride mixture (1 : 1 v/v) at 60 °C for 1 h. The reaction mixture was neutralized with 5% m/v aqueous NaHCO₃. Sterols were extracted with ether and purified on TLC.

We have used the following mobile phases for the TLC separation of the lipid classes on silica gel G:

- monogalactosyldiacylglycerol (MGDG), CHCl₃ – MeOH – Me₂CO – AcOH (3.5 : 1.2 : 1.2 : 0.05 v/v)
- triacylglycerols (TG), n-hexan – Et₂O (3 : 1 v/v)
- Phospholipids (PL), CHCl₃ – MeOH – H₂O (65 : 25 : 4 v/v)
- Sterols, n-hexan – Et₂O (1 : 1 v/v)
- Sterol acetates, n-hexane – Et₂O (10 : 1 v/v)

The lipid spots were identified using reference compounds. The spots of reference compounds were stained with H₂SO₄ – EtOH (2 : 3 v/v) and heated at 110 °C.

Gas chromatography of fatty acid methyl esters was carried out on a 30 m long Supelcowax-10 capillary column at 195 °C. The methyl ester of pentadecanoic acid (15 : 0) was used as an internal standard for the quantification of the fatty acids. Sterols were separated on a 1.82 m, 2.7% OV-17 packed column at 280 °C.

Cystoseira humilis Kütz. was collected at the same location as *C. abies-marina* and the fatty acids were isolated according to the procedures described above.

Results and Discussion

Lipid, fatty acid and sterol contents of *C. abies-marina* are shown in Table I. The lipid content was much greater than that found in *C. barbata* (1.1%) by Alifimov (1963). The differences in the lipid content of fresh and dried material are due to the loss of volatile substances and to a more difficult penetration of solvents in dry material. Wetting the material prior to extraction procedures leads to more complete extraction of the lipids (Georgiev *et al.* 1992).

The lipid yield of milled, water extracted material significantly decreases. This is a result of the action

of liberated hydrolases. For this reason, delipidisation of the material should be carried out before the water extraction, as previously described (Petkov and Dilov 1987).

The fatty acid composition of *C. abies-marina* differs substantially from that of other species studied. The comparison of our data and data obtained by other authors is valid because all of them have used the same pretreatment of algal material. Fatty acids 16 : 3 and 16 : 4 are most abundant in the total lipids (Table II). Our experience with microalgae, as well as data in the literature, indicate that 16 : 4 is localised predominantly in the thylacoid membranes as a component of MGDG, digalactosyldiacylglycerols (DGDG) and sulfoquinovosyldiacylglycerols (SQDG). Moreover, the high concentration of 16 : 4 in the total fatty acids is evidence for a good physiological state of photosynthesis. Some physiological stress conditions: nitrogen starvation, temperatures above optimum, heterotrophic nutrition, provoked a decrease of 16 : 4 and even its total disappearance in *Scenedesmus*, *Dunaliella* and *Coelastrum* (Ben-Amotz *et al.* 1985, Petkov *et al.* 1986, 1990, Furnadzhieva *et al.* 1987). The data published in these papers lead to the conclusion that a low content of 16 : 4 and the high one of 18 : 0, 18 : 2, 20 : 4, 20 : 5 is possibly connected to seasonal changes of heterotrophic nutrition, because of water pollution with organic substances. As shown in Table II, 16 : 3 and 16 : 4 constitute more than 90% of the composition of MGDG; phospholipids (PL) are built mainly of unsaturated 20 : 4 and 20 : 5 acids. Triacylglycerols (TG), which are storage substances, increase at nitrogen starvation or unfavourable conditions. In our case, the acid 20 : 5 prevails in TG. Our data confirm the results of Hulanicka *et al.* (1964) with *Euglena*, who found that autotrophic cultivation increased the percentage of

Table I. Lipid composition of *C. abies-marina*.

Substances	%
Lipids in oven dried material	9.6
Lipids in sun-dried material	8.5
Lipids in water-extracted material	2.0
Fatty acids in fresh material	4.3
Fatty acids in lipids	48.8
Unsaponifiable fraction of lipids	7.0
Sterols in unsaponifiable fraction	5.4

Table II. Fatty acid composition of *Cystoseira* species.

Fatty acids	<i>Cystoseira abies-marina</i>					<i>C. humilis</i>
	Total	TG	MGDG	PL	Sun dried	Total
14 : 0	0.5	2.7	0.5	5.7	24.9	3.1
14 : 1	—	—	—	—	5.7	—
16 : 0	1.2	18.0	1.2	25.6	25.1	8.1
16 : 1	0.1	7.9	0.3	5.8	2.4	6.2
16 : 1	0.1	—	—	—	—	—
16 : 2	7.4	3.8	3.7	2.2	—	0.6
16 : 3	40.7	—	30.7	1.2	—	0.8
16 : 4	47.0	4.6	60.3	1.4	—	1.2
18 : 0	0.1	3.9	0.1	3.7	1.5	6.2
18 : 1	0.5	9.2	0.6	11.8	14.4	9.1
18 : 2	0.4	8.5	0.5	4.2	10.4	7.8
18 : 3	tr.	—	tr.	—	—	1.9
18 : 3	0.2	1.5	0.2	—	3.5	19.3
18 : 4	0.1	—	tr.	3.7	—	13.4
20 : 4	0.9	4.9	0.7	9.8	11.5	11.4
20 : 5	0.5	34.9	1.4	24.8	—	10.9

16 : 4 whereas heterotrophic cultivation increased the percentage of 20 : 4 and 20 : 5. The data are in a good agreement with the results of Stefanov *et al.* (1988, 1990) for *Cystoseira barbata* from the Black Sea.

Neither seasonal changes nor heterotrophic nutrition completely explain the simultaneous absence of 16 : 3, 16 : 4 and 20 : 4, 20 : 5 reported in some of the publications on *Cystoseira* species (Piatek *et al.* 1978, Riguera *et al.* 1984, Kanas *et al.* 1992). For a comparison we studied the fatty acid composition of another Canarian alga *Cystoseira humilis* and found 16 : 3 and 16 : 4 acids, even if at a low percentage. In this case, the concentration of 18 : 4, 20 : 4, 20 : 5 was rather high (Table II). It is important to mention that *C. abies-marina* was collected at the beginning of October and the *C. humilis* in March.

The sterol composition of *C. abies-marina* is typical for an alga of the genus *Cystoseira* (Table III). The UV-spectrum of the sterols from fresh material and quick analytical procedures showed an absence of sterols with conjugated $\Delta^{5,7}$ -double bonds. So, the sterol composition of *C. trinodes* studied by El Easa *et al.* (1995) appears to be an exception in the genus *Cystoseira*.

Table III. Percentage of sterols of *C. abies-marina*

Sterol	%
22-Dehydrocholesterol	tr.
Cholesterol	0.7
Brassicasterol	1.2
24-methylenecholesterol*	1.1
Fucosterol	96.9

* together with campesterol

References

- Al Easa, H. S., J. M. Kornprobst and A. M. Rizk. 1995. Major sterol composition of some algae from Qatar. *Phytochemistry* 39: 377–374.
- Alfimov, N. N. 1963. Biochemistry of some macrophytes of the Black Sea. *Botan. Zh.* 48: 132–135.
- Amico, V. 1995. Marine brown algae of family Cystoseiraceae: chemistry and chemotaxonomy. *Phytochemistry* 39: 1257–1279.
- Ben-Amotz, A., T. Tornabene and W. Thomas. 1985. Chemical profile of selected species of microalgae with emphasis on lipids. *J. Phycol.* 21: 72–81.
- Combaut, G. and P. Saenger. 1984. Sterols of the Amanesiaceae (Rhodomelaceae: Rhodophyta). *Phytochemistry* 23: 781–782.
- Combaut, G., A. Yacoubou, L. Piovetti and J. M. Kornprobst. 1985. Sterols of the Senegalese brown alga *Padina vickersiae*. *Phytochemistry* 24: 618–619.
- Francisco, C., G. Combaut, J. Teste and B. F. Maume. 1977. Etude des sterols d'algues brunes du genre *Cystoseira*. *Biochim. Biophys. Acta* 487: 115–121.
- Furnadzhieva, S., G. Petkov, R. Andreeva and K. D. Dang. 1987. Physiological and biochemical characteristic of *Coelastrum sphaericum* Kom. 64/64. *Proc. IV Nat. Conf. Bot. Sofia*. pp. 305–311.
- Georgiev, D., K. Minkova, G. Petkov and M. Sholeva. 1992. Lipid extraction from *Porphyridium carentum* dry biomass. *Comptes rendus Acad. bulg. Sci.* 45: 131–134.
- Hulanica, D., J. Erwin and K. Bloch. 1964. Lipid metabolism of *Euglena gracilis*. *J. Biol. Chem.* 239: 2778–2787.
- Iatrides, M. C., J. Artaud and N. Vincente. 1983. Sterol composition of Mediterranean plants. *Oceanol. Acta* 6: 73–77.
- Kanas, G., H. Skaltsa, E. Tsitsa, A. Loukis and J. Bitis. 1992. Study of the correlation between trace elements, sterols and fatty acids in brown algae from the Saronikos Gulf of Greece. *Fresenius' J. Anal. Chem.* 344: 334–339.
- Kolattukudy, P. E. 1976. *Chemistry and Biochemistry of Natural Waxes*. Elsevier, Amsterdam. 459 pp.
- Milkova, T., G. Talev, R. Christov, S. Dimitrova and S. Popov. 1997. Secondary metabolites in *Cystoseira bar-*

Kanas *et al.* (1992) have reported campesterol from *C. compressa*. Unfortunately, under the GC-conditions they used, there is an almost full overlapping of the peaks of 24-methylenecholesterol and campesterol. Studies of Milkova *et al.* (1997) confirm this. Al Easa *et al.* (1995), using a 30 m DB 1 column, have separated 24-methylenecholesterol and campesterol but they showed that campesterol was absent in *C. trinodes*. It has to be accepted that in *Cystoseira* there is no campesterol, or if there is any, it is in trace amounts. Authors who did not separate these two sterols, gave a small value for their sum (Kanas *et al.* 1992). We may conclude that all the species of *Cystoseira* studied, have one and the same qualitative sterol composition and show quantitative differences only.

Sterols, except $\Delta^{5,7}$, are more stable to peroxidation compared to polyunsaturated fatty acids. We consider, that this is one of the reasons why the data on fatty acid composition differ significantly in different publications, while the data on sterol composition are similar. If sterols, which are secondary metabolites, coincide in the species of the same genus, it is very unlikely that primary metabolites such as fatty acids, will differ so much. For instance, *Chlorella* was subdivided by Kolattukudy (1976) into Δ^5 , Δ^7 , $\Delta^{5,7}$ -genotypes according to its sterol composition but all species of the genera had the same fatty acid composition.

We have to conclude that all species of *Cystoseira* have the same fatty acids but with different percentages, depending on the physiological and ecological conditions.

Accepted 26 February 1998

- bata* and *Cystoseira crinita* from the Black Sea 1997. *Phytochemistry* 45: 93–95.
- Petkov, G. and C. Dilov. 1987. On the composition of the alcoholic extract of microalgae of the genus *Scenedesmus* Meyen. *Khidrobiologiya* 29: 41–44.
- Petkov, G., K. D. Dang and S. Fournadjieva. 1986. Lipid composition of *Coelastrum sphaericum* and *Coelastrum cambricum*. *Compt. rend. Acad. bulg. Sci.* 39: 127–128.
- Petkov, G., G. Klyachko-Gurvich, S. Furnadzhieva, N. Pronina and Z. Ramazanov. 1990. Genotypic differences and phenotypic changes of lipid fatty acid composition in strains of *Dunaliella salina*. *Sov. Plant. Physiol.* 37: 268–272.
- Piatak, D. M., J. Schwartzinger, H. D. Lee, J. Stankovic and M. J. Gasic. 1978. Study of the lipid fractions of some Adriatic Sea algae. *Trans. Ill. State Acad. Sci.* 71: 392–397.
- Piattelli, M. 1990. Chemistry and taxonomy of Sicilian *Cystoseira* species. *New J. Chem.* 14: 777–782.
- Riguera, R., L. Castedo, J. M. Quintela and R. Vilalta. 1984. Acids, esters, and hydrocarbons in algae of the Galician coasts. *Acta Cient. Vompstelana* 21: 13–26.
- Riguera, R., L. Castedo, J. M. Quintela and R. Vilalta. 1985. Sterols from red and brown algae from the Galician coast. *An. Quim. Ser. C* 81: 113–115.
- Stefanov, K., M. Konaklieva, E. Y. Brechany and W. W. Christie. 1988. Fatty acid composition of some algae from the Black Sea. *Phytochemistry* 27: 3495–3497.
- Stefanov, K., K. Seisova, M. Konaklieva, S. Popov, G. Petkov and W. Christie. 1990. Fatty acids of Black Sea organisms. In: (A. Usov, ed.) *Biological Active Substances of Marine Organisms*. Inst. Okeanologii, AN, Moscow. pp. 51–73.
- Vilalta, R., J. M. Quintela, R. Riguera and L. Castedo. 1984. Natural marine products from algae and cnidaria of the Galician estuaries. *Cuad. Area Cienc. Mar.*: 617–625.

EL TRABAJO DE LOS DÍAS*

José Miguel Pacheco Castelao

Departamento de Matemáticas
Universidad de Las Palmas de Gran Canaria

El título de esta intervención imita intencionadamente el de una de las más conocidas obras del poeta griego Hesiodo (Siglo VIII A.C.), cuyo nombre es “Los trabajos y los días”. En tiempos de cambio en los modelos educativos de nuestro país, creo importante recordar que la cultura clásica es un patrimonio que no debe perderse y merece un lugar en los proyectos de futuras enseñanzas. El poema de Hesiodo a que hago referencia es una bella descripción de la vida diaria en la antigua Grecia, con especial interés en las labores del campo.

Leído por un matemático, son interesantísimas las referencias al paso de los astros que marcan los días para las diferentes labores. Ello nos muestra que muchos saberes matemáticos eran conocidos y aplicados por la sociedad civil en cuestiones de la vida cotidiana, sugiriendo que existía desde tiempo atrás y de modo más o menos oficial, algún organismo –muy posiblemente de carácter religioso– dedicado a la observación y utilización de esas informaciones a efectos prácticos. La lectura de Hesiodo, por tanto, nos indica que el concepto de un calendario solar era conocido y aplicado en la cultura griega, aunque coexistía en la práctica y en especial para transacciones comerciales, con un calendario lunar, tal como muestra el comediógrafo Aristófanes (Siglo V A.C.) en su divertidísima obra “Las nubes”, donde además de una cruda sátira contra los filósofos socráticos podemos enterarnos pormenorizadamente de las costumbres de los prestamistas o banqueros y de cómo esas transacciones se regían por este último tipo de calendario. Evidentemente, el desarrollo de un calendario no es sino una más de las muchas cuestiones matemáticas desarrolladas entre Grecia y el Próximo Oriente y por tanto, el terreno estaba culturalmente preparado en la Antigüedad para que, unos doscientos años después del entretenido Aristófanes, Euclides (Siglo III A.C.) compilara los “Elementos” in-

* Conferencia pronunciada en Abril de 1997 en la inauguración de las Jornadas anuales de la Sociedad «Isaac Newton», en Las Palmas de Gran Canaria. El texto que se presenta está corregido y ampliado con referencias más exactas, que no afectan esencialmente al original.

troduciendo en ellos y con ellos las bases de una cultura matemática que aún mantiene su actualidad.

Ya se habrá intuido que el objetivo de esta exposición es indagar, por supuesto de manera sencilla y que podría desarrollarse sin duda alguna en niveles elementales de la enseñanza, sobre el calendario solar, pero antes intentaré reflexionar un momento acerca del origen de las Matemáticas. No me refiero aquí a las Matemáticas antiguas o clásicas que nos han legado los griegos, sino a estadios muy anteriores a ellas, relacionados muy directamente con actividades cotidianas.

Las manifestaciones culturales más antiguas pueden datarse, y para eso está la Arqueología, en la época neolítica, cuando se desarrolla la conciencia social en los primeros grupos humanos, lo que ocurre hace alrededor de veinte mil años y viene a coincidir con el hecho de que algunos grupos nómadas deciden establecerse tras descubrir los rudimentos de la Agricultura y la Ganadería. Este conjunto de técnicas o saberes condujo pronto a plantear problemas cargados de sentido matemático: ¿Cuántas reses tenemos? ¿Qué cueva es bastante grande para guarecerlas? ¿Cuánto hay que sembrar para obtener suficientes resultados? ¿Qué cantidad de terreno se necesita para obtener una cosecha adecuada? ¿Cuándo hay que sembrar y recoger?

Preguntas como la última que se ha formulado muestran que la explotación de la Naturaleza tiene un papel capital en el desarrollo de la medida del tiempo, que es –como ya señalé antes– otra de las actividades matemáticas más antiguas y se halla relacionada, desde luego, con la observación de fenómenos repetitivos en la Naturaleza: Los más evidentes, en las zonas templadas donde se originaron las primeras civilizaciones –aparte de la sucesión trivial de días y noches– son los ciclos de las estaciones (que determinan cosas tales como las cosechas y las crecidas anuales del Nilo) y las fases de la Luna. Una observación más atenta llevaría a reconocer la variación periódica de la duración del día y a establecer su correlación con las estaciones y ciertos fenómenos vitales en la actividad explotadora. Por poner un ejemplo, se sabe que el estro de las ovejas depende de la duración del día, y lo mismo puede decirse de los ciclos reproductivos de muchas plantas, con exactitud del orden de segundos. Estos ciclos no se pueden calibrar bien con un calendario basado en la Luna, pues la duración del día no guarda relación con la fase lunar, así que para acomodar las épocas de siembra, cosecha y otras labores agropecuarias se buscó basar el calendario en el ciclo solar, más largo pero no menos claro. De manera curiosa, un calendario solar se establece mejor por la noche, y ello llevó a la observación de los astros: Las noches largas o cortas se corresponden con la aparición de algunas constelaciones o estrellas en posiciones concretas de la bóveda celeste, que pueden ser contrastadas con algún tipo de observatorio delimitado por montañas, piedras u otros accidentes naturales o artificiales. Todavía se conservan antiquísimos observatorios como el de Stonehenge en Gran Bretaña, construido entre los años 2400 y 1700 A.C., muchos siglos antes de que Hesiodo escribiera su famoso poema.

En cualquier caso, en fecha muy antigua ya se sabía que el año tenía una duración de $365 \frac{1}{4}$ días. He aquí una pregunta interesante para el aula: Parece fácil contar los 365 días, pero ¿y el cuarto de día? En una época sin relojes es necesaria una finura de observación poco corriente para establecer esa fracción. La solución al problema es, sin duda, la más obvia: Si se podía calcular un año comprobando que

cada 365 días el Sol salía tras tal piedra o árbol, el observador avezado podría reconocer que al cabo de cuatro años ya se producía un error, pues el Sol salía por el sitio correspondiente un día más tarde de lo esperado. Así se justifica ese cuarto de día, aunque es de suponer que con instrumentos de observación tan poco desarrollados no se pudiera obtener más exactitud en esa medida. De paso, conviene recordar aquí que se llama “año trópico” al tiempo invertido por el Sol entre dos pasos consecutivos por un mismo punto, la tradición utiliza el punto de Aries o equinoccio de Primavera.

Al irse creando una cultura ciudadana ya ajena a las labores del campo, se transfiere el control del tiempo a un calendario o tabla de carácter convencional para ser utilizada en las diferentes actividades. Tal calendario, que podemos denominar civil, consta de un número entero de días, por lo que con relación al paso de los astros se comete un error cuyo efecto se describe a continuación. Dado que la tabla debería ser concordante con los usos de la Agricultura, ello equivale a decir que por lo menos alguna efeméride importante, tal como el equinoccio de Primavera, debería ocurrir siempre en la misma fecha. Pero al utilizarse como año una unidad de medida más corta que el año trópico, la fecha del equinoccio se va retrasando, por lo que al cabo de unos cuantos años el desfase llega ser perceptible, y la fecha prevista para el equinoccio según el calendario civil vendría a caer en pleno verano. Es de suponer que esto no resultaría de ninguna utilidad para los agricultores.

Alrededor del año 45 A.C., siendo Julio César Emperador de Roma -y por consiguiente de casi todo el mundo conocido- el desastre del calendario era tan evidente que se hicieron estudios para arreglar la cuestión. El astrónomo griego Sosígenes se encargó del problema y el Emperador decretó que ese año duraría 484 días y que a partir de él se empezaran a contar años de 365 días, pero introduciendo uno de 366 días cada cuatro, con lo que la duración media del año quedaba en los antes citados 365 1/4 días. Los años que se añadían se denominaron “bisiestos” pues el día añadido era un segundo 6 (bis-sextil) de Marzo. En aquella época el año nuevo se celebraba en Marzo, y de eso queda todavía el recuerdo en los nombres de los últimos meses del año (Octubre = mes octavo, Noviembre = mes noveno y Diciembre = mes décimo). El primero de año se celebró durante siglos el 25 de Marzo en Europa, incluso hasta mediados del Siglo XVIII en los países protestantes.

Con la reforma Juliana pareció haberse arreglado la cuestión, pero el paso de los años y de los siglos llevó a reconocer que se había utilizado un año civil demasiado largo, por lo que la fecha del equinoccio de Primavera retrocedía hacia el invierno (por supuesto que estamos hablando del hemisferio norte de la Tierra). Con los instrumentos de medida más perfeccionados, hacia el Siglo XVI ya se había afinado la medida de la duración del año trópico, según se ve en la tabla siguiente:

Tablas Alfonsíes ¹ , 1272-1500	365d 5h 49' 15" 58'''
Ulugh Beg ² , ca. 1430	365d 5h 49' 15"
<i>De Revolutionibus</i> (Copérnico), 1543	365d 5h 49' 16" 28'''
Tablas Pruténicas ³ (Reinhold), 1551	365d 5h 49' 15" 45'''

Todas las mediciones son menores de $365 \frac{1}{4}$ días y difieren entre sí menos de segundo y medio, lo que da una idea tanto del desarrollo de los mecanismos de observación como del dominio del cálculo trigonométrico en esas épocas. Los casi once minutos de diferencia con el año civil medio de $365 \frac{1}{4}$ días se traducían en un día de retraso con respecto al ciclo de las estaciones cada 131 años, por lo que los días de retraso se iban acumulando. El matemático inglés Johannes de Sacrobosco⁴ afirmaba ya en 1232 que existía un error de diez días (no era tanto aún). Finalmente, el dominico Egnatio Danti demostró en 1574 que los días de retraso eran once en esa fecha.

Naturalmente el poder fáctico más importante de aquel tiempo, la Iglesia Católica, no podía permanecer callado ante este hecho, entre otras causas porque la Pascua, la más importante de las festividades católicas, se determina según la tradición bíblica para que tenga lugar tras la primera luna llena después del equinoccio de Primavera, y éste había sido fijado en el 21 de Marzo por el Concilio de Nicea en fecha tan remota como el año 325. Por eso, ya a mediados del Siglo XV se iniciaron estudios para corregir esta anomalía: Incluso Copérnico fue invitado a trabajar en ello en 1514 por el Papa León X. Sin embargo, la Reforma luterana —que a partir de 1530 dividió a los cristianos en protestantes y católicos— era un quebradero de cabeza más importante para los Papas de mediados del Siglo XVI que el asunto del calendario, y el estudio del problema se pospuso hasta el Papado de Gregorio VIII, quien nombró una comisión, presidida por el matemático y jesuita alemán Cristóbal Clavius para encontrar una solución a un conjunto de problemas relacionados con el calendario:

1. Acomodar el calendario al ciclo de las estaciones.
2. Fijar el día primero del año.
3. Modificar el método de inserción de los años bisiestos.
4. Determinar la fecha de la Pascua.

La reforma del calendario se llamó Gregoriana por razones evidentes y fue publicada en una bula papal en 1582 con el título *Inter gravissimas*, que viene a significar “De capital importancia”.

El punto primero se arregló ordenando que el día siguiente al 4 de Octubre de 1582 fuera el 15 de Octubre del mismo año, con lo que se ajustaron los diez días de retraso que se llevaban acumulados en esa fecha. Para convencer al Papa hubo

1. Las Tablas Alfonsíes se denominaron así por haber sido ordenada su compilación por el Rey de Castilla Alfonso X el Sabio en 1272. Fueron corregidas y ampliadas durante años, siendo muy conocida la contribución de Nicolás de Cusa en la primera mitad del Siglo XV.

2. Beg fue un astrónomo persa del Siglo XV, que construyó un observatorio en Samarkanda.

3. Erasmus Reinhold, astrónomo alemán de la primera mitad del siglo XVI. Sus *Tabulae prutenicae caelestium motuum*, o Tablas Pruténicas, son una corrección de los cálculos de Copérnico.

4. Fue muy conocido por su tratado «De Sphæra» (la celeste, se entiende), usando durante siglos en las Universidades europeas. En su autobiografía Torres Villarroel lo cita como texto en Salamanca a mediados del Siglo XVIII.

que construir una habitación especial en el Vaticano para observar el tránsito del Sol por el meridiano el día del equinoccio, que tuvo lugar el 11 de Marzo de 1582, tal como predecían los astrónomos, en vez del 21 de Marzo como obligaba el Concilio de Nicea.

El primero de año se fijó en el 1 de Enero y se determinó que habría que suprimir algunos bisiestos para que la fecha del equinoccio quedase lo más fija posible. La regla elegida fue eliminar tres bisiestos cada 400 años, siendo los eliminados los años finiseculares cuyo número no es divisible por 400. Por eso el año 2000 es bisiesto, como también lo fué el 1600, pero no lo fueron los 1700, 1800 y 1900. De este modo el calendario Gregoriano se organiza en ciclos de 400 años con 97 bisiestos por ciclo con lo que el año Gregoriano consta, en promedio, de $365 \frac{97}{400} = 365,2425$ días, ligeramente menor que el año Juliano de $365 \frac{1}{4} = 365,25$ días.

El cuarto problema, que era el más interesante para el Papa –determinar la fecha de la Pascua– se resolvió inventando un algoritmo, donde aparecen cosas tales como la Epacta y los Números de Oro, que puede consultarse en viejos manuales escolares, pero no lo explicaré aquí. En esencia se trata de coordinar el ciclo de 19 años de repetición de las fases lunares con el ciclo de años bisiestos, ya sea Juliano o Gregoriano. Este trabajo ya fue emprendido en la Antigüedad por el astrónomo Metón en el Siglo V A.C. Por ponerlo en un lenguaje que nos toca de cerca, la fecha de los Carnavales se calcula con ese algoritmo.

La reforma Gregoriana fue adoptada lentamente (ver tabla al final) y no siempre de buen grado. En la ciudad alemana de Frankfurt se produjeron motines contra el Papa y sus matemáticos⁵, acusándolos de robar once días a la vida de los amotinados. Las protestas obligaron a Clavius a escribir y publicar en 1595 un texto titulado *Novi calendarii romani apologia* para solucionar el asunto. Sin embargo, desde el punto de vista científico no se habían acabado los problemas...

A finales del Siglo XIX se sabía ya que el año Gregoriano es “demasiado largo”, habiéndose medido la duración, redondeada a cuatro cifras decimales⁶, del año trópico en 365,2422 días, esto es, unos ¡24 segundos! más corto que el año Gregoriano. Tal cosa indica que al cabo de unos 4000 años el equinoccio de Primavera retrocede un día. Esta cuestión, que no afecta especialmente a nuestras vidas, puede inducirnos a proponer una reforma del calendario por nuestra cuenta. Veremos que una vez conocidos los datos de los astrónomos sobre la duración del año trópico, una reforma consistente en ubicar los bisiestos no es más que un elegante ejercicio⁷ sobre números racionales.

Comenzaremos con una observación. El quebrado que acompaña a la parte entera 365 en el número mixto que representa la duración de los distintos tipos de años se puede leer de la siguiente manera:

5. Esto muestra que la profesión de matemático puede no ser demasiado tranquila.

6. Hoy sabemos que la duración del año trópico fluctúa, variando la sexta cifra decimal en plazos que no superan los 100 años.

7. Consúltense el interesante artículo: Rickey V F (1985) Mathematics of the Gregorian Calendar, *Math. Intell.*, 7(1), 53-56.

Año	fracción de día	interpretación
Juliano	1/4	un bisiesto cada 4 años
Gregoriano	97/400	97 bisiestos cada 400 años
Trópico	2422/10000	2422 bisiestos cada 10000 años

Nuestro problema se reduce a encontrar un quebrado con un denominador razonablemente pequeño y que se halle más próximo a 2422/10000 que 97/400, lo que nos dará una regla de bisiestos más ajustada al año trópico. Para ello partimos del propio 2422/10000, creando a partir de él una familia de quebrados aproximantes, mediante el siguiente cálculo, que se llama “desarrollo de un número racional en forma de fracción continua”:

$$\begin{aligned}
 365 \frac{2422}{10000} &= 365 + \frac{2422}{10000} = 365 + \frac{1}{\frac{10000}{2422}} = \\
 365 + \frac{1}{4 + \frac{1288}{10000}} &= 365 + \frac{1}{4 + \frac{1}{\frac{10000}{1288}}} = \\
 &= 365 + \frac{1}{4 + \frac{1}{7 + \frac{7640}{10000}}} = \\
 &= 365 + \frac{1}{4 + \frac{1}{7 + \frac{1}{1 + \dots}}} = \\
 &= 365 + [4; 7; 1; 3; 4; 1; 1; 1; 2]
 \end{aligned}$$

donde los números entre corchetes representan los sucesivos cocientes. Este desarrollo se termina al cabo de un número finito de pasos, en este caso 9, pues no es otra cosa que el algoritmo de Euclides. Si se va calculando “por pisos” la parte no entera obtendremos una serie de fracciones –llamadas reducidas– que se van aproximando a la dada, alternativamente por defecto y por exceso, siendo la última que se obtiene la fracción original:

$$\frac{1}{4} ; \frac{7}{29} ; \frac{8}{33} ; \frac{31}{128} ; \frac{132}{545} ; \frac{163}{673} ; \frac{295}{1218} ; \frac{458}{1891} ; \frac{1211}{5000} = \frac{2422}{10000}$$

y que se ordenan de mayor a menor de la siguiente manera:

$$\frac{1}{4} > \frac{8}{33} > \frac{132}{545} > \frac{295}{1218} > \frac{1211}{5000} > \frac{2422}{10000} > \frac{458}{1891} > \frac{163}{673} > \frac{31}{128} > \frac{7}{29}$$

Podemos considerar, por ejemplo, las aproximaciones por exceso. La primera de ellas es $1/4$, que corresponde a usar un año de $365 \frac{1}{4}$ días, esto es, el año Juliano. Usar la segunda sería equivalente a utilizar un año de $365 \frac{8}{33}$ días, o lo que es lo mismo, a implantar una regla de poner 8 bisiestos cada 33 años. Una observación importante es que $365 \frac{8}{33} = 365,2424$, y recordando las duraciones del año trópico y del año Gregoriano tendremos:

$$\text{Año trópico} = 365,2422 \text{ días} < 365,2424 \text{ días} < 365,2425 \text{ días} = \text{Año Gregoriano}$$

luego una regla de implantar 8 años bisiestos cada 33 años ¡es mejor aproximación al año trópico que la regla Gregoriana! Lo mismo puede decirse de las demás aproximaciones por exceso, pero al ser números tan “poco agradables” no parecen dar lugar a reglas de alguna utilidad práctica. Las aproximaciones por defecto pueden ser incluso mejores: Por ejemplo, $31/128$ conduce a un año civil de 365,242185 días, muy próximo al valor aceptado para el año trópico de 365,24219879 días⁸, del cual sacamos el redondeo 365,2422. Para completar la cuestión les diré que la propuesta $8/33$ fue hecha más de 500 años antes de la reforma Gregoriana por el matemático y poeta árabe Omar Khayyam⁹, en 1079, así que juzguen Uds. mismos en qué partes del mundo estaban más avanzadas las Matemáticas en la alta Edad Media. Ahora nos haremos una pregunta que es casi obligada: ¿De dónde salió la propuesta Gregoriana de $97/400$? Evidentemente no se obtuvo de un cálculo como el anterior, pero sí a partir de otros métodos no menos ingeniosos.

Para contestar a nuestra pregunta necesitamos contar en base 60, esto es, usar fracciones sexagesimales de día para representar la duración del año. Recordemos la tabla de duraciones del año trópico:

Tablas Alfonsíes, 1272-1500	365d 5h 49' 15" 58'''
Ulugh Beg, ca. 1430	365d 5h 49' 15"
<i>De Revolutionibus</i> (Copérnico), 1543	365d 5h 49' 16" 28'''
Tablas Pruténicas (Reinhold), 1551	365d 5h 49' 15" 45'''

8. Este valor corresponde a mediciones hechas por Newcomb a finales del Siglo XIX. Ya se ha dicho antes que sólo las cinco primeras cifras decimales son fiables.

9. Este matemático calculó la duración del año trópico con cinco decimales exactos, lo que es asombroso para su época (ver la nota anterior). El calendario que propuso iba a inaugurar la «era Jalali», pero no se aplicó en la práctica.

y traduzcamos la fracción de día a base 60, de modo que si redondeamos a las dos primeras “cifras sexagesimales” nos quedará:

$$\text{duración del año trópico} \approx 365\text{d } 14; 33 = 365\text{d} + \frac{14}{60} + \frac{33}{60^2} = 365 \frac{97}{400}$$

lo cual explica el origen de tan curiosa fracción. No olviden Uds. que no siempre es la base diez la más útil.

El calendario Gregoriano se usa habitualmente sin mayores dificultades en la vida cotidiana. Sin embargo, a efectos científicos no es todavía lo bastante preciso, y por eso a partir del día 1 de Enero de 1972 el tiempo está dado por los relojes atómicos. A veces se oye por la radio o la televisión que hay que adelantar o atrasar un segundo los relojes para acomodar el tiempo atómico al tiempo astronómico: Esa sería una especie de versión moderna de “segundos bisiestos”.

Otras culturas no basadas en la tradición grecolatina también desarrollaron calendarios solares; tal vez el más conocido sea el de los Mayas en el antiguo México, aunque la cultura china también está bien provista de estudiosos del calendario: En fecha tan antigua como 123 D.C. el astrónomo Zhang Heng ya propuso un calendario adaptado a las estaciones, y en 1074, contemporáneo de Omar Khayyam, Shen Kua efectuó otra propuesta de calendario... Por tanto, desde aquí les invito a rebuscar en enciclopedias, viejos textos, antiguas leyendas e Internet el rastro de las investigaciones sobre el calendario.

Ya para terminar, veamos una tabla cronológica con el resumen de las principales fechas del desarrollo de los calendarios:

hace 20.000 años	Agricultura
hace 4.000 años	Medidas de la duración del año
Siglo VII A.C.	Hesiodo
Siglo V A.C.	Aristófanes, Metón
Siglo III A.C.	Euclides
año 45 A.C.	Reforma Juliana
año 325	Concilio de Nicea
año 1079	Omar Khayyam
año 1582	Reforma Gregoriana Adopción por España y Francia
año 1752	Adopción por Inglaterra ¹⁰
año 1918	Adopción por Rusia
año 1927	Adopción por Turquía
año 1972	Relojes atómicos

10. También hubo motines en Inglaterra con este motivo.

En ella se puede ver cómo el poder de los Papas, aunque grande, no lo era tanto como para obligar al mundo a adoptar la reforma Gregoriana de manera inmediata: Y es que los avances de la ciencia dependen mucho de la sensibilidad de los gobernantes para que sean reconocidos.

Y con esto, acabamos nuestro breve repaso al trabajo de los días volviendo al principio para recordar de nuevo a Hesiodo, quien define el verano con estas hermosas palabras:

Comienza la siega cuando nazcan las Pléyades engendradas por Atlas, y la siembra cuando se pongan...

MATEMÁTICAS Y BIOLOGÍA*

José Miguel Pacheco Castelao
Departamento de Matemáticas
Universidad de Las Palmas de Gran Canaria



RESUMEN. La relación entre las Matemáticas y las Ciencias de la Vida es mucho más intensa de lo que permite suponer la habitual subdivisión –en el fondo de carácter artificial– de las Ciencias. El origen de las Matemáticas está profundamente enraizado en las Ciencias de la Vida, tanto de la vida biológica como de hipotéticas vidas futuras más espirituales, que son el objeto de la Teología. El desarrollo de las Matemáticas corre parejo a la evolución de los conocimientos biológicos y de las especulaciones teológicas, produciéndose intercambios muy fructíferos en los momentos de crisis intelectuales profundas. En el momento presente existen una cantidad de disciplinas intermedias entre las Ciencias de la Vida y las Matemáticas, que representan la forma actual de ofrecer una visión global de la estructura del mundo.

1. INTRODUCCIÓN

La pregunta que surge al considerar las Matemáticas como un hecho cultural es: ¿existen razones para justificar la aparición de Matemáticas entre las actividades humanas? De ella se derivan inevitablemente otras, tales como ¿es ineludible la matematización de ciertas pautas de comportamiento? o –avanzando aún un poco más– ¿resulta una obligación hacer Matemáticas o existe libertad para ello? Ninguna de estas cuestiones es ociosa ni de fácil respuesta: Sólo la ubicación de las Matemáticas en un marco cultural nos dará la estructura formal necesaria para aventurar algunas conclusiones al respecto.

En lo que sigue intentaremos contestar a las cuestiones recién formuladas mediante la consideración de ciertos hechos culturales de primera magnitud. Comenzaremos estableciendo una definición: La cultura es el conjunto de actividades, actitudes y

* Conferencia pronunciada, en el marco del ciclo «Matemáticas y Cultura», en las Universidades de La Laguna y Las Palmas de Gran Canaria en el mes de Marzo de 1998.

comportamientos propios de una sociedad en una determinada época. Notemos que la inclusión de lo temporal en el concepto de cultura es esencial a la hora de efectuar análisis serios. En efecto, es bien conocido que en una cultura se pueden distinguir niveles de perdurabilidad: Baste como ejemplo la consideración de actitudes de tipo político –cuya vida es de naturaleza efímera, poco más que modas– frente a costumbres de la vida cotidiana que se mantienen con independencia del poder político. Esa variabilidad contribuye a la complejidad del hecho cultural, que resulta ser un compendio de datos de diferentes escalas. Para verlo, pensemos en que por lo general hablamos de “la cultura griega” o “la cultura norteamericana” como si fuesen entidades cerradas y perfectamente decantadas, olvidando que muchas de las características que creemos sobresalientes son sólo recuerdos de una cotidianidad sin pretensiones de duración.

Es casi una obviedad decir que lo más característico y duradero de la actividad humana es que se desarrolla entre seres vivos, que incluyen tanto a la humanidad como al resto de la biosfera, pues raros son los organismos que de un modo u otro no poseen interacción con el hombre; incluso, si se da un paso más allá se podrían incluir en esta constatación muchas Cosmogonías y Teologías y buena parte de los avances en Informática. Por tanto, vamos a estudiar la relación entre las Ciencias de la Vida y las Matemáticas como vehículo para intentar construir una contestación, aunque sólo sea fragmentaria, a alguna de las preguntas anteriores.

2. LOS ORÍGENES

Las manifestaciones culturales más antiguas pueden datarse en la época prehistórica cuando se desarrolla la conciencia social en los primeros grupos humanos¹, siendo la Arqueología la ciencia que se ocupa de estos asuntos. La siguiente etapa en el desarrollo cultural tiene lugar cuando algunos grupos nómadas deciden establecerse tras descubrir los rudimentos de la Agricultura y la Ganadería (conviene notar aquí que la etimología de Cultura y la de Cultivo es la misma)². En esta fase el conjunto de técnicas o saberes aplicados debió conducir muy pronto a plantear problemas que hoy reconocemos como cargados de sentido matemático: ¿Cuánto y cuándo hay que sembrar para obtener suficientes resultados? ¿Qué cantidad de terreno es necesario, o basta, para obtener una cosecha adecuada? ¿Cuántas cabezas de ganado tenemos? ¿Qué cueva es lo bastante grande para guarecerlas?, etc., etc. Estas preguntas nos conducen a pensar en la existencia de métodos intelectivos capaces de tratar los datos observados y de formular predicciones a partir de ellos. En palabras más vulgares, pero no menos precisas, asistimos a la aparición de mecanismos para contar y medir que permiten manejar informaciones de importancia fundamental para la supervivencia del grupo.

1. Véase una exposición interesantísima en Bernal, J. (1972). *Historia social de la ciencia* (2 volúmenes), Ediciones 62, Barcelona.

2. Se estima que esto ocurrió durante el Neolítico, hace entre 6.000 y 20.000 años, según zonas. Una exposición muy original y novedosa puede verse en Cavalli-Sforza, L. (1997), *Genes, Pueblos y Lenguas*, Editorial Crítica, Barcelona.

Paralelamente a lo anterior se plantea cómo transmitir esos conocimientos y habilidades —que ya llamaremos matemáticos— a generaciones posteriores. Dando por descontada la existencia de un lenguaje comunitario, no es arriesgado formular aquí una hipótesis importantísima: Las Matemáticas, en ciertas formas elementales tales como los rudimentos del contar y medir, son anteriores al lenguaje como vehículo cultural³. En efecto, la operación “establecer una correspondencia biunívoca” se realiza de manera inmediata —desde nuestro punto de vista— haciendo marcas en un palo o hueso, o nudos en una cuerda, o poniendo piedras en una olla, para contar reses o frutas. Además, uno de esos objetos —palo, hueso, cuerda, olla— pudo usarse como documento al enviar el ganado o las frutas con pastores o servidores, haciéndose el recuento final de modo parecido a como se pasan las cuentas de un rosario en los rezos de varias religiones. Y todo ello no necesita una explicación en la lengua usual, que muy posiblemente no estaría desarrollada hasta ese extremo. De todas maneras, estas técnicas sólo serían aplicadas por o entre individuos de cierta capacidad intelectual, quienes serían los encargados de preservar y transmitir esos conocimientos.

Con estas herramientas, las operaciones de sumar y restar aparecen de forma muy natural, así que los elementos fundamentales de la Aritmética se detectan ya en épocas primitivas. Sin embargo, y esto justifica la hipótesis que avanzábamos un poco antes, la expresión lingüística de las cantidades —y por tanto de las operaciones entre ellas— es en general muy pobre: La mayoría de los lenguajes primitivos que se conocen carecen de numerales, a lo más algunos de ellos distinguen entre “uno”, “dos” y “muchos”. En las lenguas evolucionadas de raíz indoeuropea se conserva todavía algo de esa confusión primitiva⁴: La raíz de “tres”; three, trois, drei, tri, etc., es la misma de “trans” (más allá). La pervivencia de duales (ambos, both, beide) en muchos idiomas modernos es un recuerdo de aquellos lejanos intentos de expresar los números con palabras. Con esto hemos mostrado, en primer lugar, que los mecanismos psicológicos de hacer Matemáticas son tremendamente primitivos, y también, que la Aritmética es uno de los rasgos ineludibles en cualquier cultura desde el momento de la aparición de las primeras comunidades humanas civilizadas. En otras palabras, el sustrato intelectual necesario para la aparición de Matemáticas pertenece a los albores de la humanidad tal como la consideramos actualmente.

El origen de la Geometría debería ser contemporáneo al de la Aritmética, y podemos considerar que reside en la necesidad práctica de determinar alineaciones para la construcción, áreas de terrenos⁵ y volúmenes de líquidos o de áridos en relación con las cosechas. Hemos de notar aquí que el concepto de proporcionalidad estaría ya en la base de la Geometría bajo la forma práctica “más terreno, más cosecha”; en cualquier caso se halla en relación con la explotación de especies cultivadas y por tanto con las Ciencias de la Vida. Sin embargo, los elementos de la Geometría son de naturaleza diferente a la de los rudimentos de la Aritmética, y su evolución de-

3. Un trabajo de gran interés y bien escrito acerca de estos problemas es Sizer, W. (1991). Mathematical notions in preliterate societies, *Math. Intell.*, 13(4), 53-60.

4. Un texto muy interesante para estas cuestiones es: Wilder, R.L. (1968). *Evolution of Mathematical Concepts*, J. Wiley & Sons, New York.

5. Por ejemplo, las inundaciones anuales del Nilo hacían desaparecer los límites de las parcelas, exigiendo un trabajo minucioso de reconstrucción.

pende de factores culturales más avanzados. La observación de que la cantidad de grano de siembra (un volumen) necesaria para un terreno (un área) dado es más o menos la misma cada temporada de cultivo nos hace comprender que muy posiblemente el concepto de volumen fue anterior al de área. Reminiscencias culturales de la prelación de volúmenes sobre áreas se hallan en las nomenclaturas muchas veces coincidentes para medidas de volumen de áridos y de extensiones de terreno que estuvieron en uso hasta hace bien pocos años en medios rurales. La introducción de medidas de carácter arbitrario basadas en el metro ha relegado ese patrimonio cultural –cuyo origen en las relaciones entre el hombre y la Naturaleza es claro– a los museos⁶. Podemos relacionar la importancia de la idea de volumen con el hecho biológico de que la visión humana es estereoscópica, un rasgo que nos emparenta lejanamente con las aves, para las que la visión tridimensional es vital.

Una cuestión más técnica y de carácter eminentemente práctico, donde la explotación de la Naturaleza tiene también un papel capital, es la introducción de los calendarios⁷. La medida del tiempo es también otra de las actividades matemáticas más antiguas y se halla relacionada con la observación de fenómenos repetitivos en la Naturaleza: Los más evidentes en las zonas templadas donde se originaron las primeras poblaciones humanas, aparte de la sucesión trivial de días y noches, son los ciclos de las estaciones y las fases de la Luna. La escala temporal de las fases de la Luna resulta muy apta para la medida del tiempo, y todavía hoy es utilizada⁸: Incluso en la cultura popular actual es corriente medir la duración de los embarazos por Lunas, lo que nos proporciona un interesante maridaje entre un hecho vital y otro astronómico.

Una observación más atenta condujo a reconocer la variación de la duración del día y su relación con las estaciones y ciertos fenómenos vitales recogidos de la actividad explotadora de la tierra. Por poner un ejemplo, se sabe que el estro de las ovejas depende de la duración del día, y lo mismo puede decirse de los ciclos reproductivos de muchas plantas, con exactitud del orden de segundos. Estos ciclos no concuerdan bien con un calendario basado en la Luna, pues ni la duración del día ni la estación del año guardan correlación con la fase lunar, así para acomodar las épocas de siembra, cosecha y otras labores agropecuarias se buscó basar el calendario en el ciclo solar, más largo y menos aparente pero más ajustado a las actividades explotadoras. De inmediato se originó la Astronomía, la observación de los astros: Las noches largas o cortas se corresponden con la aparición de ciertas constelaciones o estrellas en posiciones concretas de la bóveda celeste, posiciones que pueden ser contrastadas con algún tipo de observatorio delimitado por montañas, piedras u otros accidentes naturales o artificiales. De esta manera vemos cómo las ciencias de la vida tuvieron un papel determinante en la creación de una nueva disciplina matemática que se utilizaría más adelante no sólo en los métodos de medida del tiempo, sino como base de la Navegación y por tanto, del devenir cultural de la humanidad.

6. Un libro de obligada lectura para quienes estén interesados es: Kula W. (1980). *Las medidas y los hombres*, Editorial Siglo XXI, Madrid.

7. Véase una breve noticia acerca del calendario y las Matemáticas en: Pacheco, J. (1998). *El trabajo de los días*, *Epsilon* (en prensa).

8. Debo muchas ideas de este apartado y varias sugerencias muy interesantes a Isabel Fernández.

Los estudios antropológicos (ver por ejemplo el libro de J.D. Bernal citado en la nota 1) no revelan diferencias sustanciales entre las distintas civilizaciones en lo referente a la relación entre desarrollo cultural y matematización en los niveles señalados en el número anterior. A fin de cuentas, en todas partes se ha cultivado la tierra, se ha almacenado sus productos y se ha comerciado con ellos. La evolución posterior a este estadio presenta, por el contrario, una bifurcación muy evidente: Se produce un salto cualitativo cuando la sociedad alcanza un grado de bienestar que permite a quienes se ocupan de Matemáticas –al poder desligarse de las tareas de supervivencias cotidianas– considerar la actividad matemática como un fin en sí misma, con lo que se produce la abstracción y comienzan a aparecer resultados en principio alejados de la aplicación práctica inmediata. Sin embargo este fenómeno no se produce en todas las culturas, y en aquéllas donde se da, cuyo paradigma es para nosotros la civilización griega, se le intenta buscar también una aplicación: Ofrecer una explicación del mundo o en otras palabras, dar una visión religiosa o mística de la Naturaleza. También esto son Ciencias de la Vida, pero de otras vidas que, según los estudiosos, se hallan más allá de la comprensión habitual: Esta huella perdurará a lo largo de toda la historia de las Matemáticas y como línea de pensamiento resurgirá más adelante de la mano de uno de los mayores matemáticos de la Historia, cuando Leibniz⁹ intente explicar importantes cuestiones teológicas utilizando su recién descubierto Cálculo Infinitesimal. De cualquier forma, tras esas etapas iniciales y con orígenes comunes se extiende un larguísimo período en el que la interacción entre Matemáticas y Ciencias de la Vida disminuye de tal forma que sólo se volverá a producir un nuevo contacto fructífero y definitivo tras el paso de muchos siglos.

3. EVOLUCIONES INDEPENDIENTES Y POSTERIOR CONFLUENCIA

Las Ciencias de la Vida, a partir de las formas primitivas de Agricultura, Ganadería, Medicina, evolucionaron hacia un conjunto de saberes empíricos que varía mucho según la cultura ambiente, manteniendo en general buenas relaciones con expresiones culturales de carácter religioso o esotérico, relaciones que se mantendrán durante muchos siglos. Las Matemáticas toman mientras tanto dos caminos divergentes: Por una parte se perfeccionan los métodos de cálculo, sistemas de numeración y nociones geométricas con vistas a las aplicaciones a una vida cotidiana cada vez más compleja. Este es un fenómeno que se da sobre todo en las culturas orientales y es transmitido hacia Occidente a través de los musulmanes. Así la Arquitectura, la Agrimensura, el Comercio, la Navegación y la Astronomía son los campos donde se aplican las Matemáticas. Por otra parte, como se apuntó un poco más arriba, ya se ha producido en ciertas culturas el proceso de abstracción y se origina un cuerpo de doctrina donde el placer estético prima sobre la utilidad inmediata de los resultados. Durante muchísimos años esta vía matemática permanece estancada: Habrá que esperar a que se origine el Álgebra para encontrar un nuevo renacer de las Matemáticas puras.

9. Leibniz publicó la Teodicea en 1710.



A partir del descubrimiento y exploración –o explotación– de América, que podemos considerar una consecuencia de los avances en materia de Navegación, los caminos de las Ciencias de la Vida y de las Matemáticas volverán lentamente a converger, teniendo lugar su primer encuentro importante con las grandes expediciones científicas –las primeras actividades en verdad multidisciplinarias en el sentido actual– realizadas sobre todo a lo largo del siglo XVIII y primera mitad del XIX. He aquí unos hechos culturales de primera magnitud¹⁰ –por supuesto no ajenos a avatares políticos– donde un número relativamente pequeño de intelectuales empeñados en empresas similares produce resultados espectaculares. El cúmulo de conocimientos aportado por esas expediciones en el marco de la Botánica, la Zoología, la Antropología, etc., va a la par con los avances que propiciaron en los campos de la Astronomía, la Geodesia, la Cartografía y la Navegación, y no es aventurado suponer que durante las largas travesías se produjeran importantes intercambios de puntos de vista entre los científicos expedicionarios, lo que proporcionaría las bases para el entendimiento entre las diversas disciplinas.

A nuestro modo de ver, el primer avance palpable producido en esta confluencia cultural es la invención e introducción de una taxonomía sistemática para animales y plantas, debida en primer lugar a Linneo¹¹ y que libera a los científicos de las primitivas catalogaciones aristotélicas: De nuevo aparecen las Matemáticas en forma de uno de sus temas más profundos –el de la clasificación–, que puede rastrearse a lo largo de los siglos anteriores bajo el disfraz, ligado a la Astrología y la Adivinación, de tratar de hallar una lengua perfecta, aquélla que permite nombrar unívocamente todo lo que existe en el mundo¹². Sin conseguir este ideal, el avance que supone introducir una clasificación onomástica es de incalculable importancia: A lo largo de todo el siglo XIX se utiliza y refina la primitiva idea de Linneo aplicándola con diversas variantes¹³ a la clasificación de cualquier ser vivo y originando multitud de investigaciones originales acerca de las verdaderas características diferenciales en las que fundamentar los nombres. Y ello se debe a que es, aunque muy en el fondo, una idea verdaderamente matemática.

Tras los grandes descubrimientos geográficos y sus consecuencias, plasmadas en la extensa literatura generada por las exploraciones recién citadas, podemos observar que las relaciones entre Biología y Matemáticas se van estrechando a lo largo del XIX en un proceso imparable que continúa hasta hoy mismo. La convergencia entre ambas sigue un camino a través de otras ciencias intermedias cuyo objeto de estudio va cambiando. En efecto, las primitivas Agricultura, Ganadería, Medicina... dieron

10. Consultar, por ejemplo, Sellés, M., Peset, J., Lafuente, A. (comps.) (1988). *Carlos III y la Ciencia de la Ilustración*, Alianza Editorial, Madrid. También véase la recopilación elemental Puig-Samper, M. (1991). *Las expediciones científicas durante el Siglo XVIII*, Akal Eds., Madrid.

11. Las obras fundamentales de Linneo se publicaron en 1737 y 1753. Son, respectivamente, *Genera Plantarum* y *Species Plantarum*.

12. La aportación más interesante a este problema es la *Ars Combinatoria* de Leibniz (1666). Para una descripción muy entretenida de este problema véase Eco, U. (1994). *La búsqueda de la lengua perfecta*, Editorial Grijalbo, Barcelona.

13. Esto quiere decir que los criterios fisiológicos o morfológicos en los que se basaba la clasificación fueron variando según los avances de la Biología. Véase una exposición apasionante en el volumen 3 de la *Historia general de las ciencias*, dirigida por René Tatón (Ediciones Destino, Barcelona, 1975).

paso, tras un proceso largo y no siempre fácil desde el punto de vista cultural, a una ciencia o denominador común más conceptual que vino a conocerse con el nombre de Fisiología. Esta nueva ciencia alcanza su mayoría de edad con la invención del microscopio hacia 1680, contemporáneo, y desde luego no casualmente, del descubrimiento del Cálculo Infinitesimal. A lo largo de dos siglos, la Fisiología ve cómo su objetivo se va traduciendo primero al lenguaje de la Química –que mientras tanto evoluciona lentamente desde la Alquimia medieval a una ciencia en el sentido actual de la palabra– y posteriormente al de la Física. Pero desde la creación del Cálculo Infinitesimal la relación entre Física y Matemáticas es íntima, con un continuo trasvase de ideas y teorías desde una a otra ciencia, en un ir y venir que en los últimos tiempos ha acabado por denominarse Modelización. Por tanto, una buena comprensión de los problemas de las Ciencias de la Vida y su posterior traducción a relaciones entre ideas físicas sencillas es la base de su matematización.

El científico Lamarck empleó ya en 1800 el término Biología con su significado actual, y desde entonces se pueden detectar puentes entre esta ciencia y las Matemáticas. Las primeras formulaciones matemáticas de la dinámica de poblaciones se deben a Malthus, contemporáneo de Lamarck, y son aún el primer peldaño en cualquier intento de analizar matemáticamente la evolución de una población de seres vivos. Curiosamente esta aproximación entre Biología y Matemáticas se produce al introducir un cambio importante de punto de vista: Las poblaciones se toman como magnitudes macroscópicas, representando lo que hoy llamaríamos biomasa, y corresponden por tanto a descripciones globales de la población estudiada. Es fácil reconocer que un mínimo paso de abstracción permite incorporar el Análisis Matemático o el Álgebra para obtener los primeros pasos de la Biología Matemática.

El proceso iniciado por Malthus –y que influyó notablemente en Darwin– culminará con la creación de una nueva ciencia, la Ecología¹⁴, hija de las Matemáticas y la Biología, y cuyo potencial se está desarrollando en nuestra época del modo que todos conocemos. Este nacimiento se produce de la mano de la Teoría de la Evolución: La teoría de Darwin necesitaba, para ser completa, alguna idea de base para fundamentar en ella los principios evolutivos. Los avances en Fisiología condujeron, por un lado, a un buen conocimiento de la estructura interna de las células (visión microscópica, de nuevo); por otro, los ingeniosos experimentos macroscópicos de Mendel¹⁵ –una sistematización de antiguas prácticas agrícolas de mejora– abren la vía de la Genética, donde radica la explicación de la Evolución. Y la Evolución, considerada como resultado de la dinámica interna de conjuntos de seres vivos en interacción, proporciona la justificación para las teorías ecológicas.

El análisis de las experiencias realizadas y de muchísimas observaciones propició que figuras como Galton, Fisher y otros crearan la moderna Estadística a finales del siglo XIX. Así, el influjo de la Biología fue determinante para que un conjunto de modestas técnicas contables (Estadística viene de Estado) ligadas a las burocracias estatales pasara a ser una respetable rama de las Matemáticas.

14. El primero en usar la palabra “Ecología” con un sentido parecido al actual fue Haeckel en 1866, muy pocos años después de la publicación (1859) del Origen de las Especies de Charles Darwin.

15. Mendel publicó sus resultados en 1865 como recopilación de experiencias realizadas durante más de veinte años. Nótese la abundancia de fechas casi coincidentes, que da una idea de la ebullición en materia de Biología durante el Siglo XIX.



4. BIOLOGÍA MATEMÁTICA

Comenzaremos este apartado comentando brevemente la idea de unidad de la Ciencia. En su etimología ciencia significa conocimiento, saber, y más exactamente, poder disponer de la verdad acerca de las cosas que no son evidentes. Esa verdad se puede intentar alcanzar mediante diversos métodos o visiones teóricas y, si se queda en eso, en la búsqueda de la verdad, se suele hablar de ciencia pura. Si, por el contrario, se utiliza para obtener fines prácticos, se hablará de ciencia aplicada o práctica. Sin embargo, las fronteras no son nítidas, y cada vez lo son menos, entre ciencia pura y ciencia práctica, lo que es prueba de la unidad de la Ciencia. Otra cosa es el uso que hacen los científicos y las escuelas científicas de las verdades parciales que constituyen el patrimonio cultural real de la Ciencia: Muchas veces se utilizan como armas o como ideologías —que vienen a ser lo mismo— empleadas con fines ajenos al progreso científico y técnico. Pero eso es otra historia¹⁶.

A pesar del comentario anterior, la distancia que aún separa a las Matemáticas de la Biología sigue siendo colosal si nos atenemos a la clasificación habitual de las ciencias. Las Ciencias Biológicas utilizan básicamente como método la descripción —aunque no sólo retórica, sino apoyada en técnicas de análisis de datos—, alcanzando los aspectos deductivos y teóricos sólo a unas pocas áreas. Es más, la formulación teórica en estas ciencias se produce tras la interpretación de resultados de experimentos en cuyo diseño el azar tiene una parte importante, lo que hace que en la cadena

...⇒ experimentos ⇒ teorías ⇒ experimentos...

sea difícil distinguir si la teoría precede y dirige la concepción del experimento o al revés. En el extremo opuesto encontramos las Matemáticas, donde todo es teoría y el convencimiento o hallazgo de la verdad se produce internamente. Sin embargo la interacción a nivel conceptual existe y tiende a hacerse cada vez más patente y fructífera. Desde luego no se trata tan sólo de aplicar más o menos directamente técnicas de recogida e interpretación de datos, sino de aplicar el método de las Matemáticas para construir modelos predictivos y explicativos en los más diversos campos de la Biología. De esta manera se construye una ciencia en la que el método matemático es utilizado en la extracción de información biológica relevante. En otras palabras, ha aparecido la Biología Matemática. Vamos a realizar un paseo, corto y necesariamente sesgado, por esta nueva ciencia¹⁷.

No debe extrañarnos, por razones históricas, que un aspecto troncal de la Biología Matemática sea el análisis de la evolución de poblaciones¹⁸. La clase de entes que conforman las poblaciones puede ser muy general: Casos típicos son especies cua-

16. Pueden consultarse dos textos importantes: Easlea, B. (1977), *La liberación social y los objetivos de la ciencia*, Editorial Siglo XXI, Madrid; y Feyerabend, P. (1982), *La ciencia en una sociedad libre*, Editorial Siglo XXI, Madrid.

17. Un resumen bastante acertado puede leerse en Hoppensteadt, F. (1995), *Getting started in Mathematical Biology*, *Notices AMS*, 42(9), 969-975.

18. Véase por ejemplo el conocido texto: Edelstein-Keshet, L. (1985), *Mathematical Models in Biology*, Random House, New York.

lesquiera de seres vivos, pero también puede aplicarse esta idea a moléculas, enzimas, genes, grupos de neuronas o de fibras musculares... Además, muchas de las técnicas y métodos de la teoría de poblaciones se pueden adaptar y utilizar provechosamente en otros campos.

En la situación más simple posible se considera una única población, siendo las cuestiones interesantes básicamente dos: Análisis de la evolución del tamaño poblacional y estudio de las distribuciones espacial y por edades de los elementos que la conforman. Ambos problemas pueden tratarse considerando la población aisladamente o sometida a influjos externos, de manera que tanto en un caso como en otro se incorporan en la descripción matemática términos o condiciones especiales que en su conjunto forman lo que conocemos como modelo matemático. La herramienta matemática esencial en el campo de la dinámica de poblaciones son los Sistemas Dinámicos, una teoría que describe el comportamiento evolutivo

$$P(t) \rightarrow P(t+h) = F(P(t),v)$$

siendo v un vector de parámetros adecuado (en cuya determinación práctica son esenciales las técnicas estadísticas), a partir de una población inicial $P(0)$. El incremento h puede considerarse discreto, lo que origina sistemas dinámicos discretos, o tomarse como un infinitésimo, dando así lugar a sistemas dinámicos descritos por ecuaciones diferenciales –ordinarias en este caso– siendo ésta, con mucho, la manera más habitual de trabajar en Biología Matemática. Conviene recordar aquí que el modelo básico de evolución de una población es la formulación malthusiana

$$\frac{dP}{dt} = kP, P(0) = P_0$$

donde k es una medida de la tasa específica de crecimiento y puede adquirir diversas formas: Así, si es una constante positiva, se tiene el crecimiento malthusiano, y si se permite que varíe con la propia población P , esto es, $k=k(P)$, se pueden reflejar comportamientos más realistas o complejos. El caso más relevante es cuando $k(P) = r(1-P/C)$, siendo C una capacidad límite para la población: Tenemos así otro clásico de estos temas, el problema logístico:

$$\frac{dP}{dt} = r\left(1 - \frac{P}{C}\right)P, P(0)=P_0$$

que es uno de los pilares teóricos –justificado experimentalmente por multitud de observaciones– de la dinámica de poblaciones¹⁹.

Para introducir la variabilidad espacial y la estructura de edad basta con que elijamos la descripción $P(t,x,a) =$ Biomasa (o densidad de ella) presente en el instante t , en la localización espacial x y con la edad a , de manera que las variaciones de P

19. Esta ecuación diferencial fue formulada por Verhulst, otro de los padres de la Ecología, hacia 1850.

según cada una de las variables se expresan mediante las derivadas parciales correspondientes. Un problema típico de esta clase es el estudio de la aparición de oleadas de información genética que fue modelizado por Fisher y Kolmogorov a finales de los años treinta mediante la conocida ecuación de Fisher

$$\frac{\partial P}{\partial t} = P(1-P) + D \frac{\partial^2 P}{\partial x^2}$$

que es un ejemplo prototípico de las llamadas ecuaciones de reacción difusión.

Una rama muy importante de la Economía, conocida como Bioeconomía Matemática, tuvo su origen en el estudio de casos particulares de una única población provenientes del campo de las pesquerías²⁰ y se ha desarrollado en un ámbito propio de la investigación a caballo entre las Matemáticas, la Biología y la Economía. La mayor parte de los problemas ecológicos, cuando afectan al desarrollo de poblaciones humanas, deben ser tratados en el marco de esta ciencia.

La riqueza del estudio crece enormemente cuando se consideran varias poblaciones en interacción, pues las pautas de interrelación llevan, al intentar modelizarlas, a formulaciones de mucha mayor complejidad que ponen a prueba el ingenio y capacidad creativa de los matemáticos. La ayuda de la Informática y los ordenadores es muy valiosa en los últimos avances en este campo, aunque la descripción matemática de estos problemas constituye uno de los cuerpos de doctrina clásicos en Matemáticas Aplicadas desde hace unos ochenta años. En su versión más primitiva debida a Lotka²¹ y Volterra, dada una población formada por n especies en interacción X_1, X_2, \dots, X_n , homogéneamente distribuidas, la dinámica conjunta se describe mediante el problema de valores iniciales

$$\frac{dX_i}{dt} = X_i F_i(X_1, \dots, X_n), \quad i=1, \dots, n$$

$$X_i(0) = X_{i0}, \quad i=1, \dots, n$$

donde $F_i(X_1, \dots, X_n) = a_{i1}X_1 + \dots + a_{in}X_n$, siendo los coeficientes a_{ij} constantes de signo cualquiera. Lo interesante es que el signo nos indica si la interacción es favorable (positivo) o desfavorable para la especie. Esta manera de representar la interacción biológica está tomada de la teoría de las reacciones químicas, donde se conoce con el nombre de principio de acción de masas. Otras formas de interacción matemáticamente más complicadas permiten simular diversas situaciones observadas dando lugar a modelos más realistas, esto es, que describen mejor las observaciones. Los casos $n=2$, $n=3$ son los más estudiados, sobre todo porque se hallan a ambos lados de una

20. El texto original es Clar, C.W. (1976), *Mathematical Bioeconomics*, Wiley, New York. Hay varias ediciones posteriores.

21. El texto básico es Lotka, A. (1924), *Elements of Mathematical Biology*, Editorial Dover, New York, 1956. La formulación actual está desarrollada en Volterra, V. (1932), *Léçons sur la théorie mathématique de la lutte pour la vie*, Gauthier-Villars, Paris.

frontera cualitativamente importante, la que separa los sistemas con posible comportamiento caótico ($n \geq 3$) de aquéllos en los que es imposible ($n=2$). La razón profunda de esta división es de carácter topológico y es una consecuencia del Teorema de la Curva Cerrada de Jordan, conocida como Teorema de Poincaré-Bendixson²².

En todo caso, la relación entre Biología y Matemáticas queda reflejada en dos aspectos concretos: En primer lugar, se expresan hechos biológicos en lenguaje formalizado, y en segundo lugar, la aplicación del método matemático a esas formalizaciones permite obtener resultados que después se utilizan para ayudar a interpretar la realidad biológica o para descubrir nuevos aspectos que habrían escapado a los análisis emprendidos con los métodos tradicionales de la Biología. Una parte importante de la Biología Matemática, la dedicada a las cuestiones de base tales como la transmisión de la información genética –y por tanto a desentrañar qué es la vida– se conoce como Biología Teórica²³, y en ella se intenta con una matematización a ultranza penetrar los todavía oscuros orígenes de la vida. Recordemos que la intuición genial de Watson y Crick²⁴, aparte del trabajo experimental correspondiente, consistió en formular un modelo geométrico previo al cual resultó adecuarse la estructura del ADN.

La introducción de la distribución espacial en los modelos de poblaciones, combinada con la observación acerca de la Biología Teórica, nos conduce a uno de los campos más interesantes y activos de la Biología Matemática²⁵. Hemos señalado antes que la evolución conjunta de n poblaciones homogéneamente distribuidas se puede representar con un sistema de ecuaciones diferenciales ordinarias

$$\frac{dX_i}{dt} = G_i(X_1, \dots, X_n), \quad i=1, \dots, n$$

junto con las condiciones iniciales $X_i(0)=X_{i0}$ que especifican el estado inicial del conjunto. La homogeneidad espacial es una simplificación excesiva, pues la Naturaleza se presenta raras veces de modo uniforme; más bien lo que caracteriza al mundo vivo es la extraordinaria complejidad de su aspecto externo, apareciendo a nuestra observación con una gran riqueza de formas o pautas de ordenación espacial. Se puede indagar en este problema, conocido como problema de la Morfogénesis²⁶, sus-

22. Consúltase el capítulo correspondiente en Hofbauer, J., Sigmund, K. (1988), *The theory of evolution and dynamical systems*, Cambridge U.P. El comportamiento caótico puede presentarse también en dimensión uno cuando se consideran sistemas dinámicos discretos. Véase el trabajo ya clásico: May, R. (1975), *Biological populations obeying difference equations, stable points, stable cycles and chaos*, *J. Theor. Biology*, 51, 511-524. Una exposición buena, aunque echada a perder por una traducción pésima, es Nicolis, G., Prigogine, I. (1994), *La estructura de lo complejo*, Alianza Editorial, Madrid.

23. Para tener una idea de los temas básicos de esta ciencia, aunque es un tanto anticuado, ver Waddington, C. (ed.) (1976), *Hacia una Biología Teórica*, Alianza Editorial, Madrid.

24. Se puede leer un interesante relato en el libro autobiográfico: Crick, F. (1989), *¡Qué loco propósito!*, Tusquets Editores, Barcelona.

25. Ver Murray, J. (1989), *Mathematical Biology*, Springer, Berlin. El grueso de este muy grueso y muy fundamental volumen está dedicado a la aplicación de ecuaciones de reacción difusión a muy diferentes campos de la Biología.

26. Puede consultarse un resumen de estas cuestiones en: Pacheco, J. (1997), *Sobre el problema de la Morfogénesis*, Conferencia pronunciada en la U. de La Laguna (inérito) y referencias citadas allí.



tituyendo las ecuaciones anteriores por una modificación de ellas que incluya términos de variabilidad espacial: Lo más corriente es añadir términos que se interpretan como difusión o dispersión –en sentido estricto estos son conceptos con diferentes orígenes e interpretaciones– de las respectivas especies por el espacio, con lo que se obtiene, considerando ahora que $X_i = X_i(t, x)$ se halla definida en un cierto conjunto espacio-temporal $\Omega \times [0, T]$ (usando en este caso una versión matemática muy simple de la idea de difusión) que:

$$\frac{\partial X_i}{\partial t} = G_i(X_1, \dots, X_n) + \text{div}[D_i(x, t) \text{grad} X_i], \quad i=1, \dots, n$$

más las condiciones iniciales $X_i(0, x) = X_{i0}(x)$ como en el caso espacialmente homogéneo, y ahora también las condiciones que rigen al comportamiento de las poblaciones en la frontera $\partial\Omega$ del recinto espacial que se considere. Estas pueden ser de diferentes clases según lo que se desee representar. Lo más habitual es suponer un recinto cerrado a través de cuya frontera se producen intercambios, lo que se expresa generalmente con condiciones del tipo

$$\frac{\partial X_i}{\partial n} = f_i(t, x),$$

donde n representa la normal a $\partial\Omega$. La variedad de pautas espaciales que pueden describirse con este simple expediente es enorme, y puede aplicarse a multitud de campos tanto dentro como fuera de la Biología. Por citar sólo unos pocos de estos últimos, tenemos: ritmos circadianos, aparición de oleadas migratorias, control de plagas, activación de la mitosis, el origen de las manchas en la piel de los animales, las agregaciones tales como cardúmenes de peces y bandadas de aves, las conexiones interneuronales, los mecanismos de ubicación y desarrollo de las extremidades y órganos de los embriones... para todos los cuales una representación basada en ecuaciones de reacción difusión ofrece explicaciones muy plausibles. Notemos que se puede aplicar tanto a problemas macroscópicos –ecología de poblaciones– como a otros de carácter microscópico relacionados, como se ha señalado antes, con los aspectos fundamentales de la Biología.

Para completar este apartado ofrecemos un reflexión sobre una cuestión que mantiene un interés permanente. Una de las amenazas más preocupantes para la Humanidad a lo largo de los siglos han sido las enfermedades epidémicas. La literatura mundial, desde la Biblia hasta hoy mismo, está llena de textos cuyo tema principal tiene que ver con tales desgracias: Ello nos da una idea de la importancia cultural de las catástrofes naturales, que han dejado su huella en las religiones, las costumbres y la ciencia. Grandes esfuerzos científicos, en los más diversos campos, se han dedicado al estudio de cómo aparecen, cómo pueden prevenirse o incluso de cómo erradicarlas (al menos en el caso de la viruela, todo parece indicar que se ha conseguido eliminarla, lo cual ha planteado después problemas éticos muy interesantes).

Por supuesto, una parte no desdeñable de la Biología Matemática se ocupa desde hace tiempo²⁷ también de aportar conocimientos sobre la dinámica de las epidemias, teniendo en los últimos tiempos al SIDA como objetivo fundamental por la enorme velocidad de su propagación y extensión espacial, así como la relativa impotencia de la Medicina y la Farmacología para hacer frente a esta plaga. Es ésta un área en continuo desarrollo y donde los esfuerzos combinados de muchas ciencias producen resultados muy interesantes, no sólo por su utilidad práctica inmediata sino por la profundidad de las investigaciones realizadas²⁸. Las técnicas matemáticas que más se acomodan con estos problemas –y han evolucionado en contacto con ellos– son la Estadística Multivariante y la teoría de Procesos Estocásticos, aunque las ideas que inspiraron los primeros estudios teóricos sobre epidemias a finales de los años 20 –no muy alejadas de las que sirvieron para formular la dinámica de poblaciones– siguen siendo utilizadas y refinadas continuamente.

Ya para terminar este apartado volvamos por un momento a los problemas de la vida trascendente, objeto de la Teología, que habíamos dejado atrás con Leibniz. Siguiendo con la misma línea de pensamiento podríamos preguntarnos, extendiendo el paralelismo entre las dos clases de vida que hemos comentado, si existe algo como la Teología Matemática.

La utilización del método matemático en estudios teológicos y humanísticos no es nueva, pues desde la recuperación de Aristóteles por Santo Tomás de Aquino²⁹ se puede considerar que existe una notable matematización del razonamiento sobre estos temas. Evidentemente, es imposible olvidar aquí el Tratado de Ética³⁰ de Baruch Spinoza, cuyo método de exposición sigue los principios de los Elementos de Euclides. Contemporáneos suyos son los Discursos de Metafísica (1686), que junto con la Teodicea, ya citadas antes, culminan los trabajos no puramente matemáticos de Leibniz.

La diferencia esencial entre los estudios acerca de ambos tipos de vida radica en que, al menos con los mecanismos de que disponemos, no nos es posible efectuar experimentos acerca de la vida trascendente del mismo modo que se pueden observar y reproducir aspectos de la Naturaleza en el laboratorio. Por tanto, la investigación teológica está basada, en primer lugar, en la fe y en segundo, en la búsqueda de evidencias indirectas. Un libro –muy popular hace algunos años– del teólogo alemán Hans Küng, titulado *¿Existe Dios?*, dedicaba larguísima pasajes a la historia de la ciencia y ponía especial énfasis en cuestiones matemáticas de base, indicio cierto de lo que acabamos de señalar. La polvareda –bien es cierto que con una cierta dosis

27. El trabajo pionero, contemporáneo de los de Lotka y Volterra es: Kermack, W., McKendrick, A. (1927). Contributions to the mathematical theory of epidemics, Proc. Roy. Soc. Edin., A115, 700-721. La época entre 1920 y 1950 se ha conocido a veces como la "Edad de oro de la Ecología Teórica". Véase la recopilación siguiente: Scudo, F., Ziegler, J. (1978). The golden age of Theoretical Ecology: 1923-1940, Lecture Notes in Biomathematics, 22, Springer, Berlin.

28. Una exposición muy clara y entretenida sobre el SIDA y la dinámica de sus tratamientos se puede consultar en Kirschner, D. (1996). Using Mathematics to understand HIV immune Dynamics, Notices AMS, 43(2), 191-202.

29. La Summa apareció en 1267.

30. *Ethica more geometrico demonstrata*, publicada en 1675. Hay una edición española muy asequible de la Editora Nacional.

de propaganda— que en su día desató el físico teórico Stephen Hawking³¹ con la conclusión de que Dios no es necesario para la existencia del Universo es señal de que se alcanzan terrenos movedizos. Muchas otras técnicas matemáticas se han empleado en los últimos años en la indagación teológica. Por ejemplo la Teoría de Juegos se ha utilizado para establecer criterios³² sobre cómo son y cómo se reconocen los Seres Superiores, y, ya para especialistas, se publicó hace un par de años un voluminoso texto³³ en el que se demuestra no sólo que existe vida futura sino que también se compara ésta con la prometida por las diversas religiones, todo ello en más de 600 páginas de deducciones y teoremas basados en los principios de la Física y los fundamentos de las Matemáticas.

Queda, pues, abierta la cuestión de si la Teología es matematizable y en caso de serlo, cuáles serían las Matemáticas más adecuadas para ello. Sí se puede afirmar que los tipos de problemas que se tratan en los textos recién citados remiten con insistencia a las cuestiones de base y de Fundamentos de las Matemáticas que hoy día se hallan más bien ya en los dominios de la Informática teórica, tales como la computabilidad, la complejidad algorítmica, la simulación del comportamiento del cerebro...

Vemos, pues, que de la mano de la Informática estos temas nos llevan de nuevo al estudio³⁴ de la estructura del cerebro humano, en otras palabras, regresamos a la Biología. Así podemos formularnos la siguiente pregunta:

5. ¿MATEMÁTICAS BIOLÓGICAS?

Hasta aquí el motivo conductor de la exposición ha sido cómo las Matemáticas han ayudado al avance de la Biología. Podría parecer, por tanto, que la situación contraria o bien es imposible o su importancia es mínima. Sin embargo, a lo largo de la Historia de las Matemáticas se han dado múltiples intentos de utilizar conocimientos de otras ciencias en la exploración de nuevos resultados y teoremas: Por citar dos casos muy conocidos, tenemos los experimentos —recordemos el caso de la corona de falso oro— de Arquímedes y las experiencias de Klein³⁵ con circuitos eléctricos para establecer ciertos resultados en el Análisis Complejo, que son ejemplos de aplicación de la Física a las Matemáticas.

Tal como muestra el ejemplo de Klein, la aplicación de otras ciencias a las Matemáticas depende en gran medida de avances conceptuales en esas ciencias y del de-

31. Fue muy popular a finales de los ochenta el libro: Hawking, S. (1988), *Historia del tiempo*, Editorial Crítica, Madrid.

32. Un libro muy curioso es Brams, S. (1983), *Superior Beings: If they exist, how would we know?*, Springer, Berlin.

33. Ver Tipler, F. (1996), *La Física de la inmortalidad*, Alianza Editorial Madrid. Tipler es el autor de conocidos textos de Física General de nivel elemental, muy extendidos en nuestro país.

34. En torno a estas ideas pueden consultarse los dos libros de Roger Penrose: *La nueva mente del Emperador* (1991), Editorial Mondadori, Madrid, y *Las sombras de la mente* (1996), Editorial Crítica, Madrid. En esencia Penrose mantiene que no será posible que una máquina pueda desarrollar razonamientos, esto es, está en contra de la "Inteligencia Artificial Fuerte".

35. Ver, por ejemplo, Klein, F. (1893), *On Riemann's theory of algebraic integrals and their integrals*, Editorial Dover, 1963, New York.

sarrollo de las tecnologías que hacen posible la manipulación de entidades físicas de diversas clases. La expansión imparable de la Biología Molecular y el refinamiento de sus técnicas de trabajo han propiciado en los últimos años el poder establecer con claridad ciertas analogías que permiten “hacer Matemáticas” con materiales y métodos biológicos, obteniendo resultados hasta ahora considerados como puramente matemáticos. De esta forma podríamos hablar de Matemáticas Biológicas, lo que tiene una indudable importancia no sólo a efectos prácticos, sino también visto desde una perspectiva cultural: Ello supondría un paso muy notable hacia la unidad de las ciencias.

La analogía que se ha revelado de capital importancia para establecer una conexión entre Biología y Matemáticas se expresa muy sencillamente diciendo sin precisión³⁶ que “lo complejo puede construirse mediante reiteración de operaciones sencillas”. Así pues, en términos biológicos un ser vivo es una estructura muy compleja, pero puede considerarse como el resultado de aplicar unas pocas operaciones tales como cortar, restringir, recombinar, etc. a las informaciones contenidas en una cadena de ADN. Por otro lado, en Matemáticas el resultado de aplicar una función computable a un argumento se obtiene aplicando una combinación de funciones elementales. La analogía se transforma en una técnica operativa cuando se utilizan cadenas de ADN como codificadores de información, de modo que mediante diversos enzimas se pueden llevar a cabo cálculos simples con las cadenas. En 1994 se consiguió probar mediante esta técnica un caso particular del Problema del Camino Hamiltoniano Dirigido. Este problema se refiere a la existencia, en un grafo G donde se hayan señalado un vértice V_e de entrada y otro vértice V_s de salida, de una sucesión de aristas a_1, a_2, \dots, a_k , “de sentido único”, que unan el vértice de entrada con el de salida pasando sólo una vez por todos los vértices del grafo. El autor del resultado, Leonard Adleman³⁷, diseñó un algoritmo aleatorio que fue realizado paso a paso implementándolos como operaciones con diferentes cadenas de ADN. Lo más importante de todo es que el Problema del Camino Hamiltoniano es un problema de los que se conocen como NP-completos, esto es de la categoría más difícil posible³⁸, lo que abrió la vía al estudio de otros problemas NP-completos con estos métodos.

Para darnos una idea de las diferencias físicas entre un ordenador de ADN y otro convencional, se estima que, por unidad de energía, un superordenador ejecuta unas 10^9 operaciones/julio, mientras que una máquina biológica podría efectuar 2×10^{19} operaciones/julio, con una capacidad de almacenamiento de memoria de 1 bit/nm³, siendo la capacidad actual de memoria de los ordenadores de 1 bit/ 10^{12} nm³. No debería resultarnos extraño que en algún futuro no lejano vuelvan las Ciencias de la Vida y las Matemáticas a un camino común.

36. Véase Kari, L. (1997), DNA Computing, Arrival of Biological Mathematics, Math. Intell., 19(2), 9-22.

37. Adleman, L. (1994), Molecular computation of solutions to combinatorial problems, Science 266, 1021-1024.

38. NP quiere decir “no polinómico”, y se refiere a que el tiempo que necesita el algoritmo que resuelve el problema no está acotado por un polinomio en una variable, siendo esta variable el tamaño de la descripción del problema. NP-completo significa que cualquier otro problema NP se puede llevar a él en tiempo polinómico. Los programas que corren en tiempo polinómico se llaman “eficientes”.



6. CONCLUSIONES

Para terminar vamos a extraer algunas conclusiones. Hemos efectuado una revisión histórica de las relaciones entre dos aspectos culturales omnipresentes: Las Ciencias de la Vida y las Matemáticas, observando que se puede considerar el origen de las Matemáticas ligado a los primeros pasos en el estudio y utilización de la Naturaleza. También se ha puesto de relieve que los avances en Matemáticas siempre se han utilizado como herramientas de progreso en las Ciencias de la Vida y que muchos problemas originados en este campo han sido decisivos en la creación de disciplinas matemáticas. Señalamos también que la imparable evolución de la Biología puede influir de manera aún no cuantificable en las Matemáticas futuras. Más aún, esta última observación es un argumento de peso para apoyar la idea de que la Ciencia (el Conocimiento, con mayúsculas) es única.

Concluimos ya con dos citas que deben hacernos reflexionar acerca de lo poco que aún sabemos de la Naturaleza y de lo endeble de nuestros métodos de aproximación a ese conocimiento. La primera nos muestra que las Matemáticas, en su relación con la Biología y con otras ciencias o actividades culturales, deben utilizarse con modestia y que son sólo un método, una mayéutica en sentido socrático. Se debe al estadístico S. Karlin³⁹ y dice así:

“The purpose of models is not to fit the data, but to sharpen the questions”

Debemos entender aquí que “models” significa exactamente “lo que las Matemáticas fabrican”, y que su utilidad es ayudar a que los científicos –de todos los campos– nos hagamos preguntas más pertinentes y agudas sobre la realidad.

La segunda son las primeras frases de un trabajo clásico tan citado como poco leído⁴⁰ del conocido matemático inglés Alan Turing. Este original artículo está en la base de la moderna Biología Matemática y su comienzo dice así:

“In this section a mathematical model of the growing embryo will be described. This model will be a simplification and an idealization, and consequently a falsification”.

Es importantísimo notar aquí la fuerza de la palabra “falsificación”: Lo que hace el científico (en este caso, el matemático) es falsificar⁴¹ o utilizar una visión distorsionada –aunque sólo sea un poco– de la realidad para poder entenderla. En suma, el científico es una especie de ilusionista⁴² que pretende, con su método y su lenguaje, convencer a sus oyentes de que existen razones suficientes para que le crean⁴³. Y todo ello, esos engaños conscientes, forman parte de todas las culturas. Así

39. Karlin, S. (1983), en el undécimo memorial de R.A. Fisher de la Royal Society.

40. Turing, A. (1952), *The chemical basis of Morphogenesis*, *Phil. Trans. Roy. Soc. London*, B237, 37-72.

41. En inglés “falsificación” no tiene el significado tan peyorativo como en castellano su equivalente “falsificación”. Más bien su traducción, libre de ese sentido, sería “distorsión” o “visión distorsionada”.

42. Véase una indagación sobre esa idea en el texto, ya citado anteriormente: Pacheco, J. (1997), *Sobre el problema de la Morfogénesis*, Conferencia pronunciada en la U. de La Laguna (inédito).

43. No me resisto a citar aquí dos textos deliciosos que avalan notablemente lo dicho: El primero es el

pues, parece que la contestación a la pregunta con que iniciábamos nuestra exposición deben ser afirmativa: Hay razones, y posiblemente la más importante sea el placer de la ensoñación en un cierto poder, para que las Matemáticas aparezcan entre las actividades culturales humanas. Una vez aceptado esto, el hacer Matemáticas debe ser una opción libre.

Con relación a esa libertad, recordemos antes de acabar que el gran Hilbert, refiriéndose a Cantor y al amplio dominio de los números transfinitos descubierto por éste, afirmaba que “Das Wesen der Mathematik ist Freiheit”⁴⁴. Y, como ciudadanos de ese país libre que son las Matemáticas, nos despedimos. Muchas gracias.



archiconocido libro de Sir D'Arcy Thompson (1917), *On growth and form* (La edición habitual es la abreviada de Cambridge University Press. Hay traducción al español en la Editorial Blume). El otro es Cook, T. (1914), *The curves of life*, Edición Dover de 1979, sobre la importancia de las espirales en la Naturaleza.

44. Literalmente la frase dice “La esencia de las Matemáticas es [la] libertad”. Aparece en un apéndice titulado “Über das Unendliche”, en la edición de 1931 de los *Grundlagen der Geometrie* (Teubner, Berlin). En ediciones posteriores Hilbert eliminó este apéndice. La frase exacta de Cantor es “Das Wesen der Mathematik liegt in inhre Freiheit”, esto es “La esencia de las Matemáticas radica en su libertad”. No he encontrado la referencia de Cantor, aunque prefiero, por fuerza expresiva, la cita de Hilbert. Debo estas informaciones y muy agudos comentarios sobre ellas a mi antiguo maestro el Prof. Cuesta (1907-1989), de la Universidad de Salamanca.

Population biology of the common pandora *Pagellus erythrinus* (Pisces: Sparidae) off the Canary Islands

J.G. Pajuelo*, J.M. Lorenzo

Departamento de Biología, Universidad de Las Palmas de Gran Canaria, Campus Universitario de Tafira,
35017 Las Palmas de Gran Canaria, Spain

Received 17 June 1997; accepted 22 March 1998

Abstract

Common pandora *Pagellus erythrinus* ($N=957$) were caught off the Canary Islands from January 1991 to September 1993. Total length ranged from 75 to 371 mm. The species was characterized by protogynous hermaphroditism. The overall ratio of males to females was 1 : 2.63. The reproductive season extended from April to September, with a peak in spawning activity in June–July. Fifty percent maturity was reached at 174 mm total length by females and 232 mm by males. The length–weight relationship for all individuals was described by the following parameters: $a=0.01279$ and $b=3.01338$. Fish aged 0–10 years were found. The von Bertalanffy growth parameters for the whole population were: $L_{\infty}=417.8$ mm, $k=0.205$ year⁻¹ and $t_0=-0.550$ year. Growth parameters differed between males and females. For all fish, the rates of mortality were: $Z=1.06$, $M=0.30$ and $F=0.76$, and the exploitation ratio $E=0.71$. The length at first capture for all individuals was 155 mm. The stock is being heavily exploited. Measures such as closed season or changes in fishing pattern would be desirable to safeguard the spawning stock and the recruits. © 1998 Elsevier Science B.V. All rights reserved.

Keywords: Common pandora (*Pagellus erythrinus*); Population biology; Canary Islands

1. Introduction

The common pandora (*Pagellus erythrinus*) (Linnaeus, 1758) is a demersal marine fish distributed along the European and African coasts of the Atlantic Ocean, from Norway to Angola, and around the Sao Tomé-Príncipe and Canary Islands. It is also present in the Mediterranean and Black seas (Bauchot and Hurteau, 1986; Mytilinéou, 1989).

In the Canary Islands, *P. erythrinus* is of a great commercial interest. It is common in the small-scale

fishery, contributing $\approx 16\%$ of the total catches of demersal fish (Pajuelo and Lorenzo, 1995), and is captured all year round with significant seasonal differences in the landings. The common pandora is exploited in this area with traps and longlines. In the Canary archipelago, where a conservation legislation on fisheries exists, a minimum size limit has been implemented for the species (220 mm TL).

Despite its fishing importance, no information on the Canary Islands common pandora population has been published. The present study fills that gap with information on sex, reproduction, age and growth, and mortality. The importance of this study is enhanced by the fact that catches of this species are declining and

*Corresponding author. Tel.: 0034 28 452903; fax: 0034 28 452922.

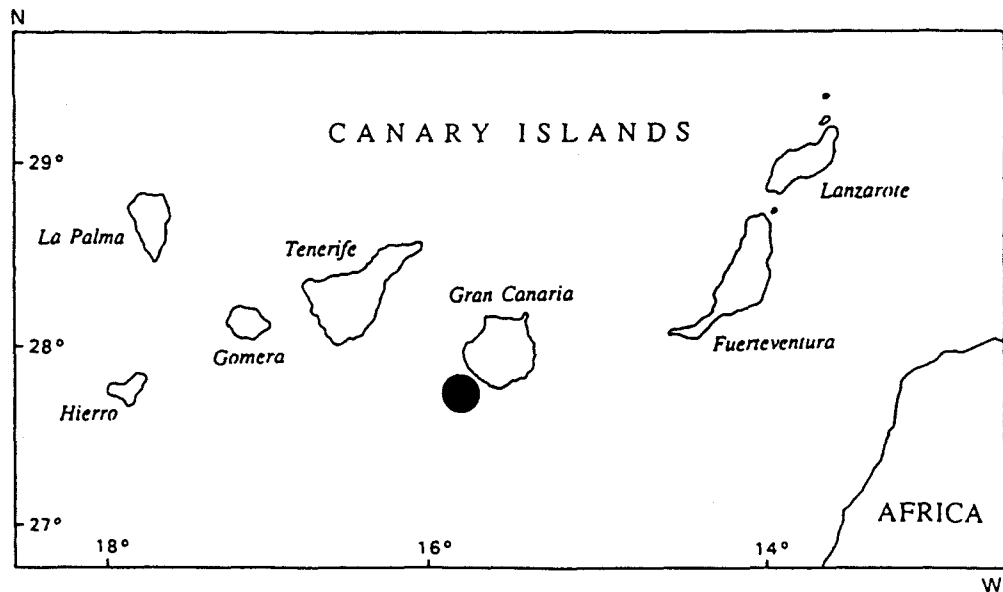


Fig. 1. Location of sampling area.

the fishing effort on it is increasing in the area (Pajuelo and Lorenzo, 1995).

2. Materials and methods

A total of 957 specimens of common pandora were obtained by a random stratified method from commercial catches at different fishing ports of the Gran Canaria Island (Fig. 1) between January 1991 and September 1993. Fish were caught with traps and longlines at depths of 12–136 m. Furthermore, 61 juveniles were collected by experimental trawl nets at depths of 0–30 m.

For each fish, the total length (TL) was measured to the mm and total weight (TW) to the 0.1 g. Sex and maturity stages were then determined macroscopically and weight of the gonads (GW) was recorded to the 0.01 g. Stages of maturation were classified as follows: I, immature; II, resting; III, ripe; IV, running ripe; and V, spent. Otoliths (sagittae) were removed from 527 individuals, cleaned and stored.

The sex-ratio of the sampled population was analyzed by size interval. The spawning season was determined following the monthly changes of the gonadosomatic index (GSI), calculated as follows (Anderson and Gutreuter, 1983):

$$\text{GSI} = 100 \text{ GW/TW}.$$

For the estimation of the mean lengths at 50% maturity, a logistic function was fitted to the proportion of the mature individuals by size class using a non-linear regression. The function used was (Saila et al., 1988):

$$P = a / \{1 + [(a - b)/b][e^{(-cl)}]\},$$

where P is the proportion of mature individuals in each size interval, and l the mean length of the interval, and a , b , and c the parameters to be estimated.

The relation of total weight to total length was calculated applying the exponential regression equation (Ricker, 1973):

$$\text{TW} = a\text{TL}^b,$$

where a and b are the parameters to be estimated. Age was determined by reading otoliths. The otoliths were embedded in a plastic resin and thin sections (0.5 mm) cut (Bedford, 1983). An index of average percent error (APE) developed by Beamish and Fournier (1981) was used to compare the accuracy of age determinations. Ageing was validated by examination of monthly changes in appearance of the edges of the otoliths (Morales-Nin, 1987). The von Bertalanffy growth curve was fitted to the observed length at age data of the resulting age-length key by means of a Marquardt's algorithm for non-linear least-squares para-

meter estimation (Saila et al., 1988). The form of the growth curve is (Beverton and Holt, 1957):

$$L_t = L_\infty(1 - e^{-k(t-t_0)}),$$

where L_t is the fish length at time t (year), L_∞ the asymptotic length to which fish tend to grow, k the growth coefficient, and t_0 the hypothetical time when fish length is zero.

Length frequency data of the catches (28 342 fish) were converted to age frequency using the von Bertalanffy growth parameters (Pauly, 1983). The total mortality rate (Z) was calculated from the length-converted catch curve using the program ELEFAN (Gayanilo et al., 1988). The equation employed was:

$$\log_e(N/dt) = a + bt,$$

where dt is the time needed to grow from the lower to the upper limit of a given length class, t the relative age corresponding to the midrange of the length class in question, and a and b the parameters to estimate. The natural mortality rate (M) was estimated from the equation of Tanaka (1960):

$$M = 3/T_{\max},$$

where T_{\max} is the age of the oldest fish sampled. Following estimation of Z and M , the fishing mortality rate (F) was estimated from:

$$F = Z - M,$$

and the exploitation ratio (E) from:

$$E = F/Z.$$

The length at first capture was determined from the selection ogive generated from the length-converted catch curve (Pauly, 1983).

Sea surface temperature data obtained from the meteorological station of Mogán (southwest Gran Canaria) were used to relate spawning seasonality and formation of growth rings on the otoliths to water temperature.

3. Results

3.1. Reproduction

Of the fish examined, 206 were males, 542 females and 61 hermaphrodites. The sex of the remaining 148

fish could not be determined macroscopically. Male gonads had residues of degenerated ovarian tissue.

The overall ratio of males to females was 1 : 2.63 and χ^2 analysis showed this to be significant ($\chi^2 \equiv 150.93 > \chi_{1,0.05}^2 = 3.84$). Females predominated in smaller size intervals and males in larger (Fig. 2). Hermaphrodites made up 6.4% of the specimens examined and were intermediate in size between females and males. Sex-ratios between males and females by size intervals had significant departures from 1 : 1 ratio ($\chi^2 > \chi_{1,0.05}^2 = 3.84$) for most size categories, except for the middle size groups (260–280 mm TL).

The GSI values of females were usually higher than those of males (Fig. 3). However, both indices followed the same pattern. The highest values occurred between April and September, with a maximum in June–July.

The parameters of sexual maturity ogive for males, females and all fish are given in Table 1. The total length at which 50% maturity is reached was 174 mm for females and 232 mm for males. There was a significant difference in length at 50% maturity between sexes (t -test, $t=13.21 > t_{0.05,746}=1.65$).

3.2. Age and growth

Fish ranged in size from 75 to 371 mm, weighing between 6.1 and 747.1 g. Males ranged from 187 to 371 mm in length and from 86.3 to 747.1 g in weight. Length of females ranged between 128 and 332 mm and weight between 11.3 and 623.4 g. Hermaphrodites ranged in size from 212 to 348 mm, weighing from 121.2 to 531.1 g.

Length–weight regression parameters for males, females and all individuals are presented in Table 2. Significant difference in the allometric coefficient was found between males and females (t -test, $t=5.09$

Table 1
Parameters of the sexual maturity ogive ($P=a/[1\{(a-b)/b\} [e^{-cL}]]$) for males, females and all individuals of *P. erythrinus* off the Canary Islands

	a	b	c	r^2
Males	103.1	0.000000297	0.845	0.991
Females	100.4	0.006951000	0.550	0.988
All fish	100.9	0.005822100	0.573	0.983

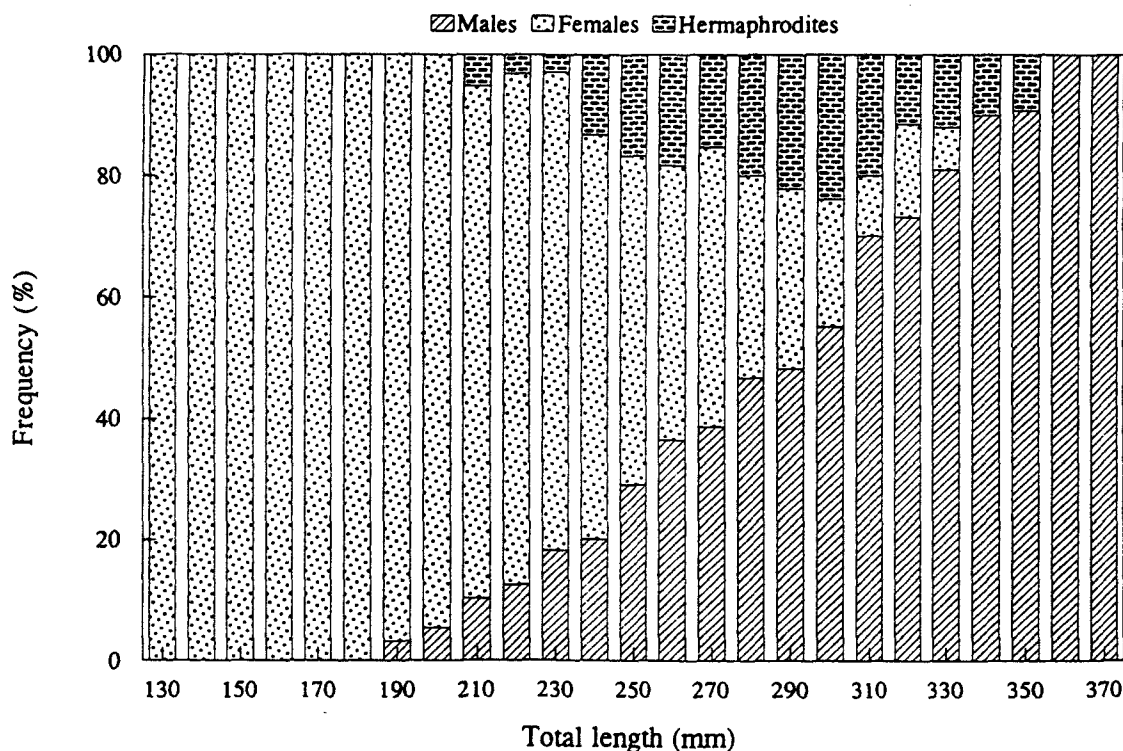


Fig. 2. Sex ratio by size intervals of *P. erythrinus* off the Canary Islands.

Table 2

Parameters of the length–weight relationship ($TW = aTL^b$) for males, females and all individuals of *P. erythrinus* off the Canary Islands

	<i>a</i>	<i>b</i>	<i>se(b)</i>	<i>n</i>	<i>r</i> ²	<i>t</i> -test
Males	0.00775	3.16805	0.03878	206	0.986	4.33 ^a
Females	0.01215	3.02741	0.06638	542	0.974	0.41
All fish	0.01279	3.01338	0.02820	957	0.990	0.47

^a (*t*-test, $t < t_{0.05, n > 200} = 1.65$).

$> t_{0.05, 746} = 1.65$). Positive allometric growth was observed for males and isometric growth for females. For all fish, weight increased isometrically with length (Table 2).

The growth rings in the otolith sections were clear when the otoliths were covered with glycerin. Eighty-two percent of the otoliths were readable. APE value was only 4.2.

Otoliths showed a seasonal variation in the formation of hyaline and opaque rings (Fig. 4). Opaque and hyaline edges were noted in all the months, but the general pattern indicated that two rings, one opaque and one hyaline, were deposited during one year. The

opaque zone is formed between April and September, mainly in June and July, and the hyaline one during the remaining months of the year. False hyaline rings were identified within the second or third annual opaque zone and in the subsequent opaque zones. These rings that are dividing the opaque zones in two parts were very thin and broke the normal growth pattern of the otoliths.

Fish aged 0–10 years were found. Age of males ranged between 2 and 10 years and of females between 1 and 7 years (Table 3). The parameters of the von Bertalanffy growth equation for males, females and all individuals are given in Table 4. Hotelling's T^2 multi-

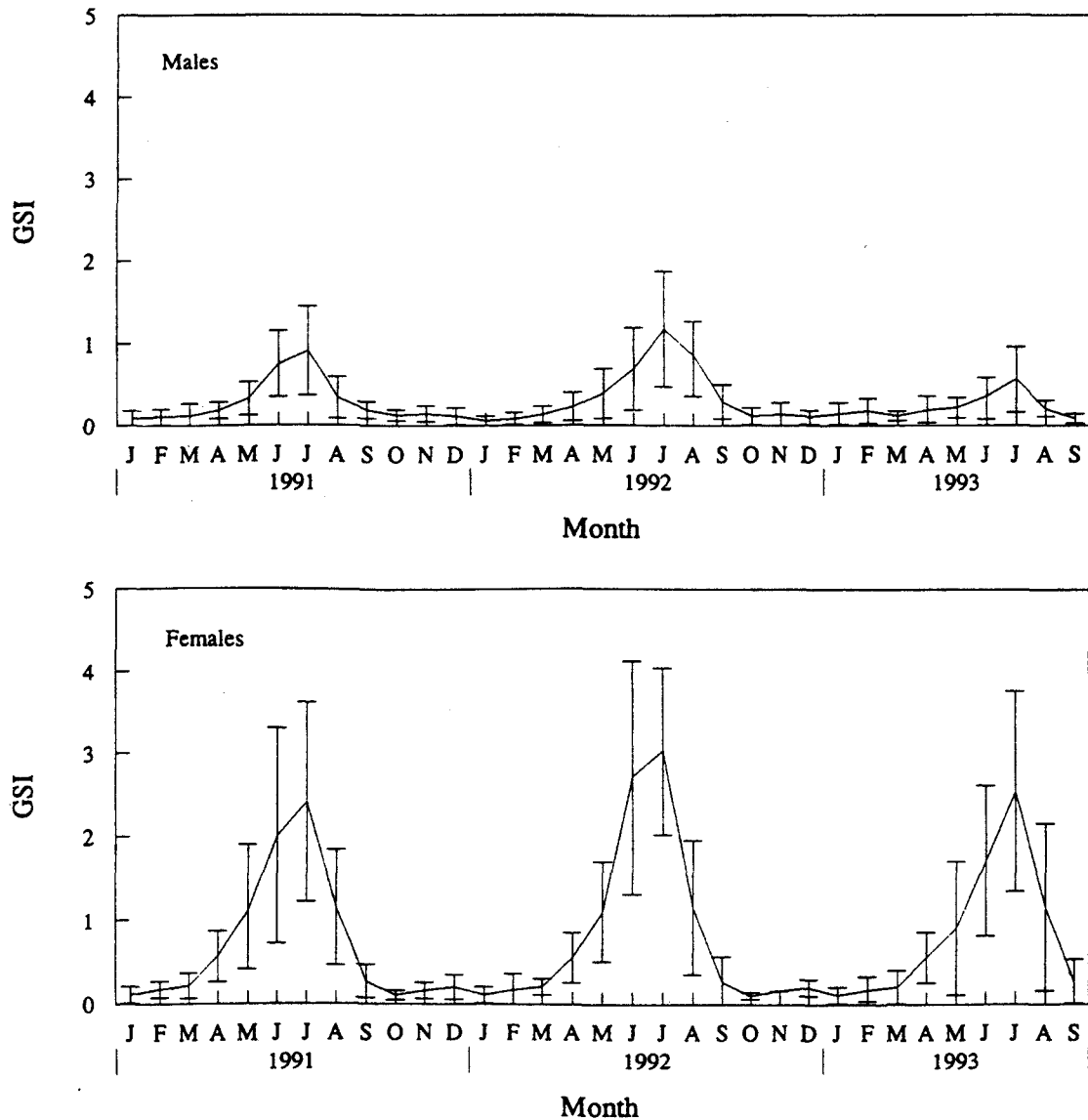


Fig. 3. Monthly change in the gonadosomatic index (GSI) for males and females of *P. erythrinus* off the Canary Islands.

variate statistical procedure (Bernard, 1981) showed significant differences between the growth parameters of males and females were found ($T^2 = 23.87 > T_{0.05,3,306}^2 = 7.91$).

3.3. Mortality

The length-converted catch curves for males, females and all individuals are shown in Fig. 5. The total, natural and fishing mortality rates, the exploitation ratio, and the length at first capture for males, females and all individuals are given in Table 5.

4. Discussion

The common pandora off the Canary Islands is hermaphroditic. This characteristic, which is common among the sparids (Alekseev, 1982; Buxton and Garratt, 1990), has also been observed for this species in other areas (Larrañeta, 1964; Papaconstantinou et al., 1988; Mytilinéou, 1989).

The presence of individuals with well-formed testes and residues of degenerated ovaries and the predominance of females at smaller sizes suggested protogynous hermaphroditism, which has been observed for

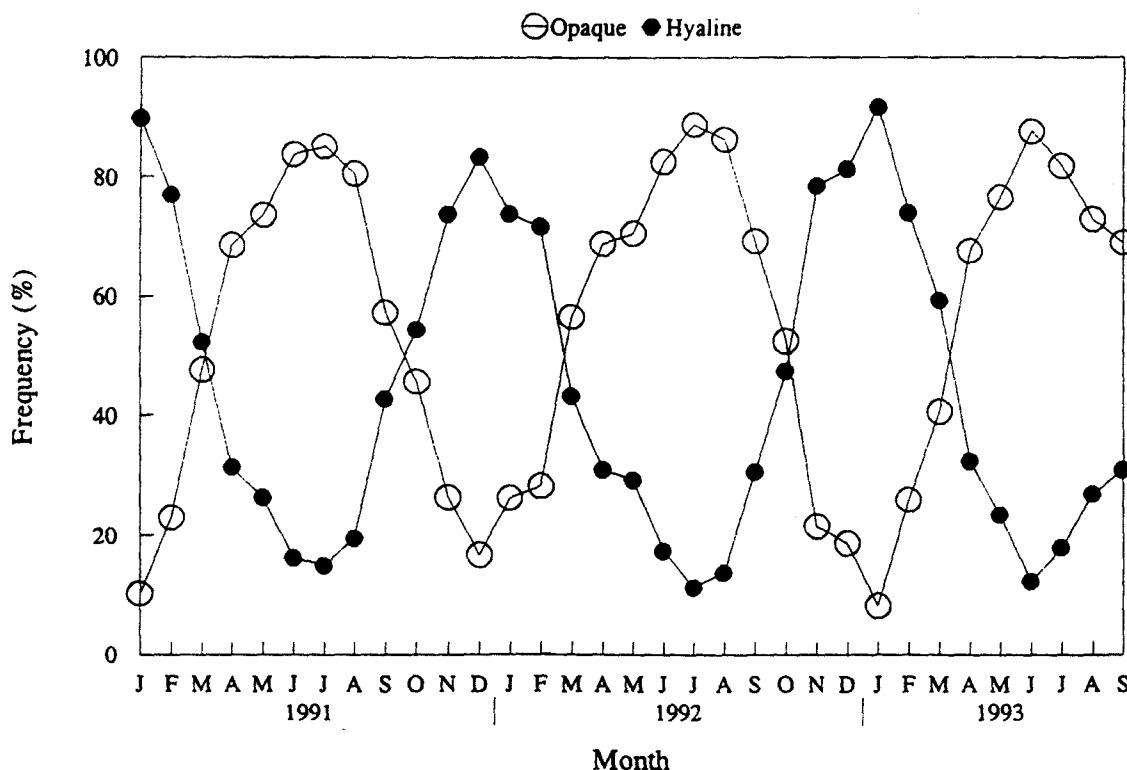


Fig. 4. Percent of otoliths of *P. erythrinus* off the Canary Islands with opaque and hyaline edges by month.

this species in the Mediterranean (Andaloro and Giarritta, 1985; Girardin and Quignard, 1985; Papaconstantinou et al., 1988; Livadas, 1989). Larrañeta (1964) reported that the ovarian region persists along the dorsoventral surface of the testes in the form of degenerated tissue in all males when the testicular region acquires the characteristic of the testis.

The size–sex structure is mainly determined by the nature of the sex change. The sex ratio was unbalanced in favour of females. The predominance of females has also been observed in the Mediterranean (Vassilopoulou et al., 1986). The absence of females in the largest size classes implies that sex conversion occurs in all fish.

Spawning takes place in the summer months. In the Atlantic, spawning occurs in spring, extending sometimes until early summer (Lloris et al., 1977). In the Mediterranean, spawning takes place from May to September (Larrañeta, 1964; Girardin and Quignard, 1985; Papaconstantinou et al., 1988; Livadas, 1989). In the Canary archipelago, the reproduction of common pandora occurs when the temperature of the sea reaches the highest values (Fig. 6).

The difference observed in sexual maturity between sexes may be explained adequately by protogyny. Fish attain maturity between the second and the third years of life. Larrañeta (1967), Girardin and Quignard (1985), Mytilinéou (1989) pointed out that this species also attains sexual maturity at the age of 2–3 years in the Mediterranean.

The length–weight relationship reveals that males are heavier than females for a given length. This may be explained by protogyny, because females predominated in smaller size classes and males in larger ones. Also, weight increases isometrically with length for all fish. Similar results have been reported from other areas (Andaloro and Giarritta, 1985; Girardin and Quignard, 1985; Livadas, 1989).

The alternative pattern of hyaline and opaque rings was easily distinguishable on the otoliths. The opaque ring is formed when the temperature of the sea is highest (Fig. 6) and food is most abundant (Hernández-León, 1988). The false rings observed are probably spawning rings, because this species spawns in summer, when the opaque zone is formed in the otoliths (Morales-Nin, 1987). Spawning rings have

Table 3
Age-length key for males, females and all individuals of *P. erythrinus* off the Canary Islands

Size (mm)	Age group (year)										
	0	I	II	III	IV	V	VI	VII	VIII	IX	X
<i>Males</i>											
190			1								
200			1	1							
210			1	4							
220				3	1						
230				2	4						
240				2	6						
250					5	1					
260					3	4					
270					1	7					
280						4	1				
290						4	2				
300						1	6				
310							13				
320							5	1	1		
330							1	3			
340								1	5		
350									6	1	
360									2	3	
370										2	1
<i>n</i>			3	12	20	21	28	5	14	6	1
<i>x</i>			193	216	240	271	311	333	346	362	371
<i>sd</i>			6	12	11	10	11	5	9	5	0
<i>Females</i>											
130		3	1								
140		1									
150		1	3								
160			12								
170			30								
180			14	1							
190			9	3							
200			4	5							
210				8							
220				22							
230				14	2						
240				4	4						
250				1	15						
260					9	1					
270					2	2					
280						11					
290						3	3				
300						1	7				
310							2	1			
320							1	2			
330								1			
<i>n</i>		5	73	58	32	18	13	4			
<i>x</i>		135	175	218	253	280	302	319			
<i>sd</i>		7	13	15	10	9	8	5			

Table 3 (continued)

Size (mm)	Age group (year)										
	0	I	II	III	IV	V	VI	VII	VIII	IX	X
All fish											
70	7										
80	16										
90	9	3									
100	1	16									
110		12									
120		8									
130		3	1								
140		1									
150		1	3								
160			12								
170			32								
180			16	1							
190			10	4							
200			5	7							
210			2	13							
220				29	1						
230				17	6						
240				9	11						
250				3	26	1					
260					14	5	1				
270					3	9					
280						19	2				
290					1	11	7				
300						3	17				
310						1	15	1			
320							6	5	1		
330							1	4			
340								2	5		
350								1	6	1	
360									2	3	
370										2	1
<i>n</i>	33	44	81	83	62	49	49	13	14	6	1
<i>x</i>	82	109	176	222	253	281	305	327	346	362	371
<i>sd</i>	8	17	15	15	13	11	12	10	9	5	0

Table 4
Parameters of the von Bertalanffy growth equation

	L_{∞} (mm)	k (year ⁻¹)	t_0 (year)	r^2
Males	420.7	0.192	-0.480	0.988
Females	382.8	0.236	-0.592	0.977
All fish	417.8	0.205	-0.550	0.967

$L_t = L_{\infty}(-1 - e^{-k(t-t_0)})$, for males, females and all individuals of *P. erythrinus* off the Canary Islands.

also been observed in the otoliths of *P. erythrinus* in the Mediterranean (Larrañeta, 1967).

The oldest fish found was 10 years old. In the Mediterranean, Larrañeta (1967) examined 15-year-

Table 5
Total (Z), natural (M) and fishing (F) mortality rates, exploitation ratio (E)

	Z	M	F	E	LC_{50} (mm)
Males	0.71	0.30	0.41	0.58	221
Females	1.41	0.43	0.98	0.69	160
All fish	1.06	0.30	0.76	0.71	155

Length at first capture (LC_{50}) for males, females and all individuals of *P. erythrinus* off the Canary Islands.

old specimens, Andaloro and Giarritta (1985) 8-year-old specimens, and Livadas (1989) 12-year-old specimens. The differences observed in mean length at age

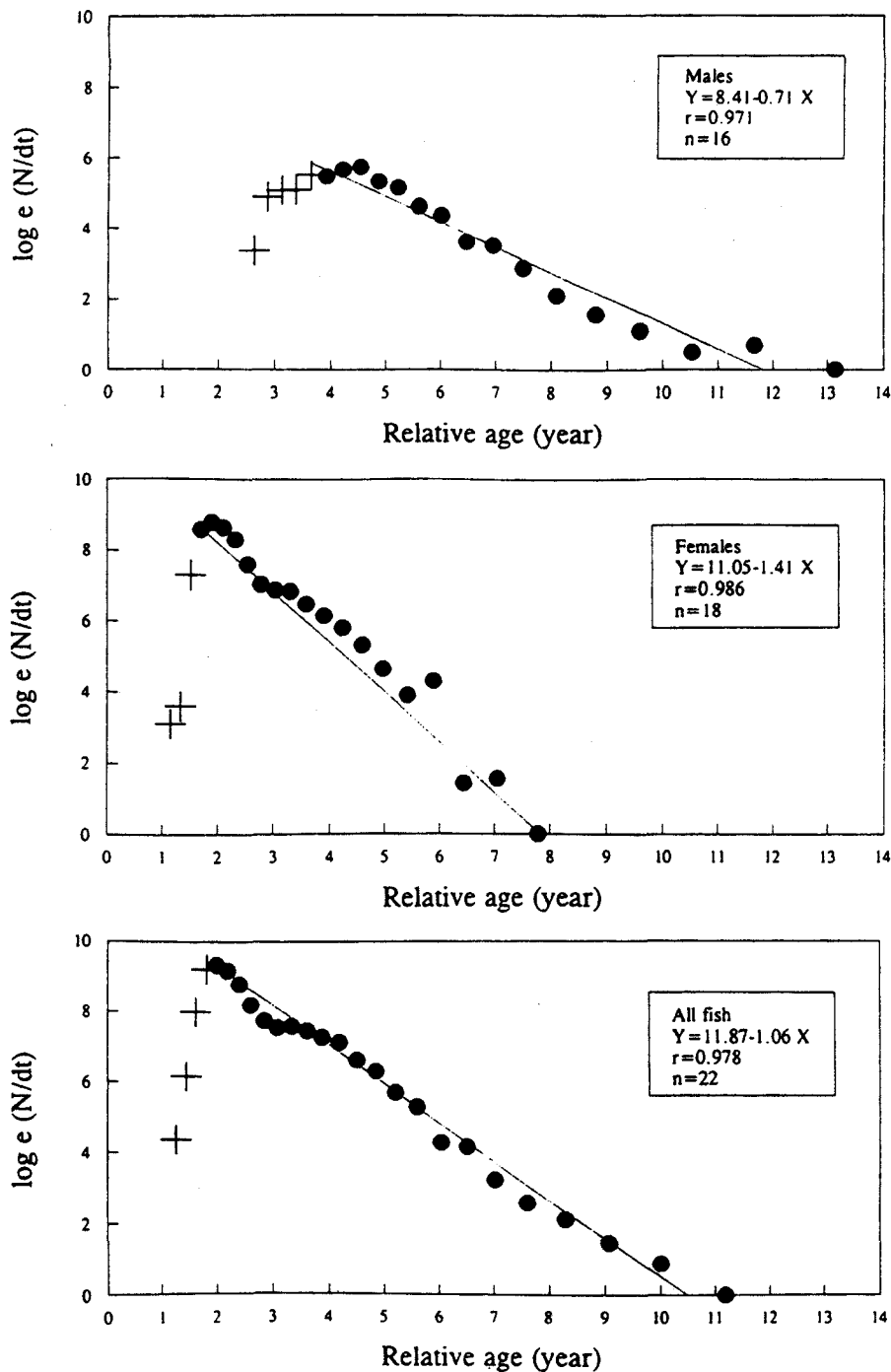


Fig. 5. Length-converted catch curves for males, females and all fish of *P. erythrinus* off the Canary Islands. The initial data points (+) were not used in the regressions.

between sexes is a characteristic of protogynous species. Alekseev (1983) indicated that the mean length of sex-reversed individuals is slightly greater than that of females at the same age. Therefore, differences in length between males and females of the same age

cannot be considered as evidence of intersexual difference in growth rates because females and males are the same individuals at different phases of sexual succession and, possibly, the largest females in an age group are the first to change sex.

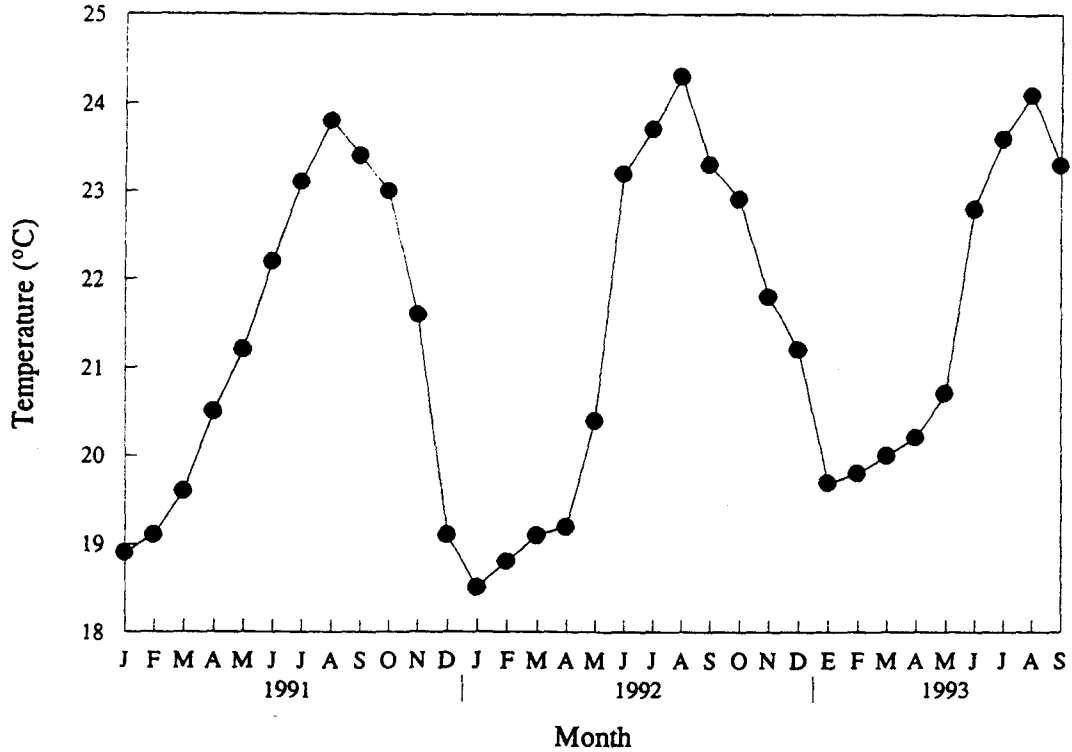


Fig. 6. Monthly course of the sea temperature in the Canary Islands.

The theoretical maximal length value ($L_{\infty} = 417.8$ mm) was close to the size of the largest fish examined and the growth coefficient value ($k = 0.205 \text{ year}^{-1}$) indicated relatively low attainment of maximal size. These parameters are similar to those reported by Juckic and Piccinetti (1981), Girardin (1981), and Andaloro and Giarritta (1985) (Table 6). However, they differ from those obtained by Girardin and Quignard (1985), Livadas (1989), and Papaconstantinou et al. (1988) (Table 6). The differences in growth between regions can be attributed to the dif-

ference in the size of the largest individual sampled in each area. The largest fish found in the studies conducted by Girardin and Quignard (1985), and Livadas (1989), and Papaconstantinou et al. (1988) was less than 300 mm TL.

The length-converted catch curves showed a typical form and justified the estimation of a single value of Z for males, females and all fish (Pauly, 1983). In all the cases, the exploitation ratio is higher than 0.50. Gulland (1971) suggested that, as a rule of thumb, a fish stock is optimally exploited at a level of fishing

Table 6
Parameters of the von Bertalanffy growth equation for *P. erythrinus* in different areas

L_{∞} (mm)	k (year^{-1})	Area	Author
405	0.24	Gulf of Lyon	Girardin (1981)
379	0.20	Adriatic Sea	Juckic and Piccinetti (1981)
367	0.16	Sicilia	Andaloro and Giarritta (1985)
345	0.33	Gulf of Lyon	Girardin and Quignard (1985)
300	0.20	Cyprus	Livadas (1989)
326	0.18	Greece	Papaconstantinou et al. (1988)
417	0.20	Canary Islands	Present study

mortality which generates $E=0.50$, where $F_{opt}=M$, but in the present study $F>F_{opt}=M$. More recently, Pauly (1987) proposed a lower optimum fishing mortality, $F_{opt}=0.4 M (F>F_{opt})$. Therefore, the stock of the common pandora of the Canary Islands is being heavily exploited.

In the Canary Islands, a minimum size limit has been implemented for target species. In the case of the common pandora, the minimum size regulation is of limited benefit because the minimum length which may be legally kept is smaller than the length at first maturity of males. The practical problem is that this species is only one component of the exploited multi-species demersal fish community (Pajuelo and Lorenzo, 1995) and it matures at a different size than the others (Pajuelo and Lorenzo, 1994, 1996). Therefore, it is susceptible to exploitation at a size when many other coexisting demersal species are mature or immature. Measures as closed season or changes in fishing pattern would be desirable to safeguard the spawning stock and the recruits.

Acknowledgements

The authors are grateful to Professor A.D. McIntyre and three anonymous reviewers for their critical and useful comments on the manuscript.

References

- Alekseev, F.E., 1982. Hermaphroditism in sparid fishes (Perciformes: Sparidae). I. Protogynyn porgies, *Pagrus pagrus*, *P. orphus*, *P. ehrenbergi* and *P. auriga*, from West Africa. *J. Ichthyol.* 22, 85–94.
- Alekseev, F.E., 1983. Hermaphroditism in porgies (Perciformes: Sparidae). II. Sexual structure of populations, mechanism of its formation and evolution in scups, *Pagrus pagrus*, *P. orphus*, *P. ehrenbergi* and *P. auriga*. *J. Ichthyol.* 23, 61–73.
- Andaloro, F., Giarritta, P.S., 1985. Contribution to the knowledge of the age, growth and feeding of pandora, *Pagellus erythrinus* (L. 1758) in the Sicilian Channel. *FAO Fish. Rep.* 336, 85–87.
- Anderson, R.O., Gutreuter, S.J., 1983. Length, weight, and associated structural indices. In: Nielsen, L.A., Johnson, D.L., (Eds.), *Fisheries Techniques*. American Fisheries Society, Bethesda, pp. 283–300.
- Bauchot, M.-L., Hureau, J.-C., 1986. Sparidae. In: Whitehead, P.J.P., Bauchot, M.-L., Hureau, J.-C., Nielsen, J., Tortonese, E., (Eds.), *Fishes of the North-Eastern Atlantic and Mediterranean*. UNESCO, Paris, pp. 883–907.
- Beamish, R.J., Fournier, D.A., 1981. A method for comparing the precision of a set of age determination. *Can. J. Fish. Aquat. Sci.* 38, 982–983.
- Bedford, B.C., 1983. A method for preparing sections of a large number of otoliths embedded in black polyester resin. *J. Cons. Perm. Int. Explor. Mer* 41, 4–12.
- Bernard, D.R., 1981. Multivariate analysis as a means of comparing growth in fish. *Can. J. Fish Aquat. Sci.* 38, 233–236.
- Beverton, R.J.H., Holt, S.J., 1957. *On the dynamics of exploited fish populations*. Fish. Inv. Ser. II, XIX. HMSO, London.
- Buxton, C.D., Garratt, P.A., 1990. Alternative reproductive styles in seabreams (Pisces: Sparidae). *Env. Biol. Fish.* 28, 113–124.
- Gayanilo, F.C., Soriano, M., Pauly, D., 1988. A draft guide to the complete ELEFAN. ICLARM Software 2, 65.
- Girardin, M., 1981. *Pagellus erythrinus* (L., 1758) et *Boops boops* (L., 1758) (Pisces, Sparidae) du Golfe du Lion. *Ecobiologie. Prises commerciales et modèles de gestion*. Ph. D. thesis, University of Languedoc, France, p. 295.
- Girardin, M., Quignard, J.P., 1985. Croissance de *Pagellus erythrinus* (Pisces: Téléostéens Sparidae) dans le Golfe du Lion. *Cybiurn* 9(4), 359–374.
- Gulland, J.A., 1971. *The Fish Resources of the Oceans*. Fishing News (Books) Ltd., West Byfleet, p. 255.
- Hernández-León, S., 1988. Ciclo anual de la biomasa del mesozooplankton sobre un área de plataforma en aguas del Archipiélago Canario. *Inv. Pesq.* 52(1), 3–16.
- Juckic, S., Piccinetti, C., 1981. GFCM report of the technical consultation on stock assessment on the Adriatic. *FAO Fish. Rep.* 253, 186.
- Larrañeta, M.G., 1964. Sobre la biología de *Pagellus erythrinus* (L.) especialmente de las costas de Castellón. *Inv. Pesq.* 27, 121–146.
- Larrañeta, M.G., 1967. Crecimiento de *Pagellus erythrinus* de las costas de Castellón. *Inv. Pesq.* 31(2), 185–258.
- Linnaeus, 1758.
- Livadas, R.J., 1989. A study of the biology and population dynamics of pandora (*Pagellus erythrinus* L., 1758), Family Sparidae, in the Seas of Cyprus. *FAO Fish. Rep.* 412, 58–75.
- Lloris, D., Allué, C., Rucabado, J., Bas, C., 1977. Fichas de identificación de especies. Atlántico Oriental. Estrecho de Gibraltar-Cabo Verde (zona CEECAF 34). Datos Informativos del Instituto de Investigaciones Pesqueras, Barcelona.
- Morales-Nin, B., 1987. Métodos de determinación de la edad en los osteíctios en base a estructuras de crecimiento. *Inf. Técn. Inst. Inv. Pesq.* 143, 30.
- Mytilinéou, C., 1989. Données biologiques sur le pageot, *Pagellus erythrinus*, des côtes orientales de la Grèce centrale. *FAO Fish. Rep.* 412, 77–82.
- Pajuelo, J.G., Lorenzo, J.M., 1994. Parámetros biológicos del besugo *Pagellus acarne* (Pisces: Sparidae) en Gran Canaria (islas Canarias). *Bol. Inst. Esp. Oceanogr.* 10, 155–164.
- Pajuelo, J.G., Lorenzo, J.M., 1995. Análisis y predicción de la pesquería demersal de las Islas Canarias mediante un modelo ARIMA. *Sci. Mar.* 59(2), 155–164.
- Pajuelo, J.G., Lorenzo, J.M., 1996. Life history of the red porgy *Pagrus pagrus* (Teleostei: Sparidae) off the Canary Islands. *Central-east Atlantic Fish. Res.* 28, 163–177.

- Papaconstantinou, C., Mytilinêou, C., Panos, T., 1988. Aspects of the life history and fishery of red pandora *Pagellus erythrinus* (Sparidae) off Western Greece. *Cybium* 13(2), 159–167.
- Pauly, D., 1983. Some simple methods for the assessment of tropical fish stock. *FAO Fish. Tech. Pap.* 234, 1–52.
- Pauly, D., 1987. A review of the ELEFAN system for analysis of length frequency data in fish and invertebrates. In: Pauly, D., Morgan, G.R. (Eds.), *Length-based Methods in Fisheries Research*. ICLARM Conference Proceedings 13. ICLARM, Manila, pp. 7–34.
- Ricker, W.E., 1973. Linear regressions in fishery research. *J. fish. Res. Bd Can.* 30, 409–434.
- Saila, S.B., Recksiek, C.W., Prager, M.H., 1988. Basic fishery science programs. A compendium of microcomputer programs and manual of operation. *Developments in Aquaculture and Fisheries Science* 18, 1–230.
- Tanaka, S., 1960. Studies on the dynamics and the management of fish populations. *Bull. Tokai Reg. Fish. Res. Lab.* 28, 1–200.
- Vassilopoulou, V., Mytilinêou, C., Papaconstantinou, C., 1986. Preliminary biological data on the red pandora (*Pagellus erythrinus* L., 1758) in the Greek seas. *FAO Fish Rep.* 361, 107–112.

A mechanism for layer formation in stratified geophysical flows

J. L. Pelegrí and P. Sangrà

Departamento de Física, Facultad de Ciencias del Mar, Universidad de Las Palmas de Gran Canaria, Canary Islands, Spain

Abstract. We discuss the possibility that steplike structures are formed in subcritical regions of vertically stratified shear flow. The mechanism we propose essentially consists of localized intense mixing in highly stratified and sheared flows, probably following frontogenesis. Its main assumption is that the vertical density flux increases monotonically with decreasing gradient Richardson numbers, which corresponds to enhanced stratification and/or diapycnal shear. This differs from Phillips' [1972] mechanism, which we argue may not apply to vertically stratified shear flow. An essential condition for the formation of constant density steps is the incorporation of a Langevin type equation which takes into account that turbulence must last for some finite characteristic time. We present numerical computations for the case of approximately constant diapycnal shear which lead to the formation of a staircase depth-density structure.

1. The Phillips Mechanism

Phillips [1972] suggested that small perturbations in an initially well stratified density profile will grow with time if a local increase in the vertical density gradient is accompanied by an even larger decrease of the (turbulent) vertical density diffusivity K . In this case, the vertical density flux will become smaller (larger) with increasing (decreasing) stratification, leading to vertical density divergence (convergence) where the density perturbation is negative (positive). The density perturbations will turn into progressively better defined steps, until the turbulent density flux becomes equal in the well-stratified and well-mixed portions of the staircase. He further parameterized K in terms of some local Richardson number, to show that the density layers will form when the turbulent density diffusivity is a large enough inverse function of this local Richardson number.

Posmentier [1977] examined the stability of the same vertically diffusive density equation used by Phillips [1972] (but with salinity rather than density):

$$\frac{\partial \rho}{\partial t} = -\frac{\partial F}{\partial z} = -\frac{\partial F}{\partial I} \frac{\partial^2 \rho}{\partial z^2}, \quad (1)$$

where ρ is density, $I = \partial \rho / \partial z$ is the local vertical density gradient, and $F \equiv w' \rho'$ is the vertical component of the turbulent density flux vector \vec{F} . (Throughout the paper we will maintain the usual decomposition of instantaneous values as equal to ensemble mean plus

fluctuating values, and we will follow the notation that primed dependent variables refer to fluctuating quantities while unprimed dependent variables refer to ensemble mean quantities.) Posmentier pointed out that the solutions of this equation are unstable if $\partial F / \partial I$ is positive, and suggested that this is the case when stratification is larger than a certain critical value. He did some numerical calculations using a parameterization for the vertical density diffusivity of the type proposed by Munk and Anderson [1948]: $K = K_0(1 + \beta Ri)^{-n}$, where K_0 is the maximum K value corresponding to vertical neutral conditions and β , n are positive constants. In this expression, Ri is the local gradient Richardson number, defined as

$$Ri = \frac{-g \left(\frac{\partial \rho}{\partial z} \right)}{\rho \left(\frac{\partial v}{\partial z} \right)^2}, \quad (2)$$

where v is the speed of the horizontal velocity, $\partial v / \partial z$ is the vertical shear, and g is the gravity acceleration (the minus sign in the definition assures Ri to be positive for stable stratification). The numerical solution was able to reproduce the formation of a depth-density staircase structure. (Hereafter, whenever we use the symbol Ri , we will refer to this local gradient Richardson number, while other possible definitions for the Richardson number will be adequately identified.)

Barenblatt *et al.* [1993] have extended Phillips' mechanism by allowing a finite time for the turbulence to adjust to the varying vertical density gradient. They specified this time delay through a linear expansion for the eddy diffusivity, which was then incorporated into the temperature vertical diffusion equation. They analyzed this equation and showed that the problem is mathematically well posed and the solution unique, and

Copyright 1998 by the American Geophysical Union.

Paper number 98JC01627.
0148-0227/98/98JC-01627\$09.00

further calculated some numerical solutions which show the formation of staircase type structures. *Kranenburg* [1996] has explored the interaction of the mean buoyancy and velocity fields in vertical diffusivity equations for both variables. He considered the slowness in the turbulence temporal adjustment by assuming that the vertical eddy diffusivity must evolve forced through a Prandtl-Kolmogorov type source term. He did a stability analysis of the equations (using generalized Munk-Anderson density and momentum diffusivity coefficients specified in terms of Ri) and obtained rather restrictive conditions on the shape of both the vertical density flux and vertical momentum flux for the development of instabilities. He further showed that under these conditions the numerical solution of the density, momentum, and eddy diffusivity equations leads to the formation of evolving staircase type structures.

The key assumption for Phillips' mechanism is the dependence of F on density stratification. This mechanism requires F to be small both for well-mixed and highly stratified conditions, with a maximum at some critical stratification value. The physical justification is that for low stratification ρ' decreases while for high stratification w' is inhibited; additionally, under high stratification the correlation $\rho'w'$ is reduced as the nature of the flow changes, with internal wave motions becoming more dominant [*Ivey and Imberger*, 1991]. *Linden* [1979, 1980] reviewed and did many laboratory experiments on grid-generated mixing across density interfaces and found that in all of them, independent of the stirring rate, the dependence was similar to that required by Phillips' mechanism. *Linden* [1980] combined the experimental data to show a similar dependence of the flux Richardson number (defined as the ratio of change in potential energy to the loss of turbulent kinetic energy) as a function of a local Richardson number expressed using some characteristic turbulent velocity scale. *Ivey and Imberger* [1991] have also found a parallel relation using data from grid-generated mixing experiments in stratified water and wind tunnels.

Ruddick et al. [1989] and *Park et al.* [1994] have recently presented laboratory experiments with mixing induced by stirring with arrays of vertical rods, leading to the formation of density steps. *Park et al.* [1994] defined an overall Richardson number depending on the initial stratification and on the speed of the rod. Their experiments clearly show that there is a critical value for this Richardson number (which depends on the Reynolds number), above which instabilities develop and turn into a set of temporally evolving and merging steps. They used a local Richardson number defined in terms of the step thickness and the speed of the rod. They found that the density flux decreased as this local Richardson number increased between 1 and 10, beyond which it became uniform, but they could not accurately confirm that the density flux decreased for values below 1. They further observed that the steps reached an equilibrium state which corresponded to a uniform density flux in the layered region.

These theoretical and experimental works appear to

confirm the formation of a staircase type structure through a Phillips type mechanism. The similarity in the evolution and merging of steps seen in both *Park et al.*'s [1994] experiments and *Barenblatt et al.*'s [1993] and *Kranenburg*'s [1996] numerical calculations is striking and rather convincing. One aspect that remains unclear, we believe, is the identification of the forcing mechanism that leads to the formation of the fine structure.

2. What Is the Role of Vertical Shear?

In the experiments reported by *Ruddick et al.* [1989] and *Park et al.* [1994] it is clear that turbulence is the result of the rods' movement, but we may wonder to what physical mechanism this corresponds in nature. In particular, it is hard to believe that this (external) source of turbulence corresponds to Kelvin-Helmholtz type instabilities, which develop in vertically stratified shear flow [*Turner*, 1986; *Thorpe*, 1987]. Hence it seems difficult to justify that the growth of the (experimentally and numerically) observed instabilities may have any dependence on Ri , which is defined in terms of the local vertical shear.

The theoretical assumptions used by *Phillips* [1972] and *Posmentier* [1977] actually do not rely on any specific dependence of F on Ri (although *Posmentier* [1977] did his numerical calculations using Ri calculated from a diagnostic depth dependence of the velocity profile). Instead they rely on the dependence of the vertical density diffusivity on a properly defined Richardson number, which is a function of the local vertical density gradient. To illustrate this, let us temporarily take a constant vertical shear, such that $Ri = Ri(l)$. In this case, equation (4) of *Phillips* [1972] may be differentiated to give

$$\begin{aligned} -\frac{\partial \overline{b'w'}}{\partial z} &= v_*^2 V' \frac{\partial [Ri^{1/2} G(Ri)]}{\partial Ri} \frac{\partial Ri}{\partial z} \quad (3) \\ &\propto -\frac{\partial g(l)}{\partial l} \frac{\partial^2 \rho}{\partial z^2} \end{aligned}$$

where $\overline{b'w'}$ is the vertical buoyancy flux (proportional to the vertical density flux F), v_* is an externally imposed characteristic velocity, $V' = \partial v / \partial z$ is the (constant) vertical shear, and g , G are undetermined functions of l which satisfy $Ri^{1/2} G(Ri) \propto l^{1/2} G(l) \equiv g(l)$; note that the change in sign takes place because Ri is always taken as a positive value.

The same argument used in equation (1) allows us now to conclude that Phillips mechanism is really independent of the amount of vertical shear, i.e., it may happen for any V' different from zero. If $V' > 0$, density perturbations are unstable when $\partial(Ri^{1/2} G) / \partial Ri < 0$ (Phillips' statement) or $\partial g / \partial l > 0$ (Posmentier's statement); the opposite occurs for $V' < 0$. Of course, V' may not be constant in z but the condition for instability does not depend on this. It may be clarifying that if we were to try the case of constant density stratification (constant l), then the instability condition could not be

obtained. We may conclude that Phillips' mechanism is not caused by turbulence induced through vertical shear and that any analysis of this mechanism is inconsistent both with the specification of the vertical density diffusivity K in terms of a local gradient Ri and with the utilization of a Munk-Anderson type of parameterization (which is supposed to apply only for stratified shear flow).

The above discussion is, of course, an oversimplification of the problem because it assumes that the vertical density flux will only depend on the density stratification, but it is illustrative of the sort of formal difficulties encountered if the density flux is left to depend on Ri . This density flux should actually depend on the local vertical density gradient, on the rate of dissipation of turbulent kinetic energy ϵ , on the kinematic viscosity ν , and on the size D and velocity V of the eddies (proportional to the diameter and velocity of the rod). The numerical and experimental evidence supporting Phillips' mechanism suggests that the dependence of the vertical density flux on the local stratification $K(I)$ should lead to a $F(I)$ type of dependence with a single maximum, as required by Phillips mechanism. The main difficulty in assessing this dependence, however, is due to the fact that most results in the literature are in terms of an overall density stratification [Linden, 1979,1980; Ivey and Imberger, 1991].

Let us now consider the behavior of the vertical density flux F for shear-induced instabilities. In this case the parameterizations employed for the vertical density diffusivity K are frequently of the Munk-Anderson type; for reviews and applications, see Pacanowski and Philander [1981], Turner [1986], Fernando [1991], and Pelegrí and Csanady [1994]. Another type of parameterization corresponds to Peters et al. [1988], who obtained a two-regime functional form $K = K(Ri)$ for the equatorial undercurrent, with a Munk-Anderson type expression for $Ri \geq 0.4$ and an expression of the form $K \sim Ri^{-9}$ for lower Ri values (Figure 1). F is usually approximated in terms of K as follows [e.g., Posmentier, 1977; Csanady, 1990; McDougall and You, 1990; Pelegrí and Csanady, 1994]:

$$F = -K \frac{\partial \rho}{\partial z} = -\frac{K}{J}, \quad (4)$$

where $J = 1/I = \partial z / \partial \rho$, or the Jacobian of the transformation from the vertical (x, y, z) to the isopycnic (x, y, ρ) reference system. An alternative expression for F is obtained introducing equation (2) into the first equality of equation (4)

$$F = \frac{\rho Ri K}{g} \left(\frac{\partial v}{\partial z} \right)^2 \quad (5)$$

This suggests that with a Munk-Anderson type of parameterization, F may have a maximum value at some low critical Ri value. However, if we accept Peters et al.'s [1988] dependence for low Ri values ($K \sim Ri^{-9}$), then F probably increases continuously with decreasing Ri . Peters et al.'s [1988] high inverse dependence of K

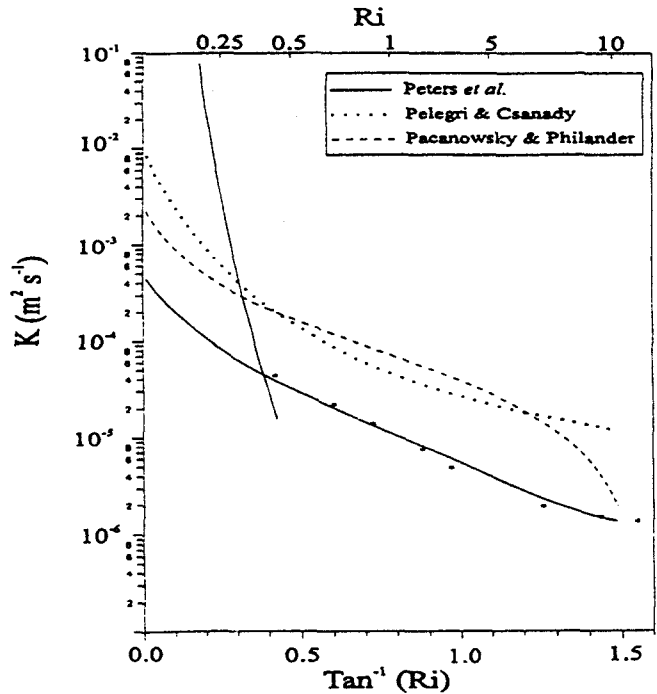


Figure 1. Vertical density diffusivity as a function of the local gradient Richardson number according to the parameterizations of Pacanowsky and Philander [1981], Peters et al. [1988], and Pelegrí and Csanady [1994]. We have adapted a curve to the Peters et al. [1988] measurements (dots) for the $Ri \geq 0.4$ region.

for low Ri values is very attractive because it conforms to a near-catastrophic shear-mixing criterion, with mixing taking place below a critical Ri value, in agreement with theoretical energy arguments [Miles, 1961; Howard, 1961; Pollard et al., 1973]. However, in both cases the exact behavior depends on how $\partial v / \partial z$ changes with decreasing Ri .

For the particular case of constant $\partial v / \partial z$, we may define

$$F_z \equiv F \left| \frac{\partial v}{\partial z} \right|$$

and use equation (5) to evaluate $\partial F_z / \partial Ri = 0$ for any parameterization of K , in order to find out if there is a value of Ri for which F is a maximum. The utilization of a Munk-Anderson relation $K = K_0(1 + \beta Ri)^{-n}$ gives a vertical density flux with a maximum at $Ri = [\beta(n-1)]^{-1}$; for example, for $n = 3/2$ and $\beta = 10$ [Pelegrí and Csanady, 1994], F_z has a maximum at $Ri = 0.2$. If we use Peters et al.'s [1988] parameterization, however, we obtain no maximum, meaning that F_z increases monotonically with decreasing Ri . Figure 2a illustrates these results using both the Pelegrí and Csanady [1994] and the Peters et al. [1988] expressions. For these calculations, we have used $\partial v / \partial z = 10^{-2} \text{ s}^{-1}$, of the same order as the maximum values reported by Bane et al. [1981] for the Gulf Stream.

Under the condition of constant vertical shear the Munk-Anderson parameterization (provided that $n > 1$) results in a $F(Ri)$ dependence which resembles the shape required for the Phillips mechanism. This pro-

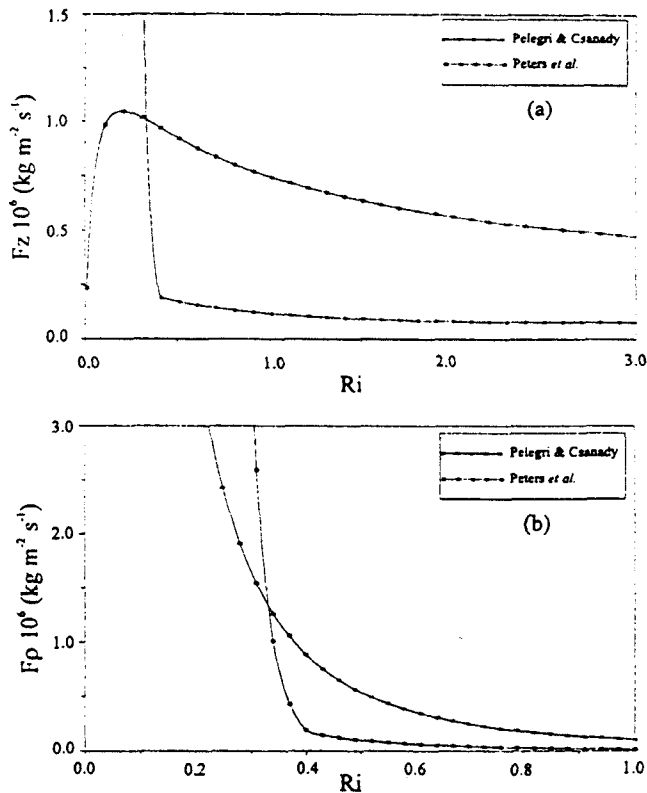


Figure 2. Vertical density flux as a function of the local gradient Richardson number for the cases of (a) constant vertical shear ($F \equiv F_z$) and (b) constant diapycnal shear ($F \equiv F_\rho$). The distributions are shown for both the Peters *et al.* [1988] and the Pelegrí and Csanady's [1994] $K(Ri)$ parameterizations.

duces a factual justification (based on the facts but not on reasoning) for relating this mechanism to shear-induced instabilities. An adequate knowledge of the exact dependence $K(I, \epsilon, \nu, V, D)$, however, is very important in order to specify the instability conditions necessary for Phillips' mechanism to develop. In particular, this knowledge is critical when taking into account the interaction between the density and velocity fields. The inadequacy of a Munk-Anderson type of K parameterization is probably the reason for the very restrictive instability conditions found by Kranenburg [1996].

A common discourse is that low- Ri values imply low vertical density gradients, which in turn, are responsible for very small density fluctuations and a decrease in F [Posmentier, 1977; Ruddick *et al.*, 1989; Park *et al.*, 1994; Kranenburg, 1996]. This is a sensible argument for a Richardson number defined in terms of a (constant) characteristic turbulent velocity, which is related to the speed of the regularly moving rods. For shear-induced instabilities, however, we find no physical reason to support the assumption that F has to decrease when Ri becomes small: these small values are only indicative of a very unstable situation, prior to very active mixing.

It must be emphasized that our purpose is not to oppose Phillips' mechanism but to warn that its origin has probably nothing to do with shear-induced mixing

and to point out the necessity of expressing the vertical density flux in terms of some properly defined local Richardson number (instead of Ri). This necessity has probably been appreciated by other authors such as Park *et al.* [1994], who always refer to a "suitably defined Richardson number" rather than to Ri , but it is fair to say that the differences have not yet been properly pointed out. In the next section we will further illustrate the role of shear by considering the problem in isopycnic coordinates. This will naturally lead to an alternative mechanism for the formation of steps in vertically stratified flow, which operates in a completely opposite fashion and has its origin on instabilities induced by vertical shear.

3. An Alternative View

There is some uncertainty on how to apply the definition for Ri (equation (2)) to adjacent layers in a staircase type of stratification. In this case we have constant density layers separated by a stratified region, both usually of similar vertical thickness [Pelegrí and Csanady, 1994], and we may wonder which is the most appropriate vertical scale δz to calculate the change in velocity δv : the thickness of the whole region (both layers and interface) or the thickness of the stratified region (interface)? The answer, however, is immediate if we consider the problem in isopycnic coordinates because both constant density layers reduce to one single ρ coordinate in the isopycnic coordinate system, each of them having an approximate constant velocity value. This practical advantage comes along with a powerful argument for using isopycnic coordinates, which was long ago clearly stated by Rossby [1936, p. 5]: "... water, because of its stratification, has a cellular structure, each cell being separated through approximately horizontal surfaces of discontinuity from the cells above and below. Each boundary surface would then act as a 'false' bottom and each cell would have a practically independent circulation" (see also Csanady [1989] and Csanady and Pelegrí [1995]).

The above reasoning suggests that the natural representation for Ri is using isopycnic coordinates [Pelegrí and Csanady, 1994]:

$$Ri = \frac{-gJ}{\rho \left(\frac{\partial v}{\partial \rho} \right)^2} \quad (6)$$

In this case the vertical density flux becomes

$$F = \frac{gK}{\rho Ri \left(\frac{\partial v}{\partial \rho} \right)^2} \quad (7)$$

and we may again ask ourselves what is the behavior of F as a function of Ri . The key factor now is not the vertical shear, but the diapycnal shear, $\partial v / \partial \rho$, i.e., the dependence of this quantity with Ri . The simplest possibility is to assume $\partial v / \partial \rho$ constant, as we did before for $\partial v / \partial z$. In this case we define

$$F_\rho \equiv F \left| \frac{\partial v}{\partial \rho} \right.$$

and we can use equation (7) to evaluate $\partial F_\rho / \partial Ri = 0$ for any particular parameterization of K . This calculation shows that F_ρ has a maximum neither for the Munk-Anderson nor for the Peters *et al.* [1988] parameterizations, in both cases F_ρ monotonically increases for decreasing Ri . Figure 2b illustrates these results using both the Pelegrí and Csanady [1994] and the Peters *et al.* [1988] expressions. For these calculations we have used $\partial v / \partial \rho = 2.5 \text{ m}^4 \text{ kg}^{-1} \text{ s}^{-1}$, of the same order as the maximum values reported by Pelegrí and Csanady [1994] for the Gulf Stream. The curve corresponding to the Pelegrí and Csanady [1994] parameterization (of the Munk-Anderson type) is strikingly different to its counterpart in Figure 2a.

Equations (2) and (6) are the expressions for Ri in vertical and isopycnic coordinates, respectively. At first sight, they may suggest very different situations: equation (2) shows that Ri increases with stratification (larger $\partial \rho / \partial z$), while equation (6) shows that Ri decreases with stratification (smaller $J = \partial z / \partial \rho$ values). The solution of this apparent paradox rests on the velocity profile, the diapycnal and vertical shears being related through the Jacobian, i.e., $\partial v / \partial \rho = J \partial v / \partial z$. For staircase type conditions, the conceptual idea of independent motions along adjacent constant density layers suggests that the difference in velocity between adjacent isopycnals will usually be a much better conserved quantity than vertical shear, which probably has a strong dependence on the evolution of the interfaces. With this assumption, equation (7) shows that the vertical density flux will have a local maximum at the position of highest stratification (the minimum in J): this is a statically stable region but it turns out to be dynamically very unstable [Pelegrí and Csanady, 1994].

In view of the lack of experimental or field data, it is clear that the assumption of constant diapycnal shear cannot be generalized, but it is attractive under frontogenetical conditions. Consider, for example, the very simple case where the isopycnals are vertically and horizontally compressed with time but maintain their slope. Recalling the thermal wind equation in isopycnic coordinates ($\rho f \partial v / \partial \rho = g \partial z / \partial x$), we may appreciate that under the geostrophic approximation a constant diapycnal shear would be appropriate. Under the same approximation, however, the increased horizontal density gradient would lead to an increase in vertical shear. Consider now a slightly more complex situation, with the isopycnals getting both compressed and tilted with time. This would cause a decrease in the Jacobian and an increase in both the diapycnal and vertical shears. In these circumstances the diapycnal shear is not constant, but it is probably more realistic to let J decrease and take a constant $\partial v / \partial \rho$ (leading to a decrease in Ri through equation 6) rather than allowing J to decrease and taking a constant $\partial v / \partial z$ (producing an increase in Ri according to equation (2)).

Following the above discussion, we are now ready to discuss an alternative process that leads to the formation of a step of constant density, i.e., to the partition of the single minimum in J into two adjacent minima

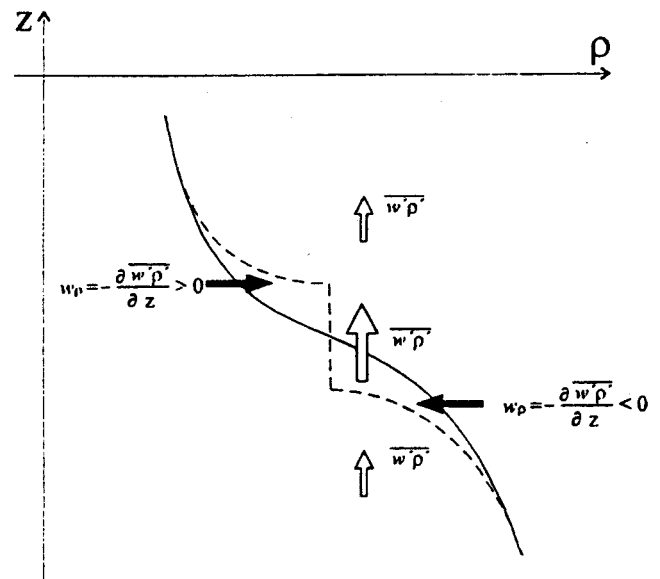


Figure 3. Schematic representation of density stratification before (solid line) and after mixing in the central region (dashed line). The arrows represent the situation previous to intense mixing: the white arrows represent the vertical density flux, and the black arrows represent the density tendency.

as illustrated in Figure 3. The density tendency, or material derivative of the density, is given by [Pelegrí and Csanady, 1994]

$$w_\rho = \frac{D\rho}{Dt} = -\frac{\partial \overline{w'\rho'}}{\partial z} \quad (8)$$

where $D\rho/Dt = \partial/\partial t + u\partial/\partial x + v\partial/\partial y + w\partial/\partial z$ is the material derivative in (x, y, z) coordinates. The solid line in Figure 3 represents the original density stratification, with a central highly stratified region which corresponds to the minimum absolute J values. The upper part of the region of high stratification corresponds to vertical convergence of density flux (positive w_ρ), while its lower part corresponds to vertical divergence (negative w_ρ). This situation, if maintained for a finite time, will cause a density increase in the upper part and a density decrease in the lower portion (dotted line). This will naturally lead to a decrease of the stratification in the central region (the creation of a well-mixed region) and to an increase at both sides of this newly formed mixed region (the creation of interfaces). A similar argument could now apply to the new interfaces, which should be prone to undergo mixing and to split into new steps of a forming staircase.

Another way to visualize the above idea is through the mass conservation equation in isopycnic coordinates. Pelegrí and Csanady [1994] showed that under the condition of dominant diapycnal convergence/divergence $\partial w_\rho / \partial \rho$, i.e., neglecting epicyclic convergence/divergence and horizontal Reynolds mass fluxes, the mass conservation equation reduces to

$$\frac{Dj}{Dt} \simeq -j \frac{\partial w_\rho}{\partial \rho} \quad (9)$$

where $j = J\rho$ is an index of separation between adjacent isopycnals and $\mathcal{D}/\mathcal{D}t = \partial/\partial t + u\partial/\partial x + v\partial/\partial y + w\rho\partial/\partial\rho$ is the material derivative in isopycnic coordinates. Applying this equation to the situation in Figure 3, we can see that it gives $\mathcal{D}j/\mathcal{D}t < 0$ for the central region, indicating that the absolute value of $J = j/\rho$ will increase with time, i.e., a decrease in the degree of stratification. Similarly, it may be appreciated that the stratification will increase with time in the upper and lower portions of the central region.

The creation of well-mixed regions following a localized maximum in the vertical density flux was already proposed by *Pelegrí and Csanady* [1994] in a simple cause-effect model. They hypothesized a distribution of the vertical density flux with a maximum on some isopycnal level and estimated the corresponding J and Ri distributions, with the Ri distribution showing a minimum below the critical Ri value. Their assumption was that this condition, if maintained for a finite time, would cause the vertical density flux to be largely reduced in the subcritical region. They simulated the modified $\overline{w'\rho'}$ distribution and recalculated the J distribution and the $z(\rho)$ profile, which showed the formation of one step. In their paper *Pelegrí and Csanady* [1994] proposed that mixing would be induced in shear unstable regions after frontogenesis, but they inaccurately mentioned that the physical process resembles Phillips' mechanism.

Figure 4 illustrates the instability processes for both the Phillips and the new mechanism, emphasizing their

completely different kinematics. In Phillips' mechanism a perturbation that reduces the stratification of the depth-density profile will grow in time until it becomes a well-mixed region and adjacent well-stratified layers are formed (Figure 4a). In the proposed alternative mechanism a highly stratified region is unstable and mixes up, splitting into a well mixed region and two adjacent interfaces (Figure 4b).

The production of local oceanic finestructure through a mechanism based on localized shear-induced mixing in stratified regions was long ago endorsed by *Woods* [1968] and *Woods and Wiley* [1972], and discussed at some length by *Turner* [1973, pp. 104, 121, 325]. They argued that the passage of long internal waves along sharp interfaces can lead to local instabilities in well stratified regions, particularly at the crests and troughs of internal waves. Portions of the stratified region are then substituted by relatively well mixed fluid, which is then elongated horizontally by vertical shear and epicycnal spreading. Some oceanic observations on local mixing in stratified regions, apparently associated to crests and troughs of traveling internal waves, have also been documented by *Woods* [1968] and *Woods and Wiley* [1972].

The mechanism here proposed does not require the passage of internal waves and can operate on horizontal scales much larger than localized regions over crests or troughs of internal waves. It is based on the creation of subcritical regions during frontogenetical situations, either because of shrinking of isopycnal layers (J is reduced) or because of tilting of the isopycnals, followed

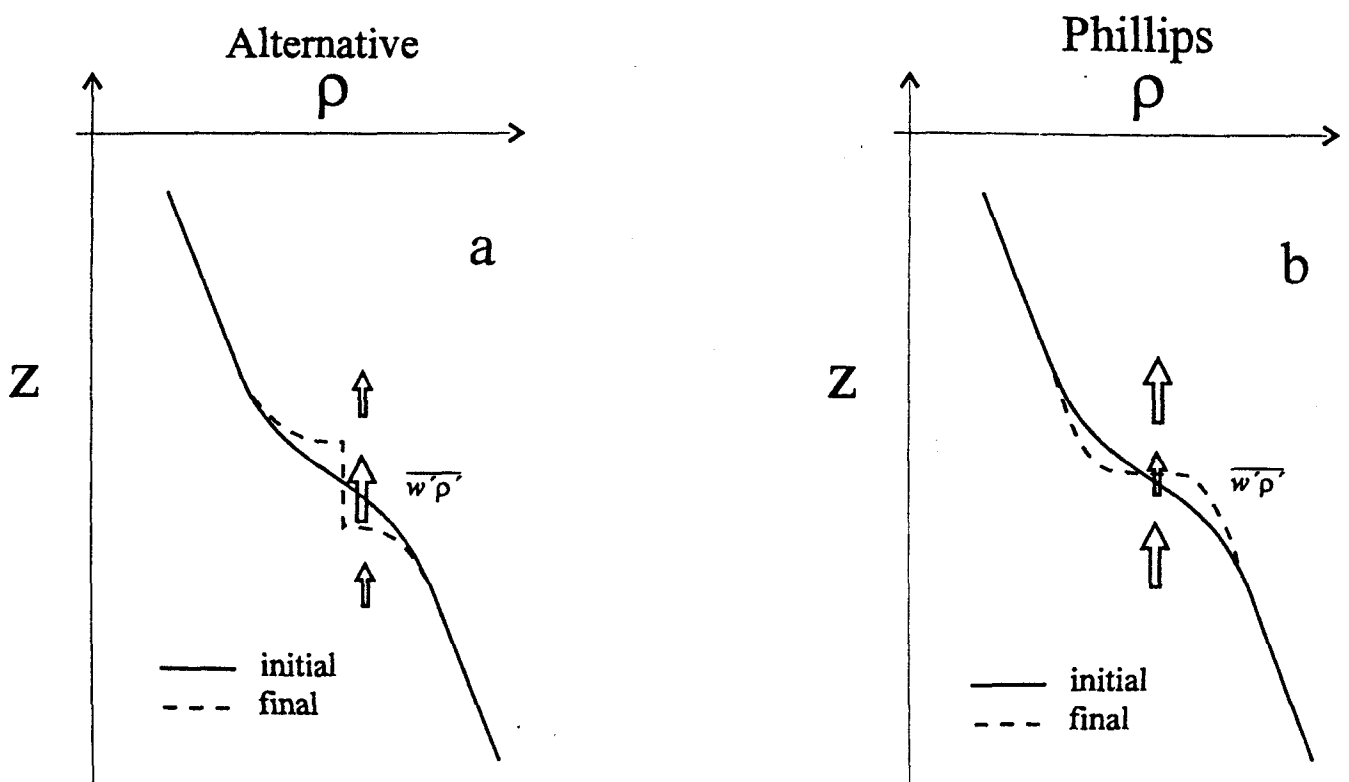


Figure 4. Schematic drawings to illustrate the kinematics of mixing for (b) Phillips' mechanism and (a) the proposed alternative mechanism.

by instabilities of the Kelvin-Helmholtz type. The actual condition for the well stratified layers to become subcritical is derived from equation (6):

$$J < \frac{\rho}{g} \left(\frac{\partial v}{\partial \rho} \right)^2 Ri_c, \quad (10)$$

where $Ri_c \simeq 0.25$ is the theoretical critical value of Ri for mixing to develop.

Some laboratory evidence that supports this mechanism can be found in a preliminary experiment reported by Thorpe [1971]. In this experiment a long tank was completely filled with two fluids of different density and tilted for a short period, just enough for the interface to become unstable, and then returned to its horizontal position. Kelvin-Helmholtz instabilities developed at the interface, which became approximately well mixed, and two interfaces were formed at the edges of this central mixed region. Several related experiments have been recently performed, and some preliminary results appear to confirm the splitting of a thin interface into a well-mixed layer and adjacent interfaces [Cisneros-Aguirre *et al.*, 1997; Fernando, 1997].

Some interesting atmospheric data were long ago presented by Browning and Watkins [1970]. They used a high power radar and simultaneous radiosonde ascents to examine the evolution of regions of high static stability. Their observations showed the formation and evolution of Kelvin-Helmholtz billows in a highly stratified region, which lead to the splitting of this region into an approximately mixed layer and two adjacent interfaces. The oceanographic field evidence, however, is limited by the difficulties in repeating hydrographic cross sections in times shorter than the passage of frontal mesoscale features. Some indirect evidence, obtained through analyses of the distribution and fluxes of properties such as nutrients and potential vorticity, is consistent with the intermittent mixing associated with this mechanism [Pelegri and Csanady, 1991; Pelegri *et al.*, 1996].

The horizontal and vertical extension of the subcritical regions depend on the frontogenetical mechanism itself, whether it is a mesoscale or basin-wide feature. Those layers with high stratification during the initial stages of frontogenesis will be susceptible to convert into well-mixed regions of the staircase, while sharp interfaces will form at the adjacent layers. If frontogenesis continues, the adjacent risers will also mix up, each splitting into a new mixed layer and two new adjacent interfaces; eventually, diapycnal mixing may become so large that it can prevent further frontogenesis to continue. The vertical and temporal scales for the formation of the well-mixed regions will arise from the corresponding scales of the Kelvin-Helmholtz billows, which depend mainly on the vertical stratification. In the laboratory, for example, stratification is usually very large, and the height of the billows may be of the order of 0.01 m, while their timescale may be of the order of 1 s; in an oceanic frontal system, however, these scales could be 1-10 m and up to 1 hour.

In general, we may expect that the strongest oceanic frontogenetical processes will be intermittent and usu-

ally associated with mesoscale features such as meanders in the Gulf Stream [e.g., Csanady, 1988; Lee and Csanady, 1994] or the coastal upwelling jet [e.g., Bane *et al.*, 1981; Csanady, 1977, 1982], evolving vortices or rings [e.g., Miller and Evans, 1985; Aristegui *et al.*, 1994], or other types of frontal structures [e.g., Csanady, 1981; Simpson, 1981]. In all these cases the temporal scale of maximum frontogenetical conditions will last long enough (of the order of several hours or days) to guarantee that subcritical conditions are attained.

4. Temporal Memory of Turbulence

One point crucial to our previous analysis is the creation of a maximum density flux in the highly stratified region. It is not enough, however, to generate such an instantaneous maximum: for our mechanism to work it is fundamental that the density flux (with convergence and divergence regions above and below, respectively) is maintained at a high level for a finite time (Figure 3). Otherwise, the convergence and divergence of density toward the neighboring regions will reduce the original density gradient (increase the Jacobian), and the density flux will consequently decrease. The result will simply be upward mass diffusion and smoothing of the original strong density gradient. The temporal maintenance of such a high-density flux at the location of the minimum in J has its physical justification on the fact that once turbulence is produced it will last for a characteristic finite time at a considerably high level. Even if the original unstable conditions disappear, turbulence will not immediately do so, i.e., once it is activated, it will decay at its own natural rate.

Barenblatt *et al.* [1993] and Kranenburg [1996] have pointed out the necessity of allowing a finite time adjustment for turbulence and have applied this idea to modify Phillips' mechanism. Such a time adjustment is not critical for their solution to work, although Barenblatt *et al.* [1993] have shown that it is necessary in order to make the problem mathematically well posed and the solution unique. Barenblatt *et al.* [1993] specified the time delay by using an elegant simple temporal expansion for the vertical density diffusivity. Kranenburg [1996] followed the same idea but justified the temporal evolution of the vertical density diffusivity through forcing by a Prandtl-Kolmogorov type source term.

In this work we essentially follow Barenblatt *et al.*'s [1993] approach to take account of the temporal memory of the turbulence field. This is done in a very simple manner, by approximating the vertical density diffusivity K with the first term of a Taylor expansion:

$$K(t) = K(t - \tau) + \left(\frac{\partial K}{\partial t} \right)_{(t-\tau)} \tau. \quad (11)$$

This equation, which relates the vertical density diffusivity at time t with those conditions that took place some time τ ago, immediately suggests equation (9) of Kranenburg [1996]:

$$\frac{\partial K_t}{\partial t} \tau = -K_t + K_f. \quad (12)$$

where we have defined two different functions which correspond to the vertical density diffusivity evaluated at different times. $K_f \equiv K(t)$ and $K_t \equiv K(t - \tau)$. Equation (12) is Langevin's equation and has its appealing physical meaning of a slowly decaying field (the turbulence with its own characteristic temporal scale) which is continuously changing due to external forcing (the local stratification); for a nice discussion see *Csanady* [1973]. If there was no external forcing, the solution would decay exponentially as $\exp(-t/\tau)$, which shows that τ corresponds to the characteristic temporal scale of the turbulence.

All that is required now is to specify a value for τ . Under the restoring force of gravity, perturbations have an angular velocity which is given by the buoyancy frequency N , defined in terms of the local vertical density gradient as $N^2 = -g/\rho$. Hence it may be expected that the natural period for the vertical density flux will be of the order of N^{-1} . This agrees well with numerical and experimental results compiled by *Gregg* [1987], which show that the age of the energy-containing eddies will be somewhere between $0.1N^{-1}$ and N^{-1} . More recent numerical calculations by *Holt et al.* [1992] also show that the vertical density flux remains large for times of the order of N^{-1} . According to these arguments, we have chosen $\tau = N^{-1}$ as the characteristic temporal scale of turbulence, to be used in the numerical calculations below. Because of the importance of local stratification in specifying the vertical density flux, we have decided to let τ vary vertically and temporally, depending on the instantaneous local vertical stratification. This has been preferred over the alternative of specifying τ in terms of the background initial stratification (as is done by *Kranenburg* [1996]).

5. Numerical Procedure

For dominant diapycnal mass transfer, the advective terms $u \partial j / \partial x + v \partial j / \partial y$ are relatively small and equation (9) may also be approximated as

$$\frac{\partial j}{\partial t} \approx -\frac{\partial(jw_\rho)}{\partial \rho} \quad (13)$$

where we have incorporated the diapycnal advection of j into the right-hand side. This equation simply states that changes in the distance between adjacent isopycnals are due to diapycnal convergence/divergence; it could have been derived from first principles by recalling that the mass flux (per unit area) through entrained water (water crossing an isopycnal with vertical speed w_e) is given by $\rho w_e = \rho J w_\rho = j w_\rho$.

Equation (12) provides the time evolution of the current density diffusivity K_t , which slowly changes as it decays and is forced by the eddy diffusivity K_f calculated from the local density field. In order to solve it, we will use a functional form $K_f = K_f(Ri)$ similar to that proposed by *Peters et al.* [1988], mainly because it conforms well to the catastrophic dependence that is expected for subcritical Ri numbers. For values of

$Ri < 0.33$, we will use exactly the same dependence as specified by *Peters et al.* [1988] ($K_f \propto Ri^{-9.2}$), while for the range $Ri \geq 0.33$, we will use *Pelegri and Csanady's* [1994] parameterization (Figure 1 illustrates that both functions intersect at $Ri = 0.33$). A second possibility would be to use a Munk-Anderson parameterization for all Ri values. The exact K_f dependence is not decisive, for constant diapycnal shear both the *Peters et al.* and the Munk-Anderson parameterizations result in K_f monotonically increasing with decreasing stratification, but some important differences arise (see the discussion at the end of section 6).

Summarizing, we will solve equations (12) and (13) together with the following parameterizations for density tendency:

$$w_\rho = \frac{\partial}{\partial z} \left(\frac{K_t}{J} \right) = \frac{1}{J} \frac{\partial}{\partial \rho} \left(\frac{K_t}{J} \right) \quad (14)$$

and for the forcing vertical density diffusivity:

$$K_f = \begin{cases} 1.1 \times 10^{-8} Ri^{-9.2} & , Ri < 0.33 \\ 2.6 \times 10^{-3} (1 + 10Ri)^{-3/2} & , Ri \geq 0.33 \end{cases} \quad (15)$$

where Ri is given by equation (6). According to the discussion in last section, we will a priori specify a value for the diapycnal shear, with the main test case corresponding to constant diapycnal shear.

These equations are solved numerically in the (t, ρ) space (forward in time and centered in ρ) to predict the temporal evolution of the vertical density diffusivity and Jacobian fields. The grid spacing is chosen as $\delta \rho = 0.005 \text{ kg m}^{-3}$ and $\delta t = 0.1 \text{ s}$. Equation (13) requires the specification of boundary conditions for j ; these have been chosen as constant j values, which imply that at the boundary isopycnals there is no diapycnal convergence/divergence. Once the Jacobian $J = j/\rho$ is known, we may immediately calculate the depth field z through integration from $z = 0$. Since we consider constant diapycnal shear, equation (15) shows that $\partial K_f / \partial \rho$ may be discontinuous at those density values where $Ri = 0.33$. This causes some small numerical instabilities, which are removed (at each time step) by applying Shapiro's running filter [*Shapiro*, 1970] three times to K_f .

The initial stratification corresponds to the depth linearly decreasing with density (from 0 to -200 m in 0.5 kg m^{-3}), over which we superimpose a sinusoidal depth fluctuation (25 m fluctuation with wavelength $\lambda_\rho = 0.5 \text{ kg m}^{-3}$). The amplitude of the fluctuation is chosen such that its maximum slope is less than the background density slope. The diapycnal shear has been taken as $2.5 \text{ m}^4 \text{ kg}^{-1} \text{ s}^{-1}$, of the same order of magnitude as the maximum values reported by *Pelegri and Csanady* [1994]. Figure 5 shows the initial conditions specified for the $z(\rho)$ field, and the corresponding initial condition for the Jacobian J , the vertical density flux w'_ρ , and the density tendency w_ρ . Hereafter, in all figures we use $\sigma \equiv \rho - 1000$, with ρ being the absolute value of density in MKS units.

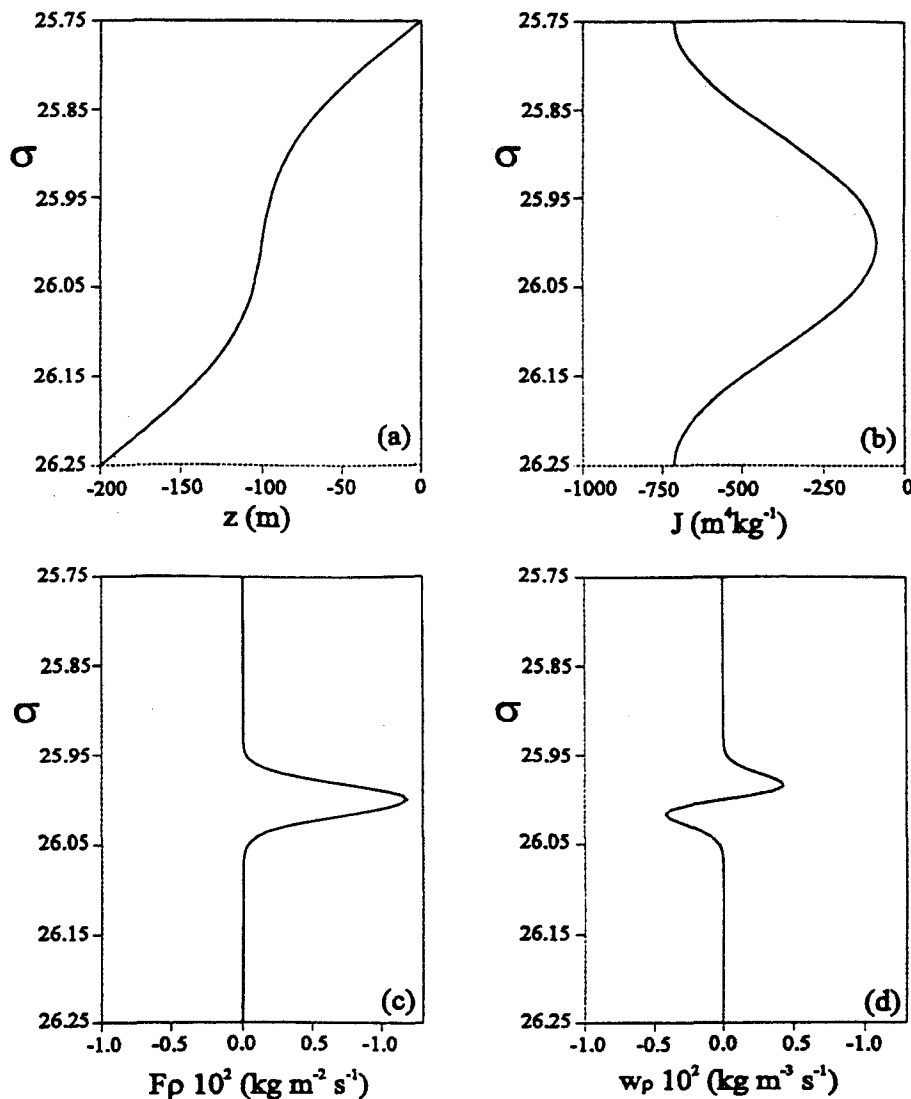


Figure 5. Initial conditions for the numerical calculations. (a) The density stratification is specified as the sum of a background linear stratification and a wave type depth-density perturbation. From the $z = z(\rho)$ field and using $\partial v / \partial \rho = 2.5 \text{ kg m}^{-3} \text{ s}^{-1}$, we obtain the initial (b) Jacobian, (c) vertical density flux, and (d) density tendency.

6. Results and Discussion

Figure 6 shows the temporal evolution of the relevant variables for the purely diffusive case, which corresponds to $\tau = 0$. In this case the system has no memory of turbulence: the maximum in the vertical density flux is responsible for the very rapid initial density convergence/divergence, but the vertical density flux decays simultaneously with the reduction of the density gradient, which inhibits the maintenance of the large density convergence/divergence necessary to produce the well-mixed region. The result is rather rapid density diffusion and the smoothing of the well-stratified region (Figures 6a and 6b), the vertical density flux (Figure 6c), the density tendency (Figure 6d), the diffusion coefficient (Figure 6e; since $\tau = 0$, this case corresponds to $K_i = K_f$), and the local gradient Richardson num-

ber (Figure 6f; since $\partial v / \partial \rho$ is constant, Ri parallels J , Figure 6b). Figure 6f illustrates that Ri remains low during a long period but it is almost constant over a large density range, implying that K_f (Figure 6e) is rather smooth.

Figures 7 and 8 show the temporal evolution for the case where we choose $\tau = N^{-1}$, as discussed in section 4. The initial τ values, for example, range somewhere between 200 s and 100 s for those regions with minimum and maximum stratification, respectively. Figure 7 presents the evolution of the depth, Jacobian, vertical density flux, and density tendency at different times. The situation is quite different from the diffusive case ($\tau = 0$), and it shows how the initially well-stratified region turns into a well-mixed region (Figures 7a and 7b). This mixed region is actually produced by the slow decrease experienced in the vertical density flux and the

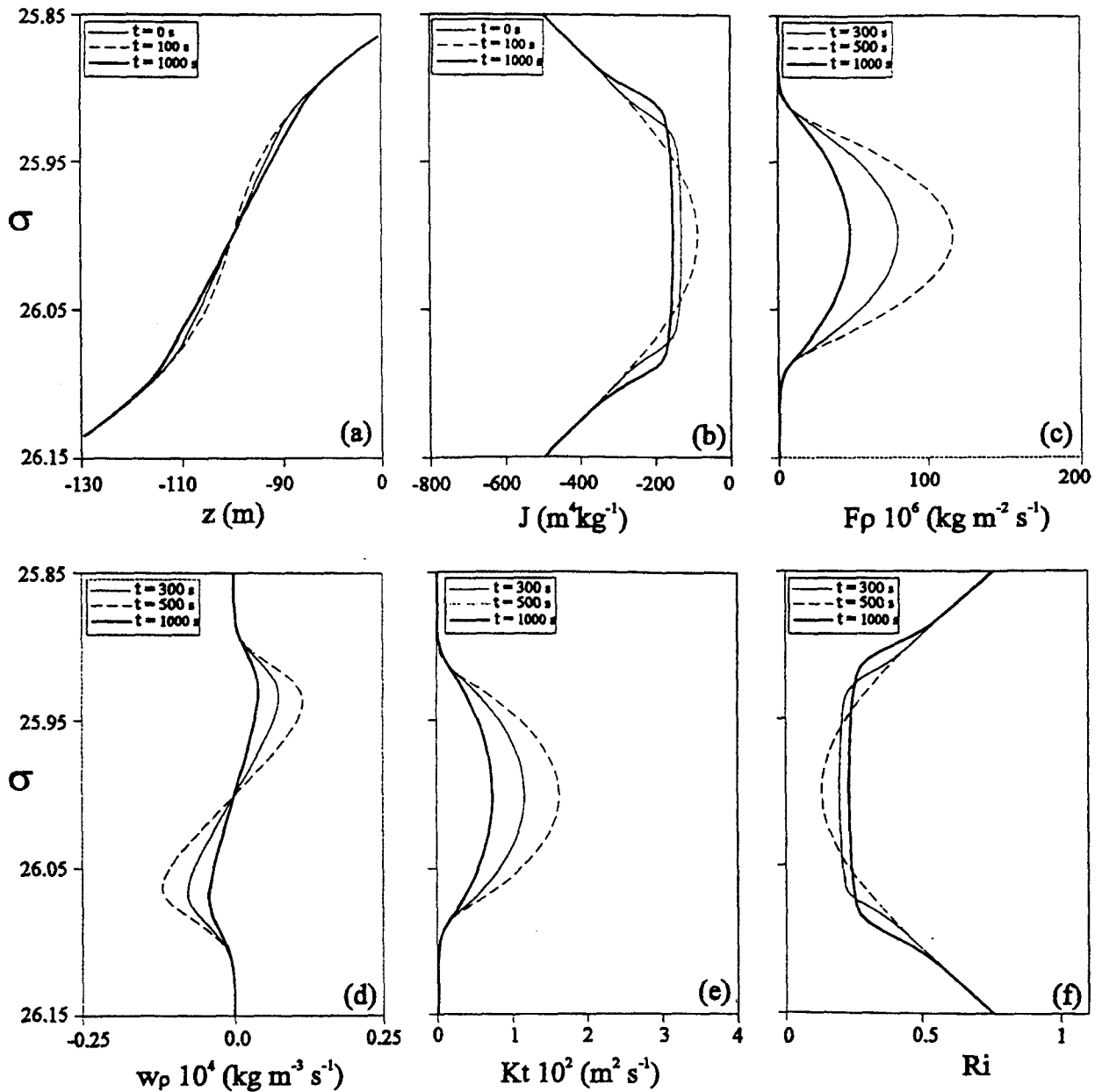


Figure 6. Case with $\tau = 0$, showing the temporal evolution of the density distribution for (a) depth, (b) Jacobian, (c) vertical density flux, (d) density tendency, (e) actual density diffusivity, and (f) local gradient Richardson number.

density tendency (Figures 7c and 7d). Figure 8 clearly illustrates the different behavior of K_t and K_f , showing how the forcing density diffusivity K_f is rapidly reduced (Figure 8b) while the actual density diffusivity K_t remains high much longer due to the temporal memory of turbulence (Figure 8a). Figure 8c shows the evolution of Ri (again paralleling the Jacobian): the initial minimum is rapidly replaced by a maximum with two adjacent minima. The maximum corresponds to the formation of the well mixed layer, while the minima indicate the locations prone to undergo future mixing.

Figures 9 and 10 correspond to the same case as before, with the difference that Shapiro's running filter is applied 30 times to Ri at each time step. Note that

averaging Ri but not J breaks the constant diapycnal shear assumption (equation (6)). The justification for doing so comes from the anisotropy associated with Kelvin-Helmholtz instabilities, which implies that they cannot take place at scales shorter than the Ozmidov scale [Miller and Evans, 1985]; by averaging only Ri , we ponder this minimum vertical size of shear-induced turbulence. Several studies [Miller and Evans, 1985; Gregg, 1987] suggest that in moderately to highly stratified regions the Ozmidov scale will be about 2 - 3 m. Taking 3 m and dividing by 100 kg m^{-3} (a characteristic value of the Jacobian in the well stratified regions) gives a corresponding density scale of 0.03 kg m^{-3} . This shows that about six density levels in our model (re-

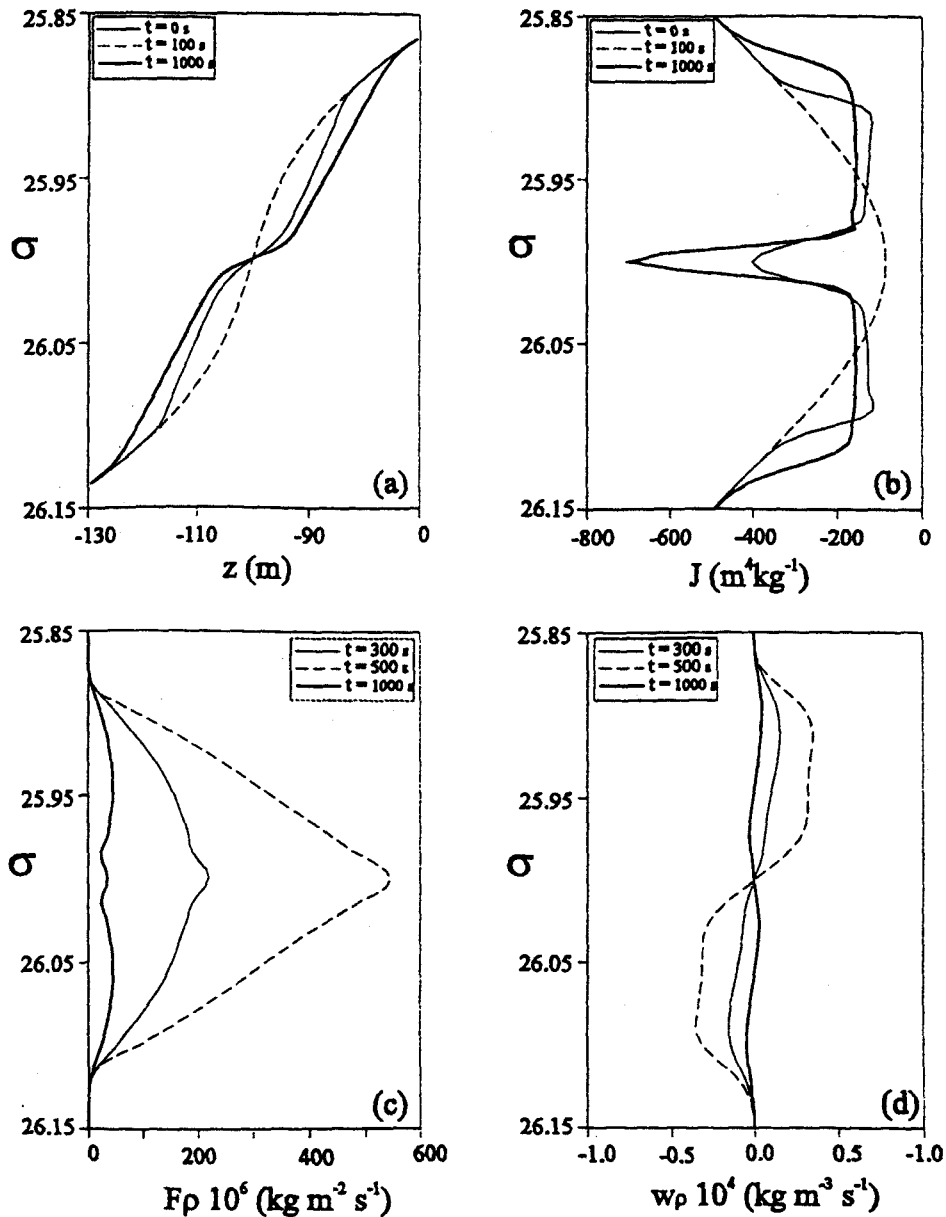


Figure 7. Case with $\tau = N^{-1}$, showing the temporal evolution of the density distribution for (a) depth, (b) Jacobian, (c) vertical density flux, and (d) density tendency.

call $\delta\rho = 0.005 \text{ kg m}^{-3}$) should be averaged to avoid contamination from small-scale turbulence; this is approximately attained with the above running filter. The vertical averaging is clear in the Ri distribution (Figure 10c), which now shows substantial differences from the J distribution (Figure 9b). The main difference with the previous calculations is that the maxima and minima in the different variables are better defined, which results in a clearer steplike structure: the central mixed layer and adjacent interfaces are sharper and additional steps of the staircase are also suggested (Figure 9a).

Several additional runs have been done (1) to examine the differences related to using either the Munk-Anderson or the Peters et al. parameterizations, and (2) to assess the sensitivity to the constant diapycnal shear assumption. The results are not shown here for

the sake of brevity, but they indicate that the Munk-Anderson parameterization can also lead to the generation of mixed layers. The difficulty with this parameterization, however, is that the above initial conditions give values of w_p which are several orders of magnitude too small for the mechanism to operate. In order to attain sufficiently large density tendency values this requires some extra forcing, either through a much larger diapycnal shear or a much smaller Jacobian. A low Jacobian, however, implies a too short turbulent temporal memory ($\tau = N^{-1}$), so the mechanism operates only with unrealistically high diapycnal shear. The second conclusion arising from the test runs is that the assumption of constant diapycnal shear is not critical for the proposed mechanism to operate. This was actually anticipated by the numerical runs shown in Fig-

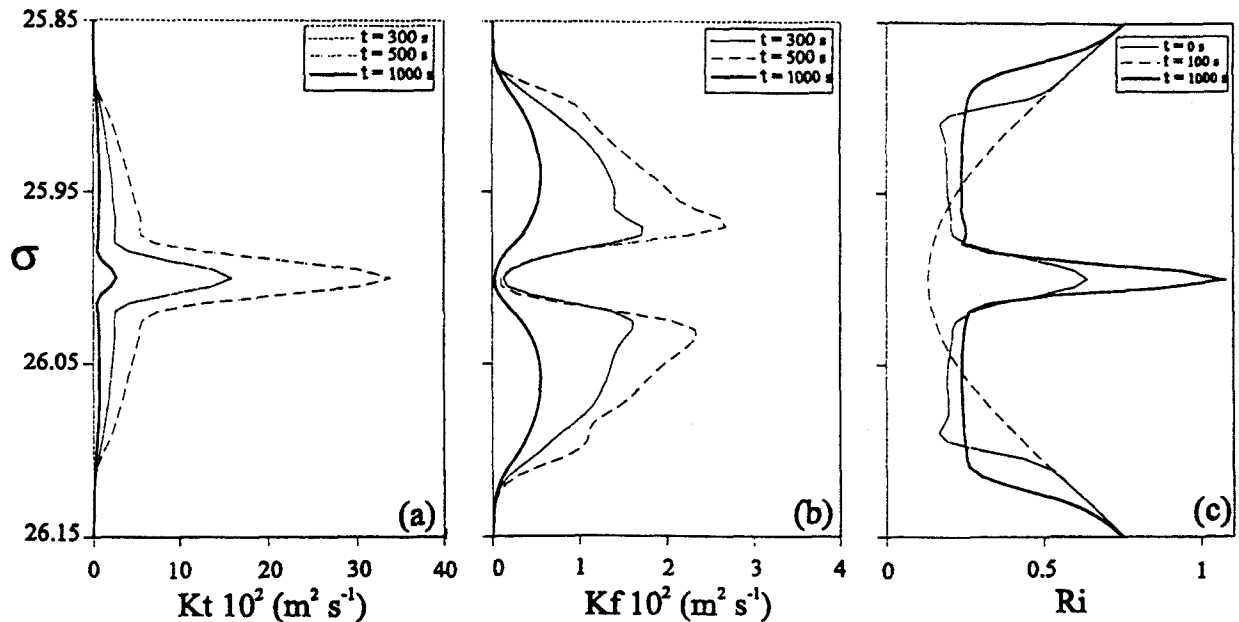


Figure 8. Case with $\tau = N^{-1}$, showing the temporal evolution of (a) actual density diffusivity, (b) instantaneous forcing density diffusivity, and (c) local gradient Richardson number.

ures 9 and 10. We have made other tests, such as letting $\partial v / \partial \rho$ decrease with time, and similar results have been obtained. The conclusion is that as long as $\partial v / \partial \rho$ remains of the same order, the level of turbulence (and hence K_f) is substantially unchanged.

Despite the conceptual justifications for a constant diapycnal shear and the relatively low sensitivity of the model to changes in $\partial v / \partial \rho$, it is clear that the lack of dynamics is a major limitation of our model. However, we believe that for geophysical flows our simple model probably reproduces the main features, leading to the evolution from continuous stratification into mixed layers. This statement is further supported by the following consideration. In our model the temporal memory of turbulence is related to the inverse buoyancy frequency. This poses a lower limit to the time required for changes in the vertical density flux, independent of faster changes in the diapycnal shear. For geostrophically balanced flows, however, this limit should actually be much larger. The reason is that rapid changes in the isopycnal slopes, such as those caused by localized mixing, are not immediately followed by a change in the geostrophic diapycnal shear. This delay is related to the relatively large characteristic timescale of geostrophic flows, much larger than the inverse buoyancy frequency, and it should be indicative of the actual time required for substantial changes in the diapycnal shear to take place.

We have argued that shear-induced, Kelvin-Helmholtz type, instabilities are the likely physical mechanism responsible for mixing in the reported numerical calculations. This conclusion is based on the fact that the eddy density flux is parameterized in terms of the gradient Richardson number, as expected for these instabilities, and that there is experimental and field

data that corroborates their presence in the development of mixed layers. It is possible, however, that our numerical simulations may also represent the generation of mixed layers by other physical mechanisms. *De Silva and Fernando* [1992], for example, have reported laboratory experiments in which a grid oscillating in an initial linearly stratified fluid produces a well-mixed turbulent patch. In their experiments, with no mean shear, the source of turbulence is clearly not related to Kelvin-Helmholtz instabilities. The main difficulty with this and other possible sources of instability is to identify how the physical mechanism operates and how the vertical density flux should be parameterized. This is clearly related to *De Silva and Fernando's* [1992] warning that "in the oceanic context the exact nature and strength of turbulent sources are not known and the extrapolation of the laboratory results to oceanic cases should be done with caution." For this reason, we believe that it is particularly important not to separate numerical solutions from physical reasoning.

7. Conclusions

We have presented a simple process-oriented model that studies the formation of mixed layers in stratified geophysical flows. The model is based on the idea that well-stratified regions with high diapycnal shear are dynamically unstable and Kelvin-Helmholtz type instabilities develop. These instabilities cause the stratified region to mix and adjacent interfaces to be formed. For this mechanism to operate the vertical density diffusivity must fulfill two conditions. First, the diffusivity must monotonically increase with decreasing gradient Richardson numbers, and second, it must have a temporal memory of turbulence.

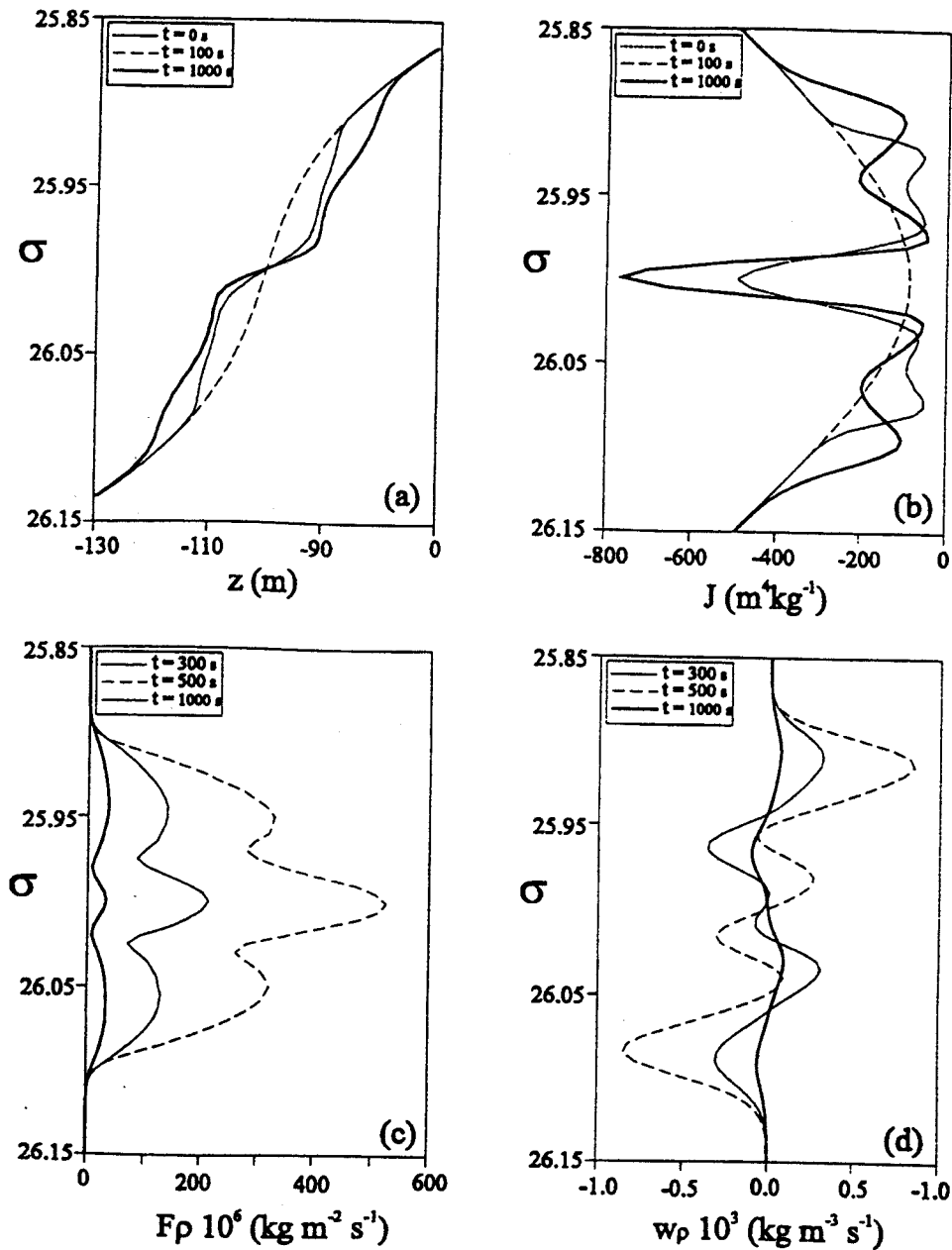


Figure 9. Case with $\tau = N^{-1}$ and a running filter applied to Ri , showing the temporal evolution of the density distribution for (a) depth, (b) Jacobian, (c) vertical density flux, and (d) density tendency.

Our numerical calculations show that an initially highly stratified but unstable region is merely diffusive if turbulence has no memory. If we allow a finite temporal adjustment for turbulence, however, the stratified region becomes well mixed and sharp interfaces are generated above and below. If we further take into account the minimum vertical scale for Kelvin-Helmholtz instabilities, then the staircase becomes clearer, with the adjacent stratified regions showing some breaking into new mixed layers.

The numerical results shown correspond to constant diapycnal shear, but several tests indicate that the results are rather robust and depend little on temporal changes of the diapycnal shear. Further studies are re-

quired to incorporate more realistic dynamics, including vertical mixing of momentum and the evolution of geostrophic shear flow in frontogenetical systems. Additional efforts are also required to obtain both laboratory and field data in order to properly validate the proposed mechanism.

The mechanism we have presented clearly differs from Phillips' in two main respects. First, the dynamics of the instability process is different: shear-induced mixing rather than mixing generated through oscillating rods. A consequence is that for Phillips, the vertical density diffusivity has a maximum as a function of some properly defined local Richardson number, which is not the local gradient Richardson number Ri . However, the

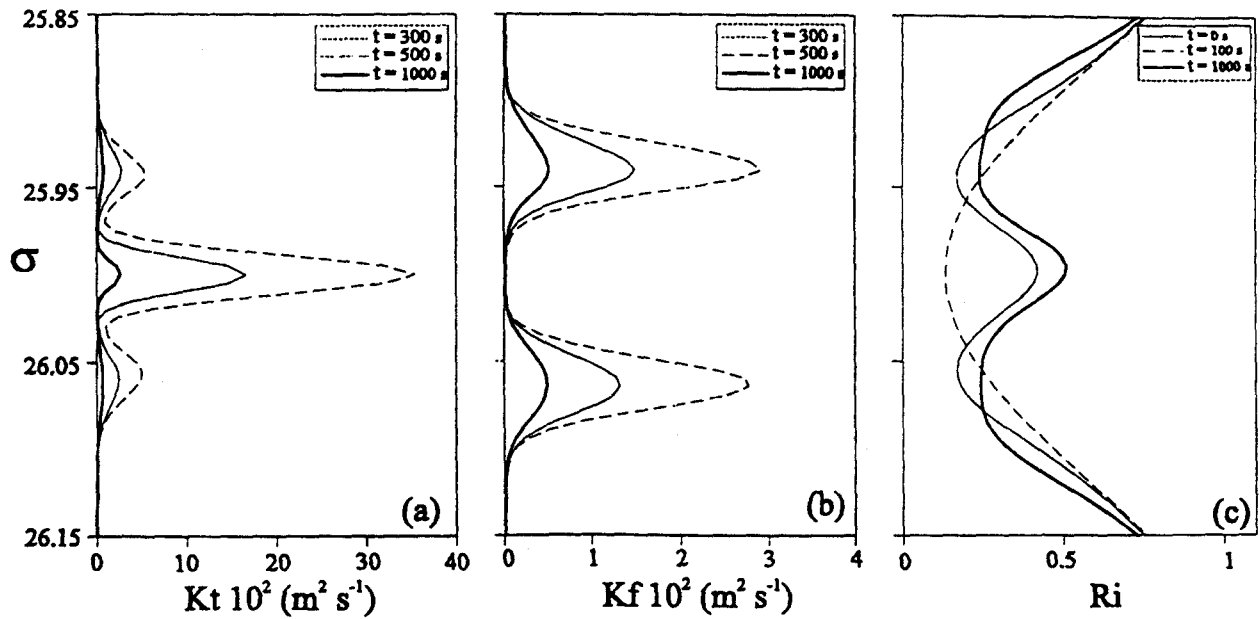


Figure 10. Case with $\tau = N^{-1}$ and a running filter applied to Ri , showing the temporal evolution of (a) actual density diffusivity, (b) instantaneous forcing density diffusivity, and (c) local gradient Richardson number.

vertical density diffusivity in the proposed mechanism monotonically increases with decreasing Ri . Second, the kinematics of mixing is totally opposite: a highly stratified region splitting into a mixed region and two adjacent interfaces rather than a growing perturbation in the depth-density profile.

Acknowledgments. This paper had its original motivation from Gabe Csanady's emphasis on thinking in terms of isopycnic coordinates. We wish to thank him for suggesting this approach as well as for his contagious enthusiasm on physical reasoning. We are also grateful to one anonymous reviewer for a number of useful comments. This work has been supported by the Spanish government through project FRENTE (CICYT grant AMB95-0731) and by the European Union through project CANIGO (MAST grant MAS3-CT96-0060).

References

- Aristegui, J., P. Sangrà, S. Hernández-León, M. Cantón, A. Hernández-Guerra, and J. L. Kerling, Island-induced eddies in the Canary Islands, *Deep Sea Res.*, **41**, 1509-1525, 1994.
- Bane, J. M., D. A. Brooks, and K. R. Lorenson, Synoptic observations of the three-dimensional structure and propagation of Gulf Stream meanders along the Carolina continental margin, *J. Geophys. Res.*, **86**, 6411-6425, 1981.
- Barenblatt, G. I., M. Bertsch, R. dal Passo, V. M. Prostokishin, and M. Ughi, A mathematical model of turbulent heat and mass transfer in stably stratified shear flow, *J. Fluid Mech.*, **253**, 341-358, 1993.
- Browning, K. A., and C. D. Watkins, Observations of clear air turbulence by high power radar, *Nature*, **227**, 260-263, 1970.
- Cisneros-Aguirre, J., J. L. Pelegrí, and P. Sangrà, Experiments on layer formation in stratified shear flows, paper presented at Meeting on Mixing in Geophysical Flows II, Universitat Politècnica de Catalunya, Barcelona, April 1997.
- Csanady, G. T., *Turbulent Diffusion in the Environment*, 248 pp., D. Reidel, Norwell, Mass., 1973.
- Csanady, G. T., Intermittent "full" upwelling in Lake Ontario, *J. Geophys. Res.*, **82**, 397-419, 1977.
- Csanady, G. T., Shelf circulation cells, *Philos. Trans. R. Soc. London, Ser. A*, **302**, 515-530, 1981.
- Csanady, G. T., On the structure of transient upwelling events, *J. Phys. Oceanogr.*, **12**, 84-96, 1982.
- Csanady, G. T., Radiation of topographic waves from Gulf Stream meanders, *Continental Shelf Res.*, **8**, 673-686, 1988.
- Csanady, G. T., Energy dissipation and upwelling in a western boundary current, *J. Phys. Oceanogr.*, **19**, 462-473, 1989.
- Csanady, G. T., Mixing in coastal regions, in *The Sea: Ocean Engineering Science*, vol. 9, edited by B. Le Mehaute and D. M. Hanes, pp. 593-629, John Wiley, New York, 1990.
- Csanady, G. T., and J. L. Pelegrí, Vorticity balance of boundary currents, *J. Mar. Res.*, **53**, 171-187, 1995.
- De Silva, L. P. D., and H. J. S. Fernando, Some aspects of mixing in a stratified turbulent patch, *J. Fluid Mech.*, **240**, 601-625, 1992.
- Fernando, H. J. S., Turbulent mixing in stratified fluids, *Annu. Rev. Fluid Mech.*, **23**, 455-493, 1991.
- Fernando, H. J. S., Experiments on some stratified and rotating flows of geophysical relevance, paper presented at the Meeting on Mixing in Geophysical Flows II, Universitat Politècnica de Catalunya, Barcelona, April 1997.
- Gregg, M. C., Diapycnal mixing in the thermocline: A review, *J. Geophys. Res.*, **92**, 5249-5286, 1987.
- Holt, S. E., J. R. Koseff, and J. H. Ferziger, A numerical study of the evolution and structure of homogeneous stably stratified sheared turbulence, *J. Fluid Mech.*, **237**, 499-539, 1992.
- Howard, L. N., Note on a paper by John W. Miles, *J. Fluid Mech.*, **95**, 509-512, 1961.

- Ivey, G. N., and J. Imberger, On the nature of turbulence in stratified fluid, Part I, The energetics of mixing, *J. Phys. Oceanogr.*, **21**, 650-658, 1991.
- Kranenburg, C., On gradient transport turbulence models for stably stratified shear flows, *Dyn. Atmos. Oceans*, **23**, 205-215, 1996.
- Lee, S., and G. T. Csanady, Instability waves in the Gulf Stream front and its thermocline layer, *J. Mar. Res.*, **52**, 837-863, 1994.
- Linden, P. F., Mixing in stratified fluids, *Geophys. Astrophys. Fluid Dyn.*, **13**, 3-23, 1979.
- Linden, P. F., Mixing across a density interface produced by grid turbulence, *J. Fluid Mech.*, **100**, 691-703, 1980.
- McDougall, T. J., and Y. You, Implications of the nonlinear equation of state for upwelling in the ocean interior, *J. Geophys. Res.*, **95**, 13,263-13,276, 1990.
- Miles, J. W., On the stability of heterogeneous shear flows, *J. Fluid Mech.*, **10**, 496-508, 1961.
- Miller, J. L., and D. L. Evans, Density and velocity enhancement in oceanic eddies, *J. Geophys. Res.*, **90**, 4793-4806, 1985.
- Munk, W. H., and E. R. Anderson, Notes on a theory of the thermocline, *J. Mar. Res.*, **7**, 276-295, 1948.
- Pacanowski, R. C., and S. G. H. Philander, Parameterization of vertical mixing in numerical models of tropical oceans, *J. Phys. Oceanogr.*, **11**, 1443-1451, 1981.
- Park, Y., J. A. Whitehead, and A. Gnanadeskian, Turbulent mixing in stratified fluids: Layer formation and energetics, *J. Fluid Mech.*, **279**, 279-311, 1994.
- Pelegrí, J. L., and G. T. Csanady, Nutrient transport and mixing in the Gulf Stream, *J. Geophys. Res.*, **96**, 2577-2583, 1991.
- Pelegrí, J. L., and G. T. Csanady, Diapycnal mixing in western boundary currents, *J. Geophys. Res.*, **99**, 18,275-18,304, 1994.
- Pelegrí, J. L., G. T. Csanady, and A. Martins, The North Atlantic nutrient stream, *J. Oceanogr.*, **52**, 275-299, 1996.
- Peters, H., M. C. Gregg, and J. M. Toole, On the parameterization of equatorial turbulence, *J. Geophys. Res.*, **93**, 1199-1218, 1988.
- Phillips, O. M., Turbulence in a strongly stratified fluid - Is it unstable?, *Deep Sea Res.*, **19**, 79-81, 1972.
- Pollard, R. T., P. B. Rhines, and R. O. R. Y. Thompson, The deepening of the wind-mixed layer, *Geophys. Fluid Dyn.*, **4**, 381-404, 1973.
- Posmentier, E. S., The generation of salinity finestructure by vertical diffusion, *J. Phys. Oceanogr.*, **7**, 298-300, 1977.
- Rosby, C. G., Dynamics of steady ocean currents in the light of experimental fluid mechanics, *Papers Phys. Oceanogr. Meteorol.*, **5**, 1-43, 1936.
- Ruddick, B. R., T. J. McDougall, and J. S. Turner, The formation of layers in a uniformly stirred density gradient, *Deep Sea Res.*, **36**, 597-609, 1989.
- Shapiro, R., Smoothing, filtering, and boundary effects, *Rev. Geophys.*, **8**, 359-387, 1970.
- Simpson, J. H., The shelf-sea fronts: Implications of their existence and behaviour, *Philos. Trans. R. Soc. London, Ser. A*, **302**, 531-546, 1981.
- Thorpe, S. A., Experiments on the instability of stratified shear flow: miscible fluids, *J. Fluid Mech.*, **46**, 299-319, 1971.
- Thorpe, S. A., Transitional phenomena and the development of turbulence in stratified fluids: A review, *J. Geophys. Res.*, **92**, 5231-5248, 1987.
- Turner, J. S., *Buoyancy Effects in Fluids*, 367 pp., Cambridge Univ. Press, New York, 1973.
- Turner, J. S., Turbulent entrainment: The development of the entrainment assumption, and its application to geophysical flows, *J. Fluid Mech.*, **173**, 431-471, 1986.
- Woods, J. D., Wave-induced shear instability in the summer thermocline, *J. Fluid Mech.*, **32**, 791-800, 1968.
- Woods, J. D., and R. L. Wiley, Billow turbulence and ocean microstructure, *Deep Sea Res.*, **19**, 87-121, 1972.

J. L. Pelegrí and P. Sangrà, Facultad de Ciencias del Mar, Campus Universitario de Tafira, Universidad de Las Palmas de Gran Canaria, 35017 Las Palmas de Gran Canaria, Spain. (e-mail: joseluis.pelegri@fisica.ulpgc.es; pablo.sangra@fisica.ulpgc.es)

(Received August 29, 1996; revised January 21, 1998; accepted January 30, 1998.)



Modeling of Shear-Induced Diapycnal Mixing in Frontal Systems

J.L. PELEGRÍ, A. RODRÍGUEZ-SANTANA, P. SANGRÀ and
A. MARRERO-DÍAZ

Departamento de Física, Facultad de Ciencias del Mar, Universidad de Las Palmas de Gran Canaria, 35017 Las Palmas de Gran Canaria, Spain

Abstract. Three shear-induced mixing models are examined and applied to oceanic frontal systems. These are a simple diagnostic model, a one-dimensional kinematical model and a two-dimensional geostrophic model. All of these are process-oriented models in isopycnic coordinates, with diapycnal mixing depending on the gradient Richardson number and mixing rapidly developing in subcritical flows. In the first model an initial subcritical condition is specified and mixing is allowed to redistribute the vertical density flux. In the second model the dynamics is specified *ad hoc* to simulate a frontal system which leads to subcritical conditions and we are left to solve the mass conservation equation. In the final model a two-dimensional density-depth field is forced through an externally imposed deformation velocity field and we solve both the mass and momentum conservation equations. In this last model diapycnal mixing controls the mass conservation equation while the momentum equations consist in cross-stream geostrophic balance. All three models produce mixed regions which probably correspond to some of the fine structure density-depth steps that are observed in geophysical flows. The very simple diagnostic and kinematical models have the merit of providing a clear picture of the physical mechanism that produces the density-depth steps, but the potential complexity of the solution is only appreciated when incorporating the dynamics, such as in the geostrophic model.

Key words: diapycnal mass transfer, frontal systems, isopycnic coordinates, process-oriented models, shear-induced mixing.

1. Introduction

Frontal systems are recognized to act as a boundary between different regions in geophysical flows, either in the atmosphere or the ocean. One large-scale example for the atmosphere is the upper level frontal system which separates the polar and subtropical air masses. Other atmospheric examples may be found at much shorter scales in the planetary boundary layer, being responsible of rapid changes in local weather. In the ocean there are numerous large-scale frontal regions which separate different oceanic waters, while at shorter scales there is a quite large variety, with fronts separating estuarine from coastal waters, coastal from oceanic waters, or different areas of shallow seas.

The importance of frontal systems as barriers between different oceanic or atmospheric regions contrasts with the possibility of cross-frontal transfer due to

dynamic instabilities [1, 5, 13, 21]. This consideration for the upper level frontal atmospheric system drew considerable attention in the 50s and 60s to the fate of radioactivity generated by nuclear testing in the stratosphere and more recently to the transfer of chlorofluoromethanes from the troposphere to the stratosphere. In the ocean, on the other hand, considerable effort has been placed to study the exchange of contaminants from the continental platform to the interior deep ocean across shelf-edge fronts, and to the vertical exchange of nutrients in coastal upwelling regions.

One difficulty in the understanding of frontal systems is that not only passive properties are transferred across them but also active properties, such as mass and potential vorticity. This redistribution modifies the kinematics and dynamics of the front and creates a feedback that considerably complicates the problem [4, 14]. Diapycnal mass transfer in oceanic fronts, for example, must affect the separation between adjacent isopycnals, placing a limit in the degree of frontogenetical compression. These type of arguments point at the need of attaining an adequate understanding on those processes which may enhance the exchange of properties across a frontal system. The best way to do this, we believe, is with a careful examination of the physical mechanisms and their analysis through process-oriented type models. These models have to be simple enough to let us understand the controlling mechanisms but they must be accurate enough to include the main physical elements. Once the mechanisms are understood we will be able to include them in more complex predictive-type models.

In the ocean there are many physical mechanisms which may be responsible for producing diapycnal mixing, such as double diffusion, convective overturning, one-way entrainment induced through boundary stresses, and shear-induced mixing. In this paper we will examine the latter of these processes (shear-induced mixing) which is likely to be very important in strong baroclinic oceanic jets. Our approach will be to examine the results of three different process-oriented models for shear-induced diapycnal mixing in frontal systems. The models are designed in isopycnic coordinates in order to examine oceanic processes; the extension to the atmospheric case, however, could be easily attained by using isentropic coordinates, with potential temperature replacing potential density. One advantage of isopycnic coordinates is their excellent resolution of regions which are highly stratified in the vertical and horizontal directions. Another advantage is that they allow us to examine mixing processes along surfaces of constant density (epipycnal mixing) and across such surfaces (diapycnal mixing) in well-stratified anisotropic fluids. These processes are well identified with physical causes, no matter how steep the isopycnals may be, in contrast to the horizontal and vertical mixing coefficients that need to be specified in Cartesian coordinates.

In Section 2 we will discuss some concepts related to the stability of stratified shear flow, with emphasis on their interpretation in isopycnic coordinates, and we will analyze how this stability may be modified in frontogenetical systems. In Sections 3 to 5 we will present the fundamentals and results for three very different

models which aim at understanding how shear-induced diapycnal mixing operates in frontal systems. An intercomparison between the simplifications involved in each model and the increasing detail of the numerical solution will allow us to appreciate both the way in which shear-induced mixing operates and the necessary elements for the model to exhibit a realistic character (Section 6).

2. Parameterization of Shear-Induced Mixing

A somehow surprising characteristic of frontogenesis is that it causes a redistribution of mass and momentum (e.g., [12]) which leads to large *static* stability (appearing as a barrier to cross-frontal advection of properties) but to low *dynamic* stability (enhancing the blending of properties across the front through mixing processes). The fact is that diapycnal mixing has been observed to be very important in both oceanic and atmospheric frontal systems [1, 6, 13–15], but still little is known on the kinematics and dynamics of this process as well as on its relative importance in diffusing properties.

A criterion for the stability of stratified shear flow may be obtained either from energy arguments [9, 20, 22] or from the stability analysis of the equations of motion [3, 8]. The criterion is expressed in terms of a gradient Richardson number Ri defined as

$$Ri = \frac{-g \frac{\partial \rho}{\partial z}}{\rho \left(\frac{\partial v}{\partial z}\right)^2} = \frac{-g \frac{\partial z}{\partial \rho}}{\rho \left(\frac{\partial v}{\partial \rho}\right)^2}, \quad (1)$$

with the first equality expressed in Cartesian coordinates and the second one in isopycnic coordinates. In this expression g is the gravity acceleration, v is the magnitude of the horizontal velocity, ρ is the potential density and z is the vertical coordinate. When Ri goes below a certain critical value, Ri_c , we may expect that Kelvin–Helmholtz type instabilities will develop. Under this condition the flow is dynamically unstable (subcritical), which means that any vertical displacement will tend to grow in time through transformation of kinetic energy into potential energy. The Ri_c value is determined from the linearized stability analysis of the mass and momentum equations, its exact value depending on the characteristics of the shear flow under consideration, with $Ri_c = 0.25$ for the case of unbounded parallel shear flow. An upper limit for Ri_c may be obtained through energy arguments, typically with a value of one [9].

Pelegrí and Sangrà [16] have recently discussed the meaning of stratification and velocity shear in the above equation for Ri , pointing out that the role of stratification appears to differ depending on whether we use Cartesian or isopycnic coordinates. In Cartesian coordinates an increase in stratification leads to supercritical conditions (an increase in Ri) while in isopycnic coordinates such an increase leads to subcritical conditions. Pelegrí and Sangrà [16] argue that the solution to this paradox lies on the behavior of the diapycnal and vertical shears, which are related by $\partial v / \partial \rho = J \partial v / \partial z$, where the Jacobian $J = \partial z / \partial \rho$ is the inverse of

the vertical density gradient. For the case of constant vertical shear an increase in stratification represents further dynamic stability. For constant diapycnal shear, however, an increase in stratification (a reduction in J) really corresponds to an increase in vertical shear, with the quadratic dependence causing a decrease in dynamic stability.

In frontogenetical situations there are several possibilities which depend on the evolution of the density field, but they all suggest a shift towards subcritical conditions. If there is an increase in the horizontal density gradient then the thermal wind relation in Cartesian coordinates ($\rho f \partial v / \partial z = g \partial \rho / \partial x$) implies that the geostrophic vertical shear will increase. In this case the maintenance of supercritical conditions will only be possible if there is a substantial increase in vertical stratification. The main difficulty with this Cartesian approach is that during a frontogenetical situation these two quantities ($\partial \rho / \partial z$ and $\partial v / \partial z$) are not really independent because of the temporal evolution of the isopycnals' slope. This is clear if we analyze the problem in isopycnic coordinates, with the thermal wind relation showing that the slope of the isopycnals is proportional to the geostrophic diapycnal shear ($\rho f \partial v / \partial \rho = g \partial z / \partial x$). In a situation in which the isopycnals become steeper and the vertical stratification increases then the resulting situation is easily appreciated through the expression for Ri in isopycnic coordinates, which shows that both these changes enhance the dynamic instability.

The vertical density flux $F \equiv \overline{w' \rho'}$ gives the rate of vertical mass transfer per unit area arising from the correlation between density and vertical velocity fluctuations (ρ' and w' , respectively). F is usually related to the vertical density diffusivity K through a relation of the type [2, 7, 14, 19]

$$F = -\frac{K}{J} . \quad (2)$$

This relation suggests that a sudden growth in vertical fluctuations (unstable behavior) has to be directly related to a growth in K .

Most parameterizations leading to oceanic K values are of the Munk–Anderson type [11]: $K = K_0(1 + \beta Ri)^{-n}$, where K_0 is the maximum K value corresponding to vertical neutral conditions, and β , n are positive constants. This $K(Ri)$ dependence suggests a considerably smooth transition from supercritical to subcritical conditions and contradicts the catastrophic-type behavior to be expected from the theoretical existence of a unique Ri_c for each flow type. There may be several reasons behind this, such as the difficulty of having a field or experimental flow with spatial homogeneity, the dependence of F on the vertical stratification (Equation (2)) and the temporal memory of turbulence which introduces a non-linear behavior.

One alternative to the Munk–Anderson $K(Ri)$ parameterization has been proposed by Peters et al. [17]. These authors analyzed stratification and energy dissipation data from the equatorial undercurrent and obtained a two-regime dependence, with a high inverse dependence on Ri ($K \propto Ri^{-9}$) for $Ri \leq 0.4$:

$$K = \begin{cases} 1.1 \times 10^{-8} \text{Ri}^{-9.2}, & \text{Ri} \leq 0.4, \\ 1.3 \times 10^{-6} + 5 \times 10^{-4} (1 + 5\text{Ri})^{-2.2}, & \text{Ri} > 0.4. \end{cases} \quad (3)$$

In this expression (with K in MKS units) we have determined the high-Ri dependence by adjusting it to the data points reported by Peters et al. [17]. This two-regime behavior has the appeal of reproducing the existence of a critical Ri value, below which instabilities must develop very rapidly. In this work (Sections 4 and 5) we will follow this representation because of its theoretical-like behavior which enhances the appearance of strong diapycnal mixing for subcritical conditions.

3. A Simple Diagnostic Approach

In this section we will examine a simple diagnostic model, similar to the one proposed by Pelegrí and Csanady [14]. Our objective will be to appreciate how frontogenesis leads to the subcritical conditions necessary for the development of strong diapycnal mixing and how this mixing can modify the density-depth distribution, creating a constant density region.

Let us consider a location where the vertical stratification is given by the Jacobian distribution shown as a solid line in Figure 1a, with a minimum located at some isopycnal (in this case at a potential density level given by $\sigma \equiv \rho - 1000 = 26.73$, with ρ in MKS units). These Jacobian values set a vertical scale characteristic of highly stratified regions in frontal systems [14]. The corresponding vertical density flux is obtained from Equations (1) and (2):

$$F = \frac{g K}{\rho \text{Ri} \left(\frac{\partial v}{\partial \rho} \right)^2}. \quad (4)$$

Equations (3) and (4) show that in subcritical conditions the vertical density flux has a very high inverse dependence with Ri, i.e., $F \propto \text{Ri}^{-10}$. This clearly suggests that under these conditions a small decrease in Ri causes a very large increase in turbulent vertical density transfer, consistent with the theoretical catastrophic behavior.

The discussion in the last section illustrated some of the possibilities taking place during frontogenesis. Two such possibilities are vertical compression of the isopycnals (a decrease in J) and the steeping up of the isopycnals (an increase in $\partial v / \partial \rho$), both leading to a decrease in Ri. Hence, we will follow the argument that the condition depicted by the solid line in Figure 1a corresponds to the vertical stratification arising after some frontogenetical period. The corresponding vertical density flux is calculated using Equation (4) (with Ri evaluated from the second equality in Equation (1)), which requires a knowledge of the diapycnal shear. In order to estimate its magnitude we will assume that the diapycnal shear is equal to $2.5 \text{ m}^4 \text{ kg}^{-1} \text{ s}^{-1}$ when the subcritical condition is reached [14], in this manner we

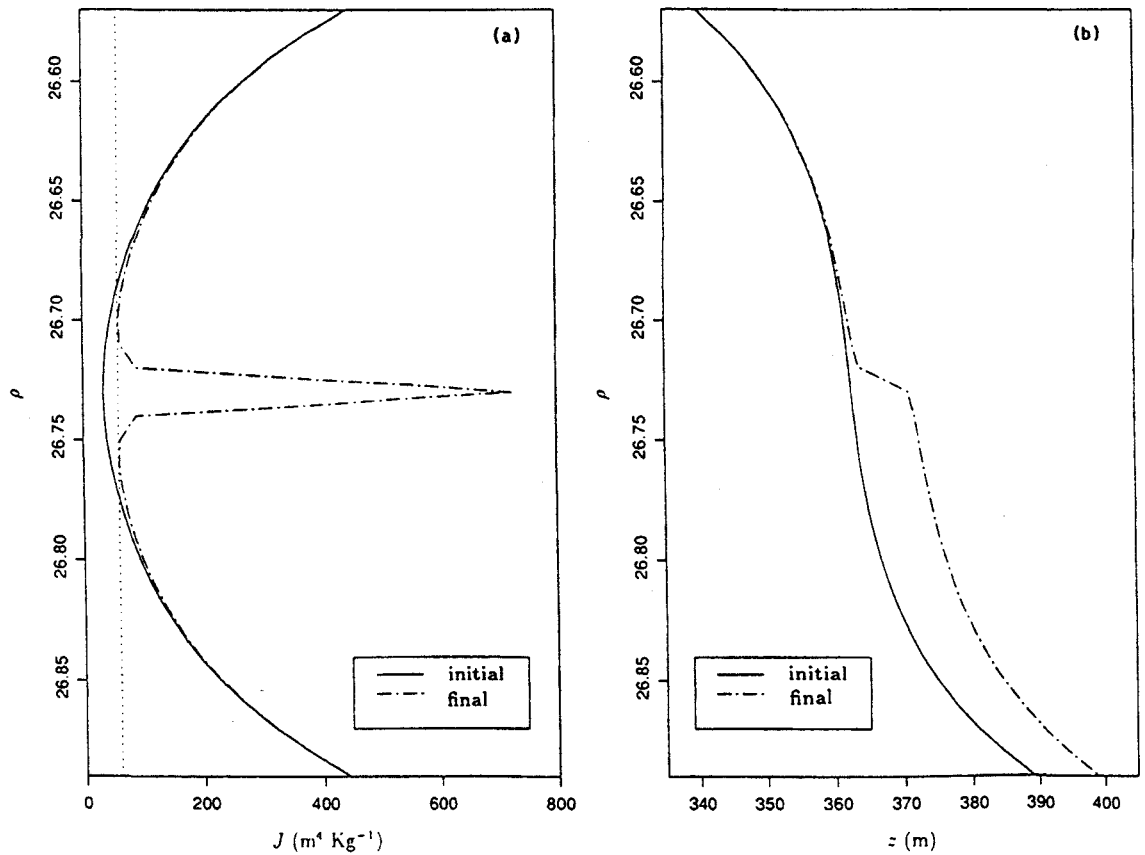


Figure 1. (a) Proposed J distributions after a period of frontogenesis and previous to the occurrence of intense mixing (solid line) and immediately after the occurrence of intense mixing (dashed line); the vertical dotted line shows the Jacobian value that leads to $Ri = 0.25$. (b) Corresponding density-depth distributions previous to mixing (solid line) and after mixing (dashed line).

obtain the F and $-\partial F/\partial z$ distributions depicted in Figure 2a (dotted and dashed lines, respectively).

Our following assumption will be to allow the high F values to mix the well stratified region. This may be understood as the result of the opposite peaks in $\partial F/\partial z$ (Figure 2a), which are responsible for the existence of a region with mass convergence next to a region with mass divergence. If this situation is maintained for a long enough period it will result in the spreading of the isopycnals. For this simulation we will simply diagnose the resulting F distribution (Figure 2b), where the previous peak in F goes to zero (the mixed region with near-zero density fluctuations) and is replaced by two adjacent maxima. The new J distribution is then obtained from Equations (1) and (4), and confirms that the previous subcritical J values have turned into supercritical (dashed line in Figure 1a). Figure 1b shows the density-depth distribution obtained after integration of the J distribution from the lowest isopycnal, before and after mixing (solid and dashed lines, respectively). These distributions illustrate how the mixing event causes the creation of a constant density region.

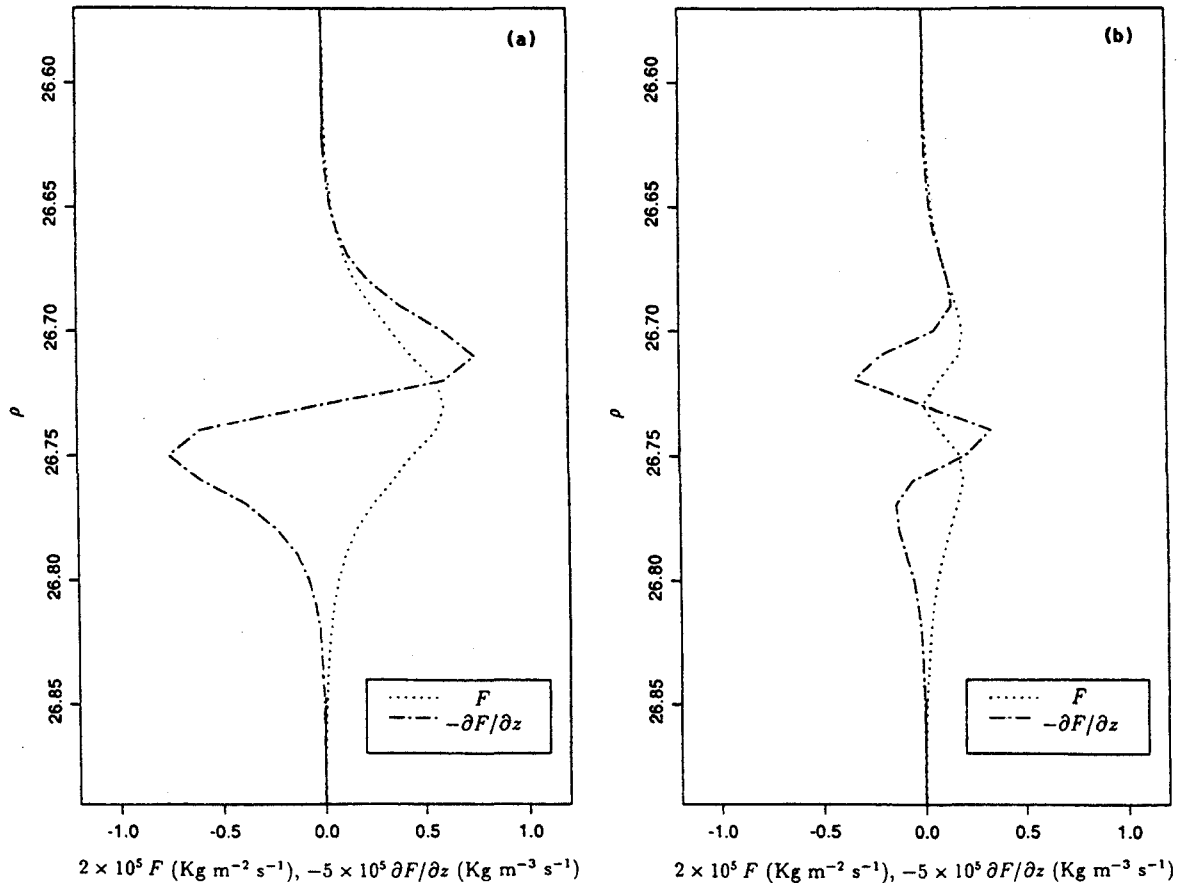


Figure 2. (a) F and $-\partial F/\partial z$ distributions immediately before intense mixing. (b) F and $-\partial F/\partial z$ distributions after the occurrence of intense mixing.

It is worth emphasizing that in the above model the well-mixed layers are created through a physical process which is completely different from Phillips–Posmentier’s mechanism [18, 19]. In the Phillips–Posmentier model a mixed layer is generated as a growing perturbation in the density–depth profile, resulting from the existence of a maximum in the functional dependence $K(\text{Ri})$. In Pelegrí and Csanady’s [14] model the vertical density diffusivity monotonically increases with decreasing Ri , which causes that the initially well stratified region is dynamically unstable and splits into a mixed layer and two adjacent interfaces.

The model we have just discussed is extremely simple because it lacks any kinematics or dynamics. In this model we dictate how the subcritical region behaves by forcing the initial peak in vertical density flux convergence to turn into near-zero values. The reason for this is the theoretical catastrophic type behavior of $K(\text{Ri})$ for subcritical Ri regions, suggesting that Kelvin–Helmholtz type instabilities will develop and mix a very localized region [23]. The limitation of the above model is that we must diagnose the initial and final F distributions, without any consideration of the transient states. In the next section we will examine how Pelegrí and Sangrà [16] have gone one step further by examining the transients with an *a priori* specified dynamics.

4. A Fully Kinematical Model

In this section we will apply Pelegrí and Sangrà's [16] model to a frontal system which is undergoing a continuous horizontal compression, i.e., an increase in the slope of the isopycnals. This model has two important additional attributes with respect to the previous one. First, the water mass redistribution caused by instabilities developing in the subcritical region is calculated according to the mass conservation equation in isopycnic coordinates and through Peters et al.'s [17] parameterization of the vertical density flux in terms of the gradient Richardson number. And second, mixing is allowed to operate during a finite interval of time through a Langevin type equation, which takes into account the temporal memory of turbulence. The model, however, lacks any iterative dynamics, in the sense that the diapycnal shear has to be externally imposed.

The mass conservation equation in isopycnic coordinates is given by [14]:

$$\frac{\partial j}{\partial t} = - \left[\frac{\partial(uj)}{\partial x} + \frac{\partial(vj)}{\partial y} \right] - \frac{\partial(j w_\rho)}{\partial \rho}, \quad (5)$$

where $j \equiv J\rho$ is a separation index between isopycnals, and w_ρ is the material derivative of density (or density tendency) given by [14]:

$$w_\rho \equiv \frac{d\rho}{dt} = - \frac{\partial F}{\partial z} = \frac{\partial}{\partial z} \left(\frac{K}{J} \right). \quad (6)$$

For the case of dominant vertical mass transfer the above mass conservation equation may be approximated by [16]:

$$\frac{\partial j}{\partial t} = - \frac{\partial(j w_\rho)}{\partial \rho}. \quad (7)$$

Pelegrí and Sangrà [16] used a $K(\text{Ri})$ parameterization which was a combination of Peters et al.'s [17] dependence for low Ri values and Pelegrí and Csanady's [14] for supercritical values. In this paper we will make use of Peters et al.'s [17] parameterization for all Ri values (Equation (3)), the differences with the one used by Pelegrí and Sangrà's [16] being relatively small. The vertical eddy density diffusivity K is calculated from the actual stratification field (through J and $\partial z/\partial x \propto \partial v/\partial \rho$). An important concept, however, is that turbulence (and K) will not immediately follow the current conditions for dynamic stability or instability, but has a temporal memory of the past conditions. This causes that subcritical conditions may be reached with turbulence taking longer to develop, or that strong turbulence can still be quite active despite the conditions are not subcritical any longer. In order to simulate the temporal memory of turbulence we will follow Pelegrí and Sangrà's [16] approach by using a Langevin type equation:

$$\frac{\partial K_t}{\partial t} = -K_t + K, \quad (8)$$

where K_t is the effective vertical density diffusivity and K is the actual (or forcing) vertical density diffusivity, calculated from the density stratification through Equation (3). τ is the characteristic temporal scale for turbulence, which we will take equal to the inverse buoyancy frequency, $N^{-1} = (-j/g)^{1/2}$. This equation shows that the effective vertical density diffusivity decays exponentially with time as it is continuously forced by the actual stratification conditions (through K).

In order to simulate the horizontal compression of the isopycnals we will exponentially shrink the cross-frontal horizontal coordinate with time, i.e., $\hat{x} = x \exp(-\gamma t)$, where \hat{x} is the horizontal coordinate after shrinking and γ is the deformation field coefficient. There are several possible choices for γ , the simplest one being to take it constant in t and ρ . For our calculations, however, we will choose $\gamma(\rho) = \gamma_0 J_0 / J_t$ where γ_0 is a constant deformation field coefficient, J_0 is a characteristic value for the Jacobian and $J_t = J(t = 0, \rho)$ is the initial Jacobian. In this way we will simulate a differential tilting in the isopycnals, with those which initially are most vertically compressed undergoing the highest tilting. The purpose of this is to reproduce the observations that suggest that frontogenesis does not take place at the same rate over a whole frontal system.

The above conditions lead to an exponential increase of the isopycnals's slope (and the diapycnal shear) in time, with a simple dependence on density. The effect of this frontogenesis is simulated by expressing the gradient Richardson number as

$$\text{Ri} = \frac{-g e^{-2\gamma t} \left(\frac{\partial z}{\partial \rho} \right)}{\rho \left(\frac{\partial v}{\partial \rho} \Big|_i \right)^2}, \quad (9)$$

where $\partial v / \partial \rho|_i$ corresponds to the diapycnal shear at the beginning of frontogenesis.

Figure 3 shows the initial distributions of depth, Jacobian, vertical density flux and density tendency as a function of the potential density anomaly σ . Figure 4 shows the temporal evolution of these properties for an initial diapycnal shear equal to $1.0 \text{ m}^4 \text{ kg}^{-1} \text{ s}^{-1}$, $\gamma_0 = 10^{-5} \text{ seg}^{-1}$ and $J_0 = 500 \text{ m}^4 \text{ kg}^{-1}$, as obtained from the numerical solution of Equations (9), (3) and (6–8) (with K_t taking the place of K in Equation (6)). The initial stratification is maximum at $\sigma = 26.0$, causing that at this isopycnal J has an absolute minimum and the vertical density flux is maximum. The time profiles at posterior times illustrate the changes undergone by these extreme values: an increase in J (Figure 4b) and a decrease in F (Figure 4c). The density tendencies attain opposite values around $\sigma_\theta = 27.0$ (Figure 4d), causing that the density-depth profile evolves towards a constant density layer (Figure 4a).

The above results reproduce the main features that were already apparent in the simple diagnostic model, but with considerably more detail and showing the temporal evolution of the dependent variables. The main limitation of this model is that the imposition of the isopycnals' slope eliminates the possibility that they get modified through mixing itself; this limitation will be largely removed in the next section by considering a case with geostrophic cross-frontal dynamics.

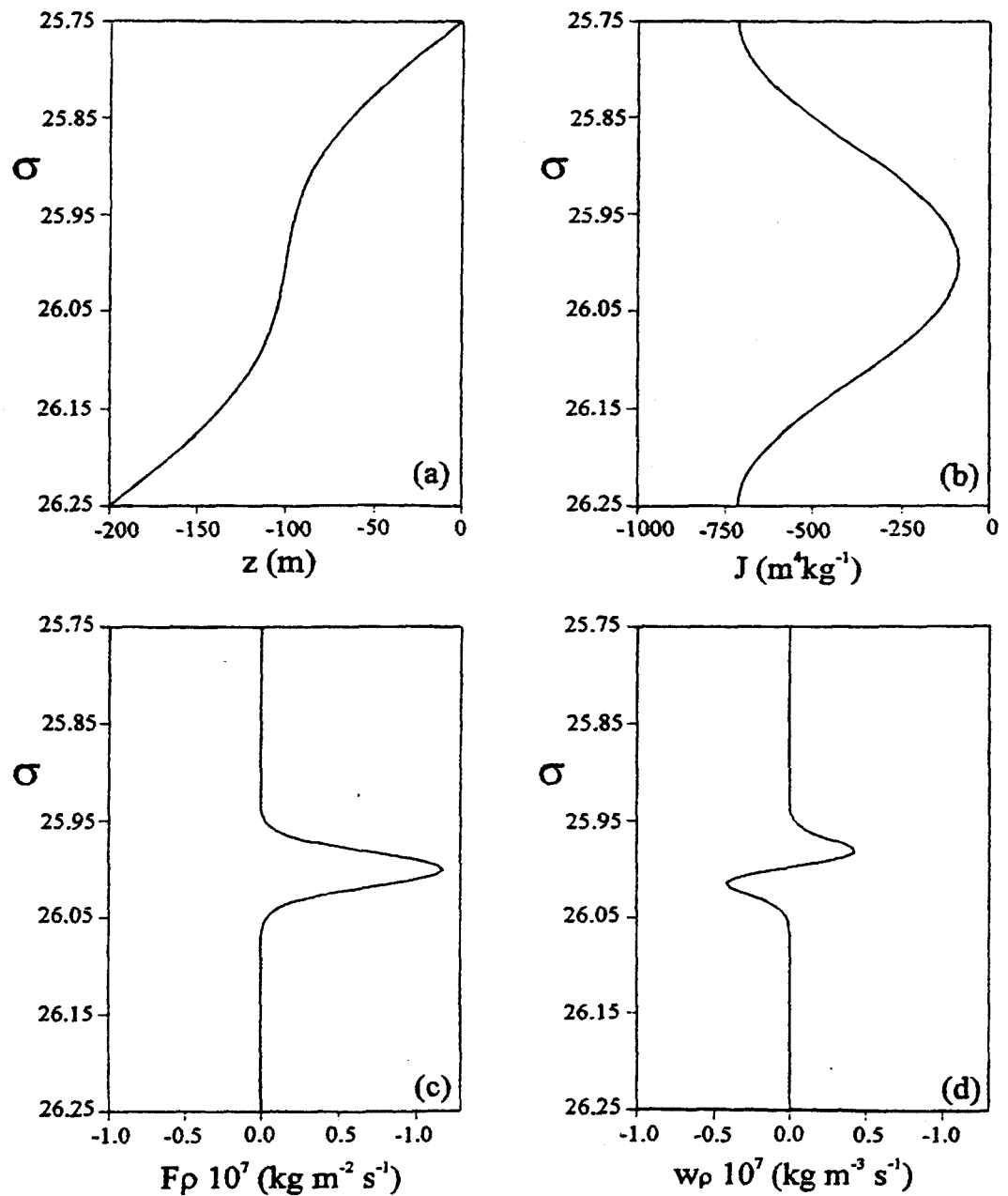


Figure 3. Initial isopycnal distribution of (a) z , (b) J , (c) F , and (d) w_ρ .

5. A Frontal System in Geostrophic Balance

The water mass redistribution through localized diapycnal mixing will necessarily modify the slope of the isopycnals at some places. The flattening or steepening up of these isopycnals will in turn modify the diapycnal shear and the gradient Richardson number, hence controlling the diapycnal mixing. In order to consider this feedback mechanism it is clearly not enough to only deal with the mass conservation equation, instead we need to include the dynamics of the system by considering both the mass and momentum conservation equations. As a first approximation we will consider a simple dynamical case, with the velocity field as the result of a cross-frontal geostrophic balance (baroclinic component),

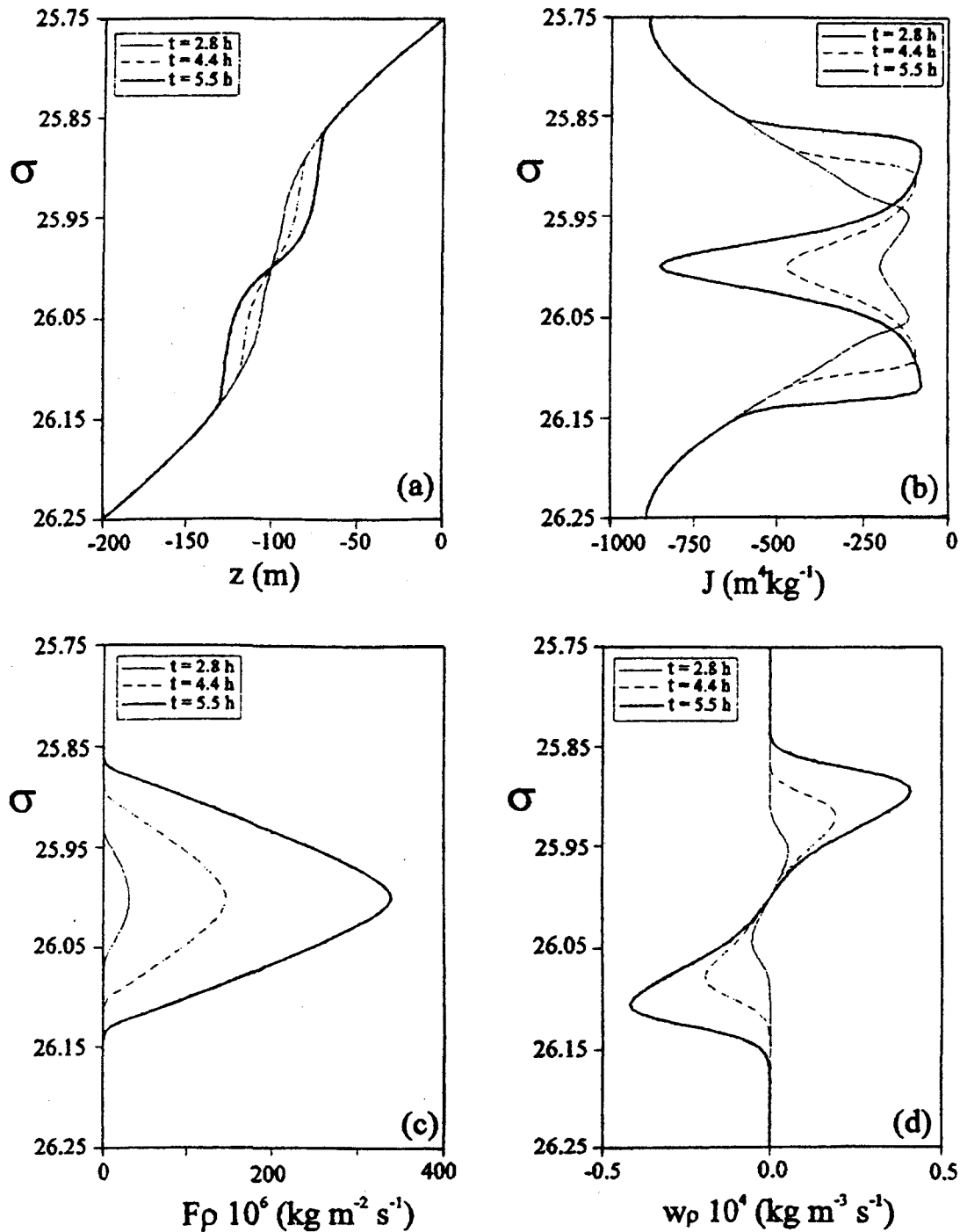


Figure 4. Temporal evolution for the isopycnic distribution of (a) z , (b) J , (c) F , and (d) $w\rho$, at $t = 2.8, 4.4$ and 5.5 hours.

$\mathbf{v} = (0, v, w\rho)$, and a pure deformation velocity field (barotropic component), $\mathbf{v}_d = (u_d, v_d, 0)$. It will become apparent that this situation, despite its simplicity, already contains all the necessary elements to incorporate an interactive process between the mass and momentum fields.

Let us consider a frontal system with (x, y) being the coordinates in the cross-frontal and along-frontal directions. By assuming that the Jacobian and the baroclinic velocity fields are independent of y , and neglecting all internal and ex-

ternal forces, we may write the momentum equations in isopycnic coordinates as follows:

$$fv = \frac{\partial \phi}{\partial x}, \quad (10)$$

$$u = 0, \quad (11)$$

where $\phi \equiv p/\rho + gz$ is the Montgomery potential [10].

The mass conservation equation is obtained after substitution of the velocity field into Equation (5):

$$\frac{\partial j}{\partial t} = - \left[\frac{\partial(ju_d)}{\partial x} + \frac{\partial(jv_d)}{\partial y} \right] - \frac{\partial(jw_\rho)}{\partial \rho}. \quad (12)$$

The deformation field is obtained from a stream function defined as $\psi = -\gamma xy$, with constant γ and such that the flow is non-divergent. In this case Equation (11) may be rewritten as follows

$$\frac{\partial j}{\partial t} + u_d \frac{\partial j}{\partial x} = - \frac{\partial(jw_\rho)}{\partial \rho}. \quad (13)$$

In a quasi-Lagrangian reference system (\hat{x}, y, ρ) moving with the deformation field ($u_d = dx/dt = -\gamma x$, with $x(t=0) = \hat{x}$), such that each fluid element is identified after its initial position, Equation (13) reduces again to Equation (7).

The equations to be numerically solved are Equations (10) and (11) together with Equations (1), (3) and (6–8) (again with K_t taking the place of K in Equation (6)). The results presented correspond to the case of $\gamma = 10^{-5} \text{ seg}^{-1}$. Figure 5 shows the initial $\rho(x, z)$ distribution (Figure 5a) and the initial $x - \rho$ distributions for the Jacobian (Figure 5b), gradient Richardson number (Figure 5c), and density tendency (Figure 5d). Figure 6 shows how these properties have evolved at $t = 11$ hours, after experimenting substantial frontogenesis (Figure 6a). The Jacobian field is modified considerably (Figure 6b) and the Richardson number becomes subcritical in the whole central region (Figure 6c; $\log \text{Ri} = -0.6$ corresponds to $\text{Ri} = 0.25$). The density tendencies are increased by almost three orders of magnitude, showing mass convergence towards the central region (Figure 6d).

With the double objective of facilitating the comparison with the results obtained from the kinematical model and obtaining a closer look at the evolution of the isopycnic structure we present the distribution of z , J , Ri and w_ρ in $x = 0$ at times $t = 12, 12.5$ and 12.6 hours (Figure 7). The agreement in the character of the solution for both models is excellent, with intense mixing taking longer to develop in the dynamical model simply due to the different initial conditions. One peculiarity of the dynamical model, however, is that the time lag between the start of intense mixing and the development of the mixed layer is considerably shorter than in the kinematical model, in a fraction of an hour instead of a few hours. This difference is due to a positive feedback mechanism: the diapycnal shear is further intensified when the isopycnals locally steep up in response to mixing itself.

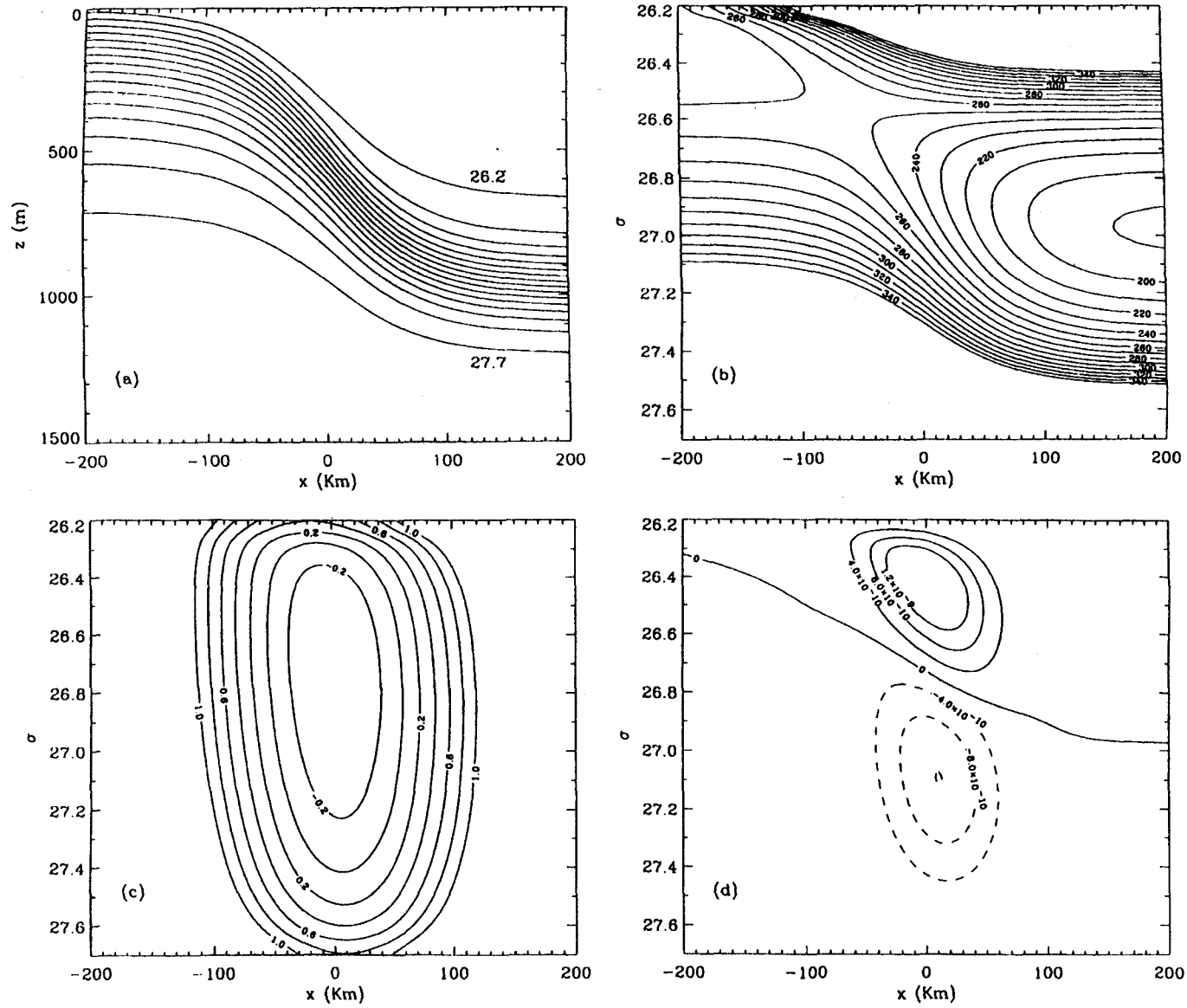


Figure 5. Initial distributions for (a) ρ , (b) J , (c) $\log Ri$, and (d) w_ρ . The ρ distribution is shown in Cartesian coordinates while the other three variables are represented in isopycnal coordinates.

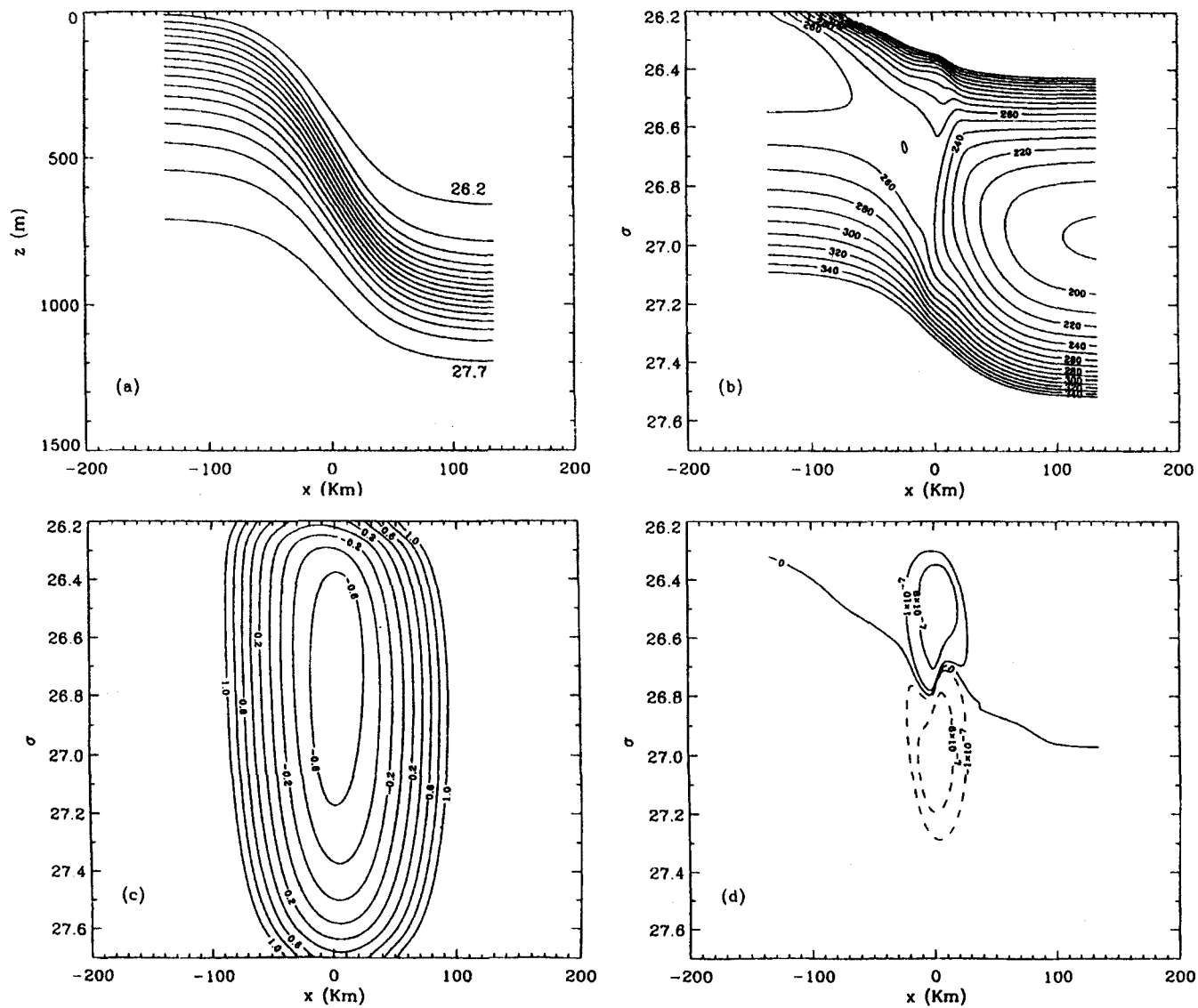


Figure 6. Distribution of (a) ρ , (b) J , (c) $\log Ri$, and (d) w_ρ at $t = 11$ hours. The ρ distribution is shown in Cartesian coordinates while the other three variables are represented in isopycnic coordinates.

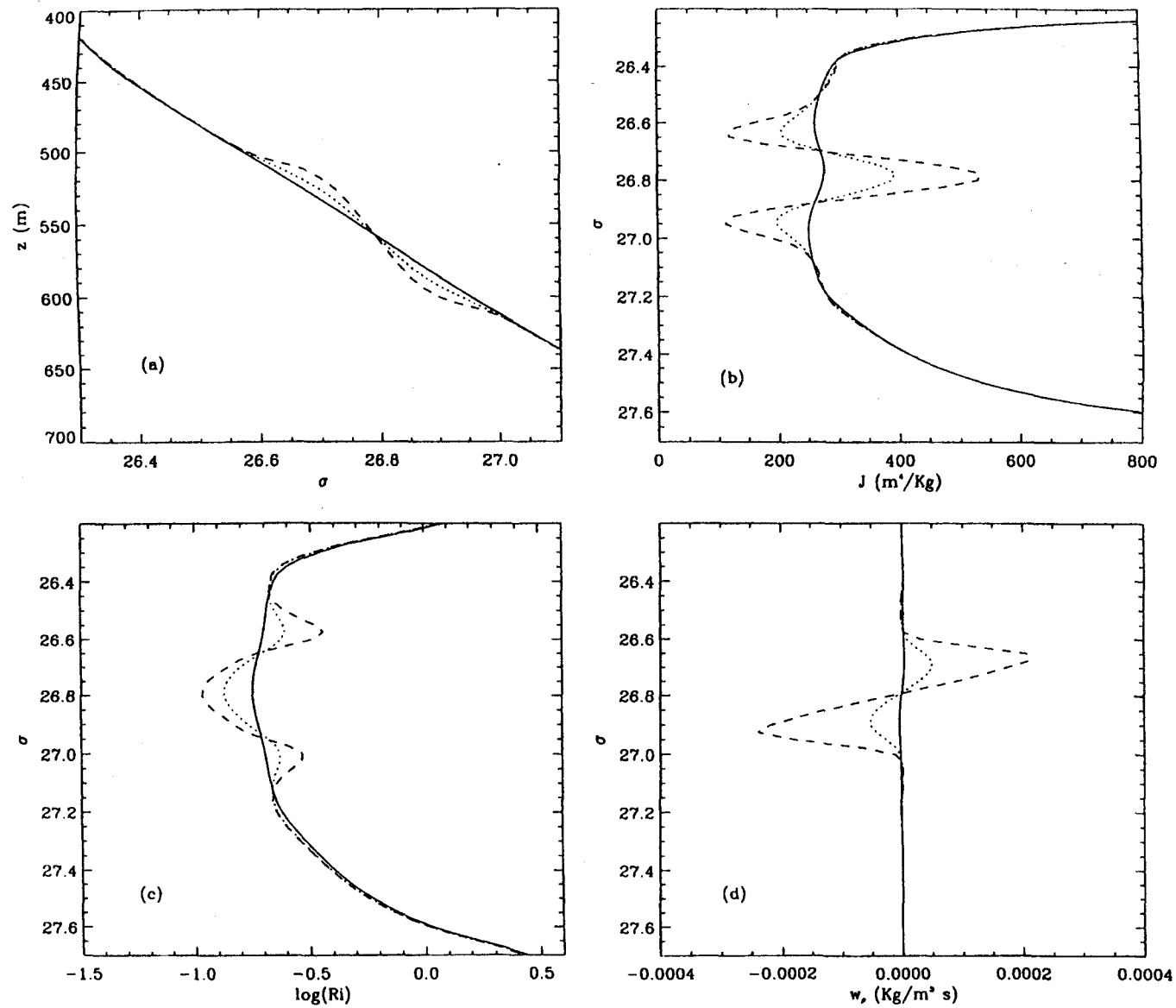


Figure 7. Temporal evolution of the isopycnic distribution at $x = 0$ for (a) z , (b) J , (c) $\log \text{Ri}$, and (d) w_ρ . The solid, dotted and dashed lines correspond to $t = 12, 12.5$ and 12.6 hours, respectively. Please note the change in scale of Figure 7a as compared with Figures 5a and 6a.

6. Conclusions

Our results show that shear-induced diapycnal mixing is a potentially important mechanism for the generation of density finestructure in geophysical flows. The simulated constant density layers indeed show many similarities with the staircase structure that is frequent in the upper thermocline or near the base of the upper mixed layer (e.g., [14] and references therein, as well as many observations we have made in the Canary Islands Basin).

The mechanism for the generation of mixed layers operates through Kelvin–Helmholtz type instabilities which develop in well stratified but highly sheared subcritical regions within frontal systems. This stratified region undergoes strong mass convergence causing the breaking of the stratification into a mixed layer, and the generation of adjacent interfaces. The shear-induced instabilities have their own characteristic life time, which means that turbulence will last despite the conditions are not subcritical any longer. This temporal memory of turbulence is a non-Newtonian characteristic of geophysical flows and turns out to be critical for the development of mixed layers, otherwise mixing relaxes once the conditions turn supercritical and the originally well stratified region simply smoothes out through diffusion.

We have examined these ideas through three process-oriented isopycnic models with a quite different degree of complexity. The diagnostic model proposes that during frontogenesis the diapycnal shear remains constant leading to the creation of a subcritical region which rapidly becomes mixed up. This very simple model already possesses the physical operating mechanism but lacks any kinematical or dynamical representation, and the duration of the instability is specified *ad hoc*, i.e., such that it mixes up the subcritical region. The second, intermediate, model introduces both the kinematics and the temporal memory of the turbulence, in such a way that it calculates the transients from the highly stratified into the well-mixed states. In this model, however, the dynamics are imposed through specification of the diapycnal shear distribution. The third model introduces the dynamics through a geostrophic cross-frontal balance and a non-geostrophic deformation velocity field. This last model, despite its simplicity, has all the fundamental elements that would need to be included in any more realistic predictive-type model. The main element is the interaction between mixing, which modifies the slope of the isopycnals, and the velocity field, which responds to the isopycnals' slope and controls the vertical density flux. Such coupling is crucial to determine the importance of diapycnal mixing in controlling the separation between isopycnals during frontogenesis.

Acknowledgments

We would like to thank Professor José M. Redondo for encouraging us to write this work. This research has been supported by the Spanish government through project FRENTEs (CICYT's grant number AMB95-0731) and by the European Union through project CANIGO (MAST's grant number MAS3-CT96-0060).

References

1. Browning, K.A., Harrold, T.W. and Starr, J.R., Richardson number limited shear zones in the free atmosphere. *Q. J. R. Meteorol. Soc.* **96** (1970) 40–49.
2. Csanady, G.T., Mixing in coastal regions. In: Le Mehaute, B. and Banes, D.M. (eds), *The Sea: Ocean Engineering Science*, Vol. 9, John Wiley, New York (1990) pp. 593–629.
3. Howard, L.N., Note on a paper by John W. Miles. *J. Fluid Mech.* **95** (1961) 509–512.
4. Keyser, D. and Rotunno, R., On the formation of potential vorticity anomalies in upper-level jet-front systems. *Mon. Weather Rev.* **118** (1990) 1914–1921.
5. Keyser, D. and Shapiro, M.A., A review of the structure and dynamics of upper-level frontal zones. *Mon. Weather Rev.* **114** (1986) 452–499.
6. Kundu, P.K. and Beardsley, R.C., Evidence of a critical Richardson number in moored measurements during the upwelling season off Northern California. *J. Geophys. Res.* **96** (1991) 4855–4868.
7. McDougall, T.J. and You, Y., Implications of the nonlinear equation of state for upwelling in the ocean interior. *J. Geophys. Res.* **95** (1990) 13263–13276.
8. Miles, J.W., On the stability of heterogeneous shear flows. *J. Fluid Mech.* **10** (1961) 496–508.
9. Miles, J.W., Richardson's criterion for the stability of stratified shear flow. *Phys. Fluids* **29** (1986) 3470–3471.
10. Montgomery, R.B., A suggested method for representing gradient flow in isentropic surfaces. *Bull. Amer. Meteorol. Soc.* **18** (1937) 210–212.
11. Munk, W.H. and Anderson, E.R., Notes on a theory of the thermocline. *J. Mar. Res.* **7** (1948) 276–295.
12. Palmén, E. and Newton, C.E., *Atmospheric Circulation Systems*. Academic, San Diego, CA (1969) 603 pp.
13. Pelegrí, J.L. and Csanady, G.T., Nutrient transport and mixing in the Gulf Stream. *J. Geophys. Res.* **96** (1991) 2577–2583.
14. Pelegrí, J.L. and Csanady, G.T., Diapycnal mixing in western boundary currents. *J. Geophys. Res.* **99** (1994) 18275–18304.
15. Pelegrí, J.L. and Richman, J.G., On the role of shear mixing during transient coastal upwelling. *Continental Shelf Res.* **13** (1993) 1363–1400.
16. Pelegrí, J.L. and Sangrà, P., A mechanism for layer formation in stratified geophysical flows. *J. Geophys. Res.* (1998) (in press).
17. Peters, H., Gregg, M.C. and Toole, J.M., On the parameterization of equatorial turbulence. *J. Geophys. Res.* **93** (1988) 1199–1218.
18. Phillips, O.M., Turbulence in a strongly stratified fluid – Is it unstable? *Deep-Sea Res.* **19** (1972) 79–81.
19. Posmentier, E.S., The generation of salinity fine structure by vertical diffusion. *J. Phys. Oceanogr.* **7** (1977) 292–300.
20. Richardson, L.F., The supply of energy from and to atmospheric eddies. *Proc. Roy. Soc. London Ser. A* **97** (1920) 354–373.
21. Roach, W.T., On the influence of synoptic development on the production of high level turbulence. *Q. J. R. Meteorol. Soc.* **96** (1970) 413–429.
22. Taylor, G.I., Internal waves and turbulence in a fluid of variable density. *Rapp. Proc. Verb. Reun. Cons. Perm. Int. d'Exploration Mer* **76** (1931) 35–42.
23. Thorpe, S.A., Experiments on the instability of stratified shear flows: Miscible fluids. *J. Fluid Mech.* **46** (1971) 299–319.

Increase of the dietary $n - 3/n - 6$ fatty acid ratio
and addition of phosphorus improves liver
histological alterations induced by feeding diets
containing soybean meal to gilthead seabream,
Sparus aurata

L. Robaina ^{a,*}, M.S. Izquierdo ^a, F.J. Moyano ^b, J. Socorro ^c,
J.M. Vergara ^a, D. Montero ^c

^a Dpto. Biología, Univ. de Las Palmas de G.C., Campus Univ. Tafira 35017, Las Palmas de Gran Canaria,
Canary Islands, Spain

^b Dpto. de Biología Aplicada, Escuela Politécnica Superior, Univ. de Almería, 04120, Almería, Spain

^c Instituto Canario de Ciencias Marinas, Apdo. 56, Telde 35200, Las Palmas de Gran Canaria,
Canary Islands, Spain

Abstract

In a previous study, several histological alterations were found in the liver of gilthead seabream fed with a diet containing 30% soybean meal (SBM). In the current study, SBM containing diets were supplemented with either potassium phosphate, zinc sulfate or phytase (*Aspergillus ficuum*), or increasing the dietary $n - 3/n - 6$ fatty acids ratio to meet that of a fish meal based diet. Diet composition did not affect fish growth, feed efficiency (FE) or protein productive value (PER). Phosphorous supplementation significantly reduced hepatosomatic indexes (HSI), although it did not alter liver lipid content. Both phosphorous supplementation and correcting the dietary $n - 3/n - 6$ fatty acid ratio significantly altered the lipid and protein content in fish muscle. Only these two treatments and principally the corrected dietary $n - 3/n - 6$ fatty acid ratio, improved

* Corresponding author.

the liver histological alterations observed in fish fed with SBM based diets. © 1998 Elsevier Science B.V.

Keywords: Soybean; Liver histology; *Sparus aurata*; Essential fatty acids

1. Introduction

In the last few years, there has been an increasing interest in the partial or complete replacement of dietary fish meal by other protein sources, animal or plant, in aquaculture feeds. Among feedstuffs of plant origin soybean meal is considered the most nutritive, being widely utilized in fish diets (Lovell, 1988; Kaushik, 1989). However, the inclusion of soybean meal in fish diets has produced contradictory results mainly because of the different heat treatments used to inactivate possible anti-nutritional factors from this feedstuff, e.g., antitrypsin activity.

In a previous experiment with gilthead seabream, it was observed that an increase in dietary level of soybean meal did not affect fish growth rate, however it did produce alterations in liver histology when compared with fish fed with a fish meal-based diet (Robaina et al., 1995). In this previous study, both trypsin inhibitor activity and essential amino acid imbalance were shown not to be the cause of the altered liver histology.

In addition to the above mentioned anti-nutritional factors, low availability of certain nutrients, such as carbohydrates (Arnesen et al., 1989; Saini, 1989; Pongmaneerat and Watanabe, 1992) and minerals (Hartman, 1979; Spinelli et al., 1983; Richardson et al., 1985; Hilton, 1989; Hossain and Jauncey, 1991) have been reported to affect soybean meal utilization by fish.

Two thirds of the soybean phosphorous is in the form of phytate phosphorous, which has low availability to fish (Riche and Brown, 1993), as these animals lack phytases which are required for its digestion (Lall, 1979; Ogino et al., 1979). In addition, presence of phytic acid in soybean meal seems to reduce the availability of zinc (Spinelli et al., 1979; Snyder and Kwon, 1987). This effect may be aggravated in the presence of excess dietary calcium (Gatlin and Phillips, 1989). The use of supplemental phytases in fish diets to increase phytate solubility, thus allowing its digestion by phosphatases in the intestine, has been suggested to overcome this problem (Campbell and Bedford, 1992).

Finally, the fatty acid composition of lipid from soybean meal, rich in $n - 6$ fatty acid, could also affect liver lipid deposition in fish. The competition between $n - 3$ and $n - 6$ fatty acids as substrates for different enzymes involved in lipid metabolism in fish has been reported, suggesting the importance of the dietary ratio of $n - 3/n - 6$ PUFA (polyunsaturated fatty acids with more than 18 carbons) (Sargent et al., 1989). One of the main indications of this essential fatty acid imbalance is an increase in liver lipid deposition (Takeuchi et al., 1979).

The aim of the present study was to determine if supplemental phosphorous or zinc or an increase in the $n - 3/n - 6$ fatty acid ratio would prevent the appearance of the histological alterations observed in gilthead seabream fed diets containing soybean meal. In addition, one of the experimental diets was supplemented with phytases in order to

increase the availability of phosphorous from soybean meal in diets for gilthead seabream.

2. Materials and methods

2.1. Diets

Sardine fish meal (69.58% crude protein, 8.35% lipid) supplied by AGRAMAR, a local producer and hexane-extracted soybean meal (43.77% crude protein, 1.18% lipid) obtained from a local importer were used as the protein sources in the experimental diets. Antitrypsin activity of the soybean meal was determined (Liu and Markakis, 1989)

Table 1
Formulation and composition of the experimental diets

	C	S30	S30+P	S30+Zn	S30+Phytase	S30+n-3/n-6
Sardine fish meal	61.80	42.50	42.50	42.50	42.50	42.50
Soybean meal	—	29.60	29.60	29.60	29.60	29.60 ^d
Sardine oil	6.60	7.30	7.30	7.30	7.30	8.00
Corn starch	12.07	12.07	8.01	12.07	12.07	12.07
Dextrin	4.03	4.03	2.68	4.03	4.03	4.03
Vitamins ^a	2.00	2.00	2.00	2.00	2.00	2.00
Minerals ^b	2.00	2.00	1.32 ^e	2.00	2.00	1.32 ^e
CMC ^c	0.50	0.50	0.50	0.50	0.50	0.50
α -Cellulose	11.00	—	—	—	—	—
P[KH ₂ PO ₄]	—	—	6.10 ^f	—	—	—
Zn [ZnSO ₄ ·7H ₂ O]	—	—	—	0.03 ^f	—	—
Phytases	—	—	—	—	0.02 ^f	—
Composition (% dry weight)						
Moisture	7.78	6.65	7.49	6.77	7.99	6.59
Crude protein	44.78	47.99	48.47	48.22	48.38	47.11
Crude lipid	11.17	11.00	11.00	10.98	10.81	11.01
Σ n-3 fatty acids	4.25	3.98	—	—	—	4.19
Σ n-6 fatty acids	0.47	0.74	—	—	—	0.40
n-3/n-6 ratio	9.09	5.39	—	—	—	9.00
Ash	10.93	10.44	15.70	10.70	10.26	10.35
Fibre	13.00	4.96	4.38	4.89	5.05	4.77
Carbohydrates ^g	20.12	25.61	20.45	25.21	25.50	26.76
Gross Energy (kJ/g)	19.01	19.39	18.40	18.82	19.42	19.31

^aVitamin premix (g/kg or IU/kg of dry diet): thiamin 40 mg, riboflavin 50 mg, pyridoxine 40 mg, calcium pantothenate 117 mg, nicotinic acid 200 mg, biotin 1 mg, folic acid 10 mg, cyanocobalamin 0.5 mg, choline chloride 2700 mg, inositol 600 mg, ascorbic acid 1000 mg, alpha tocopherol 250 mg, menadione 20 mg, cholecalciferol 2000 IU, ethoxyquin 100 mg, retinol acetate 5000 IU.

^bMineral premix (g/kg of dry diet): calcium orthophosphate 1.6 g, calcium carbonate 4 g, ferrous sulfate 1.5 g, magnesium sulfate 1.6 g, potassium phosphate 2.8 g, sodium phosphate 1 g, aluminum sulfate 0.02 g, zinc sulfate 0.24 g, copper sulfate 0.20 g, manganese sulfate 0.08 g, potassium iodate 0.02 g.

^cCarboxymethyl cellulose.

^dSoybean meal re-extracted with chloroform.

^eMinerals mix without α -cellulose.

^fAmount added instead of the α -cellulose in the mineral premix.

^gCalculated by difference (100-rest ingredients).

to be less than 3 TIA (mg of inhibited trypsin per g of soybean meal), a value which is considered acceptable for inclusion in fish diets (Akiyama, 1988). Sardine oil was used as the lipid source and corn starch and dextrin in a proportion of 3:1 were used as carbohydrate sources.

Six experimental diets were prepared: Diet 1 (C), positive control, where sardine fish meal was the only protein source; Diet 2 (S30), negative control, where 30% of the fish meal protein was replaced by soybean meal protein; Diet 3 (S30 + P), where diet 2 was supplemented with P in the form of KH_2PO_4 up to the theoretical available P level in diet 1 (it was assumed that approximately 70% of the phosphorus from the fish meal (NRC, 1983) was available for the fish, Hepher, 1988); Diet 4 (S30 + Zn), where diet 2 was supplemented with Zn in the form of $\text{ZnSO}_4 \cdot 7\text{H}_2\text{O}$ at a level of 200 mg/kg diet; Diet 5 (S30 + phytase), where diet 2 was supplemented with an amount of exogenous phytases (SIGMA P-9792) estimated to release P from the dietary phytic acid; Diet 6 (S30 + $n - 3/n - 6$), where the $n - 3/n - 6$ fatty acid ratio of diet 2 was adjusted to be similar to that of diet 1. The latter was achieved by extracting the commercial hexane-extracted soybean meal with chloroform in order to remove residual lipids, as this solvent does not extract phytic acid. Table 1 shows the formulation and composition of the experimental diets, including total lipid, $n - 3$ and $n - 6$ fatty acid composition.

Dietary essential amino acid profiles were calculated and compared with the essential amino acid profile of gilthead seabream fingerlings as a reference of dietary requirements for amino acids (NRC, 1983; New, 1986; Moyano, 1990; Vergara, 1992). As a result, no supplemental amino acids were added to the diets.

Mixed ingredients were pelleted in a 2 HP (Mobba, Milano, Italy) pellet mill with a 3 mm die. The pellets were dried and stored in a freezer at -20°C until used.

2.2. Experimental conditions

Gilthead seabream (*Sparus aurata*) juveniles of 50 g mean body weight were randomly stocked at 15 fish per 100-l tank, three tanks per treatment, after an acclimation period of 2 weeks. Natural seawater ($18.4 \pm 0.45^\circ\text{C}$) entered each tank at a rate 1 l/min; mean values for dissolved oxygen and pH during the experimental period were 7.25 ± 0.65 mg/l and 7.8 ± 0.2 , respectively. Each diet was fed to satiation four times per day, 6 days per week. The feeding trial was conducted for 75 days; the experimental period was extended to 90 days for fish fed with diets 1 and 2 in order to assess differences in fish growth.

2.3. Biochemical analysis

Crude protein ($\%N \times 6.25$) was determined by the Kjeldahl method and total lipid by petroleum ether extraction (Soxhlet technique). Gross energy content of the diets was determined using an IKA oxygen bomb calorimeter (Heitersheim, Germany). Gross energy content of the fish was calculated using theoretical indices (Brafield, 1985).

Lipids were extracted as described by Folch et al. (1957) and fatty acid analysis of total lipids were carried out as described in Izquierdo et al. (1990).

Table 2
Growth, nutrient utilization and hepatosomatic indices of fish fed with the experimental diets¹

	C	S30	S30+P	S30+Zn	S30+ phytase	S30+ n-3/n-6
Mean initial body weight (g)	52.31 ± 9.72	51.78 ± 8.33	51.09 ± 9.54	50.56 ± 9.85	52.60 ± 9.81	51.93 ± 8.49
Mean final body weight(g)	87.68 ± 14.00	85.95 ± 13.99	79.65 ± 15.65	82.35 ± 13.66	86.96 ± 15.36	86.14 ± 12.93
Weight increase (%initial weight)	67.73 ± 7.33	65.84 ± 5.59	55.94 ± 2.73	62.69 ± 6.74	65.77 ± 5.02	66.01 ± 5.71
Feed intake(g)	1411.10 ± 40.20 ^b	1095.57 ± 73.22 ^a	1042.57 ± 59.14 ^a	1119.63 ± 68.59 ^a	1153.67 ± 86.34 ^a	1125.20 ± 44.69 ^a
Protein intake(g)	583.27 ± 18.73 ^b	490.83 ± 32.81 ^a	467.50 ± 26.52 ^a	502.50 ± 30.67 ^a	513.50 ± 38.45 ^{ab}	495.20 ± 19.66 ^a
FE	0.41 ± 0.05	0.50 ± 0.05	0.45 ± 0.04	0.46 ± 0.06	0.49 ± 0.03	0.49 ± 0.05
PER	0.92 ± 0.11	1.04 ± 0.10	0.92 ± 0.08	0.94 ± 0.12	1.01 ± 0.07	1.04 ± 0.11
HSI	1.82 ± 0.08 ^b	1.59 ± 0.05 ^b	1.30 ± 0.17 ^a	1.67 ± 0.03 ^b	1.58 ± 0.12 ^b	1.57 ± 0.07 ^{ab}

¹ Values in the same row with different superscript are significantly different ($P < 0.05$).

Table 3

Muscle composition of fish fed the experimental diets (g/100 g dry weight)¹

	C	S30	S30+P	S30+Zn	S30+Phytase	S30 + n - 3/n - 6
Protein	73.88 ± 1.41 ^{ab}	75.31 ± 1.99 ^b	79.26 ± 2.81 ^c	74.06 ± 1.36 ^{ab}	75.24 ± 0.80 ^b	72.06 ± 0.77 ^a
Lipid	19.86 ± 0.91 ^c	17.57 ± 1.82 ^b	15.40 ± 0.84 ^a	20.09 ± 1.37 ^c	18.87 ± 0.85 ^{bc}	22.89 ± 0.84 ^d
Ash	5.22 ± 0.12 ^{bc}	5.51 ± 0.13 ^{cd}	5.55 ± 0.05 ^d	5.14 ± 0.10 ^b	5.28 ± 0.35 ^{bcd}	4.78 ± 0.12 ^a
Moisture	71.83 ± 1.42 ^{ab}	72.28 ± 1.37 ^{abc}	73.56 ± 0.73 ^c	71.30 ± 0.76 ^{ab}	72.48 ± 1.03 ^{bc}	70.88 ± 1.21 ^a

¹ Values in the same row with different superscript are significantly different ($P < 0.05$).

2.4. Histological studies

At the end of the experiment, livers from five fish from each tank were weighed for hepatosomatic index and fixed in 10% neutral-buffered formalin. Samples were stained with hematoxylin and eosin and periodic acid-Schiff (PAS) for histological examination (Martoja and Martoja-Pierson, 1970).

2.5. Statistical analysis

In both experiments all the data were subjected to One-way analysis of variance (ANOVA) and differences between means compared by the Tukey test at a 95% interval of confidence ($P < 0.05$).

3. Results

3.1. Growth performance and nutrient utilization

All experimental diets were well accepted by the fish, except Diet 3 at the beginning of the experiment. Table 2 shows the growth performance and nutrient utilization of the experimental diets. There were no significant differences in final body weights among fish fed with the various treatments. After 90 days, weight gains of fish fed with Diets 1 and 2 were 90.70 and 91.58%, respectively.

When comparing total feed and protein intake of fish, only those fed with Diet 1 was significantly higher than the other treatments. Feed efficiency and protein efficiency ratio values were very similar for all treatments.

Hepatosomatic index values were markedly affected by the different treatments. The addition of P in diet S30 resulted in significantly lower liver weights.

Table 4

Liver composition of fish fed the experimental diets (g/100 g dry weight)¹

	C	S30	S30+P	S30+Zn	S30+Phytase	S30 + n - 3/n - 6
Lipid	18.12 ± 1.57	17.10 ± 2.92	15.97 ± 2.51	16.10 ± 0.69	16.81 ± 1.90	17.00 ± 1.90
Moisture	69.48 ± 1.24 ^a	70.87 ± 1.37 ^a	73.52 ± 1.09 ^b	71.17 ± 0.36 ^a	71.01 ± 0.84 ^a	71.08 ± 0.75 ^a

¹ Values in the same row with different superscript are significantly different ($P < 0.05$).

3.2. Fish composition

Composition of fish muscle after the experiment is shown in Table 3. In general, values were similar for fish fed with Diets 1 and 2, except for significantly higher lipid

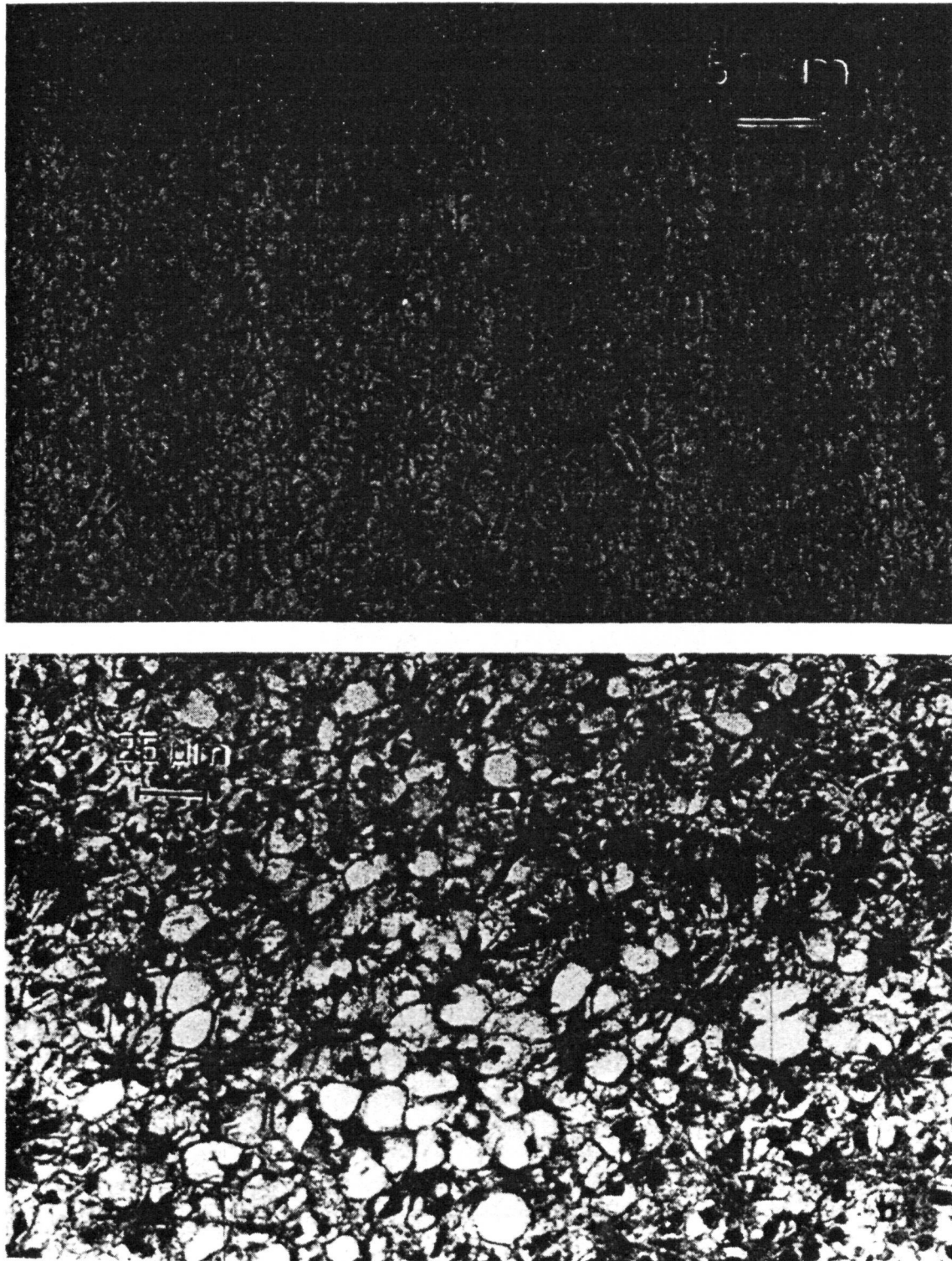


Fig. 1. Hepatic and pancreatic tissue of fish fed the experimental diets:(a) control diet; (b) diet S30; (c) diet S30 + P; (d) diet S30 + Zn; (e) diet S30 + phytase; (f) diet S30 + $n-3/n-6$.

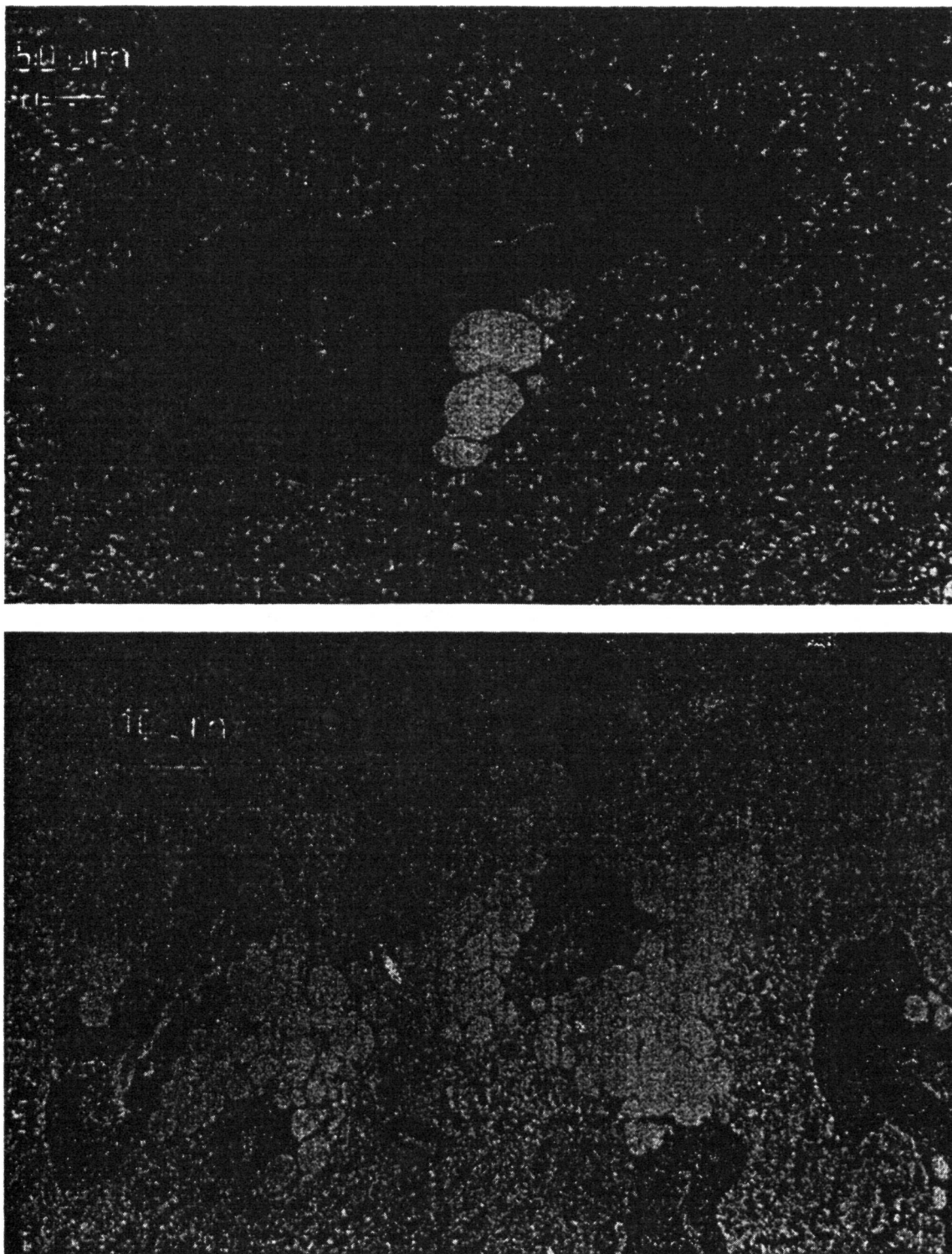


Fig. 1 (continued).

content for the positive control diet. When comparing diets containing soybean meal, muscle composition was very similar for fish fed with Diets 2 and 5. On the contrary, feeding Diet 6 produced an increase in lipid and a decrease in protein content of muscle compared to feeding Diet 2, while feeding Diet 3 resulted in a significant decrease in

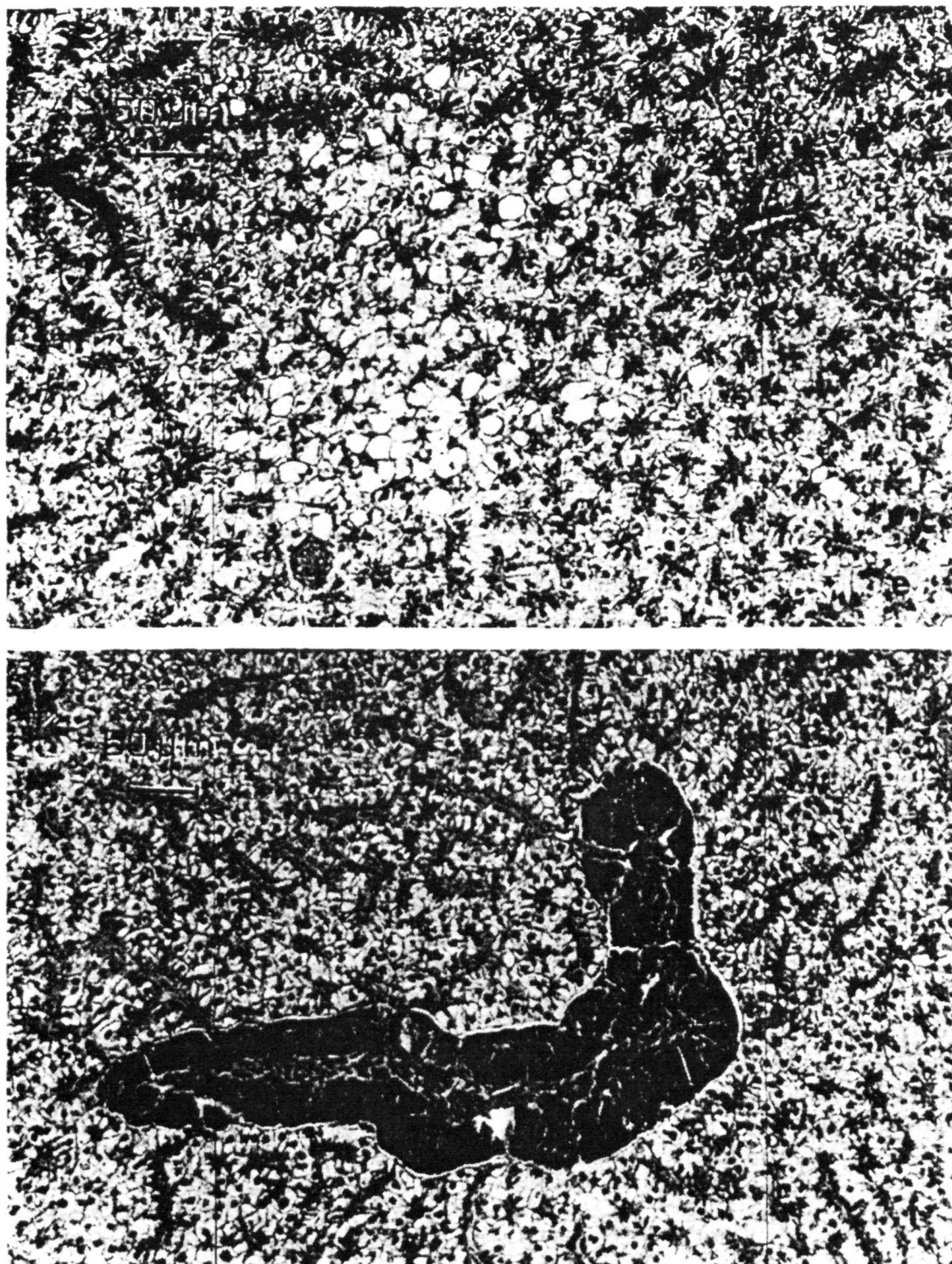


Fig. 1 (continued).

lipid and an increase in protein content. Muscle lipid content ranged from approximately 15% in fish fed with Diet 3 to 22% in fish fed with Diet 6.

Liver composition of fish fed with the different experimental diets is shown in Table 4. Values for fish fed with Diet 2 were only affected when soybean meal was supplemented with P (Diet 3), with significantly higher moisture values.

3.3. *Histological studies*

Liver samples from fish fed with the different dietary treatments were compared with those from fish fed the positive control diet (Fig. 1a) which showed a normal histology.

As previously reported (Robaina et al., 1995), Diet 2 (S30) produced livers with areas of hepatocyte nucleus polarization, as well as lipid vacuolization and isolated necrosis (Fig. 1b). Only Diet 6 (Fig. 1f) and to a lesser extent Diet 3 (Fig. 1c, small lipid deposits and condensed cytoplasm in generally small hepatocytes), seemed to improve the liver histological alterations observed in fish fed with Diet 2 (S30).

Supplementation of Diet 2 with Zn (Fig. 1d) and phytases (Fig. 1e) produced similar liver histological alterations to those found in fish fed with Diet 2. PAS-positive staining was much more intense for Diet 3 than for the other treatments, including the positive control diet.

4. Discussion and conclusions

Results for growth and nutrient utilization of all diets containing 30% soybean meal were similar to those from the control fish meal diet, as previously reported for this species (Robaina et al., 1995). Similarly, no significant differences were found among hepatosomatic indexes, except that statistically lower values were observed in fish fed with Diet 3 (S30 + P). This may be related to an altered lipid and protein metabolism in fish fed with the other diets which had a lower P availability and subsequent higher liver lipid deposition, thus increasing the HSI values. Sakamoto and Yone (1978) and Sakamoto (1981) have observed a similar effect of supplemental P in red seabream. These workers also reported an increase in liver lipid content associated with an increase in liver size. In the current study, the addition of P to the diet produced a slight decrease in liver lipid, although not significant.

The composition of fish muscle at the end of the experiment showed a reduction in lipid for those fish fed with Diet 2 (S30) as compared to the control diet. This is in agreement with results reported by Richardson et al. (1985) for salmon, Hossain and Jauncey (1991) for carp and Pfeffer and Beckmann (1991) for trout. This effect can be explained by a reduction in dietary digestible energy due to the carbohydrates in the soybean meal. Lee and Putman (1973) and Kaushik et al. (1989) have also found a decrease in trout body lipid content when digestible energy of the diets was reduced.

The addition of Zn and phytases to Diet 2 did not alter its nutrient utilization and produced similar histological characteristics. The level of Zn in this diet (200 mg/kg diet), has been reported to be adequate for channel catfish, even in the presence of high dietary phytate (Gatlin and Phillips, 1989) and is not considered as a toxic level for fish (Wekell et al., 1983). The fact that the water temperature during the experiment was below the optimum considered for the action of phytases (35–40°C), may explain the lack of any positive effect of this diet, as reported by other authors (Spinelli et al., 1979; Brown, 1991; Schäfer et al., 1994; Cain and Garling, 1995).

Histological results showed morphological differences in the hepatopancreatic parenchyma between fish fed the control diet and the S30 diet, as previously reported in

this species (Robaina et al., 1995). These differences seemed to be more related to the distribution of lipids within the hepatopancreatic tissue than to different lipid content, since no significant difference in liver total lipid content was found. Similarly, Alexis et al. (1985) found that increased levels of soybean meal in diets for trout did not produce biochemical liver alterations. On the contrary, other authors have reported a decrease in liver lipid content in yellowtail fed soybean meal-containing diets (Watanabe et al., 1992; Shimeno et al., 1993).

The lower $n-3/n-6$ fatty acid ratio in Diet 6 (S30 + $n-3/n-6$) may have improved the utilization of liver lipids, thus reducing liver histological alterations. This effect could be associated to a more favourable $n-3/n-6$ fatty acid ratio in phospholipids (PL) of the hepatic membranes, affecting its function (Bell et al., 1986). In addition, the higher ratio of dietary essential polyunsaturated fatty acids may have produced an inhibitory effect on hepatic lipogenesis, as has been demonstrated for other vertebrates (Jeffcoat et al., 1979; Sargent et al., 1989).

In summary, only the increase in the $n-3/n-6$ fatty acid ratio and P supplementation reduced liver lipid deposits around the pancreatic tissue, the level of hepatocyte vacuolization and the isolated points of necrosis observed in liver of gilthead seabream fed with diets containing high levels of soybean meal.

Acknowledgements

This study was partially supported by a grant from the University of Las Palmas de Gran Canaria.

References

- Akiyama, M., 1988. Soybean Meal Utilization in Fish Feeds. American Soybean Association, 1988, 15 pp.
- Alexis, M.N., Papaparaskeva, E., Theochari, V., 1985. Formulation of practical diets for rainbow trout (*Salmo gairdneri*) made by partial or complete substitution of fish meal by poultry by-products and certain plant by-products. Aquaculture 50, 61–73.
- Arnesen, P., Brattas, L.E., Olli, J., Krogdahl, A., 1989. Soybean carbohydrates appear to restrict utilization of nutrients by Atlantic salmon (*Salmo salar* L.). In: Takeda, M., Watanabe, T. (Eds.), The Current Status of Fish Nutrition in Aquaculture, Tokyo Univ., Fisheries, Tokyo, pp. 273–280.
- Bell, M.V., Henderson, R.J., Sargent, J.R., 1986. The role of polyunsaturated fatty acids in fish. Comp. Biochem. Physiol. 83B, 711–719.
- Brafield, A.E., 1985. Laboratory studies of energy budgets. In: Tytler, P., Calow, P. (Eds.), Fish Energetics New Perspectives. Croom Helm, London. pp. 257–307.
- Brown, P.B., 1991. Comparison of fecal collection methods for determining phosphorus absorption in rainbow trout. In: Kaushik, S.J., Luquet, P. (Eds.), Fish Nutrition in Practice (Les Colloques, no. 61), INRA, Paris, pp. 443–447.
- Cain, K.D., Garling, D.L., 1995. Pretreatment of soybean meal with phytase for salmonid diets to reduce phosphorus concentrations in hatchery effluents. Prog. Fish-Cult. 57, 114–119.
- Campbell, G.L., Bedford, M.R., 1992. Enzyme applications for monogastric feeds: a review. Ann. J. Anim. Sci. 72, 449–466.

- Folch et al., 1957.
- Gatlin, D.M. III, Phillips, H.F., 1989. Dietary calcium, phytate and zinc interactions in channel catfish. *Aquaculture* 79, 259–266.
- Hartman, G.H., 1979. Removal of phytate from soy protein. *J. Am. Oil Chem. Soc.* 56, 731–735.
- Hepher, B., 1988. *Nutrición de peces comerciales en estanques*. Limusa Ed., México, 1988, 406 pp.
- Hilton, J.W., 1989. The interaction of vitamins, minerals and diet composition in the diet of fish. *Aquaculture* 79, 223–244.
- Hossain, M.A., Jauncey, K., 1991. The effect of varying dietary phytic acid, calcium and magnesium levels on the nutrition of common carp, *Cyprinus carpio*. In: Kaushik, S.J., Luquet, P. (Eds.), *Fish Nutrition in Practice (Les Colloques, no. 61)*, INRA, Paris, pp. 705–715.
- Izquierdo, M.S., Takeuchi, T., Arakawa, T., Kitajima, C., Watanabe, T., 1990. Optimum EFA levels in *Artemia* to meet the EFA requirements of red sea bream (*Pagrus major*). In: Takeda, M., Watanabe, T. (Eds.), *The Current Status of Fish Nutrition in Aquaculture*. Japan Translation Center, Tokyo, pp. 221–232.
- Jeffcoat, R., Roberts, P.A., James, A.T., 1979. *Eur. J. Biochem.* 101, 447–453.
- Kaushik, S.J., 1989. Use of alternate protein sources for intensive rearing of carnivorous fish. In: Shiau, S.-Y. (Ed.), *Progress in Fish Nutrition. Proceedings of the Fish Nutrition Symp.* Keelung, Taiwan, ROC, Sept. 6–7, 1989. *Marine Food Science Series no. 9*, pp. 183–200.
- Kaushik, S.J., Medale, F., Faunconneau, B., Blanc, D., 1989. Effect of digestible carbohydrate on protein/energy utilization and on glucose metabolism in rainbow trout (*Salmo gairdneri* R.). *Aquaculture* 79, 63–74.
- Lall, S.P., 1979. Minerals in finfish nutrition. In: Halver, J.E., Tiews, K. (Eds.), *Proc. World Symp. on Finfish Nutrition and Fishfeed Technology*, Hamburg. Vol. I, Heenemann, Berlin, pp. 85–97.
- Lee, D.J., Putman, G.B., 1973. The response of rainbow trout to varying P:E ratios in a test diet. *J. Nutr.* 103, 916–922.
- Liu, K., Markakis, P., 1989. An improved calorimetric method for determining antitryptic activity in soy bean products. *Am. Assoc. Cereal Chem.* 66, 415–422.
- Lovell, R.T., 1988. Use of soybean products in diets for aquaculture species. *J. Aquat. Products* 2, 27–52.
- Martoja, R., Martoja-Pierson, M., 1970. *Técnicas de Histología Animal*. Toray-Masson, Barcelona, 350 pp.
- Moyano, F.J., 1990. *Utilización nutritiva de fuentes proteicas vegetales por la trucha arco iris (Oncorhynchus mykiss)*. Tesis Doctoral, Univ. de Granada, 236 pp.
- New, M.B., 1986. Aquaculture diets of postlarval marine fish of the superfamily *Percoidae*, with special reference to sea bass, sea breams, groupers and yellowtail: a review. *Kuwait Bull. Mar. Sci.* 7, 75–148.
- NRC (National Research Council), 1983. *Nutrient Requirements of Warmwater Fishes and Shellfishes*. National Academy Press, Washington, DC, 102 pp.
- Ogino, C., Takeuchi, L., Takeda, H., Watanabe, T., 1979. Availability of dietary phosphorus in carp and rainbow trout. *Bull. Jpn. Soc. Sci. Fish.* 45, 1527–1532.
- Pfeffer, E., Beckmann, J., 1991. Hydrothermically treated soy beans as source of dietary protein for rainbow trout (*Salmo gairdneri*, R.). *Arch. Anim. Nutr.*, Berlin 41, 223–228.
- Pongmaneerat, J., Watanabe, T., 1992. Utilization of soybean meal as protein source in diets for rainbow trout. *Nippon Suissan Gakkaishi* 58, 1983–1990.
- Richardson, N.L., Higgs, D.A., Beames, R.M., McBride, J., 1985. Influence of dietary calcium, phosphorus, zinc and sodium phytate level on cataract incidence, growth and histopathology in juvenile chinook salmon (*Oncorhynchus tshawytscha*). *J. Nutr.* 115, 553–567.
- Riche, M., Brown, P.B., 1993. Determination of phosphorus absorption coefficients for rainbow trout (*Oncorhynchus mykiss*) fed commercially used protein sources. Abstract of the World Aquaculture '93. Torremolinos, Spain, May 26–28, 1993, p. 258.
- Robaina, L., Izquierdo, M.S., Moyano, F., Socorro, J., Vergara, J.M., Montero, D., Fernández-Palacios, H., 1995. Soybean and lupin seed meals as protein sources in diets for gilthead seabream (*Sparus aurata*): nutritional and histological implications. *Aquaculture* 130, 219–233.
- Saini, H.S., 1989. Legumes seeds oligosaccharides. In: Huisman, J., Van der Poel, T.F.B., Liener, I.E. (Eds.), *Recent Advances of Research in Anti-nutritional Factors in Legume Seeds*. Pudoc. Wageningen, pp. 329–341.
- Sakamoto, S., 1981. Requirements and deficiency symptoms of dietary minerals in red sea bream. Report of Fish. Res. Lab., Kyushu Univ. Vol. 5, pp.1–99.

- Sakamoto, S., Yone, Y., 1978. Effect of dietary phosphorus level on chemical composition of red sea bream. *Bull. Jpn. Soc. Sci. Fish.* 44, 227–229.
- Sargent, J., Henderson, R.J., Tocher, D.R., 1989. The lipids. In: Halver, J.E. (Ed.), *Fish Nutrition*. Academic Press, San Diego, pp. 154–218.
- Schäfer, A., Koppe, W.M., Meyer-Burgdorff, K.-H., Günther, K.D., 1994. Effects of microbial phytase on the utilization of native phosphorus in a soybean meal based diet in carp. Abstract, II Intern. Symp. on Nutritional Strategies and Management of Aquaculture Waste. April 24–27, 1994, Aalborg, Denmark.
- Shimeno, S., Kumon, M., Ando, H., Ukawa, M., 1993. The growth performance and body composition of young yellowtail fed with diets containing defatted soybean meal for a long period. *Nippon Suissan Gakkaishi* 59, 821–825.
- Snyder, H.E., Kwon, T.W., 1987. *Soybean Utilization*. Van Nostrand-Reinhold, New York, 346 pp.
- Spinelli, J., Mahnken, C., Steinberg, M., 1979. Alternate sources of protein for fish meal in salmonid diets. In: Halver, J.E., Tiews, K. (Eds.), *Proc. World Symp. on Finfish Nutrition and Fishfeed Technology*, Hamburg. Vol. II, Heenemann, Berlin, pp. 131–142.
- Spinelli, J., Houle, C.R., Wekell, J.C., 1983. The effect of phytates on the growth of rainbow trout (*Salmo gairdneri*) fed purified diets containing varying quantities of calcium and magnesium. *Aquaculture* 30, 71–83.
- Takeuchi, L., Takeda, H., Watanabe, T., 1979. Availability of dietary phosphorus in carp and rainbow trout. *Bull. Jpn. Soc. Sci. Fish.* 45, 1527–1532.
- Vergara, J.M., 1992. Studies on the utilization of dietary protein and energy by gilthead sea bream (*Sparus aurata*). PhD thesis, Univ. Stirling, 162 pp.
- Watanabe, T., Viyakarn, V., Kimura, H., Ogawa, K., Okamoto, N., Iso, N., 1992. Utilization of soybean meal as a protein source in a newly developed soft-dry pellet for yellowtail. *Nippon Suissan Gakkaishi* 58, 1761–1773.
- Wekell, J.C., Shearer, K.D., Houle, C.R., 1983. High zinc supplementation of rainbow trout diet. *Prog. Fish Cult.* 48, 205–212.



Genetic structure of natural populations of *Gelidium* species: A re-evaluation of results

P. A. Sosa^{1*}, M. Valero², F. Batista¹ & M. A. Gonzalez-Pérez¹

¹Departamento de Biología, Universidad de Las Palmas de Gran Canaria, Campus Universitario de Tafira, 35017 Las Palmas, Canary Islands, Spain

²Laboratoire de Génétique et Evolution des Populations Végétales, Université de Lille-1, URA CNRS 1185, Bâtiment SN2, 59655 Villeneuve d'Ascq cedex, France

(* Author for correspondence: e-mail: pedro.sosa@biologia.ulpgc.es)

Received 1 January 1998; revised 1 June 1998; accepted 2 June 1998

Key words: Canary Islands, electrophoresis, F-statistics, *Gelidium canariensis*, *Gelidium arbuscula*, genetic distance, genetic structure, isozymes

Abstract

Twenty-two loci were re-evaluated to assess genetic variation and differentiation in three natural populations (two from Gran Canaria and one from Tenerife) of *Gelidium* (*G. canariensis* and *G. arbuscula*). The new data using exclusively the diploid subpopulation gene frequencies confirm that dispersal was restricted over short distances for the two species, but contrary to previous conclusions, the data reveal that these two closely related species differed markedly by their mating systems and patterns of genetic differentiation. Genetic differentiation among populations was twice as high in *G. arbuscula* as in *G. canariensis*. It was confirmed that the main way of reproduction is asexual in *G. arbuscula* and a discussion included as to how clonal propagation may explain the difference in haploid and diploid allele frequencies in this species. There was no evidence for asexual reproduction in *G. canariensis*. Heterozygote deficiency could be explained simply by spatial sub-structuring within populations. The importance of the sampling design in determining the level and pattern of genetic differentiation within a species is discussed.

Introduction

Most studies that have investigated genetic structure in haplo-diploid algae (Fujio et al., 1985; Lindstrom, 1993; Sosa & Garcia-Reina, 1992, 1993; Williams & Di Fiori, 1996) have attributed the co-occurrence of low levels of genetic diversity and high levels of genetic differentiation to selfing and/or asexual reproduction. The only exception is *Halidrys dioica*, reported by Lu & Williams (1994); this is diploid and obligately outcrossing.

Most of the species considered are heteromorphic with an alternation of macroscopic and microscopic phases, though only the macroscopic phases were sampled. *Gelidium*, in contrast, is isomorphic so that both haploid and diploid phases could be sampled.

Sosa and Garcia-Reina (1992, 1993) analysed and compared separately the genetic variation of haploid (female gametophytes) and diploid (tetrasporophytes) life stages in *G. canariensis* and *G. arbuscula* through isozyme electrophoresis. The authors calculated the Hardy-Weinberg departure and F-Statistics using the gene frequencies obtained from the haploid phases. The number of genes analysed for the haploid subpopulation was four times less than for the diploid one, leading to a possible bias. Therefore it was decided to re-evaluate the data using only the diploid subpopulation gene frequencies. Moreover, several procedures have been recently proposed in the literature to test for population structure (see Rousset & Raymond, 1997) which give additional and complementary information about the population structure of natural populations.

Table 1. Average genetic variation detected in *Gelidium arbuscula* and *G. canariensis* from natural populations of the Canary Islands. NG, Average Number of genes. NP, Number of analysed populations. NL, Number of loci. NA: Average Number of alleles. NPL: Average Number of polymorphic loci. A: Average number alleles per locus. P, Average Polymorphism. H, Average Expected heterozygosity. S, Sporophytic subpopulations. G, Gametophytic subpopulations. Data from Sosa and Garcia-Reina (1992, 1993).

		NP	NG	NL	NPL	NA	A	P	H
<i>G. arbuscula</i>	S	3	80	22	7	27	1.24	21.2	0.070
	G	3	15	22	2	23	1.06	6.0	0.018
<i>G. canariensis</i>	G	3	74	22	5	26	1.18	18.2	0.050
	G	3	15	22	3	22	1.10	9.1	0.031

Table 2. Tests for population differentiation among sporophytes and gametophytes within *Gelidium canariensis*. ns, not significant; -, no data; * $p < 0.05$; *** $p < 0.001$.

Populations	ALP-1	DIA-3	EST-2	MDH-1	PGI-3
Gáldar	-	ns	*	-	***
Agate	ns	ns	ns	ns	ns
Puerto Cruz	-	ns	ns	ns	ns

The aim of this paper was to compare the two *Gelidium* species using these new tools for statistical analyses of population genetic data using diploid data. As no comparison of these two *Gelidium* species using isozyme variation has been published previously, their taxonomic status of was re-examined using Nei's genetic distance (Nei, 1978) for the isozyme data.

Material and methods

Species studied and sampling localities

Analysis of the genetic diversity of three natural populations of the Canary Islands, Galdar and Agate from Gran Canaria, and Puerto de la Cruz from Tenerife of two *Gelidium* species (*G. arbuscula* and *G. canariensis*) was carried out by Sosa and Garcia-Reina (1992, 1993) using isozyme variation. The allelic frequencies for sporophytic and gametophytic phases were obtained separately. Twenty-three to 29 alleles were detected for *G. arbuscula*, and 23 to 27 alleles for *G. canariensis*, corresponding to twenty-two loci for both species (Table 1).

Statistical analyses

Deviation from Hardy-Weinberg expectations, genotypic linkage disequilibrium and differentiation among tetrasporophytic and gametophytic sub-populations were tested using the package GENEPOP, version 3.1 (Raymond & Rousset, 1995). For the two species, the test of HardyWeinberg proportions is an exact test, performed on the diploid sub-population data set, for each locus within each population. For both species, a Markov chain method was used to test for genotype linkage disequilibrium for each locus pair within each population using the diploid sub-population data set. Exact test for population differentiation among sporophytes and gametophytes within each species analyses the differences between haploid and diploid gene pools. For both species, exact tests for population differentiation were performed for each locus and within each population, also using a Markov chain method. In all cases, the Markov chain was set to 50,000 and 1000 steps of dememorization. The standard error was always < 0.005 .

The distribution of genetic variation within and among the natural populations of *Gelidium* species was analysed using F-statistics (Wright, 1965). F-statistics were computed according to Weir and Cockerham (1984) using the software FSTAT, version 1.2 (Goudet, 1995) on the diploid sub-population data set. GDA (Genetic Data Analysis: Lewis & Zaykin, 1997) software was used to calculate Nei's genetic identity (Nei, 1978). Nei's genetic identity and genetic distances (Nei, 1978) pair comparisons were calculated among populations, using diploid data set, within and among species to obtain the genetic relationship between both species.

Table 3. Tests for population differentiation among sporophytes and gametophytes within *Gelidium arbuscula*. ns, not significant; - no data; * $p < 0.05$; ** $p < 0.01$; *** $p < 0.001$.

Populations	ALP-1	DIA-2	EST-2	GDH-1	MDH-1	MDH-2	PGI-3
Gáldar	-	***	***	ns	-	-	-
Agacte	ns	ns	**	ns	ns	ns	-
Puerto Cruz	-	ns	ns	-	*	ns	ns

Table 4. Tests for Hardy-Weinberg deviation for *Gelidium canariensis*. -: Not possible (monomorphic locus); * $p < 0.05$; ** $p < 0.01$; *** $p < 0.001$.

Populations	ALP-1	DIA-3	EST-2	MDH-1	PGI-3	Mean
Gálda	-	-0.28	-0.02	-	1.00***	0.49
Agacte	-0.14	0.37	0.03	0.00	-0.08	0.12
Puerto Cruz	-	0.09	0.02	-0.10	0.51**	0.20
Mean	-0.14	0.07	0.03	-0.09	0.65***	0.23***

Results

Exact test for sub-population differentiation among diploids and haploids gene frequencies

In *Gelidium canariensis* significant differences between the two phases were found only in the Gáldar population (Table 2). This population showed significant heterogeneity among haploid and diploid gene frequencies for two of the three loci studied: although the test showed only marginal significance for locus EST-2, the result was highly significant for locus PGI-3 (Table 2). Conversely, in *G. arbuscula*, a significant heterogeneity among haploid and diploid sub-populations was found within each population for at least one locus (MDH-1 in Puerto de la Cruz, DIA-2 and EST-2 in Gáldar, and EST-2 in Agacte: Table 3). Moreover, three of these comparisons were highly significant (Table 3).

Hardy-Weinberg tests

In *Gelidium canariensis*, only one locus (PGI-3: Table 4) showed significant deviations from the Hardy-Weinberg equilibrium (heterozygote deficiency). In *G. arbuscula*, four loci (ALP-1, EST-2, MDH-1, GDH-1: Table 5) showed significant deviations from Hardy-Weinberg expectations. For this species, heterozygote excesses were revealed for two loci (EST-2 and MDH-1) within each of the population studied.

Heterozygote deficiencies were observed at the ALP-1 and GDH-1 loci within two of the three populations studied (Table 5).

Linkage disequilibrium

In *Gelidium canariensis*, only one test was marginally significant (MDH-1 and DIA-3 locus pair, data not shown) within Puerto de la Cruz population. In *G. arbuscula*, significant linkage disequilibria were detected within two of the three populations studied (Gáldar and Agacte for GDH-1/DIA-2 and MDH-2/DIA-2 locus pairs respectively (data not shown).

F-statistics

The significant heterozygote deficiency observed within *G. canariensis* species ($F_{IT} = 0.33$) was partially due to the within population component ($F_{IS} = 0.23$ essentially explained by locus PGI-3) and to the occurrence of differentiation among populations ($F_{ST} = 0.13$), (Table 6). In *Gelidium arbuscula*, the partitioning of total genetic variation observed within the species (Table 7) is very different than for *G. canariensis*. F_{IT} was essentially explained by a significant genetic differentiation among populations with a mean F_{ST} value of 0.28 being two times higher than in *G. canariensis*. The mean within population statistics was not significant because as we shown before, there was a strong discrepancy among loci and the ef-

Table 5. Tests for Hardy-Weinberg deviation in *Gelidium arbuscula*. –impossible (monomorphic locus); * $p < 0.05$; ** $p < 0.01$; *** $p < 0.001$.

Populations	ALP-1	DIA-2	EST-2	GDH-1	MDH-1	MDH-2	PGI-3	Mean
Gáldar	–	0.26	–0.46**	0.17*	–	–	–	–0.06
Agaete	0.64***	–0.10	–0.54***	0.81***	0.25	–0.01	–	0.11
Puerto Cruz	–	–0.22	–0.26	–	–0.43*	–0.22	–0.06	–0.26
Mean	0.64***	–0.04	–0.45***	0.39***	–0.06	–0.19	–0.06	–0.06

fects of heterozygote deficits were counterbalanced by heterozygote excesses (Table 7).

Genetic identity

Table 8 shows the Nei's genetic identity, I , and the genetic distance, D , between all the populations of both *Gelidium* species. The average genetic identity between both species of *Gelidium* was 0.848, with values ranging from 0.824 to 0.876. These values were always less than 0.880 (Table 8). In contrast, the I values obtained between populations of the same species were always higher than 0.960. As shown with the F-statistics analysis, genetic identities among populations were lower for *G. arbuscula* than for *G. canariensis*. Thus, I within *G. canariensis* populations ranged from 0.986 to 0.998 (average = 0.992) and the I range within *G. arbuscula* was 0.960 to 0.978 (average = 0.972).

Discussion

Mating systems and within population structure

In a species with an alternation of diploid and haploid generations, sexual reproduction balances allele frequencies among the haploid and diploid subpopulations so that no genetic differentiation among the two phases should be expected (Coyer et al., 1994; Wattier et al., 1997). Conversely, asexual reproduction (haploids producing directly haploids and *vice versa* for diploids) should lead to a reduction of gene flow between the two generations. While asexual reproduction would tend to favour genetic differentiation *via* genetic drift (the effective size of an asexual population being reduced in comparison with a sexual reproducing one), sexual reproduction would tend to homogenise allele frequencies among haploid and diploid subpopulations. It might then be expected

Table 6. F-statistics within *Gelidium canariensis*. *** $p < 0.001$.

Locus	F_{IS}	F_{ST}	F_{IT}
ALP-1	–0.01	0.01	0.00
DIA-3	0.07	–0.01	0.06
EST-2	0.03	0.29	0.30
MDH-1	–0.09	0.07	–0.02
PGI-3	0.65	0.09	0.68
All loci	0.23***	0.13***	0.33***

Table 7. F-statistics within *Gelidium arbuscula*. *** $p < 0.001$.

Locus	F_{IS}	F_{ST}	F_{IT}
ALP-1	0.64	0.07	0.67
DIA-2	–0.04	0.50	0.48
EST-2	–0.45	0.08	–0.34
GDH-1	0.40	0.30	0.58
MDH-1	–0.06	0.16	0.11
MDH-2	–0.19	0.16	0.00
PGI-3	–0.06	0.16	0.00
All loci	–0.06	0.28***	0.24***

that genetic differentiation could occur between sporophytic and gametophytic subpopulations only if recruitment *via* sexual reproduction is lower than genetic drift. Thus, significant differentiation among diploid and haploid gene frequencies could be a good indicator of the extent of asexual reproduction in the two *Gelidium* species studied.

For *Gelidium arbuscula*, differences in allele frequencies were detected among sporophytes and gametophytes subpopulations in all of the three populations studied. These results confirm those described previously (Sosa & Garcia-Reina, 1992). Asexual reproduction was considered as an important way of

Table 8. Genetic distance (below) and genetic identity (above) (Nei, 1978) detected between sporophytic subpopulations of *Gelidium arbuscula* and *G. canariensis* from the Canary Islands. Average genetic identity within *G. canariensis* populations: 0.992. Average genetic identity within *G. arbuscula* populations: 0.972. Average genetic identity between *G. arbuscula* and *G. canariensis* populations: 0.848.

	Population	<i>Gelidium canariensis</i>			<i>Gelidium arbuscula</i>		
		Gáldar	Agate	Pto. Cruz	Gáldar	Agate	Pto. Cruz
<i>G. canariensis</i>	Gáldar		0.986	0.998	0.838	0.856	0.824
	Agate	0.014		0.993	0.851	0.876	0.850
	Puerto Cruz	0.002	0.007		0.842	0.864	0.837
<i>G. arbuscula</i>	Gáldar	0.176	0.161	0.171		0.978	0.960
	Agate	0.155	0.132	0.145	0.021		0.978
	Puerto Cruz	0.193	0.163	0.177	0.041	0.022	

propagation within *G. arbuscula* populations from the Canary Islands. Although we did not have experimental data about the importance of the sexual and asexual reproduction for *Gelidium arbuscula*, the introduction of new genotypes through sexual recruitment was apparently rare in most species of *Gelidium*. As discussed by Sosa and Garcia-Reina (1992) stoloniferous outgrowths of creeping axes was a common way of propagation of *Gelidium* species. In addition, the populations of *G. arbuscula* were stable in time (personal observation); therefore, locally adapted clones could propagate asexually and became predominant through competitive advantage, thereby minimizing the availability of unoccupied substratum and limiting opportunities for recruitment of new genotypes (via sexual reproduction). In this species, the detection of heterozygote excesses within all the populations studied in conjunction with linkage disequilibrium (observed for two of the three populations analyzed) confirmed clonal reproduction of this species. Even if inbreeding or spatial sub-structuring might be occurring, these results strongly suggested that *G. arbuscula* was mainly characterized by a high level of clonal reproduction.

In contrast, the significant differences in allele frequencies among sporophytic and gametophytic subpopulations for *G. canariensis* species were only observed for the Gáldar population. In addition, only one locus (PGI-3) showed a significant deviation from Hardy-Weinberg equilibrium, and the deviation was always towards a heterozygote deficiency. These results contradict those obtained by Sosa and Garcia-Reina (1992). Even if clonal propagation via fragmentation could not be totally rejected from these analyses, the results suggested that other reproductive strategies were influencing the within population genetic structure of this species. The significant differences

in allele frequencies among sporophytic and gametophytic subpopulations for *G. canariensis* observed for Gáldar population could be explained by the occurrence of spatial sub-structuring (or Wahlund effect). Mixing of populations that differ in allele frequency would result in significant heterozygote deficiencies in the pooled or total population. In fact, the individuals analyzed for the Gáldar population belonged to five distinct successive samplings performed over two years within an area of less than one hundred square meters. Thus, for this population, the results could be explained by either a significant spatial or a temporal differentiation occurring within the site Gáldar. The observed heterozygote deficiency could be explained by selfing or inbreeding (sib-mating). However, the fact that heterozygote deficiency was only observed for a single locus suggested that this argument was relatively weak. A hierarchical and stratified sampling strategy would help to determine more accurately the spatial scale factors influencing the within population structure and to discriminate between the within-sub-population heterozygote deficiencies due to the breeding behaviour of the species (e.g. inbreeding) and the among sub-populations deficits due to the Wahlund effect (see Goudet et al., 1994 for more details). Finally, we could not exclude the hypothesis that selection (via hitch-hiking) was occurring at the PGI-3 locus to explain the discrepancy of the results among loci.

Genetic differentiation among populations within the species

Significant genetic differentiation among populations separated by 30 to 100 km was demonstrated in the two species. F_{ST} values ranged from 0.13 in *Gelidium canariensis* to 0.28 in *Gelidium arbuscula* indicating

low level of gene flow between populations. These values are higher than those described previously for diploid subpopulations (G_{ST} was 0.073 and 0.147, respectively, for *G. canariensis* and *G. arbuscula*: Sosa & Garcia-Reina 1992, 1993), and revealed that long distance dispersal seemed to be insufficient to prevent genetic differentiation among populations. Consequently, we would expect that *Gelidium arbuscula* with vegetative reproduction would exhibit a higher level of differentiation among populations than *Gelidium canariensis* because genetic drift is more efficient in an asexual species characterised by a reduced effective population size. Data confirmed this prediction since F_{ST} was two times greater in *G. arbuscula* than in *G. canariensis*. Spatial genetic differentiation among algal populations have been recently discussed by Lu & Williams (1994) and Benzie et al. (1997). Even if little is known on population biology of seaweed, they suggested that as in terrestrial plants, most populations are structured geographically at different scales, resulting from a variety of factors including mating system and dispersal capabilities. In this paper, the re-evaluation of data obtained on the mating system of both *Gelidium* species gave a new insight for the observed patterns of population spatial structure.

Genetic distances between *Gelidium* species

Species boundary was confirmed by allozyme data. The genetic identities detected among populations of the same species were always greater than those between species. As discussed by Sosa & Garcia-Reina (1992, 1993), the conspecific genetic identity values for *Gelidium* populations were high, and comparable to those reported for other seaweeds and some land plants. At the same time, congeneric values detected for *Gelidium* species ($I = 0.848$) were also in the range described for other boundaries species (Cheney & Babbel, 1978; Benzie et al., 1997).

Acknowledgments

We thanks Carolyn Engel for helpful comments on the manuscript. This work has been carried out from the collaboration within the European Community project 'BIOGAP'. MAST-III program. MAS3-CT95-0019.

References

- Benzie JAH, Price IR, Ballment E (1997) Population genetics and taxonomy of *Caulerpa* (Chlorophyta) from the great barrier reef, Australia. *J. Phycol.* 33: 491–504.
- Cheney DP, Babbel GR (1978) Biosystematic studies of the red algal genus *Eucheuma*. I. Electrophoretic variation among Florida populations. *Mar. Biol.* 47: 251–264.
- Coyer JA, Robertson DL, Alberte RS (1994) Genetic variability within a population and between diploid/haploid tissue of *Macrocystis pyrifera* (Phaeophyta). *J. Phycol.* 30: 545–552.
- Fujio Y, Kodaka PL, Hara M (1985) Genetic differentiation and amount of genetic variability in natural populations of the haploid laver *Porphyra yezoensis*. *Jap. J. Genet.* 60: 347–354.
- Goudet J (1995) Fstat Version 1.2. A computer program to calculate F-statistics. *J. Hered.* 86: 485–486.
- Goudet J, De Meeüs T, Day AJ, Gliddon C (1994) The different levels of population structuring of dogwhelks, *Nucella lapillus*, along the south Devon coast. In Beaumont A (ed.), *Genetics and Evolution of Aquatic Organisms*. Chapman & Hall, London, UK 81–95.
- Lewis PO, Zaykin D (1997) Genetic Data Analysis: Computer program for the analysis of allelic data. Version 1.0. Free program distributed by the authors over the internet from the GDA Home Page at <http://chee.unm.edu/gda/software>.
- Lindstrom SC (1993) Inter- and intrapopulation genetic variation in species of *Porphyra* (Rhodophyta: Bangiales) from British Columbia and adjacent waters. *J. appl. Phycol.* 5: 53–62.
- Lu TT, Williams SL (1994) Genetic diversity and genetic structure in the brown alga *Halidrys dioica* (Fucales: Cystoseiraceae) in southern California. *Mar. Biol.* 121: 363–371.
- Nei M (1978) Estimation of average heterozygosity and genetic distance from a small number of individuals. *Genetics* 89: 583–590.
- Raymond M, Rousset F (1995) GENEPOP (version 1.2): population genetics software for exact tests and eucumenism. *J. Hered.* 86: 248–249.
- Rousset F, Raymond M (1997) Statistical analyses of population genetic data: new tools, old concepts. *Trends Ecol. Evol.* 12: 313–317.
- Sosa PA, Garcia-Reina G (1992) Genetic variability and differentiation of sporophytes and gametophytes in populations of *Gelidium arbuscula* (Gelidiaceae: Rhodophyta) determined by isozyme electrophoresis. *Mar. Biol.* 113: 679–688.
- Sosa PA, Garcia-Reina G (1993) Genetic variability of *Gelidium canariensis* (Rhodophyta) determined by isozyme electrophoresis. *J. Phycol.* 29: 118–124.
- Wattier R, Dallas JF, Destombe C, Saumitou Laprade P, Valero M (1997) Single locus microsatellites in *Gracilariales* (Rhodophyta): high level of genetic variability within *Gracilaria gracilis* and conservation in related species. *J. Phycol.* 33: 868–880.
- Weir BS, Cockerham CC (1984) Estimating the F-statistics for the analysis of population structure. *Evolution* 38: 1358–1370.
- Williams SL, Di Fiori RE (1996) Genetic diversity and structure in *Pelvetia fastigiata* (Phaeophyta: Fucales): does a small effective neighborhood size explain fine-scale genetic structure. *Mar. Biol.* 126: 371–382.
- Wright S (1965) The interpretation of population structure by F-statistics with special regard to systems of mating. *Evolution* 19: 395–420.

Spatial Distribution of Shelf- and Slope-Dwelling Fishes Collected by Bottom Longline off Lanzarote and Fuerteventura, Canary Islands

FRANZ UIBLEIN¹, FERNANDO BORDES², RICARDO CASTILLO² & ANTONIO G. RAMOS³

¹Institut für Zoologie der Universität Salzburg, Hellbrunnerstr. 34, A-5020 Salzburg, Austria. E-mail: franz.uiblein@sbg.ac.at

²Instituto Canario de Ciencias Marinas, Aptdo. de Correos 56, E-35200 Telde, Gran Canaria, Spain.

³Departamento de Biología, Facultad de Ciencias del Mar, Universidad de Las Palmas de Gran Canaria, P.B. 550, Las Palmas de Gran Canaria, Spain.

With 6 figures and 2 tables

Key words: Depth distribution, depth-size, spawning aggregation, reproductive timing, *Mora moro*, topography, hydrography, local upwelling, satellite imagery.

Abstract. A total of 1789 fish belonging to 38 families and 73 species were collected at depths between 18 and 1102 m during 216 bottom longline operations off Lanzarote and Fuerteventura, Canary Islands, between February 1994 and December 1995. For each species the depth distribution is provided. Length-weight and depth-size relationships are reported for three shelf-dwelling species. The bigger-deeper relationship found in two of them contrasts with the bigger-shallower pattern of the deeper living trichiurid *Lepidopus caudatus*. In November 1997, nine additional bottom longline operations were carried out off eastern Fuerteventura at depths between 805 and 1217 m. In this area, after earlier studies in October 1995, a spawning aggregation of the morid *Mora moro* was encountered for the second time. The catches of 1997 revealed a strongly male-biased sex ratio. Also, the males showed a significantly lower gonadosomal index than two years earlier. These findings indicate slight interannual variations in reproductive timing and an earlier arrival of male *Mora moro* at the spawning grounds. Clear variations in the number of fish collected at adjacent sites possibly reflect a preference for distinct microhabitats. Preliminary evidence of local upwelling of cold water above the spawning grounds is provided by satellite imagery.

Problem

The Canary Islands region, situated in the northernmost part of the Eastern Central Atlantic, shows distinctive topographic and hydrographic conditions which may affect the spatial distribution of both shallow- and deep-water fishes to a considerable extent. The rather narrow shelf and the steep upper slope, typical for oceanic islands of volcanic origin, set spatial limits to the demersal fish assemblage. The hydrography of this region is characterized by countercurrents at different

depth zones with different temperature and salinity regimes and a strong upwelling activity off the adjacent north-west African coast (*e.g.*, MANN & LAZIER, 1991). Compared to topography, the effects imposed by water temperature, salinity or current velocity on fish distribution patterns may be less constraining. However, many fish species have been observed to migrate vertically or horizontally in response to local or temporal variations of water temperature (*e.g.*, NEILSON & PERRY, 1990; UIBLEIN & JAGSCH, 1994; RAMOS *et al.*, 1996).

During the last years, efforts have been increased in the Canary Islands to study the ecology of shelf- and slope-dwelling fish in detail (GONZÁLEZ *et al.*, 1988; BORDES *et al.*, 1991; BRITO *et al.*, 1993; BORDES *et al.*, 1995; UIBLEIN *et al.*, 1996). In one of these studies, the results of four bottom longline cruises off Lanzarote and Fuerteventura with special emphasis on the deep-water ichthyofauna from 100 to 1100 m depth were reported and discussed with respect to possible environmental effects on diversity, depth distribution and local abundance (UIBLEIN *et al.*, 1996). At depths of less than 100 m, an additional 48 bottom longline operations were carried out during these cruises. The present study analyses the results from these shallow-water catches and provides a complete overview of the depth distribution and abundance of fish species collected at a total of 216 localities between 18 and 1102 m. Furthermore, depth-size relationships of the most abundant shelf-dwelling species are determined and compared with the findings from deeper zones.

A special effort was made to more closely investigate a locality off Gran Tarajá in eastern Fuerteventura. In October 1995, a spawning aggregation of the moronid *Mora moro* was discovered there at about 1000 m depth (UIBLEIN *et al.*, 1996). Two years later, in early November 1997, nine bottom longline operations were carried out to examine if this spawning aggregation occurs consistently in the same area and during the same season. The results from this fishing experiment were compared with those obtained in October 1995. To detect possible interrelationships between the occurrence of the spawning aggregation and local hydrography, satellite-derived sea-surface temperature images were examined.

Material and Methods

The collections were made during four cruises with the local fishing vessel *Alkartasuna*, a boat of 12 m length and an engine power of 85 kW. It is equipped with a Furuno 50 kHz sounder, a Furuno GPS/Plotter as position indicator, and an OSA hydraulic winch. Between February 1994 and December 1995 a total of 216 localities off Lanzarote and Fuerteventura (Fig. 1) were sampled by bottom longline at depths between 18 and 1102 m. The gear was of the following type: the main line, a 2 mm diameter nylon rope (600 m length) was anchored at intervals of 50 m by stones weighing 500–600 g and at the ends by stones with 3–4 kg weight. Every two meters a 0.9 mm diameter snood, 100 cm long and terminating in a MUSTAD 3/0 hook, was attached to the main line by a swivel, giving a total of 36 hooks. The bait used was imported *Cololabis saira* (Scomberesocidae; 20 cm total length), cut into four longitudinal pieces of fillet. The time that the longline was set at the bottom ranged between 23 and 46 min (mean 30.9 min).

On 6–8 November 1997, during cruise “La Bocaina 11-97” a bottom longline experiment consisting of nine hauls was carried out off eastern Fuerteventura at depths between 805 and 1217 m (Fig. 1). In contrast to the longline operations carried out earlier, a slightly modified gear was used which allowed sampling of a larger bottom area: the main line had a total length of 1000 m, resulting in larger intervals for the anchoring stones and swivels. Size and number of hooks were identical with the gear described above. The bottom resting time of the longline ranged between 45 and 46 min.

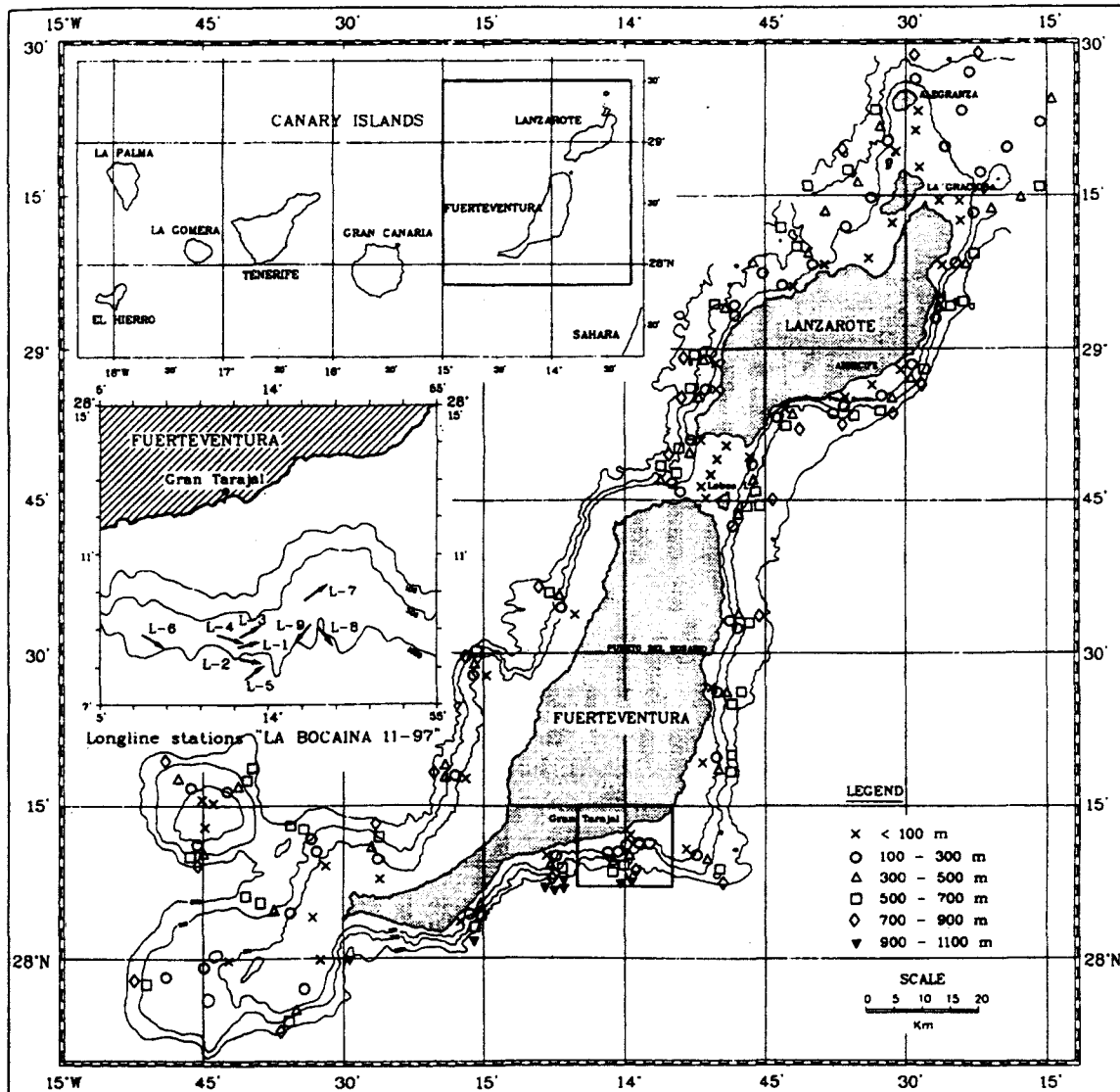


Fig. 1. Chart of the survey area off Fuerteventura and Lanzarote, Canary Islands, indicating longline station positions for six different depth zones sampled during the four earlier cruises (1994–1995) and the stations of the nine longline operations carried out during cruise “La Bocaina 11–97”.

The exact station position, initial and final depth and duration of the respective longline operation, species identity and number of individuals were recorded for each operation. The samples were stored in ice. Family identity was determined according to NELSON (1994) and species identity was re-examined (based on WHITEHEAD *et al.*, 1984–86; BRITO, 1991; NAKAMURA & PARIN, 1993; FRANQUET & BRITO, 1995; among others). In addition, total length and total weight were determined.

An additional depth zone of less than 100 m was added to the five depth zones already described by UIBLEIN *et al.* (1996). This resulted in a total of six different depth zones, with Zone 0 ranging from 0–100 m, Zone 1 from 100–300 m, Zone 2 from 300–500 m, Zone 3 from 500–700 m, Zone 4 from 700–900 m and Zone 5 from 900–1100 m.

Length-weight relationships were calculated using the regression function

$$W = aL^b$$

where W is the total weight and L is the total length.

To detect significant depth-size relationships, the most abundant species ($n > 60$) were analysed using two different methods, SPEARMAN rank correlation based on the raw data set and linear regression

function based on the geometric mean weight and length per haul. Hauls consisting of only one individual were excluded from the latter analysis.

The species collected in the longline experiment were identified and of all *Mora moro* collected, sex, total length, total weight and gonad weight were determined.

The gonadosomal index (I_G)

$$I_G = 100 \cdot W_G \cdot W^{-1}$$

was calculated, where W_G is the gonad weight and W is the total weight. In addition, ovarian maturity stage based on macroscopic characteristics was determined (c.f. UIBLEIN *et al.*, 1996).

Between August 1996 and November 1997, satellite imagery of the Advanced Very High Resolution Radiometer (AVHRR/NOAA) was received from a ground station (UTIS-ULPGC) and processed. Radiance values of channels 4 (10.5–11.3 nm) and 5 (11.5–12.5 nm) were converted to sea-surface temperatures and corrected for atmospheric effects using a multichannel algorithm. SST maps were then geometrically corrected using orbital parameters and fixed points on the ground and completed with a legend and frame. Due to frequent cloud accumulations in the study area only a relatively small sample of good quality images appropriate to show the surface temperature conditions was obtained. From this sample four representative images from different seasons or years were selected.

Results

Of the total 216 bottom longline operations carried out between February 1994 and December 1995, 175 (81%) were successful. A total of 1789 fishes were collected, resulting in 1627.9 kg of fish and means of 10.2 individuals and 9.3 kg fish per successful haul. Of the total 48 hauls carried out in Zone 0 (0–100 m depth), 47 (97.9%) resulted in the capture of at least one fish specimen. Six hundred twenty-two individuals belonging to 38 species and 19 families were collected in this depth zone, with an average of 13 individuals and 11.38 kg of fish per successful haul. Compared to the catches from the deeper zones studied earlier (UIBLEIN *et al.*, 1996), the results from Zone 0 closely resemble those of Zone 1 and clearly differ from the much lower capture success at depths between 500 and 900 m (Zone 3, Zone 4). They also differ from the increasingly lower numbers of species and families collected with increasing depth from Zone 2 (300–500 m) to Zone 5 (900–1100 m).

Four families are new among those 34 reported by UIBLEIN *et al.* (1996): Gymnuridae (*Gymnura altavela*), Myliobatidae (*Myliobatis aquila*), Synodontidae (*Synodus saurus*) and Haemulidae (*Parapristipoma octolineatum*). The depth distribution of all 73 species collected in the six depth zones, with the most abundant ones emphasized, is shown in Fig. 2.

The capture of a great number of *Serranus atricauda*, *Trachinus radiatus* and *Pagrus pagrus* in Zone 0 enabled a detailed analysis of length-weight and depth-size relationships; this supplements earlier statistical treatments of the data from deep-water fish (UIBLEIN *et al.*, 1996). The following length-weight relationships were obtained: *S. atricauda*: $W = 0.0081 L^{3.1602}$ ($n = 94$, 19–43 cm TL); *T. radiatus*: $W = 0.0035 L^{3.2923}$ ($n = 93$, 23–54 cm TL); *P. pagrus*: $W = 0.0184 L^{2.9695}$ ($n = 476$, 18–64 cm TL). Both methods of correlation analysis revealed a clear bigger-deeper pattern in *S. atricauda* and *P. pagrus* (Figs 3 and 4). For *T. radiatus* no significant correlations were discovered. These findings contrast with the depth-body size relationship of *Lepidopus caudatus*, which indicates a bigger-shallower pattern (Fig. 4; see also UIBLEIN *et al.*, 1996).

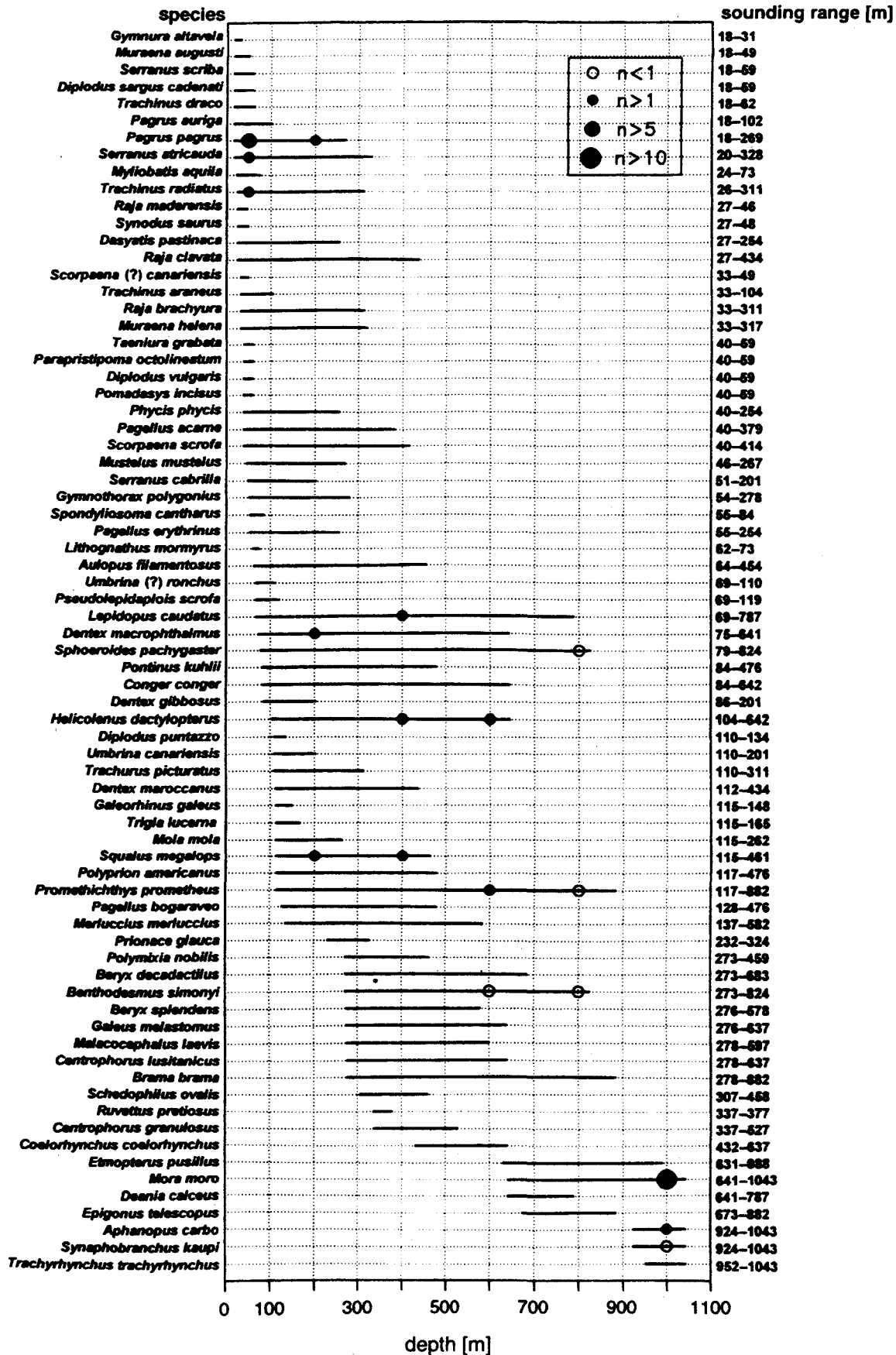


Fig. 2. Bathymetric distribution of the species collected and sounding range. Symbols indicate the three most abundant species for each of the six depth zones and the mean number of individuals per successful haul. In two cases species identity was uncertain. For further information see text.

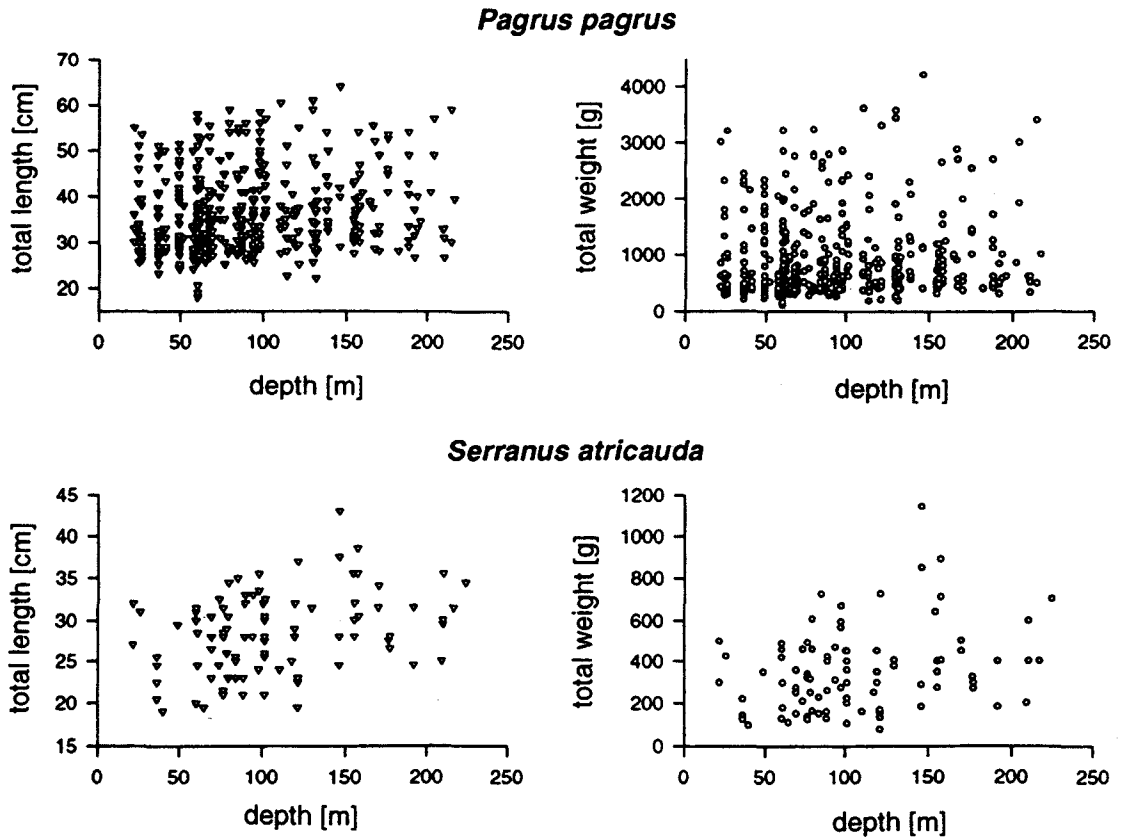


Fig. 3. Relationship between depth and two measures of body size, total length and total weight based on the raw data set in *Pagrus pagrus* ($n = 476$; $P < 0.01$ in both cases) and *Serranus atricauda* ($n = 94$; $P < 0.01$ in both cases).

The results of the bottom longline experiment carried out in November 1997 are given in Table 1. All nine longline hauls were successful. Eight of the nine hauls resulted in capture of *Mora moro*, at varying but mostly high numbers. The three other species collected, *Synaphobranchus kaupi*, *Aphanopus carbo* and *Trachyrhynchus trachyrhynchus*, occurred only at low numbers of maximally two individuals per longline operation. Closer observations during hauling in of the gear showed that during the last two operations, nr. 8 and nr. 9 (c.f. Table 1), all *M. moro* were concentrated on the hooks of the first half of the longline, whereas the second 500 m section of the main line was empty. In both cases, the initial position of the gear had been close to the entrance of a canyon-like structure of the slope, while the other end had been placed more offshore (Fig. 1).

In most catches, females were rare and males were numerically dominant. Consequently, the overall sex ratio of the *Mora moro* collected was strongly male-biased with 1 female:8.22 males ($n = 83$). This result differs significantly from the sex ratio obtained in October 1995 (1:0.94; $n = 66$; c.f. UIBLEIN *et al.*, 1996).

Total length of *Mora moro* ranged between 42 and 65.5 cm TL, which is close to the range obtained earlier (38.5–67.5 cm). Neither females nor males showed significant differences in total length between the two fishing dates (Table 2). As in 1995, males were smaller than females, and both sexes showed an advanced gonadal maturity (stages III, III–IV and IV), but no indication of completely ripened or running gonads (stage V). Interestingly, males showed a significantly lower GSI in 1997 compared to 1995 (one-way ANOVA, $P < 0.005$; Table 2).

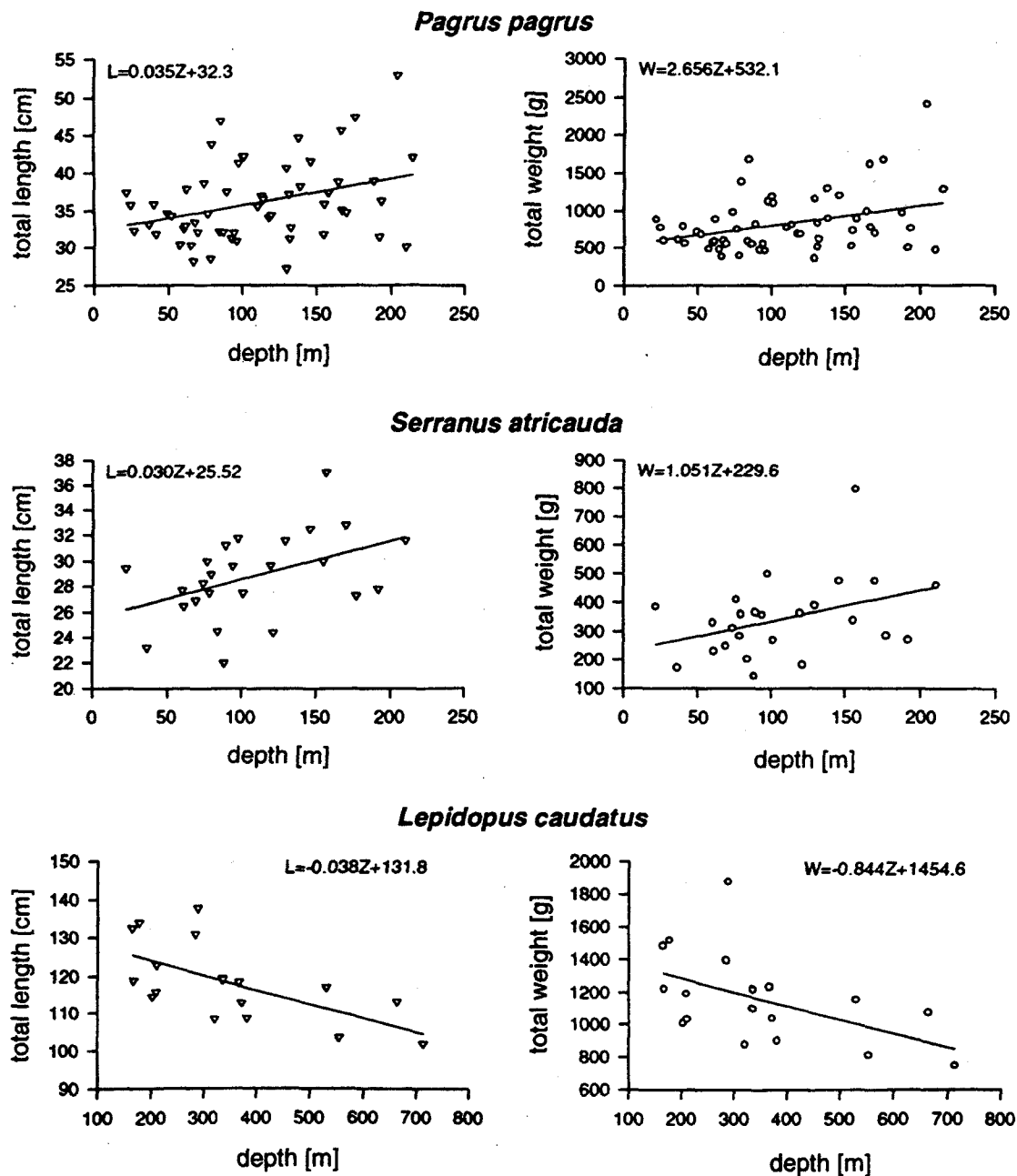


Fig. 4. Relationship between depth and two measures of body size, total length and total weight based on the geometric means of those hauls that resulted in capture of more than one individual in *Pagrus pagrus* ($n = 57$; $P < 0.01$ in both cases), *Serranus atricauda* ($n = 25$; $P < 0.05$ and $P = 0.06$, respectively), and *Lepidopus caudatus* ($n = 18$; $P < 0.01$ and $P < 0.05$, respectively). The results of linear regression analysis are also shown.

Satellite-derived sea-surface temperature images of 16 August 1996, 30 April 1997 and 1 August 1997 (Fig. 5a–c) demonstrate the repeated occurrence of a locally restricted, cool water mass surrounded by warmer surface water off eastern/southeastern Fuerteventura. This pattern is not evident from the image of 17 November 1997 (Fig. 5d). Additional observations made by examining time series of images from the different seasons and years showed that mainly between April and late September warm surface-water masses moved in a southward direction. Whereas these warm-water layers remained rather large and compact along the

Table 1. Number, date, position, depth and capture results of the bottom longline operations performed in November 1997 off Gran Tarajal, Fuerteventura.

haul nr.	date	initial position		mid-depth (initial-final depth)	number of <i>M. moro</i>	
		final position			(females)	other (number)
1	06-11-97	28°08.58'N, 14°00.93'W		947 m	4	-
		28°08.68'N, 14°00.49'W		(933-961 m)	(0)	
2	06-11-97	28°08.37'N, 14°00.89'W		1075 m	1	<i>S. kaupi</i> (1)
		28°08.26'N, 14°00.38'W		(1052-1098 m)	(1)	
3	06-11-97	28°08.73'N, 14°00.88'W		837 m	9	<i>S. kaupi</i> (1)
		28°09.02'N, 14°00.48'W		(869-805 m)	(0)	
4	06-11-97	28°08.80'N, 14°01.30'W		896.5 m	7	<i>S. kaupi</i> (1)
		28°08.62'N, 14°00.71'W		(915-878 m)	(0)	
5	07-11-97	28°07.89'N, 14°00.69'W		1208 m	-	<i>A. carbo</i> (1)
		28°08.22'N, 14°00.30'W		(1199-1217 m)		
6	07-11-97	28°08.87'N, 14°03.73'W		892.5 m	8	<i>A. carbo</i> (1)
		28°08.66'N, 14°03.29'W		(897-888 m)	(1)	<i>S. kaupi</i> (2)
7	07-11-97	28°09.75'N, 13°58.95'W		879 m	22	<i>T. trachyrhynchus</i>
		28°10.06'N, 13°58.45'W		(878-880 m)	(0)	(2)
8	08-11-97	28°09.23'N, 13°58.67'W		1020 m	14	<i>A. carbo</i> (2)
		28°08.87'N, 13°58.16'W		(1016-1024 m)	(5)	<i>S. kaupi</i> (2)
9	08-11-97	28°09.20'N, 13°58.78'W		961 m	16	-
		28°08.98'N, 13°59.14'W		(1007-915 m)	(2)	

Table 2. Number of individuals, mean total length (logarithmized, with 95% confidence limits), and mean gonadosomal index (GSI, with 95% confidence limits) for female and male *Mora moro* caught by bottom longline off Gran Tarajal, Fuerteventura, in October 1995 and November 1997.

n	28-29 October 1995		6-8 November 1997	
	females 34	males 32	females 9	males 74
log TL [cm]	1.75	1.71	1.78	1.72
(95% conf. limits)	(1.74-1.77)	(1.70-1.73)	(1.75-1.82)	(1.71-1.72)
GSI	8.74	1.84	9.51	1.38
(95% conf. limits)	(7.42-10.05)	(1.60-2.08)	(6.94-12.06)	(1.22-1.53)

northeastern coastline of Fuerteventura, a cold-water pocket appeared repeatedly at about 14° W very close to the area where the spawning aggregation of *Mora moro* was found (e.g., Fig. 5a,b). Surrounded by the warmer surface water, this pocket drifted further southward during the following days. In October/November 1996 and 1997, respectively, this situation changed drastically. The southward-directed displacement of surface water decreased, being interrupted by a rather wide-ranging spread of a uniform warm-water layer that was penetrated only by the upwelling activity off the north-west African coast (Fig. 5d).

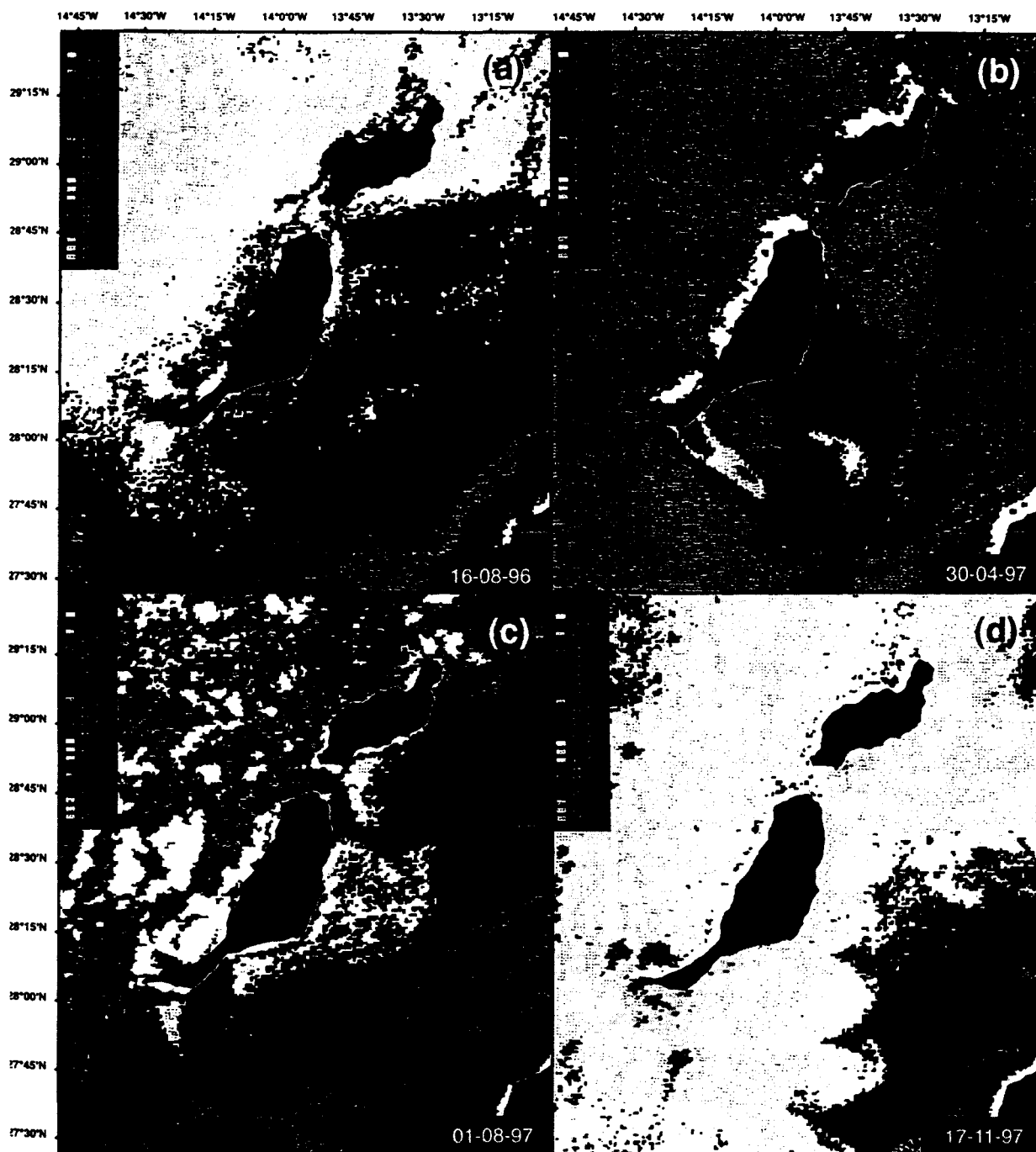


Fig. 5. Satellite-derived sea-surface temperature in the region of Lanzarote and Fuerteventura on 16 August 1996 (a), 30 April 1997 (b), 01 August 1997 (c) and 17 November 1997 (d).

Discussion

Among the 73 fish species collected, four major bathymetric groups can be roughly distinguished: shelf dwellers with rather narrow depth ranges (species occurring exclusively at less than about 200 m depth, *e.g.*, *Serranus scriba*), shelf and upper slope dwellers with rather wide depth ranges (*e.g.*, *Squalus megalops*), upper slope dwellers (*e.g.*, *Beryx decadactylus*) and middle slope dwellers (*e.g.*, *Trachyrhynchus trachyrhynchus*). Further representatives of the three latter bathymetric groups

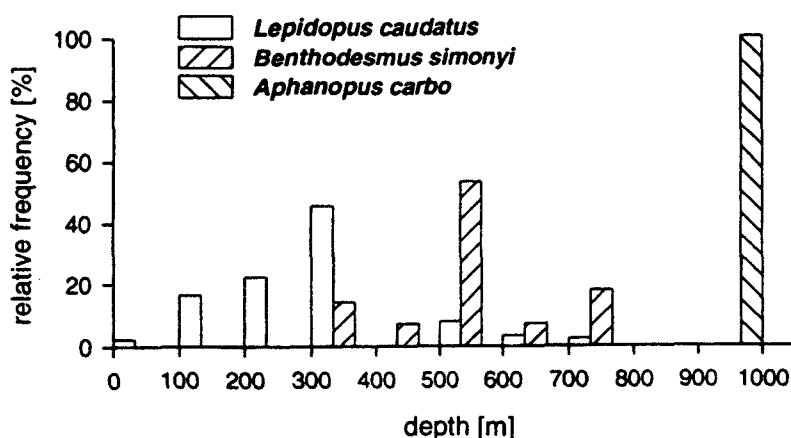


Fig. 6. Relative frequency of depth distribution in the three trichiurid species: *Lepidopus caudatus*, *Benthodesmus simonyi* and *Aphanopus carbo*.

are the three trichiurid species *Lepidopus caudatus*, *Benthodesmus simonyi* and *Aphanopus carbo*, which show a generic replacement down the slope (Fig. 6; see also NAKAMURA & PARIN, 1993). Several other slope-dwelling species, however, show great overlap in depth distribution.

Depth-body size relationships have received considerable attention in deep-sea research, as they may reveal certain intrinsic patterns or processes of adaptation to ecological variation among different depth zones (e.g., THIEL, 1979; MACPHERSON & DUARTE, 1991; MERRETT *et al.*, 1991; STEFANESCU *et al.*, 1992; UIBLEIN *et al.*, 1994; GORDON & MAUCLINE, 1996). The bigger-deeper pattern found in *Pagrus pagrus* and *Serranus atricauda* may be a consequence of either downwards directed ontogenetic migrations, depth-dependent growth rates, or overfishing in the upper shelf with size-selective gear such as bottom longline (c.f. LØKKEBORG & BJORDAL, 1992; CONNOLLY & KELLY, 1996). In the event of ontogenetic migrations, a clear bathymetric separation between size classes would be expected (cf. UIBLEIN *et al.*, 1994). The finding of a bigger-shallower pattern in *Lepidopus caudatus*, which co-occurs with the other two species at the middle and lower shelf and below the margin of the shelf, could be taken as an argument against possible overfishing effects. Therefore, of the three explanations offered, bathymetric variation in growth rates is the most plausible cause for the observed distribution patterns.

The smaller body size of *Lepidopus caudatus* at greater depth may indicate a reduced growth rate along the steeper parts of the slope, where living space and benthic food abundance should be reduced. At this depth, spatial or trophic interactions with another close relative, the trichiurid *Benthodesmus simonyi*, may occur. The latter species has a slimmer body and thus may have lower energy requirements (cf. KOSLOW, 1996) enabling it to better adapt to limited food availability. However, as both species are benthopelagic foragers (NAKAMURA & PARIN, 1993; SALDANHA *et al.*, 1995), they may obtain additional energy from feeding excursions into the open water. Off Lanzarote and Fuerteventura, at depths between 400 and 700 m, a deep-scattering layer composed of mesopelagic fish and various invertebrate species has been identified during acoustic and pelagic fishing investigations (e.g., BADCOCK, 1970; BORDES *et al.*, 1995; BORDES *et al.*, 1997).

The transition zone between the shallower, steeper, and the deeper, flatter parts

of the slope – as it occurs off eastern Fuerteventura at *ca.* 850 to 1000 m depth – may be a particularly interesting habitat for demersal fishes to settle. This zone provides more living space and probably also an increased food intake via slumps, turbidity currents, or other ways of rapid transport from the shelf and the steeper parts of the upper slope (c.f. GORDON, 1979). In this zone, the spawning aggregation of *Mora moro* was encountered for the second time in November 1997. However, as the present study suggests, this aggregation is not uniformly distributed, but shows considerable fluctuations in fish density among adjacent sites. Such a “patchy” distribution pattern may reflect the selection of distinct microhabitats within the same depth zone and area. In this respect the observation of an increased abundance close to the entrance of a submarine canyon is of particular interest.

In November 1997, as in October 1995, *Mora moro* showed an advanced gonadal maturity. However, the lower gonadosomal index of the males indicates a delay in the timing of reproduction in 1997. In contrast to such slight interannual changes in reproductive timing within one area, *Mora moro* may show considerable variations in spawning seasonality among different regions of the Atlantic. In a study on the biology of three morid species living on the continental slope of the Rockall Trough (north-east Atlantic, 53°N), GORDON & DUNCAN (1985) found clear indications of a spawning peak for *Mora moro* in June/July. Such geographical variation in spawning seasonality could reflect an environmentally induced, phenotypically plastic response (WINTERS & WHEELER, 1996) or may be genetically based (BYE, 1984). In the north-east Atlantic there is considerable latitudinal variation in seasonal food input from the surface which – apart from effects on species composition, foraging behaviour, growth and fecundity (MERRETT, 1987) – may also influence the timing of reproduction in deep-sea fishes.

Whereas males were highly abundant in the 1997 longline catches, females were much less frequent compared to the findings of two years before. As bottom longline operations carried out in the same depth zone and area during other seasons led to the capture of only a few *M. moro* (UIBLEIN *et al.*, 1996), the following scenario of two temporally separated, sex-specific spawning migrations may be hypothesized: first, the males travel to this area, select certain microhabitats, and terminate the last phase of gonad growth; later, the females arrive at these sites and then spawning takes place over a period of a few weeks. In another gadiform species, the macrourid *Coryphaenoides acrolepis*, it has been suggested that the males hold territories and females move up the slope to these areas to spawn (see GORDON, 1979).

This study provides preliminary evidence for the formation of a cold-water pocket off eastern Fuerteventura. This indicates a local upwelling activity just above the spawning grounds of *Mora moro*. Several factors have been identified to cause upwelling such as opposing undercurrents, shelf breaks, shelf-edge canyons, strong winds, capes and coastal mountains (HUTHNANCE, 1995). Most of these factors also deserve consideration for the area under study.

In gadiform fish, local hydrography has been suggested to be associated with the formation of spawning aggregations. Hoki (*Macruronus novaezelandiae*), for instance, spawn in the eastern Cook Strait, New Zealand, in dense concentrations in deep canyons at more than 200 m depth; here deep currents and local upwelling carry the eggs and larvae into shallow coastal regions of Clifford Bay (LIVINGSTON, 1990; MURDOCH *et al.*, 1990). *Mora moro* spawn at much greater depths than hoki,

where upwelling may be less influential or exert no effects at all. Furthermore, the upwelling activity off eastern Fuerteventura seems to diminish before the start of the spawning period. Fine-scaled investigations of the hydrography, topography and nutrient input at and in the immediate surroundings of the spawning grounds are needed to identify the environmental cues these deep-sea fish may use to locate the spawning area and to aggregate and reproduce there during a limited period of the year.

Summary

- (1) An analysis of 48 bottom longline operations from depths of less than 100 m is accompanied by a complete overview of the results of four bottom longline cruises carried out off Lanzarote and Fuerteventura between February 1994 and December 1995 at 216 localities between 18 and 1102 m depth. A total of 1789 fishes belonging to 38 families and 73 species were collected. The depth distribution for each species is provided, with the most abundant ones being emphasized.
- (2) For the species encountered at high frequency at less than 100 m, the length-weight and depth-size relationships are reported. Two inhabitants of the shelf and uppermost parts of the upper slope, *Pagrus pagrus* and *Serranus atricauda*, show a bigger-deeper pattern, whereas in the trichiurid *Lepidopus caudatus* a bigger-shallower pattern had been discovered during an earlier study of the deep-water fishes collected during these cruises (UIBLEIN *et al.*, 1996). The possible effects of the narrow shelf and a steep upper slope typical for the Canary Islands on the depth distribution and local abundance of demersal fish are discussed.
- (3) In November 1997, nine bottom longline operations were carried out off Gran Tarajal, eastern Fuerteventura, at depths between 805 and 1217 m. In this area, a spawning aggregation of the morid *Mora moro* had been discovered at about 1000 m depth during an earlier cruise in October 1995. Two years later, this spawning aggregation was encountered again. Interestingly, the 1997 catches revealed a strongly male-biased sex-ratio (1 female : 8.22 males versus 1 : 0.94 in 1995). Furthermore, the males showed a significantly lower gonadosomal index in 1997. These findings indicate slight interannual variations in reproductive timing and an earlier arrival of male *Mora moro* at the spawning grounds. Clear variations in the numbers of fish collected at adjacent sites within the study area may reflect a patchy distribution pattern within the spawning aggregation.
- (4) Sea-surface temperature data derived from satellite imagery indicate a zone of local upwelling of cold water just above the spawning grounds of this species. This upwelling activity, however, seems to diminish before the start of the spawning season.

Acknowledgements

We thank the crew of the fishing vessel *Alkartasuna* for assistance in the field, ANTONIO BARRERA LUJÁN and JOSÉ A. GÓMEZ BETHENCOURT for indispensable help in data collection, JOSÉ CARILLO MOLINA and FELIPE PÉREZ ARTILES for their collaboration in the analysis of catches, and JOSEP COCA for help in image processing. We thank NIGEL MERRETT, JOHN D. M. GORDON and JØRGEN G. NIELSEN for many

valuable comments on earlier versions of the manuscript. Financial support was provided by the Gobierno de Canarias.

References

- BADCOCK, J., 1970: The vertical distribution of mesopelagic fishes collected on the SOND cruise. *J. Mar. Biol. Assoc. U.K.*, **50**: 1001–1044.
- BORDES, F., A. BARRERA, R. CASTILLO, J. A. GÓMEZ, A. OJEDA & F. PÉREZ, 1991: Cartografía y evaluación de recursos pesqueros de la plataforma y talud de Gran Canaria (Islas Canarias). Consejería de Pesca y Transportes, Gobierno de Canarias, Telde, Las Palmas GC; 28 pp.
- , A. BARRERA, J. CARILLO, R. CASTILLO, J. A. GÓMEZ, K. HANSEN, F. PÉREZ & F. UIBLEIN, 1995: Cartografía y evaluación de los recursos pesqueros en la plataforma y talud de Fuerteventura y Lanzarote (Islas Canarias). Consejería de Agricultura, Pesca y Alimentación, Telde, Las Palmas GC; 56 pp.
- , A. BARRERA, J. CARILLO, R. CASTILLO, J. J. CASTRO, J. A. GÓMEZ, K. HANSEN, V. HERNÁNDEZ, T. MORENO, F. PÉREZ & F. UIBLEIN, 1997: Evaluación acústica de los recursos epipelágicos y estudio de la capa profunda de reflexión en Lanzarote, Fuerteventura y Gran Canaria (Islas Canarias). Viceconsejería de Pesca. Consejería de Agricultura, Pesca y Alimentación, Telde, Las Palmas GC; 63 pp.
- BRITO, A., 1991: Catálogo de los peces de la Islas Canarias. Ed. Francisco Lemus, La Laguna TF; 230 pp.
- , J. I. LOZANO, R. RABANAL, P. PASCUAL, M. HERNÁNDEZ, J. M. FALCÓN, J. A. GONZÁLEZ, J. I. SANTANA, J. BARQUÍN, G. GONZÁLEZ, F. I. PÉREZ & V. FERNÁNDEZ, 1993: Prospección de las poblaciones de condriictios (Tiburones) de los fondos batiales profundos de Canarias, con especial atención a su posible aprovechamiento pesquero. Consejería de Pesca y Transportes, Gobierno de Canarias, Las Palama GC; 63 pp.
- BYE, V. J., 1984: The role of environmental factors in the timing of reproductive cycles. In: G. W. POTTS & R. J. WOTTON (Eds.), *Fish reproduction: strategies and tactics*. Academic Press, London: 187–222.
- CONOLLY, P. L. & C. J. KELLY, 1996: Catch and discards from experimental trawl and longline fishing in the deep water of the Rockall Trough. *J. Fish. Biol.*, **49A**: 132–144.
- FRANQUET, F. & A. BRITO, 1995: Especies de interés pesquero de Canarias. Consejería de Pesca y Transportes, Gobierno de Canarias, Telde, Las Palmas GC; 143 pp.
- GONZÁLEZ, J. A., I. J. LOZANO, M. A. CALDENTEY, J. I. SANTANA, J. A. GÓMEZ & R. CASTILLO, 1988: Resultados de la campaña de prospección pesquera “Canarias 85”. *Inf. Téc. Inst. Esp. Oceanogr.*, **57**: 1–93.
- GORDON, J. D. M., 1979: Lifestyle and phenology in deep sea anacanthine teleosts. *Symp. Zool. Soc. London*, **44**: 327–359.
- & J. A. R. DUNCAN, 1985: The biology of fish of the family Moridae in the deep-water of the Rockall Trough. *J. Mar. Biol. Assoc. U.K.*, **65**: 475–485.
- & J. MAUCLINE, 1996: The distribution and diet of the dominant, slope-dwelling eel, *Synaphobranchus kaupi*, of the Rockall Trough. *J. Mar. Biol. Assoc. U.K.*, **76**: 493–503.
- HAEDRICH, R. L. & N. R. MERRETT, 1990: Little evidence for faunal zonation or communities in deep sea demersal fish faunas. *Prog. Oceanogr.*, **24**: 239–250.
- HUTHNANCE, J. M., 1995: Circulation, exchange and water masses at the ocean margin: the role of physical processes at the shelf edge. *Prog. Oceanogr.*, **35**: 353–431.
- KOSLOW, J. A., 1996: Energetic and life-history patterns of deep-sea benthic, benthopelagic and seamount-associated fish. *J. Fish. Biol.*, **49A**: 54–74.
- LIVINGSTON, M. E., 1990: Spawning hoki (*Macruronus novaezelandiae* HECTOR) concentrations in Cook Strait and off the east coast of South Island, New Zealand, August–September 1987. *N. Z. J. Mar. Freshwater Res.*, **24**: 503–517.
- LØKKEBORG, S. & Å. BJØRDAL, 1992: Species and size selectivity in longline fishing: a review. *Fish. Res.*, **13**: 311–322.
- MACPIHERSON, E. & C. M. DUARTE, 1991: Bathymetric trends in demersal fish size: is there a general relationship? *Mar. Ecol. Prog. Ser.*, **71**: 103–112.
- MANN, K. H. & J. R. N. LAZIER, 1991: *Dynamics of marine ecosystems*. Blackwell Scientific Publications, Boston; 466 pp.
- MERRETT, N. R., 1987: A zone of faunal change in assemblages of abyssal demersal fish in the eastern north atlantic: a response to seasonality in production? *Biol. Oceanogr.*, **5**: 137–151.
- MURDOCH, R., R. GUO & A. McCRONE, 1990: Distribution of hoki (*Macruronus novaezelandiae*) eggs

- and larvae in relation to hydrography in eastern Cook Strait, September 1987. *N. Z. J. Mar. Freshwater Res.*, **24**: 529–539.
- NAKAMURA, I. & N. V. PARIN, 1993: FAO species catalogue vol. 15. Snake mackerels and cutlass fishes of the world (Families Gempylidae and Trichiuridae). *FAO Fish. Synop.*, **15**: 1–136.
- NEILSON, J. D. & R. I. PERRY, 1990: Diel vertical migrations of marine fishes: an obligate or facultative process? *Adv. Mar. Biol.*, **26**: 115–168.
- NELSON, J. S., 1994: *Fishes of the World*. 3rd edition. John Wiley & Sons, NY: 600 pp.
- RAMOS, A. G., J. SANTIAGO, P. SANGRA & M. CANTON, 1996: An application of satellite-derived sea surface temperature data to the skipjack (*Katsuwonus pelamis* LINNAEUS, 1758) and albacore tuna (*Thunnus alalunga* BONATERRE, 1788) fisheries in the north-east Atlantic. *Int. J. Remote Sensing*, **4**: 749–759.
- SALDANHA, L., A. J. ALMEIDA, F. ANDRADE & J. GUERREIRO, 1995: Observations on the diet of some slope dwelling fishes of Southern Portugal. *Int. Rev. ges. Hydrobiol.*, **80**: 217–234.
- STEFANESCU, C., J. RUCABADO & D. LLORIS, 1992: Depth-size trends in western Mediterranean demersal deep-sea fishes. *Mar. Ecol. Prog. Ser.*, **81**: 205–213.
- THIEL, H., 1979: Structural aspects of the deep-sea benthos. *Ambio (Special Report)*, **6**: 25–31.
- UIBLEIN, F. & A. JAGSCH, 1994: Wassertemperatur, Laichaktivität und Laichplatzwahl-Beobachtungen an der Salzach-Äsche, *Thymallus thymallus* (Pisces: Salmonidae). *Artenschutzreport*, **4**: 38–41.
- , J. G. NIELSEN & W. KLAUSEWITZ, 1994: Depth dependent morphological variation in two ophiidiiform fishes from the deep Red Sea: evidence for species-specific structure in vertical distribution. *Cybium*, **18**: 15–23.
- , F. BORDES & R. CASTILLO, 1996: Diversity, abundance and depth distribution of demersal deep-water fishes off Lanzarote and Fuerteventura, Canary Islands. *J. Fish Biol.*, **49A**: 75–90.
- WHITEHEAD, P. J. P., M.-L. BAUCHOT, J.-C. HUREAU, J. NIELSEN & E. TORTONESE (Eds.), 1984–86: *Fishes of the north-eastern Atlantic and the Mediterranean*. Vol I–III. UNESCO, Paris: 1473 pp.
- WINTERS, G. H. & J. P. WHEELER, 1996: Environmental and phenotypic factors affecting the reproductive cycle of Atlantic herring. *ICES J. Mar. Sci.*, **53**: 73–88.

ULPGC.Biblioteca Universitaria



622808
BIG 574.5 COL 001

